New Scandium and Titanium Borylimido Chemistry

Benjamin A. Clough

MChem, AMRSC

St Edmund Hall

Thesis submitted to the University of Oxford for the degree of Doctor of Philosophy in Inorganic Chemistry, February 2017.

The work described in this Thesis was carried out in the Chemistry Research Laboratory, University of Oxford from October 2013 to December 2016 under the supervision of Professor Philip Mountford. All work is my own unless stated to the contrary, and has not previously been submitted for any degree at this or any other university.

Benjamin A. Clough

February 2017

Abstract

Benjamin A. Clough
St Edmund Hall

Hilary 2017
D.Phil. Thesis

This Thesis reports the synthesis and reactivity of scandium and titanium borylimides. New, versatile synthetic routes to such complexes of these two metals were targeted, and their reactions with small, unsaturated compounds were explored, with a particular focus being the reactivity of alkynes with these systems.

Chapter One provides a background on Group 4 imido and hydrazido complexes. Group 4 alkoxyimides are also reviewed, as well as the developing field of rare earth imides. The Chapter focuses on the synthesis, structure, and stoichiometric and catalytic reactions of these complexes with unsaturated substrates, and ends with a description of the handful of known transition metal borylimides.

Chapter Two first describes the synthesis and structures of new titanium borylimido synthons prepared from $Ti(NMe_2)_2Cl_2$. From the borylimide $Ti\{NB(NAr'CH)_2\}Cl_2(py)_3$ are then formed five new compounds supported by a range of tridentate, nitrogen-based ligands.

Chapter Three describes the synthesis of half-sandwich titanium borylimides through *tert*-butylimide/borylamine exchange. A sandwich compound is also described, and the electronic structures of these complexes are analysed by DFT, QTAIM and NBO studies. Reactivity with heteroallenes, and exchange reactions with amines are also explored.

Chapter Four describes the reactivity of diamide-donor-supported titanium borylimides with terminal alkynes. The principal reaction outcomes are [2+2] cycloadditions and C–H bond activations, and an interesting C–F bond activation is also described. Kinetic studies of some reactions are presented, and will be supported by further DFT studies.

Chapter Five explores attempts to prepare the first rare earth borylimide. Kinetic and computational evidence is presented for the existence of a transient scandium borylimide which rapidly undergoes interesting sp, sp^2 and sp^3 C–H bond activations.

Chapter Six presents full experimental procedures and characterising data for the new complexes reported.

CD Appendix contains CIF files for all new crystallographically characterised complexes.

Acknowledgements

First and foremost, I must extend my sincere gratitude to Prof. Philip Mountford for giving me the opportunity to study in this amazing place – not just once, but twice over. The project that became this DPhil Thesis started out as a real challenge, but flourished into a highly rewarding endeavour of which I could not be more proud, and I thank you for all your support and guidance over the last eight years and your enduring passion for metal–nitrogen multiple bonds!

The last three and a half years would not have been possible without the support of all of my colleagues in the Mountford group. The coffee area lunches and evenings in the Uni Club have been essential for the maintenance of sanity. In particular, I would like to thank Dr Laura Stevenson for all of her initial help and knowledge about titanium chemistry, and newer members of "Team Borylimide", Bowen Xie and Martin Slusarczyk, for the discussions about chemistry and keeping me distracted with an endless To Do list for crystallography – I love it really(!) Massive thanks must go to Dr Matthew Blake and Dr Insun Yu for all of their advice and their hard work for the lab, as well as to Dr Andrey Protchenko for his chemical wizardry and his initial work on this borylimido project. Simona Mellino, Bowen Xie, Martin Slusarczyk and Theresa Scharbert are also thanked for proof-reading of this Thesis, and Simona additionally for performing DFT calculations.

Thanks also go to Dr Nick Rees for maintenance of the NMR facilities, and Dr Amber Thompson and Prof. Richard Cooper for assistance with X-ray crystallography, as well as to all of the support staff of the CRL for keeping it running. Additionally, Dr Terrance Hadlington (Monash) and Prof. Simon Aldridge are thanked for their advice on boryl chemistry, and Dr Eric Clot for the collaboration on DFT calculations.

The love and support of my parents, and the rest of my family, have been invaluable whilst I've been in Oxford, and I take this opportunity to thank you all – I'll never forget everything you've done for me.

Finally, this Thesis is dedicated to my love and best friend Becky, and all of her support over these last few years – *My a'th kar!*

Contents

Chapter Two: Titanium borylimido synthons and N_2N-supported complexes: synthesis, structure and bonding

Chapter Three: Sandwich and half-sandwich titanium borylimides: synthesis, structure, bonding and reactivity

Chapter Four: Reactions of diamide-donor-supported titanium borylimides with terminal alkynes

Chapter Five: Evidence for the formation of a transient scandium borylimide and its small molecule reactivity

Chapter Six: Experimental details and characterising data

Abbreviations

General

Å	Ångstrom
atm	atmosphere(s)
Avg.	average
ca	*circa*, about
cf.	*confer*, compared to
CSD	Cambridge Structural Database
^{o}	degrees
^{o}C	degrees Celsius
d	day(s)
e	elementary charge
Fac	facially coordinating
g	grams
h	hour(s)
η	hapticity
K	Kelvin
kcal mol^{-1}	kilocalorie(s) per mole
M	molarity, mol dm^{-3}
mbar	millibar(s)
Mer	Meridonally coordinating
min	minute(s)
mL	millilitre(s)
mmol	millimole(s)
MOCVD	Metal-Organic Chemical Vapour Deposition
RDS	rate determining step
RT	room temperature
s	second(s)
μ	bridging
μmol	micromole(s)
vs	versus

Chemical

9-BBN	9-borabicyclo[3.3.1]nonane
Ad	adamantyl
Ar	aryl group
Ar'	2,6-$C_6H_3{}^{i}Pr_2$
Ar^F	C_6F_5
bipy	2,2'-bipyridine
^{n}Bu	*n*-butyl
$^{t}Bupy$	di-*tert*-butyl pyridine
CCC^{Bu}	2-(1,3-bis(N-butylimidazol-2-ylidene)-phenylene
cent	ring centroid
Cp	C_5H_5
Cp*	C_5Me_5
Cp'	C_5H_4Me
Cy	Cyclohexyl
DMAP	4-dimethylaminopyridine
E	generic chalcogen atom
EIE	equilibrium isotope effect
Et	Ethyl
H_2Me_4taa	tetramethyl dibenzotetraaza[14]annulene
H-hpp	1,3,4,6,7,8-hexaydro-2*H*-pyrimido[1,2-*a*]pyrimidine
Hpypyr	2-(2′-pyridyl)-3,5-dimethylpyrrole
IDipp	*N*,*N*'-bis(2,6-diisopropylphenyl)imidazol-2-ylidene
^{i}Pr	*iso*-propyl
KIE	kinetic isotope effect(s)
L	a supporting ligand (set)
L^1	$(Ar')NC(Me)CHC(Me)NCH_2CH_2NMe_2$
L^2	$(Ar')NC(Me)CHC(Me)NCH_2CH_2N(Me)CH_2CH_2NMe_2$
Me	methyl
Me_2pz	3,5-dimethylpyrazolyl
$Me_3[6]aneN_3$	1,3,5-trimethyltriazacyclohexane
$Me_3[9]aneN_3$	1,4,7-trimethyltriazacyclononane
Mes	2,4,6-$C_6H_2Me_3$
Mes*	2,4,6-$C_6H_2{}^{t}Bu_3$

Np	*neo*-pentyl, $-CH_2{}^tBu$
N_2NN'	$(2\text{-}C_5H_4N)CH_2N(CH_2CH_2NSiMe_3)_2$
N_2N^R	generic diamide-amine ligand
N_2N^{py}	$MeC(2\text{-}C_5H_4N)(CH_2NSiMe_3)_2$
$N_2{}^{SiMe_3}N^{Me}$	$MeN(CH_2CH_2NSiMe_3)_2$
$N_2{}^{ArF}N^{Me}$	$MeN(CH_2CH_2NAr^F)_2$
N_2N^{Me,C_3}	$MeN(CH_2CH_2CH_2NSiMe_3)_2$
$N_2N^{SiMe_3}$	$Me_3SiN(CH_2CH_2NSiMe_3)_2$
$N_2{}^{iPr}N^{Me}$	$MeN(CH_2CH_2N{}^iPr)_2$
$N_2{}^{TBS}N^{py}$	$MeC(2\text{-}C_5H_4N)\{CH_2N(Si{}^tBuMe_2)\}_2$
$N_2{}^{TFAP}N^{py}$	$MeC(2\text{-}C_5H_4N)\{CH_2NH(2\text{-}C_6F_4NMe_2)\}_2$
$N_2{}^{3,5\text{-}Xyl}N^{py}$	$MeC(2\text{-}C_5H_4N)\{CH_2NH(3,5\text{-}C_6H_3Me_2)\}_2$
$N^{3,5\text{-}Xyl}N^{pyr}$	2-(3,5-dimethylphenylamino)pyrrolinato
$N_2{}^{pyr}N^{Me}$	*N*,*N*-di(pyrrolyl-α-methyl)-*N*-methylamine
$N_2{}^{SiMe3}O$	$O\text{-}(CH_2CH_2NSiMe_3)_2$
$N_2{}^{Ar}O$	$O\text{-}(2\text{-}C_6H_4NSiMe_3)_2$
$N^{pyr}N^{Me_2}$	$Me_2NCH_2(2\text{-}NC_4H_3)$
Ph	phenyl
Pin	2,3-dimethyl-2,3-butanediol
PNP	$N\{2\text{-}P{}^iPr_2\text{-}4\text{-}C_6H_3Me\}_2$
py	pyridine
py'	4-pyrrolidinopyridine
R	generic aryl or alkyl
^tBu	*tert*-butyl
^tBu-bipy	4,4'-di-*tert*-butyl-2,2'-bipyridine
^{tBu}NacNac	$HC\{C(^tBu)NAr'\}_2$
THF	tetrahydrofuran
TMEDA	N,N,N',N'-tetramethylethylenediamine
Tol	$4\text{-}C_6H_4Me$
$Tp^{tBu,Me}$	tris(3-methyl-5-*tert*-butylpyrazolyl)borate
TTP	*meso*-tetra-*p*-tolylporphyrinato dianion
X	generic anionic ligand
Xyl	$2,6\text{-}C_6H_3Me_2$
ZPE	zero point energy
‡	transition state or activation parameter

Calculations

BCP	bond critical point
BD	bond dissociation
DFT	density functional theory
δ	delocalisation index
ε	ellipticity
G	kinetic energy density
H	energy density
HOMO	highest occupied molecular orbital
k	bond force constant
LUMO	lowest unoccupied molecular orbital
MO	molecular orbital
NBO	natural bonding orbital
NLMO	natural localised molecular orbital
TS	transition state
ρ	electron density
Q	charge
QTAIM	Quantum Theory of Atoms in Molecules
V	potential energy density
$\nabla^2\rho$	electron density Laplacian

Mass Spectrometry

EI	electron impact
FI	field impact
HR	high-resolution
m/z	mass to charge ratio
MS	mass spectrometry

Nuclear Magnetic Resonance Spectroscopy

$^{13}C\{^{1}H\}$	proton-decoupled ^{13}C
$^{11}B\{^{1}H\}$	proton-decoupled ^{11}B
$^{19}F\{^{1}H\}$	proton-decoupled ^{19}F

app.	apparent
br.	broad
COSY	correlation spectrocopy
d	doublet
HMBC	heteronuclear multiple-bond correlation
HSQC	heteronuclear single quantum correlation
Hz	Hertz
i	*ipso*
J	coupling constant
m	*meta*
m	multiplet
MHz	Megahertz
NMR	nuclear magnetic resonance
NOE	nuclear Overhauser effect
o	*ortho*
p	*para*
ppm	parts per million
q	quartet
ROESY	Rotating-frame nuclear Overhauser Effect spectroscopy
s	singlet
sept.	septet
t	triplet
VT	variable temperature
δ	chemical shift in ppm

Infrared Spectroscopy

br.	broad
FT-IR	fourier transform infrared
IR	infrared
cm^{-1}	wavenumber
m	medium
s	strong
w	weak
ν	frequency

Notes

Literature compounds described in this Thesis are numbered **1.x**, **2.x**, **3.x**, **4.x**, **5.x** according to the Chapter in which they first occur. The new compounds described in this Thesis are numbered **1** – **45**. Density functional theory (DFT) calculated compounds are clearly stated in the text.

X-ray crystallography data was collected, solved and refined by the Author with the help and guidance of Prof. Philip Mountford. For compounds **3**, **17** and **20**, data was collected by Dr Laura Stevenson, and for compound **9**, data was collected by Dr Matthew Blake. Molecular drawings were produced by Prof. Philip Mountford.

DFT calculations were performed by Simona Mellino and Prof. Philip Mountford of the University of Oxford in collaboration with Dr Eric Clot of Université Montpellier, France.

Chapter One

Introduction

1.1 General introduction

Over the past four decades, the field of transition metal–ligand multiple bonding has been the focus of a sustained research effort by many researchers in inorganic and organometallic chemistry. This has resulted in major advances in structure, bonding and reactivity in complexes containing these bonds. Of particular interest to our research group, as well as many others, are transition metal–nitrogen multiple bonds. This was initially based on the proposed existence of imido and hydrazido functional groups, M=NR and $M=NNR_2$ (R = alkyl or aryl) respectively, as intermediates in the biological fixation of dinitrogen to ammonia at transition metal centres. However, research on transition metal imido and hydrazido compounds has since flourished in its own right, with the structure and bonding of these systems now being well understood, and a wide range of useful stoichiometric and catalytic reactions with small molecules being discovered, in addition to industrial applications. These include the stoichiometric and catalytic reduction of dinitrogen,[1–6] carbodiimide metathesis,[7] olefin polymerisation,[8–12] MOCVD (Metal-Organic Chemical Vapour Deposition)[9,13,14] and new C–N bond forming reactions including hydroamination and hydrohydrazination (N–H bond addition across the multiple bonds of alkenes, alkynes, allenes and carbodiimides).[15–28]

This Thesis describes new approaches to the formation of complexes containing the related borylimido functionalities, $M=NBR_2$. Prior to this study, there were no established versatile synthetic routes to these complexes, with those few examples reported originating from either serendipitous N–B couplings or an oxidative route of limited synthetic scope. The Author therefore initially targeted the synthesis of titanium borylimides using analogous methodologies to those which have been successful in preparing titanium imides and hydrazides within our research group. The synthesis and structure of fourteen such titanium borylimido complexes will be described in Chapters Two and Three. The first reactivity studies of any borylimido complex will then be explored, focussing particularly on reactions with heteroallenes (Chapter Three) and terminal alkynes (Chapter Four). In the last six years, the first terminal imido complexes of rare earth metals have been reported. Chapter Five explores evidence for the formation of the first rare earth metal borylimide, namely of scandium.

1.2 The imido ligand

Transition metal complexes containing terminal imido ligands have been known since the late 1950s. Depending on the identity of the metal to which it binds, the imido ligand may function as either an inert spectator ligand or as a centre of diverse reactivity. Generally speaking, later transition metal imido linkages are often known to be robust supporting ligands, whilst for early metals (Groups 3 and 4) the increased polarity of the M–N multiple bond makes these complexes much more reactive.[29] The field has been covered in a number of reviews,[30–34] to which the reader is directed for a wide coverage of metal imides in general. Subsequent Sections of this Chapter will provide an overview of Group 3 and 4 metal imido chemistry, as these are of direct relevance to the borylimido complexes described in later Chapters. Firstly, however, a valence bond description of the metal–imido linkage will be provided.

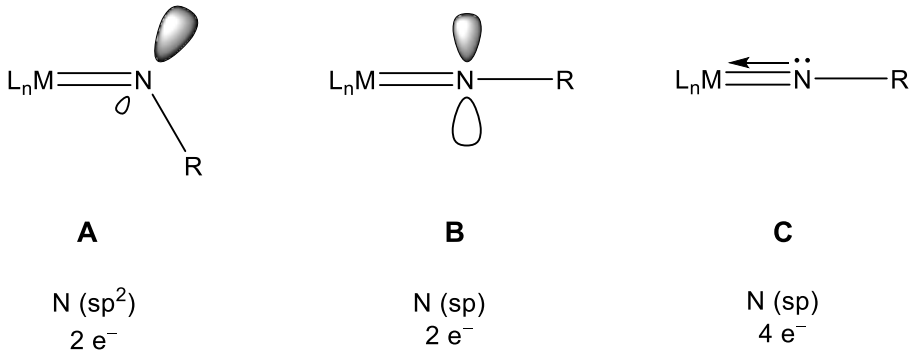

Figure 1.1. Bonding modes of the terminal imido ligand, along with orbital hybridisation of the N atom, and the neutral valence electron count of the ligand.[32]

Depending on the bonding mode present, a dianionic imido ligand is considered to bond to a transition metal with one σ-bond and either one or two π-interactions.[32] Structure A of Figure 1.1 depicts a bent M–N–R linkage with an sp^2-hybridised nitrogen atom which gives an M=N double bond ($\sigma^2\pi^2$). In this case, the nitrogen lone pair resides in an sp^2 orbital. This bonding situation is rare; one example is found in the bis(imide) $Mo(NPh)_2(S_2CNEt_2)_2$ (**1.1**, Figure 1.2), in which one phenylimido ligand is near-linear (Mo–N–C = 169.4(4)°) and one is bent (Mo–N–C = 139.4(4)°).[35] Taking a general view, the vast majority of structurally characterised imides are near-linear. This suggests sp hybridisation at nitrogen meaning that the lone pair resides in a pure p orbital (Structure B, Figure 1.1), and a formal M=N double bond ($\sigma^2\pi^2$). This situation arises in complexes where the lone pair cannot effectively donate to the metal centre due to a lack of acceptor orbitals of suitable symmetry

or energetic match. For example, in so-called π-loaded imido complexes, such as $Cp_2Ti(N^tBu)(py)$ (**1.2**, Figure 1.2), what appears to be a twenty valence electron count is rationalised by considering that competition of the imido π-components against the π-donor orbitals of the Cp ligands prevents full donation of the lone pair to the metal.[36] However, in the vast majority of imido complexes, donation of the lone pair to the metal centre is effective, which gives rise to Structure C. Here, a formal triple bond ($\sigma^2\pi^4$) is formed, in which the imido dianion now acts as a four electron donor (using the neutral electron counting method). Throughout this Thesis, the imido linkage is drawn as a double bond for simplicity. This signifies the dianionic nature of the ligand and does not imply a formal bond order of 2.

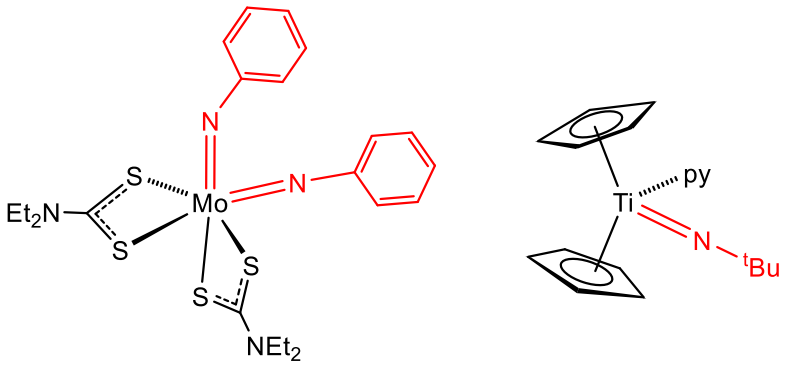

1.1 **1.2**

Figure 1.2. Examples of bent (**1.1**) and π-loaded (**1.2**) imido complexes.

1.3 Group 4 imido complexes

1.3.1 Synthesis of titanium imido complexes

In 1990, Roesky *et al.* synthesised the first titanium imido complex, $Ti\{NP(S)Ph_2\}Cl_2(py)_3$ (**1.3**), by reaction of $TiCl_4$ with $Ph_2P(S)NSiMe_3$, Me_3SiCl and pyridine.[37] In the same year, Rothwell and co-workers prepared the imido complex $Ti(Ar'O)_2(py')_2(NPh)$ (**1.4**, Ar' = 2,6-$C_6H_3{}^iPr_2$, py' = 4-pyrrolidinopyridine) through thermolysis of $Ti(Ar'O)_2(py')_2\{\eta^2\text{-}N(Ph)N(Ph)\}$, and alternatively also through addition of py' and H_2NPh to $Ti(Ar'O)_2\{\eta^2\text{-}N(^tBu)C(CH_2Ph)_2\}(py)$.[38] Both **1.3** and **1.4** were fully characterised, including through X-ray crystallography. Soon afterwards, the titanium congener of one of the early zirconium imides (*vide infra*), $Ti(NSi^tBu_3)(NHSi^tBu_3)_2$ (**1.5**), was synthesised through dehydrohalogenation of $Ti(NHSi^tBu_3)_3Cl$ with MeLi, although it was found to be a transient complex which could not be isolated.[39] Other reported routes to monomeric

imido complexes include the oxidation of Ti(II) species and reaction of (L)$TiCl_2$ complexes with 2 equivalents of MNHR (M = Li or K).[7,40–42]

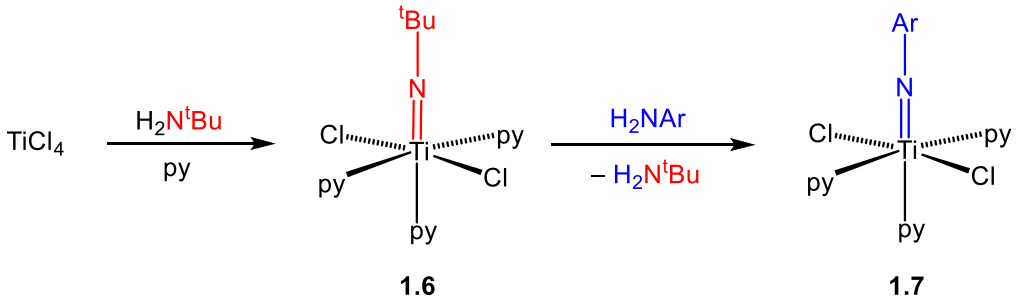

1.6 **1.7**

Scheme 1.1. Synthesis of complexes of the type $Ti(NR)Cl_2(py)_3$ (R = ^{t}Bu (**1.6**) or aryl (**1.7**)).[43]

In a more general route published by Mountford and co-workers in 1994, the high yielding, multi-gram synthesis of $Ti(N^tBu)Cl_2(py)_3$ (**1.6**) from $TiCl_4$, H_2N^tBu and pyridine was described (Scheme 1.1).[43] The analogous reactions of $TiCl_4$ with a selection of anilines and pyridine were unsuccessful. Arylimido complexes of the type $Ti(NAr)Cl_2(py)_3$ (**1.7**; examples of Ar = Ph, Xyl (2,6-$C_6H_3Me_2$) and Tol (4-C_6H_4Me)) were successfully obtained, however, by aniline/*tert*-butylimide exchange reactions with **1.6**.[34,43–45] Such tris(pyridine) imido compounds revolutionised research into titanium imido compounds, as they provided versatile entry points into a wide range of compounds following reactions with a variety of lithiated ligands (Scheme 1.2).[7,34,36,45–48] To highlight only a few examples, salt metathesis reactions of **1.6** with sodiated or lithiated Cp-type ligands $M[C_5R_5]$ (M = Li or Na, R = H or Me) resulted in sandwich or half-sandwich complexes such as $Cp_2Ti(N^tBu)(py)$ (**1.2**) and $Cp^*Ti(N^tBu)Cl(py)$ (**1.8**).[36] Similarly, salt metathesis reactions between **1.6** and the lithiated diamide-donor ligands $Li_2N_2N^{py}$ (N_2N^{py} = (2-C_5H_4N)$CMe(CH_2NSiMe_3)_2$) and $Li_2N_2N^{SiMe_3}$ ($N_2N^{SiMe_3}$ = $Me_3SiN\{(CH_2)_2NSiMe_3\}_2$) produced the complexes $Ti(N_2N^{py})(N^tBu)(py)$ (**1.9**) and $Ti(N_2N^{SiMe_3})(N^tBu)(py)$ (**1.10**) respectively.[49,50]

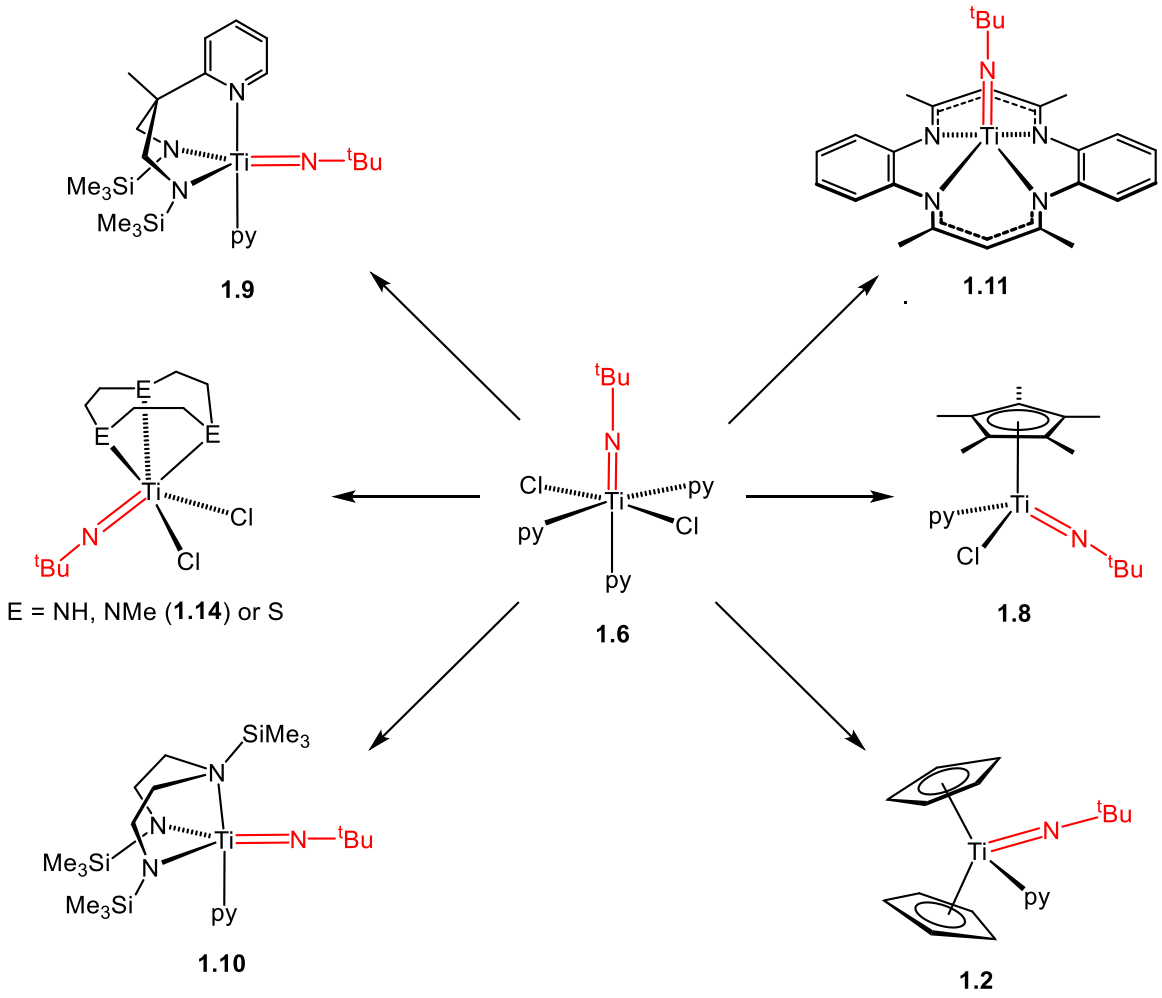

Scheme 1.2. Examples of titanium *tert*-butylimido complexes synthesised from Ti(N^{t}Bu)Cl$_2$(py)$_3$ (**1.6**).[7,34,36,45–50]

In a number of cases it was reported that the aniline/*tert*-butylimide exchange reaction could be carried out after the incorporation of the desired supporting ligand set. For example, reaction of the tetraazamacrocycle-supported *tert*-butylimido complex Ti(N^{t}Bu)(Me$_4$taa) (**1.11**, H$_2$Me$_4$taa = tetramethyl dibenzotetraaza[14]-annulene) with a range of anilines (H$_2$NAr; Ar = Ph, Tol, Xyl, 4-C$_6$H$_4$NO$_2$ and 4-C$_6$H$_4$NMe$_2$) yielded the corresponding arylimido compounds cleanly.[46,47] Similarly, the half-sandwich *tert*-butylimide **1.8** also forms a range of complexes of the type Cp*Ti(NAr)Cl(py) (Ar = Ar', 2,6-C$_6$H$_3$Br$_2$, 2-C$_6$H$_4$^{t}Bu, 2-C$_6$H$_4$^{i}Pr) upon reaction with the respective aniline.[51]

The compound $Ti(NMe_2)_2Cl_2$ has also proved to be a useful synthetic entry point into titanium imido compounds, in particular those with neutral, N_3-tridentate supporting ligands. This starting material is prepared through a simple redistribution reaction between $TiCl_4$ and $Ti(NMe_2)_4$,[52] and yields a wide range of imido complexes of the type $Ti(NR)Cl_2(NHMe_2)_2$ (R = alkyl (**1.12**) or aryl (**1.13**)) upon protonolysis with the respective alkylamine or aniline (Scheme 1.3).[53] Subsequent ligand displacement reactions with neutral ligands then produced the respective dichloride imido compounds. For example, reaction with Me_3[9]aneN_3 (1,4,7-trimethyltriazacyclononane) yields the compounds $Ti(NR)Cl_2(Me_3[9]aneN_3)$ (R = alkyl (**1.14**) or aryl (**1.15**)).[8] In some cases the previously described tris(pyridine) imido compounds **1.6** and **1.7** could be synthesised from **1.12** and **1.13** following reaction in neat pyridine. This synthetic method allowed access to some previously unknown imido synthons of the type **1.7** and also produced the first titanium compound to contain a chiral imido ligand, namely $Ti\{N\text{-}(S)\text{-}(-)\text{-}CH(Me)Ph\}Cl_2(py)_3$.[54] Structural studies of complexes of the type **1.6** and **1.7** have shown that the imido ligand exerts a relatively strong *trans* influence, quantified as the lengthening of the $Ti–N_{pyridine}$ bond of the *trans* pyridine relative to the bond distance to the *cis*-positioned pyridine ligands.[37,43] This results in a relatively labile *trans* pyridine ligand which can be removed under reduced pressure to form the chloride-bridged dimers $[Ti(NR)Cl(py)_2(\mu\text{-}Cl)]_2$ (R = alkyl or aryl).[43]

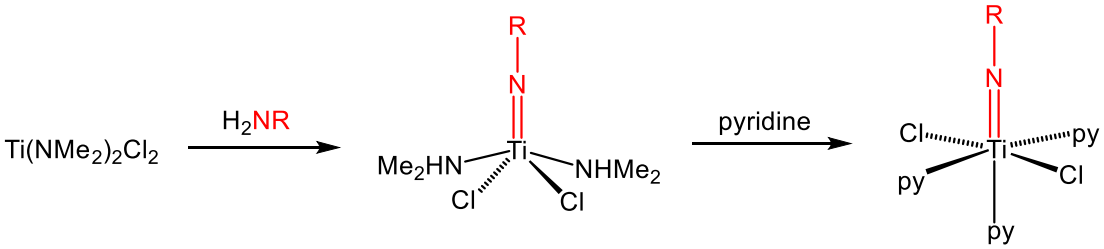

Scheme 1.3. Synthesis of $Ti(NR)Cl_2(NHMe_2)_2$ (R = alkyl (**1.12**) or aryl (**1.13**)), and reactions with pyridine.[43]

1.3.2 Synthesis of zirconium and hafnium imido complexes

The first terminal imido compounds of zirconium, $Cp_2Zr(NR)$ (R = ^{t}Bu (**1.16**), Xyl (**1.17**), 4-$C_6H_4{}^t$Bu (**1.18**); Figure 1.3), were prepared by Bergman and co-workers in 1988.[55] This family of compounds were reported to be transient species formed by thermolysis of the respective methyl-amido complex $Cp_2Zr(Me)(NHR)$, which then rapidly dimerise in hydrocarbon solutions to give complexes with bridging imido ligands. A THF adduct of the *tert*-butylimide, $Cp_2Zr(N^tBu)(THF)$ (**1.19**), could be isolated, however, when the thermolysis was performed in THF solution.[56] Dimeric zirconium and hafnium complexes containing bridging imido ligands had been previously observed by Nugent and Harlow in 1979 from the reaction of $M(NMe_2)_4$ (M = Zr or Hf) with H_2N^tBu.[57] The larger radius of zirconium and hafnium compared to titanium renders the synthesis of monomeric terminal imido compounds more difficult, as more steric protection is required at the reactive metal–nitrogen multiple bond. The same thermolytic method used to synthesise **1.19** was later used by Bergman and co-workers to prepare a mixed-sandwich complex, Cp*CpZr(N^{t}Bu)(THF).[58]

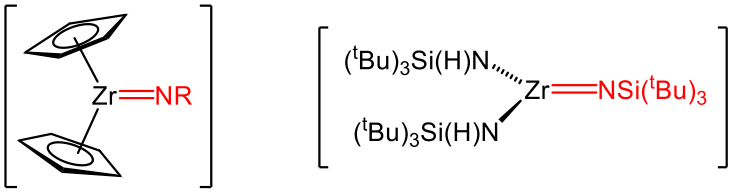

R = ^{t}Bu (**1.16**)
Xyl (**1.17**)
4-$C_6H_4{}^t$Bu (**1.18**)

1.20

Figure 1.3. Early examples of transient zirconium imido complexes.[55,59]

The transient imide $[Zr(NSi^tBu_3)(HNSi^tBu_3)_2]$ (**1.20**, Figure 1.3) was similarly prepared by Wolczanski and co-workers using a thermolysis procedure. Subsequent trapping with THF produced the isolable compound $Zr(NSi^tBu_3)(NHSi^tBu_3)_2(THF)$.[59] In 1992, Wigley and co-workers reported the preparation of a zirconium analogue of the titanium synthons $Ti(NAr)Cl_2(py)_3$ (**1.7**), namely $Zr(NAr')Cl_2(py)_3$ (**1.21**), from the reaction of $ZrCl_4(THF)_2$ with LiNHAr', Me_3SiCl and pyridine.[60] They were, however, unable to extend this result to a wider range of alkyl- or arylimido functionalities. In the absence of pyridine, the compound $Zr(NAr')Cl_2(THF)_2$ was formed, and later crystallographic characterisation by Mountford and co-workers showed that this was a dimeric species containing bridging imido ligands.[61] The analogous hafnium compound $Hf(NAr')Cl_2(THF)_2$ was also reported

by Wigley's research group.[60] Attempts were later made within our research group to access a more versatile zirconium synthon which would allow access to a wider range of alkyl- or arylimido ligands. Protonolysis methodologies based on the reactions of $Zr(CH_2SiMe_3)_2Cl_2(Et_2O)_2$ and $Zr(NMe_2)_2Cl_2(THF)_2$ with a range of primary alkylamines and anilines were found to provide general entry points to dimeric zirconium imido dichloride compounds.[53] However, addition of pyridine to such compounds did not result in monomeric compounds and the addition of lithiated ligands was also unsuccessful.

Complex **1.21** was shown by Wigley and co-workers to be a precursor to other zirconium imido complexes, namely the dimeric compounds $[(\eta^8\text{-}C_8H_8)Zr(\mu\text{-}NAr')]_2$ and $[Cp'ZrCl(\mu\text{-}NAr')]_2$ ($Cp' = \eta^5\text{-}C_5H_4Me$).[60] Our research group later used complex **1.21** for the synthesis of a number of further 2,6-diisopropylphenylimido complexes.[50,62] Zirconium and hafnium imido compounds can also be synthesised from dichloride precursors. For example, reaction of the macrocycle-supported dichloride compounds $(TTP)MCl_2$ (M = Zr or Hf, TTP = *meso*-tetra-*p*-tolylporphyrinato dianion) with two equivalents of LiNHAr' produced M(NAr')(TTP) (M = Zr (**1.22**) or Hf).[63] Our research group also reported the synthesis of the imido compound $Zr(N_2NN')(N^tBu)(py)$ ($N_2NN' = (2\text{-}C_5H_4N)CH_2N(CH_2CH_2NSiMe_3)_2$) from the dichloride precursor $Zr(N_2NN')Cl_2$ and 2 equiv. $LiCH_2SiMe_3$, followed by H_2N^tBu and pyridine.[64]

1.3.3 Structural features

During the course of research into titanium imido compounds, several studies into the geometric and electronic structures of such compounds have emerged. The results of some of these studies will be discussed here; all compounds described are monomeric, and contain a terminal imido ligand with a formal $\sigma^2\pi^4$ metal–nitrogen triple bond. For the families of compounds $Ti(NR)Cl_2(py)_3$ (R = ^{t}Bu (**1.6**) or aryl (**1.7**)), $Ti(NR)Cl_2(NHMe_2)_2$ (R = alkyl (**1.12**) or aryl (**1.13**)) and $Ti(NR)Cl_2(Me_3[9]aneN_3)$ (R = alkyl (**1.14**) or aryl (**1.15**)), short Ti–N bond lengths (range 1.672(2) – 1.7420(13) Å) and linear Ti–N–R bond angles (range 164.46(17) – 180^o) are indicative of such a triple bond.[43,53,65,66] In general, the alkylimido compounds have shorter Ti–N bonds than their arylimido counterparts (avg. Ti–NR bond length for R = alkyl: 1.690(1) Å and R = aryl: 1.7183(7) Å). A clear example of this is found in the series of compounds $Ti(NR)Cl_2(NHMe_2)_2$ (R = ^{i}Pr (**1.12a**), Ph (**1.13a**), $C_6F_5 = Ar^F$ (**1.13b**), 2,3,5,6-C_6HCl_4 (**1.13c**), 2-$C_6H_4CF_3$ (**1.13d**) and 2-$C_6H_4{}^t$Bu (**1.13e**))[53] and the series of compounds $Ti(NR)Cl_2(Me_3[9]aneN_3)$ (R = ^{t}Bu (**1.14a**), Xyl

(**1.15a**), Ar' (**1.15b**), Ph (**1.15c**), and Ar^F (**1.15d**)),[66] where the Ti–N bonds lengths increased in the order R = alkyl < aryl < electron-withdrawing aryl (see below for the origin of Ti–N bond lengthening in arylimides). The Ti–N bond lengthening effect of the electron-withdrawing substituent was also observed in the family of compounds $Ti(NR)Cl_2(py)_3$ (R = ^{t}Bu (**1.6**), 4-C_6H_4Me (**1.7a**) and 4-$C_6H_4NO_2$ (**1.7b**)), in which compound **1.7b** was found to have a much longer bond length than **1.6** and **1.7a** (1.722(3) *vs* 1.705(3) and 1.705(4) Å, respectively).[43] For this latter series of compounds, the higher coordination number and *trans* influence of the pyridine ligand generally result in a longer Ti–N bond distance than the other examples described above.

In 2011, a DFT study was carried out in order to better understand the structure and bonding in a range of cyclopentadienyl-amidinate-supported imido and hydrazido compounds.[67] The model system $CpTi\{MeC(NMe)_2\}(NR)$ (R = alkyl, aryl or NR_2) was employed, and it was found that the Ti=N bond length was significantly shorter when R = Me compared to R = Ph (1.688 *vs* 1.709 Å), which was consistent with the results obtained from crystallography discussed above. When R = Ph, donation from the Ti=N π orbital into a π* orbital of the phenyl ring can occur. Donation from a filled π orbital of the phenyl ring into the π* orbital of Ti=N can also take place, with both effects combining to result in a relative lengthening of the Ti=N bond.

As mentioned previously, the *trans* influence of the imido ligand can result in loss of the *trans*-pyridine ligand under vacuum and the formation of chloride-bridged dimers. In 1999, a computational study investigating this *trans* influence in compounds of the type $Ti(NR)Cl_2(py)_3$ (R = ^{t}Bu (**1.6**) or aryl (**1.7**)) was published, which employed model compounds of the type $Ti(NR)Cl_2(NH_3)_3$ (R = ^{t}Bu, Ph, 4-$C_6H_4NO_2$).[68] It was found that the *trans* influence arises from a complex balance of two factors. The major consideration (*ca* 75% of the influence) is purely electronic in origin; analysis of the electronic structures of the models shows that there are two filled antibonding MOs between the Ti and the *trans* NH_3 group, whilst there are no occupied MOs which are *cis* Ti–NH_3 antibonding. The second factor (*ca* 25%) arises from the fact that the HOMO is Ti–NR π-bonding, but π-antibonding between the Ti and the *cis* Cl atoms. The bending of the Cl atoms away from the imido ligand reduces the unfavourable Ti–Cl interaction and strengthens the Ti=N multiple bond. Steric repulsion between the Cl atoms and the *trans*-positioned NH_3 ligand then results in a lengthening of that Ti–NH_3 bond.

1.3.4 Stoichiometric reactions

The main point of interest for Group 4 imido compounds are reactions at the unsaturated M=NR linkage. The hallmark of the majority of Group 4 imido reaction chemistry is [2+2] cycloaddition reactivity of unsaturated substrates at the metal–nitrogen multiple bond. However, some examples involving C–H bond activations have also been reported. Bergman's zirconocene imido complex $Cp_2Zr(N^tBu)(THF)$ (**1.19**) displays extensive reaction chemistry with small molecules, some examples of which are shown in Scheme 1.4, and highlighted below.[56,69–73]

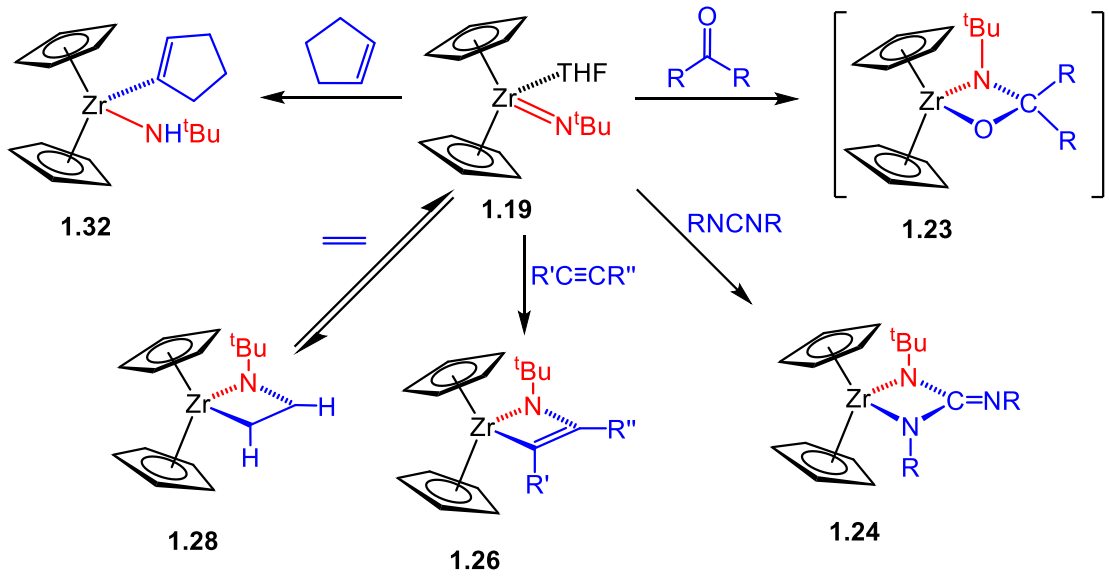

Scheme 1.4. Reactions of $Cp_2Zr(N^tBu)(THF)$ (**1.19**).[56,73]

The reactions of **1.19** with carbonyl compounds and carbodiimides produced complexes of the types $Cp_2Zr\{N(^tBu)C(R)(R)O\}$ (**1.23**) and $Cp_2Zr\{N(^tBu)C(NR)N(R)\}$ (**1.24**), respectively, through [2+2] cycloaddition of these unsaturated substrates at the metal–nitrogen multiple bond. Other examples include reactions with alkenes, alkynes and allenes which, in some cases, can lead to hydroamination of the substrate, *vide infra*. For instance, $Cp_2Zr(NR)(THF)$ (R = ^{t}Bu (**1.19**) or Xyl (**1.25**) gave [2+2] cycloaddition products with both internal and terminal alkynes, R'CCR" (R', R" = H, Me or aryl), namely $Cp_2Zr\{N(R)C(R")C(R')\}$ (R = ^{t}Bu (**1.26**, Scheme 1.4) or Xyl (**1.27**)).[56] In the case of $Cp_2Zr\{N(Xyl)C(Ph)C(Ph)\}$ (**1.27a**), the reaction was found to be reversible under certain conditions (85 – 110 °C), and on addition of TolCCTol was shown to form an equilibrium mixture of **1.27a** and the corresponding tolyl-substituted cycloaddition product $Cp_2Zr\{N(Xyl)C(Tol)C(Tol)\}$.[56] The *tert*-butylimido complex **1.19** also gave cycloaddition

products with alkenes, such as ethylene (**1.28**) and norbornene, in equilibrium with the starting material.[56]

Reaction of the cyclopentadienyl-amidinate-supported arylimido complexes Cp*Ti($N^{3,5\text{-}Xyl}N^{pyr}$)(NAr) (Ar = Xyl (**1.29**) or Mes (**1.30**), $N^{3,5\text{-}Xyl}N^{pyr}$ = 2-(3,5-dimethylphenylamino)pyrrolinato) with terminal alkynes also produced azatitanacyclobutene products. In contrast, the *tert*-butylimide Cp*Ti($N^{3,5\text{-}Xyl}N^{pyr}$)($N^tBu$)($^tBuNH_2$) (**1.31**) was found to give a C–H bond activation of HCCAr (Ar = Ph or Tol), producing the acetylide complexes Cp*Ti($N^{3,5\text{-}Xyl}N^{pyr}$)($NH^tBu$)(CCAr) instead.[28] The transient complexes M(NSi^tBu_3)($NHSi^tBu_3$)$_2$ (M = Ti (**1.5**) or Zr (**1.20**))[39,59] and $Cp_2Zr(N^tBu)(THF)$ (**1.19**)[55] were also found to activate C–H bonds. In particular, **1.19** can activate the C–H bonds of benzene when heated in that solvent, whereas no reaction was observed for the arylimido complex Cp_2Zr(NXyl)(THF) (**1.25**). Indeed, compound **1.19** was found to activate a range of sp^2 C–H bonds including those of cyclopentene (**1.32**, Scheme 1.4), norbornene (above 45 °C) and the Cp ring of various Cp-supported transition metal complexes.[73]

The diamide-amine-supported complex Ti(N_2N^{py})(N^tBu)(py) (**1.9**) also exhibits a particularly rich reaction chemistry,[7,45,74–78] and selected transformations are outlined in Scheme 1.5. Reactions of **1.9** with terminal alkynes yielded azatitanocyclobutene compounds of the type **1.33**,[75] whereas reaction with methyl-substituted internal alkynes or allenes led to the formation of titanaazetidines **1.34**.[74,78] Interestingly, reaction of **1.9** with 2 equiv. XylNC resulted in coupling of the isocyanides in the novel metallacycle **1.35**.[76]

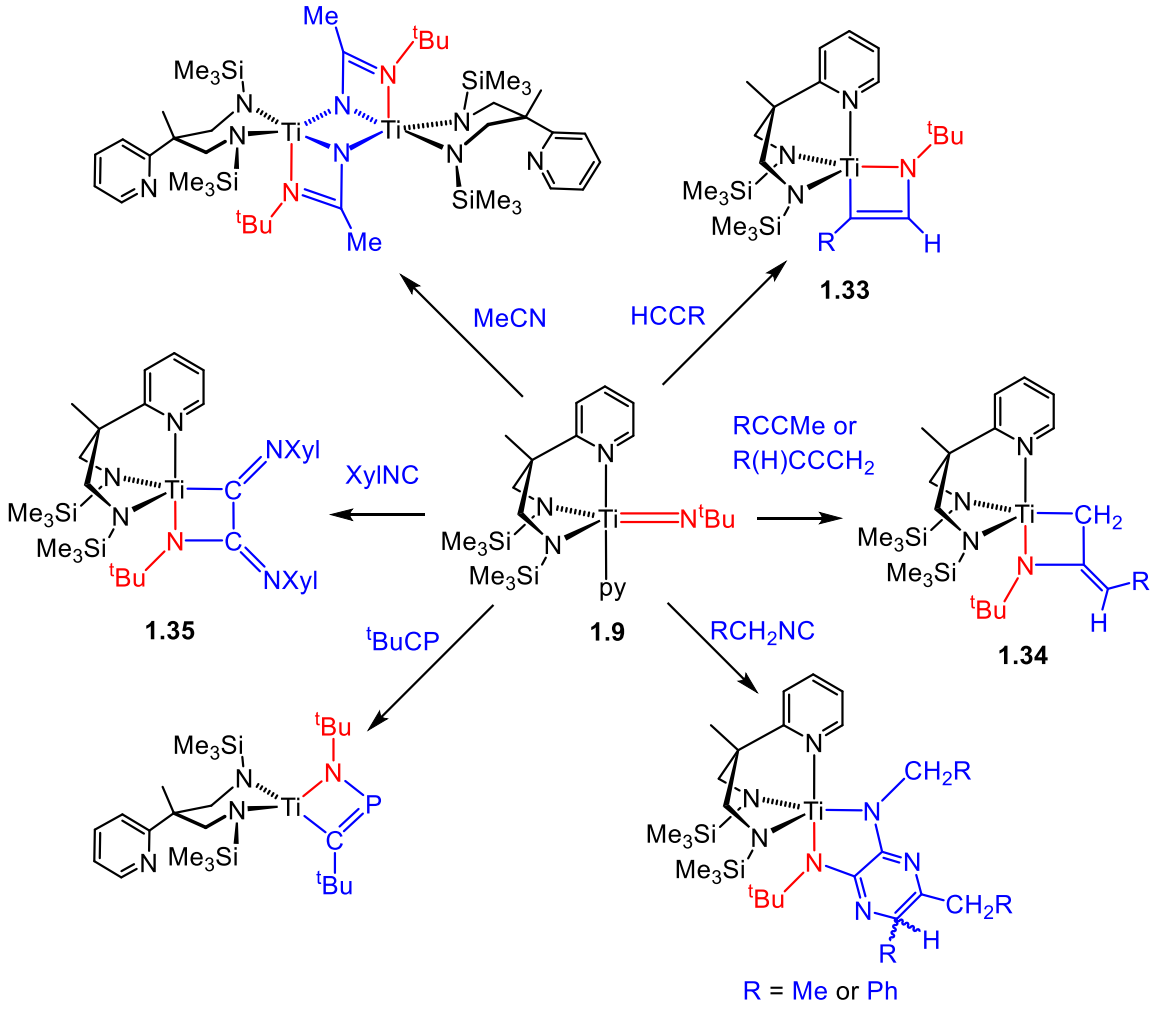

Scheme 1.5. Selected reactions of Ti(N_2N^{py})(N^tBu)(py) (**1.9**) with unsaturated compounds.[74–78]

The reactivity of several other Group 4 imido complexes with a range of organic substrates have been reported. For example, the reactions of Zr(NAr')(TTP) (**1.22**) with isocyanates proceed *via* a [2+2] cycloaddition reaction, which is followed by isomerisation and a subsequent extrusion, to generate carbodiimides.[63] The structurally similar set of compounds Ti(NAr)(Me_4taa) (Ar = Ph, Tol, Xyl, 4-$C_6H_4NO_2$, 4-$C_6H_4NMe_2$) gave an alternative reaction to produce the κ^2-N,N-bound ureate complexes Ti{N(Ar)C(O)N(Ar)}(Me_4taa) which were stable to extrusion. In some cases, this reaction was found to be reversible.[46]

Titanium imido complexes have also been shown to be capable of activating H–H, S–H and Si–H bonds. The compounds {η^5-1,3-$C_5H_3(SiMe_3)_2$}$_2$Ti(NR) (R = $SiMe_3$ or Mes) add H_2 in a 1,2-fashion across the metal–nitrogen multiple bond, yielding hydride-amide compounds.[42] The compound Cp_2Ti(N^tBu)(py) (**1.2**) reacts with MeSH to yield

$Cp_2Ti(SMe)_2$, and with SH_2 to yield the dimer $Cp_2Ti(\mu\text{-}S)_2TiCp_2$ or the monomer $Cp_2Ti(SH)_2$.[79] The corresponding reaction of $Ti(N^tBu)(Me_4taa)$ (**1.11**) with H_2S gave the terminal sulfide compound $Ti(Me_4taa)(S)$.[47] Another interesting reaction was observed for the cyclopentadienyl-amidinate-supported compound $Cp^*Ti\{MeC(N^iPr)_2\}(NTol)$ with $PhSiH_2X$ (X = Cl or Br), in which cleavage of the silicon–halogen bond gave silylamido-chloride complexes which were unstable in solution.[80]

1.3.5 Catalytic hydroamination

Since 2000, imido ligands have found applications as spectator ligands on titanium catalysts in the polymerisation of ethylene, for instance $Ti(NR)Cl_2(TMEDA)$ (R = ^{t}Bu, 2-$C_6H_4{}^t$Bu or 2-C_6H_4Ph; TMEDA = N,N,N',N'-tetramethylethylenediamine).[7,81] $Ti(NR)Cl_2(Me_3[9]aneN_3)$ (R = alkyl (**1.14)** or aryl (**1.15**))[8] and the cationic complexes $[Ti(N^tBu)(Me_3[9]aneN_3)R]^+$ (R = Me or CH_2SiMe_3)[7,82,83] have also proved effective.

Alongside ethylene polymerisation, Group 4 imido complexes have also found applications in the catalytic hydroamination of alkynes. Hydroamination is the addition of an N–H bond across an unsaturated C–C bond, and is an atom-economical method for the efficient formation of new N–C bonds. Group 4 metal complexes have been widely studied as catalysts in such processes and, through a series of mechanistic studies, three mechanisms have been established.[16–18,73,84–91] The most commonly found mechanism, the "imide route" proceeds through a [2+2] cycloaddition at the metal–nitrogen multiple bond. Protonolysis with an equivalent of amine then takes place to regenerate the imido catalyst and release an enamine, which then may tautomerise to an imine (Scheme 1.6).[20,92–95] Some exemplar catalytic systems are discussed below.

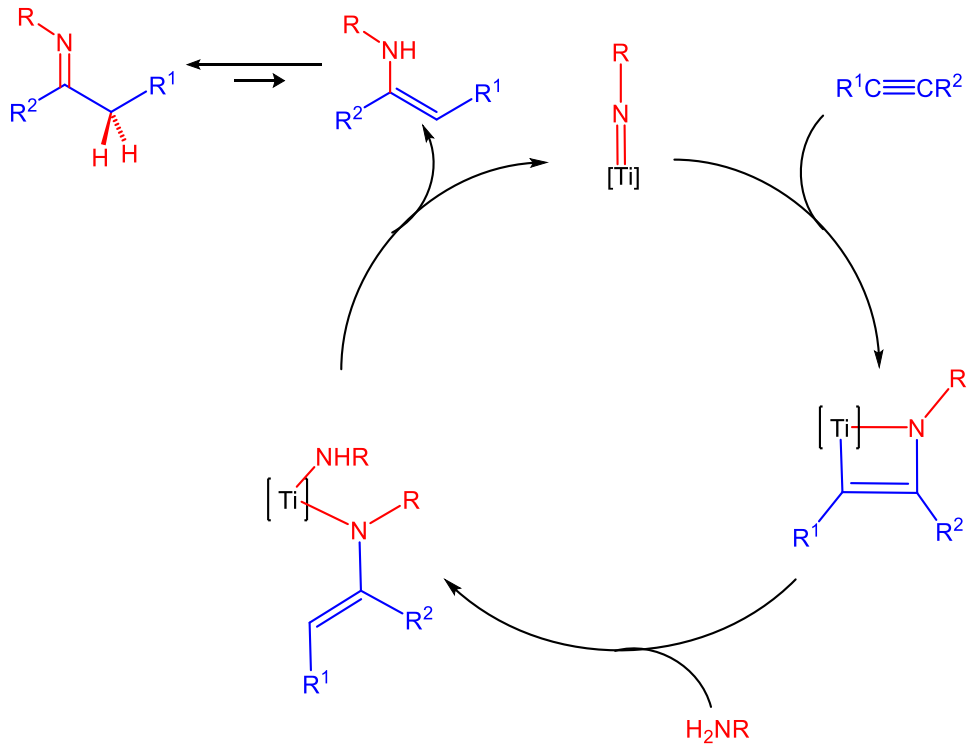

Scheme 1.6. General catalytic cycle for hydroamination (R = alkyl or aryl).

The titanium complexes, Cp*Ti($N^{3,5\text{-Xyl}}N^{pyr}$)(NXyl) (**1.29**) and Cp*Ti($N^{3,5\text{-Xyl}}N^{pyr}$)($N^{t}$Bu)(^{t}BuNH$_2$) (**1.31**), catalyse the hydroamination of both terminal and internal alkynes over a period of 24 h at 5 mol% catalyst loading, although high temperatures of 105 °C were required, and mixtures of linear and branched amines were isolated.[28] The parent compound Cp*Ti($N^{3,5\text{-Xyl}}N^{pyr}$)Me$_2$, from which both **1.29** and **1.30** are synthesised was also found to be an active hydroamination catalyst (the imido species are generated *in situ* upon addition of amine). These compounds were also shown to catalyse intramolecular hydroamination reactions. Other active catalysts reported in the literature include Cp$_2$Ti(η^2-Me$_3$SiC$_2$SiMe$_3$),[85] Ti($N_2^{pyr}N^{Me}$)(NMe$_2$)$_2$ (**1.36**, $N_2^{pyr}N^{Me}$ = *N*,*N*-di(pyrrolyl-α-methyl)-*N*-methylamine)[19] and Ti(NMe$_2$)$_4$,[96–98] with the proposed catalytic cycles proceeding *via* imido intermediates in all cases.

Bergman and co-workers have pioneered research into zirconium catalysts for the hydroamination of alkynes, alkenes and allenes. In 1992, the bis(amido) complex Cp$_2$Zr(NHXyl)$_2$ (**1.37**) was shown to catalyse the coupling of diphenylacetylene, 2-butyne and allene with H$_2$NXyl.[92] More recently, Zr(NMe$_2$)$_4$, Cp$_2$Zr(NMe$_2$)$_2$ and sulfonamide-supported zirconium complexes were also shown to be effective hydroamination catalysts of allenes, including those which are tri-substituted.[96] There are few reports, published only recently, on the use of hafnium complexes as hydroamination catalysts.[99–101] These include

the NHC-supported diiodide complex (CCC^{Bu})Hf(NMe_2)I_2 (**1.38**, CCC^{Bu} = 2-(1,3-bis(N-butylimidazol-2-ylidene)-phenylene, Figure 1.4),[101] which is able to catalyse the intramolecular hydroamination/cyclisation of a range of aminoalkene substrates, although in all of these reports the hafnium catalysts were much less active than their zirconium congeners.

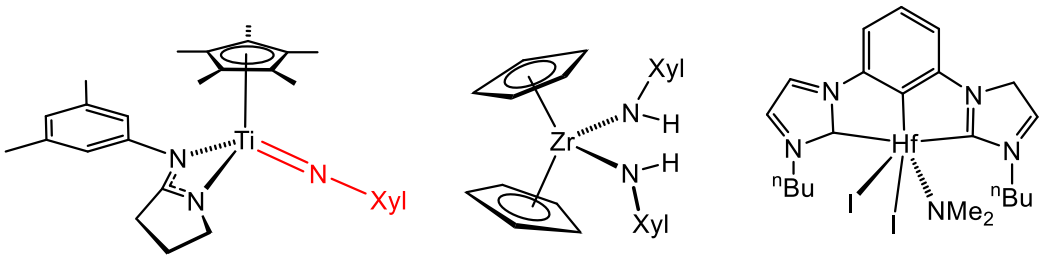

1.29 **1.37** **1.38**

Figure 1.4. Examples of Group 4 metal hydroamination catalysts.[28,92,101]

1.4 Rare earth metal imido complexes

Compared with their Group 4 counterparts, terminal imido complexes of rare earth metals are much more scarce, and advances in their successful synthesis and reactivity have taken place only in the last seven years.[102] Prior to this, the field was limited to the isolation of dimeric complexes or higher-nuclearity clusters which contained bridging imido ligands, as the putative first-formed monomeric complexes had a tendency to form these more stable structures, especially for the larger lanthanides and yttrium.[29,103–114] For example, treatment of the lanthanide naphthalide complexes Ln($C_{10}H_8$)(THF)$_3$ (Ln = Yb, Sm) with azobenzene resulted in formation of the tetranuclear complexes Ln$_4$(μ-η^2:η^2-N_2Ph_2)$_4$(μ^3-NPh)$_2$(THF)$_x$, which contain two phenylimido ligands that bridge three metal centres each, capping the tetranuclear core.[106,115] The four-electron reduction of an azobenzene unit to form the two imido ligands is accompanied by oxidation of the four metal centres from Ln(II) to Ln(III).

A number of complexes containing an Ln$_2$(μ^2-NR)$_2$ core have also been reported.[109–111] For example, treatment of Yb(NHAr')$_4${Na(THF)} with 2 or 4 equiv. ^{n}BuLi yields the mixed amido-imido complex {(Ar'N)(Ar'NH)Yb(μ-NAr')}$_2${[Li(THF)][Na(THF)]}$_2$ (**1.39**, Figure 1.5) or the related imido complex {(Ar'N)$_2$Yb(μ-NAr')}$_2${[Li$_2$(THF)][Na(THF)]}$_2$, respectively, which both incorporate an Yb$_2$(μ^2-NAr')$_2$ core.[109] Hessen and co-workers then extended this chemistry to a scandium system; reaction of the 2,3-dimethylbutadiene complex {η^5,η^1-$C_5H_4(CH_2)_2NMe_2$}Sc(C_6H_{10}) with PhCN gave the complex

[{η^5,η^1-$C_5H_4(CH_2)_2NMe_2$}Sc{μ^2-NC(Ph)C_6H_{10}}]$_2$ (**1.40**, Figure 1.5) *via* insertion of the nitrile into an Sc–C bond and attack of the other methylene group of the diene to force a cyclisation.[111] Rapid dimerisation of the three-coordinate imido complex then results in the dimeric **1.40**.

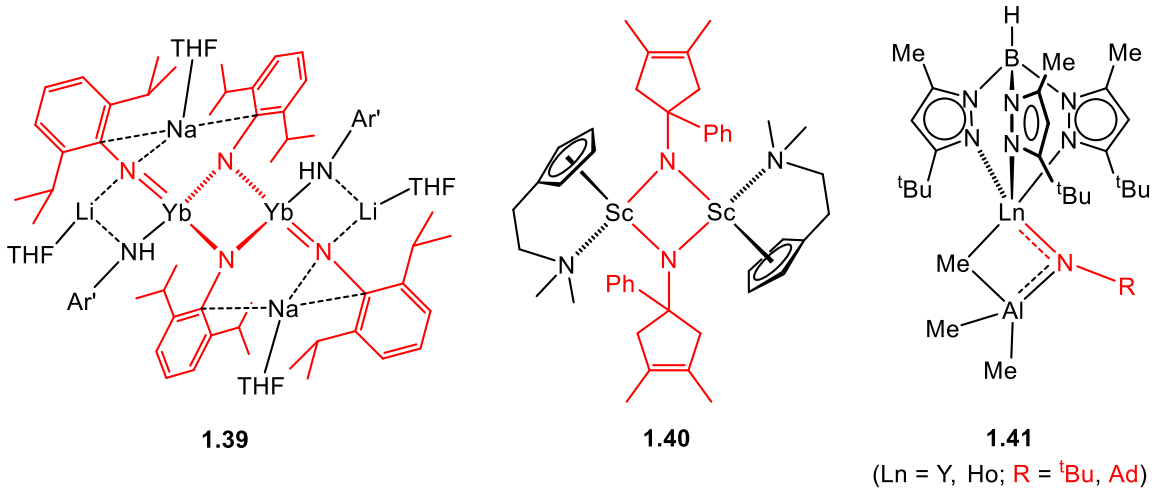

1.39 **1.40** **1.41**

(Ln = Y, Ho; R = ^{t}Bu, Ad)

Figure 1.5. Examples of rare earth complexes containing bridging and Lewis acid-supported imido ligands.[109,111,116]

Related μ^2-imido motifs have also been described in Lewis acid-stabilised imido complexes, a number of which have been prepared in recent years by Anwander and co-workers.[103,110,116–120] For example, reaction of Ln($AlMe_4$)$_3$ (Ln = Y, Nd, Lu) with H_2NMes* (Mes* = 2,4,6-$C_6H_2{}^t$Bu) ultimately yields the dimeric complexes [Ln($AlMe_4$)(μ^2-NMes*)]$_2$ which contain an Ln$_2$(μ^2-NMes*)$_2$ core.[103] Several heterobimetallic imido complexes containing an imido functional group which itself is supported by a Lewis acid have been prepared in a similar manner. For example, reaction of ($Tp^{tBu,Me}$)LnMe($AlMe_4$) (Ln = Y, Ho; $Tp^{tBu,Me}$ = tris(3-methyl-5-*tert*-butylpyrazolyl)borate) with H_2N^tBu or H_2NAd (Ad = adamantyl) produced the respective monomeric complex ($Tp^{tBu,Me}$)Ln{(μ^2-Me)$AlMe_2$}(μ^2-NR) (**1.41**, R = ^{t}Bu, Ad; Figure 1.5).[116] A similar reaction, reported by Mindiola and co-workers, formed the Lewis acid-stabilised complex (PNP)Sc{(μ^2-Me)$AlMe_2$}(μ^2-NAr') (**1.42**, PNP = N{2-P^iPr_2-4-C_6H_3Me}$_2$) from (PNP)Sc(Me)(NHAr') (**1.43**) and $AlMe_3$.[119]

Mindful that removal of the supporting $AlMe_3$ from **1.42** could result in the first terminal imido complex of scandium, Mindiola's research group subsequently added excess pyridine to that complex. This did displace the $AlMe_3$, although resulted in C–H bond activation of pyridine to yield the pyridyl complex (PNP)Sc(NHAr')(η^2-NC_5H_4) (**1.44**). The

same product was also obtained from reaction of **1.43** directly with pyridine, and mechanistic studies showed that this proceeds *via* a transient imido complex (PNP)Sc(NAr')(py) (**1.45**) which rapidly undergoes intramolecular C–H bond activation.

Whilst **1.45** was found to be too short-lived to be characterised, Chen and co-workers successfully formed the first isolable terminal imido complex of a rare earth metal in 2010.[121] This was achieved using DMAP as a very strong external Lewis base, in combination with the introduction of a new bulky β-diketiminate (NacNac)-type supporting ligand with a pendant NMe_2 donor; heating of (L^1)Sc(Me)(NHAr') (**1.46**, L^1 = (Ar')NC(Me)CHC(Me)$NCH_2CH_2NMe_2$) in the presence of DMAP gave the terminal imido complex (L^1)Sc(NAr')(DMAP) (**1.47**, Scheme 1.7). The short Sc–N_{im} distance (1.881(5) Å) and near-linear Sc–N_{im}–C angle (169.6(5)°) in **1.47** are consistent with a triple bond, as described for Group 4 imides above. DFT calculations also indicated the presence of two orthogonal π bonds and the $\sigma^2\pi^4$ nature of the triple bond.[121]

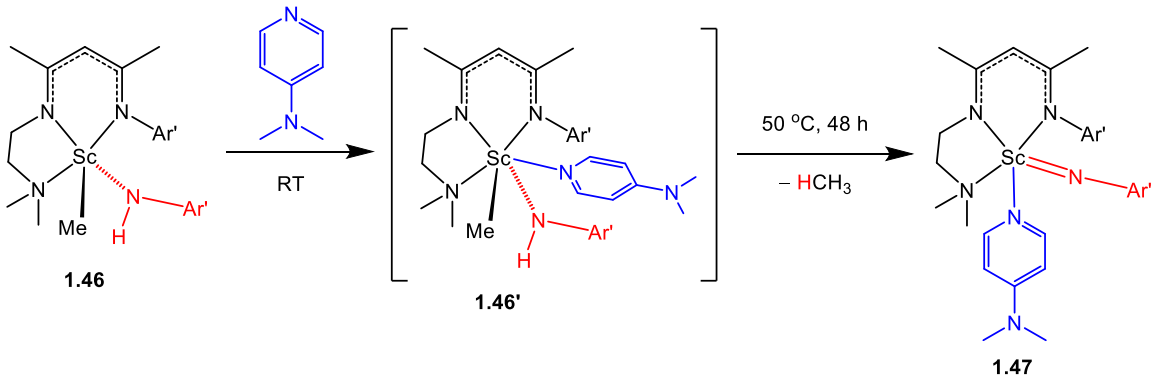

Scheme 1.7. Synthesis of (L^1)Sc(NAr')(DMAP) (**1.47**).[121]

Following the preparation of **1.47**, a number of other research groups used a similar strategy to prepare further terminal imido complexes of scandium. That is, using DMAP to stabilise the complexes, as well as incorporating a large amount of steric bulk into both the supporting ligand and the imido ligand itself. As reported by Piers and co-workers, (^{tBu}NacNac)Sc(Me)(NHAr') (^{tBu}NacNac = HC{C(^{t}Bu)NAr'}$_2$) was reacted with DMAP at 50 °C over 5 days to form (^{tBu}NacNac)Sc(NAr')(DMAP) (**1.48**, Figure 1.6), with mechanistic studies showing that this proceeds *via* an intermediate in which intramolecular C–H bond activation of an Ar' methyl group has taken place at the Sc centre.[122] Cui and co-workers also reported that the phosphazene ligand-supported alkyl-anilide {$N(PPh_2NPh)_2$}Sc(CH_2SiMe_3)(NHAr') in the presence of 2 equiv. DMAP underwent α-hydrogen abstraction over 4 h at RT to yield the imide {$N(PPh_2NPh)_2$}Sc(NAr')(DMAP)$_2$

(**1.49**, Figure 1.6).[123] Anwander and co-workers were later able to extend this methodology to other rare earth metals. In the presence of DMAP, the methyl-anilides ($Tp^{tBu,Me}$)Ln(Me)(NHAr) (Ln = Y, Ar = Xyl; Ln = Lu, Ar = 3,5-$C_6H_3(CF_3)_2$) converted to the DMAP-supported imido complexes ($Tp^{tBu,Me}$)Ln(NAr)(DMAP).[118]

Chen and co-workers were also able to prepare an isolable terminal scandium imide without the need for DMAP. This was achieved through modification of their ligand set to incorporate a second pendant amine donor, making this now a (potential) tetradentate ligand. From the alkyl-anilide (L^2)Sc(CH_2SiMe_3)(NHAr') (L^2 = (Ar')NC(Me)CHC(Me)$NCH_2CH_2N(Me)CH_2CH_2NMe_2$) in which the fourth donor atom of L^2 does not coordinate to the metal, heating at 50 °C for 3 days formed the imide (L^2)Sc(NAr') (**1.50**, Figure 1.6) in which L^2 has become tetradentate through the coordination of the second pendant amine donor.[124]

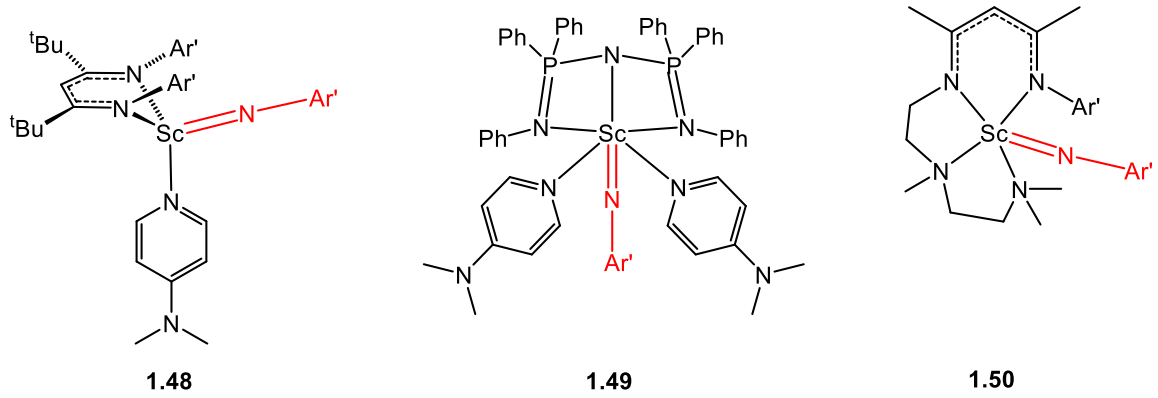

1.48 **1.49** **1.50**

Figure 1.6. Further examples of terminal imido complexes of scandium.[122–124]

With the emergence of isolable terminal imido complexes of scandium, the reactivity of this highly polar metal–nitrogen multiple bond has begun to be studied.[124–129] Firstly, imide **1.50** was subjected to a reactivity study with a range of unsaturated substrates,[128] a small number of which are highlighted here (Scheme 1.8). Generally, initial [2+2] or [2+4] cycloadditions are followed by other processes such as hydrogen transfer, Michael addition or an isomerisation. For example, reaction of **1.50** with CO_2 gave the first example of a rare earth dicarboxylate complex (L^2)Sc{$(O_2C)_2$NAr'} (**1.51**), and reaction with the isocyanate PhNCO resulted in the N,O-bound ureate complex (L^2)Sc{η^2-PhNC(NAr')O} (**1.52**) through an isomerisation which is driven by minimisation of steric interaction between the Ar' group and the L^2 supporting ligand. Additionally, the reaction of **1.50** with

cyclopentadiene gave a Cp-complex (L^2)Sc(Cp)(NHAr') (**1.53**) through C–H bond activation of the substrate.

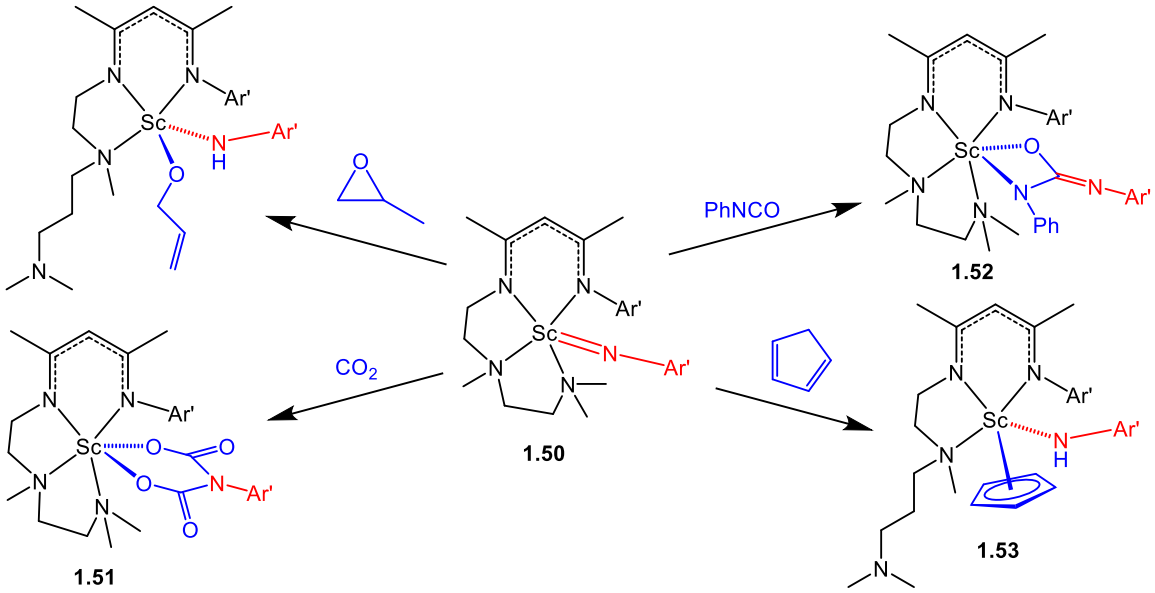

Scheme 1.8. Reactions of (L^2)Sc(NAr') (**1.50**) with unsaturated substrates.[128]

After having initial problems separating the by-product DMAP from the products of reactions of **1.47**,[128] Chen and co-workers later found that DMAP could be abstracted from this complex using 9-BBN (9-borabicyclo[3.3.1]nonane), or an alkyl derivative, to produce a base-free imide (L^1)Sc(NAr') (**1.47'**) that could then undergo reactions with added substrates, some examples of which are highlighted here (Scheme 1.9).[129] Addition of 9-BBN and MeCCPh to **1.47** at RT produced the first reported azascandacyclobutene (L^1)Sc{N(Ar')C(Me)C(Ph)} (**1.54**) *via* [2+2] cycloaddition of the alkyne at the metal–nitrogen multiple bond. Complex **1.47** reacts with 9-BBN and the terminal alkenes H_2C=C(H)R (R = ^{t}Bu, ^{n}Pr) to form the *trans*-alkenyl complexes (L^1)Sc(NHAr'){C(H)=C(H)R} (**1.55**) *via* C–H bond activation at the terminal methylene group of the alkene. When **1.47'** was generated from **1.47** with the addition of ^{t}Bu$CH_2CH_2BC_8H_{14}$, and heated at 50 °C without the addition of another reagent, a "tuck-in" complex (**1.56**, Scheme 1.9) was formed *via* C–H bond activation of a supporting ligand isopropyl group at the metal–nitrogen bond in a 1,2-fashion, which regenerates a protonated anilido ligand. Interestingly, addition of THF to **1.47'** results in the THF-coordinated imide (L^1)Sc(NAr')(THF) (**1.57**) as an isolable complex. This implies that DMAP is required kinetically to drive the α-abstraction step that forms **1.47** from the methyl-anilide **1.46**, but the strong base is not necessary to stabilise the final imido product.

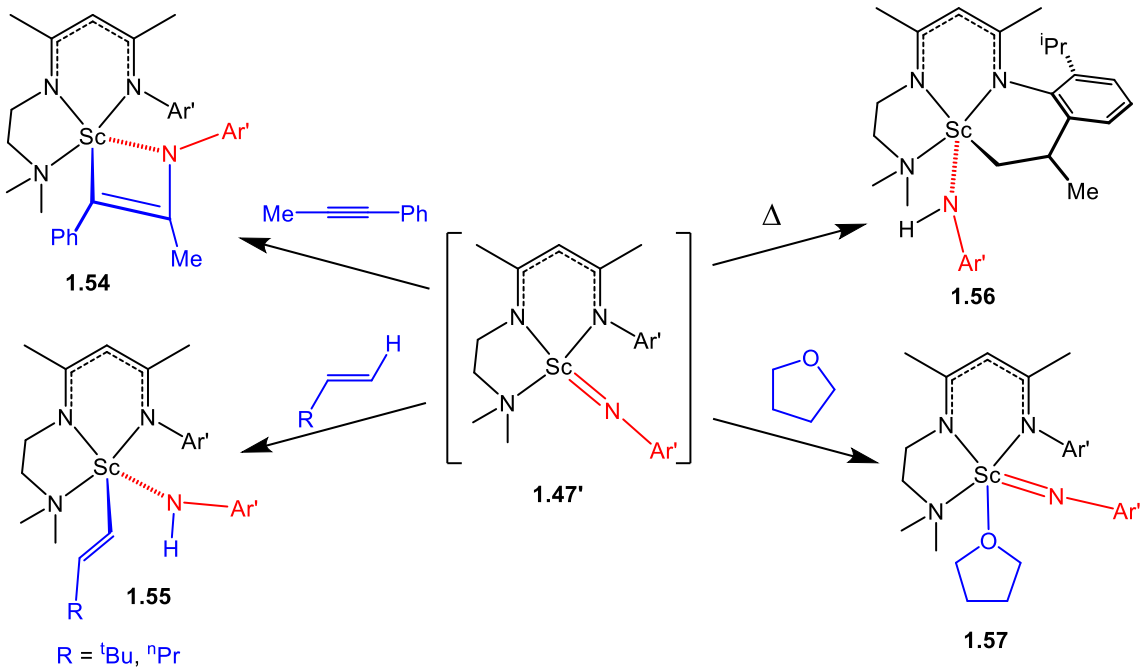

Scheme 1.9. Reactions of the *in situ*-generated imide (L^1)Sc(NAr') (**1.47'**).[129]

1.5 The hydrazido ligand

Terminal hydrazido complexes of transition metals have been known for as long as their imido counterparts, although early research into these compounds focussed on their relationship to the fixation of nitrogen in biology, particularly in Group 6 metal systems. In comparison, more recent work on Group 4 metal hydrazides has revolved around their richer reactivity with organic substrates when compared with the imides. The presence of the β-heteroatom, and a reducible N–N bond, have resulted in the discovery of a plethora of novel C–N bond-forming reactions. Section 1.6 will, therefore, focus exclusively on developments in the synthesis and reactivity of Group 4 hydrazido complexes.

Firstly, however, the potential structural diversity of the hydrazido ligand is noted. Having an $N_\beta R_2$ group enables a number of different bonding modes to metal centres (Figure 1.7).[19] The formal charge can be –1 or –2 depending on the presence or absence of an N_α-substituent, and N_β may also coordinate to a metal centre. However, all hydrazido ligands described in the following Section, and the rest of this Thesis, will be of the η^1-hydrazido(2–) variety, which are four-electron donors and isoelectronic with the imido ligand.[67,130]

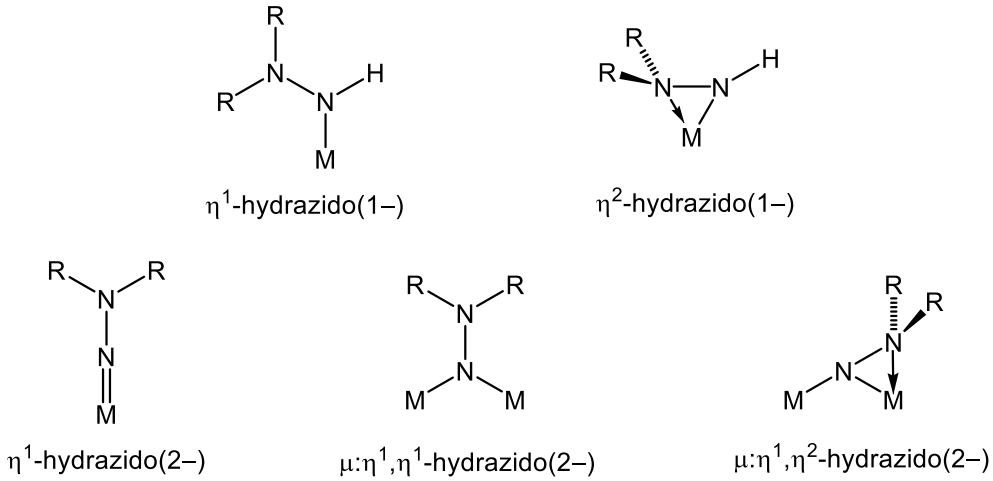

Figure 1.7. Bonding modes of hydrazido ligands.

1.6 Group 4 hydrazido complexes

1.6.1 Synthesis of titanium hydrazido complexes

The preparation of the first monomeric terminal hydrazido complex of titanium was reported by Wiberg *et al.* in 1978.[131] The reaction of Cp_2TiCl_2 with two equivalents of $Me_3SiN{=}NSiMe_3$ produced $Cp_2Ti\{NN(SiMe_3)_2\}$. It was not until 1999, however, that the next terminal titanium hydrazide was reported by our research group, this being the complex $Ti(NNPh_2)(Me_4taa)$ (**1.58**).[46] The first structural characterisation of a terminal titanium hydrazide was performed by Odom and co-workers in 2004 on the complex $Ti(N_2{}^{pyr}N^{Me})(NNMe_2)(^tBu\text{-bipy})$ (^tBu-bipy = 4,4'-di-*tert*-butyl-2,2'-bipyridine).[19] The successful syntheses of the diphenylhydrazido analogues of the imido synthons **1.6** and **1.12**, $Ti(NNPh_2)Cl_2(py)_3$ (**1.59**) and $Ti(NNPh_2)Cl_2(NHMe_2)_2$ (**1.60**) respectively,[130,132] through a hydrazine/*tert*-butylimide exchange methodology, subsequently allowed access to a wide range of diphenylhydrazido complexes.

Compound **1.59** was synthesised through a reaction of **1.6** with H_2NNPh_2, and **1.60** from $Ti(N^tBu)Cl_2(NHMe_2)_2$ (**1.12b**) and H_2NNPh_2, by analogy with those reactions with anilines described in Section 1.3.1 which produced arylimido complexes. Attempts to synthesise dimethylhydrazido analogues of **1.59** and **1.60** using H_2NNMe_2 resulted in the formation of dimeric complexes containing bridging dimethylhydrazido ligands.[130,132] These dimers were found to be inert to protonolysis or salt metathesis, indicating that the hydrazido bridges are not easily cleaved. Salt metathesis reactions of **1.59** with lithiated ligands produced the respective hydrazides with a number of supporting ligands. In subsequent

reactivity studies, dianionic, tridentate N- or O-donor ligands have been of particular use. Compounds **1.61** – **1.64** are examples of hydrazides containing such supporting ligand sets (Scheme 1.10).[132]

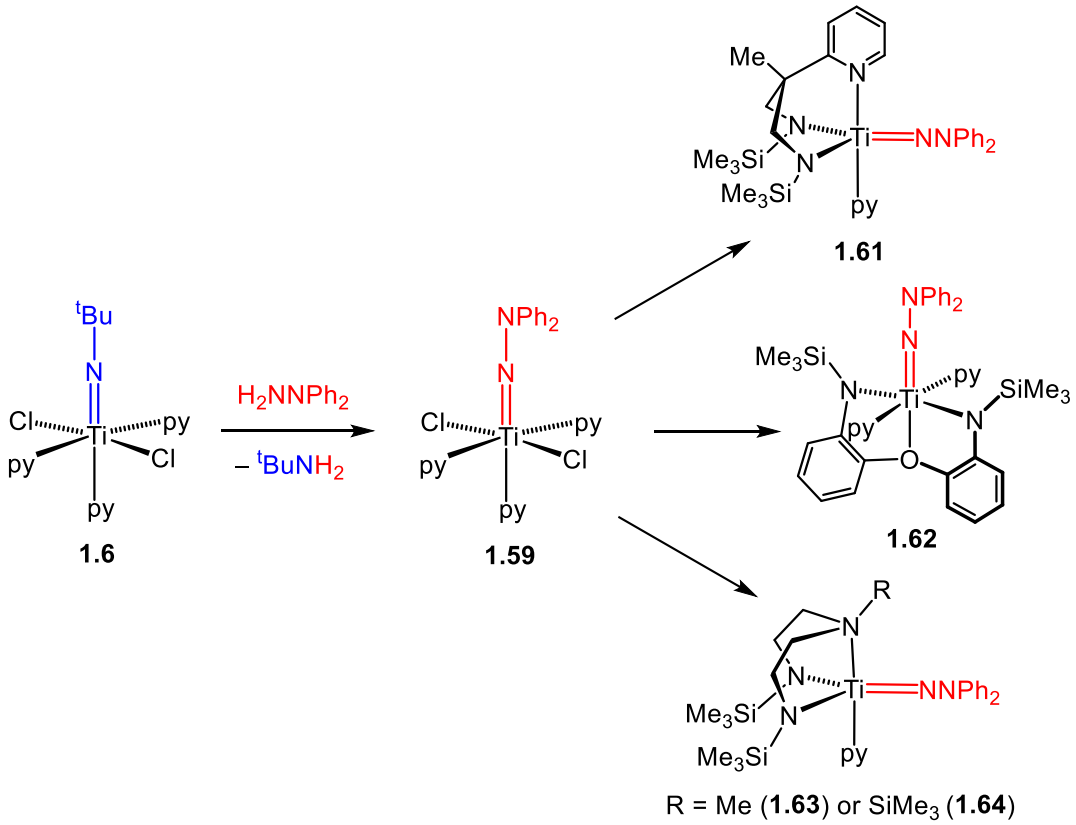

Scheme 1.10. Synthesis of $Ti(NNPh_2)Cl_2(py)_3$ (**1.59**) and examples of its salt metathesis reactions with lithiated ligands.[132]

Cyclopentadienyl-amidinate-supported hydrazido complexes have also been a focus of attention, as this supporting ligand set has proved itself as being relatively robust and suitable for reactivity studies of the hydrazido ligand. The complexes $Cp^*Ti\{MeC(N^iPr)_2\}(NNRR')$ (R = R' = Me (**1.65**) or Ph (**1.66**); R = Me, R' = Ph (**1.67**); Figure 1.8) were prepared in our research group by reaction of the *tert*-butylimide **1.8** with the corresponding hydrazine.[67] Other examples of Cp-supported hydrazides include $Cp_2Ti(NNPh_2)(py)$ (**1.68**) and $Cp^*Ti(NNPh_2)Cl(py)$ (**1.69**), both of which are prepared from the *tert*-butylimido analogue and H_2NNPh_2.[133]

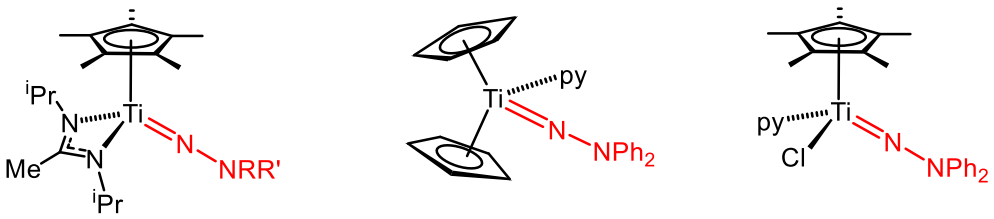

R = R' = Me (**1.65**) or Ph (**1.66**);
R = Me, R' = Ph (**1.67**)

1.68

1.69

Figure 1.8. Examples of Cp-supported titanium hydrazides.[67,133]

1.6.2 Synthesis of zirconium and hafnium hydrazido complexes

The first monomeric terminal hydrazido complex of zirconium was reported by Bergman and co-workers in 1991.[134] $Cp_2Zr(NNPh_2)$ (**1.70**) was observed to be a transient complex obtained from thermolysis of $Cp_2Zr(NHNPh_2)(CH_2CH_2{}^tBu)$, which then rapidly dimerises in solution to form a complex with bridging hydrazido ligands. When prepared in the presence of DMAP, however, the isolable hydrazide $Cp_2Zr(NNPh_2)$(DMAP) (**1.71**) was successfully formed.

The diamide-pyridine-supported hydrazide $Zr(N_2{}^{TBS}N^{py})(NNPh_2)$(py) (**1.72**, $N_2{}^{TBS}N^{py}$ = $MeC(2\text{-}C_5H_4N)(CH_2NSiMe_2{}^tBu)_2$) was prepared by Gade and co-workers in 2007 through reaction of $Zr(N_2{}^{TBS}N^{py})Cl_2$ with $LiNHNPh_2$, and subsequent dehydrohalogenation with $LiN(SiMe_3)_2$.[135] In 2008, the same method was used to prepare the first hafnium hydrazido compound $Hf(N_2{}^{TBS}N^{py})(NNPh_2)$(py) (**1.73**).[136] Unfortunately, no zirconium or hafnium hydrazido synthon, to which a wide range of supporting ligands can be added, has been successfully prepared. This has meant that a desired supporting ligand is usually added to the metal prior to addition of the hydrazido ligand. For example, $Zr(NMe_2)_4$ has proved to be a useful starting material, and addition of the protioligand $H_2N_2{}^{3,5\text{-}Xyl}N^{py}$ ($MeC(2\text{-}C_5H_4N)(CH_2N(H)\text{-}3,5\text{-}C_6H_3Me_2)_2$) yields the bis(amido) compound $Zr(N_2{}^{3,5\text{-}Xyl}N^{py})(NMe_2)_2$. A second protonolysis reaction can then be carried out with two cyclic hydrazines H_2NNR_2 in the presence of DMAP to yield the hydrazido compounds $Zr(N_2{}^{3,5\text{-}Xyl}N^{py})(NNR_2)(DMAP)_2$ ($R_2 = C_9H_{10}$ (**1.74**, Figure 1.9) or $C_{12}H_8$).[137] Interestingly, reaction of the protioligand $H_2N_2{}^{ArF}N^{py}$ ($MeC(2\text{-}C_5H_4N)(CH_2N(H)Ar^F)_2$), which bears electron-withdrawing aryl substituents on the N_{amide} atoms, with $Zr(NMe_2)_2$ at 90 °C resulted in the formation of the difluoride compound $Zr(N_2{}^{TFAP}N^{py})F_2$ (**1.75**, $N_2{}^{TFAP}N^{py}$ = $MeC(2\text{-}C_5H_4N)\{CH_2N(2\text{-}C_6F_4NMe_2)\}_2$).[138] Compound **1.75** is formed from the exchange of one of the *ortho*-fluorine substituents on both aryl rings with a dimethylamido group

originating from $Zr(NMe_2)_4$. However, it was still possible to obtain a hydrazido compound, $Zr(N_2^{TFAP}N^{py})(NNPh_2)$, from **1.75** *via* reaction with $LiNHNPh_2$ and then $LiN(SiMe_3)_2$.

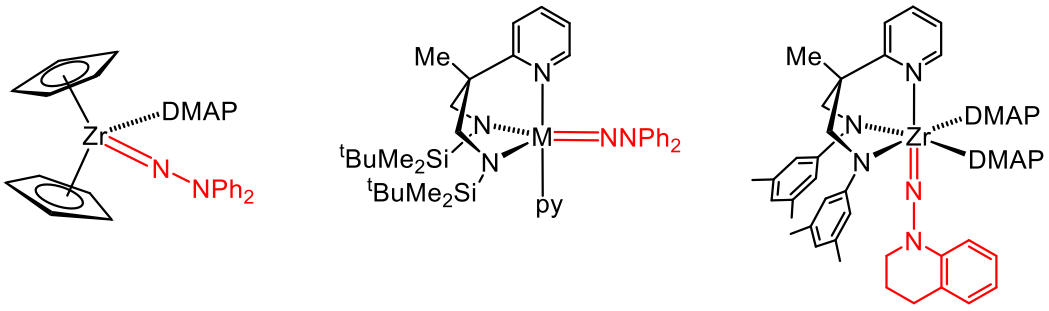

1.71 M = Zr (**1.72**), Hf (**1.73**) **1.74**

Figure 1.9. Examples of zirconium and hafnium hydrazido complexes.[134–137]

1.6.3 Stoichiometric reactions involving the $M{=}N_{im}$ bond

Group 4 hydrazido compounds exhibit a wealth of reactivity with small molecules, and reaction at the $M{=}N_{im}$ multiple bond *via* a [2+2] cycloaddition, as in Group 4 imides, is a common first step. In many cases the products of this initial cycloaddition can be isolated and characterised, and then undergo further reaction. These secondary reactions can include insertion of a second substrate into the now single $M–N_{im}$ bond or extrusion of a new organic compound.

The first examples of isolable compounds resulting from [2+2] cycloaddition reactions of a titanium hydrazido compound were the reactions of the macrocycle-supported complex $Ti(NNPh_2)(Me_4taa)$ (**1.58**) with CO_2 or TolNCO. However, neither metallacyclic product was structurally authenticated.[46] The sandwich compound $Cp_2Ti(NNPh_2)(py)$ (**1.68**) underwent a [2+2] cycloaddition reaction with ^{t}BuCP to give one of the first examples of a structurally authenticated cycloaddition product for any metal hydrazide, as well as the first reported reactivity of a hydrazido compound with a phosphaalkyne.[139] Since these early examples, the stoichiometric reactivity of Group 4 hydrazides has progressed rapidly and selected examples will be discussed below.

As found for their imido analogues, the stoichiometric reactions of the cyclopentadienyl-amidinate-supported hydrazido compounds $Cp^*Ti\{MeC(N^iPr)_2\}(NNR_2)$ (R = Me (**1.65**) or Ph (**1.66**)) have been particularly fruitful. Selected reactions and their products are shown in Scheme 1.11. With CE_2 (E = O or S), [2+2] cycloaddition reactions occurred, initially

yielding the carbamate-type compounds **1.76**. When E = O, a second insertion occurred into the now single Ti–N_{im} bond resulting in "double insertion" complexes of the type **1.77**.[67] Reactions of **1.65** and **1.66** with isocyanates gave different reaction outcomes. The reaction of the diphenylhydrazido compound **1.66** yielded isolable cycloaddition products with both alkyl and aryl isocyanates (**1.78**), whereas the dimethylhydrazido analogue **1.65** reacted with Ar'NCO and ^{t}BuNCO to give the oxo-bridged dimer [Cp*Ti{MeC(N^{i}Pr)$_2$}(μ-O)]$_2$ (**1.79**), and the organic compounds ^{t}BuNCNNMe$_2$ (**1.80**) and cyclic N(Me)$_2$NC(NAr')N(Ar')C(O) (**1.81**) respectively, following extrusion from the inherently unstable cycloaddition intermediates (Scheme 1.11).[67] Interestingly, reaction of **1.65** with two equivalents of TolNCO gave Cp*Ti{MeC(N^{i}Pr)$_2$}{OC(NNMe$_2$)N(Tol)C(NTol)O} (**1.82**) following the same cycloaddition-extrusion pathway as with Ar'NCO and ^{t}BuNCO. However, in this case, rapid cycloaddition of the extruded organic fragment to Ti=O (instead of dimerisation) formed Cp*Ti{MeC(N^{i}Pr)$_2$}{N(Tol)C(NNMe$_2$)O} (not observed), which then reacts with a second equivalent of TolNCO to give **1.82**.

Reactions of zirconium hydrazides with isocyanates and isothiocyanates are also known. Gade and co-workers reported that the reactions of Zr(N$_2$^{TBS}N^{py})(NNPh$_2$)(py) (**1.72**) with MesNCS and PhNCS gave isolable cycloaddition products in which the new ligand is bound in a κ^2-N,S-fashion.[140] Cycloaddition reactions of **1.72** and its hafnium congener **1.73** with alkyl- and aryl-substituted allenes were also described, which proceeded with Markovnikov regioselectivity (*vide infra*) in both cases. Additionally, **1.72** underwent [2+3] cycloadditions with organic azides to generate azazirconacyclopentene-type complexes, the first compounds of any metal to contain that functional group.[141]

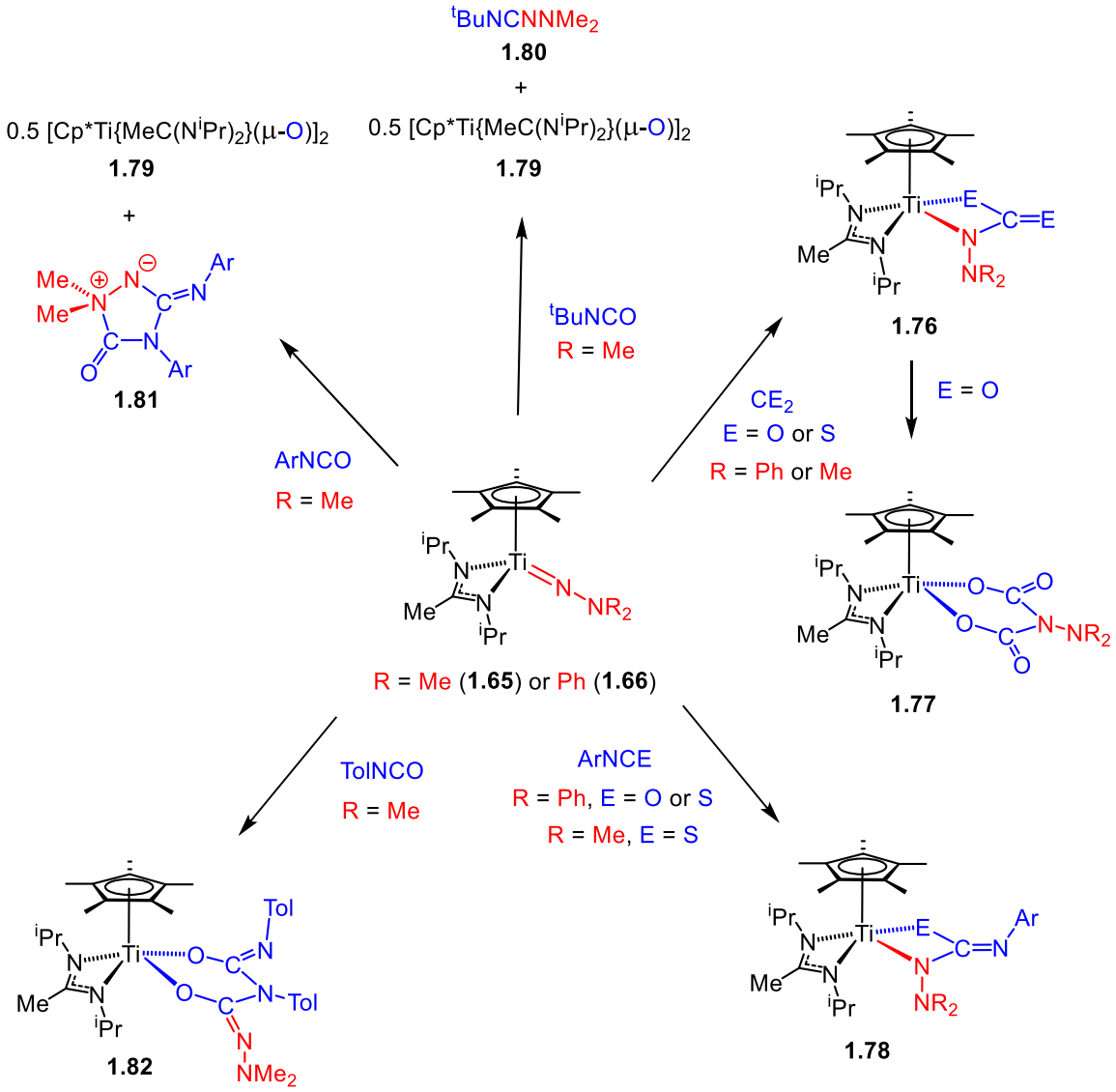

Scheme 1.11. Reactions of Cp*Ti{MeC(N^{i}Pr)$_2$}(NNR$_2$) (R = Me (**1.65**) or Ph (**1.66**) with unsaturated substrates.[67]

Compounds **1.65** and **1.66** showed no reaction with alkynes. In comparison, Gade's more open cyclopentadienyl-amidinate-supported compound Cp*Ti(N$^{3,5\text{-Xyl}}$N^{pyr})(NNMe$_2$)(DMAP) reacts with one equivalent of HCCPh to yield Cp*Ti(N$^{3,5\text{-Xyl}}$N^{pyr}){N(NMe$_2$)C(Ph)C(H)}, in which the C(H) carbon is bound to titanium (the Markovnikov regioisomer).[26] Although calculations showed that the anti-Markovnikov regioisomer with the C(Ph) bound to titanium is electronically favoured, the steric bulk of the Cp*-amidinate supporting ligand set prevents the alkyne from approaching with this orientation, and in the case of **1.65** and **1.66**, from reacting at all. In contrast, the diamide-pyridine-supported compound Ti(N$_2$N^{py})(NNPh$_2$)(py) (**1.61**) reacts with both terminal and internal alkynes to give azametallacyclic compounds of the type

Ti(N_2N^{py}){N(NPh_2)C(R)C(Ar)} (**1.83**, Ar = phenyl or substituted phenyl; R = H or Me, Equation 1.1) with exclusively anti-Markovnikov regiochemistry.[142]

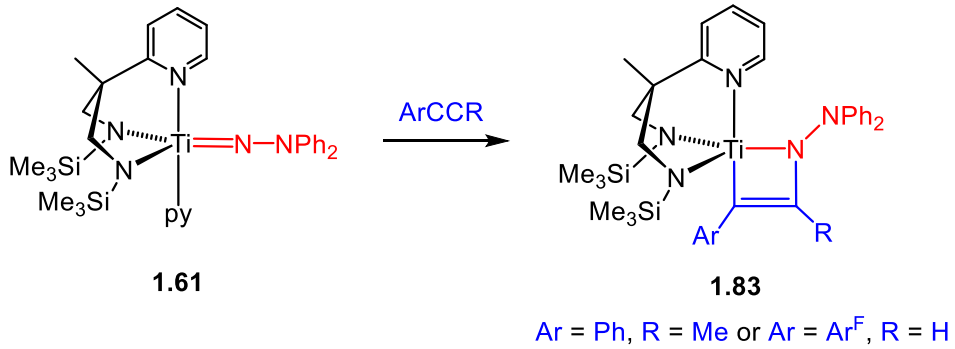

1.61 **1.83**

Ar = Ph, R = Me or Ar = Ar^F, R = H

Equation 1.1[142]

1.6.4 Stoichiometric reactions involving N_α–N_β bond cleavage

Notwithstanding the rich reactivity at the M=N_{im} bond described above, Group 4 hydrazido chemistry came into its own with the discovery of a wide range of processes involving reductive cleavage of the N_α–N_β bond by oxidisable substrates such as isonitriles. For example, the diamide-donor-supported compounds Ti(N_2N^{py})($NNPh_2$)(py) (**1.61**) and Ti($N_2^{SiMe_3}N^{Me}$)($NNPh_2$)(py) (**1.63**) both react with one equivalent of XylNC to give the N_α–N_β bond cleavage products Ti(N_2N^{py})(NPh_2)(NCNXyl) and Ti($N_2^{SiMe_3}N^{Me}$)(NPh_2)(NCNXyl) (**1.84**, Figure 1.10) respectively.[143] DFT calculations indicated that loss of pyridine, then formation of an isonitrile adduct occur, prior to the formation of a three-membered intermediate which is supported by coordination of the N_β atom to the metal centre. From here, N_α–N_β bond cleavage is facile and results in formation of the final products.[143] An analogous isonitrile insertion reaction had previously been reported for the zirconium hydrazide Zr($N_2^{TBS}N^{py}$)($NNPh_2$)(py) (**1.72**) and ^{t}BuNC,[135] and was later reported for the reaction of Ti($N_2^{SiMe_3}O$)($NNPh_2$)$(py)_2$ (**1.85**, $N_2^{SiMe_3}O$ = $O(CH_2CH_2NSiMe_3)_2$) with ^{t}BuNC.[144] Compound **1.85** also reacts with XylNC, consuming two equivalents of the substrate. The first equivalent results in N_α–N_β bond cleavage as above and the second equivalent reacts with one of the N–$SiMe_3$ ligand bonds yielding **1.86** (Figure 1.10). N_α–N_β bond cleavage is also observed in the reactions of complex **1.72** with propylene sulfide or Ph_3PSe, which form the dimeric compounds {Zr($N_2^{TBS}N^{py}$)(NPh_2)}$_2$(μ-N_2E) (E = S (**1.87**) or Se (**1.88**), Figure 1.10).[135]

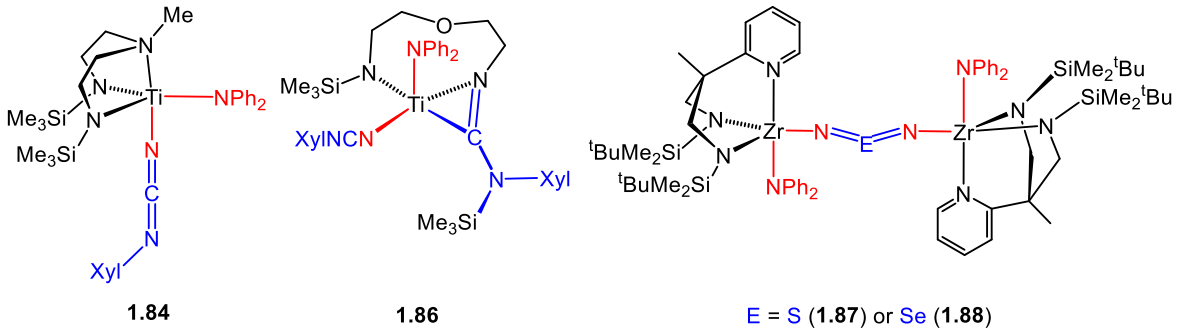

Figure 1.10. N_α–N_β bond cleavage products of Group 4 hydrazido compounds.[135,143,144]

These reactions with isonitriles are reminiscent of an early example of Group 4 hydrazido reactivity which was reported by Bergman and co-workers. The *in situ*-generated hydrazide $Cp_2Zr(NNPh_2)$ (**1.70**) undergoes N_α–N_β bond cleavage upon reaction with CO to form the mixed zirconium amide-isocyanate $Cp_2Zr(NCO)(NPh_2)$ (**1.89**, Scheme 1.12).[134] **1.70** also reacted with symmetrical internal alkynes RCCR (R = Et, Ph or Tol) to yield the complexes **1.90**, **1.91** and **1.92**, respectively (Scheme 1.12). These complexes contain seven-membered metallacycles formed from N_α–N_β bond cleavage followed by a C–H bond activation. Similar reactions with internal alkynes were reported for the diamide-pyridine-supported **1.72**, for which the products were either seven-membered metallacycles as above or (in the case of MeCCMe) a vinylimido complex, $Zr(N_2^{TBS}N^{py})\{NC(Me)=C(Me)NPh_2\}$, which represents insertion of the alkyne into the N_α–N_β bond.[145]

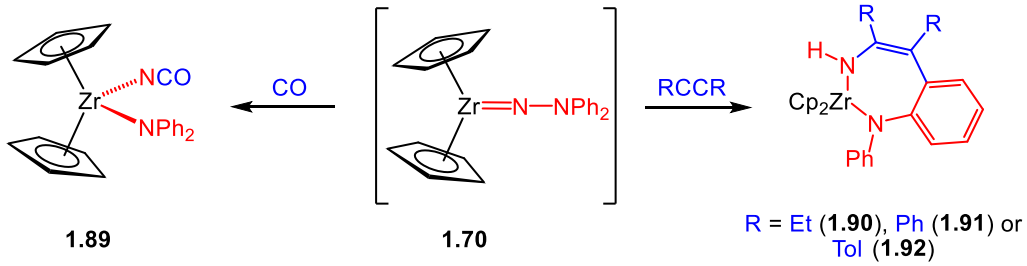

Scheme 1.12. Reactions of $Cp_2Zr(NNPh_2)$ (**1.70**) with CO and internal alkynes.[134]

Following on from the cycloaddition reactions of alkynes with $Ti(N_2N^{py})(NNPh_2)(py)$ (**1.61**) to give metallacycles **1.83** as described in the previous Section, it was found that the azametallacyclic product $Ti(N_2N^{py})\{N(NPh_2)C(Me)C(Ph)\}$ (**1.83a**) converted to the vinylimido compound $Ti(N_2N^{py})\{NC(Ph)=C(Me)NPh_2\}(py)$ when left in solution for 3 days at RT.[139] Similarly, reaction of $Ti(N_2^{SiMe_3}N^{Me})(NNPh_2)(py)$ (**1.63**) with a range of internal alkynes resulted in the formation of analogous vinylimido compounds $Ti(N_2^{SiMe_3}N^{Me})\{NC(R)=C(Me)NPh_2\}$ (**1.93**, R = alkyl or aryl).[142] However, when the

diarylalkynes ArCCAr (Ar = Ph or 4-C_6H_4OMe) were used, the compounds Ti{MeN($CH_2CH_2NSiMe_3$)(CH_2CH_2NH)}{N($SiMe_3$)C(Ar)C(Ar)-1,2-C_6H_4N(Ph)} (Ar = Ph (**1.94**) or 4-C_6H_4OMe (**1.95**)) were observed as well as the expected vinylimido compounds Ti($N_2^{SiMe_3}N^{Me}$){NC(Ar)=C(Ar)NPh_2}(py) (Ar = Ph (**1.96**) or 4-C_6H_4OMe (**1.97**)). Compounds **1.94** and **1.95** are similar to the seven-membered metallacycles **1.90**, **1.91** and **1.92** described above, and are thought to form *via* the same mechanism, followed by a 1,3-$SiMe_3$ sigmatropic shift (Figure 1.11).[146]

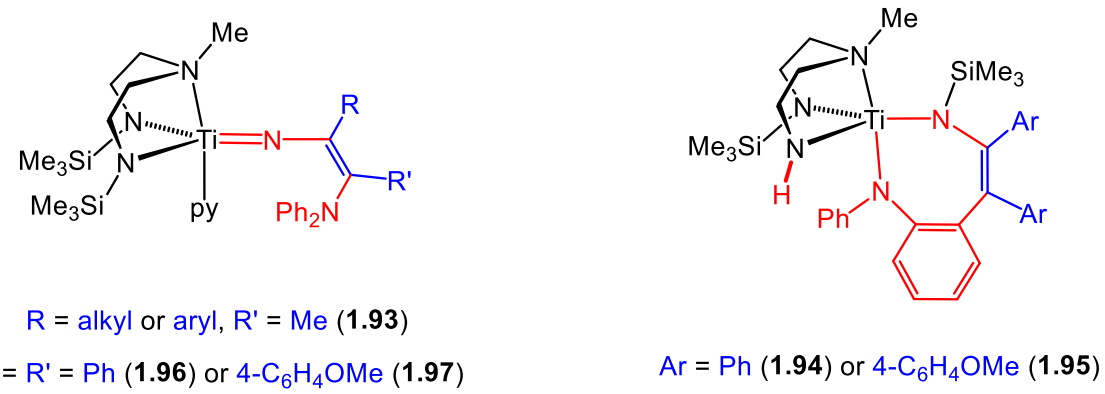

Figure 1.11. Reaction products of Ti($N_2^{SiMe_3}N^{Me}$)($NNPh_2$)(py) (**1.63**) with alkynes.[142]

1.6.5 Catalytic reactions

Given the widespread use of Group 4 imido complexes as catalysts for the hydroamination of alkynes, described in Section 1.3.5, a large body of work has subsequently been built around analogous processes which may be catalysed by Group 4 hydrazido complexes. Firstly, a direct extension of hydroamination catalysis known as hydrohydrazination, in which the N–H bonds of an N,N-disubstituted hydrazine are added across an alkyne to form hydrazones, has received much attention, and several examples of Group 4 catalytic systems have been reported.[19–21,25,26,84,85] Like hydroamination, hydrohydrazination is postulated to proceed through metallacycles of the type **1.98** (Figure 1.12) which can then undergo protonolysis of the Ti–C and Ti–N bonds upon addition of an equivalent of hydrazine to form hydrazones (**1.99**). This second step is proposed to proceed *via* a transient mixed bis(hydrazido(1–)) intermediate, in analogy to the mechanism for hydroamination shown in Scheme 1.6.

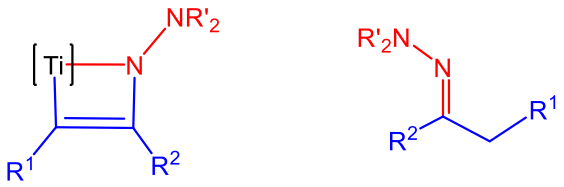

1.98 **1.99**

Figure 1.12. Metallacyclic intermediates of hydrohydrazination (**1.98**), and resulting hydrazones (**1.99**).

Such catalytic reactions have typically been found to require high temperatures (> 75 °C) and long reaction times (2 – 75 h), with harsher conditions being necessary for internal alkynes. In many cases, the active hydrazido catalyst is synthesised *in situ* from the corresponding diamide pre-catalyst (L)Ti(NMe_2)$_2$ upon introduction of the hydrazine.[20,21,25,84] In 2011, Gade and co-workers reported that the cyclopentadienyl-amidinate-supported compounds Cp*Ti($N^{3,5\text{-Xyl}}N^{pyr}$)(NNRR')(L) (R = R' = Ph or Me; R = Ph, R' = Me; L = py, DMAP or H_2N^tBu) were capable of catalysing the hydrohydrazination of a range of alkynes with quantitative conversion taking place within 1 h at RT (at 5 mol% catalyst loading).[26] In some cases, further reactions of the hydrazones can take place to form other nitrogen-containing organic compounds. The formation of indoles,[19,21,22,84,85] pyrroles[84] and tryptamines[23] in this way have been reported, with these cyclisations usually requiring the addition of an external Lewis acid such as $ZnCl_2$ for their successful catalysis.

Furthermore, an iminohydrazination reaction has been developed using the pre-catalysts **1.100** and **1.101** (Figure 1.13), where an alkyne, hydrazine and organic isocyanide are coupled in a single reaction to form a 1,3-iminohydrazone.[24,147] This process has since been developed further, and the precatalyst Ti(NMe_2)$_2$(pypyr)$_2$ (**1.102**, Hpypyr = 2-(2'-pyridyl)-3,5-dimethylpyrrole, Figure 1.13) can be used in the multicomponent coupling of alkynes, isonitriles and monosubstituted hydrazines to yield pyrroles in a single step, without the need for an external Lewis acid.[148]

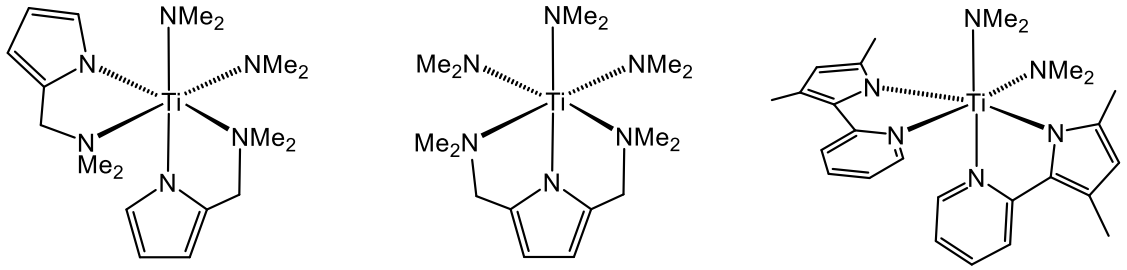

Figure 1.13. Titanium pre-catalysts for hydrohydrazination and iminohydrazination processes.[24,147,148]

As discussed in the previous Section, reaction of Ti($N_2^{SiMe_3}N^{Me}$)($NNPh_2$)(py) (**1.63**) with a range of internal alkynes resulted in the formation of vinylimido compounds of the type **1.93**, through insertion into the N_α–N_β bond.[142] Addition of one equivalent of H_2NNPh_2 to such vinylimido compounds regenerates the starting hydrazide **1.63**, along with the organic product $RC(NH_2)=C(Me)NPh_2$ (Equation 1.2). This was the first example of this type of coupling of a hydrazine with an alkyne, and can be performed catalytically from either **1.63** or **1.93**, with the overall result being the 1,2-diamination of the alkyne, a previously unknown process.

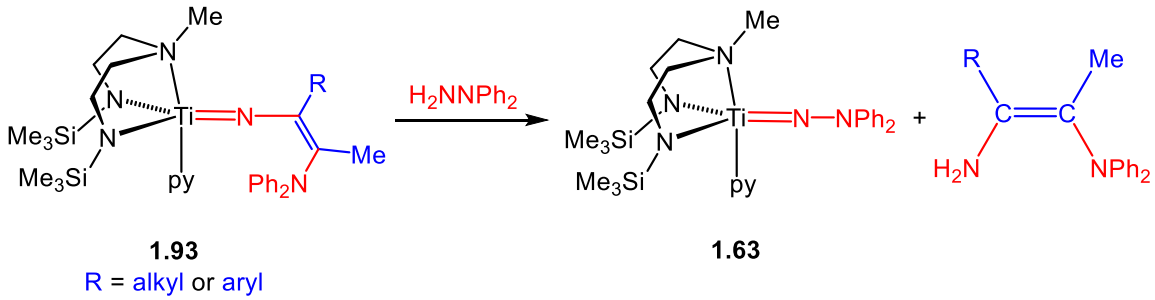

Equation 1.2[142]

Subsequent work has sought to elucidate the mechanism of this process and extend the scope of alkynes and hydrazines for which it is successful.[146,149] Recent work has also shown that replacing the –$SiMe_3$ substituents on the N_{amide} atoms of the supporting ligand in **1.63** with the less sterically demanding –^{i}Pr substituents results in a switch in catalytic process back to the more usual hydrohydrazination.[150]

1.7 Group 4 alkoxyimido complexes

The wide range of Group 4 imido and hydrazido compounds that have been prepared, and their rich reactivity with small molecules, in particular catalytic C–N bond forming reactions, have prompted more recent work in our research group on the preparation of new imido-type functionalities with different heteroatoms acting as the N_{im}-substituent. To this end, a focus has been placed on the synthesis of alkoxyimido complexes, M=NOR, with the ultimate aim in this case being the discovery of novel C–O bond forming processes.

The first Group 4 alkoxyimides were prepared in 2011 by our research group. A reaction between $Ti(NMe_2)_2Cl_2$ and H_2NO^tBu successfully formed the alkoxyimido complex $Ti(NO^tBu)Cl_2(NHMe_2)_2$ (**1.103**) in analogy to its imido and hydrazido counterparts.[151,152] Addition of a range of neutral, tridentate ligands to **1.103** resulted in the corresponding dichloride compounds $Ti(NO^tBu)Cl_2(L)$ (L = $Me_3[9]aneN_3$, $HC(Me_2pz)_3$ (Me_2pz = 3,5-dimethylpyrazolyl) and $Me_3[6]aneN_3$ (trimethyl-1,3,5-triazacyclohexane, **1.104**). Addition of H_2NO^tBu to $Ti(N^tBu)Cl_2(py)_3$ (**1.6**) in an attempted *tert*-butylimide/alkoxyamine exchange did not cleanly form the desired alkoxyimido analogue, and neither could this be formed through direct addition of pyridine to **1.103**. However, it was found that $Ti(NO^tBu)Cl_2(py)_3$ (**1.105**) could be formed by reaction of **1.104** with neat pyridine, releasing the free neutral, tridentate ligand in the process (Scheme 1.13).

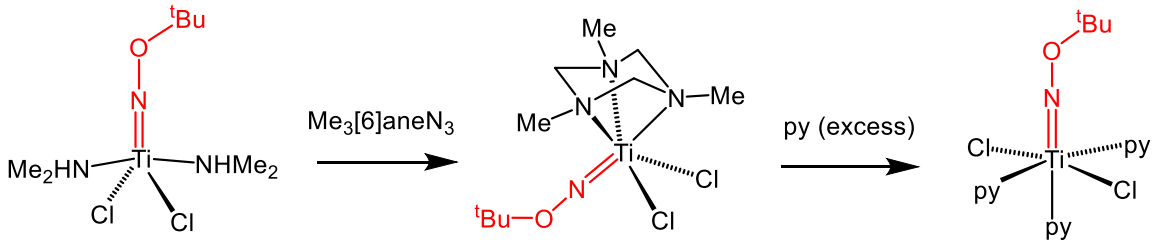

1.103 **1.104** **1.105**

Scheme 1.13. Synthesis of the titanium alkoxyimido synthon $Ti(NO^tBu)Cl_2(py)_3$ (**1.105**).[152]

As previously described for its imido and hydrazido counterparts, complex **1.105** proved to be a useful synthon for the addition of a range of supporting ligand sets through salt metathesis reactions. The diamide-amine-supported complex $Ti(N_2^{SiMe_3}N^{Me})(NO^tBu)(py)$ (**1.106**) is one such compound formed in this way. In a first reactivity test of the alkoxyimido functional group, the reaction of **1.106** with MeCCPh gave net insertion of

the alkyne into one of the Ti–$NSiMe_3$ bonds as well as N–O bond cleavage to yield **1.107** (Equation 1.3).[151] This contrasts with the reactivity of the diphenylhydrazido analogue **1.63**, which was found to be a catalyst for the 1,2-diamination of alkynes (described in the previous Section). Unfortunately, the activation of the supporting ligand of **1.106** precludes the possibility of an analogous catalytic process in this system.

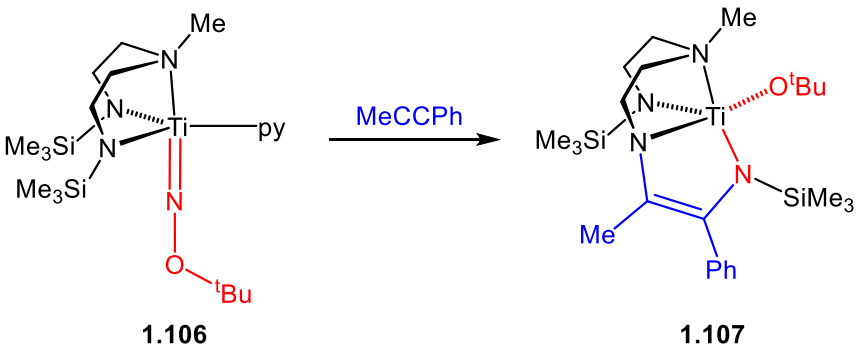

1.106 **1.107**

Equation 1.3[151]

Encouraged by the wide range of reactivity observed with imido and hydrazido complexes supported by cyclopentadienyl-amidinate ligand sets, the preparation of an alkoxyimido analogue was next targeted by our research group in an attempt to further the reactivity of this functional group. To this end, Cp*Ti{$PhC(N^iPr)_2$}(NO^tBu) (**1.108**) was prepared through a *tert*-butylimide/*tert*-butoxyamine exchange reaction from the corresponding imido complex.[153] The reactivity of **1.108** with a range of unsaturated substrates including CS_2, isocyanates, aldehydes, ketones and nitriles has been reported, and is the only detailed reactivity study of an alkoxyimido compound to date. Generally, the reactivity of **1.108** was not found to differ dramatically from its imido and hydrazido counterparts.

Interestingly, however, the reaction of **1.108** with the terminal alkyne $HCCAr^F$ resulted in the quantitative formation of the product **1.109** (Equation 1.4).[153] This is proposed to form through an initial [2+2] cycloaddition across the metal–nitrogen multiple bond followed by N–O bond cleavage to give an azirinyl intermediate, which in turn undergoes nucleophilic attack by one of the amidinate nitrogen atoms to form a seven-membered metallacycle. Unfortunately, attempted reactions between **1.108** and internal alkynes such as MeCCPh and MeCC-4-$C_6H_4CF_3$ gave complicated mixtures of products.[153]

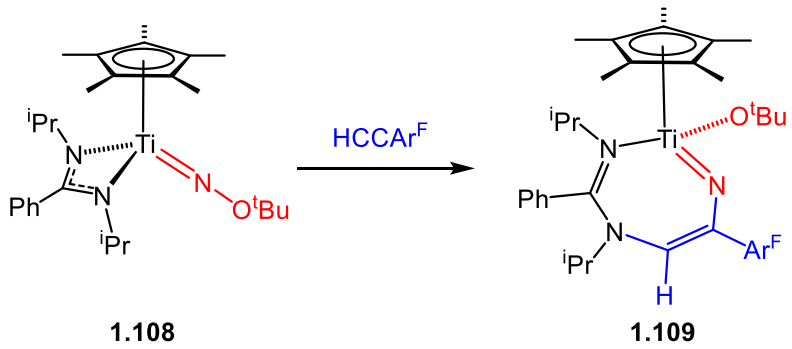

1.108 **1.109**

Equation 1.4[153]

1.8 Transition metal borylimido complexes

The substitution of a BR_2 group at the N_{im} atom of a metal–nitrogen multiply bonded functional group forms a borylimido moiety. A handful of transition metal complexes containing a terminal borylimido ligand have been reported, although these represent a disparate field in which no well-established synthetic routes are known. Those compounds that have been reported have generally been prepared through serendipitous N–B couplings, or through an oxidative route utilising a borylazide; both routes will be described below. Additionally, to date there have been no reports of the reactivity of any borylimido complex with small molecules.

The first known borylimido complex was described by Wilkinson and co-workers in 1993. Reaction of the tungsten(II) complex $WCl_2(PMe_3)_4$ with 2 equivalents of Mes_2BN_3 formed the tungsten(VI) bis(borylimido) complex $W\{NB(Mes)_2\}_2Cl_2(PMe_3)_2$ (**1.110**, Figure 1.14).[154] This oxidative process is driven by the accompanying reductive formation of 2 equivalents of N_2. In 2003, Sundermeyer and co-workers used the same methodology to prepare two further borylimido complexes. The reaction of the bis(imide) $W(NMes)_2(PMe_3)_3$ with Mes_2BN_3 formed the mixed borylimido-bis(imido) complex $W\{NB(Mes)_2\}(NMes)_2(PMe_3)_2$ (**1.111**, Figure 1.14), and the reaction of the vanadium(III) complex $V(Mes)_3(THF)$ with Mes_2BN_3 formed the vanadium(V) imide $V\{NB(Mes)_2\}(Mes)_3$ (**1.112**, Figure 1.14).[155]

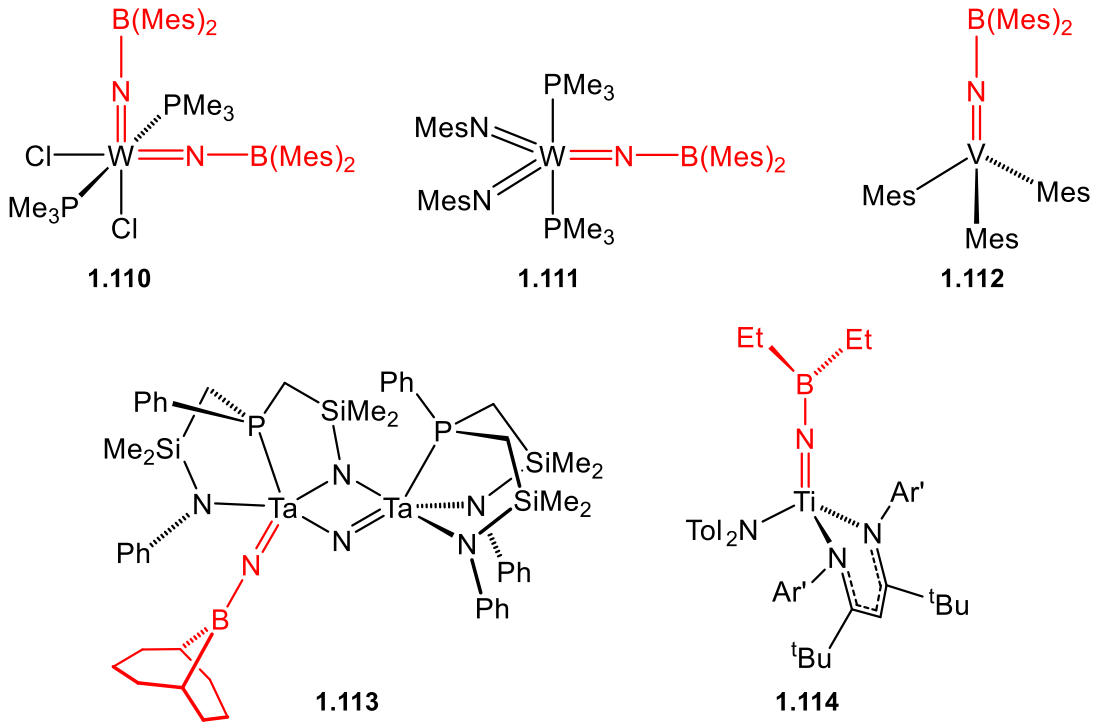

Figure 1.14. Previously reported terminal borylimido complexes.[154–157]

Two further terminal borylimido complexes were prepared through investigations of dinitrogen reactivity with a borane at a transition metal centre. In 2002, Fryzuk *et al.* communicated the rearrangement of a 9-BBN adduct of a tantalum dinitrogen complex to form the BBN-imido complex **1.113** (Figure 1.14).[156] Addition of another equivalent of 9-BBN monomer to **1.113** formed a Lewis acid–base adduct at its bridging nitride atom, but left the borylimido ligand intact.[158] Also, Semproni and Chirik have reported the formation of bimetallic zirconocene and hafnocene complexes containing bridging borylimido ligands through rearrangement of a BPin (Pin = 2,3-dimethyl-2,3-butanediol) adduct of the respective bridging-dinitrogen complex (which contains a μ^2-N_2BPin ligand).[159]

The first report of a Group 4 complex containing a terminal borylimido ligand came from Mindiola and co-workers in 2014: (^{tBu}NacNac)Ti(NBEt$_2$)(NTol$_2$) (**1.114**, Figure 1.14) was prepared through a serendipitous reaction of the parent imido (terminal NH) compound with 2 equivalents of NaHBEt$_3$.[157] Recently, our research group communicated the preparation of a second terminal borylimido complex of titanium through the reaction of a diphenyl- or dimethylhydrazide (**1.66** or **1.65**, respectively) with 1 equivalent of 9-BBN dimer. The formation of Cp*Ti{MeC(N^{i}Pr)$_2$}(NBC$_8$H$_{14}$) (**1.115**) was accompanied by elimination of the respective diphenyl- or dimethylaminoborane and H_2 (Equation 1.5).[160]

This reaction was initially postulated to proceed *via* 1,2-B–H addition to the Ti–N multiple bond to give a titanium hydride species with an η^2-borylhydrazido ligand, followed by hydride transfer and N_α–N_β cleavage leaving a mixed amido-borylamido compound. Finally, 1,2-elimination of HNR_2 (R = Ph or Me) forms the borylimido multiple bond, and the released amine undergoes dehydrogenation with the other half of the 9-BNN dimer to leave $R_2NBC_8H_{14}$.[160] However, a later observation that the dehydrogenation occurs more rapidly than an independent reaction between 9-BBN and HNR_2 suggests that the reaction proceeds *via* an alternative mechanism, and attempts to elucidate this through DFT calculations are ongoing.[161] A computational study of **1.115** confirmed the presence of a Ti–N triple bond ($\sigma^2\pi^4$), and found the two Ti–N π interactions by MO and NBO analyses, one of which is significantly stabilised by delocalisation into the otherwise vacant 2p AO of boron.[160]

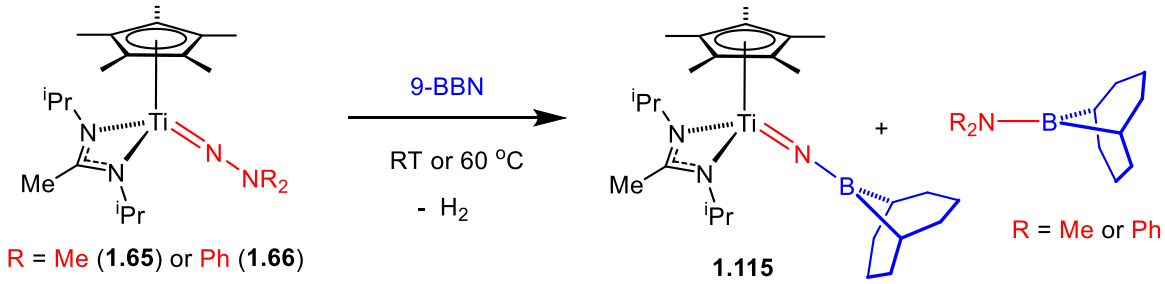

Equation 1.5[160]

Finally, some structurally related complexes of titanium have been prepared by Lancaster and co-workers. Reaction of $Ti(NMe_2)_3Cl$ with the ammonia borane $H_3NB(Ar^F)_3$ gave the ion pair $[Ti(NMe_2)_2(NHMe_2)_2Cl][Ti\{NB(Ar^F)_3\}Cl_2(NHMe_2)_2]$ in which the anion (**[1.116]**$^-$) incorporates a nitridoborane ligand $–NB(Ar^F)_3$, formed through three N–H bond activations.[162,163] This is considered a Lewis acid-stabilised nitrido ligand, and not a borylimido ligand, as it has a formal 3– charge. Subsequently, cation exchanges were performed to yield three new ion pairs: these being the salts of **[1.116]**$^-$ and $[Me_4N]^+$, $[Ph_4P]^+$ and $[(PhCH_2)Ph_3P]^+$.[163] Structural and computational characterisation of the nitridoborane ligand in **[1.116]**$^-$ confirmed the presence of a formal Ti–N triple bond.

1.9 Summary and Objectives

This Chapter has explored the well-established chemistry of Group 4 imido and hydrazido complexes, including their synthesis, reactivity and structure, as well as practical applications in catalysis. Additionally, the more recent evolution of rare earth imido

chemistry, through new strategies aimed at stabilising this more reactive metal–nitrogen multiple bond, was described. The Chapter concluded with a survey of the handful of terminal borylimido complexes which are known across the transition metals, with these compounds not yet constituting an established field.

It is apparent that one current direction of effort in metal–nitrogen multiple bond chemistry is the investigation of functional groups with new heteroatoms bonded at the N_{im} group, such as alkoxyimides. With two borylimido complexes of titanium having been prepared in the past two years, although by somewhat serendipitous N–B couplings, one aim of this Thesis is to develop versatile synthetic routes to titanium borylimides, taking inspiration from our research group's rich history in titanium imido and hydrazido chemistry.

Another focus of metal–nitrogen multiple bond chemistry has been the development of novel catalytic C–N bond-forming reactions. Thus, a second aim of this Thesis is to investigate the reactivity of titanium borylimides with small molecules, particularly alkynes, and test the feasibility of analogous catalytic processes in these systems.

Finally, a third aim of this Thesis is to extend the recent developments in the synthesis and reactivity of rare earth imides (particularly those of scandium) to form the borylimido complex of a rare earth metal. It was postulated that the electron richness and steric bulk of the borylimido ligand employed here may stabilise such a compound.

1.10 References

1 J. Chatt, A. J. Pearman and R. L. Richards, *J. Chem. Soc. Dalton Trans.*, 1977, 2139–2142.

2 M. Hidai, *Coord. Chem. Rev.*, 1999, **185**–**186**, 99–108.

3 R. R. Schrock, *Angew. Chem. Int. Ed.*, 2008, **47**, 5512–22.

4 R. R. Schrock, *Acc. Chem. Res.*, 2005, **38**, 955–62.

5 W. W. Weare, X. Dai, M. J. Byrnes, J. M. Chin, R. R. Schrock and P. Muller, *Proc. Natl. Acad. Sci.*, 2006, **103**, 17099–17106.

6 D. V. Yandulov and R. R. Schrock, *Inorg. Chem.*, 2005, **44**, 1103–1117.

7 N. Hazari and P. Mountford, *Acc. Chem. Res.*, 2005, **38**, 839–849.

8 N. Adams, H. J. Arts, P. D. Bolton, D. Cowell, S. R. Dubberley, N. Friederichs, C. M. Grant, M. Kranenburg, A. J. Sealey, B. Wang, P. J. Wilson, A. R. Cowley, P. Mountford and M. Schröder, *Chem. Commun.*, 2004, 434–435.

9 P. D. Bolton and P. Mountford, *Adv. Synth. Catal.*, 2005, **347**, 355–366.

10 H. R. Bigmore, S. R. Dubberley, M. Kranenburg, S. C. Lawrence, A. J. Sealey, J. D. Selby, M. A. Zuideveld, A. R. Cowley and P. Mountford, *Chem. Commun.*, 2006, 436–438.

11 H. R. Bigmore, M. A. Zuideveld, A. M. Kowalczyk, A. R. Cowley, M. Kranenburg, E. J. L. McInnes and P. Mountford, *Inorg. Chem.*, 2006, **45**, 6411–6423.

12 P. J. Wilson, A. J. Blake, P. Mountford and M. Schroder, *Chem. Commun.*, 1998, 1007–1008.

13 C. H. Winter, P. H. Sheridan, T. S. Lewkebandara, M. J. Heeg and J. W. Proscia, *J. Am. Chem. Soc.*, 1992, **114**, 1095–1097.

14 T. S. Lewkebandara, P. H. Sheridan, M. J. Heeg, A. L. Rheingold and C. H. Winter, *Inorg. Chem.*, 1994, **33**, 5879–5889.

15 I. Bytschkov and S. Doye, *Eur. J. Org. Chem.*, 2003, **2003**, 935–946.

16 S. Doye, *Synlett*, 2004, **2004**, 1653–1672.

17 A. V. Lee and L. L. Schafer, *Eur. J. Inorg. Chem.*, 2007, 2243–2255.

18 T. E. Müller, K. C. Hultzsch, M. Yus, F. Foubelo and M. Tada, *Chem. Rev.*, 2008, **108**, 3795–892.

19 Y. Li, Y. Shi and A. L. Odom, *J. Am. Chem. Soc.*, 2004, **126**, 1794–1803.

20 J. S. Johnson and R. G. Bergman, *J. Am. Chem. Soc.*, 2001, **123**, 2923–2924.

21 C. Cao, Y. Shi and A. L. Odom, *Org. Lett.*, 2002, **4**, 2853–2856.

22 L. Ackermann and R. Born, *Tetrahedron Lett.*, 2004, **45**, 9541–9544.

23 V. Khedkar, A. Tillack, M. Michalik and M. Beller, *Tetrahedron Lett.*, 2004, **45**, 3123–3126.

24 S. Banerjee, Y. Shi, C. Cao and A. L. Odom, *J. Organomet. Chem.*, 2005, **690**, 5066–5077.

25 S. Banerjee, E. Barnea and A. L. Odom, *Organometallics*, 2008, **27**, 1005–1014.

26 K. Weitershaus, H. Wadepohl and L. H. Gade, *Organometallics*, 2009, **28**, 3381–3389.

27 P. D. Schweizer, H. Wadepohl and L. H. Gade, *Organometallics*, 2013, **32**, 3697–3709.

28 K. Weitershaus, B. D. Ward, R. Kubiak, C. Müller, H. Wadepohl, S. Doye and L. H. Gade, *Dalton Trans.*, 2009, 4586–602.

29 G. R. Giesbrecht and J. C. Gordon, *Dalton Trans.*, 2004, 2387–2393.

30 W. A. Nugent and B. L. Haymore, *Coord. Chem. Rev.*, 1980, **31**, 123–175.

31 W. A. Nugent and J. M. Mayer, *Metal-Ligand Multiple Bonds*, Wiley-Interscience,

New York, 1988.

32 D. E. Wigley, in *Progress in Inorganic Chemistry*, ed. K. D. Karlin, Wiley-Interscience, New York, 1994, vol. 42, pp. 239–482.

33 M. H. Chisholm and I. P. Rothwell, in *Comprehensive Coordination Chemistry*, Pergamon Press, Oxford, 1987, vol. 2, pp. 161–184.

34 P. Mountford, *Chem. Commun.*, 1997, 2127–2134.

35 B. L. Haymore, E. A. Maatta and R. A. D. Wentworth, *J. Am. Chem. Soc*., 1979, **101**, 2063–2068.

36 S. C. Dunn, P. Mountford and D. A. Robson, *J. Chem. Soc. Dalton Trans.*, 1997, **2**, 293–304.

37 H. W. Roesky, H. Voelker, M. Witt and M. Noltemeyer, *Angew. Chem. Int. Ed. Engl.*, 1990, **29**, 669–670.

38 J. E. Hill, R. D. Profilet, P. E. Fanwick and I. P. Rothwell, *Angew. Chem. Int. Ed. Engl.*, 1990, **29**, 664–665.

39 C. C. Cummins, C. P. Schaller, G. D. Van Duyne, P. T. Wolczanski, A. W. E. Chan and R. Hoffmann, *J. Am. Chem. Soc.*, 1991, **113**, 2985–2994.

40 A. R. Fout, U. J. Kilgore and D. J. Mindiola, *Chem. Eur. J.*, 2007, **13**, 9428–9440.

41 R. Duchateau, A. J. Williams, S. Gambarotta and M. Y. Chiang, *Inorg. Chem.*, 1991, **30**, 4863–4866.

42 T. E. Hanna, I. Keresztes, E. Lobkovsky, W. H. Bernskoetter and P. J. Chirik, *Organometallics*, 2004, **23**, 3448–3458.

43 A. J. Blake, P. E. Collier, S. C. Dunn, W. Li, P. Mountford and O. V Shishkin, *J. Chem. Soc. Dalton Trans.*, 1997, 1549–1558.

44 S. C. Dunn, A. S. Batsanov and P. Mountford, *J. Chem. Soc. Chem. Commun.*, 1994, **724**, 2007–2008.

45 L. H. Gade and P. Mountford, *Coord. Chem. Rev.*, 2001, **216**–**217**, 65–97.

46 A. J. Blake, J. M. McInnes, P. Mountford, G. I. Nikonov, D. Swallow and D. J. Watkin, *J. Chem. Soc. Dalton Trans.*, 1999, 379–392.

47 D. Swallow, J. M. McInnes and P. Mountford, *J. Chem. Soc. Dalton Trans.*, 1998, 2253–2260.

48 E. Müller, J. Müller, F. Olbrich, W. Brüser, W. Knapp, D. Abeln and F. T. Edelmann, *Eur. J. Inorg. Chem.*, 1998, 87–91.

49 P. E. Collier, S. M. Pugh, H. S. C. Clark, J. B. Love, A. J. Blake, F. G. N. Cloke and P. Mountford, *Inorg. Chem.*, 2000, **39**, 2001–2005.

50 A. J. Blake, P. E. Collier, L. H. Gade, P. Mountford, J. Lloyd, S. M. Pugh, M. Schubart, M. E. G. Skinner and D. J. M. Trösch, *Inorg. Chem.*, 2001, **40**, 870–877.

51 C. T. Owen, P. D. Bolton, A. R. Cowley and P. Mountford, *Organometallics*, 2007, **26**, 83–92.

52 M. Froneman, D. L. Cheney and T. A. Modro, *Phosphorus. Sulfur. Silicon Relat. Elem.*, 1990, **47**, 273–281.

53 N. Adams, H. R. Bigmore, T. L. Blundell, C. L. Boyd, S. R. Dubberley, A. J. Sealey, A. R. Cowley, M. E. G. Skinner and P. Mountford, *Inorg. Chem.*, 2005, **44**, 2882–2894.

54 C. Lorber, R. Choukroun and L. Vendier, *Eur. J. Inorg. Chem.*, 2006, 4503–4518.

55 P. J. Walsh, F. J. Hollander and R. G. Bergman, *J. Am. Chem. Soc.*, 1988, **110**, 8729–8731.

56 P. J. Walsh, F. J. Hollander and R. G. Bergman, *Organometallics*, 1993, **12**, 3705–3723.

57 W. A. Nugent and R. L. Harlow, *Inorg. Chem.*, 1979, **18**, 2030–2032.

58 R. L. Zuckerman, S. W. Krska and R. G. Bergman, *J. Am. Chem. Soc.*, 2000, **122**, 751–761.

59 C. C. Cummins, S. M. Baxter and P. T. Wolczanski, *J. Am. Chem. Soc.*, 1988, **110**, 8731–8733.

60 D. J. Arney, M. A. Bruck, S. R. Huber and D. E. Wigley, *Inorg. Chem.*, 1992, **31**, 3749–3755.

61 S. R. Dubberley, S. Evans, C. L. Boyd and P. Mountford, *Dalton Trans.*, 2005, 1448–1458.

62 A. J. Blake, P. Mountford, G. I. Nikonov and D. Swallow, *Chem. Commun.*, 1996, 1835–1836.

63 J. L. Thorman, I. A. Guzei, Young and L. K. Woo, *Inorg. Chem.*, 1999, **38**, 3814–3824.

64 M. E. G. Skinner, T. Toupance, D. A. Cowhig, B. R. Tyrrell and P. Mountford, *Organometallics*, 2005, **24**, 5586–5603.

65 A. E. Guiducci, C. L. Boyd and P. Mountford, *Organometallics*, 2006, **25**, 1167–1187.

66 N. Adams, H. J. Arts, P. D. Bolton, D. Cowell, S. R. Dubberley, N. Friederichs, C. M. Grant, M. Kranenburg, A. J. Sealey, B. Wang, P. J. Wilson, M. Zuideveld, A. J. Blake, M. Schröder and P. Mountford, *Organometallics*, 2006, **25**, 3888–3903.

67 P. J. Tiong, A. Nova, L. R. Groom, A. D. Schwarz, J. D. Selby, A. D. Schofield, E. Clot and P. Mountford, *Organometallics*, 2011, **30**, 1182–1201.

68 N. Kaltsoyannis and P. Mountford, *J. Chem. Soc., Dalton Trans.*, 1999, 781–789.

69 S. Y. Lee and R. G. Bergman, *Tetrahedron*, 1995, **51**, 4255–4276.

70 K. E. Meyer, P. J. Walsh and R. G. Bergman, *J. Am. Chem. Soc.*, 1995, **117**, 974–985.

71 S. Y. Lee and R. G. Bergman, *J. Am. Chem. Soc.*, 1995, **117**, 5877–5878.

72 S. A. Blum, V. A. Rivera, R. T. Ruck, F. E. Michael and R. G. Bergman, *Organometallics*, 2005, **24**, 1647–1659.

73 A. P. Duncan and R. G. Bergman, *Chem. Rec.*, 2002, **2**, 431–445.

74 D. J. M. Trösch, P. E. Collier, A. Bashall, L. H. Gade, M. McPartlin, P. Mountford and S. Radojevic, *Organometallics*, 2001, **20**, 3308–3313.

75 B. D. Ward, A. Maisse-Francois, P. Mountford and L. H. Gade, *Chem. Commun.*, 2004, 704–705.

76 A. Bashall, P. E. Collier, L. H. Gade, M. McPartlin, P. Mountford, S. M. Pugh, S. Radojevic, M. Schubart, I. J. Scowen and D. J. M. Trösch, *Organometallics*, 2000, **19**, 4784–4794.

77 S. M. Pugh, D. J. M. Trösch, D. J. Wilson, A. Bashall, F. G. N. Cloke, L. H. Gade, P. B. Hitchcock, M. McPartlin, J. F. Nixon and P. Mountford, *Organometallics*, 2000, **19**, 3205–3210.

78 A. Bashall, P. E. Collier, L. H. Gade, M. McPartlin, P. Mountford and D. J. M. Trösch, *Chem. Commun.*, 1998, 2555–2556.

79 P. Mountford, *J. Organomet. Chem.*, 1997, **528**, 15–18.

80 P. J. Tiong, A. Nova, A. D. Schwarz, J. D. Selby, E. Clot and P. Mountford, *Dalton Trans.*, 2012, **41**, 2277–2288.

81 A. J. Nielson, M. W. Glenny and C. E. F. Rickard, *J. Chem. Soc. Dalton Trans.*, 2001, 232–239.

82 P. D. Bolton, E. Clot, N. Adams, S. R. Dubberley, A. R. Cowley and P. Mountford, *Organometallics*, 2006, **25**, 2806–2825.

83 P. D. Bolton, E. Clot, A. R. Cowley and P. Mountford, *Chem. Commun.*, 2005, 3313–3315.

84 A. L. Odom, *Dalton Trans.*, 2005, 225–233.

85 A. Tillack, H. Jiao, I. G. Castro, C. G. Hartung and M. Beller, *Chem. Eur. J.*, 2004, **10**, 2409–2420.

86 B. F. Straub and R. G. Bergman, *Angew. Chem. Int. Ed.*, 2001, **40**, 4632–4635.

87 S. Tobisch, *Dalton Trans.*, 2006, **13**, 4277.

88 S. Tobisch, *Chem. Eur. J.*, 2007, **13**, 4884–4894.

89 C. Müller, R. Koch and S. Doye, *Chem. Eur. J.*, 2008, **14**, 10430–10436.

90 S. Tobisch, *Chem. Eur. J.*, 2008, **14**, 8590–8602.

91 K. C. Hultzsch, *Adv. Synth. Catal.*, 2005, **347**, 367–391.

92 P. J. Walsh, A. M. Baranger and R. G. Bergman, *J. Am. Chem. Soc.*, 1992, **114**, 1708–1719.

93 A. M. Baranger, P. J. Walsh and R. G. Bergman, *J. Am. Chem. Soc.*, 1993, **115**, 2753–2763.

94 F. Pohlki and S. Doye, *Angew. Chem.*, 2001, **113**, 2361–2364.

95 L. E. N. Allan, G. J. Clarkson, D. J. Fox, A. L. Gott and P. Scott, *J. Am. Chem. Soc.*, 2010, **132**, 15308–15320.

96 L. Ackermann, R. G. Bergman and R. N. Loy, *J. Am. Chem. Soc.*, 2003, **125**, 11956–11963.

97 D. Duncan and T. Livinghouse, *Organometallics*, 1999, **18**, 4421–4428.

98 L. Ackermann and R. G. Bergman, *Org. Lett.*, 2002, **4**, 1475–1478.

99 K. Manna, W. C. Everett, G. Schoendorff, A. Ellern, T. L. Windus and A. D. Sadow, *J. Am. Chem. Soc.*, 2013, **135**, 7235–7250.

100 L. Luconi, A. Rossin, G. Tuci, S. Germain, E. Schulz, J. Hannedouche and G. Giambastiani, *ChemCatChem*, 2013, **5**, 1142–1151.

101 J. Cho, T. K. Hollis, E. J. Valente and J. M. Trate, *J. Organomet. Chem.*, 2011, **696**, 373–377.

102 O. T. Summerscales and J. C. Gordon, *RSC Adv.*, 2013, **3**, 6682–6692.

103 D. Schädle, C. Schädle, K. W. Törnroos and R. Anwander, *Organometallics*, 2012, **31**, 5101–5107.

104 D. Schädle, C. Schädle, D. Schneider, C. Maichle-Mössmer and R. Anwander, *Organometallics*, 2015, **34**, 4994–5008.

105 K. D. Conroy, W. E. Piers and M. Parvez, *Organometallics*, 2009, **28**, 6228–6233.

106 A. A. Trifonov, M. N. Bochkarev, H. Schumann and J. Loebel, *Angew. Chem. Int. Ed. Engl.*, 1991, **30**, 1149–1151.

107 Z. Xie, S. Wang, Q. Yang and T. C. W. Mak, *Organometallics*, 1999, **18**, 1578–1579.

108 S. Wang, Q. Yang, T. C. W. Mak and Z. Xie, *Organometallics*, 1999, **18**, 5511–

5517.

109 H. Chan, H. Li and Z. Xie, *Chem. Commun.*, 2002, 652–653.

110 J. C. Gordon, G. R. Giesbrecht, D. L. Clark, P. J. Hay, D. W. Keogh, R. Poli, B. L. Scott and J. G. Watkin, *Organometallics*, 2002, **21**, 4726–4734.

111 D. J. Beetstra, A. Meetsma, B. Hessen and J. H. Teuben, *Organometallics*, 2003, **22**, 4372–4374.

112 A. G. Avent, P. B. Hitchcock, A. V Khvostov, M. F. Lappert and A. V Protchenko, *Dalton Trans.*, 2004, 2272–2280.

113 D. Cui, M. Nishiura and Z. Hou, *Angew. Chem. Int. Ed.*, 2005, **44**, 959–962.

114 C.-L. Pan, W. Chen, S. Song, H. Zhang and X. Li, *Inorg. Chem.*, 2009, **48**, 6344–6346.

115 N. S. Emelyanova, M. N. Bochkarev, H. Schumann, J. Lebel and L. Esser, *Koord. Khim.*, 1994, **20**, 789–793.

116 D. Schädle, C. Maichle-Moessmer, C. Schädle and R. Anwander, *Chem. Eur. J.*, 2015, **21**, 662–670.

117 C. Schädle, D. Schädle, K. Eichele and R. Anwander, *Angew. Chem. Int. Ed.*, 2013, **52**, 13238–13242.

118 D. Schädle, M. Meermann-Zimmermann, C. Schädle, C. Maichle-Mössmer and R. Anwander, *Eur. J. Inorg. Chem.*, 2015, **2015**, 1334–1339.

119 J. Scott, F. Basuli, A. R. Fout, J. C. Huffman and D. J. Mindiola, *Angew. Chem. Int. Ed.*, 2008, **47**, 8502–8505.

120 D. Schädle, C. Maichle-Mössmer, K. Törnroos and R. Anwander, *Inorganics*, 2015, **3**, 500–510.

121 E. Lu, Y. Li and Y. Chen, *Chem. Commun.*, 2010, **46**, 4469–4471.

122 T. Chu, W. E. Piers, J. L. Dutton and M. Parvez, *Organometallics*, 2013, **32**, 1159–1165.

123 W. Rong, J. Cheng, Z. Mou, H. Xie and D. Cui, *Organometallics*, 2013, **32**, 5523–5529.

124 E. Lu, J. Chu, Y. Chen, M. V Borzov and G. Li, *Chem. Commun.*, 2011, **47**, 743–745.

125 J. Chu, C. E. Kefalidis, L. Maron, X. Leng and Y. Chen, *J. Am. Chem. Soc.*, 2013, **135**, 8165–8168.

126 J. Chu, E. Lu, Y. Chen and X. Leng, *Organometallics*, 2013, **32**, 1137–1140.

127 E. Lu, Q. Zhou, Y. Li, J. Chu, Y. Chen, X. Leng and J. Sun, *Chem. Commun.*, 2012,

48, 3403–3405.

128 J. Chu, E. Lu, Z. Liu, Y. Chen, X. Leng and H. Song, *Angew. Chem. Int. Ed.*, 2011, **50**, 7677–7680.

129 J. Chu, X. Han, C. E. Kefalidis, J. Zhou, L. Maron, X. Leng and Y. Chen, *J. Am. Chem. Soc.*, 2014, **136**, 10894–10897.

130 T. B. Parsons, N. Hazari, A. R. Cowley, J. C. Green and P. Mountford, *Inorg. Chem.*, 2005, **44**, 8442–8458.

131 N. Wiberg, H.-W. Häring, G. Huttner and P. Friedrich, *Chem. Ber.*, 1978, **111**, 2708–2715.

132 J. D. Selby, C. D. Manley, A. D. Schwarz, E. Clot and P. Mountford, *Organometallics*, 2008, **27**, 6479–6494.

133 J. D. Selby, M. Feliz, A. D. Schwarz, E. Clot and P. Mountford, *Organometallics*, 2011, **30**, 2295–2307.

134 P. J. Walsh, M. J. Carney and R. G. Bergman, *J. Am. Chem. Soc.*, 1991, **113**, 6343–6345.

135 H. Herrmann, J. L. Fillol, H. Wadepohl and L. H. Gade, *Angew. Chem. Int. Ed.*, 2007, **46**, 8426–8430.

136 H. Herrmann, J. L. Fillol, T. Gehrmann, M. Enders, H. Wadepohl and L. H. Gade, *Chem. Eur. J.*, 2008, **14**, 8131–8146.

137 S. A. Scholl, H. Wadepohl and L. H. Gade, *Organometallics*, 2013, **32**, 937–940.

138 S. A. Scholl, G. T. Plundrich, H. Wadepohl and L. H. Gade, *Inorg. Chem.*, 2013, **52**, 10158–10166.

139 J. D. Selby, C. Schulten, A. D. Schwarz, A. Stasch, E. Clot, C. Jones and P. Mountford, *Chem. Commun.*, 2008, 5101–5103.

140 T. Gehrmann, G. T. Plundrich, H. Wadepohl and L. H. Gade, *Organometallics*, 2012, **31**, 3346−3354.

141 T. Gehrmann, J. L. Fillol, H. Wadepohl and L. H. Gade, *Angew. Chem. Int. Ed.*, 2009, **48**, 2152–2156.

142 A. D. Schofield, A. Nova, J. D. Selby, C. D. Manley, A. D. Schwarz, E. Clot and P. Mountford, *J. Am. Chem. Soc.*, 2010, **132**, 10484–10497.

143 A. D. Schofield, A. Nova, J. D. Selby, A. D. Schwarz, E. Clot and P. Mountford, *Chem. Eur. J.*, 2011, **17**, 265–285.

144 J. Unruangsri, H. Morgan, A. D. Schwarz, A. D. Schofield and P. Mountford, *Organometallics*, 2013, **32**, 3091–3107.

145 T. Gehrmann, S. A. Scholl, J. L. Fillol, H. Wadepohl and L. H. Gade, *Chem. Eur. J.*, 2012, **18**, 3925–3941.

146 A. D. Schofield, DPhil Thesis, University of Oxford, 2012.

147 S. Banerjee and A. L. Odom, *Organometallics*, 2006, **25**, 3099–3101.

148 A. A. Dissanayake and A. L. Odom, *Chem. Commun.*, 2012, **48**, 440–442.

149 L. R. Groom, DPhil Thesis, University of Oxford, 2014.

150 A. D. Schwarz, C. S. Onn and P. Mountford, *Angew. Chem. Int. Ed.*, 2012, **51**, 12298–12302.

151 A. D. Schwarz, A. Nova, E. Clot and P. Mountford, *Chem. Commun.*, 2011, **47**, 4926–4928.

152 A. D. Schwarz, A. Nova, E. Clot and P. Mountford, *Inorg. Chem.*, 2011, **50**, 12155–12171.

153 L. R. Groom, A. D. Schwarz, A. Nova, E. Clot and P. Mountford, *Organometallics*, 2013, **32**, 7520–7539.

154 A. A. Danopoulos, C. Redshaw, A. Vaniche, G. Wilkinson, B. Hussain-Bates and M. B. Hursthouse, *Polyhedron*, 1993, **12**, 1061–1071.

155 K. Weber, K. Korn, A. Schorm, J. Kipke, M. Lemke, A. Khvorost, K. Harms and J. Sundermeyer, *Z. Anorg. Allg. Chem.*, 2003, **629**, 744–754.

156 M. D. Fryzuk, B. A. MacKay, S. A. Johnson and B. O. Patrick, *Angew. Chem. Int. Ed. Engl.*, 2002, **41**, 3709–3712.

157 R. Thompson, C.-H. Chen, M. Pink, G. Wu and D. J. Mindiola, *J. Am. Chem. Soc.*, 2014, **136**, 8197–8200.

158 B. A. MacKay, S. A. Johnson, B. O. Patrick and M. D. Fryzuk, *Can. J. Chem.*, 2005, **83**, 315–323.

159 S. P. Semproni and P. J. Chirik, *Eur. J. Inorg. Chem.*, 2013, **2**, 3907–3915.

160 L. C. Stevenson, S. Mellino, E. Clot and P. Mountford, *J. Am. Chem. Soc.*, 2015, **137**, 10140–10143.

161 S. Mellino and P. Mountford, Unpublished results.

162 A.-M. Fuller, W. Clegg, R. W. Harrington, D. L. Hughes and S. J. Lancaster, *Chem. Commun.*, 2008, 5776–5778.

163 A.-M. Fuller, D. L. Hughes, G. A. Jones and S. J. Lancaster, *Dalton Trans.*, 2012, **41**, 5599–5609.

Chapter Two

Titanium borylimido synthons and N_2N-supported complexes: synthesis, structure and bonding

2.1 Overview

This chapter will first describe the synthesis of three titanium borylimido compounds, including the synthons Ti{NB(NAr'CH)$_2$}Cl$_2$(NHMe$_2$)$_2$ (**1**) and Ti{NB(NAr'CH)$_2$}Cl$_2$(py)$_3$ (**3**) from Ti(NMe$_2$)$_2$Cl$_2$, this being the first of two new routes to access titanium borylimido compounds to be introduced in this Thesis. Subsequently, the installation of five tridentate nitrogen-based ligands onto **3** will be explored. Structural characterisation of all of these compounds will be presented, and particular emphasis will be placed on comparisons of the Ti–N–B linkage with the previously reported imido and hydrazido analogues. DFT and QTAIM analyses will also be explored, with comparisons made between a model borylimide and its alkyl- and arylimido counterparts.

2.2 Introduction

As discussed in Chapter One of this Thesis, the synthesis, characterisation and reactivity of Group 4 metal complexes containing a metal–nitrogen multiple bond have been studied in considerable depth over recent decades.[1–15] One particular seminal area of interest were the Group 4 imido compounds (L)M=N–R (R = alkyl or aryl), which formally contain a metal–nitrogen triple bond ($\sigma^2\pi^4$).[13,16–22] The characterisation of the structure and bonding of this functional group has been achieved in a large number of compounds, containing a wide range of auxiliary ligand sets. In addition, many reactivity studies of these compounds have been published, in some cases the imide being an inert supporting ligand, and in others it being the centre of reactivity. The related Group 4 terminal hydrazido(2–) compounds (L)M=NNRR' (R and/or R' = H, alkyl, aryl or SiMe$_3$) have been known for as long as the imides,[7,23–25] but detailed study of their reactivity has been much more recent, having been mostly developed within the last 10 years. Whilst research into Group 6 hydrazides has focussed on their links to the fixation of dinitrogen at biological metal centres,[26] their Group 4 counterparts display reactivity with a rich array of small molecules, as discussed fully in Chapter One.

Given this diverse range of reactivity, work within our research group over recent years has begun to focus on the substitution of the hydrazide N$_\beta$ atom with other heteroatoms, X, in order to develop new functional groups, M=N–XR$_n$, and to test their capacity for novel N–C and X–C bond forming reactions. To this end, the first Group 4 alkoxyimido compounds, (L)Ti=NO^{t}Bu, were reported by our research group in 2011.[27,28] Later, the first detailed reactivity study of an alkoxyimido complex, namely Cp*Ti{PhC(N^{i}Pr)$_2$}(NO^{t}Bu)

(**1.108**), was also published.[29] This compound demonstrated a wide range of reactivity with unsaturated substrates although, disappointingly, no synthetically useful reactions occurred with either terminal or internal alkynes.

Incorporation of a boron atom as the β-heteroatom in a metal–nitrogen multiply bonded functional group forms a borylimido moiety. Only two examples of terminal Group 4 borylimides have been reported to date, both arising from serendipitous N–B coupling reactions. The first, (^{tBu}NacNac)Ti(NBEt$_2$)(NTol$_2$) (**1.114**, ^{tBu}NacNac = HC{C(^{t}Bu)NAr'}$_2$), was produced through reaction of 2 equiv. NaHBEt$_3$ with the parent imido (terminal NH) compound by Mindiola and co-workers.[30] A second was prepared in our research group through reaction of either a dimethyl- or diphenylhydrazide with 1 equiv. 9-BBN dimer; the formation of Cp*Ti{MeC(N^{i}Pr)$_2$}(NBC$_8$H$_{14}$) (**1.115**) was accompanied by elimination of dimethyl- or diphenylaminoborane, respectively, and H$_2$.[31]

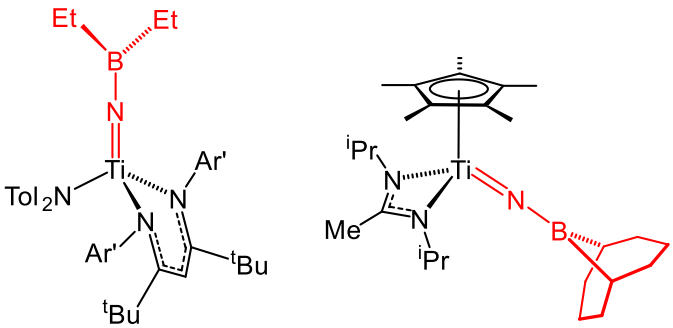

1.114 **1.115**

Figure 2.1. Group 4 borylimido complexes reported to date.[30,31]

Across the rest of the transition metals, borylimido complexes remain very poorly explored, with no established synthetic routes, and no reactivity reported. Indeed, only a further four borylimides have been reported, three of which were synthesised *via* an oxidative methodology using Mes$_2$BN$_3$, with formation of the –NBMes$_2$ functional group being accompanied by N$_2$ extrusion (see Chapter One).[32,33] Chapters Two and Three of this Thesis will discuss the realisation of the Author's aim to develop new, versatile pathways to borylimido complexes, taking inspiration from analogous routes which are well established in titanium imido, hydrazido and alkoxyimido chemistry.

In work previously developed by this research group and others, synthons of the type Ti(NR)Cl$_2$(L)$_n$ (R = ^{t}Bu, aryl, NPh$_2$, O^{t}Bu; L = py, 4-NC$_5$H$_4$^{t}Bu; n = 2 or 3)[27,28,34,35] and Ti(NR)Cl$_2$(NHMe$_2$)$_2$ (R = alkyl, aryl, NPh$_2$, NO^{t}Bu)[27,28,36–38] proved to be versatile entry points to new complexes through displacement of the Cl or Lewis base ligands with anionic

or neutral donors. A general route to the latter type involves the reaction of $Ti(NMe_2)_2Cl_2$ with the required amine, N,N-disubstituted hydrazine or alkoxyamine,[27,28,36–39] and in some cases, reaction of those compounds with pyridine results in the pyridine-coordinated complexes $Ti(NR)Cl_2(py)_3$.[36,40] This Chapter will discuss the extension of this route to the formation of titanium borylimido complexes using borylamines.

Throughout previous studies of metal–nitrogen multiply bonded compounds, the choice of supporting ligand set has been of particular importance in obtaining systems that exhibit controlled reactivity. The dianionic, tridentate diamide-amine ligands $RN\{(CH_2)_nNSiMe_3\}_2$ (R = Me, n = 2 ($N_2N^{SiMe_3}N^{Me}$) or n = 3 (N_2N^{Me,C_3}); R = $SiMe_3$, n = 2 ($N_2N^{SiMe_3}$)) have been demonstrated to be one of the most effective for promoting chemistry at the Group 4 metal–nitrogen multiple bond, along with the related diamide-pyridine ligands $(2\text{-}C_5H_4N)CMe(CH_2NSiMe_2R)_2$ (R = Me (N_2N^{py}) or R = ^{t}Bu ($N_2^{TBS}N^{py}$)) and diamide-ether ligands $O(CH_2CH_2NSiMe_3)_2$ ($N_2^{SiMe_3}O$) and $O(2\text{-}C_6H_4NSiMe_3)_2$ ($N_2^{Ar}O$).[34,41–55] These chelating ligands provide a well-defined, but flexible environment around the metal centre and have found extensive utility in early transition metal chemistry generally, and in metal–ligand multiple bond chemistry in particular.[12,31,55–62] For example, $Ti(N_2^{SiMe_3}N^{Me})(NNPh_2)(py)$ (**1.63**) catalyses the *cis*-diamination of alkynes by diphenylhydrazine,[41] whilst changing the N_{amide}-substituent to an isopropyl group in $Ti(N_2^{iPr}N^{Me})(NNPh_2)(py)$ (**2.1**) instead gave catalytic hydrohydrazination of alkynes by the same substrate.[63] Structural and computational studies of these systems have shown that the N_{amide} π-donors destabilise the $M{=}N_\alpha$ multiple bond by competing for the metal π-acceptor orbitals, thus activating the multiple bond towards reactivity with organic substrates.[34,62] This Chapter will describe the synthesis of three diamide-amine-supported borylimido complexes, as well as a diamide-pyridine-supported borylimide. The relative level of disruption of the titanium–nitrogen multiple bond by these ligands will be discussed, drawing evidence from crystallographic studies.

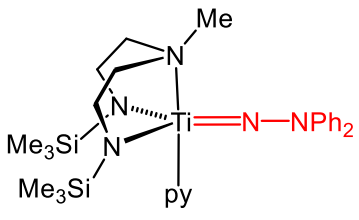

1.63

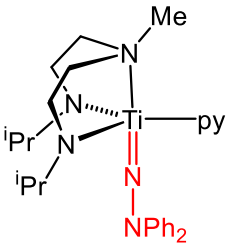

2.1

Figure 2.2. Examples of diamide-amine-supported hydrazido complexes.[41,63]

2.3 Selection of a borylamine starting material

Preliminary reactions using conventional dialkyl- or diarylborylamines, including H_2NBMes_2 and H_2N–BBN, as precursors to borylimido ligands were first attempted. If formed, such borylimido complexes would be the analogues of the previously reported tungsten (**1.110** and **1.111**) and vanadium (**1.112**) dimesitylborylimido complexes (formed from Mes_2BN_3), and **1.115** described above (formed from H-BBN), respectively. However, under the protonolysis methodologies applied here (*vide infra*), no success was found in the formation of titanium borylimides from these borylamines. It was initially speculated that, in these borylamines, significant donation of electron density from the nitrogen lone pair to the boron empty 2p orbital occurs, thus reducing the ability of the amine to pre-coordinate to the metal. Furthermore, the electropositive nature of boron reduces the acidity of the borylamine, making protonolysis reactivity less likely. DFT calculations (B3PW91 functional and Def2TZVP basis set) were performed by Prof. Philip Mountford on the pyramidalisation of the lone pair in two model borylamines, H_2NBMe_2 and H_2NBPh_2, with the SCF energies of these processes calculated to be 6.9 and 6.7 kcal mol^{-1}, respectively. Considering a typical entropic contribution to free energy of *ca* 12 – 13 kcal mol^{-1} for an associative reaction, the formation of a borylamine adduct of $Ti(NMe_2)_2Cl_2$ (which is expected to be virtually activationless) should be accessible at RT. The alternative outcomes of these reactions will be discussed further in Section 2.4.

However, success has been found with the borylamine $H_2NB(NAr'CH)_2$ (**2.2**). In this compound, which incorporates a 1,3,2-diazaborole moiety, the boron atom is part of a five-membered heterocycle, and is flanked by the two nitrogen atoms in this ring, in addition to the amine nitrogen. The SCF energy of pyramidalisation here was calculated to be 1.6 kcal mol^{-1}, indicating reduced donation of the terminal amine lone pair to the boron 2p orbital. Further stabilisation of this unit is provided by the unsaturation in the C_2 backbone imparting 6π-aromatic character on the boryl ring.[64] Recently, Jones and co-workers reported a high-yielding, multi gram-scale preparation of this borylamine; bubbling of ammonia through a hexane solution of $BrB(NAr'CH)_2$ yields **2.2** and NH_4Br, which are easily separated by filtration (Equation 2.1).[65] With such convenient access, **2.2** became the focus of study, and all borylimido complexes reported in Chapters Two and Three of this Thesis are derived from this borylamine.

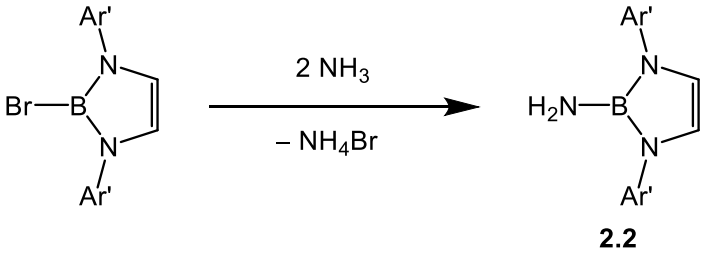

2.2

Equation 2.1[65]

2.4 Synthesis of Ti{NB(NAr'CH)$_2$}Cl$_2$(NHMe$_2$)$_2$ (1)

Previous work within this research group demonstrated the preparation of monomeric species of the type Ti(NR)Cl$_2$(NHMe$_2$)$_2$ (R = alkyl, aryl, NPh$_2$, O^{t}Bu) from reaction of Ti(NMe$_2$)$_2$Cl$_2$ with the respective primary amine, aniline, diphenylhydrazine or *tert*-butoxyamine.[27,28,34,35,40] In the same way, the borylamine H$_2$NB(NAr'CH)$_2$ (**2.2**) reacted cleanly with Ti(NMe$_2$)$_2$Cl$_2$ on the NMR tube scale in C$_6$D$_6$, forming the borylimido complex Ti{NB(NAr'CH)$_2$}Cl$_2$(NHMe$_2$)$_2$ (**1**) *via* proton transfer (Equation 2.2). When synthesised on the preparative scale in toluene solution, **1** was isolated as a red-brown solid in 79% yield. The ^{1}H NMR spectrum in C$_6$D$_6$ solution displays resonances for a *C$_s$* symmetric species containing one NB(NAr'CH)$_2$ and two NHMe$_2$ ligands. The resonances attributed to the borylimido moiety include a singlet at 5.73 ppm for the NCH units of the boryl ring, a septet at 3.53 ppm for the isopropyl methine and two doublets (1.56 and 1.24 ppm) for the diastereotopic isopropyl methyl groups. The ^{11}B chemical shift of the borylimido ligand in **1** is 14.2 ppm, which compares with 23.0 ppm for H$_2$NB(NAr'CH)$_2$ (**2.2**). DFT calculations on the full complex **1** gave a computed ^{11}B NMR shift of 13.7 ppm, which is in good agreement with the experimental value. The majority of titanium borylimido complexes to be reported in this Thesis have ^{11}B resonances in the range *ca* 13 – 16 ppm.

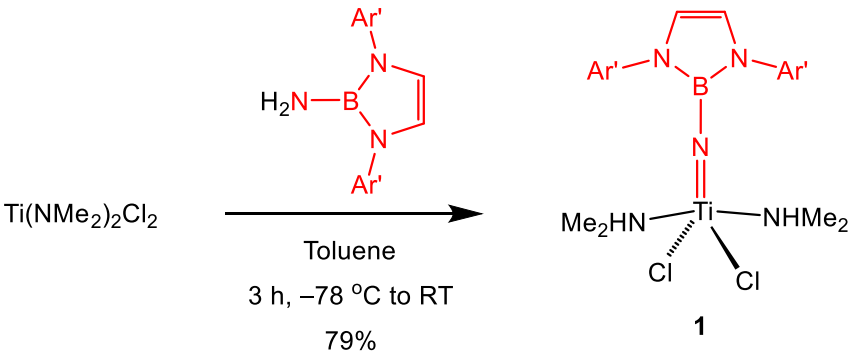

1

Equation 2.2

Diffraction-quality crystals of **1** were grown from a hexane solution at RT. The molecular solid state structure, which confirms that depicted in Equation 2.2, is shown in Figure 2.3, and selected bond lengths and angles are listed in Table 2.1. In the solid state, $Ti\{NB(NAr'CH)_2\}Cl_2(NHMe_2)_2$ (**1**) has an approximately trigonal bipyramidal geometry in which the two $NHMe_2$ ligands occupy axial positions and the Cl and $NB(NAr'CH)_2$ ligands occupy equatorial positions. The orientation of the borylimido ligand is such that it lies between the planes defined by the mutually *trans* Cl atoms and the mutually *trans* amine ligands; the angle between the Cl(1)–Ti(1)–Cl(2) plane and the {N(1),B(1),N(2),N(3)} plane is *ca* 61.0°. **1** can be compared with the array of previously structurally characterised complexes of the type $Ti(NR)Cl_2(NHMe_2)_2$ (R = alkyl, aryl, O^tBu),[27,28,36–40] all of which share a largely similar molecular geometry. Of particular interest here is the Ti–N–B linkage. The short Ti(1)–N(1) distance of 1.7027(11) Å and the near-linear Ti(1)–N(1)–B(1) angle of 178.19(9)°, which implies sp hybridisation at N(1), are both consistent with a titanium–nitrogen triple bond ($\sigma^2\pi^4$). The N(1)–B(1) distance of 1.4374(16) Å is consistent with a single bond, falling within the range (*ca* 1.34 – 1.51 Å) of all N–B single bonds with sp hybridised N and three-coordinate B in the Cambridge Structural Database.[66] Past experimental and computational work has found that $Ti–N_{im}$ bond lengths typically follow the trend $Ti–N_{alkyl} < Ti–NO^tBu < Ti–N_{aryl} < Ti–NNPh_2$ (N_{im} is used to represent the multiply-bonded nitrogen in imido, hydrazido, alkoxyimido and borylimido compounds), and this is indeed the case for the respective analogues of **1** (although no hydrazide has been structurally characterised). The Ti(1)–N(1) bond length of 1.7027(10) Å in **1** places within the range reported for a series of eight arylimido complexes $Ti(NAr)Cl_2(NHMe_2)_2$ (avg. $Ti–N_{im}$ = 1.703 Å, range 1.694(4) – 1.708(2) Å),[36,40] and is longer than in both the alkylimide $Ti(N^iPr)Cl_2(NHMe_2)_2$ (1.672(2) Å) and the *tert*-butoxyimido analogue (1.688(3) and 1.691(3) Å for the two crystallographically independent molecules).[28,36]

In the solid state, molecules of **1** form hydrogen-bonded dimers across crystallographic inversion centres, as illustrated in Figure 2.4. Within each molecule, only one of the Cl ligands and one $N\underline{H}Me_2$ is involved in an N–H···Cl hydrogen bond, the H(1)···Cl(2A) distance being 2.861(18) Å, thus lying within the expected range for an "intermediate" strength N–H···Cl hydrogen bond.[67]

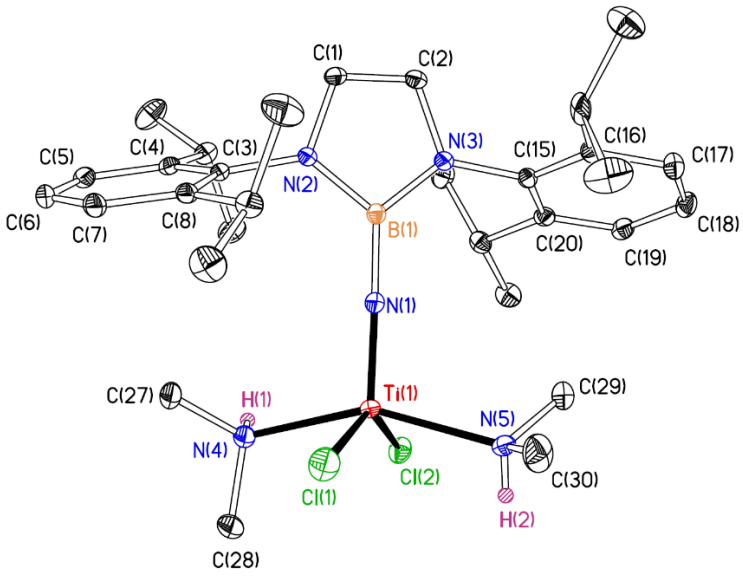

Figure 2.3. Displacement ellipsoid plot (25% probability) of $Ti\{NB(NAr'CH)_2\}Cl_2(NHMe_2)_2$ (**1**). C-bound H atoms are omitted for clarity. H(1) and H(2) are drawn as spheres of an arbitrary radius.

Table 2.1. Selected bond distances (Å) and angles (°) for $Ti\{NB(NAr'CH)_2\}Cl_2(NHMe_2)_2$ (**1**).

Ti(1)–N(1)	1.7027(10)	N(1)–Ti(1)–N(4)	104.60(4)
Ti(1)–N(4)	2.2235(11)	N(1)–Ti(1)–N(5)	102.30(4)
Ti(1)–N(5)	2.2447(11)	N(4)–Ti(1)–N(5)	152.65(4)
Ti(1)–Cl(1)	2.3224(4)	N(1)–Ti(1)–Cl(1)	110.35(4)
Ti(1)–Cl(2)	2.3730(4)	N(4)–Ti(1)–Cl(1)	85.72(3)
N(1)–B(1)	1.4374(16)	N(5)–Ti(1)–Cl(1)	89.57(3)
B(1)–N(2)	1.4466(16)	N(1)–Ti(1)–Cl(2)	108.21(4)
B(1)–N(3)	1.4449(16)	N(4)–Ti(1)–Cl(2)	81.57(3)
N(4)–H(1)	0.898(18)	N(5)–Ti(1)–Cl(2)	85.47(2)
N(5)–H(2)	0.849(19)	Cl(1)–Ti(1)–Cl(2)	141.288(17)
		Ti(1)–N(1)–B(1)	178.19(9)
		N(1)–B(1)–N(2)	127.00(11)
		N(1)–B(1)–N(3)	129.11(11)

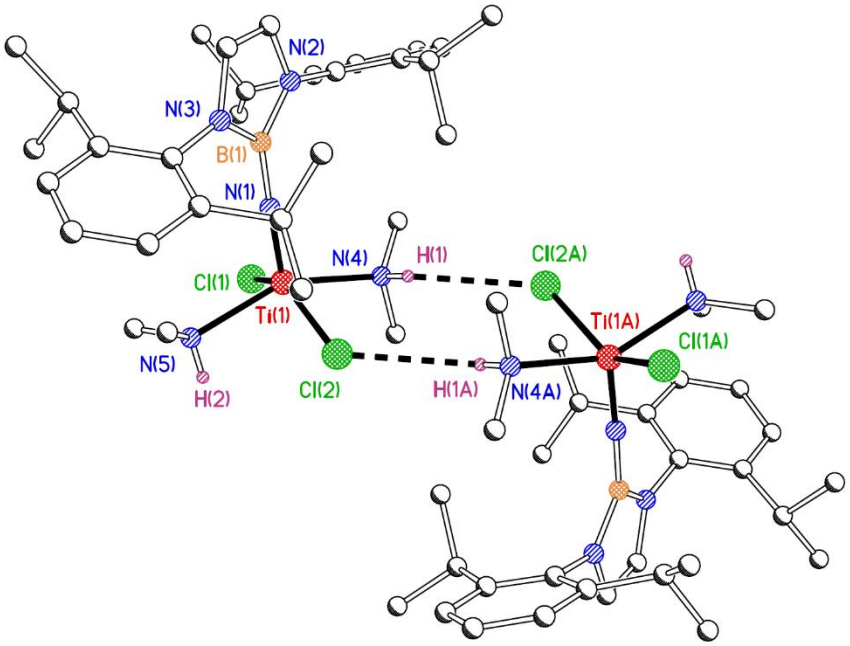

Figure 2.4. View of Ti{NB(NAr'CH)$_2$}Cl$_2$(NHMe$_2$)$_2$ (**1**) showing hydrogen-bonded dimers. C-bound H atoms are omitted and all atoms are drawn as spheres of an arbitrary radius. Selected distance: H(1)···Cl(2A) = 2.861(18) Å. Cl(1) and H(2) form no hydrogen bonds. Atoms carrying the suffix 'A' are related to their counterparts by the symmetry operator [1–*x*, 2–*y*, 1–*z*].

The formation of hydrogen-bonded dimers in the solid state contrasts with the majority of the imido compounds Ti(NR)Cl$_2$(NHMe$_2$)$_2$, which generally form extended hydrogen-bonded chains in the solid state through both Cl ligands and both N<u>H</u>Me$_2$ atoms.[36] However, the compound Ti(N-2-C$_6$H$_4$^{t}Bu)Cl$_2$(NHMe$_2$)$_2$ forms dimers in the same manner as **1**,[36] and this similarity is attributed to the steric disruption caused by the *ortho*-^{t}Bu substituent in the imide, and the very large BN(Ar'CH)$_2$ moiety in **1**, which both prevent the formation of extended chains. The solid state IR spectrum (Nujol mull) of **1** is consistent with the hydrogen-bonded dimers shown above, displaying two overlapping ν(N–H) bands at 3289 and 3277 cm^{-1}, assigned to the non-bridging N–H bond and the hydrogen bonding N–H respectively. In dichloromethane solution, a single ν(N–H) band is observed at 3288 cm^{-1}.

Reactions were also attempted between Ti(NMe$_2$)$_2$Cl$_2$ and two other borylamines: (μ-H$_2$N)$_2$(BC$_8$H$_{14}$)$_2$ and H$_2$NBMes$_2$. The reaction of the latter borylamine with Ti(NMe$_2$)$_2$Cl$_2$ on the NMR tube scale in C$_6$D$_6$ resulted in a large amount of precipitation from the solution and the gradual decay of all resonances from the ^{1}H NMR spectrum when

heated at 50 °C. Attempts to redissolve the precipitate in CD_2Cl_2 to ascertain its identity resulted only in the observation of a complex mixture of products. The former reagent, the amino-derivative of 9-BBN, which exists as a dimer in C_6D_6 solution, also resulted in precipitation from the solution on the NMR tube scale. In this case, however, one species remained in the ^{1}H NMR spectrum after 6 h at RT, which was confirmed to be $Me_2NBC_8H_{14}$ by inspection of the resonances.[31,68] Thus, in both of these cases, it appears that an amine transfer process takes place, causing the decomposition of the titanium starting material, and the loss of all titanium species from solution.

Given the failure of the reactions of $(\mu\text{-}H_2N)_2(BC_8H_{14})_2$ and H_2NBMes_2 with $Ti(NMe_2)_2Cl_2$ to form the desired borylimido complexes, the energetics of these hypothetical reactions (Equation 2.3 depicts the former case) were compared with the (experimentally successful) formation of $Ti\{NB(NAr'CH)_2\}Cl_2(NHMe_2)_2$ (**1**) through DFT calculations (including dispersion and solvent corrections), which were performed by Simona Mellino and Prof. Philip Mountford. When considering the formation of **1**, **1_BBN** and **1_BMes$_2$** from $Ti(NMe_2)_2Cl_2$ and the respective borylamine monomer, the Δ_rG values for the three reactions were calculated to be –4.3, 2.3 and –2.0 kcal mol^{-1} respectively. Given that $(\mu\text{-}H_2N)_2(BC_8H_{14})_2$ is known to exist in solution as a dimer, the energy of its dissociation to a monomer should be accounted for. This was calculated to be 2.2 kcal mol^{-1} for each half dimer forming one monomer. Therefore, including this dissociation, the total free energy change for the formation of **1_BBN** becomes 4.5 kcal mol^{-1}. Thus it can be seen that the formation of **1_BBN** is thermodynamically disfavoured compared with **1**, somewhat explaining the different reaction outcome in this case. In contrast, the formation of **1_BMes$_2$** was calculated to be exergonic. It is therefore postulated that an amide-exchange route analogous to that found experimentally for $(\mu\text{-}H_2N)_2(BC_8H_{14})_2$ may be thermodynamically favoured over the desired reaction. However, Me_2NBMes_2 could not be observed in the ^{1}H NMR spectrum of the final reaction mixture. Furthermore, it was established earlier that pyramidalisation at the nitrogen atom of the borylamines, which is necessary for their coordination to the metal centre, is kinetically accessible, therefore ruling out the suspected involvement of donation of the nitrogen lone pair to the boron 2p orbital as a factor in these reaction outcomes.

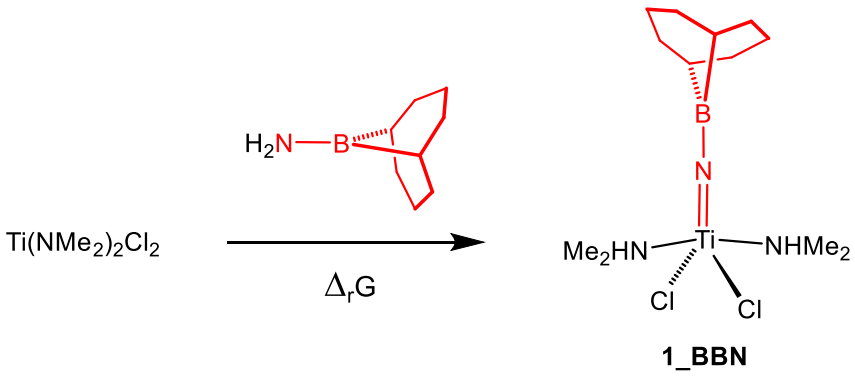

Equation 2.3

In Section 2.8, DFT calculations will be presented which give a bonding analysis of the Ti–N multiple bond in model diamide-pyridine-supported borylimido complexes. Furthermore, in Section 3.7, calculations will provide a full analysis of imido/borylamine and borylimido/amine exchanges in model half-sandwich complexes, with the findings also being of relevance to the reactions of $Ti(NMe_2)_2Cl_2$ with $H_2NB(NAr'CH)_2$ (**2.2**), $(\mu\text{-}H_2N)_2(BC_8H_{14})_2$ and H_2NBMes_2 as described above.

2.5 Amine substitution reactions of $Ti\{NB(NAr'CH)_2\}Cl_2(NHMe_2)_2$ (1)

Substitution of the $NHMe_2$ ligands of **1** was successfully achieved with the neutral, *fac*-N_3 donor ligand $Me_3[6]aneN_3$ (trimethyl-1,3,5-triazacyclohexane), the application of which in titanium imido chemistry is well established.[69,70] Reaction of **1** with $Me_3[6]aneN_3$ proceeded smoothly in toluene at room temperature to afford the complex $Ti\{NB(NAr'CH)_2\}Cl_2(Me_3[6]aneN_3)$ (**2**) in 58% isolated yield (Scheme 2.1). The ^1H NMR spectrum of **2** in C_6D_6 solution is characteristic of a C_s symmetric species; in addition to the resonances attributed to the borylimido ligand, there are two singlets in a 2:1 integration ratio for the N-methyl groups which are *trans* to the Cl ligands or to the borylimido ligand, and similarly two pairs of doublets in a 2:1 ratio attributed to the methylene protons of the $Me_3[6]aneN_3$ ring.

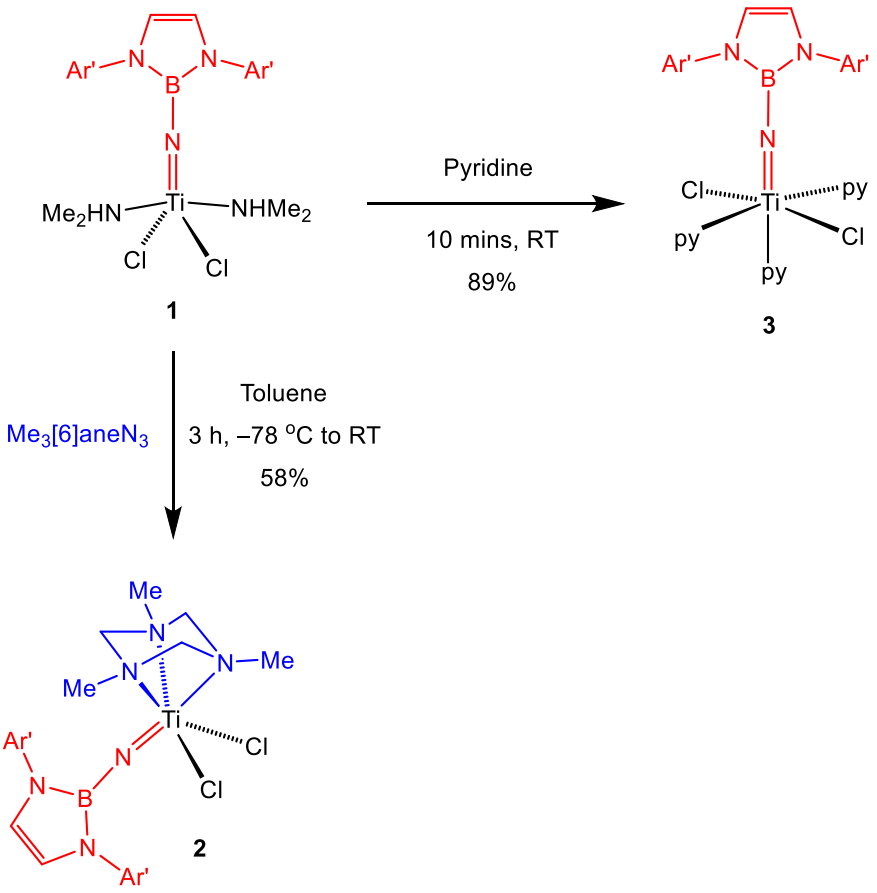

Scheme 2.1. Synthesis of Ti{NB(NAr'CH)$_2$}Cl$_2$(Me$_3$[6]aneN$_3$) (**2**) and Ti{NB(NAr'CH)$_2$}Cl$_2$(py)$_3$ (**3**) from Ti{NB(NAr'CH)$_2$}Cl$_2$(NHMe$_2$)$_2$ (**1**).

In this research group's previously reported alkoxyimido chemistry it was found that the NHMe$_2$ ligands of Ti(NO^{t}Bu)Cl$_2$(NHMe$_2$)$_2$ (**1.103**) could not be cleanly displaced through direct reaction with pyridine. Instead, reaction of the Me$_3$[6]aneN$_3$-bound alkoxyimido analogue of **2** with pyridine releaseed the *fac*-N$_3$ donor, thus forming the useful alkoxyimido synthon Ti(NO^{t}Bu)Cl$_2$(py)$_3$ (**1.105**).[27,28] However, in these investigations of titanium borylimido chemistry, the converse was found to be true. That is, attempted reactions of Ti{NB(NAr'CH)$_2$}Cl$_2$(Me$_3$[6]aneN$_3$) (**2**) with pyridine did not cleanly form the pyridine-bound compound, perhaps due to greater steric hindrance in this case. Gratifyingly, however, direct reaction of **1** with neat pyridine did result in clean formation of the desired compound Ti{NB(NAr'CH)$_2$}Cl$_2$(py)$_3$ (**3**) in 89% isolated yield. Compound **3** was also prepared *via* a "one-pot" reaction from Ti(NMe$_2$)$_2$Cl$_2$ without the need to purify the intermediate **1**, yielding 5.3 g of product from 1.5 g of Ti(NMe$_2$)$_2$Cl$_2$ and 3.0 g of borylamine **2.2** (94% overall yield). The ^{1}H NMR spectrum of **3** in C$_6$D$_6$ solution (Figure 2.5) features the expected resonances for the borylimido ligand, as well as two sets of

resonances in a 2:1 integration ratio corresponding to the pyridine ligands positioned *cis* and *trans* to the borylimido group respectively. Those signals belonging to the *trans*-positioned pyridine are significantly broadened, an effect which has also been described in the analogous imido, hydrazido and alkoxyimido complexes,[28,35,38] and is attributed to a dissociative exchange of *trans* pyridine ligands between molecules of **3** in solution.

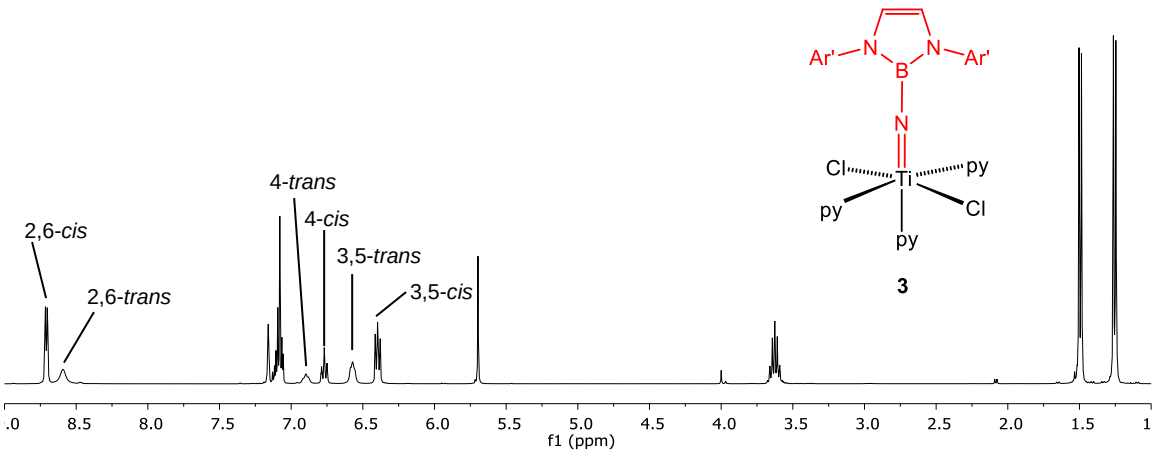

Figure 2.5. ^{1}H NMR spectrum (400.1 MHz) of Ti{NB(NAr'CH)$_2$}Cl$_2$(py)$_3$ (**3**) in C_6D_6 at 298 K.

Diffraction-quality crystals of **3** were successfully grown from a hexane solution at 5 °C, and the solid state structure obtained. The molecular structure is shown in Figure 2.6, and selected bond lengths and angles listed in Table 2.2. The borylimide **3** has an approximately octahedral titanium centre about which the three pyridine ligands are coordinated in a meridional fashion and the two Cl atoms are mutually *trans*, and thus its geometry is entirely analogous to those complexes of the type Ti(NR)Cl$_2$(py)$_3$ (R = alkyl, aryl, NPh$_2$, O^{t}Bu) which have previously been structurally characterised.[28,34,35,40,71–73] The borylimido ligand is oriented such that its N–Ar' substituents almost eclipse the *cis*-positioned pyridine ligands; the angle between the N(5)–Ti(1)–N(6) plane and the plane of the boryl ring is *ca* 8.9°. Ti(1) lies *ca* 0.27 Å above the {Cl(1),Cl(2),N(5),N(6)} least-squares plane in order to augment the Ti(1)–N(1) multiple bond, as described previously in d^0 metal imido and nitrido complexes.[19,74] It is also observed that the borylimido ligand exerts a very strong *trans* influence on the N(4) pyridine ligand. This is defined quantitatively as the difference between the Ti–N bond lengths for the pyridine ligands *cis* and *trans* to the borylimido ligand. The two independent values are 0.318(2) and 0.314(2) Å, giving an average of 0.316(1) Å. This value is significantly greater than that generally reported for the analogous imides Ti(NR)Cl$_2$(py)$_3$ (R = ^{t}Bu, Ph, Tol, P(S)Ph$_2$; range = 0.18 – 0.21 Å),[35,73] hydrazides

$Ti(NNPh_2)Cl_2(L)_3$ (L = py, 4-$NC_5H_4{}^tBu$; avg. value *ca* 0.160 Å)[34] and alkoxyimide $Ti(NO^tBu)Cl_2(py)_3$ (**1.105**, 0.170(2) Å).[28]

Previous experimental and computational studies have reported that the *trans* influence in these complexes depends on a number of factors which include the identity of the N-substituent and the Ti–N bond distance.[19,35] The very large *trans* influence in this case points to the borylimido ligand having a very high σ-donor ability as compared to its imido, hydrazido and alkoxyimido analogues. This is consistent with the well-developed chemistry of the 1,3,2-diazaborolyl moiety ($B(NAr'CH)_2$) itself, in which the lithium boryl reagent $Li\{B(NAr'CH)_2\}(THF)_2$ has been extensively utilised as a nucleophilic source of boron.[75–77] In one particular result, the extremely strong σ-donor properties of this anionic 1,3,2-diazaborolyl unit were responsible for the stabilisation of the first acyclic silylene complex $Si\{B(NAr'CH)_2\}\{N(SiMe_3)Ar'\}$.[78] In the case of the borylimido ligand $–NB(NAr'CH)_2$, the strongly σ-donating boryl group raises the energy of the σ-donor orbital on the nitrogen, thus making it a stronger σ-donor itself. Despite the strong *trans* influence observed structurally and by NMR spectroscopy in **3**, it was found experimentally that the *trans*-positioned pyridine is not susceptible to removal, even after extended periods under dynamic vacuum.

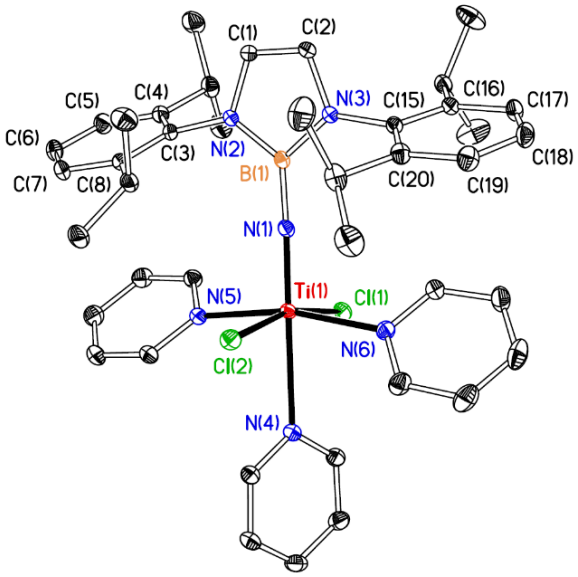

Figure 2.6. Displacement ellipsoid plot (30% probability) of $Ti\{NB(NAr'CH)_2\}Cl_2(py)_3$ (**3**). H atoms are omitted for clarity.

The Ti(1)–N(1) bond length of 1.7118(9) Å and N(1)–B(1) bond length of 1.4216(14) Å are again consistent with a titanium–nitrogen triple bond and nitrogen–boron single bond

respectively, and this is also the case for all further borylimido compounds for which the solid state structures are reported herein (*vide infra*). As was also the case for the analogues of **1**, the Ti(1)–N(1) distance of 1.7118(9) Å in **3** falls within the range of those Ti–N_{im} distances in the previously structurally characterised arylimides $Ti(NAr)Cl_2(py)_3$ (avg. Ti–N_{im} = 1.718 Å, range 1.705(4) – 1.730(2) Å for six examples),[35,40,71,79] is longer than in both the alkylimide $Ti(N^tBu)Cl_2(py)_3$ (**1.6**, 1.697(3) or 1.705(3) Å for two independent structure determinations)[35,72] and in the alkoxyimide $Ti(NO^tBu)Cl_2(py)_3$ (**1.105**, 1.7087(18) Å),[28] and shorter than in the hydrazide $Ti(NNPh_2)Cl_2(py)_3$ (1.727(2) Å).[34]

Table 2.2. Selected bond distances (Å) and angles (°) for $Ti\{NB(NAr'CH)_2\}Cl_2(py)_3$ (**3**).

Ti(1)–N(1)	1.7118(9)	N(1)–Ti(1)–N(4)	179.37(3)
Ti(1)–N(4)	2.5411(9)	N(1)–Ti(1)–N(5)	94.77(4)
Ti(1)–N(5)	2.2229(9)	N(1)–Ti(1)–N(6)	98.41(4)
Ti(1)–N(6)	2.2268(9)	N(4)–Ti(1)–N(5)	85.85(3)
Ti(1)–Cl(1)	2.4106(3)	N(4)–Ti(1)–N(6)	80.97(3)
Ti(1)–Cl(2)	2.3861(3)	N(5)–Ti(1)–N(6)	166.62(3)
N(1)–B(1)	1.4216(14)	N(1)–Ti(1)–Cl(1)	96.30(3)
B(1)–N(2)	1.4507(14)	N(4)–Ti(1)–Cl(1)	93.80(2)
B(1)–N(3)	1.4452(13)	N(5)–Ti(1)–Cl(1)	89.18(2)
		N(6)–Ti(1)–Cl(1)	87.15(2)
		N(1)–Ti(1)–Cl(2)	97.34(3)
		N(4)–Ti(1)–Cl(2)	82.55(2)
		N(5)–Ti(1)–Cl(2)	90.37(2)
		N(6)–Ti(1)–Cl(2)	90.18(2)
		Cl(1)–Ti(1)–Cl(2)	166.343(12)
		Ti(1)–N(1)–B(1)	177.85(9)
		N(1)–B(1)–N(2)	128.85(9)
		N(1)–B(1)–N(3)	126.96(9)

The preparation of borylimide **3** was particularly desired because of the ability of its imido, hydrazido and alkoxyimido analogues to act as versatile synthons for the installation of a wide range of supporting ligand sets.[27,28,34,35] Previous work has shown that the analogues of **1** can be poor starting materials in reactions with anionic reagents such as lithiated amide ligands due to side-reactions arising from the somewhat acidic $NHMe_2$ groups.[13,34] Therefore the aprotic borylimido compound **3** was exclusively used for the installation of amide ligands through salt metathesis, as explored in Sections 2.6 and 2.7.

2.6 Installation of diamide-amine supporting ligands

Salt metathesis reactions of $Ti\{NB(NAr'CH)_2\}Cl_2(py)_3$ (**3**) with the respective dilithiated ligand produced three diamide-amine-supported borylimido compounds $Ti(N_2{}^RN^{Me})\{NB(NAr'CH)_2\}(py)$ (R = $SiMe_3$ (**4**), Ar^F = C_6F_5 (**5**), ^{i}Pr (**6**); Equation 2.4). After mixing in toluene at –78 °C, the three reactions proceeded smoothly over 1 – 3 h at RT, and the pure products were isolated after removal of the volatiles from pentane extractions. The ^{1}H (Figure 2.7) and ^{13}C NMR spectra of all three compounds indicate that they have C_s symmetric structures in which the diamide-amine ligands are *fac*-coordinated, as well as containing a borylimido ligand and a pyridine donor. The diamide-amine ligand methylene proton signals present as four multiplet resonances (relative intensity 2 H each) in each case. For R = $SiMe_3$ and ^{i}Pr, one set of signals is observed for the respective N_{amide} substituents, these being one 2 H septet and two 6 H doublets in **6**, and a single 18 H $SiMe_3$ singlet in **4.** Additionally for R = Ar^F, a single set of resonances is observed in the ^{19}F spectrum of **5**, i.e. three multiplets.

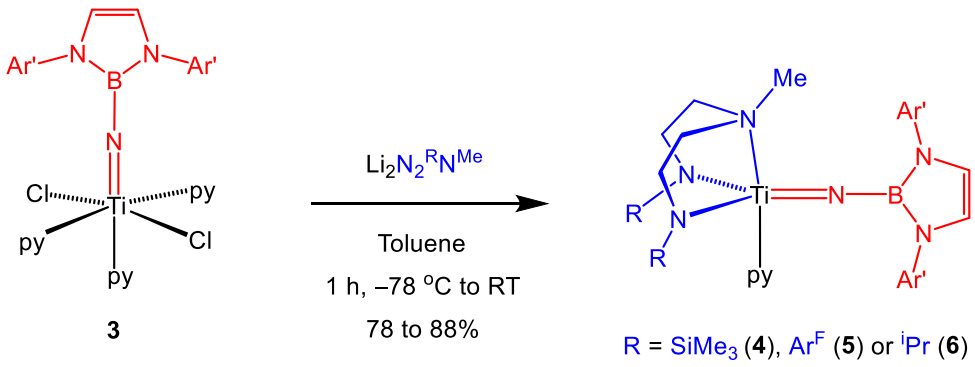

Equation 2.4

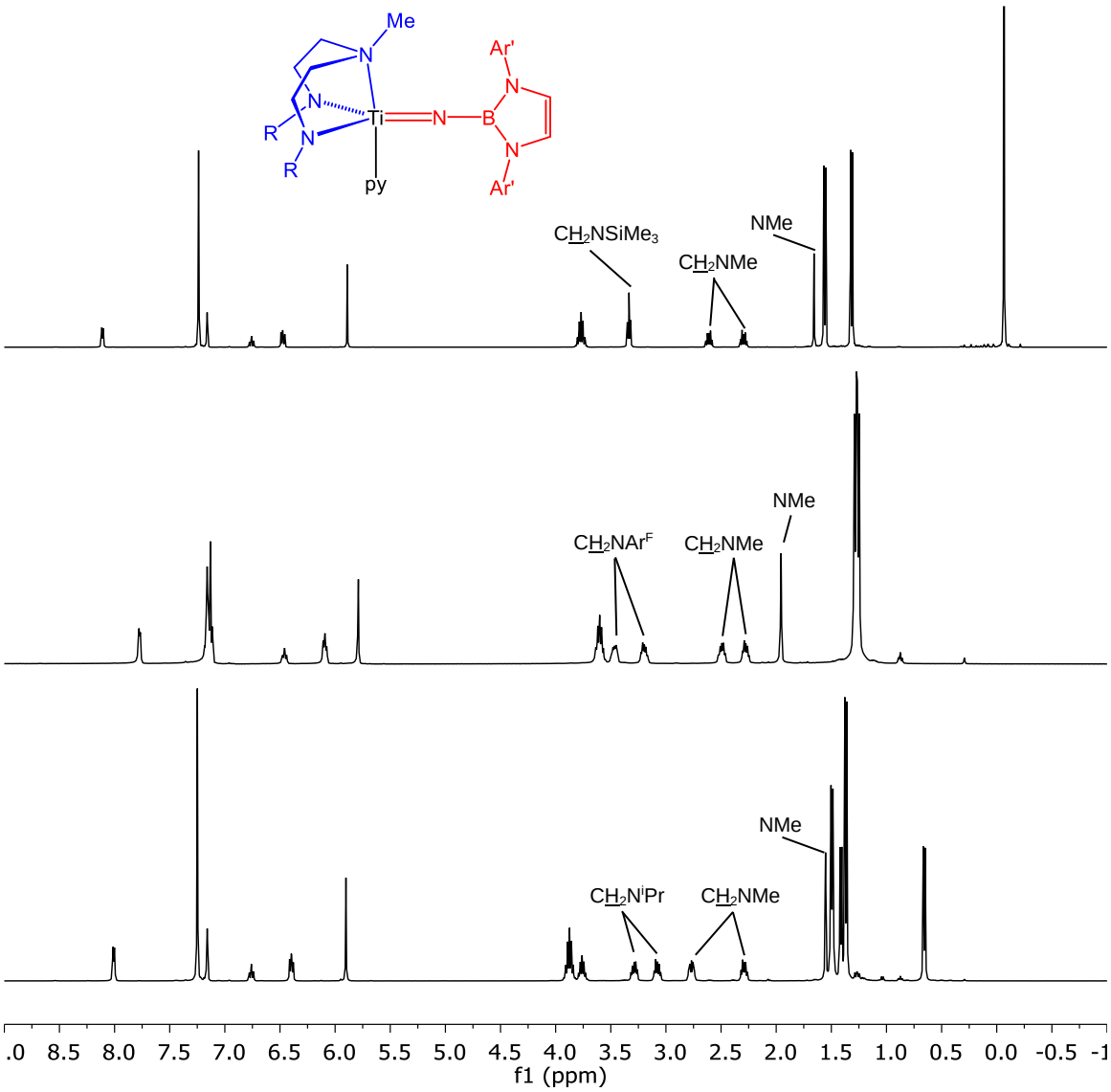

Figure 2.7. ^{1}H NMR spectra (400.1 MHz) of Ti($N_2^RN^{Me}$){NB(NAr'CH)$_2$}(py) (R = $SiMe_3$ (**4**, top), Ar^F (**5**, middle), ^{i}Pr (**6**, bottom)) in C_6D_6 at 298 K.

Diffraction-quality crystals of compounds **4**, **5** and **6** were grown from saturated hexane or pentane solutions at 5 °C, and the molecular solid state structures are shown in Figure 2.8 along with selected bond lengths and angles in Table 2.3. The three complexes all have trigonal-bipyramidal geometries, in which the diamide-amine ligands coordinate facially, and the borylimido ligands occupy an equatorial site *cis* to the axial NMe donor. The positioning of the titanium–nitrogen multiple bond in such complexes depends on both steric and electronic considerations. The electronic preference is for the multiple bond to be oriented axially (termed the *trans* arrangement), as when it is oriented in the equatorial site (termed the *cis* arrangement), the π-donor components of the bond must compete with the N_{amide} lone pairs for the π-acceptor orbitals on the metal centre,[62] and this axial

positioning was found to be the case for two analogues of **6**: the hydrazide Ti($N_2^{iPr}N^{Me}$)($NNPh_2$)(py) (**2.1**) and the imide Ti($N_2^{iPr}N^{Me}$)(NXyl)(py) (**2.3**).[63,80] However, the equatorial orientation is often preferred because steric clash between the bulky N_{amide}-substituents and the imido (or analogous) ligand is reduced;[43] for example, as in Ti($N_2^{SiMe_3}N^{Me}$)($NNPh_2$)(py) (**1.63**).[34] It is thus unsurprising, given the very large steric profile of the borylimido moiety, that in compounds **4**, **5** and **6**, the steric demands dominate, placing the borylimido ligand *cis* to the NMe donor. In all three structures, the boryl moiety is oriented such that the boryl ring lies nearly coplanar with the N(4)–Ti(1)–N(7) axis, this presumably being to avoid steric clash between the bulky Ar' groups and the N_{amide}-substituents. The angles between the two planes are *ca* 24.8 (**4**), 4.6 (**5**) and 12.5° (**6**) respectively.

The short Ti–N_{im} distances in the range 1.730(2) – 1.760(2) Å and nearly linear Ti–N_{im}–B angles in the range 160.05(10) – 170.38(18)° establish sp hybridisation at N_{im} and formal Ti≡N triple bonds in all three cases. All of the N_{amide} atoms are sp^2 hybridised and have approximately trigonal planar geometry as indicated by the sum of the angles subtended at the N_{amide} atoms being *ca*. 360° in each case, this being typical for early transition metal complexes.[81–83] The Ti–N_{py} bond lengths in the range 2.2040(11) – 2.219(3) Å are typical of neutral σ-only interactions between the titanium centre and the pyridine donor.[66]

Further discussion of the bond metrics of these three solid state structures will take two directions. Firstly, comparisons will be drawn between each compound in turn with its respective titanium–nitrogen multiple bonded structural analogues (i.e. imides, hydrazides and alkoxyimides), and secondly, the three solid state structures will be compared with each other, paying particular attention to the structural changes of the borylimido unit as the N_{amide}-substituent is varied.

For the complex in which the N_{amide}-substituents are $SiMe_3$ groups (**4**), there exist two crystallographically characterised analogues: the hydrazide Ti($N_2^{SiMe_3}N^{Me}$)($NNPh_2$)(py) (**1.63**) and the alkoxyimide Ti($N_2^{SiMe_3}N^{Me}$)(NO^tBu)(py) (**1.106**). The hydrazide **1.63** exists solely as the *cis*-isomer (like **4**), and has a shorter Ti–N_{im} distance of 1.733(5) Å (*vs* 1.7537(12) Å in **4**).[34] This is in contrast to the hydrazido analogue of Ti{$NB(NAr'CH)_2$}$Cl_2(py)_3$ (**3**) described above, which had a longer Ti–N_{im} bond length than its borylimido counterpart. Considering the bonding situation elucidated by DFT calculations in **1.63**,[34] as well as related diamide-donor-supported borylimides (*vide infra*),

the best Ti–N_{im} π-bonding match is found when the boryl ring is oriented along the equatorial plane containing the anionic N_{amide} atoms. This is because the nitrogen $2p_\pi$ AO perpendicular to the plane of the boryl ring is destabilised by an antibonding interaction with a filled π orbital of the ring, thus making it high in energy and the best match with the $1b_2$ acceptor on the metal (to form the π_v MO). Thus, the steric requirement, in the case of **4**, for the boryl moiety to be rotated 90° to the electronically preferred orientation results in the significant lengthening of the Ti–N_{im} bond of the borylimide, making this longer than in the hydrazide **1.63** which was shown to have its NPh_2 substituent oriented in the electronically preferred manner.[34] The alkoxyimide **1.106** exists as both the *cis* and *trans* forms, although only the *trans* isomer was structurally characterised.[28] Thus, as the electronically preferred form, the Ti–N_{im} distance of 1.721(2) Å is, as expected, much shorter than in the borylimide counterpart **4**.

The complex in which the N_{amide}-substituents are C_6F_5 (Ar^F) groups (**5**) also has two crystallographically characterised analogues: the hydrazide Ti($N_2^{ArF}N^{Me}$)($NNPh_2$)(py) (**2.4**) and the alkoxyimide Ti($N_2^{ArF}N^{Me}$)(NO^tBu)(py) (**2.5**).[84] The molecular solid state structures of both of these compounds show that the multiply bonded nitrogen ligand occupies the axial position *trans* to the NMe donor, this being allowed by the planar nature of the Ar^F ring. The Ti–N_{im} bond length of 1.731(3) Å in the hydrazide **2.4** is comparable to that in the borylimide **5** (1.730(2) Å), whilst as above for **1.106**, the alkoxyimide **2.5** has a much shorter bond length of 1.7088(16) and 1.7128(16) Å (for two crystallographically independent molecules). Similarly, the borylimido complex with ^{i}Pr groups as N_{amide}-substituents (**6**) also has two crystallographically characterised analogues, the hydrazide Ti($N_2^{iPr}N^{Me}$)($NNPh_2$)(py) (**2.1**) and the imide Ti($N_2^{iPr}N^{Me}$)(NXyl)(py) (**2.3**),[63,80] which both have the *trans*-oriented structure, with the multiply bonded ligand in the axial position. Again, the hydrazide has a shorter Ti–N_{im} bond length than the borylimido counterpart (1.7444(14) *vs* 1.760(2) Å),[63] whilst the arylimido compound has a comparable bond length to the borylimide of 1.7581(19) Å.[80]

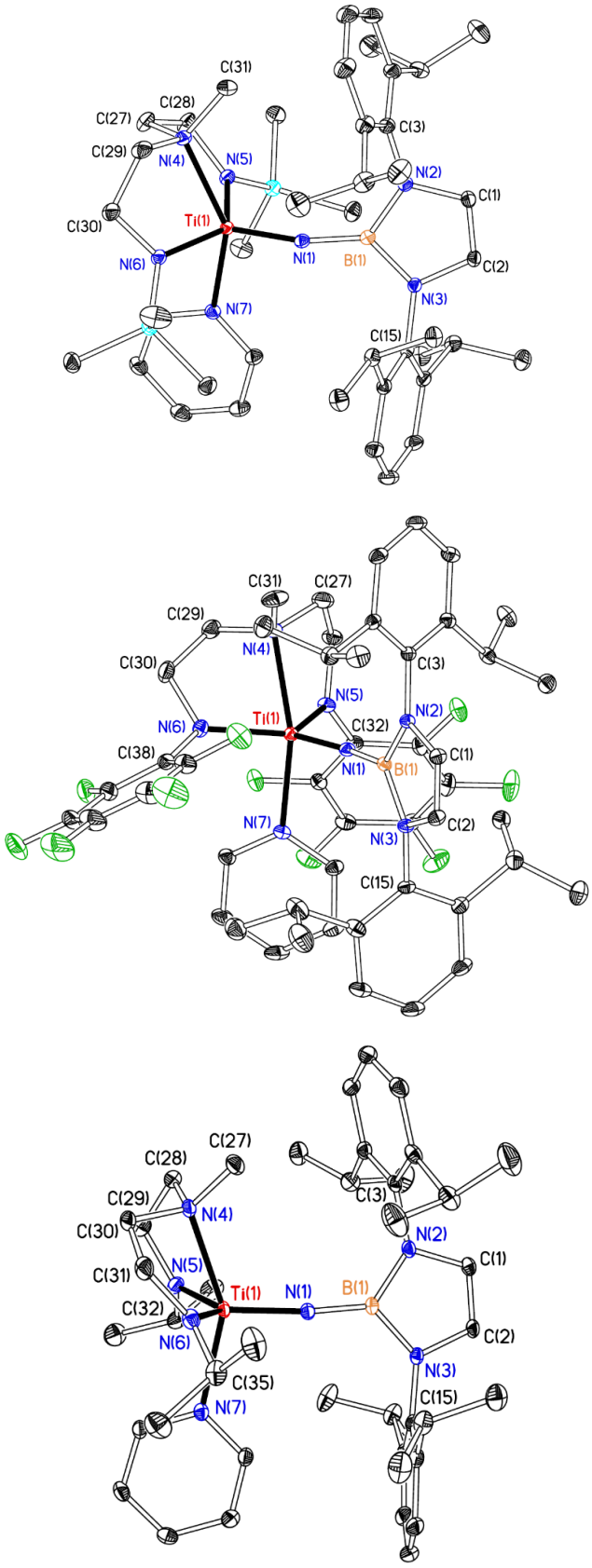

Figure 2.8. Displacement ellipsoid plots (20% probability) of Ti($N_2^RN^{Me}$){NB(NAr'CH)$_2$}(py) (R = $SiMe_3$ (**4**, top), Ar^F (**5**, middle), ^iPr (**6**, bottom)). H atoms are omitted for clarity.

Table 2.3. Selected bond lengths (Å) and angles (°) for Ti($N_2^RN^{Me}$){NB(NAr'CH)$_2$}(py) (R = $SiMe_3$ (**4**), Ar^F (**5**), ^{i}Pr (**6**)).

Parameter	**4**	**5**	**6**
Ti(1)–N(1)	1.7537(12)	1.730(2)	1.760(2)
Ti(1)–N(4)	2.2577(11)	2.2279(19)	2.245(3)
Ti(1)–N(5)	2.0193(12)	2.047(2)	1.998(3)
Ti(1)–N(6)	2.0278(12)	2.015(2)	1.974(3)
Ti(1)–N(7)	2.2040(11)	2.2042(19)	2.219(3)
N(1)–B(1)	1.4190(19)	1.418(3)	1.417(4)
B(1)–N(2)	1.4628(19)	1.453(3)	1.462(4)
B(1)–N(3)	1.4690(18)	1.457(3)	1.463(4)
N(1)–Ti(1)–N(4)	114.49(5)	107.11(8)	110.94(11)
N(1)–Ti(1)–N(5)	112.52(5)	115.23(9)	116.07(13)
N(1)–Ti(1)–N(6)	113.22(5)	116.28(9)	114.45(12)
N(1)–Ti(1)–N(7)	101.33(5)	96.86(8)	99.95(11)
N(5)–Ti(1)–N(6)	133.70(5)	126.98(9)	128.60(12)
N(5)–Ti(1)–N(7)	88.43(5)	91.24(7)	90.58(11)
N(6)–Ti(1)–N(7)	89.47(5)	94.40(8)	89.65(11)
Ti(1)–N(1)–B(1)	160.05(10)	170.38(18)	169.9(2)
N(1)–B(1)–N(2)	128.27(12)	128.1(2)	128.9(3)
N(1)–B(1)–N(3)	129.08(12)	128.6(2)	128.7(3)

It can be seen that there are significant variations in the bond metrics of the borylimido units in the three complexes **4**, **5** and **6**, particularly the differences in the Ti–N_{im} bond lengths which range from 1.730(2) Å in **5** to 1.760(2) Å in **6**. The short Ti–N_{im} length in **5** arises from the Ar^F group being the most σ-electron withdrawing substituent, which allows greater σ donation from the borylimido ligand and causes the contraction of the bond. The long Ti–N_{im} bond length in **6** arises from the N_{amide} atoms of this complex being the most π-basic, thus disrupting the π-components of the metal–nitrogen multiple bond to the

highest degree and causing the bond to lengthen. These differences in Ti–N_{im} bond lengths, and by extension the bond strengths will later be related to differences in the reactivity of the three complexes with terminal alkynes (Chapter Four). Although the Ti–N_{im} bond length varies with the N_{amide}-substituent, the N_{im}–B bond lengths are invariant within error, the values being 1.4190(19), 1.418(3) and 1.417(4) Å in **4**, **5** and **6**, respectively. The three Ti–N_{im}–B bond angles in the borylimido compounds are all close to linearity, and it is proposed that the observed variation between the minimum of 160.05(10) (**4**) and maximum of 170.38(18)° (**5**) primarily reflects steric requirements for the borylimido Ar' groups to orient around the N_{amide}-substituents. Accompanying the variation in the Ti–N_{im} bond lengths between **4**, **5** and **6**, are corresponding variations in the Ti–N_{amide} bond distances. Borylimide **5**, which has the shortest Ti–N_{im} bond distance as described above, has the longest Ti–N_{amide} distances, at 2.047(2) and 2.015(2) Å, whilst complex **6**, which, of the three, had the longest Ti–N_{im} bond distances correspondingly has the shortest Ti–N_{amide} bond distances at 1.998(3) and 1.973(3) Å. This effect arises from the "π-loaded" nature of the complexes, as previously explored through DFT calculations on diamide-amine supported titanium hydrazides;[34] the π components of the metal–nitrogen multiple bond must compete with the amide SALCs for the same π-acceptor orbital at the metal centre.

2.7 Installation of related N_2N supporting ligands

To further extend this chemistry, and study the effect that supporting ligand sets have on the structure, bonding and reactivity of titanium borylimido compounds, two similar dianionic, tridentate ligands were incorporated. Salt metathesis reactions between $Ti\{NB(NAr'CH)_2\}Cl_2(py)_3$ (**3**) and both $Li_2N_2N^{py}$ and $Li_2N_2{}^{pyr}N^{Me}$ ($N_2{}^{pyr}N^{Me}$ = *N*,*N*-di(pyrrolyl-α-methyl)-*N*-methylamine) gave the respective borylimido complexes.

Mixing of **3** and $Li_2N_2N^{py}$ in toluene at –78 °C, followed by 3 h stirring at RT and subsequent extraction into pentane produced pure $Ti(N_2N^{py})\{NB(NAr'CH)_2\}(py)$ (**7**, Equation 2.5). The ^1H (Figure 2.9) and ^{13}C NMR spectra of **7** indicate that the complex has a C_s symmetric structure in the solution phase. In addition to those resonances expected for the borylimido and pyridine ligands, two singlets corresponding to the methyl (3 H) and trimethylsilyl (18 H) groups of the diamide-pyridine ligand are observed, as well as two mutually coupled doublets corresponding to the diastereotopic $NC\underline{H}_2C(Me)$ protons and four inequivalent multiplets corresponding to the pyridyl unit.

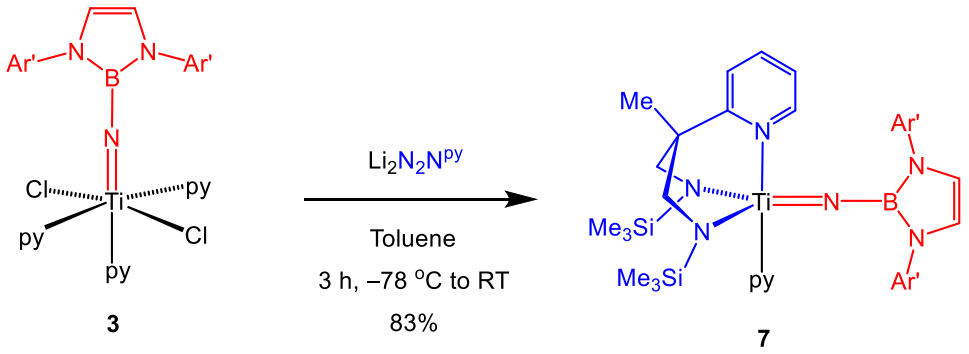

Equation 2.5

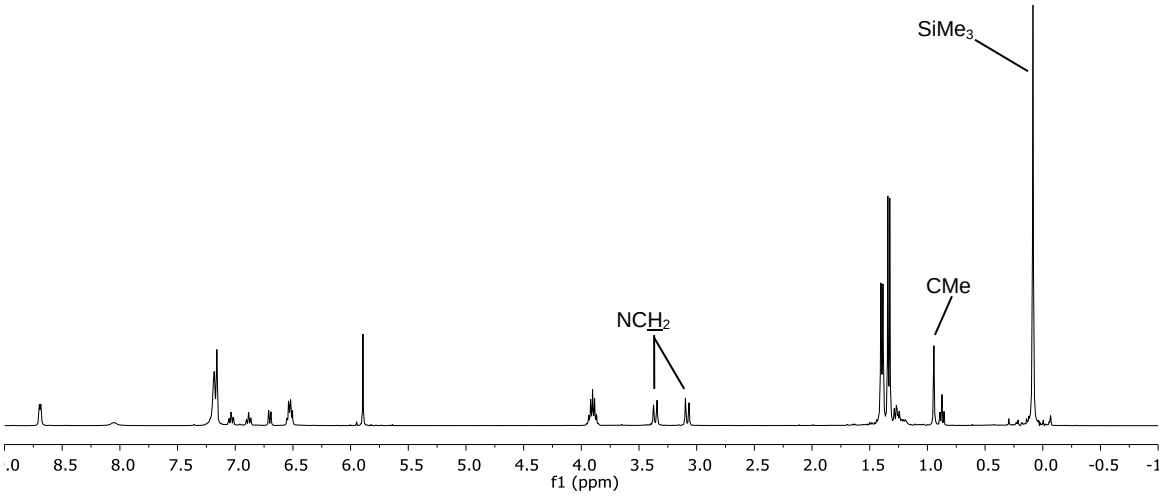

Figure 2.9. ^{1}H NMR spectrum (400.1 MHz) of Ti(N_2N^{py}){NB(NAr'CH)$_2$}(py) (**7**) in C_6D_6 at 298 K.

Diffraction-quality crystals of **7** were grown from a saturated pentane solution at 5 °C, and the molecular solid state structure is shown in Figure 2.10 along with selected bond lengths and angles in Table 2.4. Molecules of **7** have a distorted trigonal bipyramidal coordination geometry in the solid state, with the arrangement of ligands about the metal being entirely analogous to compounds **4** – **6**; i.e. the equatorial plane contains the two N_{amide} atoms and the borylimido ligand, which sits *cis* to the axial pyridyl donor of the tridentate ligand. The Ti–N_{im} bond lengths of 1.7727(6) and 1.7604(7) Å (for two crystallographically independent molecules) are comparable to that of the $N_2{}^{iPr}N^{Me}$-coordinated **6**; i.e. it appears that this N_2N^{py} ligand also results in greater than usual lengthening of the Ti–N_{im} bond length. These are also longer than the Ti–N_{im} lengths in two crystallographically characterised analogues of **7**, the imide Ti(N_2N^{py})(N^{t}Bu)(py) (**1.9**) and the hydrazide Ti(N_2N^{py})($NNPh_2$)(py) (**1.61**), at 1.724(2) and 1.759(2) Å, respectively.[34,59]

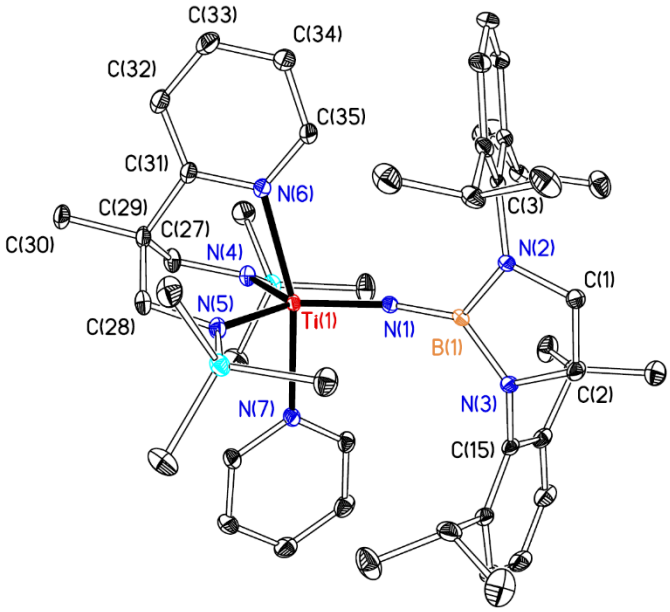

Figure 2.10. Displacement ellipsoid plot (20% probability) of $Ti(N_2N^{py})\{NB(NAr'CH)_2\}(py)$ (**7**). H atoms are omitted for clarity.

Table 2.4. Selected bond distances (Å) and angles (°) for $Ti(N_2N^{py})\{NB(NAr'CH)_2\}(py)$ (**7**). Values in brackets are for the second crystallographically independent molecule.

Ti(1)–N(1)	1.7727(6) [1.7604(7)]	N(1)–Ti(1)–N(4)	125.35(3) [122.36(3)]
Ti(1)–N(4)	1.9860(7) [1.9757(7)]	N(1)–Ti(1)–N(5)	123.39(3) [123.95(3)]
Ti(1)–N(5)	1.9648(7) [1.9734(7)]	N(1)–Ti(1)–N(6)	102.94(3) [101.50(3)]
Ti(1)–N(6)	2.2105(7) [2.2002(7)]	N(1)–Ti(1)–N(7)	92.93(3) [96.89(3)]
Ti(1)–N(7)	2.2450(7) [2.2576(7)]	N(5)–Ti(1)–N(6)	82.07(3) [81.44(3)]
N(1)–B(1)	1.4149(11) [1.4185(11)]	N(5)–Ti(1)–N(7)	90.35(3) [90.66(3)]
B(1)–N(2)	1.4744(10) [1.4686(11)]	N(6)–Ti(1)–N(7)	164.07(2) [161.39(2)]
B(1)–N(3)	1.4718(11) [1.4701(11)]	Ti(1)–N(1)–B(1)	159.95(6) [167.32(6)
		N(1)–B(1)–N(2)	126.32(7) [128.61(7)]
		N(1)–B(1)–N(3)	131.78(7) [129.19(7)]

A related dipyrrolide-amine ligand was next incorporated in an analogous manner. The $N_2^{pyr}N^{Me}$ ligand has previously been utilised in a number of compounds prepared by Odom and co-workers,[28,85–90] often focussing on hydroamination catalysis in particular. In a similar manner to above, mixing of **3** and $Li_2N_2^{pyr}N^{Me}$ in toluene at –78 °C, followed by stirring at RT for 45 minutes and subsequent extraction and crystallisation from Et_2O produced $Ti(N_2^{pyr}N^{Me})\{NB(NAr'CH)_2\}(py)_2$ (**8**, Equation 2.6). Again, the ^1H (aromatic region shown in Figure 2.11) and ^{13}C NMR spectra of **8** indicate that the complex has a C_s symmetric structure in the solution phase. Only one set of resonances corresponding to the two pyrrolyl groups of the tridentate ligand are observed, meaning that these are chemically equivalent by symmetry, whilst the spectrum also displays resonances belonging to two chemically inequivalent pyridine donors (as well as the borylimido ligand).

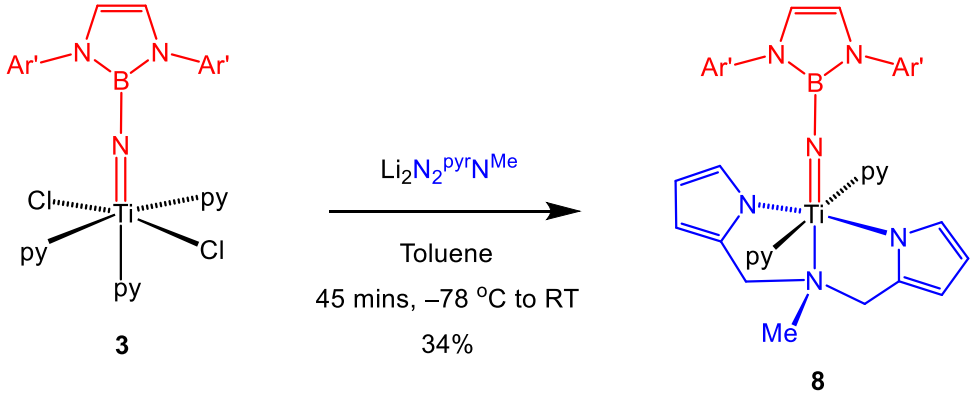

Equation 2.6

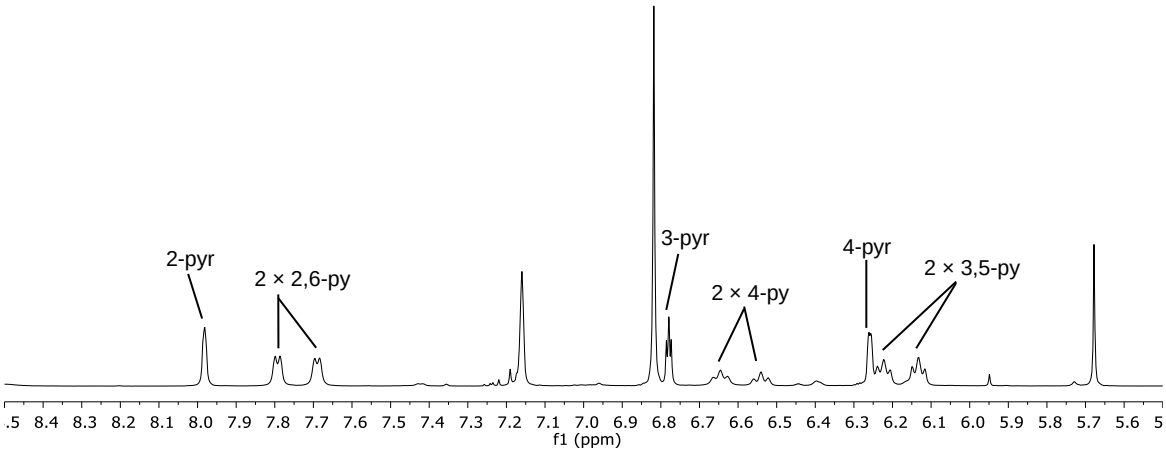

Figure 2.11. Aromatic region of the ^1H NMR spectrum (400.1 MHz) of $Ti(N_2^{pyr}N^{Me})\{NB(NAr'CH)_2\}(py)_2$ (**8**) in C_6D_6 at 298 K.

Diffraction-quality crystals of **8** were grown from a concentrated Et_2O solution at 5 °C, and the molecular solid state structure is shown in Figure 2.12 along with selected bond lengths and angles in Table 2.5. Unlike complexes **4** – **7**, the tridentate ligand in **8** is coordinated in a meridional fashion as part of an overall distorted octahedral geometry, and the borylimido ligand now sits *trans* to the central NMe donor. The Ti–N_{im} bond length of 1.732(4) Å is relatively short when compared with the previous four compounds, this being comparable to the bond length in **5** (of 1.730(2) Å). Furthermore, the structure confirms that two (rather than one) pyridine ligands are retained from **3**, allowed presumably by the reduced steric profile of the tridentate ligand. It also makes clear the reason for the inequivalence of the two pyridine ligands in the solution phase NMR spectra: the methyl group at the NMe position of the tridentate ligand points towards only one of these pyridine groups.

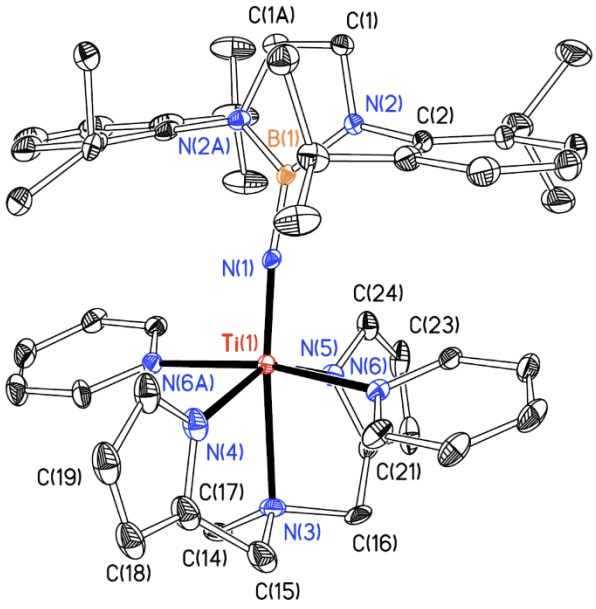

Figure 2.12. Displacement ellipsoid plot (20% probability) of $Ti(N_2^{pyr}N^{Me})\{NB(NAr'CH)_2\}(py)_2$ (**8**). H atoms are omitted for clarity. Atoms carrying the suffix 'A' are related to their counterparts by the symmetry operator [–*x*, –*y*, 1+*z*].

Table 2.5. Selected bond distances (Å) and angles (°) for Ti($N_2^{pyr}N^{Me}$){NB(NAr'CH)$_2$}(py)$_2$ (**8**).

Ti(1)–N(1)	1.732(4)	N(1)–Ti(1)–N(3)	170.6(2)
Ti(1)–N(3)	2.440(5)	N(1)–Ti(1)–N(4)	114.2(3)
Ti(1)–N(4)	2.064(6)	N(1)–Ti(1)–N(5)	98.0(2)
Ti(1)–N(5)	2.047(5)	N(1)–Ti(1)–N(6)	94.67(9)
Ti(1)–N(6)	2.258(3)	N(3)–Ti(1)–N(6)	85.99(9)
N(1)–B(1)	1.421(8)	N(4)–Ti(1)–N(5)	147.8(3)
B(1)–N(2)	1.449(5)	N(4)–Ti(1)–N(6)	84.76(9)
		N(5)–Ti(1)–N(6)	92.96(9)
		Ti(1)–N(1)–B(1)	167.9(4)
		N(1)–B(1)–N(2)	128.1(2)

2.8 Computational studies of bonding in a diamide-pyridine-supported borylimide

A number of computational studies into the bonding of Group 4 imido, hydrazido and alkoxyimido complexes have previously been carried out, and the electronic structure of the metal–nitrogen multiple bond is well understood.[16–18,20–22,28,29,34,38,86,91–93] Recently, the bonding in the borylimide Cp*Ti{MeC(N^iPr)$_2$}(NBC_8H_{14}) (**1.115**) was analysed by molecular orbital (MO) and natural bond orbital (NBO) studies,[31] although no comparisons have yet been made between borylimides and analogous imides. Additionally, related calculations on a hypothetical borylnitrene complex of iron have been reported by Bettinger.[94] The isoelectronic relationships of the model borylnitrene ligand, $–NBH_2$, with the vinylidene $–CCH_2$ and aminoborylene $–BNH_2$ were explored, with the iron complex of the former predicted to have a small HOMO–LUMO gap (compared with the other two model ligands) and hence be highly reactive.

To gain further understanding into the bonding of titanium borylimido complexes, DFT calculations were carried out on the model systems Ti($N_2^{SiH_3}N^{py}$)(NR)(py) (R = Me (**1Q_Me**), Xyl (**1Q_Xyl**), B(NMeCH)$_2$ (**1Q_B(NMeCH)$_2$**) by Prof. Philip Mountford, using the B3PW91 functional and the Def2TZVP basis set. In order to study the underlying

electronic interactions (without contribution from steric effects), the real N_2N^{py} supporting ligand was modelled as $N_2^{SiH_3}N^{py}$, in which the N_{amide}-substituents are SiH_3 groups rather than $SiMe_3$ groups. Additionally, in **1Q_B(NMeCH)$_2$**, a model of the real borylimide **7**, the boryl functionality was modelled as the smaller $NB(NMeCH)_2$ group. The geometries, key orbital representations and associated energies are shown in Figure 2.13.

Considering first the bonding in the model methylimide **1Q_Me**, Figure 2.13 (top) shows the two π components that make up the formal Ti–N triple bond. Despite the symmetry of the methyl group, these two MOs are not degenerate because they involve interactions with two metal d orbitals of different symmetry and energy. Figure 2.14 depicts the σ-only frontier MOs (d orbitals only, arbitrary energies) for a hypothetical trigonal bipyramidal complex $M(NR)(NR'_2)_2(L_{ax})_2$ (L_{ax} is a generic σ-only donor).[95] The $2a_1$ MO is strongly σ* antibonding, and cannot engage in metal–ligand π interactions. The $1a_1$ and $1b_1$ levels are slightly σ* metal–ligand antibonding and higher in energy than the strictly σ non-bonding $1b_2$ and $1a_2$ levels. Of these four orbitals, the $1b_1$ and $1b_2$ MOs are the best suited for π-bonding with an imido-type ligand in the equatorial position. Thus, it is the higher energy $1b_1$ MO which forms the HOMO in **1Q_Me** (assigned as the π_h component) with an imido nitrogen lone pair, while the $1b_2$ forms the HOMO–1 (π_v).

Turning next to **1Q_Xyl**, the HOMO (in this case π_v) is significantly destabilised compared to that in **1Q_Me** (–4.84 *vs* –5.29 eV). This arises from an antibonding interaction between the Ti–N π bond and a filled π MO of the aryl ring, and also drives the electronic preference for the ring to lie in the equatorial plane as it is the N lone pair perpendicular to the ring which finds the best energy match with the acceptor orbital on the metal. The HOMO–1 (π_h) is formed with the N lone pair in the plane of the aryl ring, and is slightly lower in energy than that in **1Q_Me** (–5.54 *vs* –5.39 eV) based on the electron-withdrawing nature of an aryl group relative to methyl. Additionally, the HOMO–6 shows backbonding from an imido π MO into a π* antibonding orbital of the aryl ring. Together, the HOMO and HOMO–6 show two effects which activate the π components of the Ti–N multiple bond in arylimides compared with alkylimides.

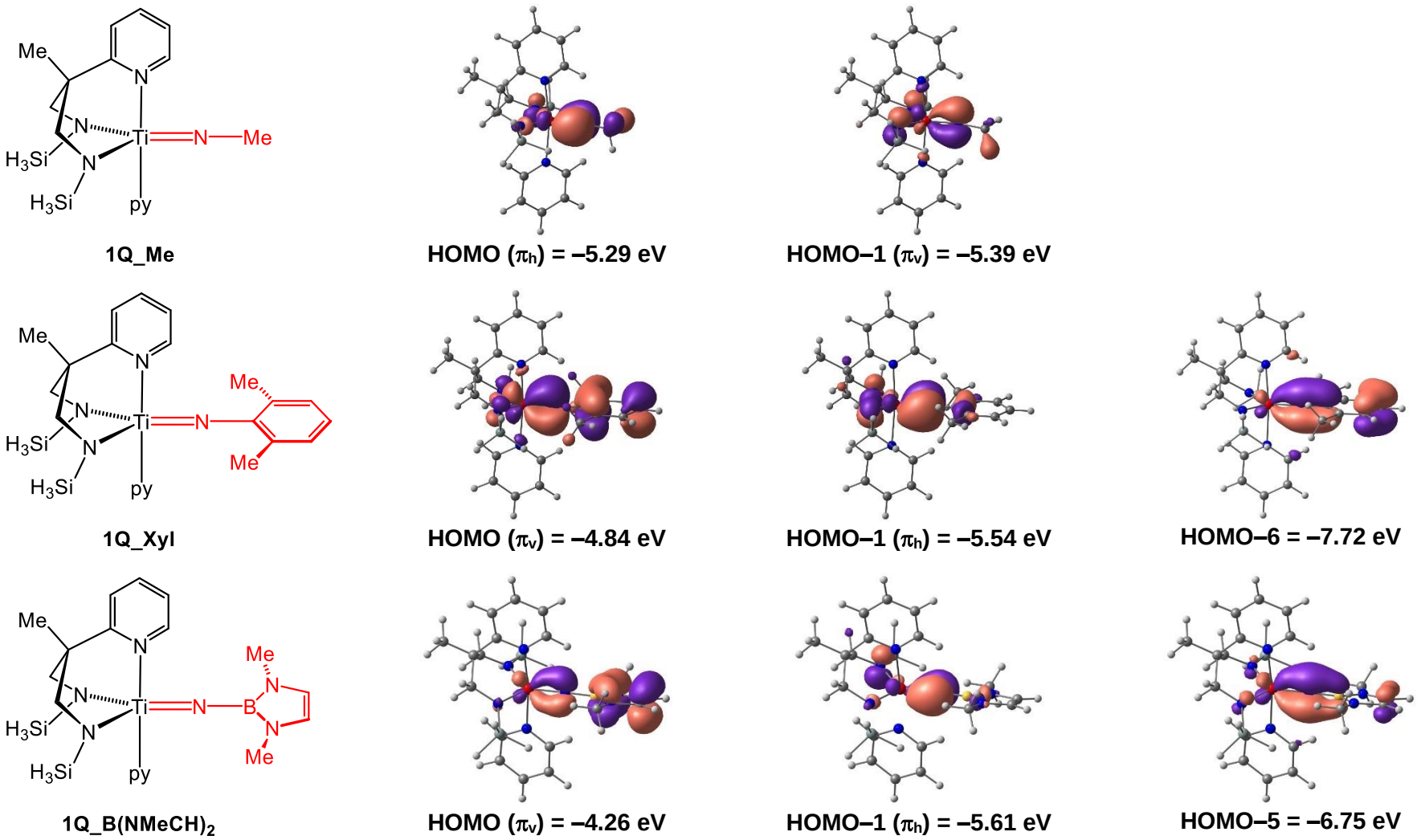

Figure 2.13. DFT model compounds Ti($N_2^{SiH_3}N^{py}$)(NR)(py) (R = Me (**1Q_Me**, top), Xyl (**1Q_Xyl**, middle), $B(NMeCH)_2$ (**1Q_B(NMeCH)$_2$**, bottom) and associated isosurfaces and energies of the π components of the Ti–N linkages.

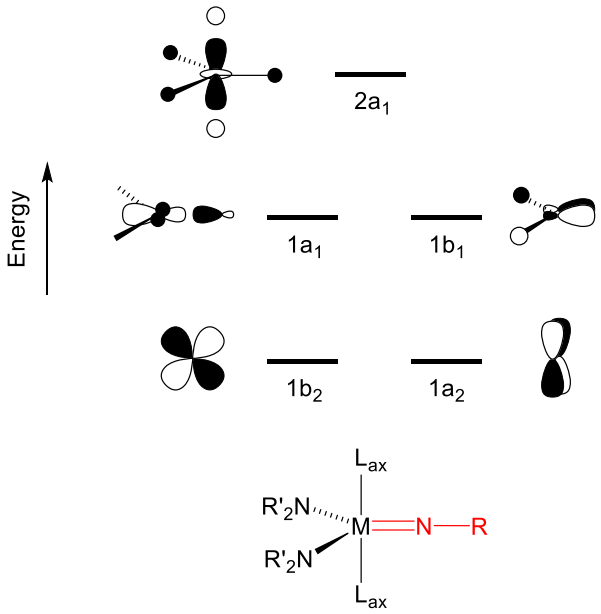

Figure 2.14. The σ-only frontier MOs (d orbitals only, arbitrary energies) for a hypothetical bis(dialkylamide)-imido system.[95] Labels are for local C_{2v} symmetry and L_{ax} represents a nominal axial ligand.

Considering now the MOs of the model borylimide **1Q_B(NMeCH)2**, these are broadly comparable in form to those of **1Q_Xyl**. Again, the HOMO is the π_v orbital, with an antibonding interaction between the Ti–N π bond and a filled π orbital of the boryl ring. This is even higher in energy than the HOMO of **1Q_Xyl** (–4.26 *vs* –4.84 eV) which is attributed to the electropositive nature of boron. The boryl ring is oriented in the equatorial plane for the same reason as the aryl ring in the model arylimido complex. Furthermore, in this case the HOMO–5 represents a backbonding interaction from a metal–nitrogen π MO into a π* MO on the boryl ring. The models **1Q_Xyl** and **1Q_B(NMeCH)2**, therefore, demonstrate the structural and electronic similarities between this borylimido group and arylimido ligands, which arise from the presence of an aromatic π system in this boryl functionality. This has been alluded to previously in the crystallographic characterisations of some of the borylimido complexes reported here, in particular those of complexes **1** and **3**, for which the bond metrics of the borylimido linkage were found to be comparable to those of their previously reported arylimido counterparts.

Quantum Theory of Atoms in Molecules (QTAIM) analyses were also performed to give further understanding of the similarities and differences in electronic structure between the three model complexes **1Q_R**.[96] Selected QTAIM data are shown in Tables 2.6 and 2.7. The delocalisation index, δ(A–B), of a bond A–B is a measure of the number of electron

pairs delocalised or shared between the two atoms and can relate to formal bond order.[97] For example, δ(C–C) values calculated for ethane, ethylene and acetylene are 1.02, 1.93 and 2.88, respectively. The correlation between δ and formal bond order does not hold for bonds between heteroatoms, although trends may still be extracted from a family of compounds containing the same pair of bonded atoms. Thus, the variation in δ(Ti–N_{im}) as R is changed may be considered, and then related to the relative strength of the multiple bonds in these complexes. Of the three model complexes **1Q_R**, **1Q_Me** has the largest δ(Ti–N_{im}) value of 1.539 and **1Q_Xyl** has the smallest value of 1.349, with that of **1Q_B(NMeCH)$_2$** being intermediate. This corresponds to the Ti–N multiple bond of the methylimido complex having the greatest bond order and that of the xylylimido complex having the smallest, and is confirmed by comparison with the Ti–N_{im} bond distances of the optimised calculated structures. The distance is shortest for **1Q_Me** (1.701 Å) and longest for **1Q_Xyl** (1.738 Å).

In QTAIM, the ellipticity (ε) of a bond is a measure of the asymmetry of π bonding in that bond.[96] For example, the C–C bonds of ethane and acetylene have ε values of 0, representing their cylindrical nature, whilst that of ethylene (having one π component) has a value of 0.22. Of the three models **1Q_R**, the ε value at the BCP of the Ti–N_{im} bond is largest (0.061) for **1Q_Me**. As the NMe group itself is cylindrically symmetrical, this represents an asymmetry in the π components of the multiple bond which can only arise from the directionality of the metal acceptor orbitals (depicted in Figure 2.14). Upon moving to **1Q_Xyl** and **1Q_B(NMeCH)$_2$**, the ε values fall to 0.023 and 0.032 respectively. In these cases, the different energies of the N lone pairs in parallel with and perpendicular to the aryl or boryl ring mean that the ellipticity now represents the asymmetry of both the metal acceptor orbitals and the imido ligand N lone pairs. The destabilisation of the π component which is perpendicular to the aryl or boryl ring in **1Q_Xyl** and **1Q_B(NMeCH)$_2$** respectively (as described in MO terms above), appears to give an electron distribution with a greater degree of overall cylindrical symmetry than **1Q_Me**. This disruption of a π component of the multiple bond is reflected in the calculated Ti–N_{im} bond distances, which are shortest for **1Q_Me** (having the largest ε) and longest for **1Q_Xyl** (having the smallest ε).

Table 2.6. Selected QTAIM data (atomic units) in model complexes of the type Ti($N_2^{SiH_3}N^{py}$)(NR)(py) (R = Me (**1Q_Me**), Xyl (**1Q_Xyl**), B(NMeCH)$_2$ (**1Q_B(NMeCH)$_2$**), and Ti–NR bond distances (*d*, Å) in the optimised structures. Values for ρ (electron density), $\nabla^2\rho$ (electron density Laplacian), *H* (energy density) and ε (ellipticity) were obtained at the bond critical point. δ(A–B) is the delocalisation index for the stated pair of atoms.

	δ(Ti–N_{im})	ρ(Ti–N_{im})	$\nabla^2\rho$(Ti–N_{im})	ε(Ti–N_{im})	*H*(Ti–N_{im})	*d*(Ti–N_{im}) / Å	δ(Ti–N_{amide}) (avg.)	ρ(Ti–N_{amide}) (avg.)	ε(Ti–N_{amide}) (avg.)
1Q_Me	1.539	0.195	0.801	0.061	–0.097	1.701	0.607	0.109	0.147
1Q_Xyl	1.349	0.178	0.763	0.023	–0.078	1.738	0.638	0.112	0.187
1Q_B(NMeCH)$_2$	1.463	0.195	0.700	0.032	–0.096	1.724	0.630	0.112	0.168

Table 2.7. QTAIM charges (*Q*, units of *e*) of fragments of model complexes of the type Ti($N_2^{SiH_3}N^{py}$)(NR)(py) (R = Me (**1Q_Me**), Xyl (**1Q_Xyl**), B(NMeCH)$_2$ (**1Q_B(NMeCH)$_2$**).

	Q($N_2^{SiH_3}N^{py}$)	*Q*(Ti)	*Q*(py)	*Q*(NR)
1Q_Me	–1.202	2.038	0.048	–0.884
1Q_Xyl	–1.141	2.069	0.060	–0.987
1Q_B(NMeCH)$_2$	–1.166	2.069	0.054	–0.965

Next, trends in the delocalisation indices of the Ti–N_{im} bonds and Ti–N_{amide} bonds may be related. The δ(Ti–N_{im}) values have an anti-correlation with the δ(Ti–N_{amide}) values. The largest δ(Ti–N_{im}) value in **1Q_Me** corresponds to the smallest δ(Ti–N_{amide}) value (averaged over the two bonds) of 0.607. Conversely, the smallest δ(Ti–N_{im}) belonged to **1Q_Xyl**, which also has the largest average δ(Ti–N_{amide}) of 0.638. This relationship reflects the fact that the imido group and the N_{amide} atoms of the supporting ligand must compete for some of the same π-acceptor orbitals on the metal centre. Therefore, a reduction in the π-donor ability of the imido ligand results in a greater bond order for the Ti–N_{amide} bonds of the supporting ligand.

The same effect can also be viewed in relation to the charges, *Q*, on the imido and diamide-pyridine fragments of the three model complexes (Table 2.7). For an anionic ligand, a less negative *Q* value reflects greater covalent interaction with the metal centre as its negative charge is partially donated to the metal centre. Like the corresponding relationship between delocalisation indices described above, **1Q_Me** shows the strongest covalent interaction of the imido ligand (*Q*(NMe) = –0.884 *e*) and the weakest of the supporting ligand (*Q*($N_2^{SiH_3}N^{py}$) = –1.202 *e*), whilst **1Q_Xyl** has a weaker imido linkage (*Q*(NXyl) = –0.987 *e*) and stronger interaction of the supporting ligand (*Q*($N_2^{SiH_3}N^{py}$) = –1.141 *e*). Again, **1Q_B(NMeCH)$_2$** has intermediate values, though is most similar to the arylimido model.

2.9 Conclusions and Outlook

This Chapter has described the synthesis and characterisation of eight borylimido complexes of titanium. Firstly, a new route to the formation of borylimido compounds was described: the reaction of the borylamine $H_2NB(NAr'CH)_2$ (**2.2**) with $Ti(NMe_2)_2Cl_2$ to form $Ti\{NB(NAr'CH)_2\}Cl_2(NHMe_2)_2$ (**1**). Subsequent reactions exchanged the amine donor ligands of **1** to form $Ti\{NB(NAr'CH)_2\}Cl_2(Me_3[6]aneN_3)$ (**2**) and $Ti\{NB(NAr'CH)_2\}Cl_2(py)_3$ (**3**). Crystallographic characterisation of **1** and **3** demonstrated that the Ti–N_{im} linkage is best considered a triple bond (as in titanium imides, hydrazides and alkoxyimides), and its bond metrics are particularly comparable to those in analogous arylimido complexes. Also, structural analysis of the octahedral complex **3** showed that the borylimido ligand exerts a very strong *trans* influence, and is thus a very strong σ donor.

Next, the use of **3** as a salt metathesis synthon was demonstrated. Reactions with three dilithiated ligands produced the diamide-amine supported compounds $Ti(N_2^RN^{Me})\{NB(NAr'CH)_2\}(py)$ (R = $SiMe_3$ (**4**), Ar^F (**5**), ^{i}Pr (**6**)). Structural

characterisation probed the effect of the varying N_{amide}-substituent on the borylimido Ti=N linkage, this bond being shortest for **5** and longest for **6**.

Finally, two further complexes supported by N_3-tridentate ligands were synthesised and characterised. The diamide-pyridine-supported complex $Ti(N_2N^{py})\{NB(NAr'CH)_2\}(py)$ (**7**) was shown to have an entirely analogous structure to compounds **4** – **6**, in which the tridentate ligands coordinate in a facial manner as part of a trigonal bipyramidal geometry. In contrast, the dipyrrolide-amine-supported complex $Ti(N_2^{pyr}N^{Me})\{NB(NAr'CH)_2\}(py)_2$ (**8**) has an octahedral geometry in which the tridentate ligand is coordinated in a meridional fashion. Compounds **4** – **8** represent a family of titanium borylimido complexes which are all supported by N_3-tridentate ligands, though with varying steric and electronic considerations. The effect of these factors on the reactivity of the five compounds with terminal alkynes will be the focus of Chapter Four.

DFT calculations performed on the model complexes $Ti(N_2^{SiH_3}N^{py})(NR)(py)$ (R = Me (**1Q_Me**), Xyl (**1Q_Xyl**), $B(NMeCH)_2$ (**1Q_B(NMeCH)$_2$**) showed that the borylimido functional group is structurally and electronically similar to an arylimido ligand. In particular, this arises from the presence of the aromatic π system in this 1,3,2-diazaborolyl-type group. QTAIM analyses of the same model complexes then explored the relative bond orders of the three Ti–N multiple bonds, as well as the competition between the imido-type ligand and the N_{amide} atoms of the supporting ligand for the π-acceptor orbitals of the metal.

One focus of ongoing work in our research group is the preparation of borylamines with reduced steric profiles compared with **2.2**, and attempts to form the corresponding Group 4 borylimido complexes. For example, some success has been found with a borylamine having isopropyl groups as N-substituents (rather than Ar' groups): $H_2NB(N^iPr)_2C_6H_4$. Zirconium borylimido complexes derived from that borylamine have already been synthesised,[98] and work to form the analogues of complexes **1** and **3** is currently underway.[99]

2.10 References

1 M. J. Carney, P. J. Walsh, F. J. Hollander and R. G. Bergman, *J. Am. Chem. Soc.*, 1989, **111**, 8751–8753.

2 M. J. Carney, P. J. Walsh and R. G. Bergman, *J. Am. Chem. Soc.*, 1990, **112**, 6426–6428.

3 M. J. Carney, P. J. Walsh, F. J. Hollander and R. G. Bergman, *Organometallics*,

1992, **11**, 761–777.

4 M. R. Smith, P. T. Matsunaga and R. A. Andersen, *J. Am. Chem. Soc.*, 1993, **115**, 7049–7050.

5 J. L. Polse, R. A. Andersen and R. G. Bergman, *J. Am. Chem. Soc.*, 1995, **117**, 5393–5394.

6 W. A. Howard, T. M. Trnka, M. Waters and G. Parkin, *J. Organomet. Chem.*, 1997, **528**, 95–121.

7 A. J. Blake, J. M. McInnes, P. Mountford, G. I. Nikonov, D. Swallow and D. J. Watkin, *J. Chem. Soc. Dalton Trans.*, 1999, 379–392.

8 I. Pappas and P. J. Chirik, *Angew. Chem. Int. Ed.*, 2014, **53**, 6241–6244.

9 D. E. Wigley, in *Progress in Inorganic Chemistry*, ed. K. D. Karlin, Wiley-Interscience, New York, 1994, vol. 42, pp. 239–482.

10 A. P. Duncan and R. G. Bergman, *Chem. Rec.*, 2002, **2**, 431–445.

11 P. Mountford, *Chem. Commun.*, 1997, 2127–2134.

12 L. H. Gade and P. Mountford, *Coord. Chem. Rev.*, 2001, **216**–**217**, 65–97.

13 N. Hazari and P. Mountford, *Acc. Chem. Res.*, 2005, **38**, 839–849.

14 A. R. Fout, U. J. Kilgore and D. J. Mindiola, *Chem. Eur. J.*, 2007, **13**, 9428–9440.

15 C. M. Kozak and P. Mountford, *Angew. Chem. Int. Ed.*, 2004, **43**, 1186 –1189.

16 T. R. Cundari, *J. Am. Chem. Soc.*, 1992, **114**, 7879–7888.

17 Z. Lin and M. B. Hall, *Coord. Chem. Rev.*, 1993, **123**, 149–167.

18 P. Mountford and D. Swallow, *J. Chem. Soc., Chem. Commun.*, 1995, 2357–2359.

19 N. Kaltsoyannis and P. Mountford, *J. Chem. Soc., Dalton Trans.*, 1999, 781–789.

20 T. R. Cundari, *Chem. Rev.*, 2000, **100**, 807–818.

21 A. D. Schwarz, A. J. Nielson, N. Kaltsoyannis and P. Mountford, *Chem. Sci.*, 2012, **3**, 819–824.

22 S. C. Dunn, N. Hazari, N. M. Jones, A. G. Moody, A. J. Blake, A. R. Cowley, J. C. Green and P. Mountford, *Chem. Eur. J.*, 2005, **11**, 2111–2124.

23 N. Wiberg, H.-W. Häring, G. Huttner and P. Friedrich, *Chem. Ber.*, 1978, **111**, 2708–2715.

24 J. L. Thorman and L. K. Woo, *Inorg. Chem.*, 2000, **39**, 1301–1304.

25 P. J. Walsh, M. J. Carney and R. G. Bergman, *J. Am. Chem. Soc.*, 1991, **113**, 6343–6345.

26 M. Hidai and Y. Mizobe, *Chem. Rev.*, 1995, **95**, 1115–1133.

27 A. D. Schwarz, A. Nova, E. Clot and P. Mountford, *Chem. Commun.*, 2011, **47**,

4926–4928.

28 A. D. Schwarz, A. Nova, E. Clot and P. Mountford, *Inorg. Chem.*, 2011, **50**, 12155–12171.

29 L. R. Groom, A. D. Schwarz, A. Nova, E. Clot and P. Mountford, *Organometallics*, 2013, **32**, 7520–7539.

30 R. Thompson, C.-H. Chen, M. Pink, G. Wu and D. J. Mindiola, *J. Am. Chem. Soc.*, 2014, **136**, 8197–8200.

31 L. C. Stevenson, S. Mellino, E. Clot and P. Mountford, *J. Am. Chem. Soc.*, 2015, **137**, 10140–10143.

32 A. A. Danopoulos, C. Redshaw, A. Vaniche, G. Wilkinson, B. Hussain-Bates and M. B. Hursthouse, *Polyhedron*, 1993, **12**, 1061–1071.

33 K. Weber, K. Korn, A. Schorm, J. Kipke, M. Lemke, A. Khvorost, K. Harms and J. Sundermeyer, *Z. Anorg. Allg. Chem.*, 2003, **629**, 744–754.

34 J. D. Selby, C. D. Manley, A. D. Schwarz, E. Clot and P. Mountford, *Organometallics*, 2008, **27**, 6479–6494.

35 A. J. Blake, P. E. Collier, S. C. Dunn, W. Li, P. Mountford and O. V Shishkin, *J. Chem. Soc. Dalton Trans.*, 1997, 1549–1558.

36 N. Adams, H. R. Bigmore, T. L. Blundell, C. L. Boyd, S. R. Dubberley, A. J. Sealey, A. R. Cowley, M. E. G. Skinner and P. Mountford, *Inorg. Chem.*, 2005, **44**, 2882–2894.

37 N. Adams, A. R. Cowley, S. R. Dubberley, A. J. Sealey, M. E. G. Skinner and P. Mountford, *Chem. Commun.*, 2001, 2738–2739.

38 T. B. Parsons, N. Hazari, A. R. Cowley, J. C. Green and P. Mountford, *Inorg. Chem.*, 2005, **44**, 8442–8458.

39 N. A. H. Male, M. E. G. Skinner, S. Y. Bylikin, P. J. Wilson, P. Mountford and M. Schroder, *Inorg. Chem.*, 2000, **39**, 5483–5491.

40 C. Lorber, R. Choukroun and L. Vendier, *Eur. J. Inorg. Chem.*, 2006, 4503–4518.

41 J. D. Selby, C. D. Manley, M. Feliz, A. D. Schwarz, E. Clot and P. Mountford, *Chem. Commun.*, 2007, **733**, 4937–4939.

42 J. D. Selby, C. Schulten, A. D. Schwarz, A. Stasch, E. Clot, C. Jones and P. Mountford, *Chem. Commun.*, 2008, 5101–5103.

43 A. D. Schofield, A. Nova, J. D. Selby, C. D. Manley, A. D. Schwarz, E. Clot and P. Mountford, *J. Am. Chem. Soc.*, 2010, **132**, 10484–10497.

44 P. J. Tiong, A. D. Schofield, J. D. Selby, A. Nova, E. Clot and P. Mountford, *Chem.*

Commun., 2010, **46**, 85–87.

45 A. D. Schofield, A. Nova, J. D. Selby, A. D. Schwarz, E. Clot and P. Mountford, *Chem. Eur. J.*, 2011, **17**, 265–285.

46 H. Herrmann, J. L. Fillol, H. Wadepohl and L. H. Gade, *Angew. Chem. Int. Ed.*, 2007, **46**, 8426–8430.

47 H. Herrmann, J. L. Fillol, H. Wadepohl and L. H. Gade, *Organometallics*, 2008, **27**, 173–174.

48 H. Herrmann, T. Gehrmann, H. Wadepohl and L. H. Gade, *Dalton Trans.*, 2008, 6231–6241.

49 T. Gehrmann, J. L. Fillol, H. Wadepohl and L. H. Gade, *Angew. Chem. Int. Ed.*, 2009, **48**, 2152–2156.

50 T. Gehrmann, J. L. Fillol, H. Wadepohl and L. H. Gade, *Organometallics*, 2012, **31**, 4504–4515.

51 T. Gehrmann, M. Kruck, H. Wadepohl and L. H. Gade, *Chem. Commun.*, 2012, **48**, 2397–2399.

52 T. Gehrmann, G. T. Plundrich, H. Wadepohl and L. H. Gade, *Organometallics*, 2012, **31**, 3346−3354.

53 A. Bashall, P. E. Collier, L. H. Gade, M. McPartlin, P. Mountford and D. J. M. Trösch, *Chem. Commun.*, 1998, 2555–2556.

54 P. E. Collier, S. M. Pugh, H. S. C. Clark, J. B. Love, A. J. Blake, F. G. N. Cloke and P. Mountford, *Inorg. Chem.*, 2000, **39**, 2001–2005.

55 A. J. Blake, P. E. Collier, L. H. Gade, M. McPartlin, P. Mountford, M. Schubart and I. J. Scowen, *Chem. Commun.*, 1997, 1555–1556.

56 S. Friedrich, M. Schubarta, L. H. Gade, I. J. Scowen, A. J. Edwards and M. McPartlin, *Chem. Ber.*, 1997, 1751–1759.

57 L. H. Gade, *Chem. Commun.*, 2000, 173–181.

58 A. Bashall, P. E. Collier, L. H. Gade, M. McPartlin, P. Mountford, S. M. Pugh, S. Radojevic, M. Schubart, I. J. Scowen and D. J. M. Trösch, *Organometallics*, 2000, **19**, 4784–4794.

59 A. J. Blake, P. E. Collier, L. H. Gade, P. Mountford, J. Lloyd, S. M. Pugh, M. Schubart, M. E. G. Skinner and D. J. M. Trösch, *Inorg. Chem.*, 2001, **40**, 870–877.

60 D. J. M. Trösch, P. E. Collier, A. Bashall, L. H. Gade, M. McPartlin, P. Mountford and S. Radojevic, *Organometallics*, 2001, **20**, 3308–3313.

61 S. M. Pugh, D. J. M. Trösch, D. J. Wilson, A. Bashall, F. G. N. Cloke, L. H. Gade,

P. B. Hitchcock, M. McPartlin, J. F. Nixon and P. Mountford, *Organometallics*, 2000, **19**, 3205–3210.

62 B. D. Ward, G. Orde, E. Clot, A. R. Cowley, L. H. Gade and P. Mountford, *Organometallics*, 2004, **23**, 4444–4461.

63 A. D. Schwarz, C. S. Onn and P. Mountford, *Angew. Chem. Int. Ed.*, 2012, **51**, 12298–12302.

64 N. Metzler-Nolte, *New J. Chem.*, 1998, **22**, 793–795.

65 T. J. Hadlington, J. A. B. Abdalla, R. Tirfoin, S. Aldridge and C. Jones, *Chem. Commun.*, 2016, **52**, 1717–1720.

66 D. A. Fletcher, R. F. McMeeking and D. Parkin, *J. Chem. Inf. Comput. Sci.*, 1996, **36**, 746 (Cambridge Structural Database version 5.37).

67 G. Aullón, D. Bellamy, L. Brammer, E. A. Bruton and A. G. Orpen, *Chem. Commun.*, 1998, 653–654.

68 K. Niedenzu, *Inorg. Chem.*, 1990, **29**, 538–541.

69 P. J. Wilson, A. J. Blake, P. Mountford and M. Schröder, *J. Organomet. Chem.*, 2000, **600**, 71–83.

70 P. D. Bolton, E. Clot, N. Adams, S. R. Dubberley, A. R. Cowley and P. Mountford, *Organometallics*, 2006, **25**, 2806–2825.

71 C. T. Owen, P. D. Bolton, A. R. Cowley and P. Mountford, *Organometallics*, 2007, **26**, 83–92.

72 C. J. Carmalt, A. C. Newport, I. P. Parkin, A. J. P. White and D. J. Williams, *J. Chem. Soc. Dalton Trans.*, 2002, 4055–4059.

73 H. W. Roesky, H. Voelker, M. Witt and M. Noltemeyer, *Angew. Chem. Int. Ed. Engl.*, 1990, **29**, 669–670.

74 P. D. Lyne and D. M. P. Mingos, *J. Chem. Soc. Dalton Trans.*, 1995, 1635–1643.

75 Y. Segawa, M. Yamashita and K. Nozaki, *Science*, 2006, **314**, 113–115.

76 Y. Segawa, Y. Suzuki, M. Yamashita and K. Nozaki, *J. Am. Chem. Soc.*, 2008, **130**, 16069–16079.

77 L. Weber, *Eur. J. Inorg. Chem.*, 2012, 5595–5609.

78 A. V. Protchenko, K. H. Birjkumar, D. Dange, A. D. Schwarz, D. Vidovic, C. Jones, N. Kaltsoyannis, P. Mountford and S. Aldridge, *J. Am. Chem. Soc.*, 2012, **134**, 6500–6503.

79 P. E. Collier, S. C. Dunn, P. Mountford, O. V Shishkin and D. Swallow, *J. Chem. Soc. Dalton Trans.*, 1995, **2**, 3743–3745.

80 L. C. Stevenson, DPhil Thesis, University of Oxford, 2015.

81 D. L. Hughes, I. A. Latham and G. J. Leigh, *J. Chem. Soc., Dalton Trans.*, 1986, 393–398.

82 J. S. M. Lehn and D. M. Hoffman, *Inorganica Chim. Acta*, 2003, **345**, 327–332.

83 A. S. Dudnik, V. L. Weidner, A. Motta, M. Delferro and T. J. Marks, *Nat. Chem.*, 2014, **6**, 1100–1107.

84 A. D. Schwarz and P. Mountford, Unpublished results.

85 A. A. Dissanayake and A. L. Odom, *Tetrahedron*, 2012, **68**, 807–812.

86 S. Patel, Y. Li and A. L. Odom, *Inorg. Chem.*, 2007, **46**, 6373–6381.

87 Y. Li, S. Banerjee and A. L. Odom, *Organometallics*, 2005, **24**, 3272–3278.

88 Y. Li, Y. Shi and A. L. Odom, *J. Am. Chem. Soc.*, 2004, **126**, 1794–1803.

89 Y. Li, A. Turnas, J. T. Ciszewski and A. L. Odom, *Inorg. Chem.*, 2002, **41**, 6298–6306.

90 S. A. Harris, J. T. Ciszewski and A. L. Odom, *Inorg. Chem.*, 2001, **40**, 1987–1998.

91 J. D. Selby, M. Feliz, A. D. Schwarz, E. Clot and P. Mountford, *Organometallics*, 2011, **30**, 2295–2307.

92 H. Herrmann, J. L. Fillol, T. Gehrmann, M. Enders, H. Wadepohl and L. H. Gade, *Chem. Eur. J.*, 2008, **14**, 8131–8146.

93 S. Kahlal, J. Saillard, J. Hamon, C. Manzur and D. Carrillo, *J. Chem. Soc. Dalton Trans.*, 1998, 1229–1240.

94 H. F. Bettinger, *Inorg. Chem.*, 2007, **46**, 5188–5195.

95 A. R. Rossi and R. Hoffmann, *Inorg. Chem.*, 1975, **14**, 365–374.

96 R. F. W. Bader, *Atoms in Molecules: A Quantum Theory*, Oxford University Press, Oxford, 1990.

97 X. Fradera, M. A. Austen and R. F. W. Bader, *J. Phys. Chem. A*, 1999, **103**, 304–314.

98 B. Xie and P. Mountford, Unpublished results.

99 H. Barrett, M. Slusarczyk and P. Mountford, Unpublished results.

Chapter Three

Sandwich and half-sandwich titanium borylimides: synthesis, structure, bonding and reactivity

3.1 Overview

This chapter will describe the synthesis and characterisation of six titanium borylimido complexes with sandwich and half-sandwich structures. To begin, a second route to access borylimido chemistry will be introduced, namely imide/borylamine exchange, to produce Cp*Ti{NB(NAr'CH)$_2$}Cl(py) (**9**). From this compound, the incorporation of two N,N-bidentate supporting ligands will then be described. The electronic structure of the borylimido linkage will be elucidated by DFT calculations, and this compared with a model dialkylborylimido complex. Next, the formation of a titanocene borylimido compound will be described, and its bonding will also be explored through computation. The synthesis of half-sandwich compounds utilising a Cp ligand will then be discussed. Finally, the reactivity of half-sandwich titanium borylimides with the heteroallenes CO_2 and CS_2 will be explored, as well as borylimide/amine and imide/borylamine exchanges. The energetics of these latter processes were calculated by DFT, and considered alongside a QTAIM analysis, with the results shedding light on the unique behaviour of borylamines and borylimido complexes in these reactions.

3.2 Introduction

Over the past six decades, sandwich and half-sandwich complexes of transition metals incorporating cyclopentadienyl (Cp) and pentamethylcyclopentadienyl (Cp*) ligands have been at the forefront of research in organometallic chemistry. Significant work has been carried out in elucidating the structure and bonding in these systems, as well as their stoichiometric and catalytic reactivity. The field has been extensively reviewed over the years.[1–5]

Of particular relevance to this Thesis are a plethora of Group 4 metal–nitrogen multiply bonded complexes with sandwich and half-sandwich structures. Indeed, the first Group 4 imido complex to be isolated was the zirconocene imide Cp$_2$Zr(N^{t}Bu)(THF) (**1.19**), which was described by Bergman and co-workers in 1988.[6] The rich reactivity of the imido functionality in this, and related, compounds was the first indication that Group 4 metal–nitrogen multiple bonds behaved very differently to their later transition metal counterparts.[1] Subsequent work in this research group led to the preparation of a titanocene imide, Cp$_2$Ti(N^{t}Bu)(py) (**1.2**),[7] and a hydrazide, Cp$_2$Ti(NNPh$_2$)(py) (**1.68**).[8]

In recent years, this research group has also utilised half-sandwich imido, hydrazido and alkoxyimido complexes for in-depth reactivity studies of these functional groups. A

common motif is the combined coordination of Cp* and a monoanionic, bidentate amidinate ligand, which together provide a robust supporting ligand set,[9–20] as in, for example, the alkoxyimide Cp*Ti{PhC(N^{i}Pr)$_2$}(NO^{t}Bu) (**1.108**). In this Chapter, the reactions of two half-sandwich borylimido complexes with CO_2 and CS_2 will be described, and compared to the reactions of Cp*-amidinate-supported imides and hydrazides with those small molecules. For example, reactions of both Cp*Ti{MeC(N^{i}Pr)$_2$}(N^{t}Bu) (**3.1**) and Cp*Ti{MeC(N^{i}Pr)$_2$}(NAr) (**3.2**; Ar = Tol, 4-$C_6H_4CF_3$, 4-$C_6H_4NMe_2$, 2,6-$C_6H_3Me_2$) with CO_2 form [2+2] cycloaddition products **3.3** and **3.4**, respectively (Figure 3.1). However, while the aryl compounds **3.4** react with a further equivalent of CO_2 to form the "double insertion" products **3.5**, the *tert*-butyl homologue does not, giving instead ^{t}BuNCO extrusion and the μ-oxo dimer [Cp*Ti{MeC(N^{i}Pr)$_2$}(μ-O)]$_2$ (**1.79**).[9,11] When this chemistry was extended to the hydrazides Cp*Ti{MeC(N^{i}Pr)$_2$}(NNR$_2$) (R = Me (**1.65**), Ph (**1.66**)), the final products obtained were "double insertion" products analogous to **3.5**.[16]

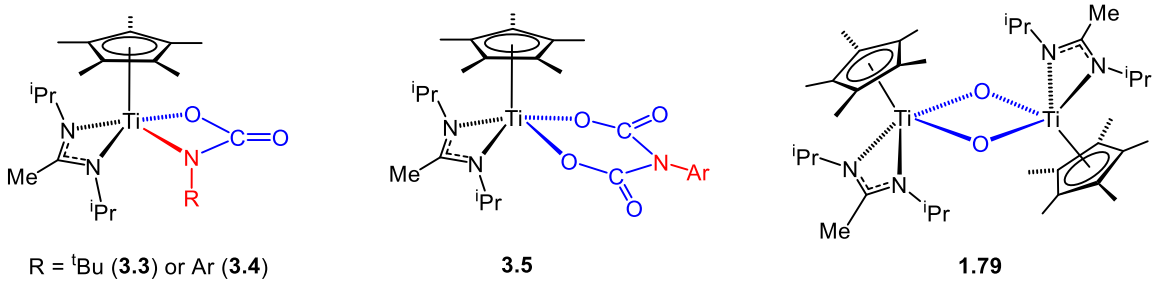

Figure 3.1. Exemplar products of reactions of Cp*-amidinate-supported imides with CO_2 and CS_2. (Ar = Tol, 4-$C_6H_4CF_3$, 4-$C_6H_4NMe_2$, 2,6-$C_6H_3Me_2$).[9,11]

As discussed in Chapters One and Two, this research group has accessed arylimido, hydrazido and alkoxyimido complexes through exchange of a *tert*-butylimido ligand with the respective aniline, hydrazine or alkoxyamine. For example, the reaction of Cp*Ti(N^{t}Bu)Cl(py) (**1.8**) with H_2NAr' produced the arylimide Cp*Ti(NAr')Cl(py) (**3.6**),[21] while reaction of **1.8** with H_2NNPh$_2$ produced the hydrazide Cp*Ti(NNPh$_2$)Cl(py) (**1.69**).[8] Consequently, the Author aimed to extend this methodology to borylimido chemistry using the borylamine H_2NB(NAr'CH)$_2$ (**2.2**), and this is now presented as the second route employed in this Thesis to access titanium borylimido compounds.

3.3 Synthesis and bonding of Cp*-half-sandwich titanium borylimido complexes

3.3.1 Synthesis of Cp*Ti{NB(NAr'CH)$_2$}Cl(py) (9)

When followed on the NMR tube scale in C_6D_6 solution at 90 °C, a mixture of Cp*Ti(N^{t}Bu)Cl(py) (**1.8**) with $H_2NB(NAr'CH)_2$ (**2.2**) resulted in very slow, partial conversion to an apparent borylimido compound. It was suspected that higher temperatures and removal of the H_2N^tBu byproduct were required in order to drive the reaction to completion, and this was ultimately achieved through a reaction in the melt, assisted by removal of H_2N^tBu by dynamic vacuum. On the preparative scale, heating of a mixture of **1.8** and **2.2** to 140 °C, with exposure to dynamic vacuum, resulted in the formation of Cp*Ti{NB(NAr'CH)$_2$}Cl(py) (**9**) in 59% isolated yield (Equation 3.1). The ^{1}H NMR spectrum of **9** is indicative of a C_1 symmetric species in solution: two Ar' isopropyl environments are observed, with two C<u>H</u>MeMe septets (2 H integration each) and four CH<u>MeMe</u> doublets (6 H integration each), this suggesting restricted rotation of the two Ar' moieties. In addition, the expected resonances for an η^5-C_5Me_5 ligand (15 H singlet) and an N-bound pyridine ligand are observed.

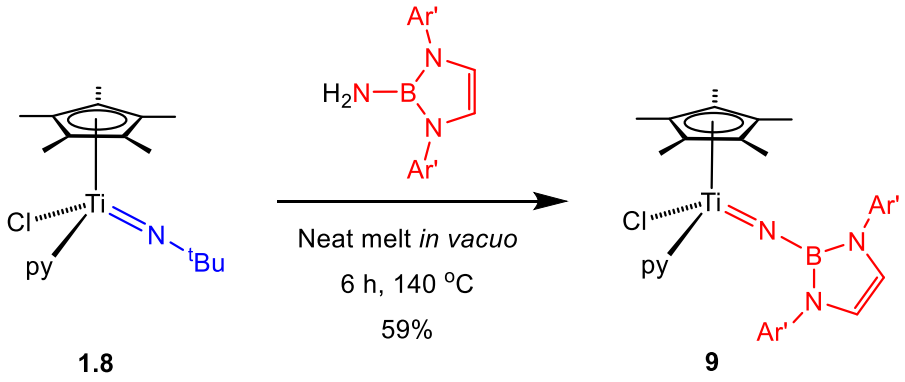

1.8 **9**

Equation 3.1

Diffraction-quality crystals of borylimide **9** were grown from a benzene/hexane mixture at RT. The molecular solid state structure is shown in Figure 3.2, along with selected bond distances and angles in Table 3.1. Solid state structures of six related titanium–nitrogen multiple bonded complexes of the type Cp*Ti(NR)Cl(py) (R = ^{t}Bu (**1.8**), Ar' (**3.6**), 2,6-$C_6H_3Br_2$, 2-$C_6H_4{}^tBu$, 2-$C_6H_4{}^iPr$, NPh_2 (**1.69**)) have been reported to date,[8,21,22] all of which are generally comparable in structure to **9**, having three-legged piano stool-type geometries. At 1.7380(11) Å, the Ti(1)–N(1) bond distance of **9** falls within the range of that distance in the four arylimido analogues (range 1.7304(19) – 1.753(2) Å)[21] and is

similar to that in the diphenylhydrazide **1.69** (1.734(2) Å),[8] although this is significantly longer than in the *tert*-butylimido compound **1.8** (1.696(4) and 1.698(4) Å for two crystallographically independent molecules).[22]

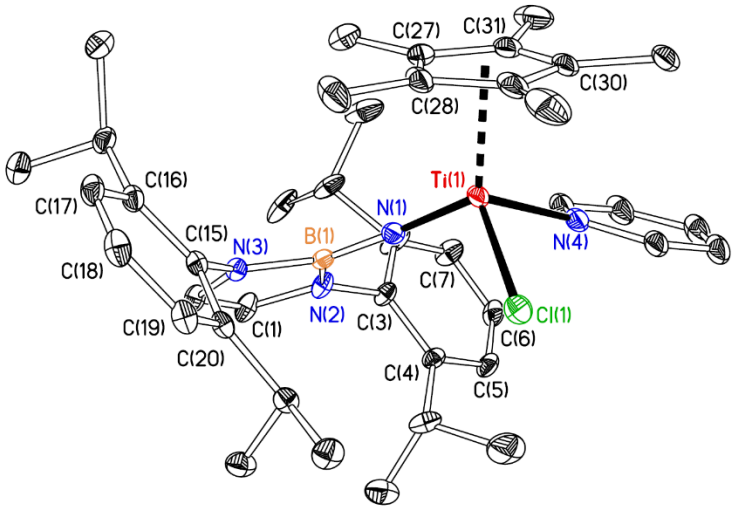

Figure 3.2. Displacement ellipsoid plot (20% probability) of Cp*Ti{NB(NAr'CH)$_2$}Cl(py) (**9**). H atoms are omitted for clarity.

Table 3.1. Selected bond distances (Å) and angles (°) for Cp*Ti{NB(NAr'CH)$_2$}Cl(py) (**9**). Cp_{cent} refers to the computed η^5-C_5Me_5 ring centroid.

Ti(1)–N(1)	1.7380(11)	Cp_{cent}–Ti(1)–N(1)	122.0
Ti(1)–N(4)	2.1649(11)	Cp_{cent}–Ti(1)–N(4)	110.1
Ti(1)–Cl(1)	2.3212(4)	Cp_{cent}–Ti(1)–Cl(1)	116.8
Ti(1)–Cp_{cent}	2.07	N(1)–Ti(1)–Cl(1)	107.68(5)
N(1)–B(1)	1.4153(17)	N(4)–Ti(1)–Cl(1)	96.77(4)
B(1)–N(2)	1.4513(16)	N(1)–Ti(1)–N(4)	99.16(5)
B(1)–N(3)	1.4545(15)	Ti(1)–N(1)–B(1)	175.01(8)
		N(1)–B(1)–N(2)	127.35(10)
		N(1)–B(1)–N(3)	129.47(10)

In the four arylimido complexes, the aryl substituents adopted a common orientation, with the normal to the C_6 ring plane being almost co-incident with the plane containing Ti, the imido N atom and the Cp ring centroid.[21] Considering the structural similarities already described between the borylimido complexes reported here and their respective arylimido analogues, the boryl ring might be expected to take up the same orientation in **9**. However, the solid state structure of **9** shows that there is a *ca* 25° deviation from that geometry (the relevant dihedral angles are N(2)–B(1)···Ti(1)–Cp_{cent} = 117° and N(3)–B(1)···Ti(1)–Cp_{cent} = 66°), and this is attributed to accommodation of the large steric bulk of the borylimido moiety.

As an alternative route to access **9**, Ti{NB(NAr'CH)$_2$}Cl$_2$(py)$_3$ (**3**) was reacted with 1 equivalent of LiCp* on the NMR tube scale. Heating for 3 days at 70 °C in C_6D_6 resulted in quantitative conversion to the desired Cp*-bound compound **9**. However, on the preparative scale in toluene, this route gave increased product decomposition (indicated by the presence of H_2NB(NAr'CH)$_2$ (**2.2**) in the reaction mixture) which was probably due to the extended reaction time at high temperature. Therefore only the previously described synthetic route *via tert*-butylimide/borylamine exchange was later used to reliably access the borylimide **9**.

Additionally, the reactions of Cp*Ti(N^{t}Bu)Cl(py) (**1.8**) with (μ-H_2N)$_2$(BC_8H_{14})$_2$ and H_2NBMes$_2$ were also investigated, with the aim of forming the respective dialkyl- or diarylborylimido complexes. Unfortunately, no success was found with either of these substrates, with both solution and melt reactions being attempted. At low temperatures in C_6D_6 solution, no reaction was observed in either case, whilst the forcing conditions employed in higher temperature solution reactions, or in melts, ultimately resulted only in decomposition of the starting material **1.8**.

3.3.2 Installation of N,N-bidentate ligands

As described in Section 1.8, this research group recently reported the formation of an amidinate-supported borylimido complex Cp*Ti{MeC(N^{i}Pr)$_2$}(NBC_8H_{14}) (**1.115**) from the related hydrazide and 9-BBN.[23] Thus, given the successful synthesis of the cyclopentadienyl borylimido synthon **9**, an analogue of **1.115** incorporating the –NB(NAr'CH)$_2$ group was targeted *via* salt metathesis with Li[MeC(N^{i}Pr)$_2$]. Unfortunately, on the NMR tube scale in C_6D_6, no reaction occurred between **9** and the

lithium amidinate, or the analogous Li[PhC(N^iPr)$_2$]. This is suspected to be due to prevention of complexation by insurmountable steric constraints.

Attention was therefore turned to alternative monoanionic, N,N-bidentate ligands with reduced steric profiles, and titanium borylimido complexes were successfully prepared with two such ligands. The first of these is the bicyclic guanidinate derived from H-hpp (1,3,4,6,7,8-hexahydro-2*H*-pyrimido[1,2-*a*]pyrimidine), which has a rich history as a bidentate ligand to a wide range of metals,[24] and has found some application in titanium imido chemistry previously.[25] Secondly, the aminopyrrolide ligand $N^{pyr}N^{Me_2}$ ($Me_2NCH_2(2\text{-}NC_4H_3)$) was employed, which, along with related pyrrolide ligands, has been used extensively in Group 4 imido and hydrazido chemistry in recent years, including in the application of alkyne hydrohydrazination.[26–33]

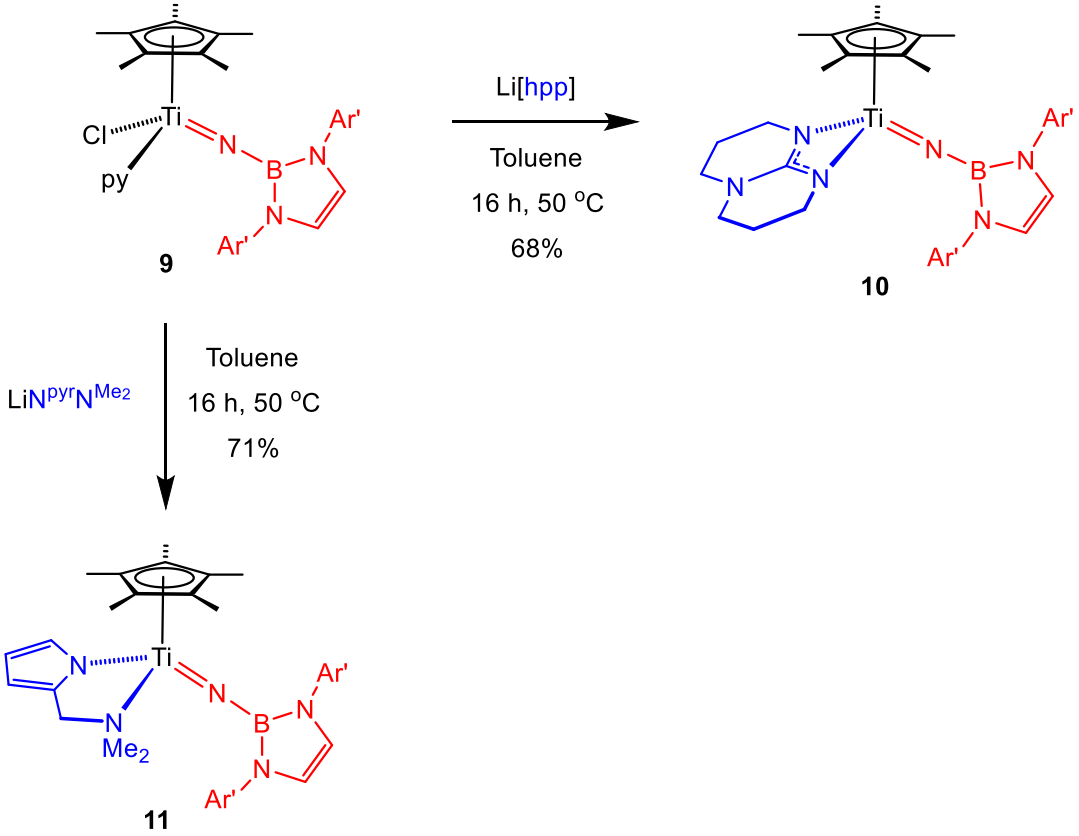

Scheme 3.1. Synthesis of Cp*Ti(hpp){NB(NAr'CH)$_2$} (**10**) and Cp*Ti($N^{pyr}N^{Me_2}$){NB(NAr'CH)$_2$} (**11**) from Cp*Ti{NB(NAr'CH)$_2$}Cl(py) (**9**).

Reaction of **9** with 1 equiv. of either Li[hpp] or Li$N^{pyr}N^{Me_2}$ proceeded smoothly in toluene solution at 50 °C. Following work-up, the two complexes Cp*Ti(hpp){NB(NAr'CH)$_2$} (**10**) and Cp*Ti($N^{pyr}N^{Me_2}$){NB(NAr'CH)$_2$} (**11**) were isolated in 68 and 71% yield respectively

(Scheme 3.1). The ^{1}H NMR spectrum of **10** (Figure 3.3, top) is indicative of a C_s symmetric species, with the resonances attributed to the six methylene groups of the hpp ligand taking the form of six partially overlapping multiplets arising from protons oriented "up" or "down" with respect to the Cp* ligand. The four isopropyl groups of the borylimido ligand are chemically equivalent, giving one septet (4 H) and two doublets (12 H each). In contrast, the ^{1}H NMR spectrum of **11** (Figure 3.3, bottom) is indicative of a C_1 symmetric species. The $N^{pyr}N^{Me_2}$ ligand gives three multiplets from the pyrrole ring as well as two methylene doublets and two NMe singlets. In this case, the four isopropyl groups of the borylimido ligand are not all chemically equivalent, with two septets (2 H each) and four doublets (6 H each) being observed, similar to the spectrum of **9**.

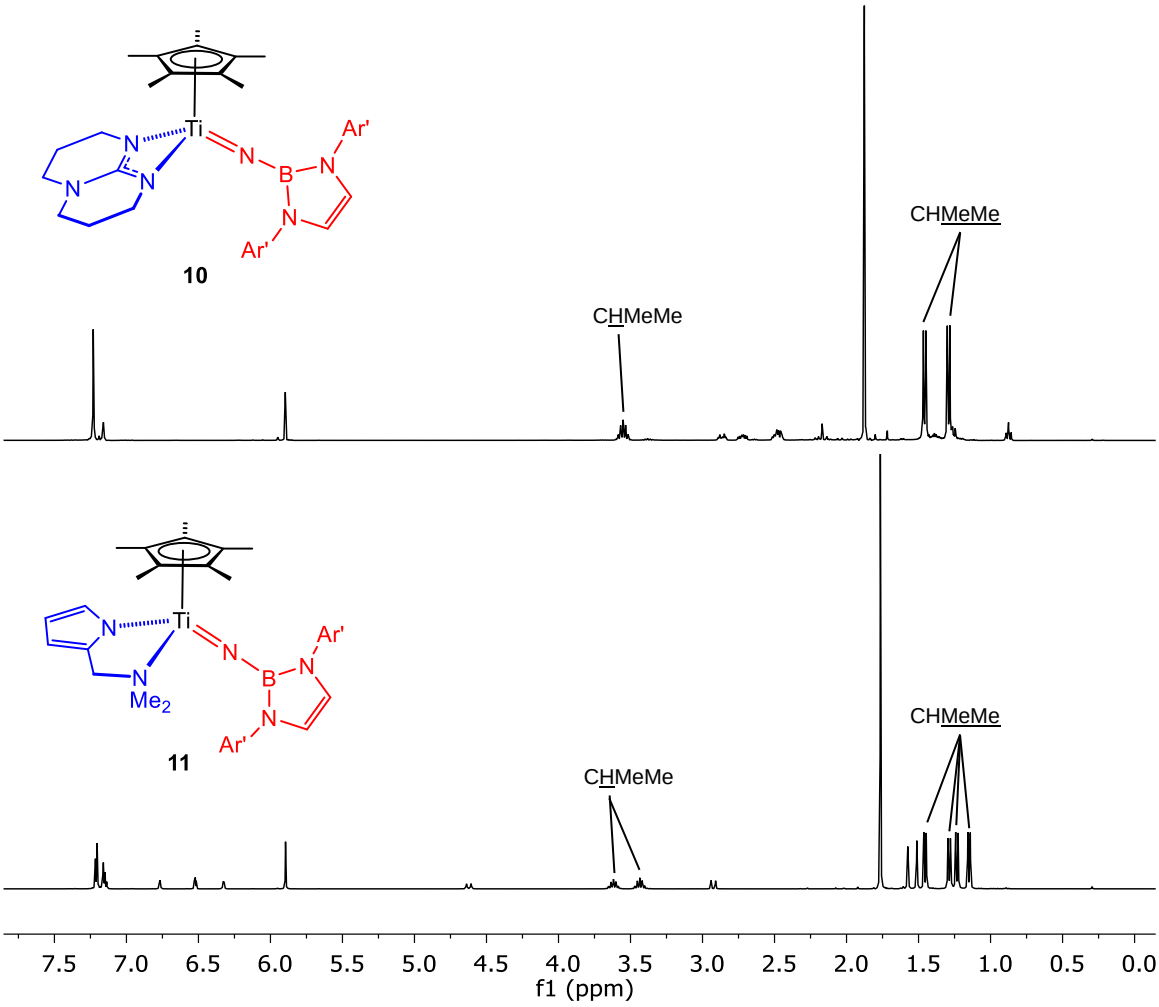

Figure 3.3. ^{1}H NMR spectra (400.1 MHz) of Cp*Ti(hpp){NB(NAr'CH)$_2$} (**10**, top) and Cp*Ti($N^{pyr}N^{Me2}$){NB(NAr'CH)$_2$} (**11**, bottom) in C_6D_6 at 298 K.

Diffraction-quality crystals of both **10** and **11** were successfully grown from hexane solutions. The molecular solid state structures are shown in Figure 3.4, and selected bond distances and angles are listed in Table 3.2.

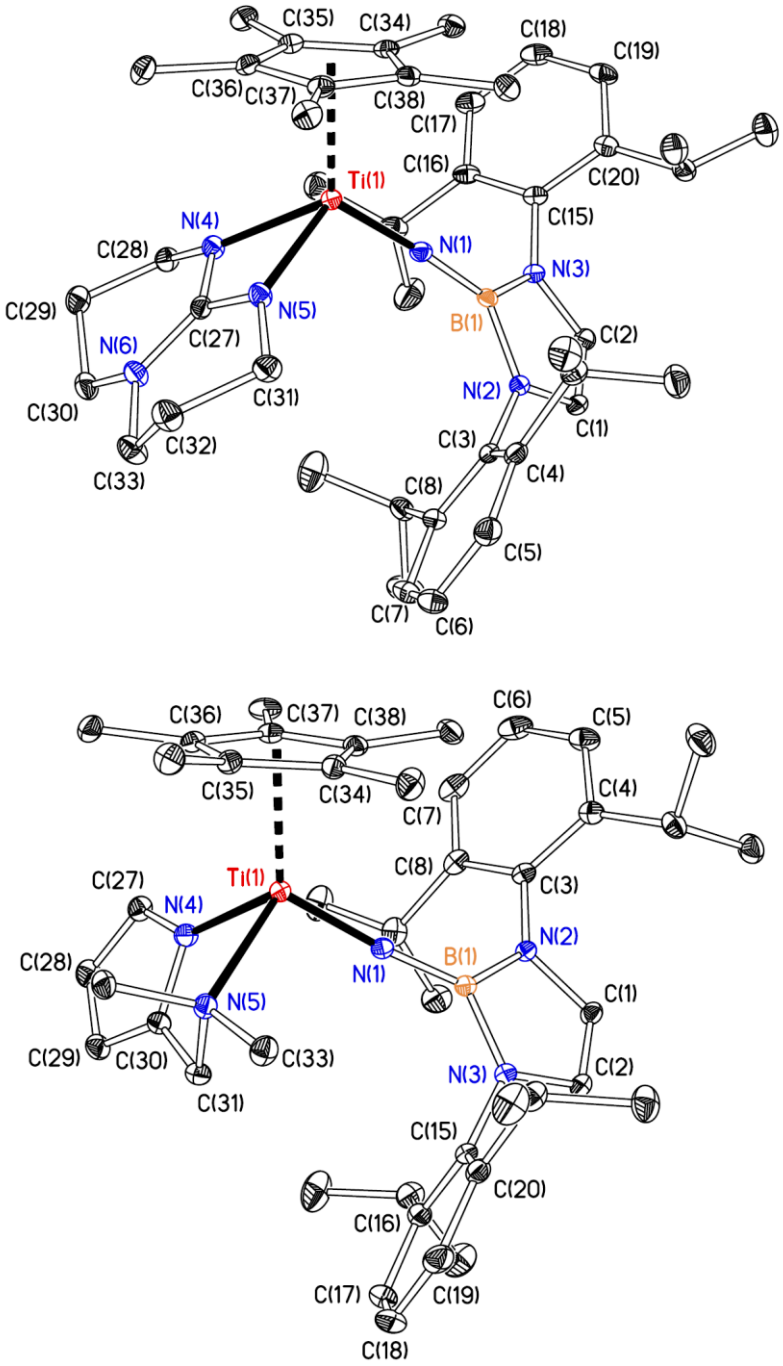

Figure 3.4. Displacement ellipsoid plots (20% probability) of Cp*Ti(hpp){NB(NAr'CH)$_2$} (**10**, top) and Cp*Ti(N^{pyr}N^{Me_2}){NB(NAr'CH)$_2$} (**11**, bottom). H atoms are omitted for clarity.

Table 3.2. Selected bond lengths (Å) and angles (°) for Cp*Ti(hpp){NB(NAr'CH)$_2$} (**10**) and Cp*Ti(N^{pyr}N^{Me_2}){NB(NAr'CH)$_2$} (**11**). Cp$_{cent}$ refers to the computed η^5-C$_5$Me$_5$ ring centroids.

Parameter	**10**	**11**
Ti(1)–N(1)	1.7433(19)	1.7444(12)
Ti(1)–N(4)	2.0790(18)	2.0740(12)
Ti(1)–N(5)	2.0753(19)	2.2319(12)
Ti(1)–Cp$_{cent}$	2.07	2.08
N(1)–B(1)	1.422(3)	1.4318(19)
B(1)–N(2)	1.452(3)	1.4668(19)
B(1)–N(3)	1.455(3)	1.4555(18)
N(1)–Ti(1)–Cp$_{cent}$	125.1	122.5
N(4)–Ti(1)–Cp$_{cent}$	117.1	118.8
N(5)–Ti(1)–Cp$_{cent}$	115.0	121.1
N(1)–Ti(1)–N(4)	109.87(8)	105.96(5)
N(1)–Ti(1)–N(5)	109.56(8)	100.13(5)
N(4)–Ti(1)–N(5)	64.95(7)	79.25(5)
Ti(1)–N(1)–B(1)	176.00(17)	174.15(10)
N(1)–B(1)–N(2)	126.7(2)	130.54(12)
N(1)–B(1)–N(3)	130.4(2)	126.52(13)

Both compounds **10** and **11** possess a three-legged piano stool geometry, with an η^5-C$_5$Me$_5$ ligand, η^1-borylimido ligand and a κ^2-N,N'-bound ligand (hpp or N^{pyr}N^{Me_2}, respectively). Comparison of the metric parameters of the Ti–N–B linkage show that the borylimido moiety is broadly similar in the two compounds: the Ti(1)–N(1) (1.7433(19) and 1.7444(12) Å in **10** and **11** respectively) and N(1)–B(1) distances (1.422(3) and 1.4318(19) Å), along with the Ti(1)–N(1)–B(1) angles (176.00(17) and 174.15(10)°) demonstrate that both complexes bear Ti–N triple bonds and N–B single bonds, in agreement with all of the structural characterisations discussed previously. As expected, the bite angle of the hpp

ligand at the metal is much smaller than in $N^{pyr}N^{Me_2}$, with respective N(4)–Ti(1)–N(5) values of 64.95(7) and 79.25(5)°. This arises from the presence of a single carbon atom bridging the N donor atoms in hpp, whilst a two-carbon bridge separates the pyrrolide nitrogen and $\underline{N}Me_2$ in $N^{pyr}N^{Me_2}$.

3.3.3 Computational studies of bonding in Cp*-half-sandwich borylimides

In Chapter Two, DFT and QTAIM analyses were presented of the model diamide-pyridine-supported complexes $Ti(N_2^{SiH_3}N^{py})(NR)(py)$ (R = Me (**1Q_Me**), Xyl (**1Q_Xyl**), $B(NMeCH)_2$ (**1Q_B(NMeCH)$_2$**)), which focussed on the comparison of the electronic structure in the latter borylimide to the two model imides, one having an alkyl substituent and one an aryl substituent. In summary, **1Q_B(NMeCH)$_2$** was shown to be most similar to an arylimide due to the presence of the aromatic π system in the boryl functionality, and this similarity has also been observed experimentally in the bond metrics of the crystallographically characterised complexes **1**, **3** and **9**. In this Section, new computational analyses of model half-sandwich complexes will be used to probe differences between the $NB(NAr'CH)_2$ ligand and dialkylborylimido ligands such as that in the BBN-substituted compound **1.115**.

DFT calculations were carried out on the model systems $CpTi\{MeC(NMe)_2\}(NR)$ (**2Q_R**; R = Me, Ph, BMe_2, $B(NMeCH)_2$) using the B3PW91 functional and Def2TZVP basis set, by Simona Mellino and Prof. Philip Mountford. The geometries, key orbital representations and associated energies are shown in Figure 3.7. **2Q_B(NMeCH)$_2$** is used as a model for the real compound **10**, although in this case the hpp ligand is approximated as the $\{MeC(NMe)_2\}$ amidinate to give direct comparisons with previously reported computational results on imides, hydrazides and alkoxyimides,[16,19] whilst **2Q_BMe$_2$** is a model of the real BBN-substituted compound **1.115**. A comparison of **2Q_Me** with an hpp-supported analogue is described in Appendix A1. Firstly, however, the frontier molecular orbitals (FMOs) of the model imido and borylimido dianions $[NMe]^{2-}$, $[NPh]^{2-}$, $[NBMe_2]^{2-}$ and $[NB(NMeCH)_2]^{2-}$ are compared, and then the FMOs of the $[CpTi\{MeC(NMe)_2\}]^{2+}$ fragment will be described. Note that, although the symmetry is less than cylindrical in the anions $[NR]^{2-}$ (with the exception of $[NMe]^{2-}$), the π notation will be used for the bonding characteristics of the respective 2p N atomic orbitals.

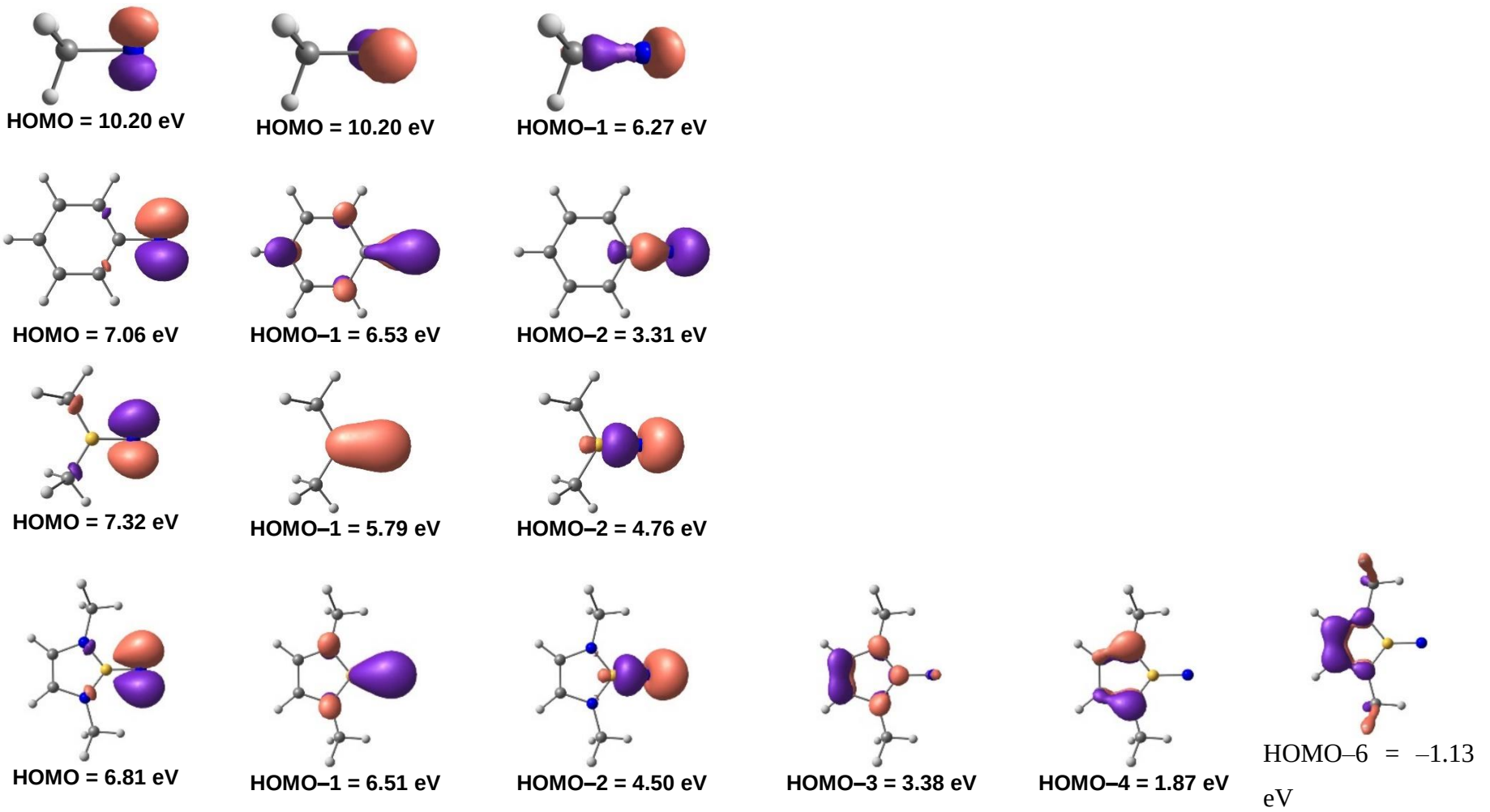

Figure 3.5. Isosurfaces and energies of frontier molecular orbitals (σ and 2 π) in the model imido-type dianions $[NMe]^{2-}$, $[NPh]^{2-}$, $[NBMe_2]^{2-}$ and $[NB(NMeCH)_2]^{2-}$, along with filled π-orbitals of the boryl ring in $[NB(NMeCH)_2]^{2-}$.

Figure 3.5 shows the three highest occupied MOs for the four model imido-type fragments $[NMe]^{2-}$, $[NPh]^{2-}$, $[NBMe_2]^{2-}$ and $[NB(NMeCH)_2]^{2-}$, these being the nitrogen-based σ-donor orbital and two π-donor orbitals in each case. Considering first $[NMe]^{2-}$, this dianionic fragment has two degenerate and orthogonal MOs (N lone pairs) at an energy of 10.20 eV. The σ-donor orbital is the HOMO–1 at 6.27 eV. Having no electron-withdrawing substituent, the FMOs of $[NMe]^{2-}$ are considerably destabilised compared with those of the three other model dianions which are next described. Moving to $[NPh]^{2-}$, now the two nominally π-symmetry N lone pairs are of different energy. The HOMO lies parallel to the phenyl ring, so does not have any interaction with the π orbitals of that ring. In contrast, the lone pair perpendicular to the ring partially donates into an unoccupied ring π orbital to form the HOMO–1 which is stabilised by 0.53 eV relative to the HOMO. Meanwhile, the HOMO–2 is the σ-donor orbital, which is stabilised by 2.96 eV relative to that of $[NMe]^{2-}$ by the electron-withdrawing phenyl group.

Moving next to the two borylimido dianions, the HOMO–1 of $[NBMe_2]^{2-}$ is stabilised by 1.53 eV relative to the HOMO due to a significant degree of donation of the N lone pair to the empty B 2p orbital. In $[NB(NMeCH)_2]^{2-}$, the lone pair perpendicular to the boryl ring is similarly stabilised by donation to the B 2p orbital, though only by 0.30 eV, due to competing donation from the nitrogen atoms that form the backbone of the borolyl ring. Comparing the two σ-donor orbitals in these model borylimido dianions, that of $[NB(NMeCH)_2]^{2-}$ is stabilised by 0.26 eV relative to that of $[NBMe_2]^{2-}$ due to the electronegativity of the adjacent nitrogen atoms in the borolyl backbone compared with the methyl substituents in the latter borylimido fragment. Additionally, Figure 3.5 displays three further occupied MOs of $[NB(NMeCH)_2]^{2-}$ which represent the 6π electrons of the aromatic boryl ring. These will be referred to later when considering the bonding in **2Q_B(NMeCH)$_2$**.

Calculations were also performed on the model dicationic fragment $[CpTi\{MeC(NMe)_2\}]^{2+}$. Selected FMOs, some of which are expected to act as the acceptor orbitals for an imido-type dianion, are depicted in Figure 3.6. The LUMO+1 and LUMO+2 are effectively the metal d orbitals which can act as π-acceptors to an imido-type ligand bonding at the vacant site, and it is noted that the LUMO+1 is also slightly δ*-antibonding to the amidinate ligand. The LUMO+3 acts as the σ-acceptor, whilst the LUMO is a purely non-bonding metal d orbital, and the LUMO+4 is a metal–ligand antibonding orbital with δ symmetry so is not involved with the bonding of an imido ligand.

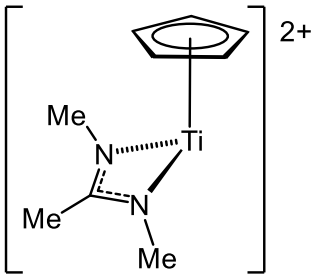

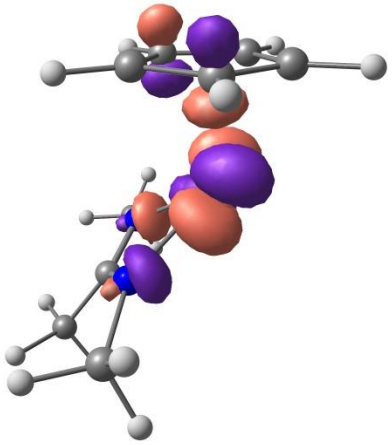

LUMO+4 = –10.4 eV

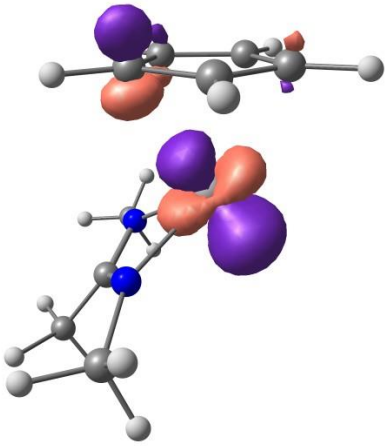

LUMO+3 = –11.6 eV

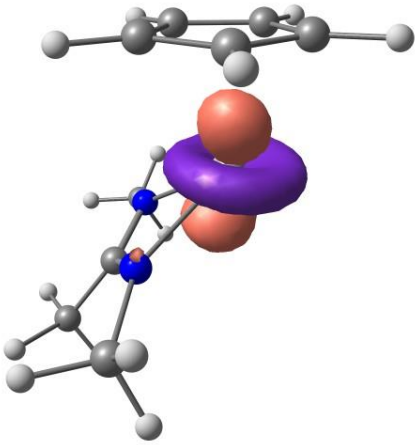

LUMO+2 = –11.9 eV

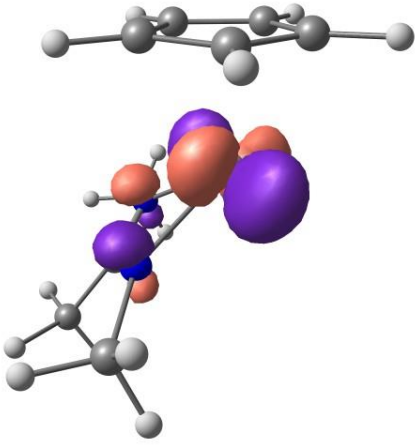

LUMO+1 = –12.3 eV

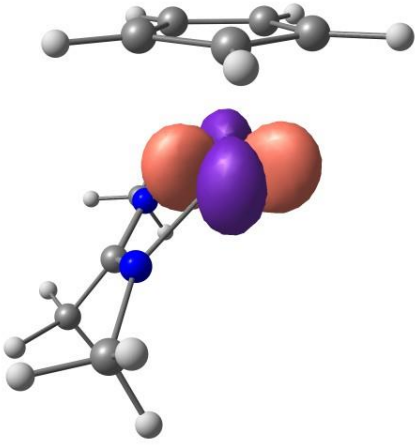

LUMO = –12.6 eV

Figure 3.6. Isosurfaces and energies of frontier molecular orbitals in the model dicationic fragment $[CpTi\{MeC(NMe)_2\}]^{2+}$.

It is also noted that, in the real compounds, the LUMO+2 and LUMO+3 mix to optimise σ and π bonding (see, for example, the HOMO of **2Q_Me**, *vide infra*). Finally, it is noted that the FMO energies for both $[NR]^{2-}$ and $[Ti\{MeC(NMe)_2\}]^{2+}$ are artificially raised and lowered by imposition of the formal 2– and 2+ charges, respectively.

With the FMOs of both imido-type dianions and the corresponding dicationic metal fragment now having been considered, the electronic structures of the model compounds **2Q_R** themselves will next be described. Although the two π-symmetry lone pairs of $[NMe]^{2-}$ are degenerate (C_{3v} symmetry), the two π-components of the metal–nitrogen multiple bond that they go on to form in **2Q_Me** are not isoenergetic as they have different symmetries and involve mixing with different acceptor orbitals at the metal centre, these being the LUMO+1 and LUMO+2 of the $[CpTi\{MeC(NMe)_2\}]^{2+}$ fragment. The HOMO–1 of **2Q_Me** has an energy of –5.68 eV and lies parallel to the vertical Ti–Cp_{cent} vector (Figure 3.7), so is denoted π_v, whilst the π_h component is the HOMO–2 with an energy of –6.17 eV. Additionally, the HOMO (–5.49 ev) is an amidinate ligand-based lone pair.

Turning next to **2Q_Ph**, the π_v component of the multiple bond is now the HOMO, with an energy of –5.23 eV (destabilised by 0.45 eV relative to the π_v of **2Q_Me**). This destabilisation arises from an antibonding interaction of the Ti–N π-bond with a filled π orbital of the phenyl ring. The HOMO–2 is the Ti–N π_h component, which is formed from the higher energy of the two π-symmetry N lone pairs depicted in $[NPh]^{2-}$ in Figure 3.5. This is 0.33 eV lower in energy than the π_h in **2Q_Me** due to the electron-withdrawing nature of the phenyl group compared with methyl. The counterpart of the HOMO in **2Q_Ph** is the HOMO–7 which is Ti–N π_v bonding and also shows significant donation of a Ti–N π component into the phenyl ring. The HOMO–1 is a mainly amidinate ligand-based lone pair, similar to the HOMO of **2Q_Me**.

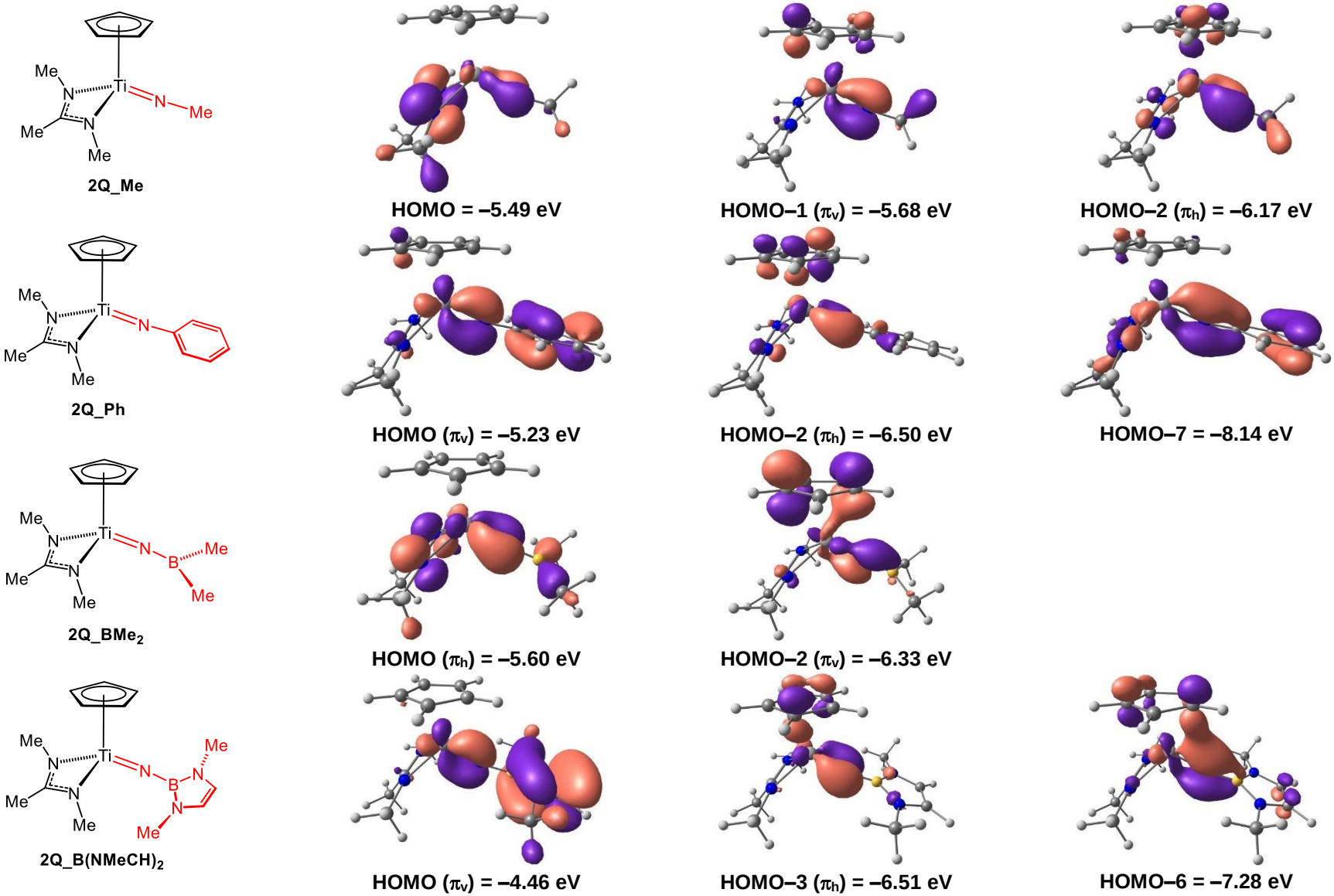

Figure 3.7. DFT model compounds CpTi{MeC(NMe)$_2$}(NR) (**2Q_R**; R = Me, Ph, BMe$_2$, B(NMeCH)$_2$), and associated isosurfaces and energies of the π components of the Ti–N linkages.

Moving on to **2Q_BMe$_2$**, the HOMO is now the π_h component of the metal–nitrogen multiple bond, at an energy of –5.60 eV. This is similar in energy to the HOMO–1 (π_v) of **2Q_Me** (–5.68 eV) due to two counteracting factors. Firstly, this π_h MO is formed from the lower in energy of the two π-acceptor orbitals of the $[CpTi\{MeC(NMe)_2\}]^{2+}$ fragment, contributing to a stabilisation relative to **2Q_Me**, and secondly, the electropositive nature of boron gives an opposing destabilising effect. Although the HOMO–2 of **2Q_BMe$_2$** shows significant mixing with Cp π-bonding orbitals, inspection of atomic contributions shows that this is the MO best considered to incorporate the π_v component. This is 0.73 eV more stable than the π_h as this is formed from the HOMO–1 of $[NBMe_2]^{2-}$ which is significantly stabilised by donation of the N lone pair into the empty B 2p orbital. As in **2Q_Ph**, the complete Ti–N π_v interaction is distributed among several MOs.

Finally, the π MOs of the model borylimide **2Q_B(NMeCH)$_2$** are comparable in form to those of the model phenylimide **2Q_Ph**. In particular, the π_v component of both models is the HOMO, which is high in energy due to an antibonding interaction between this component of the multiple bond and a filled π orbital of the respective phenyl or borylimido ring. However, that of **2Q_B(NMeCH)$_2$** is significantly higher in energy than that of **2Q_Ph** (–4.46 *vs* –5.23 eV), this being due to the electropositive nature of boron. The π_h component is much lower in energy (–6.51 eV) as it is perpendicular to the B 2p orbital so has no interaction with it; this is formed from the HOMO of $[NB(NMeCH)_2]^{2-}$ as depicted in Figure 3.5. Similar to **2Q_Ph**, the HOMO–6 of **2Q_B(NMeCH)$_2$** represents a backbonding interaction from a metal–nitrogen π component into an empty π orbital of the boryl ring, this effect originating from the HOMO–1 of the $[NB(NMeCH)_2]^{2-}$ fragment.

These computational results have highlighted some electronic differences between borylimido ligands of the 1,3,2-diazaborolyl form and ones in which the boron atom has a naked empty 2p orbital, such as that derived from BBN. In particular, in the latter case, one π component is stabilised by significant donation to the empty B 2p orbital, whilst for the former case, this effect is somewhat lessened and is accompanied by a destabilisation of a multiple bond π component by the filled boryl π system, similar to the π-effect in an arylimide. In Sections 2.4 and 3.3.1 the failure of $(\mu\text{-}H_2N)_2(BC_8H_{14})_2$ to form titanium borylimido complexes through protonolysis reactions where $H_2NB(NAr'CH)_2$ (**2.2**) succeeded was described. Later, in Section 3.7, a combined DFT and QTAIM study will be presented to explain exchange reactions of borylimido complexes with amines to give imides, and *vice versa*. In particular, the bond dissociation energies of the Ti–N multiple

bonds, and relevant N–H bond strengths will be considered in order to shed light on these observed outcomes.

3.4 Synthesis and bonding of $Cp_2Ti\{NB(NAr'CH)_2\}(py)$ (12)

Further to the use of $Ti\{NB(NAr'CH)_2\}Cl_2(py)_3$ (**3**) as a titanium borylimido synthon as described in Chapter Two, and mindful of the fact that no metallocene borylimido complex has been reported to date, the reaction of **3** with NaCp was next targeted. On the preparative scale in toluene, the reaction of **3** with two equivalents of NaCp cleanly formed the desired titanocene borylimide $Cp_2Ti\{NB(NAr'CH)_2\}(py)$ (**12**) in 58% isolated yield (Equation 3.2). The ^1H NMR spectrum in C_6D_6 solution demonstrates the presence of two η^5-bound Cp ligands as a 10 H singlet, and one pyridine donor ligand, in addition to the borylimido ligand.

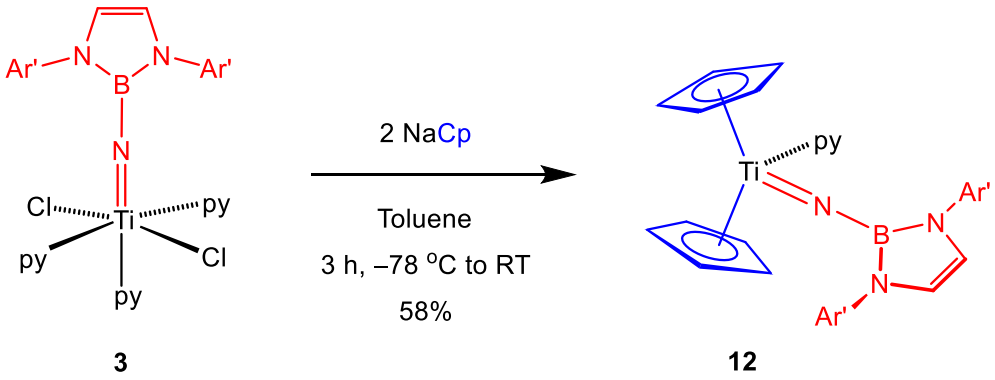

3 **12**

Equation 3.2

Diffraction-quality crystals of **12** were grown from a pentane solution at 5 °C. The molecular solid state structure is shown in Figure 3.8, and selected bond distances and angles are listed in Table 3.3. Molecules of **12** contain a bent Cp_2Ti moiety which is coordinated to both the borylimido ligand and a pyridine donor ligand. Although this is the first borylimido sandwich compound of any metal, its structure may be compared to the wide range of metal–ligand multiply bonded Group 4 metallocenes of the type $Cp^R_2M(E)(L)$ (M = Ti, Zr, Hf; E = NR, PR, O, S, Se, Te; L = Lewis base).[6–8,34–45] The Cp rings of **12** are η^5-coordinated to the metal with Ti–C bonds in the range 2.4022(18) – 2.6053(18) Å, and an average Ti–Cp centroid distance of 2.18 Å, which is comparable to those in the analogous imide $Cp_2Ti(N^tBu)(py)$ (**1.2**, 2.22 Å) and hydrazide $Cp_2Ti(NNPh_2)(py)$ (**1.68**, 2.18 Å).[7,8] This is, however, *ca* 0.1 Å longer than the Ti–Cp centroid distances generally found in titanocene complexes of the type $Cp^R_2TiX_2$ (X = Cl,

alkyl).[46] Close inspection of the Ti–C bonds of **12** reveals that the upper Cp ring (as drawn in Figure 3.8) has a considerable tilt away from the borylimido ligand and the ideal geometry (of five equal Ti–C distances). That is, C(28) and C(29) have Ti–C distances of 2.6050(18) and 2.6053(18) Å respectively, whilst those for C(27), C(30) and C(31) are shorter at 2.4943(17), 2.4423(18) and 2.4325(18) Å. Thus the bonding situation for this Cp ring may be viewed as moving toward an η^3-coordination mode. As a comparison, the Ti–C lengths in the "lower" Cp ring are in the range *ca* 2.402 – 2.503 Å and so the tilting effect is not appreciable in that ring. The Ti(1)–N(1) bond length of 1.7549(13) Å is comparable to the Ti–N_{im} distance in the hydrazide **1.68** (1.757(2) Å),[8] and longer than in the imide **1.2** (1.723(6) Å),[7] and is consistent with a Ti–N triple bond. A small departure from linearity is encountered in the Ti(1)–N(1)–B(1) angle, which has the value 159.65(12)°. This is likely due to unavoidable steric constraints imposed by the large substituents of the borylimido ligand, in addition to electronic effects which will be discussed below with the aid of DFT calculations.

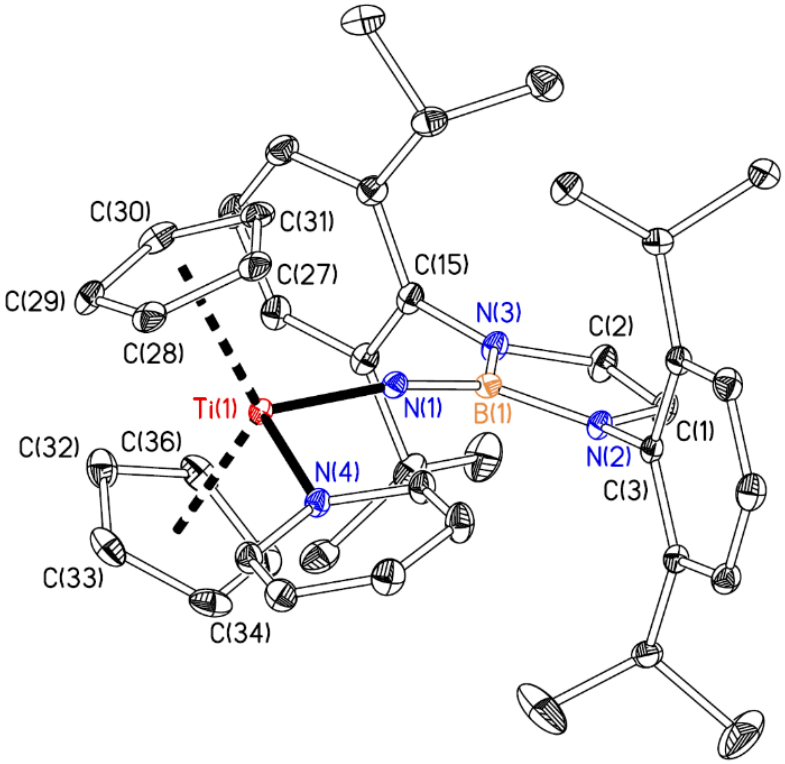

Figure 3.8. Displacement ellipsoid plot (20% probability) of $Cp_2Ti\{NB(NAr'CH)_2\}(py)$ (**12**). H atoms are omitted for clarity.

Table 3.3. Selected bond distances (Å) and angles (°) for $Cp_2Ti\{NB(NAr'CH)_2\}(py)$ (**12**). $Cp_{cent(1)}$ and $Cp_{cent(2)}$ refer to the computed Cp ring centroids for "upper" and "lower" Cp rings, respectively, as depicted in Figure 3.8.

Ti(1)–N(1)	1.7549(13)	$Cp_{cent(1)}$–Ti(1)–N(1)	113.8
Ti(1)–N(4)	2.2523(14)	$Cp_{cent(2)}$–Ti(1)–N(1)	111.3
Ti(1)–$Cp_{cent(1)}$	2.22	$Cp_{cent(1)}$–Ti(1)–N(4)	99.2
Ti(1)–$Cp_{cent(2)}$	2.14	$Cp_{cent(2)}$–Ti(1)–N(4)	106.4
N(1)–B(1)	1.426(2)	$Cp_{cent(1)}$–Ti(1)–$Cp_{cent(2)}$	125.1
B(1)–N(2)	1.455(2)	N(1)–Ti(1)–N(4)	95.11(5)
B(1)–N(3)	1.462(2)	Ti(1)–N(1)–B(1)	159.65(12)
		N(1)–B(1)–N(2)	128.69(14)
		N(1)–B(1)–N(3)	128.45(14)

The molecular structures of **12** and its imido and hydrazido analogues **1.2** and **1.68** appear, at first sight, to be twenty valence electron species.[7,8] Using the neutral counting method, the titanium centre provides four electrons, the two Cp rings provide five electrons each, pyridine provides two electrons and imido ligands (and derivatives) are considered to donate four electrons. Previous computational studies of titanocene complexes have described the frontier orbitals of the Cp_2Ti^{2+} fragment.[47,48] The LUMO, LUMO+1 and LUMO+2 are all Ti–Cp non-bonding orbitals within the equatorial plane. The LUMO+3 and LUMO+4 are Ti–Cp π* anti-bonding orbitals which lie perpendicular to the equatorial plane. Considered together, these MOs allow for two σ interactions and one π interaction with donor ligands in the equatorial plane, and a second π interaction may only feasibly take place using the Ti–Cp π* LUMO+3. Considering the coordination environment of **12**, coordination of the pyridine donor ligand takes place using one σ orbital in the equatorial plane with the other involved in the σ bond of the borylimido ligand. To elucidate the π bonding situation, DFT calculations (B3PW91) were performed on a model of the borylimide **12**, $Cp_2Ti\{NB(NMeCH)_2\}(py)$ (**12_B(NMeCH)$_2$**), by Simona Mellino of this research group. The HOMO and HOMO–1 are shown in Figure 3.9. The HOMO is a Ti–N π bond in the equatorial plane which uses the N lone pair perpendicular to the boryl ring

and is destabilised by an antibonding interaction with the filled π orbitals of the ring, like the model half-sandwich compound **2Q_B(NMeCH)$_2$** described above. In contrast, the HOMO–1 is a formally non-bonding orbital based on the borylimido and two Cp ligands, with little electron density at the Ti centre. This is the basis of the apparent twenty valence electron count, where in fact the two "excess" electrons are found in this non-bonding orbital. Partial donation of electron density into the Ti–Cp π* orbitals does take place, however, and this results in incomplete donation from both the borylimido ligand and the Cp rings, giving an overall lengthening of the respective bond distances in the real compound **12**. This effect has previously been described in the hydrazide **1.68**, and other Group 4 – 6 complexes of the type $Cp^R_2M(E)(L)$ (E = O, or NR; L = two- or one-electron donor or none).[8,48–54] In this case, this also explains the significant tilting of one of the Cp rings in **12**, as the ligands compete for the same acceptor orbitals on the Ti centre, as well as the degree of non-linearity in the Ti–N–B linkage.

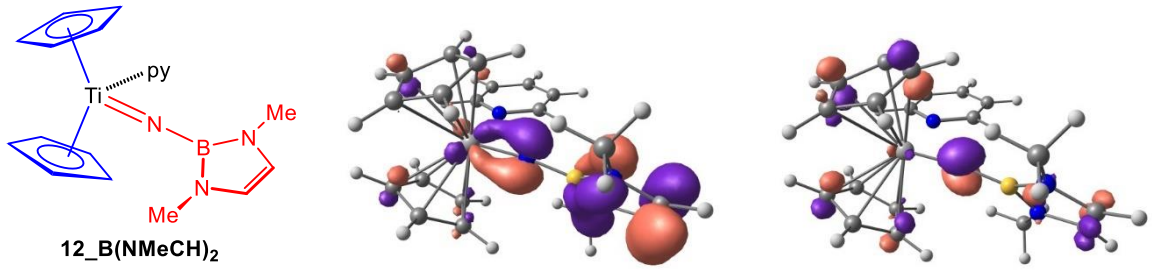

Figure 3.9. DFT model compound $Cp_2Ti\{NB(NMeCH)_2\}(py)$ (**12_B(NMeCH)$_2$**) and associated isosurfaces and energies of the two π components of the Ti–N linkages.

3.5 Synthesis of Cp-half-sandwich borylimido complexes

Given the formation of the sandwich compound **12** from $Ti\{NB(NAr'CH)_2\}Cl_2(py)_3$ (**3**) and 2 equiv. NaCp, the formation of a half-sandwich complex from the same starting material and 1 equiv. NaCp was next targeted. However, when this reaction was attempted on the NMR tube scale, the resulting ^{1}H NMR spectrum showed a mixture of the starting material **3**, the sandwich compound **12**, and a species that was assigned as the desired half-sandwich compound (based on NMR signal integrations). Instead, a redistribution methodology was employed, in which a 1:1 mixture of **3** and **12** in toluene solution was heated at 70 °C over 5 days, resulting in conversion of the two starting materials to $CpTi\{NB(NAr'CH)_2\}Cl(py)$ (**13**) in 75% isolated yield (Scheme 3.2). The analogous reaction in a *tert*-butylimido system, between $Ti(N^tBu)Cl_2(py)_2$ and $Cp_2Ti(N^tBu)(py)$ (**1.2**)

was reported to be much more facile, taking only 12 h at RT.[7] Considering the lability of the Cp ligand in **12** as discussed above, the more forcing conditions and longer reaction time required in this case are presumably due to the greater steric bulk of the borylimido ligand raising the barrier to reaction. This seems especially important when it is noted that this reaction involves the approach of – and ligand exchange between – two molecules which *both* contain a bulky borylimido ligand. The ^{1}H NMR spectrum of **13**, being analogous to that of the Cp* homologue **9**, indicates a C_1 symmetric species in solution: restricted rotation of the Ar' moieties results in four CHMeMe doublets (although two are partially overlapped and are observed as an apparent triplet).

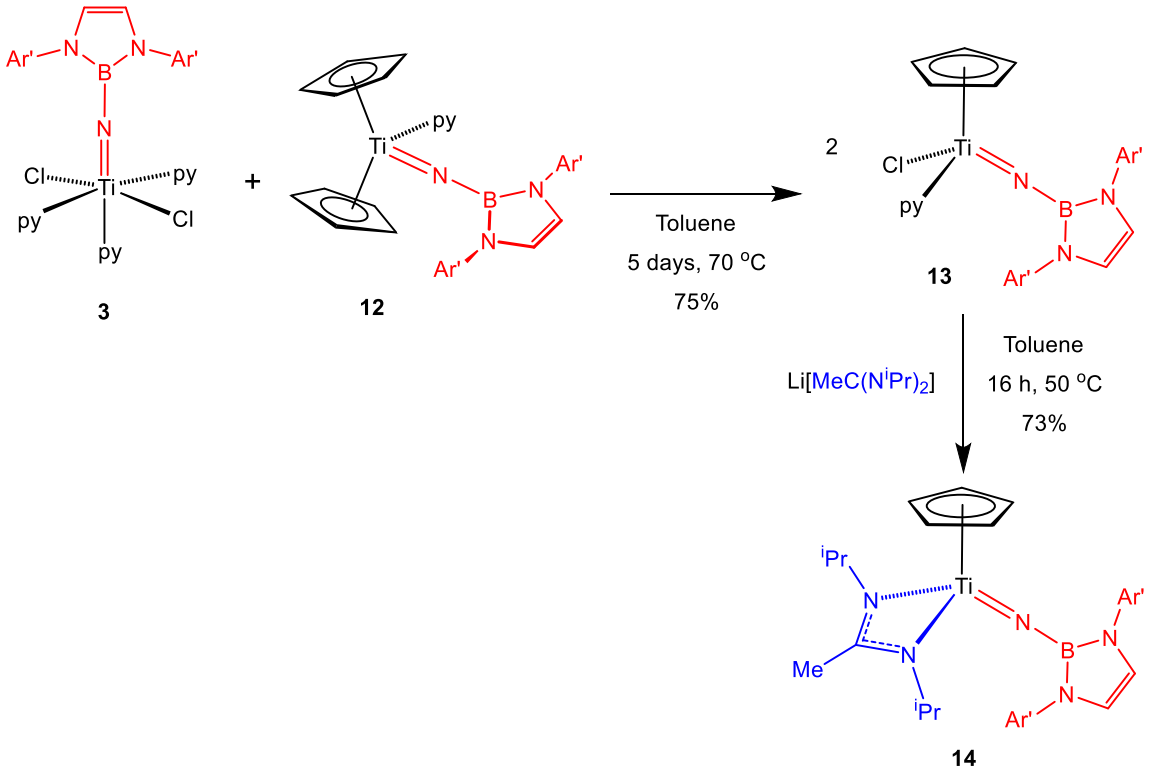

Scheme 3.2. Synthesis of CpTi{NB(NAr'CH)$_2$}Cl(py) (**13**) and CpTi{MeC(N^{i}Pr)$_2$}{NB(NAr'CH)$_2$} (**14**).

Mindful of the earlier failure of the Cp* analogue **9** to react with Li[MeC(N^{i}Pr)$_2$], which was ascribed to steric constraints, the use of **13** as a borylimido synthon was tested through its reaction with that lithiated ligand. Interestingly, reaction of **13** and Li[MeC(N^{i}Pr)$_2$] in toluene solution at 50 °C over 16 h resulted in the formation of CpTi{MeC(N^{i}Pr)$_2$}{NB(NAr'CH)$_2$} (**14**) in 73% isolated yield. The ^{1}H NMR spectrum of **14** in C_6D_6 solution is consistent with a C_s symmetric structure: the N-bound isopropyl groups of the supporting ligand are chemically equivalent, giving one CHMeMe septet and

two CHMeMe doublets, as are the isopropyl groups on the borylimido moiety. Unfortunately, diffraction-quality crystals of neither **13** nor **14** could be obtained from a variety of crystallisation methods, presumably due to the reduced domination of molecular shape and packing by the Cp ligand (compared to Cp*).

3.6 Reactivity of Cp*-half-sandwich titanium borylimido complexes

3.6.1 Reactions with CO_2 and CS_2

When a C_6D_6 solution of Cp*Ti(hpp){NB(NAr'CH)$_2$} (**10**) in an NMR tube was exposed to an atmosphere of CO_2, and the reaction progress followed by ^{1}H NMR spectroscopy, slow conversion to a single product was observed over 2.5 days at RT. The appearance of a yellow precipitate and change in the colour of the solution from deep red to orange were accompanied by the gradual loss of all signals corresponding to the hpp ligand from the reaction ^{1}H NMR spectra. In contrast, no reaction occurred between **10** and CS_2 at RT on the NMR tube scale, although a reaction between the two progressed smoothly over 3.5 days at 80 °C. In this case, no precipitate was formed, and the reaction ^{1}H NMR spectra showed new resonances corresponding to the hpp ligand.

In view of analogous reactions of titanium imido and hydrazido complexes with CO_2 and CS_2 (Section 3.2),[9,11,13,16] initial [2+2] cycloaddition of the heteroallene with the Ti–N multiple bond was expected, potentially followed by extrusion of a boryl-functionalised organic. Scaling up of the two above reactions, and separation of the two products formed in each case, confirmed the reactions to be overall functional group transfer of the borylimido unit onto CE_2 to form ECNB(NAr'CH)$_2$ (E = O (**15**), S (**16**)), a borylisocyanate and borylisothiocyanate, respectively. The second E atom of CE_2 goes to form one half of the respective oxo- or sulfido-bridged titanium dimer [Cp*Ti(hpp)(μ-E)]$_2$ (E = O (**17**), S (**18**); Scheme 3.3). On the preparative scale, the boryl-functionalised organics were obtained as the filtrate of hexane separations, with the relatively insoluble titanium dimers remaining behind. The oxo-bridged dimer **17** was found to be insoluble also in benzene, explaining its precipitation from C_6D_6 on the NMR tube scale and the loss of its signals from the ^{1}H NMR spectrum, whilst the sulfido-bridged **18** was much more soluble in benzene, explaining the differing observations in this respect.

The organic reaction products **15** and **16** were also prepared through an alternative route, inspired by previous work on boryliso(thio)cyanates by Lappert and Weber (*vide infra*).[55,56]

Salt metathesis reactions of $BrB(NAr'CH)_2$ with AgOCN or AgSCN in MeCN solution produced **15** and **16** in 71 and 81% isolated yields, respectively (Equation 3.3).

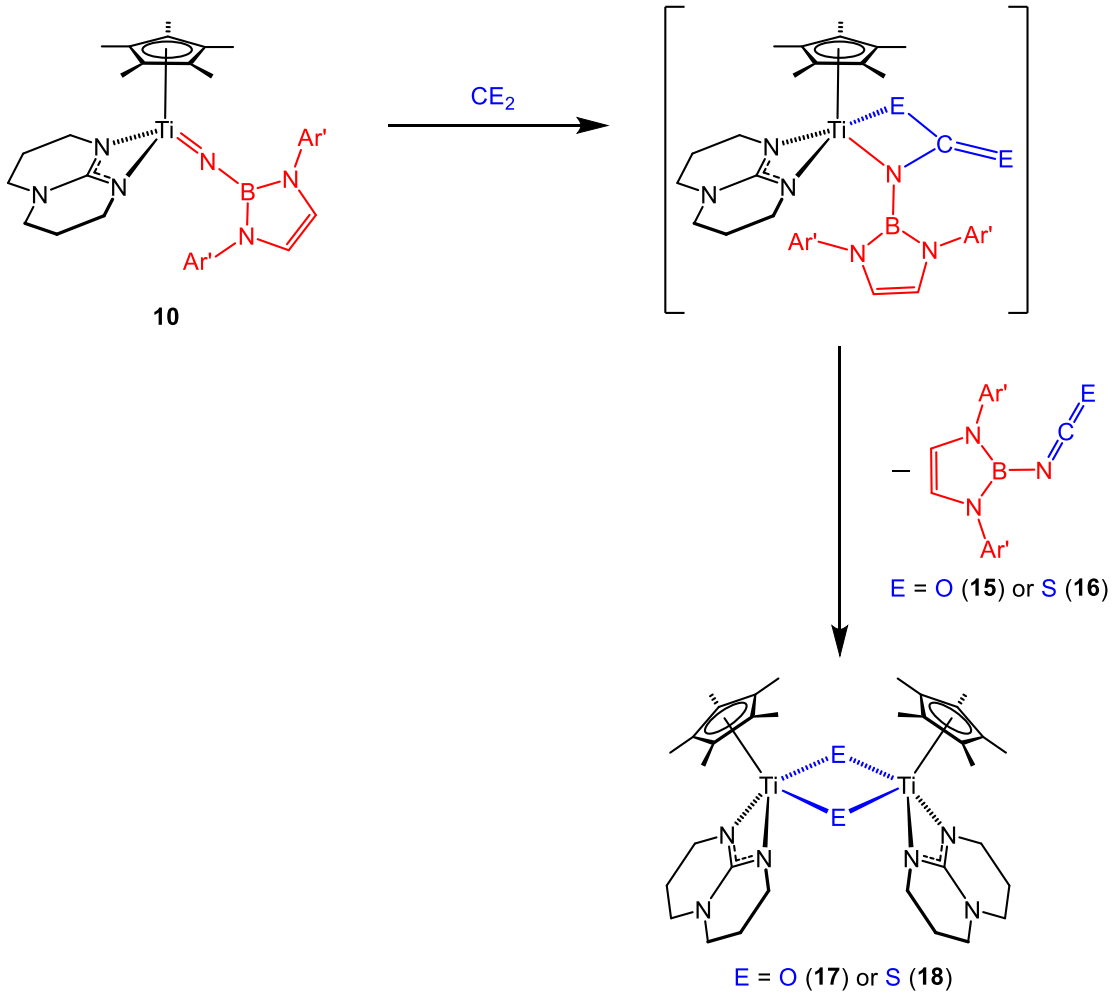

Scheme 3.3. Reactions of Cp*Ti(hpp){NB(NAr'CH)$_2$} (**10**) with CO_2 and CS_2. Reaction conditions: E = O: Benzene, RT, 2.5 days; E = S: Toluene, 80 °C, 3.5 days. Note: **17** exists as both *cis* and *trans* isomers.

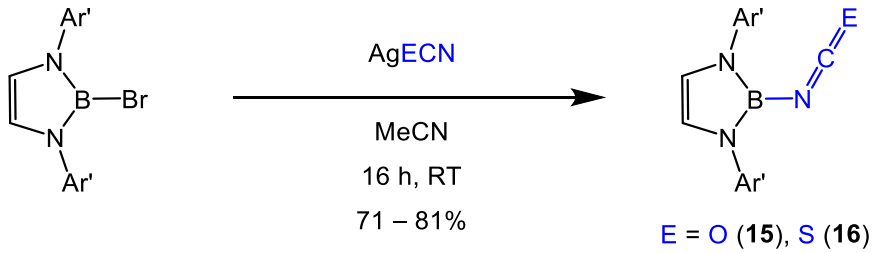

Equation 3.3

The characterisation of all four of these compounds will now be described, starting with the boryl-functionalised organics **15** and **16**, then followed by the titanium dimers **17** and **18**. The ^{1}H NMR spectra of the borylisocyanate **15** and the borylisothiocyanate **16** both display the expected resonances of the boryl moiety, including a septet (4 H) and two doublets (12 H each) attributed to the four isopropyl groups, and a singlet (2 H) attributed to the protons on the boryl ring backbone, in addition to overlapping multiplets in the aromatic region. In the ^{13}C NMR spectra, very low intensity signals corresponding to the central carbon in the iso(thio)cyanate moiety are observed at 125.7 and 143.2 ppm, in **15** and **16**, respectively. These are similar to those reported in the analogous compounds ECNB(N^{t}BuCH)$_2$ (E = O (**3.7**), S (**3.8**)) which were synthesised by Weber *et al.* through salt metathesis reactions of ClB(N^{t}BuCH)$_2$ with AgECN, these ^{13}C chemical shifts being 123.9 and 140.5 ppm respectively.[56] These are all comparable to those values found in organic iso(thio)cyanates generally; for example, the corresponding ^{13}C signal is 121.5 ppm in MeNCO, and 128.7 ppm in MeNCS.[57] IR spectroscopy was also used to characterise the compounds **15** and **16**. Of particular note are the very intense bands at 2305 and 2092 cm^{-1}, respectively, which are assigned to the antisymmetric stretches of the NCE units.[57] Again, these values are comparable to those reported by Weber *et al.* in **3.7** and **3.8**: 2317 and 2122 cm^{-1} respectively.[56] In 1965, Lappert *et al.* reported the preparation of a wide range of boryliso(thio)cyanates *via* salt metathesis reactions of boryl halides with the respective silver salt,[55] and these were later characterised by IR spectroscopy.[58] The reported NCE antisymmetric stretches in these compounds are also found at similar frequencies; to highlight just two examples, (Me$_2$N)$_2$BNCO has a sharp band at 2289 cm^{-1} and (Me$_2$N)$_2$BNCS has a similar band at 2105 cm^{-1}. The corresponding symmetric stretches of the NCE units in **15** and **16** would be expected to give relatively weak bands around 1400 and 700 cm^{-1} respectively.[57] However, given the presence of many other bands in these regions of the IR spectra, assignments were not possible.

Diffraction-quality crystals of both **15** and **16** were grown from hexane solutions at –30 °C, and the compounds then structurally characterised. The molecular solid state structures are shown in Figure 3.10, along with selected bond lengths and angles in Table 3.4. Both of the NCE units are very close to linearity, with N(1)–C(1)–E(1) angles of 176.76(16) (E = O) and 175.4(3)° (E = S). The B(1)–N(1)–C(1) angles of the two compounds are also similar (159.55(13) and 156.0(6)° respectively), although it is noted that these angles are closer to those expected for sp-hybridised N (180°) than for sp^2-hybridised N (120°).

Similar observations have been made in the previously reported NHC-supported boryliso(thio)cyanates {IDipp}–BH_2NCE (**3.9**, IDipp = *N*,*N*'-bis(2,6-diisopropylphenyl)imidazol-2-ylidene), and were ascribed to stabilisation of a resonance form containing an N≡C triple bond in which a positive charge on the nitrogen sits next to the negative boron (**3.9b**, Equation 3.4).[59] In both compounds **15** and **16**, the iso(thio)cyanate moiety is almost coplanar with the boryl ring, presumably to maximise conjugation of the N=C=E π bonds with the boryl π-system. The associated N(2)–B(1)···N(1)–C(1) dihedral angles are *ca* 23° in **15** and *ca* 5 or 14° in **16** (the two different values arising from positional disorder of the NCS group in the solid state structure).

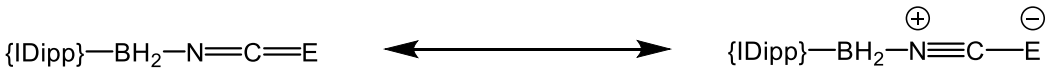

3.9a **3.9b**

Equation 3.4[59]

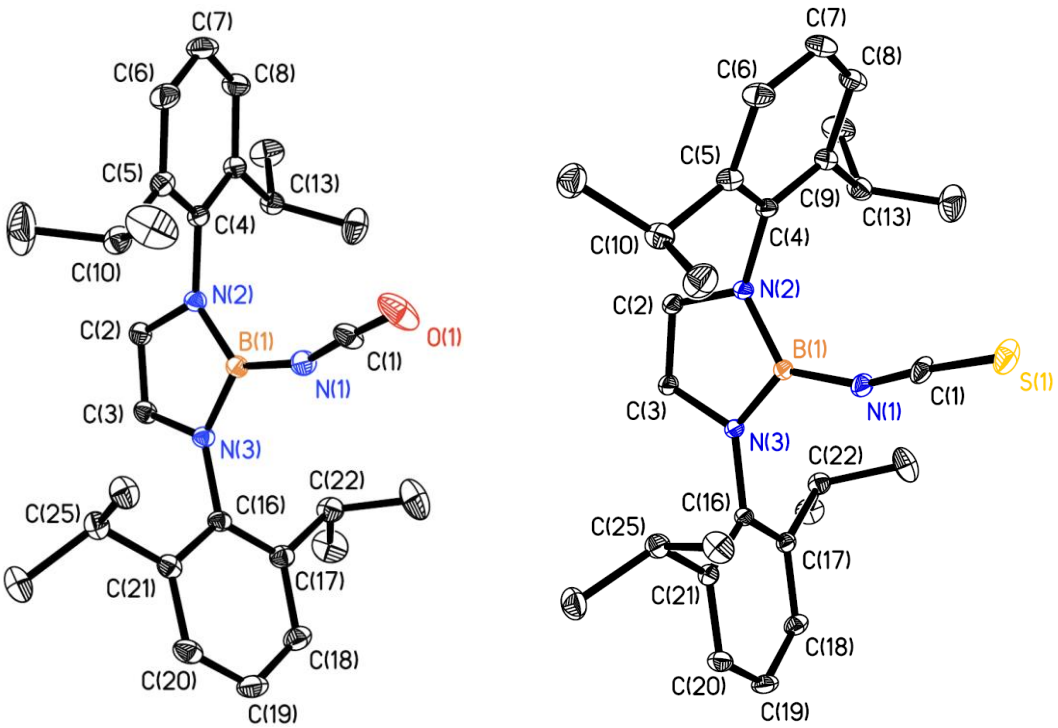

Figure 3.10. Displacement ellipsoid plots (25% probability) of ECNB(NAr'CH)$_2$ (E = O (**15**, left), S (**16**, right)). H atoms are omitted for clarity.

Table 3.4. Selected bond lengths (Å) and angles (°) for ECNB(NAr'CH)$_2$ (E = O (**15**), S (**16**)).

Parameter	**15**	**16**
B(1)–N(1)	1.4388(16)	1.4429(16)
B(1)–N(2)	1.4201(16)	1.4164(16)
B(1)–N(3)	1.4161(16)	1.4151(16)
N(1)–C(1)	1.1688(16)	1.169(5)
C(1)–E(1)	1.1754(17)	1.585(2)
N(1)–B(1)–N(2)	127.23(11)	125.09(11)
N(1)–B(1)–N(3)	126.14(11)	127.93(11)
B(1)–N(1)–C(1)	159.55(13)	156.0(6)
N(1)–C(1)–E(1)	176.76(16)	175.4(3)

Next, attention is turned to the characterisation of the oxo- and sulfido-bridged dimeric complexes **17** and **18**. The ^{1}H NMR spectrum of oxo-bridged **17** in CD_2Cl_2 is consistent with the presence of two isomeric forms of the complex; two $C_5\underline{Me}_5$ singlets are observed, as well as two sets of resonances belonging to the hpp ligands. It is proposed that these are *cis* and *trans* isomers arising from differing substitution of the Cp* and hpp ligands around the Ti_2O_2 core. In contrast, the ^{1}H NMR spectrum of the sulfido-bridged **18** in C_6D_6 displays resonances consistent with only one compound; one $C_5\underline{Me}_5$ singlet and one set of hpp resonances. To shed more light on the respective structures, diffraction-quality crystals of both compounds were successfully grown and then were structurally characterised. The molecular solid state structures are shown in Figure 3.11, and selected bond lengths and angles in Table 3.5.

The solid state structure obtained of **17** contains only the *trans* isomer (***trans*-17**) of the two observed by ^{1}H NMR spectroscopy (although it is not known if this is the major or minor isolated isomer). In contrast, the crystallographic characterisation of **18** shows that its single isolated structure is the *cis*-oriented form. Furthermore, whilst all four atoms of the $Ti_2(\mu\text{-}O)_2$ core of ***trans*-17** are coplanar (this being necessary due to the molecule sitting on a crystallographic inversion centre), the $Ti_2(\mu\text{-}S)_2$ core of **18** has a puckered or "butterfly"

geometry with, instead, a crystallographic mirror plane passing through the S atoms of the molecule. The fold angle here is *ca* 155°, with the puckering appearing to be necessary to prevent steric clash between the two *cis*-oriented Cp* ligands.

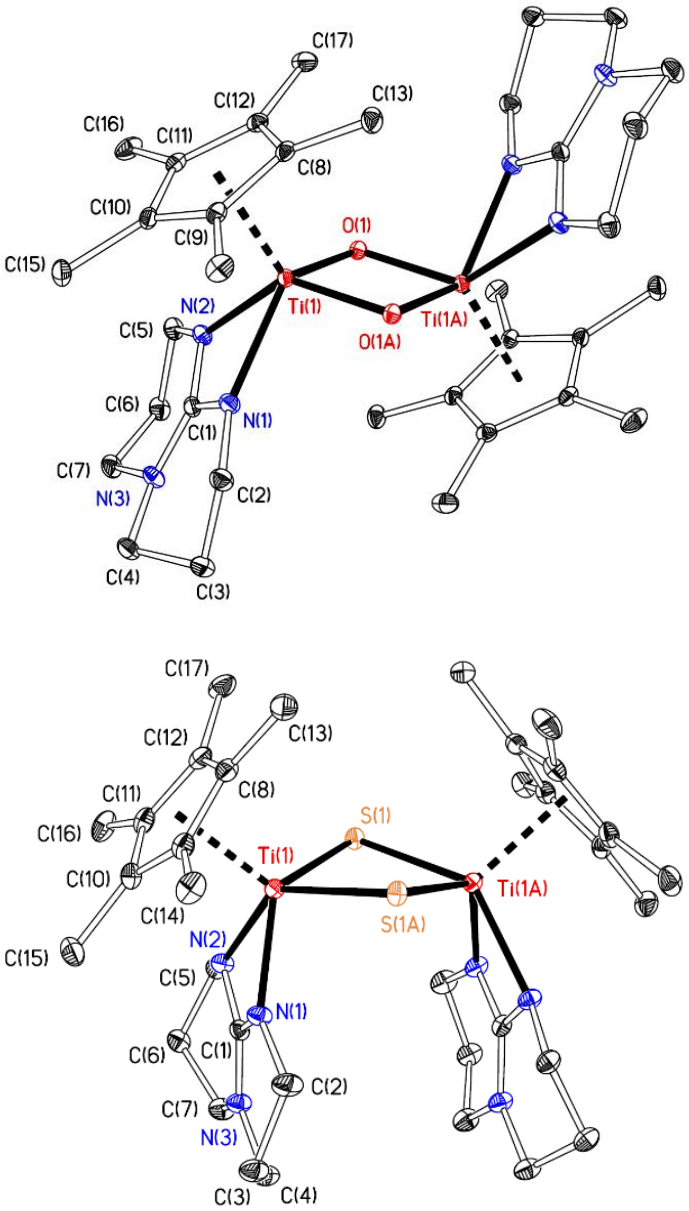

Figure 3.11. Top: Displacement ellipsoid plot (20% probability) of *trans*-[Cp*Ti(hpp)(μ-O)]$_2$ (***trans*-17**). H atoms are omitted for clarity. Atoms carrying the suffix 'A' are related to their counterparts by the symmetry operator [1–*x*,1–*y*, –*z*]. Bottom: Displacement ellipsoid plot (20% probability) of [Cp*Ti(hpp)(μ-S)]$_2$ (**18**). H atoms are omitted for clarity. Atoms carrying the suffix 'A' are related to their counterparts by the symmetry operator [–*x*, *y*, ½–*z*].

Table 3.5. Selected bond lengths (Å) and angles (°) for *trans*-[Cp*Ti(hpp)(μ-O)]$_2$ (***trans*-17**) and [Cp*Ti(hpp)(μ-S)]$_2$ (**18**). E = O or S, respectively. Cp$_{cent}$ refers to the computed η^5-C$_5$Me$_5$ ring centroids.

Parameter	***trans*-17**	**18**
Ti(1)–E(1)	1.8506(11)	2.3025(5)
Ti(1)–E(1A)	1.8825(11)	2.3965(5)
Ti(1)–N(1)	2.1240(15)	2.0864(16)
Ti(1)–N(2)	2.1623(14)	2.1600(15)
Ti(1)–Cp$_{cent}$	2.09	2.08
E(1)–Ti(1)–E(1A)	83.04(5)	88.644(18)
E(1)–Ti(1)–N(1)	128.76(6)	137.24(5)
E(1)–Ti(1)–N(2)	89.71(5)	86.02(4)
N(1)–Ti(1)–N(2)	61.61(6)	62.23(6)
E(1)–Ti(1)–Cp$_{cent}$	114.4/117.8	111.3/119.8
N(1)–Ti(1)–Cp$_{cent}$	111.5	112.3
N(2)–Ti(1)–Cp$_{cent}$	108.5	107.1
Ti(1)–E(1)–Ti(1A)	96.96(5)	88.694(17)

Both ***trans*-17** and **18** may also be compared with structural analogues of the type [Cp*Ti{RC(NR')$_2$}(μ-E)]$_2$ which contain bidentate amidinate ligands. Two such analogues exist for ***trans*-17** (E = O), where R' = ^{i}Pr, and R = Me (**3.10**) or Ph (**3.11**).[9,11,19] The bond metrics of the Ti$_2$(μ-O)$_2$ core in ***trans*-17** are comparable to those of both literature compounds. However, the Ti–Cp$_{cent}$ distance in ***trans*-17** of 2.093 Å is slightly shorter than those in **3.10** and **3.11**: 2.130 and 2.138/2.143 Å, respectively. Likewise, the Ti–N bond lengths to the bidentate ligand are slightly shorter in ***trans*-17** than in **3.10** and **3.11**. These effects are attributed to the reduced steric demand of the hpp ligand when compared to the amidinate ligands of the latter two complexes, and are similar to cases where the Cp* ligands are replaced with less bulky Cp-derivatives such as C$_5$H$_4$Me.[11] Only one amidinate-bound analogue of the sulfido-bridged **18** has been structurally characterised: [Cp*Ti{PhC(NSiMe$_3$)$_2$}(μ-S)]$_2$ (**3.12**), this being exclusively the *trans* isomer. The Ti–S

bond lengths of **18** (2.3025(5) and 2.3965(5) Å) are longer than those in **3.12** (2.259(1) Å), and this may be attributed to reduced orbital overlap due to the aforementioned puckering of the molecule. It is noted that this puckering, combined with differing isomerism (*cis* rather than *trans*-arrangement) may preclude any further direct comparison between the structures of **18** and **3.12**.

The mechanism of the reactions of titanium imides and hydrazides with CO_2 and CS_2 are well established.[11,13,16] As described above, initial cycloaddition to form a (thio)carbamate complex takes place (this compound often being isolable), with further reaction resulting in extrusion of an iso(thio)cyanate *via* retro-[2+2], or (for CO_2 only) giving a "double insertion" product such as **3.5** (Figure 3.1). In an attempt to observe a carbamate-type intermediate in the reaction of the borylimide **10** with CO_2, the reaction was monitored at 198 K by NMR spectroscopy. Although the ^{1}H spectra obtained at this temperature appeared rather complex, resonances attributed to the borylisocyanate **15** (one of the final products) were observed, showing that, even at this low temperature, any carbamate-type intermediate must be very short-lived. Nevertheless, a low intensity multiplet was observed at 4.64 ppm and assigned to an hpp methylene proton, with such a high chemical shift for this ligand being indicative of a crowded metallacycle, based on other results obtained within our research group.[60] Although the reaction of **10** with CS_2 required high temperatures, the reaction was monitored on the NMR tube scale and a ^{1}H NMR spectrum obtained at RT part-way through the reaction. However, no evidence of any intermediate could be observed this way. Thus, the extremely short-lived nature of the putative carbamate-type intermediates precluded isolation of these compounds.

Previous work from our research group has investigated the effect of different imido functionalities on the outcome and rate of reactions with CO_2.[11] It was shown that increased steric bulk favours isocyanate extrusion (rather than "double insertion") by stabilising the extrusion product, as well as increasing the energy of the transition state on the path to a second CO_2 insertion. With this in mind, it is unsurprising that the very bulky borylimide **10** gives only extrusion of the borylisocyanate **15**. Futhermore, the transition state on the final step of isocyanate extrusion is stabilized by increased steric bulk, thus this explains why the carbamate-type intermediate was observed to be very short-lived and was not isolable in this case.

In the same way as with **10**, reactions were attempted between Cp*Ti($N^{pyr}N^{Me_2}$){NB(NAr'CH)$_2$} (**11**) and both CO_2 and CS_2. When **11** was exposed to an atmosphere of CO_2 on the NMR tube scale in C_6D_6, smooth formation of the borylisocyanate **15** was observed, along with a new set of resonances belonging to the bidentate ligand; in this case no precipitate was formed. In contrast, no reaction was observed between **11** and CS_2 on the NMR tube scale, even with extended heating at 80 °C. It is proposed that the absence of any reaction with CS_2 in this case is steric in origin, with the NMe_2 group of the $N^{pyr}N^{Me_2}$ ligand giving greater steric protection at the metal centre compared with hpp. This is sufficient to prevent CS_2 from approaching the metal centre, but not the smaller CO_2. The reaction between **11** and CO_2 was performed on the preparatory scale in benzene, and the two products separated using pentane: **15** was isolated from a recrystallisation of the pentane solution, whilst the oxo-bridged dimer [Cp*Ti($N^{pyr}N^{Me_2}$)(μ-O)]$_2$ (**19**) was isolated through a recrystallisation of the remaining yellow solid from warm hexane. Analysis of the ^{1}H NMR spectrum of **19** shows the presence of only one isomer. However, given that the solid state structure could not be obtained, it is not known if this is the *cis* or *trans* isomer.

3.6.2 Reactions of Cp*Ti(hpp){NB(NAr'CH)$_2$} (10) with primary amines

In Section 3.3.1, the failure of a solution phase reaction between Cp*Ti(N^tBu)Cl(py) (**1.8**) and H_2NB(NAr'CH)$_2$ (**2.2**) to form the borylimido complex Cp*Ti{NB(NAr'CH)$_2$}Cl(py) (**9**) was described. Instead, a melt reaction was required to drive the desired reaction to completion. This was in stark contrast to our research group's previous work, where exchange of the *tert*-butylimido group of **1.8** with an aniline or H_2NNPh_2 was found to be relatively facile, yielding the respective arylimide or hydrazide.[8,21] It was suspected that the differing behaviour in this case was due to the borylamine being insufficiently acidic to effect protonolytic exchange of the *tert*-butylimido ligand, as compared to other amine derivatives (including anilines and N,N-diphenylhydrazine) for which this type of reaction is successful. Computational work later in this Chapter probes in detail the underlying factors for the success or failure of these amine/imide exchange reactions.

As a comparison to the hpp-supported borylimide **10**, the *tert*-butylimido analogue, Cp*Ti(hpp)(N^tBu) (**20**), was prepared from **1.8** and Li[hpp]. Given access to both **10** and **20** independently of each other, these hpp-supported compounds were used as a platform to investigate imido/borylimido ligand exchange reactions by protonolysis. A 1:1 mixture

of the imide **20** and borylamine **2.2** in C_6D_6 solution with gentle heating settled to an equilibrium mixture of **20** and Cp*Ti(hpp){NB(NAr'CH)$_2$} (**10**) in the ratio *ca* 70:30 (by NMR integration). The reverse reaction (i.e. starting with a 1:1 mixture of the borylimide **10** and H_2N^tBu) also formed the same equilibrium mixture (Equation 3.5). The Gibbs free energy change (Δ_rG) of the forward reaction was calculated to be 1.0 kcal mol^{-1} at 298 K from the measured equilibrium constant (K_{eq}) of 0.184. DFT calculations (B3PW91 functional and Def2TZVP basis set with solvent and d3(bj) dispersion correction, by Prof. Philip Mountford) gave a Δ_rG value of –0.6 kcal mol^{-1}, which is in good agreement with a reaction in finely balanced equilibrium.

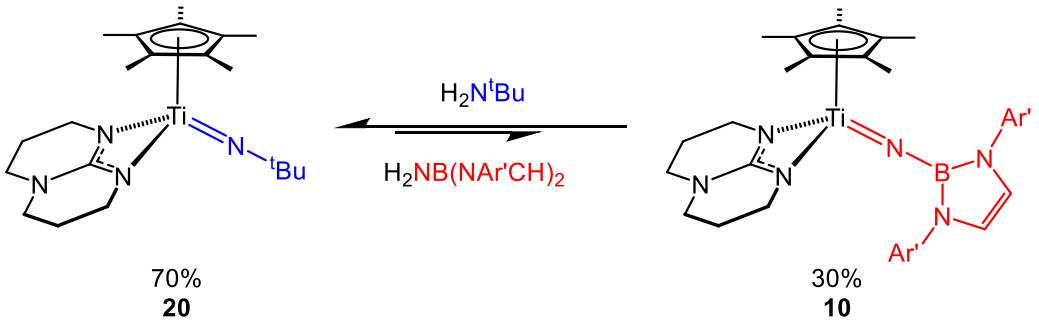

Equation 3.5

Next, the borylimide **10** was reacted with two anilines, H_2NTol and H_2NXyl (Xyl = 2,6-$C_6H_3Me_2$), on the NMR tube scale. Complex **10** underwent immediate 50% conversion to the bis(anilido) compound Cp*Ti(hpp)(NHTol)$_2$ (**21**) when reacted with 1 equiv. of H_2NTol, and quantitative conversion to the same compound was achieved with 2 equiv. of the amine (Scheme 3.4). In contrast, **10** reacted instantaneously with 1 equiv. of H_2NXyl to quantitatively form the xylylimido complex Cp*Ti(hpp)(NXyl) (**22**). The DFT-computed Δ_rG value of –6.1 kcal mol^{-1} for this reaction is consistent with a quantitative process. Further DFT studies are described in the following Section. Both **21** and **22** were also independently synthesised on the preparative scale from the *tert*-butylimide **20** and the respective aniline in toluene. The preference of H_2NTol to form the bis(anilide) **21** (from both imido and borylimido starting materials) rather than an arylimide like **22** is proposed to be due to the reduced steric profile of the *p*-tolyl moiety compared with the 2,6-disubstituted Xyl group.

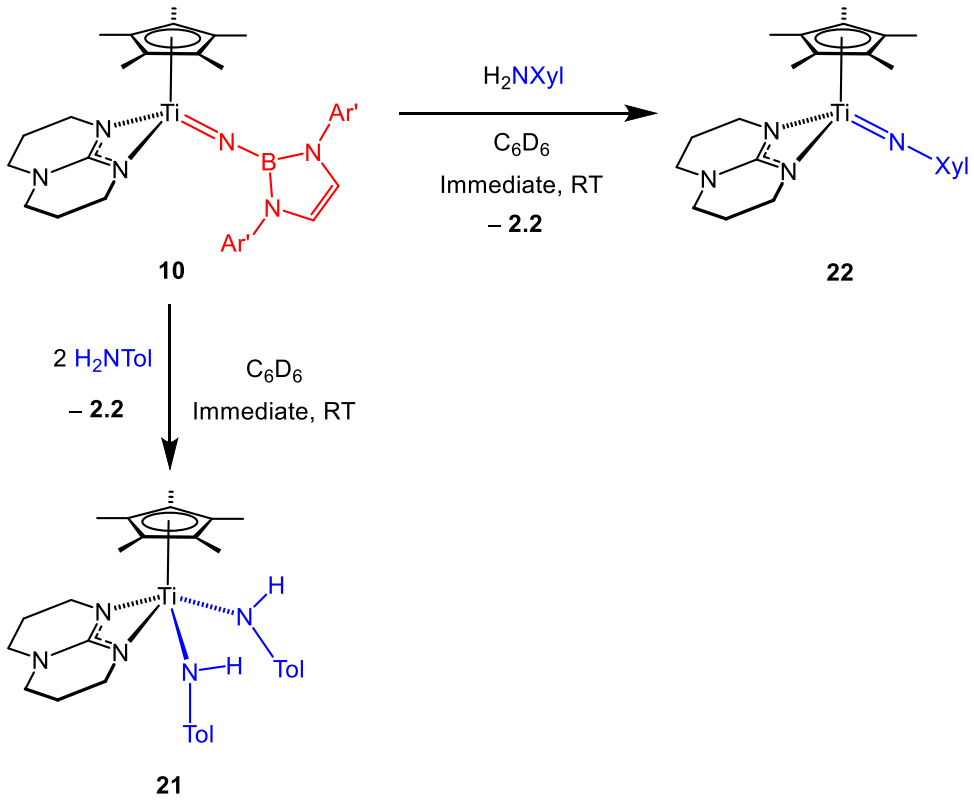

Scheme 3.4. Borylimido ligand exchange reactions of Cp*Ti(hpp){NB(NAr'CH)$_2$} (**10**) with H_2NXyl and H_2NTol.

Diffraction-quality crystals of both the *tert*-butylimide **20** and the bis(anilide) **21** were successfully grown, and the solid state structures obtained. The molecular structures are depicted in Figure 3.12, and selected bond lengths and angles are listed in Table 3.6. The Ti–N_{im} bond length in **20** of 1.7081(18) Å is much shorter than that in the borylimido analogue **10** (1.7433(19) Å), this difference being in line with previous discussion of trends in titanium–nitrogen multiple bond lengths in the borylimides **1**, **3** and **9**, with their respective imido analogues.

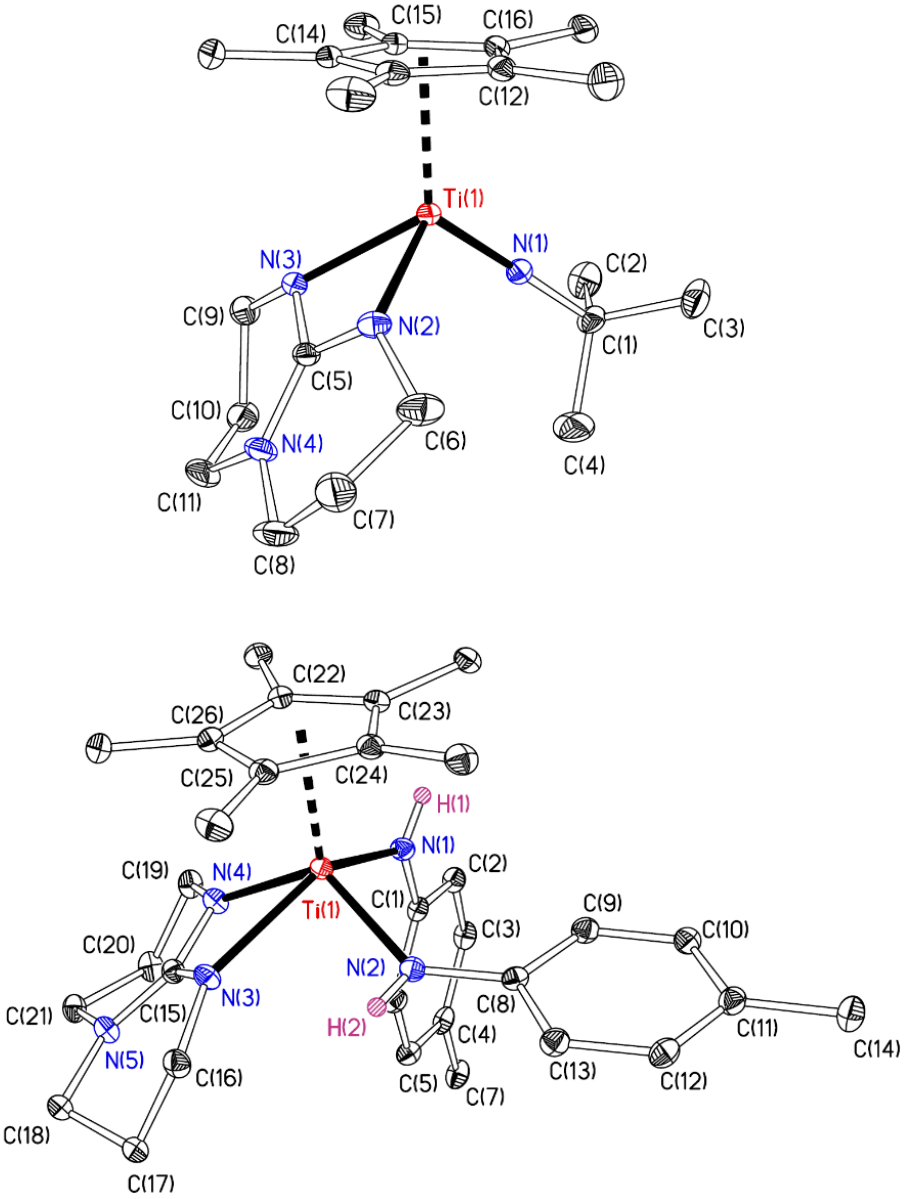

Figure 3.12. Displacement ellipsoid plots (20% probability) of Cp*Ti(hpp)(N^{t}Bu) (**20**, top) and Cp*Ti(hpp)(NHTol)$_2$ (**21**, bottom). C-bound H atoms are omitted for clarity. H(1) and H(2) of **21** are drawn as spheres of an arbitrary radius.

Table 3.6. Selected bond lengths (Å) and angles (°) for Cp*Ti(hpp)(N^{t}Bu) (**20**) and Cp*Ti(hpp)(NHTol)$_2$ (**21**). Cp$_{cent}$ refers to the computed η^5-C$_5$Me$_5$ ring centroids.

Parameter	**20**	**21**
Ti(1)–N(1)	1.7081(18)	1.9769(15)
Ti(1)–N(2)	2.0748(19)	1.9956(15)
Ti(1)–N(3)	2.0875(18)	2.1910(14)
Ti(1)–N(4)	-	2.0680(15)
Ti(1)–Cp$_{cent}$	2.08	2.07
N(1)–C(1)	1.449(3)	1.389(2)
N(2)–C(8)	-	1.388(2)
N(1)–H(1)	-	0.86(2)
N(2)–H(2)	-	0.82(2)
N(1)–Ti(1)–Cp$_{cent}$	127.3	109.0
N(2)–Ti(1)–Cp$_{cent}$	116.6	118.1
N(3)–Ti(1)–Cp$_{cent}$	117.9	110.9
N(4)–Ti(1)–Cp$_{cent}$	-	113.7
N(1)–Ti(1)–N(2)	106.37(9)	94.58(6)
N(1)–Ti(1)–N(3)	106.83(8)	136.58(6)
N(1)–Ti(1)–N(4)	-	86.72(6)
N(2)–Ti(1)–N(3)	65.23(8)	81.55(6)
N(2)–Ti(1)–N(4)	-	124.44(6)
N(3)–Ti(1)–N(4)	-	61.96(6)
Ti(1)–N(1)–C(1)	178.32(18)	128.23(12)
Ti(1)–N(2)–C(8)	-	137.95(12)
Ti(1)–N(1)–H(1)	-	121.0(16)
Ti(1)–N(2)–H(2)	-	106.0(16)

3.7 Computational studies of imido ligand exchange reactions

The facile protonolysis of the borylimido ligand by the two anilines as described above, along with the equilibrium mixture obtained with H_2N^tBu, are noted as being examples of behaviour very different to previously studied arylimido and hydrazido ligands. The particularly strong basicity of the borylimido ligand was previously discussed in Section 2.5, and DFT calculations will now be employed to investigate the energetics of bond scission and formation in these amine exchange reactions.

In DFT calculations performed by Simona Mellino and Prof. Philip Mountford, gas-phase electronic SCF energies were calculated for the hypothetical isodesmic reactions depicted in Figure 3.13, in which the methylimido ligand of **2Q_Me** is exchanged with two borylamines to give the respective model borylimido complex and methylamine. It can be seen that the reaction with the model dialkylborylamine, H_2NBMe_2, has a highly positive Δ_rE of 11.7 kcal mol^{-1}, while the reaction with $H_2NB(NMeCH)_2$ has a much smaller Δ_rE of 0.8 kcal mol^{-1}. These two calculated energies are in accordance with the experimental results in which no exchange took place between Cp*Ti(hpp)(N^tBu) (**20**) and $(\mu\text{-}H_2N)_2(BC_8H_{14})_2$, while **20** and $H_2NB(NAr'CH)_2$ (**2.2**) gave an equilibrium mixture of the *tert*-butylimide and the borylimide **10**. The values obtained can also be compared with those from previous calculations, although performed with a slightly different computational methodology, of the isodesmic reactions of **2Q_Me** with H_2NPh, H_2NNPh_2 and H_2NOMe,[16,19] these being –2.5, –5.1 and –3.9 kcal mol^{-1}, respectively. In contrast to those Δ_rE values for the two borylamines, these are much more negative, and experimentally, exchange reactions between Cp*Ti{$MeC(N^iPr)_2$}(N^tBu) (**3.1**) and H_2NNPh_2, H_2NO^tBu or anilines are quantitative.[11,16,19]

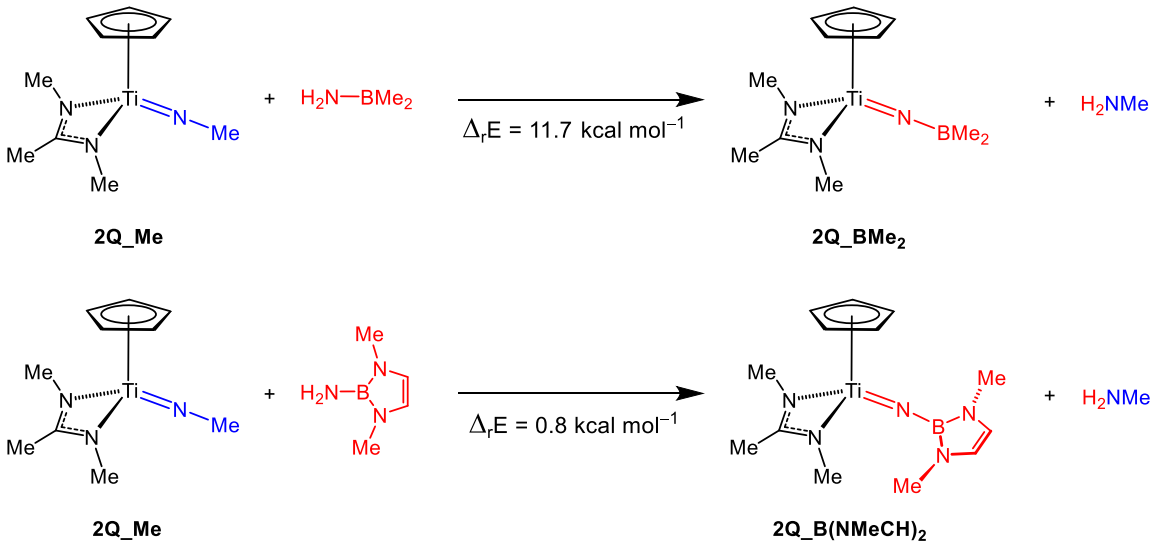

Figure 3.13. DFT computed electronic energies for the isodesmic reactions illustrated.

To further elucidate these differences in energetics between borylamines and other amine derivatives, bond dissociation energies of the model titanium–nitrogen multiple bonds were calculated. The bond dissociation energy is considered the sum of three components: the interaction energy ($E_{interaction}$) of the multiple bond itself, in addition to the relaxation energies (E_{relax}) of the two resulting fragments (Equation 3.6). The three components and the summed bond dissociation energies are all listed in Table 3.7. From this table it is clear that the model borylimides have the greatest bond dissociation energies, so are considered to be the strongest titanium–nitrogen linkages by this measure. In particular, **2Q_B(NMeCH)$_2$** and **2Q_BMe$_2$** have ΔE_{BD} values of 119.6 and 132.3 kcal mol^{-1}, respectively, which compare to 109.7 and 108.2 kcal mol^{-1} for the model imides **2Q_Me** and **2Q_Ph**.

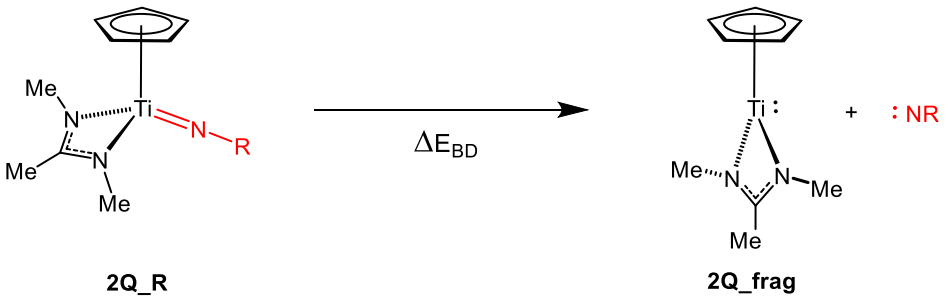

Equation 3.6

Table 3.7. Relaxation energies (E_{relax}), interaction energies ($E_{interaction}$) and bond dissociation energies (ΔE_{BD} = E_{relax} (**2Q_frag**) + E_{relax} (NR) + $E_{interaction}$) for a range of titanium–nitrogen multiply bonded model complexes. All fragments are in the triplet state, and all energies are given in kcal mol^{-1}.

NR	E_{relax} (**2Q_frag**)	E_{relax} (NR)	$E_{interaction}$	ΔE_{BD}
NMe	–7.9	–1.2	118.8	109.7
NPh	–7.9	–2.2	118.3	108.2
$NBMe_2$	–7.9	–5.9	146.1	132.3
$NB(NMeCH)_2$	–7.9	–1.2	128.7	119.6

The bond dissociation energies described above showed that the model borylimides actually have stronger Ti–N multiple bonds than their imido counterparts. However, experimentally it is observed that borylamines do not readily exchange with a *tert*-butylimido ligand, and in the reactions of **10**, that H_2N^tBu and anilines do give exchange with a borylimido ligand. To obtain the full picture, the N–H bond energies of the relevant amine and borylamine substrates must now be considered. In Scheme 3.5, a modified version of the isodesmic reactions of Figure 3.13 is presented, in which ΔE_{exch} is decomposed into four components: the bond dissociation energies of both the substrate and product Ti–N multiple bonds, and the bond dissociations of two H atoms from both reagent and product amine derivatives. The energies of the four processes, along with the total ΔE_{exch} are listed in Table 3.8. It can be seen that both borylamines give positive ΔE_{exch} values: 0.8 and 11.7 kcal mol^{-1} for $H_2NB(NMeCH)_2$ and H_2NBMe_2 respectively (the same values as given in Figure 3.13). In contrast, exchange with the model aniline H_2NPh gives –1.8 kcal mol^{-1}. Inspection of how the ΔE_2 and ΔE_3 values vary with the R group show that there is greater variation in the former, that is the breaking of the N–H bonds in the H_2NR reagent, implying that this is the dominant component of ΔE_{exch}. In particular, for H_2NBMe_2, ΔE_2 is very large (225.8 kcal mol^{-1}), and it is only slightly smaller for $H_2NB(NMeCH)_2$ (202.3 kcal mol^{-1}). To summarise, the strong N–H bonds in the model borylamines appear to outweigh the effect of the stronger Ti–N bonds in the respective model borylimido complexes. These ΔE_2 values for the borylamines may be compared with 188.2 kcal mol^{-1} for H_2NPh, whilst the corresponding ΔE_3 value is 108.2 kcal mol^{-1}. Given that anilines are known experimentally to give exchange with the *tert*-butylimide, this

supports the statement that the strength of the borylamine N–H bonds outweighing the stronger Ti–N bonds is the basis of the experimental failure to produce borylimides through exchange of an imido ligand with a borylamine, and also explains how the borylimido ligand in **10** is so readily displaced by H_2N^tBu. These findings may also be of relevance to the failure of the reaction between $Ti(NMe_2)_2Cl_2$ and $(\mu\text{-}H_2N)_2(BC_8H_{14})_2$ as described in Section 2.4. Whilst reaction with $H_2NB(NAr'CH)_2$ (**2.2**) produces **1**, the analogous compound **1_BBN** cannot be prepared. These findings imply that this failure may be due to the stronger N–H bonds in $(\mu\text{-}H_2N)_2(BC_8H_{14})_2$ relative to the other borylamine, making this protonolysis reaction unfeasible, and allowing instead the observed deleterious side reaction which forms $Me_2NBC_8H_{14}$.

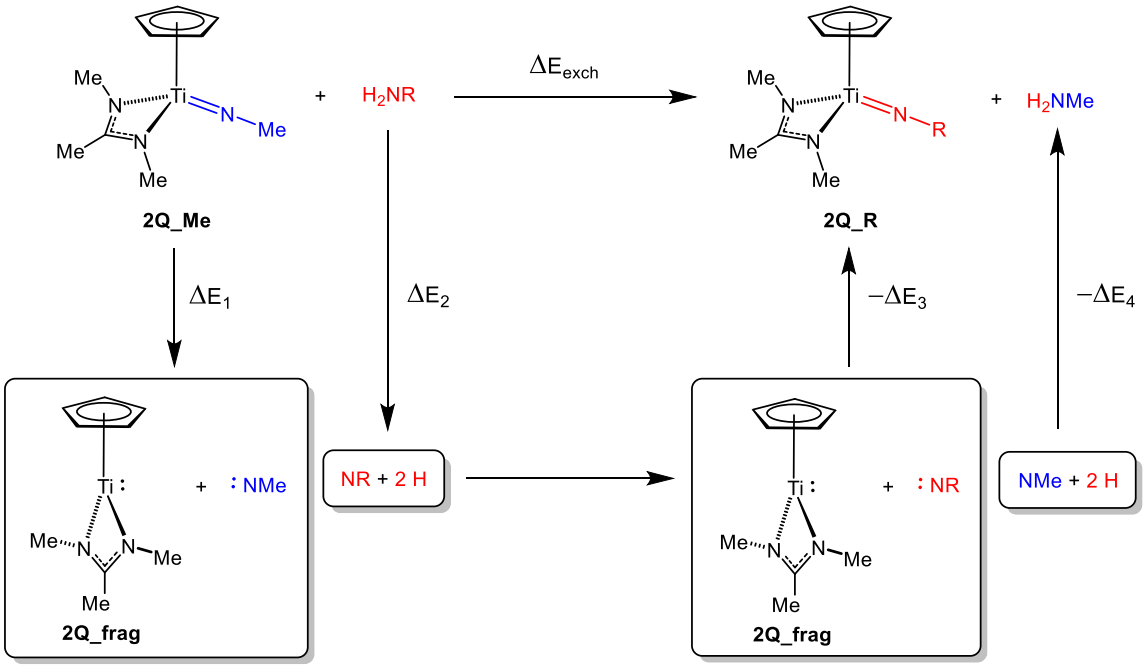

Scheme 3.5. Energy decomposition scheme for the exchange reactions of **2Q_NMe** with amine derivatives H_2NR.

Table 3.8. ΔE values (kcal mol^{-1}) for the four processes depicted in Scheme 3.5, along with the total ΔE_{exch} (= $\Delta E_1 + \Delta E_2 - \Delta E_3 - \Delta E_4$). All fragments are in the triplet state.

NR	ΔE_1	ΔE_2	ΔE_3	ΔE_4	ΔE_{exch}
NPh	109.7	188.2	108.2	191.5	–1.8
$NBMe_2$	109.7	225.8	132.3	191.5	11.7
$NB(NMeCH)_2$	109.7	202.3	119.6	191.5	0.8

Returning to experiment, reactions of Cp*Ti(hpp)(N^{t}Bu) (**20**) with H_2NBMes_2 and $(\mu\text{-}H_2N)_2(BC_8H_{14})_2$ in C_6D_6 solution were also attempted. For the former substrate, no reaction was observed after heating at 90 °C for a prolonged period, whilst for the latter the forcing conditions employed led only to decomposition of **20**. Furthermore, the attempted reaction of Cp*Ti(hpp){NB(NAr'CH)$_2$} (**10**) and $(\mu\text{-}H_2N)_2(BC_8H_{14})_2$ was also unsuccessful, similarly leading to decomposition of the starting material **10** after heating up to 90 °C gave no other reaction. In the context of the computational results presented above, these reaction outcomes are now unsurprising. It was found that the model dialkylborylamine H_2NBMe_2 has the strongest N–H bonds of those calculated, with this outweighing the accompanying high Ti–N bond strength of the desired product. Thus, it is clear that imido exchange by protonolysis is not a suitable reaction for the formation of such borylimido complexes. Future attempts to form borylimides of this type may instead focus on salt metathesis reactions using a lithium borylamide reagent, or alternatively oxidative reactions with a borylazide derivative in analogy to the syntheses of **1.110**, **1.111** and **1.112**.

To shed more light on these exchange reactions and their relationship to the strength of the respective metal–nitrogen multiple bonds, a combined DFT (computed bond dissociation energies, ν(N–H) and force constants) and QTAIM study was performed by Prof. Philip Mountford on the same family of model complexes **2Q_R**, and including a wider range of R substituents to test various features of the bonding.[61] The key QTAIM parameters are listed in Tables 3.9 and 3.10, along with calculated stretching frequencies (ν) and force constants (*k*) of the N–H bonds in the respective amines H_2NR which will be discussed below. In the following tables and plots, a colour coding scheme is employed to visually highlight the different types of metal–nitrogen multiple bonded functional groups. Blue

data correspond to borylimido functional groups, red to arylimides and green to hydrazides, whilst the black data refer to the model methylimide **2Q_Me**.

There exist (in principle) two measures of the titanium–nitrogen multiple bond strength which may be accessed both experimentally and through computation: the Ti–N bond distance and the bond dissociation energy (ΔE_{BD}). Here, each of these will be correlated with QTAIM parameters and their variation with R discussed. Firstly, however, it is noted that the Ti–N bond distances and bond dissociation energies in the family of compounds **2Q_R** are not themselves correlated, as shown in Figure 3.14 (top left). Indeed, when the Ti–N_{im} bond distance in **2Q_Me** is moved to 1.750 Å from its value of 1.679 Å in the optimised structure, the total electronic energy of the resulting model complex is found to be only 1.3 kcal mol^{-1} more, signifying that the electronic energy of the system (and by extension, ΔE_{BD}) is not strongly dependent on the value of this metric, which relates mainly to π interactions with the substituent R.

Next, the variation in the Ti–N_{im} bond distance in this family of model complexes is considered. This distance anti-correlates with the delocalisation index δ(Ti–N_{im}) of that bond, as seen in Figure 3.14 (top right, r^2 = 0.866). As discussed in Chapter Two, the delocalisation index, δ(A–B), of a bond A–B is a measure of the number of electron pairs delocalised or shared between the two atoms and can relate to formal bond order.[62] This trend follows the same reasoning which has previously been used to explain the variation of crystallographically-measured Ti–N_{im} bond distances, as well as bond energies in the model diamide-pyridine-supported complexes **1Q_R**. Using the Ti–N_{im} distance of 1.679 Å in **2Q_Me** as a starting point, the model arylimides **2Q_4-C$_6$H$_4$CF$_3$**, **2Q_Ph** and **2Q_C$_6$H$_4$NH$_2$** all have longer distances, and correspondingly smaller delocalisation indices. In an arylimide, there are two contributing π effects. Firstly, a backbonding interaction exists from a Ti–N π bond to an unoccupied π* orbital of the aryl ring, and secondly, there is donation from a filled π orbital of the aryl ring into a π* orbital of the Ti–N bond. Together, these two effects result in a reduction of the bond order of the Ti–N multiple bond and a lengthening of the bond. The data here suggest that the former effect is dominant, as this effect is greatest for the electron-poor ring in **2Q_4-C$_6$H$_4$CF$_3$** group, giving a bond distance of 1.708 Å and δ(Ti–N_{im}) of 1.498, and least for the electron-rich ring in **2Q_4-C$_6$H$_4$NH$_2$**, giving a bond distance of 1.700 Å and δ(Ti–N_{im}) of 1.550.

Table 3.9. Selected QTAIM data (atomic units) in model complexes of the type CpTi{MeC(NMe)$_2$}(NR) (**2Q_R**; R = BMe$_2$, B(NMeCH)$_2$, BMe$_2$NH$_3$, Me, 4-C$_6$H$_4$CF$_3$, Ph, 4-C$_6$H$_4$NH$_2$, NMe$_2$, NMe$_2$_planar), associated Ti–N$_{im}$ and N$_{im}$–R bond distances (*d*, Å) in the optimised structures, and energies (kcal mol^{-1}) for Ti–N bond dissociation (ΔE_{BD}), amine exchange from **2Q_Me** (ΔE_{exch}) and double N–H bond dissociation of the respective amine (ΔE_{2N-H}). Values for ρ (electron density), $\nabla^2\rho$ (electron density Laplacian), and ε (ellipticity) were obtained at the bond critical point. δ(A–B) is the delocalisation index for the stated pair of atoms.

2Q_R	*d*(Ti–N$_{im}$)	*d*(N$_{im}$–R)	ΔE_{BD}	ΔE_{exch}	ΔE_{2N-H}	δ(Ti–N$_{im}$)	ρ(Ti–N$_{im}$)	$\nabla^2\rho$(Ti–N$_{im}$)	ε(Ti–N$_{im}$)	δ(N$_{im}$–R)
2Q_BMe$_2$	1.706	1.415	132.3	11.7	225.8	1.590	0.206	0.712	0.211	0.535
2Q_B(NMeCH)$_2$	1.694	1.429	119.6	0.8	202.3	1.632	0.212	0.727	0.063	0.482
2Q_BMe$_2$NH$_3$	1.674	1.504	117.2	5.7	204.7	1.772	0.222	0.765	0.032	0.407
2Q_Me	1.679	1.417	109.7	0.0	191.5	1.673	0.209	0.819	0.091	1.046
2Q_4-C$_6$H$_4$CF$_3$	1.708	1.361	111.6	–2.4	191.0	1.498	0.196	0.770	0.152	1.128
2Q_Ph	1.702	1.366	108.2	–1.8	188.2	1.534	0.199	0.780	0.134	1.112
2Q_4-C$_6$H$_4$NH$_2$	1.700	1.369	103.3	–2.8	182.4	1.550	0.200	0.781	0.110	1.107
2Q_NMe$_2$	1.699	1.346	94.6	–6.5	170.0	1.551	0.193	0.811	0.041	1.287
2Q_NMe$_2$_planar	1.712	1.320	93.3	–7.0	168.1	1.501	0.182	0.841	0.210	1.351

Table 3.10. QTAIM charges (*Q*, units of *e*) of fragments of model complexes of the type CpTi{MeC(NMe)$_2$}(NR) (**2Q_R**; R = BMe$_2$, B(NMeCH)$_2$, BMe$_2$NH$_3$, Me, 4-C$_6$H$_4$CF$_3$, Ph, 4-C$_6$H$_4$NH$_2$, NMe$_2$, NMe$_2$_planar), and average ν(N–H) (cm^{-1}) and force constants *k*(N–H) (mDyne Å^{-1}) associated with the respective amine H$_2$NR.

2Q_R	*Q*(NR)	*Q*(Ti)	ν(N–H) (avg.)	*k*(N–H) (avg.)
2Q_BMe$_2$	–0.887	1.972	3644.2	8.4
2Q_B(NMeCH)$_2$	–0.851	1.967	3684.2	8.6
2Q_BMe$_2$NH$_3$	–0.747	1.940	3606.2	8.2
2Q_Me	–0.802	1.944	3555.0	8.0
2Q_4-C$_6$H$_4$CF$_3$	–0.912	1.967	3646.5	8.4
2Q_Ph	–0.874	1.958	3630.5	8.3
2Q_4-C$_6$H$_4$NH$_2$	–0.838	1.950	3609.5	8.2
2Q_NMe$_2$	–0.749	1.910	3479.1	7.6
2Q_NMe$_2$_planar	–0.695	1.884	3443.5	7.5

The same effect is seen in the model hydrazides, though in this case arises from donation of the N$_\beta$ lone pair into a π* orbital of the Ti–N multiple bond. This effect is greatest when N$_\beta$ is forced to be planar as a more linear alignment of the lone pair with the Ti–N π bond is possible. Turning to the model borylimides, **2Q_B(NMeCH)$_2$** and **2Q_BMe$_2$**, these have longer Ti–N$_{im}$ distances than **2Q_Me** due to delocalisation of an N$_{im}$ lone pair to the 2p orbital of boron. This effect is lessened for **2Q_B(NMeCH)$_2$** as there is competing donation to the 2p orbital by the nitrogen atoms in the backbone of the borolyl moiety, and is also found to be negated by the coordination of NH$_3$ to boron in the model **2Q_BMe$_2$NH$_3$**. This latter model borylimide is isoelectronic with a *tert*-butylimide, and has a comparable Ti–N$_{im}$ bond distance to the model **2Q_^{t}Bu** (not shown in Table 3.9; 1.674 *vs* 1.681 Å).

Considering next the bond dissociation energies of the Ti–N$_{im}$ linkages in the model complexes, these have a strong negative correlation with the Laplacian of the electron density, $\nabla^2\rho$(Ti–N$_{im}$), at the bond critical point (BCP), as seen in Figure 3.14 (centre left,

r^2 = 0.801). The electron density Laplacian is a degree of the concentration of electron density at a particular point (in this case the BCP).[63] Generally speaking, where $\nabla^2\rho > 0$ electron density is locally depleted compared to its average, and where $\nabla^2\rho < 0$ the electron density is locally concentrated compared to its average, and a negative $\nabla^2\rho$ at the BCP is often used to signify a covalent bond. For polar bonds, however, the Laplacian may be of either sign.[64] In the model complexes **2Q_R**, the $\nabla^2\rho$(Ti–N_{im}) values are all positive and, given the relationship with bond dissociation energies, a smaller (i.e. less positive) value here corresponds to a stronger Ti–N_{im} bond.

It is also found that the Ti–N bond dissociation energies of **2Q_R** correlate extremely well with the calculated N–H bond dissociation energies of the corresponding amines H_2NR, as shown in Figure 3.14 (centre right, r^2 = 0.988), and in turn with the average N–H bond force constants which reflect only N–H σ-bonding effects. The anti-correlation between the average force constant *k*(N–H) and the electron density Laplacian is also shown in Figure 3.14 (bottom left). These results therefore confirm a relationship between the strength of the N–H bonds of an amine H_2NR and the metal–nitrogen multiple bond strength in the corresponding imido derivative, arising from the σ-donor ability of the NR fragment. In cases where NR is a strong σ-donor, such as for R = BMe_2 and $B(NMeCH)_2$ (due largely to the electropositive nature of boron, and shown by the high energies of the σ-donor HOMO–2 orbitals of $[NBMe_2]^{2-}$ and $[NB(NMeCH)_2]^{2-}$ in Figure 3.5), the N–H bonds of the amine are strongest (avg. *k* = 8.4 and 8.6 mDyne $Å^{-1}$ respectively) and ΔE_{BD} values are the greatest (132.3 and 119.6 kcal mol^{-1} respectively). When considering the much smaller ΔE_{BD} values in the model hydrazides **2Q_NMe$_2$** and **2Q_NMe$_2$_planar** (94.6 and 93.3 kcal mol^{-1} respectively) it is now apparent that these are due to the poorer σ-donor ability of the $NNMe_2$ fragments, which arises largely from the electronegativity of the N_β-containing group.

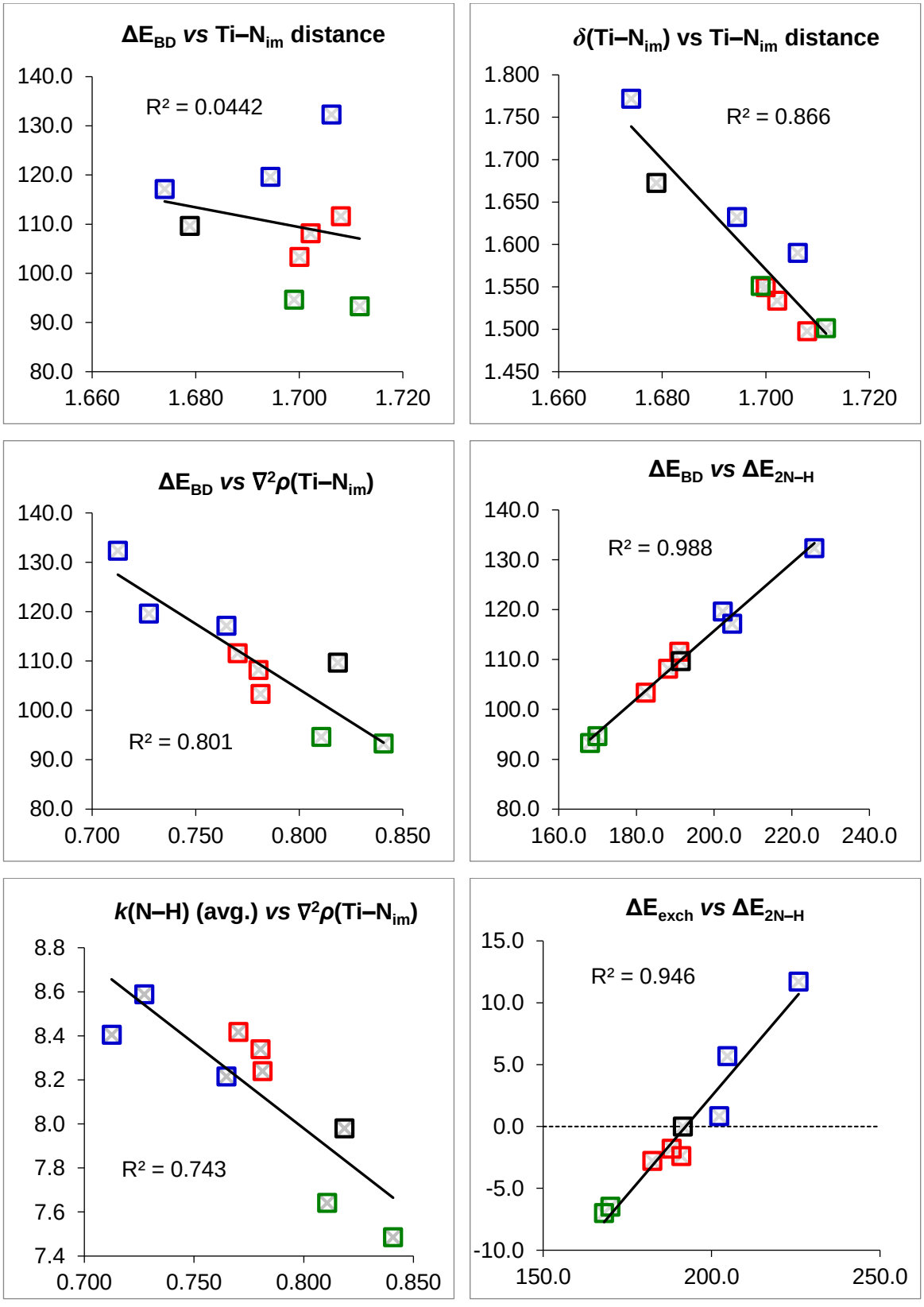

Figure 3.14. Selected relationships of QTAIM parameters (atomic units) with bond dissociation and exchange energies (kcal mol^{-1}), N–H bond force constants (*k*, mDyne $Å^{-1}$) and Ti–N_{im} bond distances (Å).

Finally, the plot at the bottom right of Figure 3.14 highlights the strong correlation (r^2 = 0.946) between the N–H bond dissociation energy in the amine H_2NR and the electronic energy change for the process in which that amine exchanges with the imido ligand of **2Q_Me** to give **2Q_R** and H_2NMe. The placing of the red and green data points below the ΔE_{exch} = 0 line indicate that these processes are favourable for anilines and hydrazines respectively, and such exchanges are known experimentally.[11,16] Meanwhile, the blue data points above the line indicate that the analogous exchange reactions with borylamines are unfavourable. However, ΔE_{exch} for the exchange reaction with $H_2NB(NMeCH)_2$ is calculated to be only slightly positive (0.8 kcal mol^{-1}), which is consistent with the experimental result in which reaction of $H_2NB(NAr'CH)_2$ (**2.2**) with Cp*Ti(hpp)(N^{t}Bu) (**20**) gives partial conversion to the borylimido analogue **10**. Meanwhile the same process with H_2NBMe_2 is clearly experimentally inaccessible, with ΔE_{exch} = 11.7 kcal mol^{-1}.

In order to see more clearly other relationships between QTAIM parameters and the Ti–N_{im} bond dissociation energies, QTAIM studies were next performed on variants of the model complexes **2Q_R** in which the Ti–N_{im} bond distances of all of the complexes were fixed at 1.700 Å which is close to the average of the optimised distances. These new models are denoted **2Q_R_fixed**, and the newly calculated QTAIM parameters for the Ti–N_{im} bond are listed in Table 3.11, along with graphical plots of their relationships with the bond dissociation energies obtained from the original models **2Q_R** in Figure 3.15. This strategy aimed to isolate the underlying donor ability of the NR fragment from the π effects which dominate variation in the Ti–N_{im} bond distance.

Firstly, there is a strong correlation (r^2 = 0.874) between the Ti–N_{im} bond dissociation energies in **2Q_R** and the electron densities at the BCP, ρ, in **2Q_R_fixed** (Figure 3.15, top left). Correlations of ρ with binding energies are known for a number of different types of bond, and can be used as a measure of bond covalency.[64] In this study, ρ is found to be greatest for the borylimides (blue data points), corresponding to the greatest ΔE_{BD} values, and smallest for the hydrazides (green data points), these having the smallest ΔE_{BD} values. Thus, ρ appears to reflect increasing covalency of the Ti–N_{im} bond with more electron-releasing NR fragments. A strong negative correlation (r^2 = 0.834) also exists between ΔE_{BD} and the Laplacian of the electron density at the BCP, $\nabla^2\rho$ (Figure 3.15, top right). The Laplacian is defined as the sum of three curvatures of electron density at the BCP: λ_1 and λ_2 are negative and lie in two coordinates perpendicular to the bond path, while λ_3, the curvature along the bond path, is positive.[64] It is the two negative components of the

Laplacian which measure the concentration of electron density along the bond path, and give the negative correlation mentioned above. Plotting ΔE_{BD} against the negative λ component which has the highest magnitude (by convention λ_1), a strong negative correlation (r^2 = 0.908) is again observed (Figure 3.15, centre left). The most electron-releasing NR fragments give the most negative λ_1 values. This, therefore, reflects the greatest degree of electron density concentration along the bond path for the strongest bond.

Turning next to measures of energy density, there is a strong correlation (r^2 = 0.873) between ΔE_{BD} and the total energy density (the sum of potential and kinetic energy densities) at the BCP, *H* (Figure 3.15, centre right). *H* is known to be negative for covalent interactions, with its increasing magnitude reflecting a greater degree of covalency.[64,65] This follows the same trends described above for the electron-releasing nature of the respective NR fragments. Inspection of the potential (*V*) and kinetic (*G*) energy components of *H* show that, in this study, the variation of the total energy density is dominated by *V*, with a plot of ΔE_{BD} against *V* giving a similarly strong correlation (r^2 = 0.826; Figure 3.15, bottom left). In contrast, there is no significant relationship between *G* and ΔE_{BD}.

A negative correlation (r^2 = 0.839) is found, however, between ΔE_{BD} and the composite QTAIM parameter G/ρ (Figure 3.15, bottom right). For a homonuclear bond, this ratio has been reported to increase with the bond order, whilst in polar bonds the increasing magnitude of this ratio corresponds to an increasing bond polarity.[63] It is the latter correlation which is relevant in this study, where the ratio is greatest for the most polar Ti–N_{im} bonds (hydrazides containing electronegative N_β) and smallest for the least polar Ti–N_{im} bonds (borylimides containing electropositive B). Interestingly, the G/ρ value of **2Q_BMe$_2$NH$_3$_fixed** is considerably smaller than that of **2Q_Me_fixed**, despite these two models being isoelectronic (1.428 *vs* 1.508). This highlights the fact that this metric is dominated by the electronegativity of the atom directly bonded to N_{im}. Indeed, the G/ρ value of **2Q_BMe$_2$NH$_3$_fixed** is closer to those of the two other model borylimides **2Q_BMe$_2$** and **2Q_B(NMeCH)$_2$** (1.400 and 1.405 respectively).

Table 3.11. Selected QTAIM data (atomic units) for the Ti–N_{im} bond (fixed at 1.700 Å) in model complexes of the type CpTi{MeC(NMe)$_2$}(NR) (**2Q_R_fixed**; R = BMe_2, $B(NMeCH)_2$, BMe_2NH_3, Me, 4-$C_6H_4CF_3$, Ph, 4-$C_6H_4NH_2$, NMe_2, NMe_2_planar). All other bond metrics remained unchanged from the optimised structures. Values for ρ (electron density), $\nabla^2\rho$ (electron density Laplacian), ε (ellipticity), H (total energy density), G (kinetic energy density) and V (potential energy density) were obtained at the bond critical point. δ is the delocalisation index of the Ti–N_{im} bond. λ_1 and λ_2 are curvatures of the electron density in two coordinates perpendicular to the bond path, while λ_3 is the curvature of the electron density along the bond path.

2Q_R_fixed	δ	ρ	$\nabla^2\rho$	ε	λ_1	λ_2	λ_3	H	G	V	G/ρ
2Q_BMe_2_fixed	1.596	0.210	0.719	0.208	–0.366	–0.303	1.388	–0.114	0.294	–0.407	1.400
2Q_$B(NMeCH)_2$_fixed	1.627	0.209	0.722	0.063	–0.339	–0.318	1.379	–0.113	0.293	–0.406	1.405
2Q_BMe_2NH_3_fixed	1.749	0.208	0.740	0.032	–0.318	–0.308	1.366	–0.112	0.297	–0.408	1.428
2Q_Me_fixed	1.653	0.199	0.793	0.096	–0.298	–0.272	1.362	–0.101	0.300	–0.401	1.508
2Q_4-$C_6H_4CF_3$_fixed	1.506	0.200	0.780	0.150	–0.321	–0.279	1.379	–0.103	0.298	–0.401	1.490
2Q_Ph_fixed	1.536	0.200	0.783	0.133	–0.315	–0.278	1.377	–0.103	0.298	–0.401	1.494
2Q_4-$C_6H_4NH_2$_fixed	1.549	0.200	0.781	0.111	–0.312	–0.281	1.374	–0.103	0.298	–0.401	1.491
2Q_NMe_2_fixed	1.550	0.192	0.809	0.041	–0.277	–0.266	1.352	–0.095	0.297	–0.391	1.545
2Q_NMe_2_planar_fixed	1.515	0.188	0.859	0.205	–0.274	–0.228	1.361	–0.089	0.304	–0.394	1.618

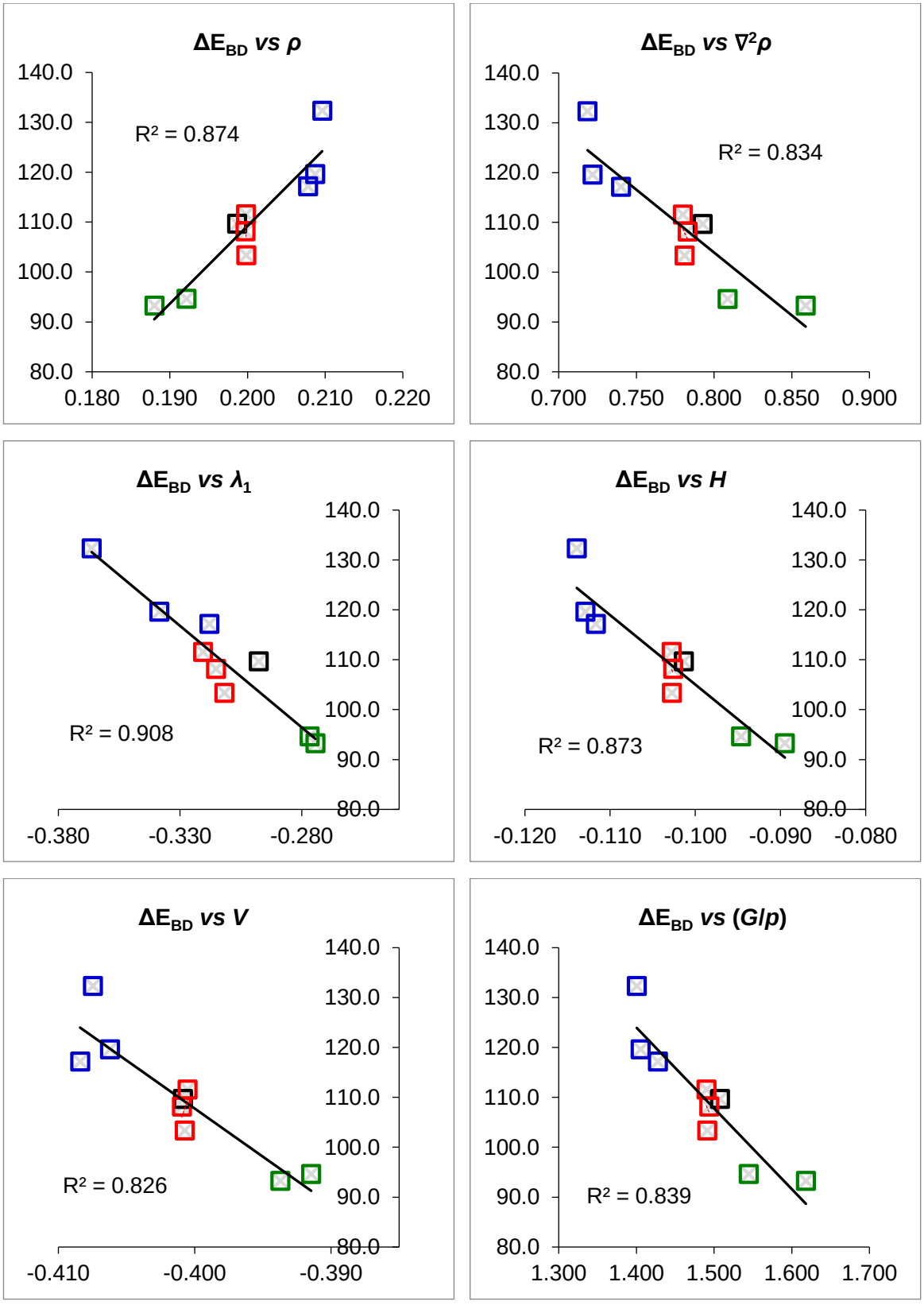

Figure 3.15. Selected relationships of QTAIM parameters (atomic units) of the Ti–N_{im} bond of the models **2Q_R_fixed** with bond dissociation energies (kcal mol^{-1}) of the models **2Q_R**.

It is also noted that the delocalisation indices (δ) in the family of fixed-distance models **2Q_R_fixed** correlate strongly with the Ti–N_{im} bond distances in the relaxed species **2Q_R** (r^2 = 0.823), whilst δ of **2Q_R_fixed** does not correlate well with the bond dissociation energies of **2Q_R** (r^2 = 0.231). This confirms that the low energy variation in the Ti–N_{im} bond distances across the range of models **2Q_R** does not have a significant effect on the calculated bond dissociation energies in those models, and validates this approach of fixing the Ti–N_{im} bond distance to reveal more underlying relationships with QTAIM parameters.

To relate these conclusions back to orbital interpretations, a natural bonding orbital (NBO) study was performed by Dr Eric Clot of Université Montpellier, France, on the family of model complexes **2Q_R_fixed**. In this methodology, the models were set up with no formal bond being present between Ti and N_{im} (although the Ti–N_{im} distance is set at 1.700 Å). Instead, N_{im} bears three NBOs which ideally contain two electrons each, these representing three N lone pairs: one with σ symmetry and two with π symmetry. These three NBOs then mix with accepting NBOs on the Ti centre to create three natural localised molecular orbitals (NLMOs) which are strictly occupied by two electrons each and represent the one σ and two π components (π_{para} and π_{perp}) of the metal–nitrogen multiple bond in a Lewis structure sense.[66] Inspection of the percentage titanium participation in each of these NLMOs is a means to evaluate the σ- or π-donor ability of the respective NBO; a greater weight on Ti indicates greater donation of electron density from N_{im}, i.e. a greater degree of covalency. This data is listed in Table 3.12.

Inspection of the titanium participation in the σ NLMO shows that this is largest for the borylimides (blue) and smallest for the hydrazides (green), indicating a relationship with the electronegativity of the substituent R. Thus, NR fragments with more electropositive R groups are stronger σ donors and, as expected from the QTAIM studies described above, a strong correlation (r^2 = 0.798) is found between ΔE_{BD} and % Ti (σ) (Figure 3.16, left). The titanium participation in π_{perp} scales in the opposite direction, due to the π effects of the R substituent which have previously been described (e.g. donation of an N_β lone pair into a Ti–N π* orbital or donation of Ti–N π electrons into an empty B 2p orbital), although this correlates less well with ΔE_{BD}. No clear relationship is seen between the identity of R and Ti participation in π_{para}.

Table 3.12. Percentage Ti participation (% Ti) in Ti–N_{im} NLMOs, and hybridisation (proportion of p character, sp^x) of the Ti–N and N–R σ bonds, obtained from NBO calculations on model complexes of the type CpTi{MeC(NMe)$_2$}(NR) (**2Q_R_fixed**; R = BMe_2, $B(NMeCH)_2$, BMe_2NH_3, Me, 4-$C_6H_4CF_3$, Ph, 4-$C_6H_4NH_2$, NMe_2, NMe_2_planar).

2Q_R_fixed	%Ti (σ)	%Ti (π_{para})	%Ti (π_{perp})	sp^x (Ti–N σ)	sp^x (N–R σ)
2Q_BMe_2_fixed	20.4	30.2	17.2	1.94	0.54
2Q_$B(NMeCH)_2$_fixed	19.4	26.1	25.7	1.53	0.78
2Q_BMe_2NH_3_fixed	20.3	25.8	30.0	1.05	1.01
2Q_Me_fixed	18.0	28.7	29.1	0.64	1.78
2Q_4-$C_6H_4CF_3$_fixed	17.4	27.1	24.6	0.83	1.43
2Q_Ph_fixed	17.6	27.4	25.8	0.81	1.45
2Q_4-$C_6H_4NH_2$_fixed	17.5	27.1	26.9	0.78	1.48
2Q_NMe_2_fixed	17.0	25.2	34.1	0.45	2.36
2Q_NMe_2_planar_fixed	16.7	22.9	37.2	0.51	2.19

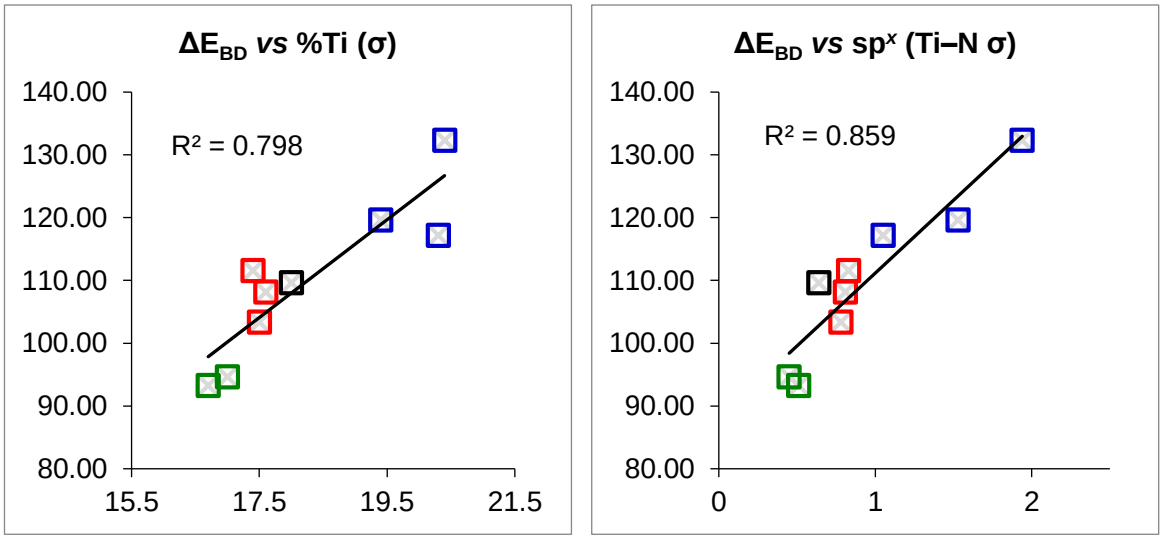

Figure 3.16. Relationships of bond dissociation energies (kcal mol^{-1}) of the models **2Q_R** with percentage titanium participation in the σ NLMO (%Ti (σ), left) and with the degree of p character (sp^x) in the same NLMO (right) in **2Q_R_fixed**.

Furthermore, the hybridisation of the N-based NLMO in the Ti–N and N–R σ bonds (data in Table 3.12) were analysed to give further insight on the effect of electronegativity of the R substituent on the NR fragment's σ-donor ability. It was found that the Ti–N bond has the greatest degree of p character for the borylimides (blue, electropositive B) and the smallest degree of p character for the hydrazides (green, electronegative N_β). The degree of p character in the N–R σ bond anti-correlates with that in the Ti–N σ bond. Greater p character in the Ti–N bond corresponds to greater polarisation of the NLMO towards the Ti centre, thus this parameter scales with the percentage of titanium participation in it. Correspondingly, ΔE_{BD} may also be related to the proportion of p character in the σ NLMO, with a strong correlation ($r^2 = 0.859$) again being observed (Figure 3.16, right).

In summary, these QTAIM and NBO studies have shown that two measures of metal–nitrogen multiple bond strength, the bond distance and the bond dissociation energy, are separable and arise from distinct electronic factors. The variation in the Ti–N_{im} bond distance is found to be dominated by π interactions with the substituent at the N_{im} atom, whilst variation in the bond dissociation energy is found to arise primarily from the underlying σ-donor ability of the NR fragment, which in turn relates to the electronegativity or electropositivity of the R substituent. It is the latter effect which controls the favourability of imido ligand exchange reactions, and the difficulties in forming borylimides through this methodology are found to arise from the high N–H bond strengths in the corresponding borylamines.

3.8 Conclusions and Outlook

This Chapter has described the synthesis and characterisation of a further six borylimido complexes of titanium, these all having sandwich or half-sandwich structures. Firstly, a new route to introduce the borylimido functional group was described: imide/borylamine exchange, which produced Cp*Ti{NB(NAr'CH)$_2$}Cl(py) (**9**) from the *tert*-butylimido analogue **1.8**. Next, **9** was used as a synthon for the installation of two supporting ligands. Salt metathesis reactions of **9** with Li[hpp] and Li$N^{pyr}N^{Me_2}$ produced the respective borylimido complexes Cp*Ti(hpp){NB(NAr'CH)$_2$} (**10**) and Cp*Ti($N^{pyr}N^{Me_2}$){NB(NAr'CH)$_2$} (**11**). DFT calculations performed on a model of **10** elucidated the electronic structure of the Ti–N multiple bond in these borylimido systems and made comparisons of this to a BMe_2-substituted analogue.

The first metallocene borylimido complex, $Cp_2Ti\{NB(NAr'CH)_2\}(py)$ (**12**) was prepared through salt metathesis of $Ti\{NB(NAr'CH)_2\}Cl_2(py)_3$ (**3**) and 2 equiv. NaCp. A redistribution reaction between **3** and **12** then gave the half-sandwich complex $CpTi\{NB(NAr'CH)_2\}Cl(py)$ (**13**), which itself reacted with $Li[MeC(N^iPr)_2]$ to yield $CpTi\{MeC(N^iPr)_2\}\{NB(NAr'CH)_2\}$ (**14**). Interestingly, no reaction occurred between that lithiated amidinate and the Cp* analogue **9**, this being ascribed to insurmountable steric constraints.

As a preliminary test of reactivity of the borylimido functional group, **10** was reacted with the heteroallenes CO_2 and CS_2, resulting in the boryliso(thio)cyanates $ECNB(NAr'CH)_2$ (E = O (**15**), S (**16**)) *via* functional group transfer of the borylimido unit, with concomitant formation of the dimeric titanium compounds $[Cp^*Ti(hpp)(\mu\text{-}E)]_2$ (E = O (**17**), S (**18**)). The exchange of the borylimido ligand of **9** with three amines was also tested, this again confirming the high basicity of this ligand. The relevant bond dissociation energies of titanium–nitrogen multiply bonded functional groups were explored through DFT and QTAIM calculations. These ultimately showed that the failure of protonolysis reactions of imides with borylamines, and the ready exchange of borylimido ligands with other amines, can be ascribed to the very high N–H bond strengths in the borylamines, which outweighs the corresponding increase in metal–nitrogen bond strength. Furthermore, QTAIM and NBO studies explored the use of the bond distance and bond dissociation energy as two measures of metal–nitrogen multiple bond strength. The variation in the former arises from π interactions with the substituent on the N_{im} atom, whilst the latter varies with the σ-donor ability of the respective NR fragment (ultimately related to the electronegativity or electropositivity of the R group) and is the factor that controls the favourability of imido ligand exchange reactions.

Currently, within our research group, a full reactivity study of $Cp^*Ti(hpp)\{NB(NAr'CH)_2\}$ (**10**) is being carried out by another DPhil student.[60] The reactions with CO_2 and CS_2 (presented in this Chapter) have been extended to reactions with other polar substrates such as isocyanates, aldehydes, ketones and esters, and the reactivity with internal and terminal alkynes has also been explored. Furthermore, where relevant, analogous reactions have been carried out with the imido analogue $Cp^*Ti(hpp)(N^tBu)$ (**20**) to investigate the differences between the imido and borylimido functional groups. Additionally, a second DPhil student has prepared zirconium and hafnium congeners of the titanocene borylimide

$Cp_2Ti\{NB(NAr'CH)_2\}(py)$ (**12**) which was presented here.[67] Reactivity studies of those complexes with a range of unsaturated small molecules are currently underway.

3.9 References

1 A. P. Duncan and R. G. Bergman, *Chem. Rec.*, 2002, **2**, 431–445.

2 N. Hazari and P. Mountford, *Acc. Chem. Res.*, 2005, **38**, 839–849.

3 G. Erker, G. Kehr and R. Fröhlich, *J. Organomet. Chem.*, 2004, **689**, 1402–1412.

4 P. C. Mohring and N. J. Coville, *J. Organomet. Chem.*, 1994, **479**, 1–29.

5 U. Rosenthal, P. Ardnt, W. Baumann, V. V. Burlakov and A. Spannenberg, *J. Organomet. Chem.*, 2003, **670**, 84–96.

6 P. J. Walsh, F. J. Hollander and R. G. Bergman, *J. Am. Chem. Soc.*, 1988, **110**, 8729–8731.

7 S. C. Dunn, P. Mountford and D. A. Robson, *J. Chem. Soc. Dalton Trans.*, 1997, **2**, 293–304.

8 J. D. Selby, M. Feliz, A. D. Schwarz, E. Clot and P. Mountford, *Organometallics*, 2011, **30**, 2295–2307.

9 A. E. Guiducci, A. R. Cowley, M. E. G. Skinner and P. Mountford, *J. Chem. Soc. Dalton Trans.*, 2001, 1392–1394.

10 C. L. Boyd, E. Clot, A. E. Guiducci and P. Mountford, *Organometallics*, 2005, **24**, 2347–2367.

11 A. E. Guiducci, C. L. Boyd, E. Clot and P. Mountford, *Dalton Trans.*, 2009, 5960–5979.

12 C. L. Boyd, A. E. Guiducci, S. R. Dubberley, B. R. Tyrrell and P. Mountford, *J. Chem. Soc. Dalton Trans.*, 2002, 4175–4184.

13 A. E. Guiducci, C. L. Boyd and P. Mountford, *Organometallics*, 2006, **25**, 1167–1187.

14 P. J. Tiong, A. Nova, E. Clot and P. Mountford, *Chem. Commun.*, 2011, **47**, 3147–3149.

15 P. J. Tiong, A. D. Schofield, J. D. Selby, A. Nova, E. Clot and P. Mountford, *Chem. Commun.*, 2010, **46**, 85–87.

16 P. J. Tiong, A. Nova, L. R. Groom, A. D. Schwarz, J. D. Selby, A. D. Schofield, E. Clot and P. Mountford, *Organometallics*, 2011, **30**, 1182–1201.

17 P. J. Tiong, A. Nova, A. D. Schwarz, J. D. Selby, E. Clot and P. Mountford, *Dalton Trans.*, 2012, **41**, 2277–2288.

18 P. J. Tiong, L. R. Groom, E. Clot and P. Mountford, *Chem. Eur. J.*, 2013, **19**, 4198–4216.

19 L. R. Groom, A. D. Schwarz, A. Nova, E. Clot and P. Mountford, *Organometallics*, 2013, **32**, 7520–7539.

20 L. R. Groom, A. F. Russell, A. D. Schwarz and P. Mountford, *Organometallics*, 2014, **33**, 1002–1019.

21 C. T. Owen, P. D. Bolton, A. R. Cowley and P. Mountford, *Organometallics*, 2007, **26**, 83–92.

22 Y. Bai, M. Noltemeyer and H. W. Roesky, *Z. Naturforsch.*, 1991, **46b**, 1357–1363.

23 L. C. Stevenson, S. Mellino, E. Clot and P. Mountford, *J. Am. Chem. Soc.*, 2015, **137**, 10140–10143.

24 M. P. Coles, *Chem. Commun.*, 2009, 3659–3676.

25 M. P. Coles and P. B. Hitchcock, *Organometallics*, 2003, **22**, 5201–5211.

26 A. L. Odom, *Dalton Trans.*, 2005, 225–233.

27 S. Banerjee and A. L. Odom, *Organometallics*, 2006, **25**, 3099–3101.

28 Y. Li, Y. Shi and A. L. Odom, *J. Am. Chem. Soc.*, 2004, **126**, 1794–1803.

29 C. Cao, Y. Shi and A. L. Odom, *Org. Lett.*, 2002, **4**, 2853–2856.

30 Y. Li, S. Banerjee and A. L. Odom, *Organometallics*, 2005, **24**, 3272–3278.

31 S. Patel, Y. Li and A. L. Odom, *Inorg. Chem.*, 2007, **46**, 6373–6381.

32 S. Banerjee, E. Barnea and A. L. Odom, *Organometallics*, 2008, **27**, 1005–1014.

33 S. Majumder, K. R. Gipson, R. J. Staples and A. L. Odom, *Adv. Synth. Catal.*, 2009, **351**, 2013–2023.

34 M. R. Smith, P. T. Matsunaga and R. A. Andersen, *J. Am. Chem. Soc.*, 1993, **115**, 7049–7050.

35 Z. K. Sweeney, J. L. Polse, R. A. Andersen, R. G. Bergman and M. G. Kubinec, *J. Am. Chem. Soc.*, 1997, **119**, 4543–4544.

36 Z. K. Sweeney, J. L. Polse, R. G. Bergman and R. A. Andersen, *Organometallics*, 1999, **18**, 5502–5510.

37 K. M. Doxsee and J. B. Farahi, *J. Chem. Soc. Chem. Commun.*, 1990, 1452–1454.

38 W. A. Howard and G. Parkin, *J. Organomet. Chem.*, 1994, **472**, c1–c4.

39 R. L. Zuckerman and R. G. Bergman, *Organometallics*, 2000, **19**, 4795–4809.

40 M. J. Carney, P. J. Walsh and R. G. Bergman, *J. Am. Chem. Soc.*, 1990, **112**, 6426–6428.

41 P. J. Walsh, A. M. Baranger and R. G. Bergman, *J. Am. Chem. Soc.*, 1992, **114**,

1708–1719.

42 Z. Hou, T. L. Breen and D. W. Stephan, *Organometallics*, 1993, **12**, 3158–3167.

43 A. M. Baranger, P. J. Walsh and R. G. Bergman, *J. Am. Chem. Soc.*, 1993, **115**, 2753–2763.

44 W. A. Howard, M. Waters and G. Parkin, *J. Am. Chem. Soc.*, 1993, **115**, 4917–4918.

45 W. A. Howard and G. Parkin, *J. Am. Chem. Soc.*, 1994, **116**, 606–615.

46 D. A. Fletcher, R. F. McMeeking and D. Parkin, *J. Chem. Inf. Comput. Sci.*, 1996, **36**, 746 (Cambridge Structural Database version 5.37).

47 J. W. Lauher and R. Hoffmann, *J. Am. Chem. Soc.*, 1976, **98**, 1729–1742.

48 J. C. Green, *Chem. Soc. Rev.*, 1998, **27**, 263–271.

49 N. D. Silavwe, M. R. M. Bruce, C. E. Philbin and D. R. Tyler, *Inorg. Chem.*, 1988, **27**, 4669–4676.

50 J. C. Green, M. L. H. Green, J. T. James, P. C. Konidaris, G. H. Maunder and P. Mountford, *J. Chem. Soc., Chem. Commun.*, 1992, 1361–1365.

51 K. A. Joergensen, *Inorg. Chem.*, 1993, **32**, 1521–1522.

52 T. E. Hanna, E. Lobkovsky and P. J. Chirik, *Inorg. Chem.*, 2007, **46**, 2359–2361.

53 A. J. Bridgeman, L. Davis, S. J. Dixon, J. C. Green and I. N. Wright, *J. Chem. Soc. Dalton Trans.*, 1995, 1023–1027.

54 L. Luo, G. Lanza, I. L. Fragalà, C. L. Stern and T. J. Marks, *J. Am. Chem. Soc.*, 1998, **120**, 3111–3122.

55 M. F. Lappert, H. Pyszora and M. Rieber, *J. Chem. Soc.*, 1965, 4256–4264.

56 L. Weber, E. Dobbert, R. Boese, M. T. Kirchner and D. Bläser, *Eur. J. Inorg. Chem.*, 1998, 1145–1152.

57 E. Pretsch, P. Buhlmann and C. Affolter, *Structure Determination of Organic Compounds*, Springer, Heidelberg, 3rd edn., 2000.

58 M. F. Lappert and H. Pyszora, *J. Chem. Soc. A*, 1967, 854–860.

59 A. Solovyev, Q. Chu, S. J. Geib, L. Fensterbank, M. Malacria, E. Lacôte and D. P. Curran, *J. Am. Chem. Soc.*, 2010, **132**, 15072–15080.

60 M. Slusarczyk and P. Mountford, Unpublished results.

61 R. F. W. Bader, *Atoms in Molecules: A Quantum Theory*, Oxford University Press, Oxford, 1990.

62 X. Fradera, M. A. Austen and R. F. W. Bader, *J. Phys. Chem. A*, 1999, **103**, 304–314.

63 P. Macchi and A. Sironi, *Coord. Chem. Rev.*, 2003, **238**–**239**, 383–412.

64 C. F. Matta and R. J. Boyd, *The Quantum Theory of Atoms in Molecules*, Wiley-VCH, Weinheim, 2007.

65 D. Cremer and E. Kraka, *Angew. Chem. Int. Ed. Engl.*, 1984, **23**, 627–628.

66 F. Weinhold and C. R. Landis, *Chem. Educ. Res. Pr.*, 2001, **2**, 91–104.

67 B. Xie and P. Mountford, Unpublished results.

Chapter Four

Reactions of diamide-donor-supported titanium borylimides with terminal alkynes

4.1 Overview

This Chapter will describe the reactivity of four diamide-donor-ligand-supported titanium borylimido complexes, Ti($N_2^RN^{Me}$){NB(NAr'CH)$_2$}(py) (R = $SiMe_3$ (**4**), Ar^F (**5**), ^{i}Pr (**6**)) and Ti(N_2N^{py}){NB(NAr'CH)$_2$}(py) (**7**), with two terminal alkynes, HCCTol and $HCCAr^F$. The reactions primarily resulted in either [2+2] cycloadditions of the alkyne across the Ti–N multiple bond or C–H bond activations at the terminal sp carbon, depending on the identity of the supporting ligand and the alkyne. Additionally, two cases of an interesting C–F activation will be described, and kinetic analyses of these processes will be presented. DFT calculations will also be presented to explain the differing outcomes of the reactions with terminal alkynes, as well as the potential for hydroamination-type reactivity in these systems.

4.2 Introduction

As introduced in Chapter One, Group 4 imido and hydrazido complexes display a broad range of reactivity with small unsaturated molecules.[1–21] In recent years, alkynes have become one focus of reactivity studies on these systems, as researchers have aimed to discover new C–N bond-forming processes that arise from reactions at the metal–nitrogen multiple bond. Additionally, for terminal alkynes, competitive 1,2-C–H bond activations may also take place across the multiple bond.[22–25] Catalytic C–N bond-forming reactions with alkynes have been of particular interest, and include hydroamination, hydrohydrazination and iminohydrohydrazination, which all involve the net addition of an N–H bond across an unsaturated C–C bond.[6,11,26–39] More recently, diamination catalysis has been reported, in which the N–N bond of N,N'-diarylhydrazines is added across the triple bond of internal alkynes.[8,12]

In many of these catalytic processes, the first step of the mechanism is the [2+2] cycloaddition of the alkyne or alkene across the metal–nitrogen multiple bond to yield an azametallacyclobutene. For example, Scheme 4.1 depicts a catalytic cycle for the hydroamination of HCCPh by H_2NXyl using an aminopyrollinato-supported titanium imido catalyst, Cp*Ti($N^{3,5\text{-Xyl}}N^{pyr}$)(NXyl) (**1.29**), as reported by Gade and co-workers.[22] Considering this catalytic cycle stepwise, addition of HCCPh to **1.29** results in the azatitanacyclobutene **4.1** *via* [2+2] cycloaddition. Next, aminolysis of the metallacycle by H_2NXyl reforms the imido functional group by two successive proton transfers, to

ultimately extrude the enamine **4.2**. In this case, the putative vinylamido ligand-containing intermediate **4.1_Int** was not observed.

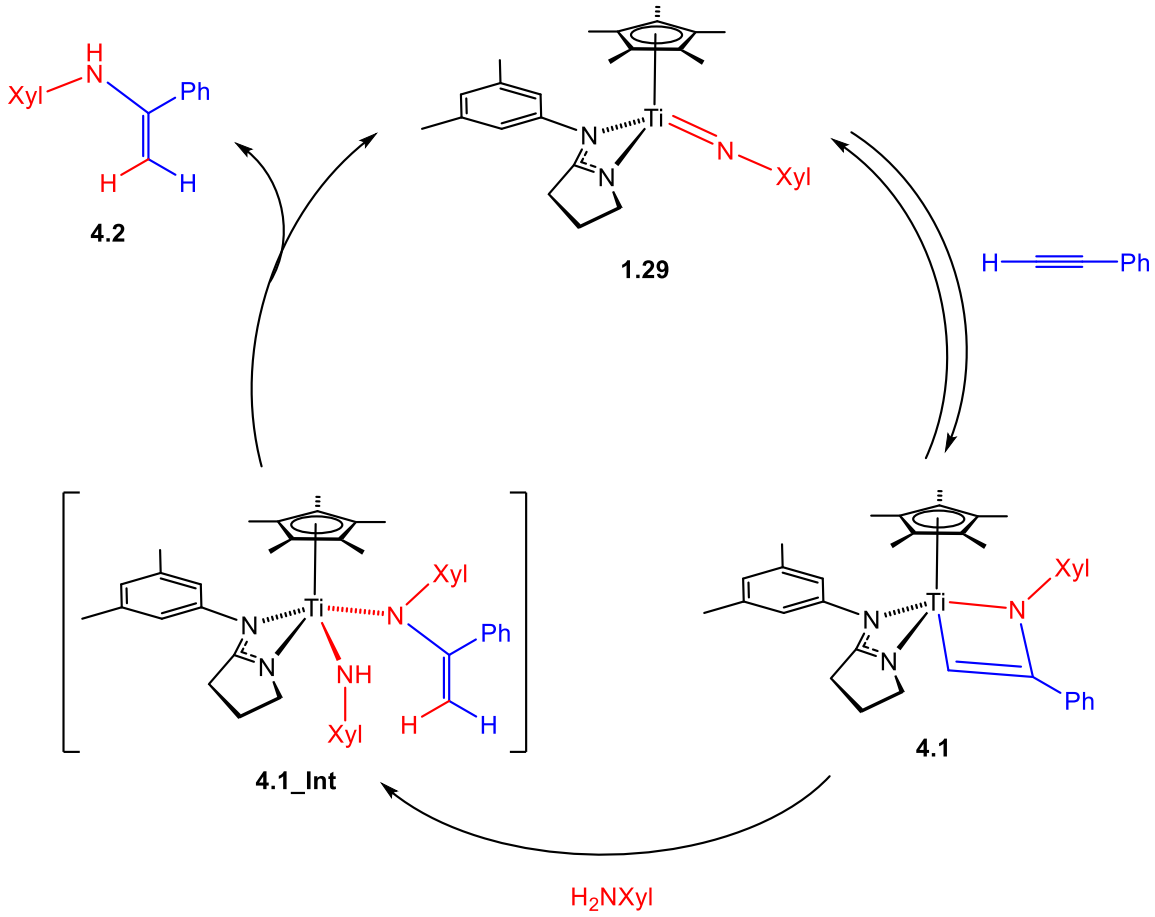

Scheme 4.1. An exemplar catalytic cycle of the hydroamination of a terminal alkyne by H_2NXyl using Cp*Ti($N^{3,5\text{-}Xyl}N^{pyr}$)(NXyl) (**1.29**) as catalyst.[22]

Within our research group, much success has been found in the reactions, both stoichiometric and catalytic, of alkynes with titanium imides and hydrazides supported by diamide-amine and diamide-pyridine ligands.[8,9,12,30,40–45] For example, the hydrazide Ti($N_2^{SiMe_3}N^{Me}$)($NNPh_2$)(py) (**1.63**) reacts with internal alkynes to yield vinylimido species of the type Ti($N_2^{SiMe_3}N^{Me}$){NC(R)C(Me)NPh_2}(py) (**1.93**, R = Me, Ph, Tol, 4-$C_6H_4{}^tBu$, 4-C_6H_4OMe, 4-$C_6H_4CF_3$) through N_α–N_β bond insertion (Equation 4.1).[8,12] With the addition of H_2NNPh_2, a catalytic cycle is set up, in which the vinylimido ligand is cleaved from the metal centre *via* protonolysis, and a hydrazido complex regenerated. This is formally the addition of the N–N bond of the hydrazine across the alkyne triple bond, a 1,2-diamination.

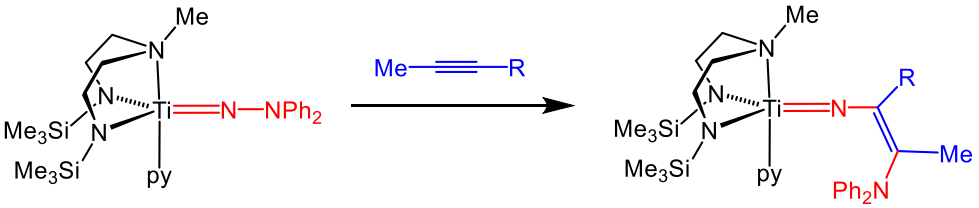

1.63 **1.93**

R = Me, Ph, Tol, 4-$C_6H_4{}^tBu$, 4-C_6H_4OMe, 4-$C_6H_4CF_3$

Equation 4.1[8]

Later, a modification of the diamide-amine supporting ligand was introduced, which incorporates isopropyl rather than trimethylsilyl groups as the N_{amide}-substituents. Reactions of the hydrazide Ti($N_2^{iPr}N^{Me}$)($NNPh_2$)(py) (**2.1**) with the internal alkynes MeCCPh and MeCCMe gave complex mixtures of products. However, reactions of **2.1** with a range of terminal alkynes were found to successfully form vinylhydrazide-acetylide compounds of the type Ti($N_2^{iPr}N^{Me}$){N(NPh_2)C(H)C(H)(R)}(CCR) (**4.3**, R = Tol, 4-$C_6H_4CF_3$, 4-C_6H_4OMe, Ar^F, $SiMe_3$; Equation 4.2).[30] With the addition of H_2NNPh_2, the hydrazide **2.1** was found to catalyse the hydrohydrazination of the terminal alkyne, which is the formal addition of the N–H bonds of the hydrazine across the alkyne triple bond to yield a hydrazone. The vinylhydrazide-acetylides **4.3** were proposed to be intermediates in the catalytic cycle.

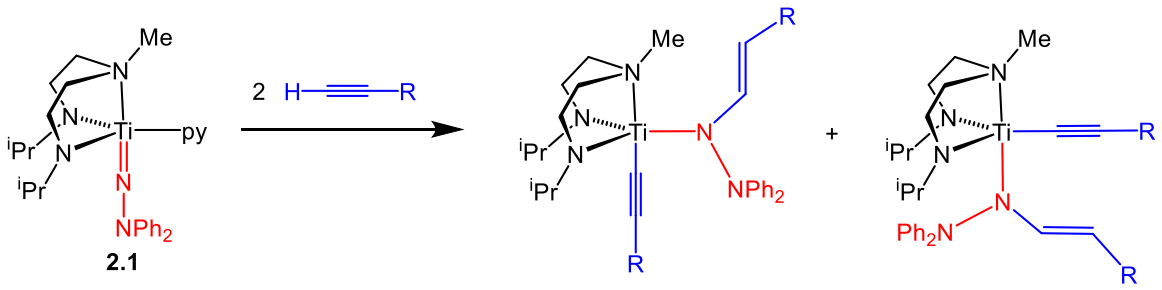

2.1

cis (thermodynamic product) *trans* (kinetic product)

4.3 (R = Tol, 4-$C_6H_4CF_3$, 4-C_6H_4OMe, Ar^F, $SiMe_3$)

Equation 4.2[30]

The examples above demonstrate the suitability of diamide-amine supporting ligand sets for controlled reactivity studies of titanium–nitrogen multiple bonds, as well as highlighting the dramatic shift in catalytic behaviour of **1.63** and **2.1** with a modification of the N_{amide}-substituent. Thus, the reactions of the diamide-amine-supported borylimides **4** – **6**, and the diamide-pyridine-supported **7**, with terminal alkynes were targeted. In this Chapter,

reactions of those four complexes with two such terminal alkynes, HCCTol and HCCAr^F, will be explored. No reactivity was observed, however, between these four borylimides and three internal alkynes; MeCCMe, MeCCPh and MeCC-4-$C_6H_4CF_3$ (see Section 4.7).

4.3 Reactions of Ti($N_2^{SiMe_3}N^{Me}$){NB(NAr'CH)$_2$}(py) (4) with terminal alkynes

When performed on the NMR tube scale, the reactions between Ti($N_2^{SiMe_3}N^{Me}$){NB(NAr'CH)$_2$}(py) (**4**) and the terminal alkynes HCCTol and HCCAr^F, were both quantitative, forming the azatitanacyclobutene complexes Ti($N_2^{SiMe_3}N^{Me}$){N{B(NAr'CH)$_2$}C(H)C(Ar)} (Ar = Tol (**23**), Ar^F (**24**)). The reactions were extremely rapid at RT, with immediate colour changes from red to red-black being observed in both cases. On the preparative scale, the reactions were carried out in toluene over 1 h at RT, with **23** and **24** being isolated as waxy solids in 68 and 66% yields, respectively (Equation 4.3).

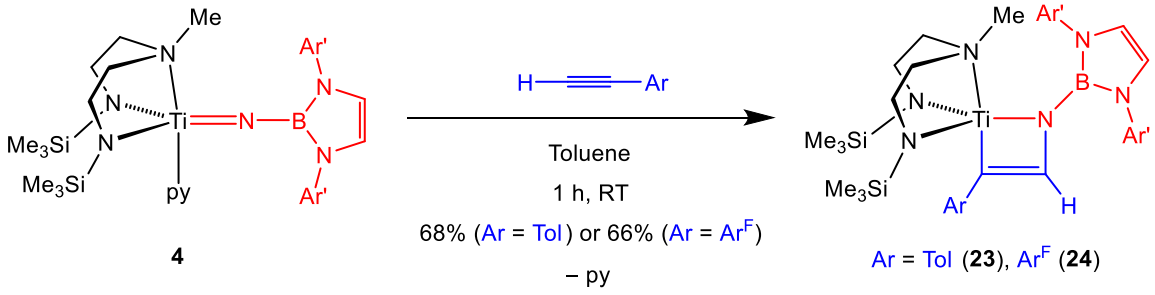

Equation 4.3

The identification of **23** and **24** as azatitanacyclobutene structures, formed by [2+2] cycloaddition of the alkyne across the Ti–N multiple bond, was initially achieved through inspection of the respective ^{1}H NMR spectrum (shown for **23** in Figure 4.1). In both spectra, a 1 H singlet is observed at a diagnostically high chemical shift: 10.51 and 10.43 ppm in **23** and **24** respectively, which corresponds to the C=CH of the azatitanacyclobutene unit. These are comparable to the methine ^{1}H chemical shifts of a number of previously reported cycloadditions with terminal alkynes.[9,12,22,41,45] Close inspection of the ^{1}H NMR spectrum of **24** reveals that this complex was actually isolated as a mixture of two isomers in a *ca* 4:1 ratio (calculated by NMR integration), with the duplication of all resonances other than the C=CH which is a single broad singlet. The isomerism is proposed to arise from the *cis* or *trans* placing of the borylamido fragment of the metallacycle with respect to the NMe donor. Analysis of the spectrum of a ROESY NMR experiment proved inconclusive in assigning which of these is the major and minor isomer. However, the

regiochemistry of the [2+2] cycloaddition itself must also be considered. In **23**, an HSQC correlation is found between C=C<u>H</u> at 10.51 ppm and a ^{13}C resonance at 162.7 ppm, whilst an HMBC correlation is observed to a ^{13}C resonance at 205.3 ppm. The latter (high δ) resonance is diagnostic of being directly bonded to the titanium centre, hence this confirms that **23** exists as a single anti-Markovnikov regioisomer (as depicted in Equation 4.3). In **24**, the analogous HSQC correlation is observed to a ^{13}C signal at 161.8 ppm, whilst the HMBC correlation is to a ^{13}C signal with a somewhat higher chemical shift of 179.4 ppm, this again being consistent with an anti-Markovnikov isomer. A second set of HSQC and HMBC correlations for the broadened C=CH singlet was not observed. It is therefore proposed that the two isomers of **24** are in exchange on the NMR timescale, with the observed shifts of the ^{1}H and ^{13}C resonances associated with the azatitanacyclobutene core being weighted means of those of the two isomers. To test this, variable temperature ^{1}H NMR experiments were performed between 298 K and 208 K in toluene-d_8. Whilst the broad C=CH singlet was observed to shift slightly further downfield with decreasing temperature, decoalescence into two signals was not observed, even at the lowest temperature measured.

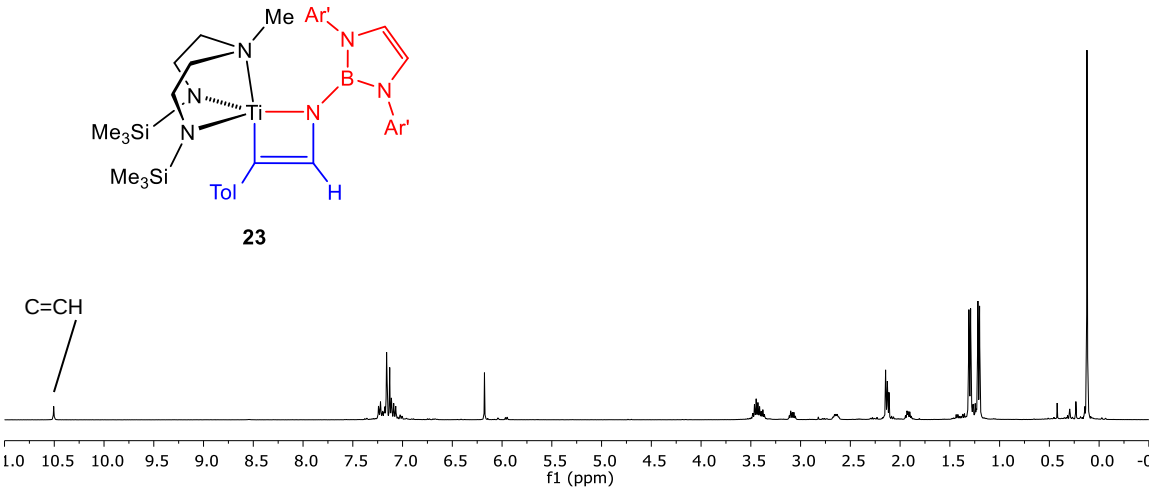

Figure 4.1. ^{1}H NMR spectrum (400.1 MHz) of Ti($N_2^{SiMe_3}N^{Me}$){N{B(NAr'CH)$_2$}C(H)C(Tol)} (**23**) in C_6D_6 at 298 K.

The origin of the regioselectivity of [2+2] cycloadditions has previously been investigated by DFT calculations on a model of the hydrazide **1.63**.[12] The HOMO of the respective azatitanacyclobutene was calculated to result from stabilisation of the four-electron repulsion between the lone pair on the N_{im} atom and the filled C–C π orbital of the alkyne by the vacant C–C π* orbital. As a result of the mixing between these orbitals, the HOMO

of the metallacycle resides primarily on the N_{im} atom and the carbon atom bonded to titanium. Where the incoming alkyne has one π-accepting substituent, such as an aryl group, its own HOMO is mostly developed on the sp carbon atom directly bonded to that substituent. Therefore, the arrangement which minimises repulsion between the alkyne π MO and the N_{im} lone pair is the one in which the aryl-substituted end of the alkyne bonds to the titanium, the so-called anti-Markovnikov regioisomer (i.e. the isomer that would give rise to the anti-Markovnikov hydroamination product upon protonolysis). Quantitatively, for HCCPh in the model hydrazido system, that regioisomer is favoured by a factor of 10^4 over the Markovnikov regioisomer, in terms of an equilibrium between the two.[12] Being a strongly σ-withdrawing group in addition to a π-acceptor, the Ar^F group is expected to give an even stronger anti-Markovnikov regioselectivity.

Diffraction-quality crystals of **23** were grown from a small sample of the isolated waxy solid left under dynamic vacuum for an extended period of time. The molecular solid state structure is shown in Figure 4.2, and selected bond distances and angles are listed in Table 4.1. Compound **23** has a distorted pentacoordinate geometry, having a τ value of 0.59. The parameter τ was defined by Addison *et al*. as $(A - B)/60$, where A and B are the two greatest L–M–L angles in the complex.[46] For a perfect square-based pyramid, $\tau = 0$, and for a perfect trigonal bipyramid, $\tau = 1$. The geometry of **23**, therefore, may be described as 59% along the pathway of distortion between square-based pyramidal and trigonal bipyramidal geometries. The diamide-amine ligand remains facially coordinated to the metal, and the κ^2-coordination of the C(38)–C(39)–N(1) unit to form the four-membered azatitanacyclobutene ring with Ti(1) is confirmed. This moiety appears comparable to those analogues which have previously been structurally characterised,[24,40,41] having a small bite angle (N(1)–Ti(1)–C(38)) of 75.52(4)°. This is, however, wider than in the compounds Ti(N_2N^{py}){N(Ar')C(H)C(Tol)} (**4.4**) and Ti($N_2^{3,5\text{-Xyl}}N^{py}$){N(^{t}Bu)C(H)C(Tol)} ($N_2^{3,5\text{-Xyl}}N^{py}$ = (2-C_5H_4N)CMe(CH_2N-3,5-$C_6H_3Me_2$)$_2$), which have bite angles of 68.3(1) and 70.63(7)° respectively,[40,41] this presumably being necessary to accommodate the steric bulk of the boryl moiety. The C=C bond length of 1.3715(16) Å is consistent with this being a carbon–carbon double bond, and the Ti(1)–N(1) and Ti(1)–C(38) bond lengths of 1.9784(10) and 2.0026(12) Å respectively are consistent with sp^2-type single bonds being formed to the metal centre. Interestingly, the shift from a Ti–N triple bond to a single bond appears to have had no significant effect on the N(1)–B(1) bond, its distance being 1.4275(16) Å in **23** and 1.4190(19) Å in the starting borylimide **4**.

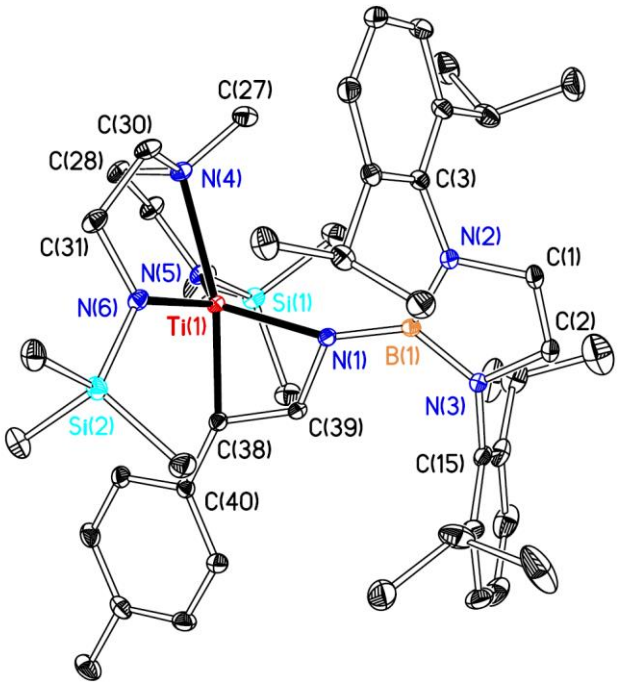

Figure 4.2. Displacement ellipsoid plot (25% probability) of Ti($N_2^{SiMe_3}N^{Me}$){N{B(NAr'CH)$_2$}C(H)C(Tol)} (**23**). H atoms are omitted for clarity.

Table 4.1. Selected bond distances (Å) and angles (°) for Ti($N_2^{SiMe_3}N^{Me}$){N{B(NAr'CH)$_2$}C(H)C(Tol)} (**23**) (τ = 0.59).

Ti(1)–N(1)	1.9784(10)	N(1)–Ti(1)–N(4)	119.26(4)
Ti(1)–N(4)	2.2900(10)	N(1)–Ti(1)–N(5)	115.69(4)
Ti(1)–N(5)	1.9798(10)	N(1)–Ti(1)–N(6)	75.84(4)
Ti(1)–N(6)	1.9880(10)	N(5)–Ti(1)–N(6)	129.88(4)
Ti(1)–C(38)	2.0026(12)	N(1)–Ti(1)–C(38)	75.52(4)
N(1)–B(1)	1.4275(16)	N(4)–Ti(1)–C(38)	165.11(4)
N(1)–C(39)	1.4277(14)	N(5)–Ti(1)–C(38)	96.65(4)
C(38)–C(39)	1.3715(16)	N(6)–Ti(1)–C(38)	99.69(4)
		Ti(1)–N(1)–B(1)	157.51(8)
		Ti(1)–C(38)–C(39)	81.22(7)
		N(1)–C(39)–C(38)	121.12(10)

4.4 Reactions of Ti($N_2^{ArF}N^{Me}$){NB(NAr'CH)$_2$}(py) (5) with terminal alkynes

With the reactions of Ti($N_2^{SiMe_3}N^{Me}$){NB(NAr'CH)$_2$}(py) (**4**) with the two terminal alkynes above acting as a starting point, attention was next given to testing whether changing the N_{amide}-substituents of the diamide-amine supporting ligand would alter the reaction outcomes. On the NMR tube scale in C_6D_6, the reaction of Ti($N_2^{ArF}N^{Me}$){NB(NAr'CH)$_2$}(py) (**5**) with HCCTol gave quantitative conversion to a single product at RT, with an immediate colour change of the solution to red-black being observed. In contrast, the NMR tube scale reaction between **5** and $HCCAr^F$ was slower at RT, with resonances belonging to two products increasing in intensity. Heating at 70 °C resulted in conversion to a single species (which was one of those found to be already forming at RT).

On the preparative scale, **5** and HCCTol were mixed in toluene over 20 minutes, yielding the azatitanacyclobutene compound Ti($N_2^{ArF}N^{Me}$){N{B(NAr'CH)$_2$}C(H)C(Tol)} (**25**) as a deep red solid in 76% yield (Scheme 4.2). The reaction with $HCCAr^F$ was also scaled up in toluene, and following heating at 60 °C for 16 h, the product was isolated as a yellow-orange solid in 57% yield (Scheme 4.3). Crystallographic characterisation (*vide infra*) showed that this compound was a titanium fluoride complex, Ti{MeN($CH_2CH_2NAr^F$){$CH_2CH_2NC_6F_4C(Ar^F)$=CHNB(NAr'CH)$_2$}}(F) (**26**), in which one of the C_6F_5 rings of the supporting ligand has become coupled to a vinyl-borylamide moiety to form a seven-membered metallacycle, accompanied by migration of a fluorine from the C_6F_5 ring onto the titanium centre. To investigate the formation of **26**, the isolation of the putative intermediate (the other observed species in the NMR tube scale reaction at RT) was sought. Exclusive formation of this intermediate was successfully achieved on the NMR tube scale by reacting the borylimide **5** with $B(Ar^F)_3$ in order to abstract the pyridine donor, followed by addition of 1 equiv. of $HCCAr^F$. This gave immediate conversion to the azatitanacyclobutene compound Ti($N_2^{ArF}N^{Me}$){N{B(NAr'CH)$_2$}C(H)C(Ar^F)} (**27**). However, on the preparative scale, **27** was found to be unstable to isolation, resulting in a large proportion of H_2NB(NAr'CH)$_2$ (**2.2**) along with unidentified titanium species, so this compound was characterised by NMR experiments only (*vide infra*). Upon heating in C_6D_6 at 60 °C, the Tol-analogue **25** underwent conversion to the titanium fluoride complex Ti{MeN($CH_2CH_2NAr^F$){$CH_2CH_2NC_6F_4C$(Tol)=CHNB(NAr'CH)$_2$}}(F) (**28**), which is entirely analogous in structure to **26**. On the preparative scale, **5** and HCCTol were mixed in toluene at 70 °C for 3.5 h, resulting in **28** as a yellow-orange solid in 47% yield.

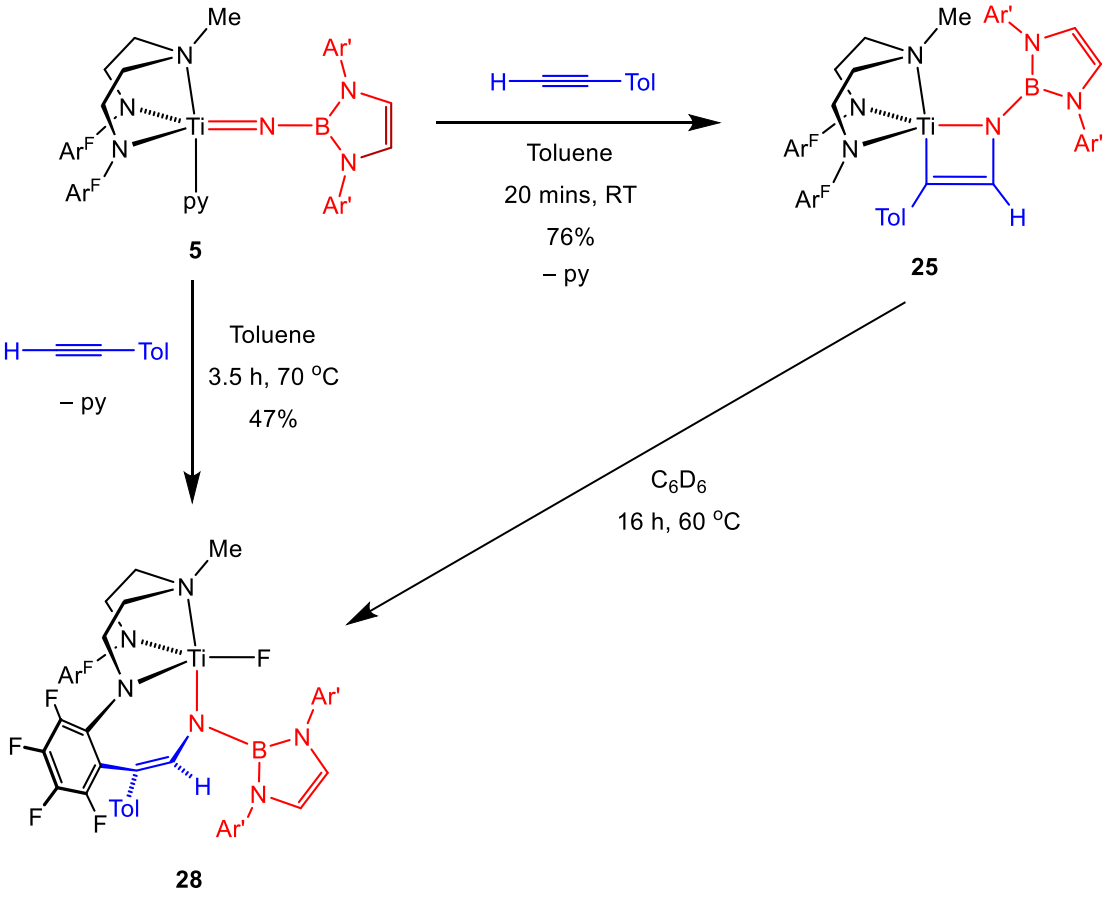

Scheme 4.2. Synthesis of Ti($N_2^{ArF}N^{Me}$){N{B(NAr'CH)$_2$}C(H)C(Tol)} (**25**) and Ti{MeN($CH_2CH_2NAr^F$){$CH_2CH_2NC_6F_4$C(Tol)=CHNB(NAr'CH)$_2$}}(F) (**28**) from Ti($N_2^{ArF}N^{Me}$){NB(NAr'CH)$_2$}(py) (**5**).

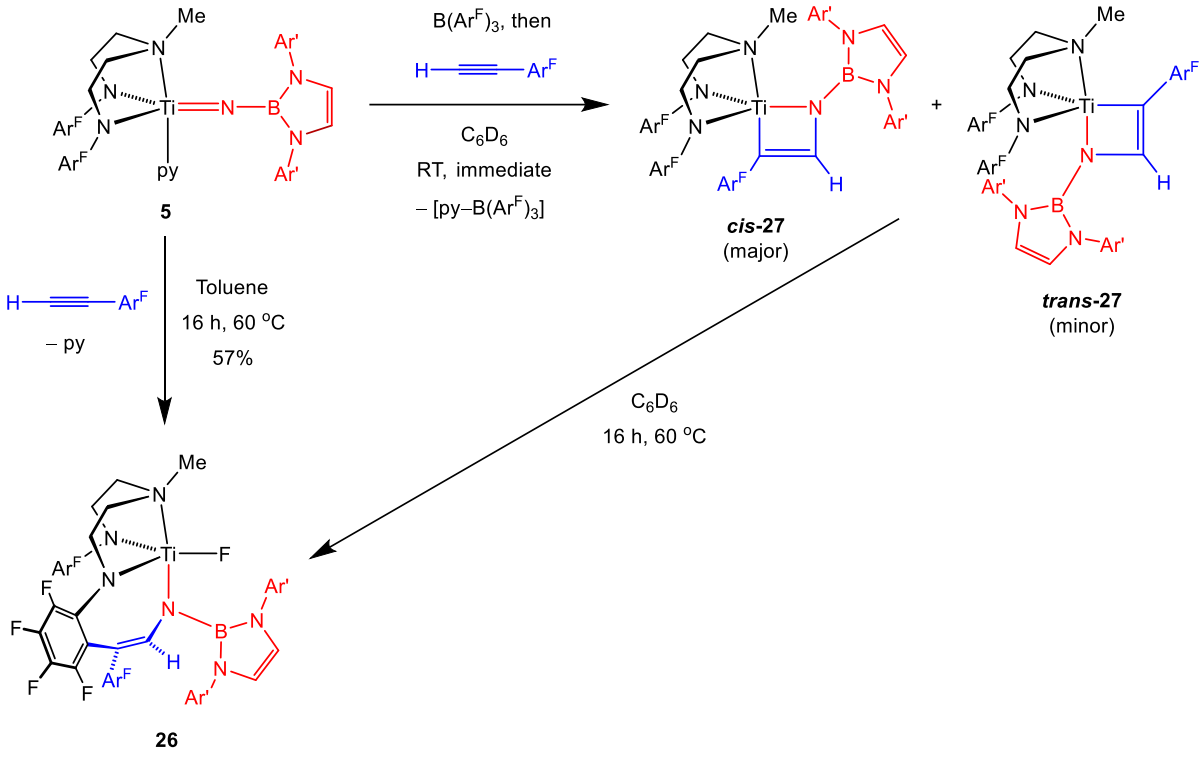

Scheme 4.3. Synthesis of Ti($N_2^{ArF}N^{Me}$){N{B(NAr'CH)$_2$}C(H)C(Ar^F)} (**27**) and Ti{MeN($CH_2CH_2NAr^F$){$CH_2CH_2NC_6F_4C(Ar^F)$=CHNB(NAr'CH)$_2$}}(F) (**26**) from Ti($N_2^{ArF}N^{Me}$){NB(NAr'CH)$_2$}(py) (**5**).

Characterisation of the two azatitanacyclobutene complexes **25** and **27** by ^{1}H and ^{13}C NMR showed that compound **25** exists as a single isomer, whilst **27** exists as two isomers in a *ca* 3:1 ratio. The molecules of both compounds (including both isomers of **27**) are C_s symmetric, with just one set of resonances for the boryl isopropyl groups, and four multiplets for the $N_2^{ArF}N^{Me}$ methylene groups signifying a mirror plane through the supporting ligand on the NMR time scale. The ^{1}H NMR spectrum of **25** is shown in Figure 4.3 (top). The ^{1}H and ^{13}C NMR spectra of both **25** and **27** show the diagnostic features of an azatitanacyclobutene structure in analogy with that of the $N_2^{SiMe_3}N^{Me}$ counterpart **23**. The metallacycle methine proton of **25** gave a singlet at 11.61 ppm, whilst the two isomers of **27** gave singlets at 11.51 and 11.30 ppm. Again, anti-Markovnikov regiochemistry for all structures was confirmed by HSQC and HMBC correlations. In **25**, an HSQC correlation was observed to a ^{13}C signal at 163.8 ppm, and an HMBC correlation observed to 217.2 ppm. For the two isomers of **27**, HSQC correlations were observed at 162.6 and 160.2 ppm, and HMBC correlations at 194.1 and 201.1 ppm. Though the two isomers of **27** are both confirmed as being of anti-Markovnikov regiochemistry, a ROESY experiment to test

which set of NMR resonances corresponds to either the *cis* or *trans* isomer unfortunately proved inconclusive.

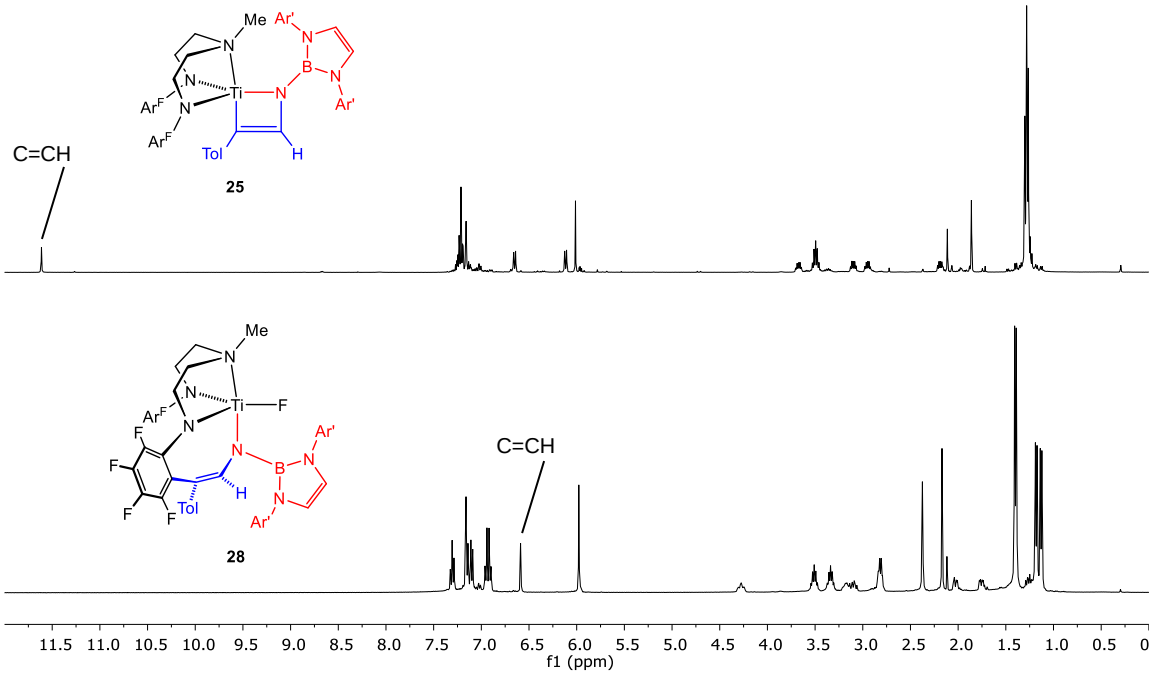

Figure 4.3. ^{1}H NMR spectra (400.1 MHz) of Ti($N_2^{ArF}N^{Me}$){N{B(NAr'CH)$_2$}C(H)C(Tol)} (**25**, top) and Ti{MeN(CH$_2$CH$_2$NAr^F){CH$_2$CH$_2$NC$_6$F$_4$C(Tol)=CHNB(NAr'CH)$_2$}}(F) (**28**, bottom) in C_6D_6 at 298 K.

Diffraction-quality crystals of **25** were successfully grown from a hexane solution at 5 °C. The molecular solid state structure is shown in Figure 4.4, and selected bond distances and angles are listed in Table 4.2. Molecules of **25** have an analogous structure to **23**, having distorted pentacoordinate geometry, with a τ value of 0.69. The diamide-amine ligand coordinates to the titanium centre in a facial arrangement, and the κ^2-C(44)–C(45)–N(1) unit is arranged with the N-boryl group *cis* to the NMe donor. The bite angle of the latter group is again larger than in the literature analogues, being 77.19(6)°. The C(44)–C(45), Ti(1)–C(44) and Ti(1)–N(1) bond distances are comparable with the corresponding values observed for **23**. However, in this case, there is a π-stacking interaction between the tolyl ring and one of the C_6F_5 rings of the supporting diamide-amine ligand which may be described as having an offset face-to-face relationship.[47] The centroid–centroid distance of the two rings is *ca* 3.73 Å, which is similar to the centroid–centroid distances between C_6H_6 and C_6F_6 rings in the solid state structure of a 1:1 mixture of those compounds, these being 3.4 – 3.6 Å.[48–50] A close C···C contact of *ca* 3.19 Å is found, this being comparable to close

contacts in previously reported complexes incorporating π-stacking of perfluorophenyl rings,[51] as well as, for example, C···C distances in the computed solid state structure of C_6F_6 itself.[47] The topic of intra- and intermolecular π-stacking between phenyl and perfluorophenyl rings has been of increasing interest to researchers in recent years due to the strong stabilisation (*ca* 7 kcal mol^{-1}) of molecular structures arising from these interactions.[52] Other similar interactions of fluorine, such as hydrogen bonds to F atoms and F···F interactions are much weaker in comparison (as summarised in a review by Hulliger and co-workers).[53]

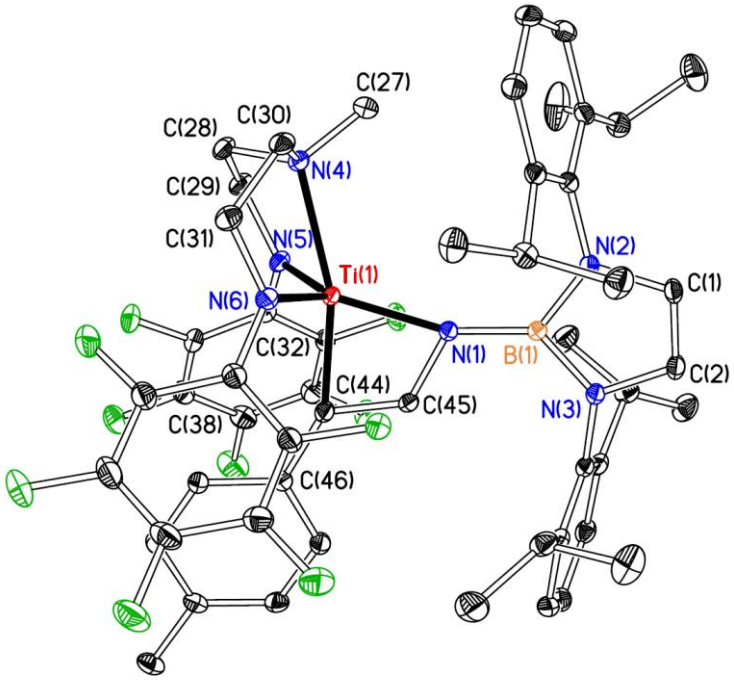

Figure 4.4. Displacement ellipsoid plot (25% probability) of $Ti(N_2^{ArF}N^{Me})\{N\{B(NAr'CH)_2\}C(H)C(Tol)\}$ (**25**). H atoms are omitted for clarity.

Table 4.2. Selected bond distances (Å) and angles (°) for Ti($N_2^{ArF}N^{Me}$){N{B(NAr'CH)$_2$}C(H)C(Tol)} (**25**) (τ = 0.69).

Ti(1)–N(1)	1.9833(13)	N(1)–Ti(1)–N(4)	119.76(5)
Ti(1)–N(4)	2.2530(14)	N(1)–Ti(1)–N(5)	120.32(6)
Ti(1)–N(5)	1.9944(15)	N(1)–Ti(1)–N(6)	118.17(6)
Ti(1)–N(6)	1.9882(15)	N(5)–Ti(1)–N(6)	121.50(6)
Ti(1)–C(44)	1.9522(17)	N(1)–Ti(1)–C(44)	77.19(6)
N(1)–B(1)	1.443(2)	N(4)–Ti(1)– C(44)	162.79(6)
N(1)–C(45)	1.402(2)	N(5)–Ti(1)– C(44)	93.63(7)
C(44)–C(45)	1.389(2)	N(6)–Ti(1)– C(44)	98.61(7)
		Ti(1)–N(1)–B(1)	161.16(11)
		Ti(1)–C(44)–C(45)	80.31(10)
		N(1)–C(45)–C(44)	123.18(15)

Turning next to the characterisation of the titanium fluoride complexes **26** and **28**, the ^{1}H NMR spectrum of **28** is shown in Figure 4.3 (bottom). Whilst the ^{1}H NMR spectrum of **25** was indicative of a C_s symmetric species, the transformation to **28** has resulted in a C_1 symmetric structure, in which two sets of resonances are observed for the isopropyl groups on the boryl moiety. Additionally, the four methylene groups of the diamide-amine ligand now give eight multiplets (some overlapping), compared with the four multiplets observed in the azatitanacyclobutene **25**. Most significantly, a 1 H singlet is observed at 6.59 ppm which corresponds to the olefinic proton adjacent to the N-boryl group in the expanded metallacycle. This is a significant shift from the 11.61 ppm signal of the azatitanacyclobutene methine proton in **25**. The ^{1}H NMR spectrum of **26** is analogous to that described for **28**. Most importantly, a similar olefinic signal is found at 6.72 ppm. In the ^{19}F spectra of **26** and **28**, very low intensity singlets were found at –100.0 and –102.5 ppm, respectively, these corresponding to the titanium-bound fluorides and being far downfield relative to the signals of those F nuclei remaining bound to the aromatic rings.

Diffraction-quality crystals of **26** and **28** were grown from hexane and benzene solutions, respectively, at RT. The molecular solid state structures are shown in Figure 4.5, and selected bond distances and angles are listed in Table 4.3. Both complexes are found to be pentacoordinate, but now have slightly distorted trigonal bipyramidal geometries (τ = 0.93 (**26**) and 0.95 (**28**)), in which the diamide-amine ligand is facially coordinating. The fluoride ligand occupies the third equatorial site, and the N-boryl group now sits *trans* to the NMe donor in the opposing axial site. Both complexes incorporate a seven-membered metallacycle, formed from the coupling of a ligand C_6F_5 group onto what was the Ti-bound carbon in the azatitanacyclobutenes **27** and **25**. The olefinic C=C bonds have distances of 1.343(3) and 1.353(3) Å in **26** and **28** respectively, so are significantly shorter than the C=C bond distance in the solid state structure of **25** (1.389(2) Å). Meanwhile, the C–C and C–N bond distances either side of the olefinic linkage are consistent with being single bonds.

The solid state structures of the fluoride complexes **26** and **28** also both display π-stacking interactions, in these cases between an Ar' group of the boryl moiety and the C_6F_4 ring of the seven-membered metallacycle. Similar to that observed in **25**, these are considered offset face-to-face interactions.[47] The centroid–centroid distances of the two interactions are *ca* 3.70 and 3.73 Å in **26** and **28** respectively, so both are comparable to that observed in **25** (3.73 Å). The closest C···C contacts of *ca* 3.34 and 3.41 Å, respectively, in the two complexes are somewhat longer than that in **25** (3.19 Å), though this appears to reflect a greater degree of lateral offset of the two rings in both of these cases, compared with the former complex.

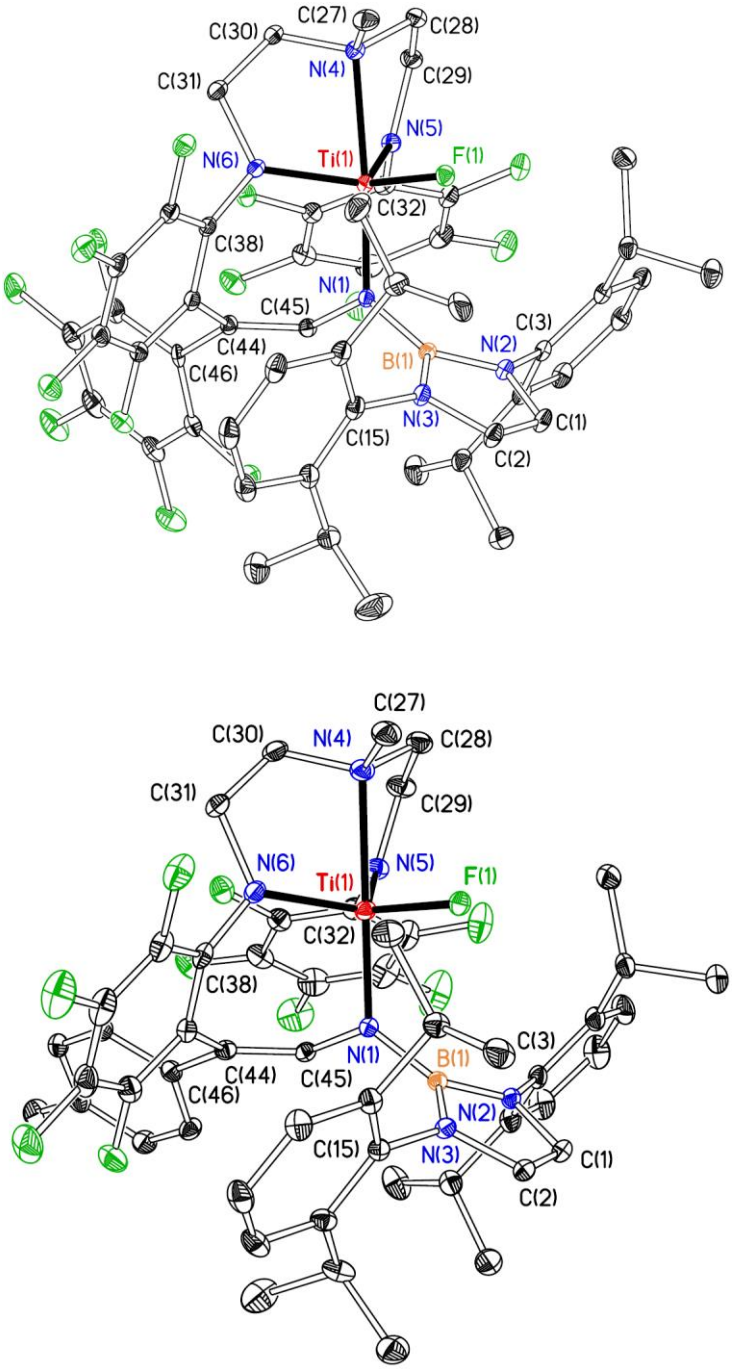

Figure 4.5. Displacement ellipsoid plots (20% probability) of Ti{MeN($CH_2CH_2NAr^F$){$CH_2CH_2NC_6F_4C$(Ar)=CHNB(NAr'CH)$_2$}}(F) (Ar = Ar^F (**26**, top), Tol (**28**, bottom). H atoms are omitted for clarity.

Table 4.3. Selected bond lengths (Å) and angles (°) for Ti{MeN($CH_2CH_2NAr^F$){$CH_2CH_2NC_6F_4C$(Ar)=CHNB(NAr'CH)$_2$}}(F) (Ar = Ar^F (**26**), Tol (**28**) (τ = 0.93 (**26**) and 0.95 (**28**)).

Parameter	**26**	**28**
Ti(1)–N(1)	1.9300(17)	1.9105(17)
Ti(1)–N(4)	2.2667(19)	2.265(2)
Ti(1)–N(5)	1.9759(18)	1.957(2)
Ti(1)–N(6)	1.9466(18)	1.936(2)
Ti(1)–F(1)	1.8016(12)	1.8226(13)
N(1)–B(1)	1.479(3)	1.470(3)
N(1)–C(45)	1.405(2)	1.404(3)
C(44)–C(45)	1.343(3)	1.353(3)
N(1)–Ti(1)–N(4)	175.29(7)	177.52(8)
N(1)–Ti(1)–N(5)	107.63(7)	106.37(8)
N(1)–Ti(1)–N(6)	98.93(7)	101.93(8)
N(5)–Ti(1)–N(6)	116.01(8)	113.22(9)
N(1)–Ti(1)–F(1)	95.62(6)	94.78(7)
N(4)–Ti(1)– F(1)	85.20(6)	83.62(6)
N(5)–Ti(1)– F(1)	114.14(7)	115.60(7)
N(6)–Ti(1)– F(1)	119.81(7)	120.65(7)
Ti(1)–N(1)–B(1)	127.01(13)	125.08(14)
Ti(1)–N(1)–C(45)	112.13(13)	110.31(13)
N(1)–C(45)–C(44)	125.97(19)	126.4(2)

Attention is now given to the mechanism of formation of the titanium fluoride complexes **26** and **28**. After initial cycloaddition of the alkyne to give the azatitanacyclobutenes **27** and **25**, it is proposed that nucleophilic attack of the Ti-bound carbon of the metallacycle unit on the *ortho* position of a supporting ligand C_6F_5 ring takes place, resulting in an expanded (seven-membered) metallacycle, and accompanied by migration of the displaced

fluorine atom to the titanium centre. A similar C–F activation was previously reported by this research group, in which [1+2] addition of XylNC to a benzimidamido complex Cp*Ti{PhC(N^{i}Pr)$_2$}{NC(Ar^{F})NO^{t}Bu} (**4.5**) was followed by nucleophilic attack of the XylNC atom of an η^2-carbodiimide intermediate (**4.5_Int**) on the *ortho* position of the nearby Ar^{F} group (Scheme 4.4).[54] Other examples of C–F bond activations by d^0 Group 4 metal species have been reported,[55,56] and titanium fluoride compounds are not uncommon.[57–61]

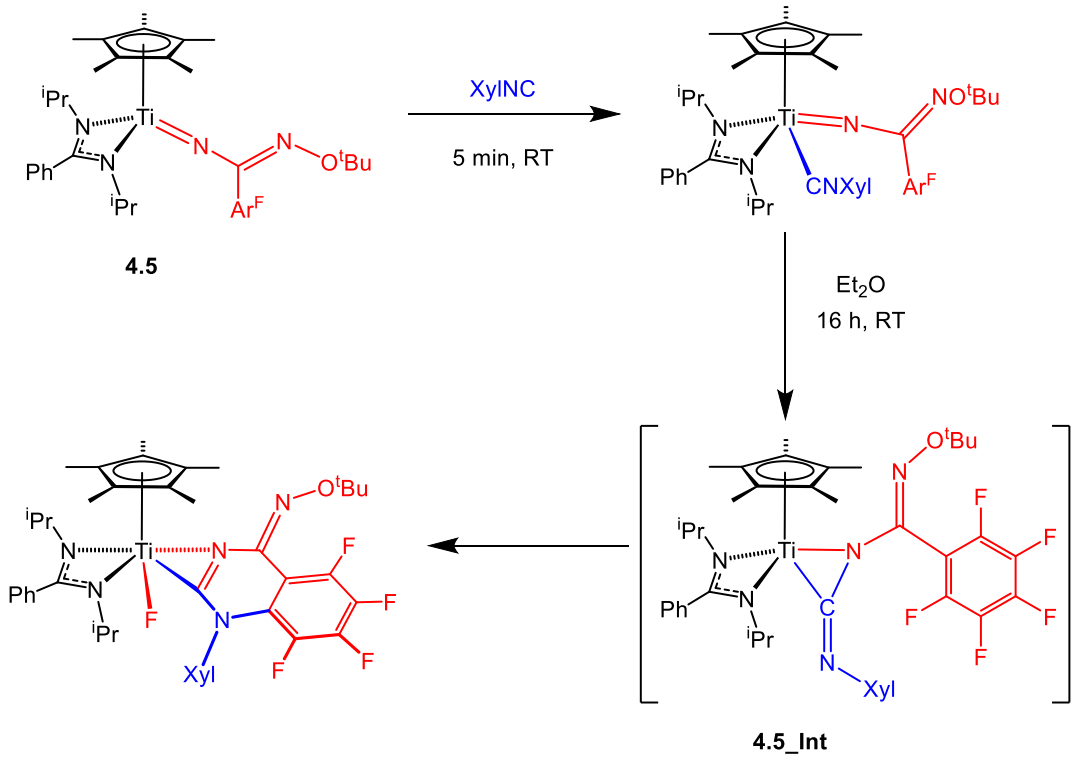

Scheme 4.4. C–F bond activation resulting from reaction of Cp*Ti{PhC(N^{i}Pr)$_2$}{NC(Ar^{F})NO^{t}Bu} (**4.5**) with XylNC.[54]

In order to support the mechanism of C–F bond activation proposed above, both transformations (**25** to **28** and **27** to **26**) were monitored by ^{1}H NMR arrays in the temperature range 327 – 339 K. The reactions followed first order kinetics over this temperature range as judged by linear semilogarithmic plots of –ln(1–([**28**]/[**28**]$_{final}$)) *vs* time (and analogously for [**26**]). This form of the rate law (in terms of the product **28**) is valid as only **25** and **28** (and no intermediates) are observed, and [**25**]$_0$ = [**28**]$_{final}$. The plots are shown in Figures 4.6 and 4.7, respectively, and all reactions are shown to at least 85% conversion (approximately three half-lives). The rates were found to be effectively independent of the concentration of starting material; for **25**, a reaction monitored at double

concentration at 333 K showed no significant variation in rate from the reaction monitored at the standard concentration (k = 12.72(2) × 10^{-5} and 11.04(3) × 10^{-5} s^{-1} for double and standard concentrations respectively), and similarly for **27** at 336 K (k = 12.63(2) × 10^{-5} and 11.82(1) × 10^{-5} s^{-1} for double and standard concentrations respectively). The extracted first order rate constants for all temperatures monitored are listed in Appendix A2 (Tables A3 (reaction of **25**) and A4 (reaction of **27**)).

An Eyring analysis of the first order rate constants, k, was carried out for both reactions. For the reaction of **25** (Figure 4.6), this gave the activation parameters $\Delta H^{\ddagger}$ = 14.1(1.5) kcal mol^{-1} and $\Delta S^{\ddagger}$ = –34.3(4.4) cal mol^{-1} K^{-1} ($\Delta G_{333}^{\ddagger}$ = 25.5(1.5) kcal mol^{-1}). For the reaction of **27** (Figure 4.7), the activation parameters obtained were $\Delta H^{\ddagger}$ = 13.9(1.0) kcal mol^{-1} and $\Delta S^{\ddagger}$ = –35.3(2.9) cal mol^{-1} K^{-1} ($\Delta G_{333}^{\ddagger}$ = 25.7(1.0) kcal mol^{-1}). The free energy of activation ($\Delta G^{\ddagger}$) values are both consistent with reactions that require elevated temperatures to proceed. Also, the entropy of activation ($\Delta S^{\ddagger}$) values are strongly negative. This is consistent with the proposed mechanism, in which nucleophilic attack of the azatitanacyclobutene carbon atom on the Ar^F ring results in a cyclisation, giving coupling of the diamide-amine supporting ligand to the alkenic moiety. This would be expected to greatly reduce the vibrational degrees of freedom of the complex, and hence give a negative $\Delta S^{\ddagger}$. It is also apparent that all three activation parameters are comparable for the two different reactions. Given the proposal that these reactions involve nucleophilic attack, the reaction in which the azatitanacyclobutene unit has a substituted electron-withdrawing Ar^F group might be expected to be slower than the reaction where this is a Tol group, as there would be less negative charge built up on that carbon in the former case. As described earlier, the molecular solid state structure of **25** contains a π-stacking interaction between an Ar^F group of the supporting ligand and the Tol group. Although **27** could not be crystallographically characterised, if that complex contained an analogous π-stacking interaction, it would be between two Ar^F rings. Computational work by Dance and co-workers has shown that the π-stacking between C_6H_6 and C_6F_6 rings is approximately twice as attractive as that between two C_6F_6 molecules,[47] and that this result may be extended to π-stacking between Ph and Ar^F groups. Therefore, it is proposed that the comparable activation parameters obtained for the C–F bond activation reactions of **25** and **27** arise from a balance of effects: the greater stabilisation of **25** relative to **27** by π-stacking offsets the greater nucleophilicity of the Tol-substituted metallacycle carbon atom relative to that which is substituted by an Ar^F group.

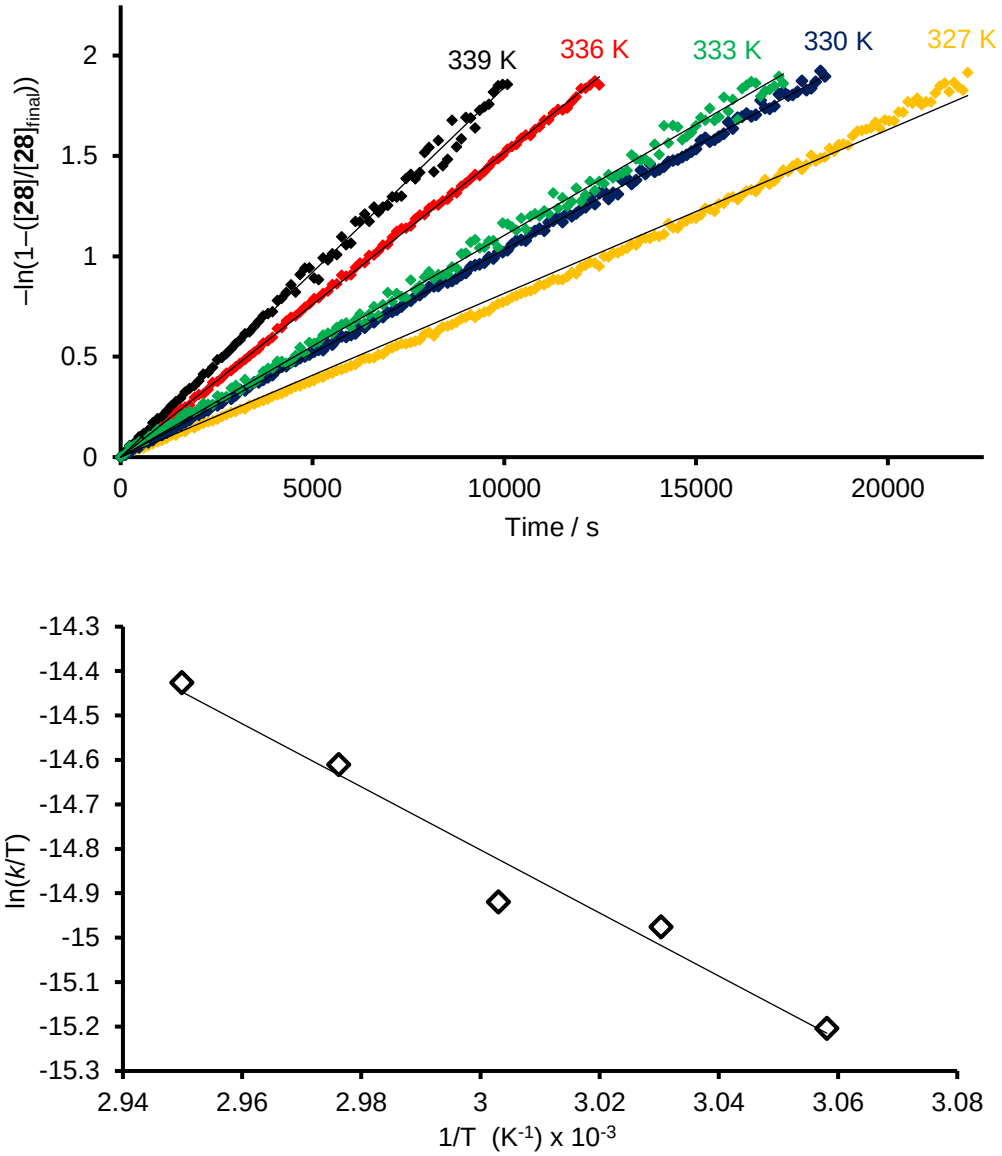

Figure 4.6. Top: first order semi-logarithmic plots for the conversion of Ti($N_2^{ArF}N^{Me}$){N{B(NAr'CH)$_2$}C(H)C(Tol)} (**25**) to Ti{MeN($CH_2CH_2NAr^F$){$CH_2CH_2NC_6F_4$C(Tol)=CHNB(NAr'CH)$_2$}}(F) (**28**) in C_6D_6. (avg. r^2 = 0.998, range 0.995 – 0.999). Bottom: Eyring plot for the conversion of Ti($N_2^{ArF}N^{Me}$){N{B(NAr'CH)$_2$}C(H)C(Tol)} (**25**) to Ti{MeN($CH_2CH_2NAr^F$){$CH_2CH_2NC_6F_4$C(Tol)=CHNB(NAr'CH)$_2$}}(F) (**28**) in C_6D_6. Activation parameters derived from linear regression analysis (r^2 = 0.969): $\Delta H^{‡}$ = 14.1(1.5) kcal mol^{-1}; $\Delta S^{‡}$ = –34.3(4.4) cal mol^{-1} K^{-1}; $\Delta G_{333}^{‡}$ = 25.5(1.5) kcal mol^{-1}. The experiment at 333 K was repeated with double [**25**], giving ln(*k*/T) = –14.8 (1/T = 3.00 × 10^{-3} K^{-1}).

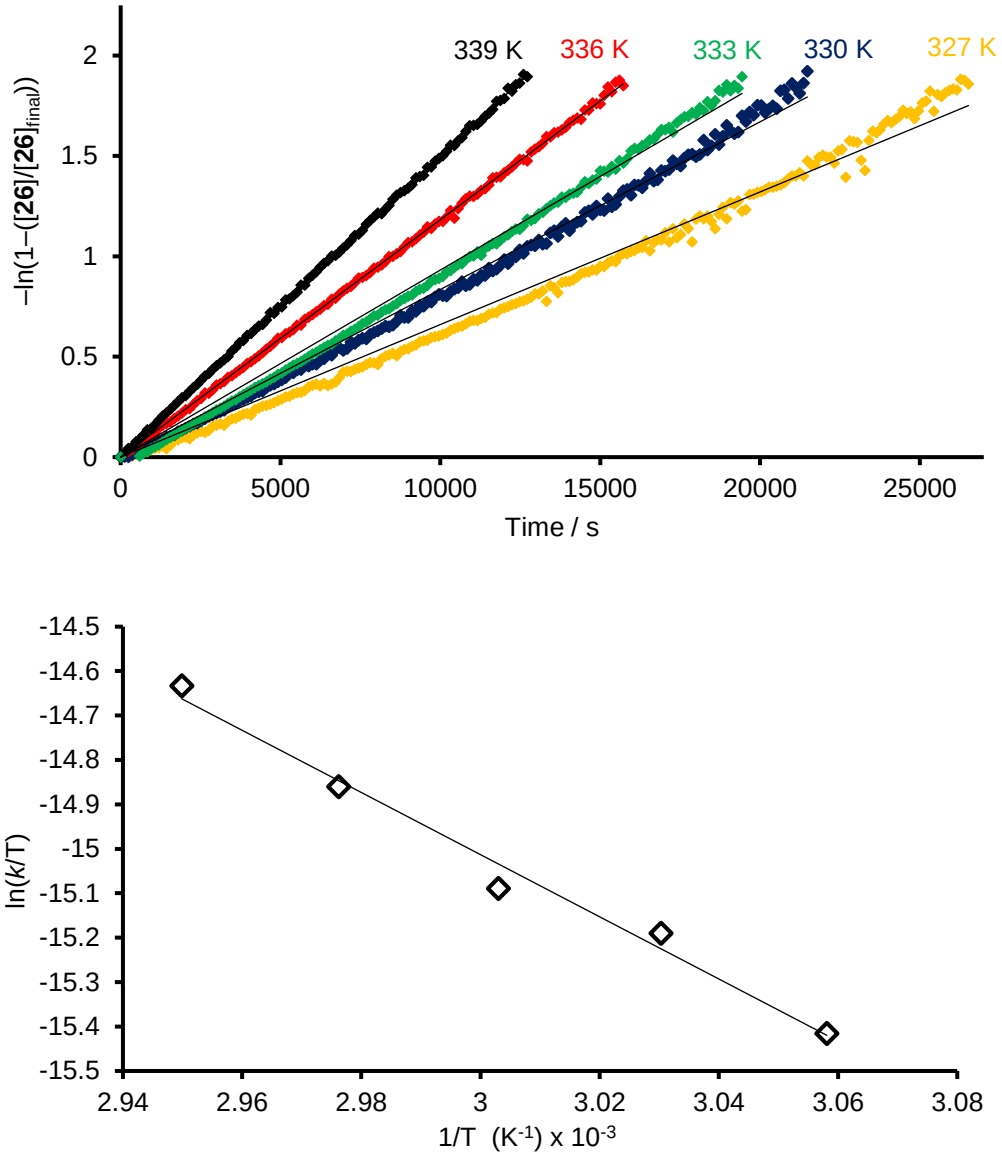

Figure 4.7. Top: first order semi-logarithmic plots for the conversion of Ti($N_2^{ArF}N^{Me}$){N{B(NAr'CH)$_2$}C(H)C(Ar^F)} (**27**) to Ti{MeN($CH_2CH_2NAr^F$){$CH_2CH_2NC_6F_4C(Ar^F)$=CHNB(NAr'CH)$_2$}}(F) (**26**) in C_6D_6. (avg. r^2 = 0.996, range 0.990 – 0.999). Bottom: Eyring plot for the conversion of Ti($N_2^{ArF}N^{Me}$){N{B(NAr'CH)$_2$}C(H)C(Ar^F)} (**27**) to Ti{MeN($CH_2CH_2NAr^F$){$CH_2CH_2NC_6F_4C(Ar^F)$=CHNB(NAr'CH)$_2$}}(F) (**26**) in C_6D_6. Activation parameters derived from linear regression analysis (r^2 = 0.985): $\Delta H^{‡}$ = 13.9(1.0) kcal mol^{-1}; $\Delta S^{‡}$ = –35.3(2.9) cal mol^{-1} K^{-1}; $\Delta G_{333}^{‡}$ = 25.7(1.0) kcal mol^{-1}. The experiment at 336 K was repeated with double [**27**], giving ln(*k*/T) = –14.8 (1/T = 2.98 × 10^{-3} K^{-1}).

4.5 Reactions of Ti($N_2^{iPr}N^{Me}$){NB(NAr'CH)$_2$}(py) (6) with terminal alkynes

Next, the borylimide Ti($N_2^{iPr}N^{Me}$){NB(NAr'CH)$_2$}(py) (**6**), in which the N_{amide}-substituents are now isopropyl groups, was reacted with the same two terminal alkynes. On the NMR tube scale in C_6D_6, addition of HCCTol to a solution of **6** gave an immediate colour change to deep red-brown, and inspection of the ^{1}H NMR spectrum indicated quantitative conversion to two species: two isomers of a [2+2] cycloaddition product. In contrast, addition of HCCAr^F to a solution of **6** resulted in an immediate colour change to orange, with the ^{1}H NMR spectrum indicating quantitative conversion to a borylamide-acetylide compound *via* C–H bond activation of the alkyne.

On the preparative scale, the two alkynes were reacted with **6** in toluene solution, and left to stir at RT for 1 h. The two products, Ti($N_2^{iPr}N^{Me}$){N{B(NAr'CH)$_2$}C(H)C(Tol)} (**29**) and Ti($N_2^{iPr}N^{Me}$){NHB(NAr'CH)$_2$}(CCAr^F) (**30**), were isolated in 43 and 51% yields, respectively (Scheme 4.5). The ^{1}H NMR spectrum of isolated **29** is consistent with this being a mixture of two isomeric forms of an azatitanacyclobutene complex in a *ca* 3:1 ratio. Two methine (1 H) singlets are observed at 10.32 and 9.35 ppm, corresponding to the major and minor isomer, respectively. The former resonance gives rise to an HSQC correlation to a ^{13}C signal at 148.9 ppm, and an HMBC correlation to a ^{13}C signal at 209.5 ppm, whilst that belonging to the minor isomer gives an HSQC correlation at 143.5 ppm and an HMBC correlation at 196.7 ppm. This confirms that both isomeric forms of **29** have anti-Markovnikov regiochemistry, in analogy with those azatitanacyclobutene complexes characterised previously. A ^{1}H–^{1}H ROESY NMR experiment showed the presence of an nOe in the major isomer between the NMe singlet and the doublet of an isopropyl group on the boryl moiety. This suggests, therefore, that the major isomer is that which has the N-boryl side of the metallacycle oriented *cis* to the NMe donor group, and that in the minor isomer the N-boryl is oriented *trans* to that group. nOe correlations in the minor isomer were too weak to give further evidence in this matter. The ^{1}H NMR spectrum of **30**, in contrast, shows the product exists as a single isomer with C_s symmetry. A slightly broadened 1 H singlet is observed at 6.58 ppm, this being assigned as the borylamide NH. The absence of any HMBC correlations to this resonance confirms that this proton sits at the borylamide site, and is not on an N_{amide} atom of the diamide-amine supporting ligand. In the ^{13}C NMR spectrum, the two acetylide functional group carbons are assigned at 162.0 and 83.7 ppm, corresponding to the carbon directly bonded to Ti, and the one adjacent to the Ar^F ring, respectively. Additionally, a band at 2094 cm^{-1} in the IR spectrum (Nujol

mull) of **30** is attributed to ν(C≡C), which is consistent with Cp-supported titanium and zirconium acetylide ligand frequencies reported previously.[24,25,62]

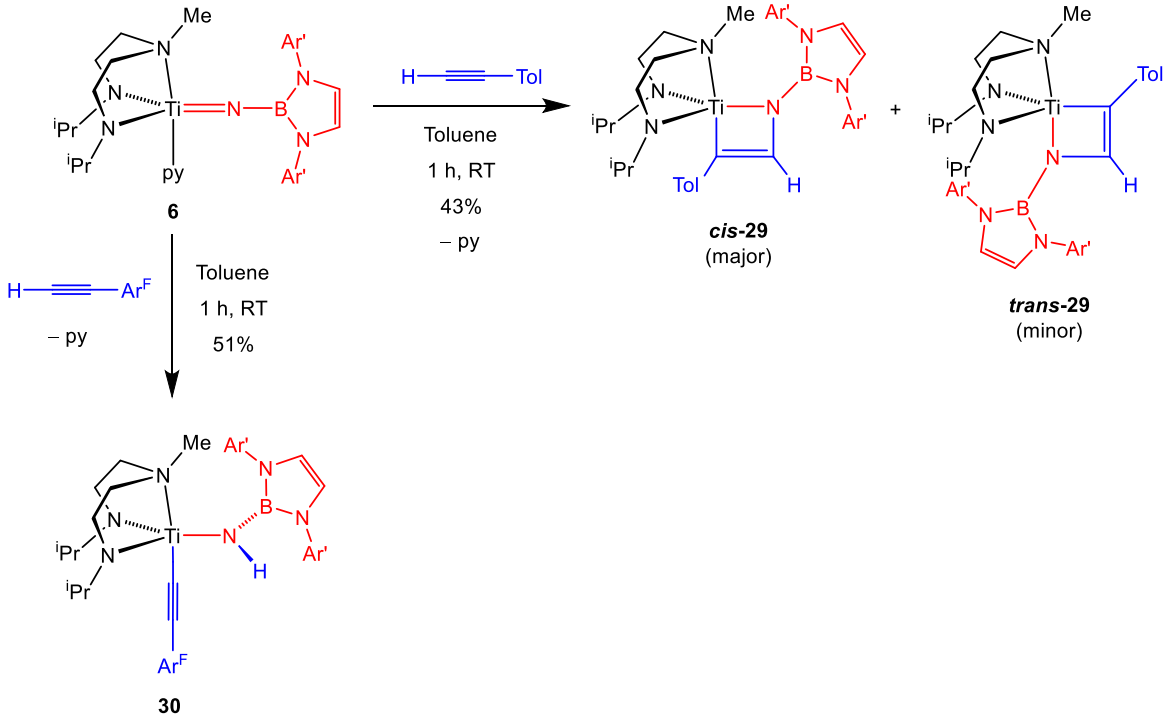

Scheme 4.5. Synthesis of Ti($N_2^{iPr}N^{Me}$){N{B(NAr'CH)$_2$}C(H)C(Tol)} (**29**) and Ti($N_2^{iPr}N^{Me}$){NHB(NAr'CH)$_2$}(CCAr^F) (**30**) from Ti($N_2^{iPr}N^{Me}$){NB(NAr'CH)$_2$}(py) (**6**).

Diffraction-quality crystals of **29** were successfully grown from a hexane solution at 5 °C. The molecular solid state structure is shown in Figure 4.8, and selected bond distances and angles are listed in Table 4.4. Molecules of **29** have an analogous structure to those of **23** and **25**; having an overall pentacoordinate geometry (τ = 0.58 and 0.63 for the two crystallographically independent molecules), the diamide-amine ligand coordinates to the titanium centre in a facial arrangement, and the κ^2-C(38)–C(39)–N(1) unit is arranged with the N-boryl group *cis* to the NMe donor. Thus, this was a selective crystallisation of the *cis* isomer of the complex (***cis*-29**) only. The bite angle of the κ^2-bound group is again larger than analogues which do not contain the very bulky boryl group, these being 75.34(10) and 75.13(10)° in the two crystallographically independent molecules. The C(44)–C(45), Ti(1)–C(44) and Ti(1)–N(1) bond distances are comparable with the corresponding values observed for **23** and **25**.

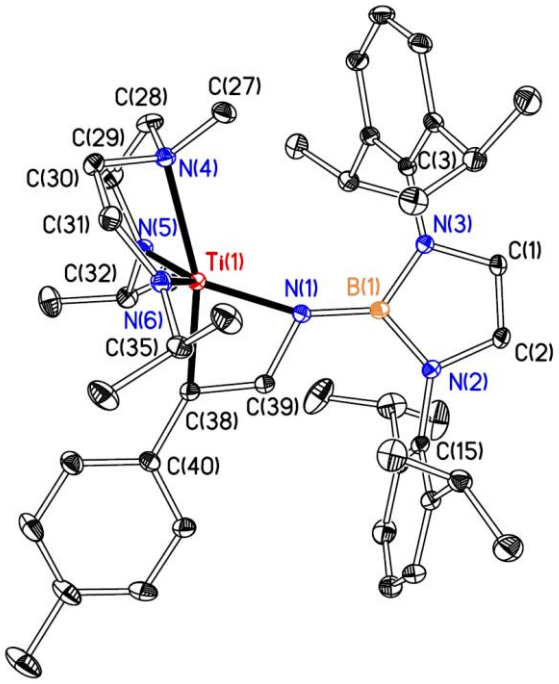

Figure 4.8. Displacement ellipsoid plot (25% probability) of *cis*-Ti($N_2^{iPr}N^{Me}$){N{B(NAr'CH)$_2$}C(H)C(Tol)} (***cis*-29**). H atoms are omitted for clarity.

Table 4.4. Selected bond distances (Å) and angles (°) for *cis*-Ti($N_2^{iPr}N^{Me}$){N{B(NAr'CH)$_2$}C(H)C(Tol)} (***cis*-29**). Values in brackets are for the second crystallographically independent molecule (τ = 0.58 [0.63]).

Ti(1)–N(1)	1.999(2) [1.996(2)]	N(1)–Ti(1)–N(4)	122.72(9) [120.68(9)]
Ti(1)–N(4)	2.294(2) [2.301(2)]	N(1)–Ti(1)–N(5)	114.38(10) [118.09(11)]
Ti(1)–N(5)	1.963(3) [1.943(3)]	N(1)–Ti(1)–N(6)	118.29(10) [115.56(11)]
Ti(1)–N(6)	1.957(2) [1.953(3)]	N(5)–Ti(1)–N(6)	127.27(10) [126.24(12)]
Ti(1)–C(38)	1.998(3) [2.007(3)]	N(1)–Ti(1)–C(38)	75.34(10) [75.13(10)]
N(1)–B(1)	1.432(4) [1.426(4)]	N(4)–Ti(1)– C(38)	161.94(10) [164.19(10)]
N(1)–C(39)	1.433(3) [1.424(4)]	N(5)–Ti(1)– C(38)	97.72(11) [97.70(12)]
C(38)–C(39)	1.358(4) [1.357(4)]	N(6)–Ti(1)– C(38)	97.57(11) [98.74(11)]
		Ti(1)–N(1)–B(1)	160.17(18) [159.24(19)]
		Ti(1)–C(38)–C(39)	82.13(17) [81.65(18)]
		N(1)–C(39)–C(38)	122.1(2) [122.6(3)]

Several examples of Group 4 acetylide complexes have previously been prepared through C–H bond activation of a terminal alkyne. These reactions usually involve transfer of the proton to the X atom of a Ti–X multiple bond (X = N or O),[22,24,37,62,63] as is the case for the borylamide-acetylide **30**. The 1,2-addition of HCCPh to a scandium imido compound has also been reported, resulting in an amido-acetylido complex,[64] and the analogous reaction also occurs with the tantalum imido complex $[Cp^*_2Ta(N^tBu)(THF)][B(Ar^F)_4]$.[65] Recently, within this research group, the reactivity of the imido complex $Ti(N_2^{iPr}N^{Me})(NXyl)(py)$ (**4.6**) with electron-deficient terminal arylalkynes was explored.[25] The first formed products were found to be acetylide complexes, for example $Ti(HN_2^{iPr}N^{Me})(NXyl)(CCAr^F)(py)$ when using $HCCAr^F$. Addition of a second equivalent of the respective terminal alkyne gave bis(acetylide) compounds, such as $Ti(H_2N_2^{iPr}N^{Me})(NXyl)(CCAr^F)_2$ (**4.7**), which could then isomerise to vinylamide-acetylides such as $Ti(N_2^{iPr}N^{Me})\{N(Xyl)C(H)C(H)Ar^F\}(CCAr^F)$ (**4.8**) upon heating.

In order to test for the formation of analogous compounds from the borylimide **6**, it was reacted on the NMR tube scale with 2 equiv. $HCCAr^F$ at RT. Rather than quantitatively forming a bis(acetylide) like **4.6** giving **4.7**, this was found to immediately result in an equilibrium mixture of the acetylide **30** and another species in a *ca* 72:28 mixture (calculated by integration of the respective boryl NCH resonances), with unreacted $HCCAr^F$ remaining in the solution. Gentle heating of the equilibrium mixture resulted only in a slight shift of the equilibrium back towards **30**. To characterise the second complex in solution, **6** was reacted with 20 equiv. $HCCAr^F$, giving *ca* 93% conversion to the new species which was confirmed to be the bis(acetylide) $Ti(H_2N_2^{iPr}N^{Me})\{NB(NAr'CH)_2\}(CCAr^F)_2$ (**31**). The ^1H NMR spectrum of **31** as the major component of this mixture is shown in Figure 4.9, and is consistent with a C_s symmetric structure as depicted in Equation 4.4. The methine resonance of the N-bound isopropyl groups has experienced a significant upfield shift relative to its position in **6** (2.37 *vs* 3.76 ppm), although is partly obscured by a ligand methylene resonance. A broad doublet of doublets (2 H) is observed at 3.71 ppm, which is assigned to the two NH groups of the now double-protonated diamide-amide ligand, with coupling to the adjacent isopropyl methine and one of the adjacent methylene protons being revealed through a COSY spectrum. The diastereotopic methylene groups of the supporting ligand give a distinctive multiplet pattern when it is neutral and has meridional coordination.[25] In **31**, this results in four 2 H multiplets, of which the two $C\underline{H}_2NMe$ multiplets are the most downfield (3.48 ppm) and

most upfield (1.64 ppm) and the two C<u>H</u>$_2$N^{i}Pr multiplets are of intermediate chemical shifts (2.37 and 2.17 ppm). Additionally, the ^{19}F and ^{13}C spectra of **31** show two sets of signals for the Ar^F groups, indicating that these are not chemically equivalent by symmetry. Finally, the ^{11}B resonance of 13.3 ppm is consistent with the complex retaining a multiply bonded borylimido ligand, in contrast with a protonated borylamido ligand which would be expected to give an ^{11}B resonance in the region of 24 – 21 ppm.

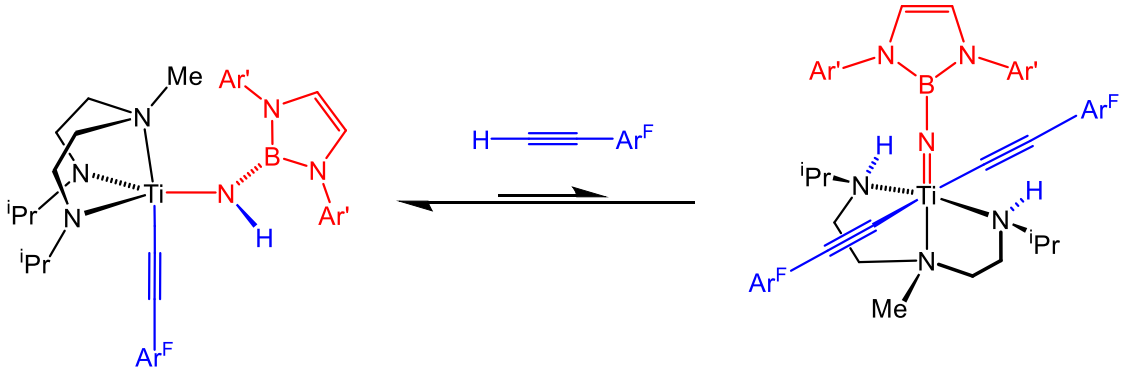

Equation 4.4

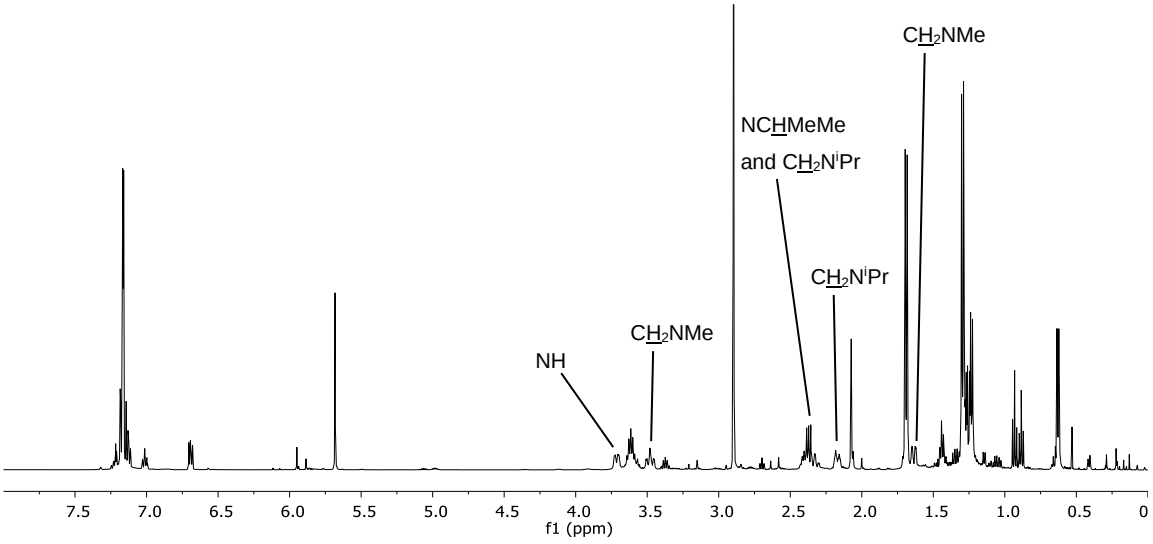

Figure 4.9. ^{1}H NMR spectrum (500.3 MHz) of a mixture containing Ti(H$_2$N$_2^{iPr}$N^{Me}){NB(NAr'CH)$_2$}(CCAr^F)$_2$ (**31**) in C$_6$D$_6$ at 298 K.

Next, the acetylide complex **30** was heated at 60 °C in C$_6$D$_6$ solution. Over 16 h this gave quantitative conversion to two new species, which were found to be two isomers of the azatitanacyclobutene complex Ti(N$_2^{iPr}$N^{Me}){N{B(NAr'CH)$_2$}C(H)C(Ar^F)} (**32**, Scheme 4.6) in a *ca* 3:1 ratio. In the ^{1}H NMR spectrum, the metallacycle methine resonances are

observed at 9.29 and 10.32 ppm, respectively, for the major and minor isomers. HSQC and HMBC correlations analogous to those described previously show that both isomers have anti-Markovnikov regiochemistry. A ^{1}H–^{1}H ROESY NMR experiment showed the presence of an nOe in the major isomer between the doublet of an isopropyl group on the boryl moiety and an N-bound isopropyl doublet. This suggests, therefore, that the major isomer is that which has the N-boryl side of the metallacycle oriented *trans* to the NMe donor group. Correspondingly an nOe was observed in the minor isomer between the NMe singlet and a boryl isopropyl doublet, implying that this is the *cis*-oriented isomer. The major and minor isomers are therefore assigned as ***trans*-32** and ***cis*-32**, respectively. On the preparative scale, **6** and HCCAr^{F} were mixed in toluene and heated at 60 °C for 16 h, giving compound **32** as a brown, waxy solid in 73% isolated yield.

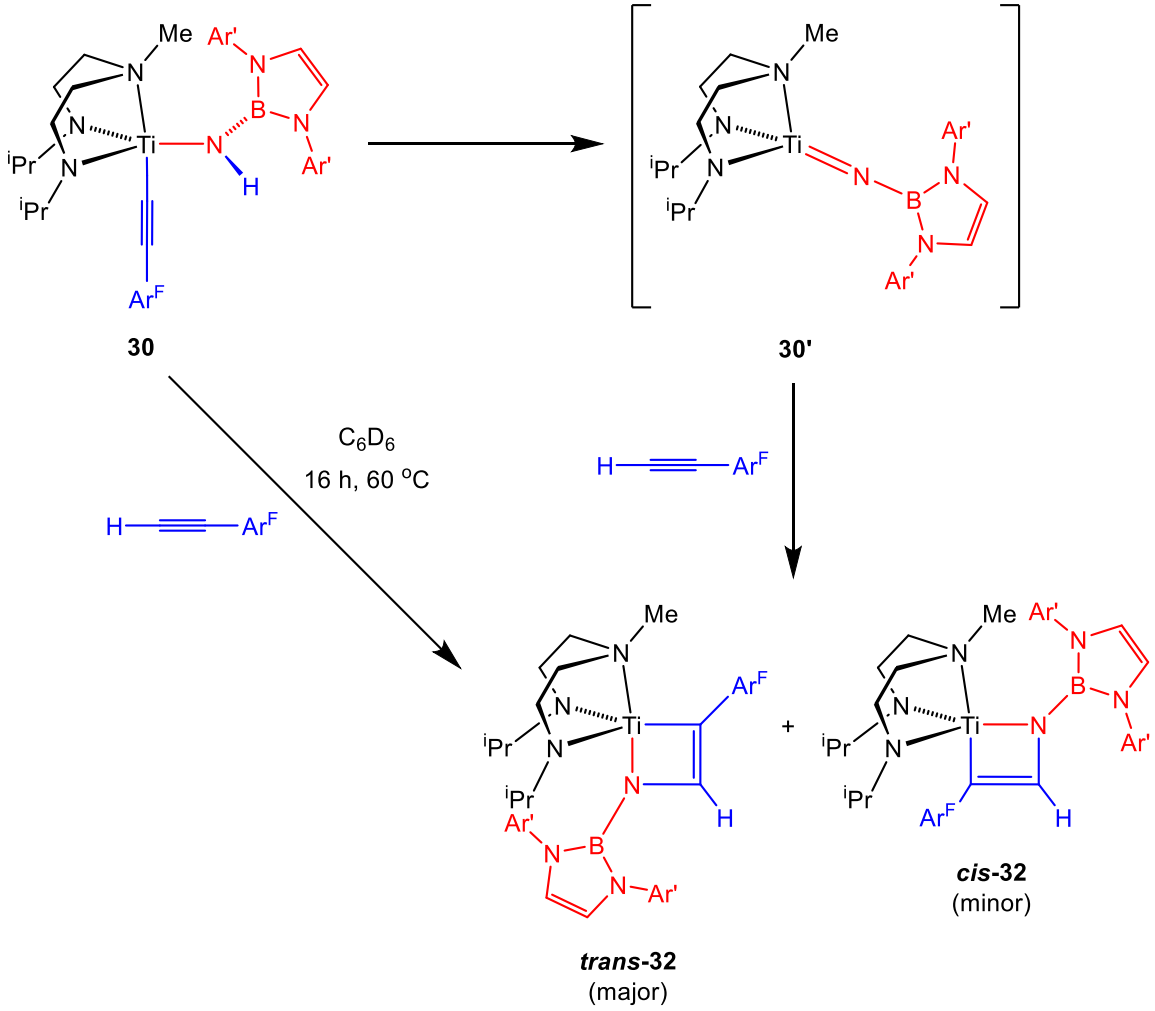

Scheme 4.6. Conversion of Ti(N$_2^{iPr}$N^{Me}){NHB(NAr'CH)$_2$}(CCAr^{F}) (**30**) to Ti(N$_2^{iPr}$N^{Me}){N{B(NAr'CH)$_2$}C(H)C(Ar^{F})} (**32**) upon heating.

Given the conversion of the acetylide complex **30** to the azatitanacyclobutene complex **32** upon heating as described above, a fuller picture of the reactivity of the borylimide **6** with the two terminal alkynes has now been realised. It appears that, in reaction with the more acidic terminal alkyne $HCCAr^F$, the first-formed acetylide **30** is obtained as the kinetic product of this reaction at RT. Upon heating, conversion to the two isomers of the azatitanacyclobutene **32** as the thermodynamic products is achieved, with the reaction presumably proceeding by reforming of the alkyne to leave a borylimido intermediate (**30'**), which then undergoes [2+2] cycloaddition with the released alkyne. It is noted that, of the three diamide-amine-supported borylimides (**4**, **5** and **6**), it was complex **6** which had the longest Ti–N_{im} bond distance due to the more π-basic N_{amide} atoms weakening the π components of the multiple bond to the greatest degree (as described in Section 2.6). It is proposed that this weakening of the Ti–N_{im} bond is sufficient to allow the breaking of the more acidic C–H bond in $HCCAr^F$, giving an acetylide complex as kinetic product, rather than an analogue of the metallacycles that were found in the reactions of this alkyne with borylimides **4** and **5**. This does not take place with HCCTol, due to the less acidic nature of the terminal C–H bond.

To clarify, trends in the acidity of alkyne C–H bonds are actually the reverse of the trend in the C–H bond strength. It has been reported that relative M–X bond enthalpies correlate with the respective H–X bond enthalpy,[66–69] and experimental results have shown that M–C bond energies increase more rapidly with changes in substituent than the corresponding difference in C–H bond strengths.[70] Thus, in potential C–H bond activations at metal centres, there is a thermodynamic preference for a stronger C–H bond to be broken. In summary, it is the stronger metal–carbon bond (which outweighs the stronger C–H bond) which increases the tendency of the electron-deficient alkyne $HCCAr^F$ to give a C–H bond activation at titanium.

Unfortunately, the C–H bond activation of $HCCAr^F$ at the Ti–N multiple bond of **6** to form **30** was found to be too rapid to precisely monitor by ^{1}H NMR arrays for the purpose of kinetic analysis and measurement of a kinetic isotope effect (KIE) for this process. Additionally, the equilibrium between the borylamide-acetylide **30** and the bis(acetylide) **31** precluded the measurement of a KIE for this C–H bond activation by competition reactions, as this would cause scrambling of the isotopologue mixture. In the next Section, reactions of the diamide-pyridine-supported borylimide **7** with the terminal alkynes HCCTol and $HCCAr^F$ will be presented, with the principal outcomes in the two cases being

analogous to those obtained for **6**. In the case of the C–H bond activation of $HCCAr^F$ by **7**, the reaction proceeded more slowly, so a KIE for this process could be successfully measured (*vide infra*).

4.6 Reactions of $Ti(N_2N^{py})\{NB(NAr'CH)_2\}(py)$ (7) with terminal alkynes

Turning now to the reactions of the diamide-pyridine-supported borylimide **7** with HCCTol and $HCCAr^F$, the first formed reaction products with both terminal alkynes were found to be analogous to those of the reaction of the respective alkyne with **6**. On the NMR tube scale in C_6D_6, the reaction of **7** with HCCTol was found to proceed more slowly than the same reaction with **6**. However, heating at 60 °C for 2 h resulted in quantitative conversion to the azatitanacyclobutene complex $Ti(N_2N^{py})\{N\{B(NAr'CH)_2\}C(H)C(Tol)\}$ (**33**). Similarly, the NMR tube scale reaction of $HCCAr^F$ with **7** proceeded more slowly than that with **6**, although after 16 h at RT, quantitative conversion to the analogous borylamide-acetylide complex, $Ti(N_2N^{py})\{NHB(NAr'CH)_2\}(CCAr^F)$ (**34**), had taken place.

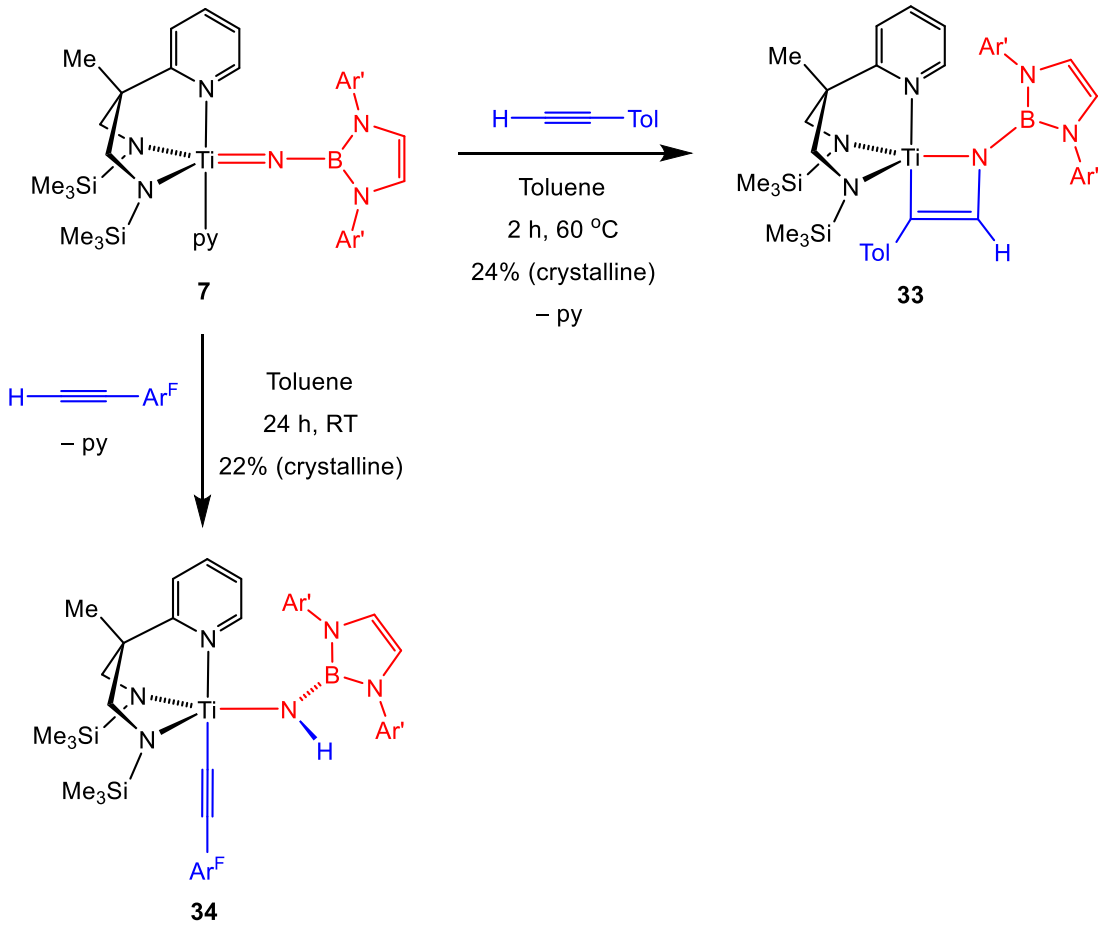

Scheme 4.7. Synthesis of $Ti(N_2N^{py})\{N\{B(NAr'CH)_2\}C(H)C(Tol)\}$ (**33**) and $Ti(N_2N^{py})\{NHB(NAr'CH)_2\}(CCAr^F)$ (**34**) from $Ti(N_2N^{py})\{NB(NAr'CH)_2\}(py)$ (**7**).

On the preparative scale, **7** was reacted with the two alkynes in toluene solutions; heating with HCCTol at 60 °C for 2 h gave **33** in 24% crystalline yield, and a reaction with $HCCAr^F$ at RT for 24 h gave **34** in 22% crystalline yield (Scheme 4.7). The low yields obtained were due to the very high solubility of these compounds in hydrocarbon solvents. The ^{1}H NMR spectrum of isolated **33** is consistent with this being a single isomer of an azatitanacyclobutene complex with anti-Markovnikov regiochemistry, as described previously for the analogues **23**, **25** and **29**. The metallacycle methine singlet is observed at 9.56 ppm, with an HSQC correlation to a ^{13}C signal at 154.9 ppm, and an HMBC correlation to a ^{13}C signal at 210.6 ppm. The ^{1}H NMR spectrum of **34** is comparable to that of its analogue **30**. A broad NH singlet is observed at 6.08 ppm, and this has no COSY or HMBC correlations. In the ^{13}C NMR spectrum, the two acetylide functional group carbons are assigned at 161.1 and 87.6 ppm, corresponding to the carbon directly bonded to Ti, and the one adjacent to the Ar^F ring, respectively. Additionally, a band at 2096 cm^{-1} in the IR spectrum (Nujol mull) of **34** is attributed to ν(C≡C), which is similar to that in **30**, as well as the previously mentioned literature compounds.[24,25,62]

Diffraction-quality crystals of both compounds **33** and **34** were grown from hexane solutions at 5 °C. The molecular solid state structures are shown in Figure 4.10, and selected bond distances and angles are listed in Table 4.5. The azatitanacyclobutene complex **33** has an analogous structure to those of **23**, **25** and **29**, having a distorted pentacoordinate geometry (τ = 0.50) in which the diamide-pyridine ligand is facially coordinating. The solid state structure confirms its anti-Markovnikov regiochemistry, and demonstrates that the single isomer has the N-boryl group oriented *cis* to the pyridyl donor group. The bite angle of the κ^2-C(42)–C(43)–N(1) unit is 69.58(9)°, which is smaller than in complexes **23**, **25** and **29** (75.52(4), 77.19(6) and 75.34(10)°, respectively), and is actually closer to that in the literature compound Ti(N_2N^{py}){N(Ar')C(H)C(Tol)} (**4.4**, 68.3(1)°) which is a direct analogue of **33** as it has the same supporting ligand set.[41] The smaller bite angle in **33** may reflect the slightly more sterically encumbering nature of the diamide-pyridine supporting ligand as there is a three-carbon bridge between each N_{amide} atom and the neutral N donor (compared to a two-carbon bridge in the diamide-amine ligands). This would be expected to give more steric restriction of the bulky boryl moiety and hence force a smaller bite angle in this case. The Ti–N(1), Ti–C and C=C bond distances are all comparable to those distances in the analogues **23**, **25** and **29**.

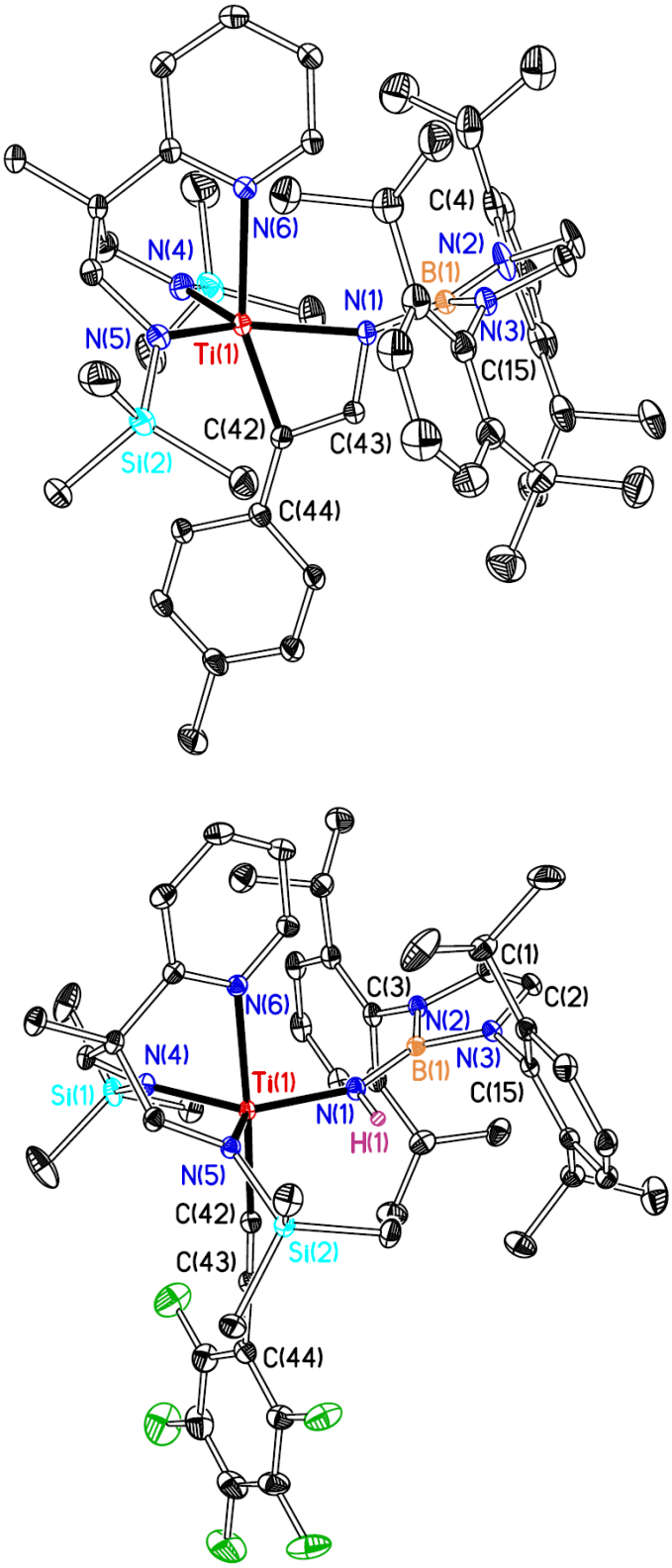

Figure 4.10. Displacement ellipsoid plots (25% probability) of $Ti(N_2N^{py})\{N\{B(NAr'CH)_2\}C(H)C(Tol)\}$ (**33**) and $Ti(N_2N^{py})\{NHB(NAr'CH)_2\}(CCAr^F)$ (**34**). C-bound H atoms are omitted for clarity. H(1) of **34** is drawn as a sphere of arbitrary radius.

Table 4.5. Selected bond lengths (Å) and angles (°) for Ti(N_2N^{py}){N{B(NAr'CH)$_2$}C(H)C(Tol)} (**33**) and Ti(N_2N^{py}){NHB(NAr'CH)$_2$}($CCAr^F$) (**34**) (τ = 0.50 (**33**) and 0.63 (**34**)).

Parameter	**33**	**34**
Ti(1)–N(1)	2.062(2)	1.9591(8)
Ti(1)–N(4)	1.911(3)	1.9236(8)
Ti(1)–N(5)	1.907(3)	1.8841(8)
Ti(1)–N(6)	2.283(2)	2.2774(8)
Ti(1)–C(42)	2.053(3)	2.1552(10)
N(1)–B(1)	1.429(3)	1.4269(13)
N(1)–C(43)	1.380(3)	-
N(1)–H(1)	-	0.908(16)
C(42)–C(43)	1.320(4)	1.2143(15)
N(1)–Ti(1)–N(4)	130.10(11)	139.09(3)
N(1)–Ti(1)–N(5)	126.52(11)	114.38(3)
N(1)–Ti(1)–N(6)	90.59(8)	89.10(3)
N(4)–Ti(1)–N(5)	102.54(12)	104.47(3)
N(1)–Ti(1)–C(42)	69.58(9)	92.96(4)
N(4)–Ti(1)– C(42)	106.60(12)	95.14(4)
N(5)–Ti(1)– C(42)	107.84(11)	96.28(4)
N(6)–Ti(1)– C(42)	159.89(9)	176.67(3)
Ti(1)–N(1)–B(1)	152.40(18)	155.66(7)
Ti(1)–C(42)–C(43)	85.61(17)	177.30(8)
N(1)–C(43)–C(42)	120.8(2)	-

The borylamide-acetylide complex **34** also has distorted pentacoordinate geometry (τ = 0.63), with the diamide-pyridine ligand being facially coordinating across two equatorial sites and an axial site. The borylamide ligand sits at the equatorial site *cis* to the pyridyl donor group, with the angle between the two ligands being 89.10(3)°, and the acetylide

ligand sits *trans* to the pyridyl group with an angle of 176.67(3)° between those two ligands. The Ti–C bond distance to the acetylide ligand is 2.1552(10) Å, which is slightly shorter than the two Ti–C distances in the bis(acetylide) **4.7** (2.2098(13) and 2.2182(13) Å), and slightly longer than that in the vinylamide-acetylide complex **4.8** (2.140(2) Å).[25] The C≡C bond distance of 1.2143(15) Å is consistent with a full triple bond, and is comparable to the C≡C distance in **4.8** (1.207(4) Å) and one of those distances in **4.7** (1.2132(18) Å), and is slightly longer than the second C≡C distance in **4.7** (1.1979(19) Å).[25]

Similar to the borylamide-acetylide **30**, heating of **34** at 70 °C for 18 h in C_6D_6 resulted in quantitative conversion to the azatitanacyclobutene complex $Ti(N_2N^{py})\{N\{B(NAr'CH)_2\}C(H)C(Ar^F)\}$ (**35**, Scheme 4.8). On the preparative scale, **35** was synthesised by heating of a mixture of **7** and $HCCAr^F$ in toluene at 60 °C for 40 h, giving the desired product as a deep brown, waxy solid in 64% yield. The ^1H and ^{13}C NMR spectra of **35** are consistent with the compound existing as a single isomer of anti-Markovnikov regiochemistry, with a metallacycle methine ^1H resonance observed at 10.05 ppm, and HSQC and HMBC correlations are found to be in analogy with those of **32**. Thus, the reactions of **7** with HCCTol and $HCCAr^F$ were broadly similar to those of **6** with the two alkynes. It is again noted that borylimide **7** had a relatively long titanium–nitrogen multiple bond length like **6**, and that as discussed above, this allows the formation of the borylamide-acetylide as a kinetic product with the more acidic $HCCAr^F$. Again, heating of this first-formed product led to complete conversion to the azatitanacyclobutene complex **35**, which is considered the thermodynamic product.

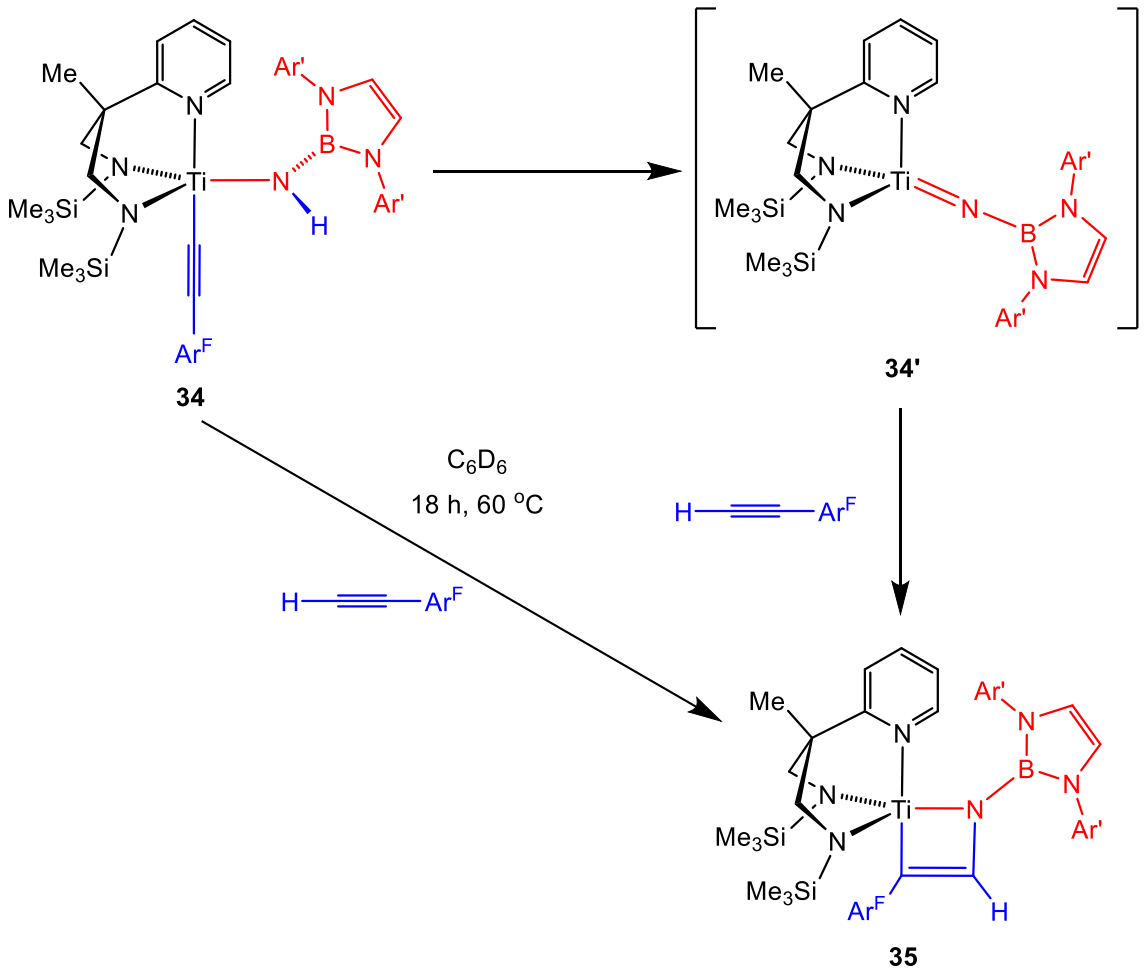

Scheme 4.8. Conversion of Ti(N_2N^{py}){NHB(NAr'CH)$_2$}($CCAr^F$) (**34**) to Ti(N_2N^{py}){N{B(NAr'CH)$_2$}C(H)C(Ar^F)} (**35**) upon heating.

Next, kinetic analysis of the initial reaction between Ti(N_2N^{py}){NB(NAr'CH)$_2$}(py) (**7**) and $HCCAr^F$ to give the borylamide-acetylide **34** was sought. In order to avoid the effect of product inhibition (i.e. the build-up of the released pyridine as the reaction progressed), the initial rates method was used to effectively measure the rate of the reaction, d[**34**]/d*t* at time = 0, t_0. The reaction of $HCCAr^F$ with **7** was monitored by a ^{1}H NMR array at 298 K. A small amount of the thermodynamic metallacycle product **35** was also observed to form, though remaining as a constant proportion of the product mixture as the reaction proceeded. Therefore, a composite initial rate was measured (see below), and was then scaled to the correct proportion of the acetylide complex **34** in the mixture, to give an initial rate reflecting only the formation of **34**. The graph of ([**34**] + [**35**]) *vs* time gave the non-linear plot drawn in Figure 4.11 (top). Graphical software (*Origin*) was used to fit a curve to all of the data points, thus describing the evolution of product throughout the kinetic study (Equation 4.5; 'y_0', 'A_n' and 'B_n' are empirical constants). The curve was then

differentiated to obtain an equation for the gradient (Equation 4.6), and the gradient calculated at time = 0 s (Equation 4.7). This allowed the initial rate of the reaction to be calculated, giving values of 21.16(7) × 10^{-6} and 19.16(4) × 10^{-6} mol dm^{-3} s^{-1} (performed in duplicate, and considering the formation of **34** only, as described above). The same reaction was carried out with $DCCAr^F$ and the initial rate of the reaction calculated to be 3.94(1) × 10^{-6} and 3.94(2) × 10^{-6} mol dm^{-3} s^{-1} (performed in duplicate). Thus the kinetic isotope effect (KIE; k_H/k_D) of the C–H bond activation is calculated to be between 4.86 and 5.37.

$$[\text{Products}] = y_0 + \text{A}_1 e^{-t/\text{B}_1} + \text{A}_2 e^{-t/\text{B}_2} \tag{4.5}$$

$$\frac{d[\text{Products}]}{dt} = -\frac{\text{A}_1 e^{-t/\text{B}_1}}{\text{B}_1} - \frac{\text{A}_2 e^{-t/\text{B}_2}}{\text{B}_2} \tag{4.6}$$

$$\left(\frac{d[\text{Products}]}{dt}\right)_{t=0} = -\frac{\text{A}_1}{\text{B}_1} - \frac{\text{A}_2}{\text{B}_2} \tag{4.7}$$

An alternative method of measuring the kinetic isotope effect was also carried out. A competition reaction of **7** with an excess of both $HCCAr^F$ and $DCCAr^F$ (1:5:5) simultaneously on the NMR tube scale allowed calculation of the KIE from the ratio of the two isotopologues **34** and **34-*d*$_1$**. After 16 h at RT, the product mixture contained approximately 87% **34** and 13% **34-*d*$_1$** as determined by integration of the NH resonance against the boryl NCH resonance, establishing a KIE of 6.5 from this method.

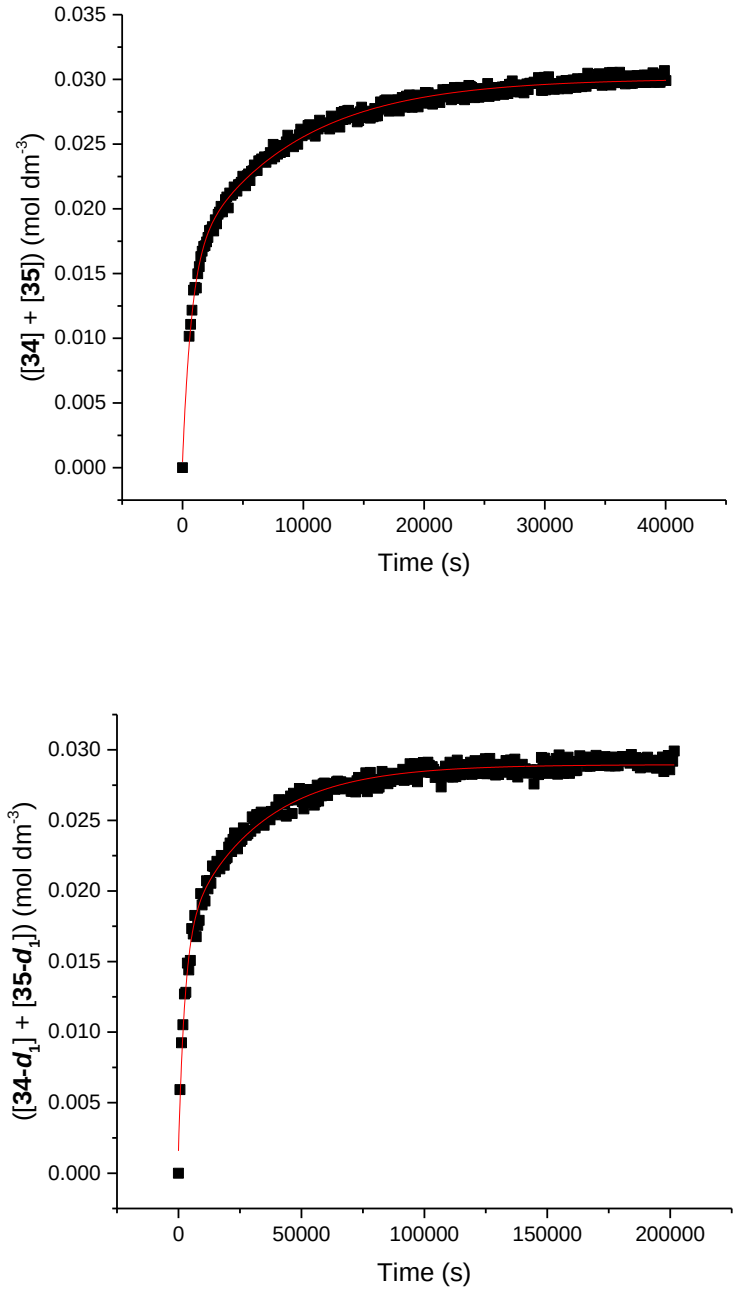

Figure 4.11. Top: plot of the sum of [Ti(N_2N^{py}){NHB(NAr'CH)$_2$}($CCAr^F$)] ([**34**]) and [Ti(N_2N^{py}){N{B(NAr'CH)$_2$}C(H)C(Tol)}] ([**35**]) *vs* time plotted in *Origin*. The best-fit line (r^2 = 0.9928) shown gave A_1 = –0.0156(4), B_1 = 733(21), A_2 = –0.0141(2), B_2 = 8792(174) giving an initial rate of 19.16(4) × 10^{-6} mol dm^{-3} s^{-1}. Bottom: plot of the sum of [Ti(N_2N^{py}){NDB(NAr'CH)$_2$}($CCAr^F$)] ([**34-*d*$_1$**]) and [Ti(N_2N^{py}){N{B(NAr'CH)$_2$}C(D)C(Tol)}] ([**35-*d*$_1$**]) *vs* time plotted in *Origin*. The best-fit line (r^2 = 0.9847) shown gave A_1 = –0.0151(4), B_1 = 2578(142), A_2 = –0.0123(3), B_2 = 30574(856) giving an initial rate of 3.94(1) × 10^{-6} mol dm^{-3} s^{-1}.

The KIE values given above are consistent with a number of previously reported KIEs of C–H bond activations and formations at Group 4 metal centres. In particular, Wolczanski and co-workers have published extensively on the release of alkanes *via* α-abstraction in Group 4 alkyl-amide complexes,[71–75] processes which have KIE values in the range *ca* 4 – 13. For example, (^{t}Bu$_3$SiNH)$_3$Zr(Me) eliminates methane under heating to give an imido product, with a reported KIE of 7.3(4).[72] Similar processes have also been studied by other research groups,[76,77] and have been covered in a number of recent reviews.[78–80] Large KIEs such as those reported for all of these cases are proposed to be a result of transition states where the transfer of H is relatively linear; i.e. where the transition state has approximately equal bond-making and -breaking character.[81,82] A number of KIEs for the reverse processes, C–H bond activations, have also been reported,[63,83,84] these being in a similar range of *ca* 6 – 11. For example, Bergman and co-workers have investigated C–H bond activations of C_6H_6, *n*-pentane, mesitylene and (*E*)-neohexene (and their deuterated counterparts) by an *in situ*-generated zirconium imide Cp*CpZr(N^{t}Bu), with KIEs of 7.4, 8.9, 8.8 and 6.9 being reported, respectively.[63]

The kinetics of the conversion of the borylamide-acetylide **34** to the azatitanacyclobutene complex **35** were also analysed. The decay of **34** and **34-*d*$_1$** were monitored by ^{1}H NMR arrays at 343 K, and were found to follow first order kinetics as judged by semi-logarithmic plots of –ln([**34**]/[**34**]$_0$) *vs* time (and analogously for **34-*d*$_1$**, Figure 4.12). The plots are shown to at least 85% conversion (approximately three half-lives). The observed rate constants (k_{obs}, in duplicate) were measured to be 3.76(1) × 10^{-5} and 4.43(1) × 10^{-5} s^{-1} for reactions of **34**, and 3.16(2) × 10^{-5} and 3.03(2) ×10^{-5} s^{-1} for reactions of **34-*d*$_1$**, giving a KIE of between 1.19 and 1.46. As none of the putative borylimido intermediate **34'** is observed during the course of the reaction (Scheme 4.9), a steady-state approximation was applied to this intermediate in order to obtain a rate equation (Equations 4.8 –4.12). The final form of the rate equation is shown in Equation 4.12. The approximation $k_{-1} >> k_2$ (Equation 4.10) has been used because, starting from the borylimide **7**, the reaction with HCCAr^F to form the acetylide **34** is known to be fast at RT, whereas formation of **35** requires elevated temperatures. Thus, the observed rate constants (k_{obs}) are a combination of the equilibrium constant (K_{eq}) between **34** and **34'** and the secondary k_2 rate constant.

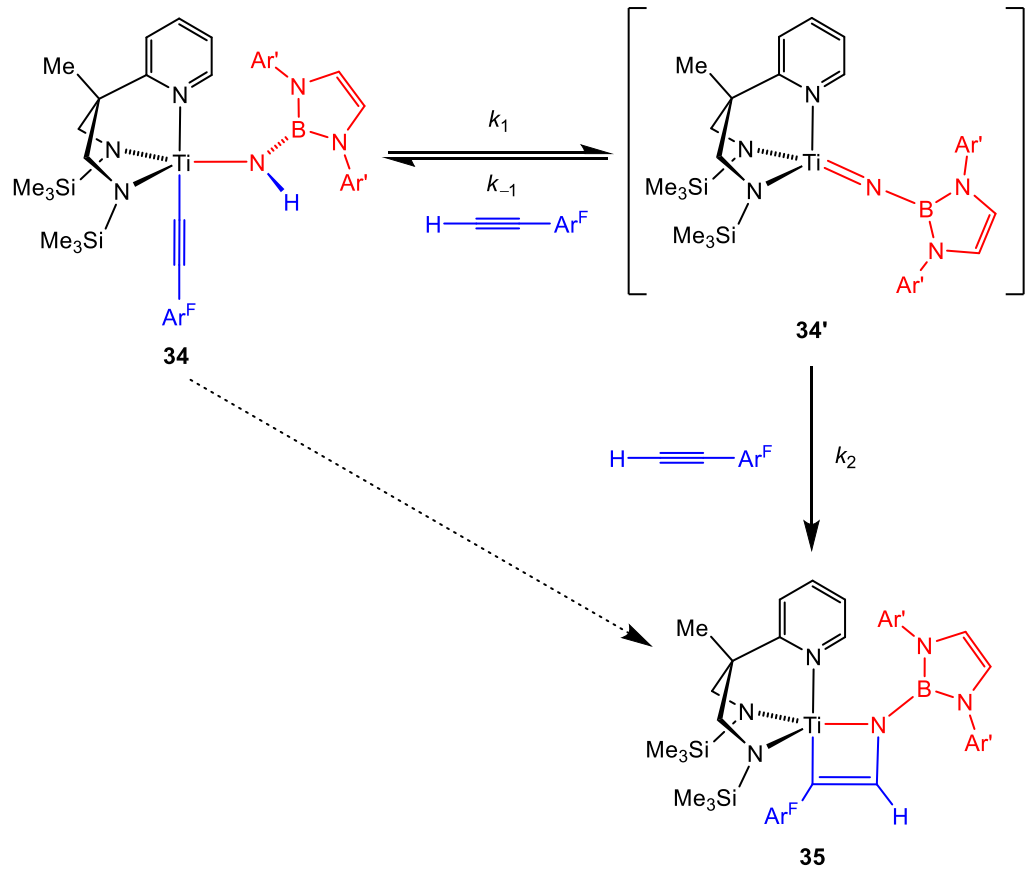

Scheme 4.9. Mechanism for the conversion of Ti(N_2N^{py}){NHB(NAr'CH)$_2$}($CCAr^F$) (**34**) to Ti(N_2N^{py}){N{B(NAr'CH)$_2$}C(H)C(Ar^F)} (**35**).

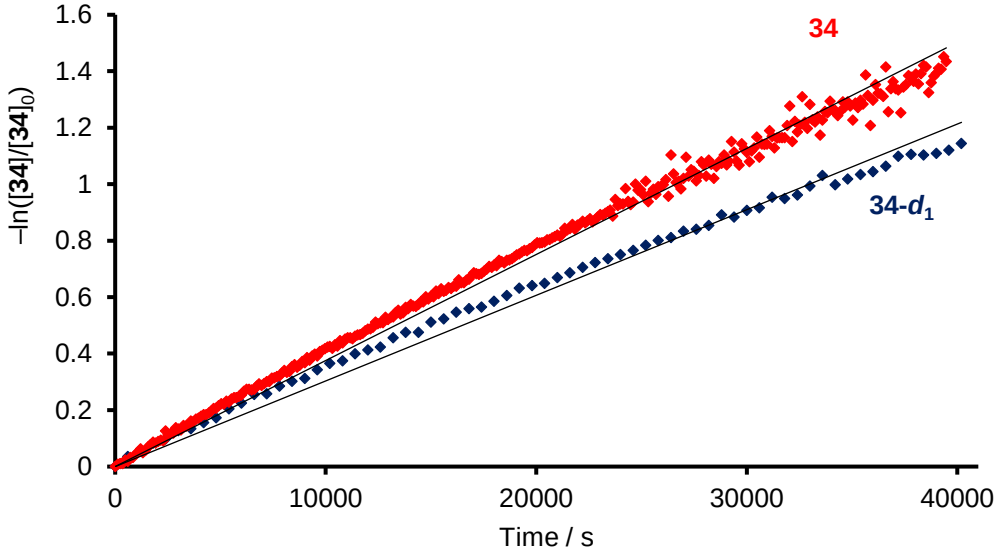

Figure 4.12. First order semi-logarithmic plots for the conversion of Ti(N_2N^{py}){NHB(NAr'CH)$_2$}($CCAr^F$) (**34**) to Ti(N_2N^{py}){N{B(NAr'CH)$_2$}C(H)C(Ar^F)} (**35**), and **34-*d*$_1$** to **35-*d*$_1$**, in C_6D_6. (avg. r^2 = 0.987, range 0.982 – 0.991).

$$\frac{d[\mathbf{34'}]}{dt} = k_1[\mathbf{34}] - k_{-1}[\mathbf{34'}][\text{alkyne}] - k_2[\mathbf{34'}][\text{alkyne}] = 0 \quad (4.8)$$

$$[\mathbf{34'}] = \frac{k_1[\mathbf{34}]}{(k_{-1} + k_2)[\text{alkyne}]} \quad (4.9)$$

$$\frac{d[\mathbf{35}]}{dt} = k_2[\mathbf{34'}][\text{alkyne}] \quad (4.10)$$

$$= \frac{k_1 k_2[\mathbf{34}]}{k_{-1} + k_2}$$

$$\frac{d[\mathbf{35}]}{dt} = \frac{k_1 k_2[\mathbf{34}]}{k_{-1}} \quad (\text{if } k_{-1} >> k_2)$$

$$K_{\text{eq}} = \frac{k_1}{k_{-1}} \quad (4.11)$$

$$-\frac{d[\mathbf{34}]}{dt} = \frac{d[\mathbf{35}]}{dt} = K_{\text{eq}} k_2[\mathbf{34}] = k_{\text{obs}}[\mathbf{34}] \quad (4.12)$$

The isotope effect for the conversion of **34** to **35** is much smaller than that previously described for the formation of **34** from **7**, which was proposed to have a relatively linear transition state. Smaller KIEs in the region 2.5 – 3.5 are expected for proton transfers occurring by non-linear transition states,[30,77,81,85–87] although even smaller values in the region of 1.5 have been reported.[88,89] The small isotope effect observed here for the conversion of **34** to **35** may reflect the presence of isotope-sensitive equilibria rather than the KIE of a single step. An inverse equilibrium isotope effect (EIE) of 0.781 was reported by Bergman and co-workers for a similar reaction.[62] Initial [2+2] cycloaddition of HCCPh with the titanium oxo compound Cp*$_2$Ti(O)(py) gave the metallacycle Cp*$_2$Ti{CH=C(Ph)O} which, upon thermolysis, underwent conversion to the hydroxoacetylide compound Cp*$_2$Ti(OH)(CCPh). Mechanistic studies showed that the process occurred by facile cycloreversion back to a terminal oxo complex, followed by proton transfer and Ti–C bond formation. The EIE value of 0.781 arises from deuterium favouring to reside in the higher energy bond (O–H), as the difference in zero point energy (ZPE) between an E–H and E–D bond increases with vibrational frequency.[81] Thus the equilibrium shifts further to the hydroxoacetylide species on substitution of H with D. As that reaction was found to be reversible, the EIE of the reverse reaction (hydroxoacetylide converting to the metallacycle) can be stated to be 1.28 (1/0.781). This reverse reaction is

analogous to the conversion of **34** to **35**, and has a comparable EIE value to this case, as the same ZPE-driven effect takes place with N–H and N–D bonds. Comparable values were also reported recently by this research group in a similar reaction: the conversion of the bis(acetylide) **4.7** to the vinylamide-acetylide complex **4.8** having an EIE of 1.4.[25]

4.7 Further reactions attempted between borylimides and alkynes

Further to the reactions of HCCTol and $HCCAr^F$ with the four borylimido complexes **4**, **5**, **6** and **7**, reactions were also attempted between those two terminal alkynes and the dipyrrolide-amine-supported borylimide $Ti(N_2^{pyr}N^{Me})\{NB(NAr'CH)_2\}(py)_2$ (**8**). Unfortunately, upon reactions on the NMR tube scale in C_6D_6, neither alkyne reacted with **8**, the starting material remaining unchanged even with extended heating up to 90 °C. This may be due to **8** having a six-coordinate structure due to it retanining two coordinated pyridine donors (unlike **4**, **5**, **6** and **7**, which retain a single pyridine donor and have five-coordinate geometries). The increased coordination number at the titanium centre presumably prevents the pre-coordination of the terminal alkyne which is necessary for any subsequent reaction to take place.

Reactions were also attempted between all five of these borylimido complexes and three internal alkynes: MeCCMe, MeCCPh and MeCC-4-$C_6H_4CF_3$. Again, no successful reaction was found in any of these cases. Suspecting that this may have been due to insurmountable steric barriers, a test reaction was performed with $Ti(N_2^{ArF}N^{Me})\{NB(NAr'CH)_2\}(py)$ (**5**), for which pyridine abstraction by $B(Ar^F)_3$ was known to be successful (Section 4.4). *In situ* formation of the base free borylimide by reaction of **5** with $B(Ar^F)_3$ was followed by addition of MeCCMe and MeCCPh, although neither gave any subsequent reaction upon heating.

In Section 4.2, the hydroamination of alkynes by titanium imido catalysts was discussed. It was shown that, in some cases, azatitanacyclobutene-type complexes were intermediates in the catalytic cycle.[6,22,26,27,29,33,35–38] Given the formation of a number of metallacycles of this type through the reactions of **4**, **5**, **6** and **7** with HCCTol and $HCCAr^F$, the Author next targeted the completion of a (stoichiometric) cycle by reactions of those metallacycles with the borylamine $H_2NB(NAr'CH)_2$ (**2.2**), with the hope that aminolysis by the borylamine would yield a hydro-borylamination product and regenerate a borylimide. Unfortunately, the attempted reactions of the metallacycles **23**, **25**, **29** and **33** with **2.2** were all unsuccessful. On the NMR tube scale at lower temperatures, no reaction was observed,

whereas upon stronger heating up to 90 °C, in most cases, this led to eventual decomposition of the metallacyclic compound, with ^{1}H NMR signals corresponding to the borylamine being observed to increase in intensity. Thus, in all of these cases, stoichiometric hydro-borylamination could not be achieved. It was initially postulated that this may be due to the high strength of the N–H bonds of the borylamine (Section 3.7) preventing it from cleaving the metallacyclic fragment through protonolytic exchange.

To investigate this further, Ti(N_2N^{py}){N{B(NAr'CH)$_2$}C(H)C(Tol)} (**33**) was reacted with two further amines with the possibility that these would cleave the metallacyclic fragment from the metal *via* protonolysis to form what would have been the product of hydro-borylamination, and generate a titanium imide. On the NMR tube scale in C_6D_6, **33** was reacted with 1 equiv. of both H_2N^tBu and H_2NAr' (as well as 1 equiv. of pyridine in each case). In the reaction of H_2N^tBu with **33**, heating at 60 °C over 24 h resulted in formation of the enamine TolC(H)=C(H)N(H)B(NAr'CH)$_2$ (**4.9**), which is the expected product of hydro-borylamination. This product has been isolated and fully characterised by another DPhil student within our group, and the ^{1}H NMR spectrum obtained here was consistent with that of the isolated material.[90] Despite this result, inspection of the other signals in the ^{1}H NMR spectrum did not show the formation of either a base-free or pyridine-supported *tert*-butylimido complex, with multiple environments being observed for the N_2N^{py} supporting ligand. Thus, the fate of the titanium in this reaction is unclear. With the addition of H_2NAr' to **33**, no reaction was observed at lower temperatures, and **33** was found to decompose upon heating to 85 °C. The failure of the reaction in this case may be due to the increased bulk of H_2NAr' relative to H_2N^tBu making the desired aminolysis unfeasible.

4.8 Computational studies of reactions of model complexes with alkynes

Building on the DFT bonding analysis in the model systems Ti($N_2^{SiH_3}N^{py}$)(NR)(py) (R = Me (**1Q_Me**), Xyl (**1Q_Xyl**), B(NMeCH)$_2$ (**1Q_B(NMeCH)$_2$**)) presented in Chapter Two, further calculations were performed by Prof. Philip Mountford to investigate the outcomes of reactions with alkynes in diamide-pyridine-supported systems, and later the feasibility of hydroamination-type reactivity from the respective metallacycles.

Firstly, the outcomes of reactions of these systems with alkynes are considered. The base-free model complexes Ti($N_2^{SiH_3}N^{py}$)(NR) (R = Me (**3Q_Me**), Xyl (**3Q_Xyl**), B(NMeCH)$_2$ (**3Q_B(NMeCH)$_2$**)) were employed, as it is well established in previously reported titanium imido and hydrazido reactivity that pyridine dissociation occurs prior to

reaction with an alkyne.[12,45] The total electronic energies of the models **3Q_R** were calculated, as well as those of the model anti-Markovnikov azatitanacyclobutenes Ti($N_2^{SiH_3}N^{py}$){N(R)C(H)C(Ar)} (**4Q_NR_HCCAr**) and acetylides Ti($N_2^{SiH_3}N^{py}$)(NHR)(CCAr) (**5Q_NR_HCCAr**) derived from hypothetical reactions with HCCPh and $HCCAr^F$ (Scheme 4.10). Subtracting the electronic energies of the starting materials from those of the respective products gives the electronic SCF energy change (ΔE) of each process, as listed in Table 4.6.

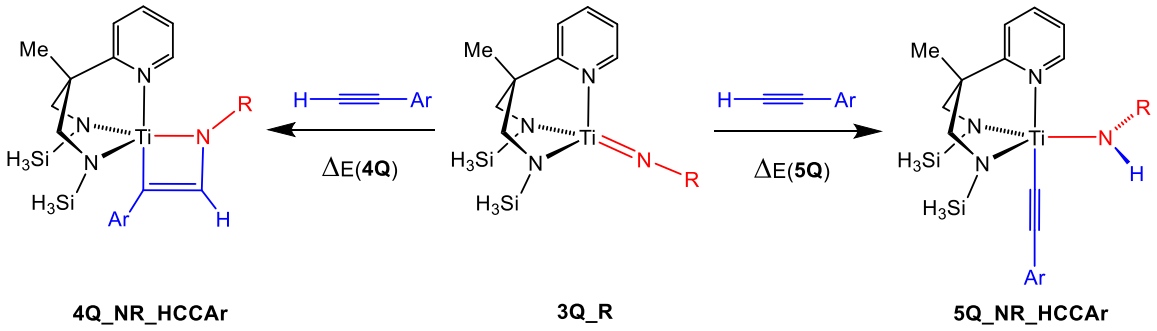

Scheme 4.10. Reaction scheme for the hypothetical reactions of Ti($N_2^{SiH_3}N^{py}$)(NR) (**3Q_R**, R = Me, Xyl, $B(NMeCH)_2$) with HCCPh and $HCCAr^F$ to give either metallacycles **4Q_NR_HCCAr** or acetylides **5Q_NR_HCCAr**.

Table 4.6. Electronic energy changes (ΔE, kcal mol^{-1}) calculated for the reactions of Ti($N_2^{SiH_3}N^{py}$)(NR) (**3Q_R**, R = Me, Xyl, $B(NMeCH)_2$) with HCCPh and $HCCAr^F$ to give metallacycles (**4Q**) or acetylides (**5Q**).

Starting model complex	Alkyne	ΔE(**4Q**)	ΔE(**5Q**)
3Q_Me	HCCPh	–24.4	–13.6
3Q_Xyl	HCCPh	–17.0	–9.1
3Q_B(NMeCH)$_2$	HCCPh	–21.1	–12.1
3Q_B(NMeCH)$_2$	$HCCAr^F$	–26.9	–15.0

Considering first the ΔE values for the reactions of the three models **3Q_R** with HCCPh, in all three cases the [2+2] cycloaddition reaction to give the metallacycles **4Q_NR_HCCPh** is strongly electronically favoured over the C–H bond activation to give

the acetylides **5Q_NR_HCCPh**. For a reaction to proceed it must outcompete the possible re-coordination of pyridine to the base-free complex **3Q_R**, for which the electronic energy changes are –9.2, –9.7 and –10.8 kcal mol^{-1} for R = Me, Xyl, B(NMeCH)$_2$, respectively. Thus, all of the processes in Table 4.6, other than formation of the acetylide **5Q_NXyl_HCCPh**, are electronically favoured over coordination of pyridine. Experimentally, the borylimide **7** reacted with HCCTol to form exclusively the metallacycle **33**, and the real imido compounds Ti(N$_2$N^{py})(NR)(py) (R = ^{t}Bu (**1.9**), Ar') reacted with HCCTol to give exclusively the metallacycles Ti(N$_2$N^{py}){N(R)C(H)C(Tol)} (R = ^{t}Bu (**4.10**), Ar' (**4.4**)) as well as with HCCPh to give the analogous metallacycles Ti(N$_2$N^{py}){N(R)C(H)C(Ph)} (R = ^{t}Bu (**4.11**), Ar').[41] The relative magnitudes of the ΔE values calculated here suggest that the model borylimide is more similar to an alkylimide, rather than an arylimide, in its reactivity with terminal alkynes.

ΔE values were also calculated for the two possible outcomes of the reaction of **3Q_B(NMeCH)$_2$** with HCCAr^F (Table 4.6). Switching to the electron-deficient alkyne results in more negative values (compared with those for HCCPh) for both the cycloaddition and C–H bond activation processes (the effect being strongest for the cycloaddition reaction). Experimentally, the acetylide **34** is formed as the kinetic product of **7** and HCCAr^F at RT, whilst conversion to the metallacycle **35** as the thermodynamic product takes place upon heating. Whilst the calculations show that an electronic preference for the cycloaddition remain, the stabilisation of the electron-deficient acetylide is sufficient to allow its isolation as the kinetic product in the experimental system.

Additionally, ΔE values for cycloadditions of the three **3Q_R** models with internal alkynes MeCCMe and MeCCPh were calculated. For **3Q_B(NMeCH)$_2$**, these were calculated to be –13.6 and –15.6 kcal mol^{-1} respectively, so significantly smaller in magnitude than the energy changes for cycloadditions of terminal alkynes shown in Table 4.6. In addition to the smaller electronic driving force, the increased sterics of an internal alkyne may make these reactions unfeasible experimentally. Indeed, no reaction was found to take place between **7** and MeCCMe or MeCCPh (*vide supra*).

Next, the electronic energy changes of reactions of **4Q_NR_HCCPh (**R = Me, Xyl, NB(NMeCH)$_2$) with amines H$_2$NR' (R' = Me, Xyl, B(NMeCH)$_2$) to generate the enamines *trans*-PhC(H)=C(H)NH(R) and the imide-type complexes **3Q_R'** (Equation 4.13) were calculated, and these are listed in Table 4.7. These hypothetical aminolysis reactions

represent the second step of a stoichiometric hydroamination-type reaction in which the imido catalyst is regenerated and the enamine is released as the desired product.

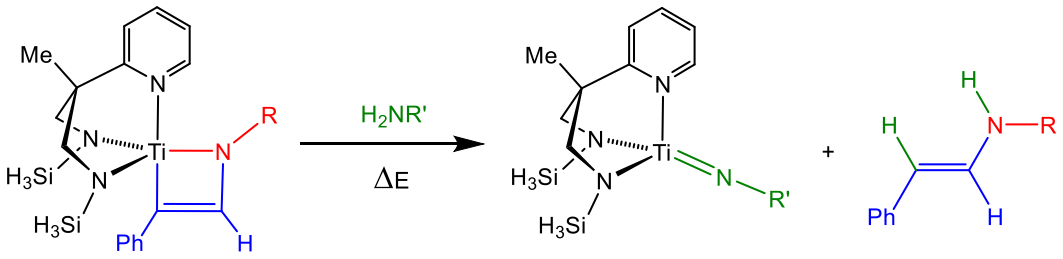

4Q_NR_HCCPh **3Q_R'**

Equation 4.13

Table 4.7. Electronic energy changes (ΔE, kcal mol^{-1}) calculated for the reactions of Ti($N_2^{SiH_3}N^{py}$){N(R)C(H)C(Ph)} (**4Q_NR_HCCPh**, R = Me, Xyl, B(NMeCH)$_2$) with amines H_2NR' (R' = Me, Xyl, B(NMeCH)$_2$) to give the imides **3Q_R'** and enamines PhC(H)=C(H)NH(R).

Starting metallacycle	Amine	ΔE
4Q_NMe_HCCPh	H_2NMe	–13.7
4Q_NXyl_HCCPh	H_2NXyl	–15.1
4Q_NB(NMeCH)$_2$_HCCPh	$H_2NB(NMeCH)_2$	–14.8
4Q_NB(NMeCH)$_2$_HCCPh	H_2NMe	–14.3

The first three rows of Table 4.7 show reactions between each model metallacycle **4Q_NR_HCCPh** and the amine (or borylamine) from which the amido (or borylamido) portion of its metallacyclic unit derives; i.e. R = R'. The ΔE values calculated are all of similar magnitude, with the reaction of **4Q_NXyl_HCCPh** with H_2NXyl being the most favourable with ΔE = –15.1 kcal mol^{-1}. A fourth calculated value, for **4Q_NB(NMeCH)$_2$_HCCPh** with H_2NMe, is found to be –14.3 kcal mol^{-1}, which is slightly less favourable than the reaction with the model borylamine (–14.8 kcal mol^{-1}). Experimentally, the metallacycle **4.11** is known to undergo aminolysis with H_2N^tBu to yield the *tert*-butylimide **1.9** and enamine PhC(H)=C(H)NH(^{t}Bu),[41] and the metallacycle **33** underwent aminolysis with H_2N^tBu to give the boryl-substituted enamine **4.9** (although

decomposition of the titanium species occurred). This implies, therefore, that hydro-borylamination using the borylamine **2.2** in this system should be thermodynamically feasible. However, as described above, no such reactions with this borylamine were found to take place. To shed more light on these reactions, additional DFT calculations including solvent and dispersion corrections were performed on the full, experimentally known systems, giving the thermodynamic parameters of these reactions, which are listed in Table 4.8. These include the known reaction of the metallacycle ***trans*-4.11** with H_2N^tBu to give the *tert*-butylimide **1.9** and PhC(H)=C(H)NH(^{t}Bu), the experimentally unsuccessful reaction of **33** with borylamine **2.2**, and the reaction of **33** with H_2N^tBu which produces the boryl-substituted enamine **4.9**.

Table 4.8. DFT-calculated thermodynamic parameters (ΔG and ΔH in kcal mol^{-1}, ΔS in cal K^{-1} mol^{-1}) for the reactions of the real metallacycles Ti(N_2N^{py}){N(R)C(H)C(Ar)} (R = ^{t}Bu, Ar = Ph (**4.11**) or Tol (**4.10**); R = B(NAr'CH)$_2$, Ar = Tol (**33**)) with H_2N^tBu or $H_2NB(NAr'CH)_2$ (**2.2**) to produce the respective enamine and imide.

Starting metallacycle	Amine	ΔG	ΔH	ΔS
***trans*-4.11**	H_2N^tBu	–4.7	–2.7	6.5
***trans*-4.10**	H_2N^tBu	–5.3	–3.1	7.3
33	H_2N^tBu	–7.5	1.2	29.0
33	$H_2NB(NAr'CH)_2$	–12.5	–11.5	3.3

Considering the first two rows of Table 4.8, these show the reactions of phenyl- and tolyl-substituted metallacycles derived from *tert*-butylimide **1.9** with H_2N^tBu to re-form **1.9** and the respective enamine. All of the thermodynamic parameters are similar in magnitude for the two reactions. The third row shows the reaction of the boryl-substituted metallacycle **33** with H_2N^tBu. Compared to the above two processes, the reaction is weakly endothermic rather than exothermic (ΔH = 1.2 kcal mol^{-1}; *cf.* –2.7 and –3.1 kcal mol^{-1} above). Most noticeably, however, this reaction has an extremely high ΔS of 29.0 cal K^{-1} mol^{-1} (*cf.* 6.5 and 7.3 cal K^{-1} mol^{-1} in the other two reactions). This arises from the release of the bulky boryl functionality from the highly crowded metallacycle, thus greatly increasing the vibrational degrees of freedom in the products. This entropic effect contributes to a more

negative ΔG value of –7.5 kcal mol^{-1} for this process. Finally, the fourth row of Table 4.8 shows the reaction of **33** with $H_2NB(NAr'CH)_2$ (**2.2**). In this case, ΔH is strongly exothermic (–12.5 kcal mol^{-1}), perhaps reflecting the formation of a stronger C–N bond in the enamine product compared with the reaction of H_2N^tBu. With a small, positive ΔS value being calculated, this gives a strongly negative ΔG of –12.5 kcal mol^{-1}, making this the most exergonic of the four processes. Knowing that **4.10** experimentally undergoes aminolysis with H_2N^tBu to complete a hydroamination cycle, it appears that the analogous process between **33** and **2.2** should be thermodynamically favoured to an even greater degree. The failure of this reaction to take place experimentally, therefore, is ascribed to the large steric bulk of the boryl functionality making the process kinetically unfeasible.

4.9 Conclusions and Outlook

This Chapter has primarily described the reactivity of four titanium borylimido complexes (supported by diamide-amine or diamide-pyridine ligand sets) with two terminal alkynes, HCCTol and $HCCAr^F$. In all four cases, reactions of the borylimides with HCCTol resulted in [2+2] cycloadditions to give the azatitanacyclobutene complexes $Ti(N_2{}^RN^{Me})\{N\{B(NAr'CH)_2\}C(H)C(Tol)\}$ (R = $SiMe_3$ (**23**), Ar^F (**25**), ^{i}Pr (**29**)) and $Ti(N_2N^{py})\{N\{B(NAr'CH)_2\}C(H)C(Tol)\}$ (**33**), all of which were shown to have anti-Markovnikov regiochemistry through NMR and crystallographic characterisations.

Meanwhile, the reactions with $HCCAr^F$ showed some differing behaviour. Whilst **4** and **5** again gave azatitanacyclobutenes $Ti(N_2{}^RN^{Me})\{N\{B(NAr'CH)_2\}C(H)C(Ar^F)\}$ (R = $SiMe_3$ (**24**), Ar^F (**27**)), **6** and **7** gave C–H bond activations of $HCCAr^F$ to yield the borylamide-acetylide complexes $Ti(N_2{}^{iPr}N^{Me})\{NHB(NAr'CH)_2\}(CCAr^F)$ (**30**) and $Ti(N_2N^{py})\{NHB(NAr'CH)_2\}(CCAr^F)$ (**34**), respectively, as kinetic products. Heating of both **30** and **34** gave conversion to the metallacycles $Ti(N_2{}^{iPr}N^{Me})\{N\{B(NAr'CH)_2\}C(H)C(Ar^F)\}$ (**32**) and $Ti(N_2N^{py})\{N\{B(NAr'CH)_2\}C(H)C(Ar^F)\}$ (**35**), respectively, as thermodynamic products. The kinetic isotope effect of the C–H bond activation to form **34** was measured to be between 4.86 and 5.37, which is consistent with a number of previously reported cases of C–H bond activations and formations at Group 4 metal centres in which transfer of H takes place in a relatively linear fashion. An equilibrium isotope effect of the conversion of **34** to **35** was measured to be between 1.19 and 1.46, with this reflecting the thermodynamic

preference of D to reside at the amide site in **35**, rather than as the metallacycle methine in **34**.

Upon heating, the $N_2^{ArF}N^{Me}$-supported metallacycles **25** and **27** both underwent a C–F bond activation reaction to yield the titanium fluoride complexes Ti{MeN($CH_2CH_2NAr^F$){$CH_2CH_2NC_6F_4C$(Ar)=CHNB(NAr'CH)$_2$}}(F) (Ar = Tol (**28**), Ar^F (**26**)). The kinetics of these reactions were studied by ^{1}H NMR arrays, and Eyring analyses subsequently carried out. The activation parameters of the two processes were found to be comparable within error, with this proposed to reflect a balance between the nucleophilicity of the attacking metallacycle carbon and stabilisation of the initial metallacycle through π-stacking. The presence of this latter effect was also supported by crystallographic characterisations.

Finally, attempts were made to investigate the feasibility of potential hydro-borylamination catalysis in these systems. In azatitanacyclobutenes **23**, **25**, **29** and **33**, the borylamine H_2NB(NAr'CH)$_2$ (**2.2**) did not successfully effect protonolysis of the metallacyclic fragment. However, reaction of **33** with H_2N^tBu did yield the enamine TolC(H)=C(H)N(H)B(NAr'CH)$_2$ (**4.9**), which would have been the product of successful hydro-borylamination. DFT calculations showed that, in a thermodynamic sense, aminolysis of the metallacycle **33** by **2.2** should be strongly favourable. Indeed, the ΔG of this process was calculated to be more negative than for the analogous reaction in an imido system which is known to be experimentally successful. The failure of this reaction is therefore ascribed to the extreme bulk of the boryl moiety making the process kinetically unfeasible.

The further investigation of reactivity of Group 4 borylimido complexes with terminal and internal alkynes by other DPhil students within this research group is ongoing. Of note are successful reactions of Cp*Ti(hpp){NB(NAr'CH)$_2$} (**10**) with some internal alkynes to give azatitanacyclobutene complexes,[91] while similar reactions of zirconocene borylimides with internal alkynes have also been successful.[90] Furthermore, in the latter system, an extended investigation of the scope of hydro-borylamination-type reactions is currently underway.

4.10 References

1 D. E. Wigley, in *Progress in Inorganic Chemistry*, ed. K. D. Karlin, Wiley-Interscience, New York, 1994, vol. 42, pp. 239–482.

2 P. Mountford, *Chem. Commun.*, 1997, 2127–2134.

3 L. H. Gade and P. Mountford, *Coord. Chem. Rev.*, 2001, **216**–**217**, 65–97.

4 P. D. Bolton and P. Mountford, *Adv. Synth. Catal.*, 2005, **347**, 355–366.

5 N. Hazari and P. Mountford, *Acc. Chem. Res.*, 2005, **38**, 839–849.

6 A. L. Odom, *Dalton Trans.*, 2005, 225–233.

7 A. R. Fout, U. J. Kilgore and D. J. Mindiola, *Chem. Eur. J.*, 2007, **13**, 9428–9440.

8 J. D. Selby, C. D. Manley, M. Feliz, A. D. Schwarz, E. Clot and P. Mountford, *Chem. Commun.*, 2007, **733**, 4937–4939.

9 J. D. Selby, C. Schulten, A. D. Schwarz, A. Stasch, E. Clot, C. Jones and P. Mountford, *Chem. Commun.*, 2008, 5101–5103.

10 K. Weitershaus, J. Lloret Fillol, H. Wadepohl and L. H. Gade, *Organometallics*, 2009, **28**, 4747–4757.

11 K. Weitershaus, H. Wadepohl and L. H. Gade, *Organometallics*, 2009, **28**, 3381–3389.

12 A. D. Schofield, A. Nova, J. D. Selby, C. D. Manley, A. D. Schwarz, E. Clot and P. Mountford, *J. Am. Chem. Soc.*, 2010, **132**, 10484–10497.

13 P. J. Tiong, A. D. Schofield, J. D. Selby, A. Nova, E. Clot and P. Mountford, *Chem. Commun.*, 2010, **46**, 85–87.

14 A. J. Blake, J. M. McInnes, P. Mountford, G. I. Nikonov, D. Swallow and D. J. Watkin, *J. Chem. Soc. Dalton Trans.*, 1999, 379–392.

15 T. Gehrmann, J. L. Fillol, H. Wadepohl and L. H. Gade, *Organometallics*, 2012, **31**, 4504–4515.

16 H. Herrmann, J. L. Fillol, H. Wadepohl and L. H. Gade, *Angew. Chem. Int. Ed.*, 2007, **46**, 8426–8430.

17 J. Unruangsri, H. Morgan, A. D. Schwarz, A. D. Schofield and P. Mountford, *Organometallics*, 2013, **32**, 3091–3107.

18 A. D. Schofield, A. Nova, J. D. Selby, A. D. Schwarz, E. Clot and P. Mountford, *Chem. Eur. J.*, 2011, **17**, 265–285.

19 P. J. Walsh, M. J. Carney and R. G. Bergman, *J. Am. Chem. Soc.*, 1991, **113**, 6343–6345.

20 R. F. Munhá, L. F. Veiros, M. T. Duarte, M. D. Fryzuk and A. M. Martins, *Dalton Trans.*, 2009, 7494–7508.

21 T. Gehrmann, J. L. Fillol, H. Wadepohl and L. H. Gade, *Organometallics*, 2010, **29**, 28–31.

22 K. Weitershaus, B. D. Ward, R. Kubiak, C. Müller, H. Wadepohl, S. Doye and L. H.

Gade, *Dalton Trans.*, 2009, 4586–602.

23 J. L. Polse, A. W. Kaplan, R. A. Andersen and R. G. Bergman, *J. Am. Chem. Soc.*, 1998, **120**, 6316–6328.

24 J. L. Polse, R. A. Andersen and R. G. Bergman, *J. Am. Chem. Soc.*, 1998, **120**, 13405–13414.

25 L. C. Stevenson, DPhil Thesis, University of Oxford, 2015.

26 S. Doye, *Synlett*, 2004, **2004**, 1653–1672.

27 T. E. Müller, K. C. Hultzsch, M. Yus, F. Foubelo and M. Tada, *Chem. Rev.*, 2008, **108**, 3795–892.

28 Y. Li, Y. Shi and A. L. Odom, *J. Am. Chem. Soc.*, 2004, **126**, 1794–1803.

29 S. Banerjee, E. Barnea and A. L. Odom, *Organometallics*, 2008, **27**, 1005–1014.

30 A. D. Schwarz, C. S. Onn and P. Mountford, *Angew. Chem. Int. Ed.*, 2012, **51**, 12298–12302.

31 P. D. Schweizer, H. Wadepohl and L. H. Gade, *Organometallics*, 2013, **32**, 3697–3709.

32 C. Cao, Y. Shi and A. L. Odom, *Org. Lett.*, 2002, **4**, 2853–2856.

33 J. S. Johnson and R. G. Bergman, *J. Am. Chem. Soc.*, 2001, **123**, 2923–2924.

34 V. Khedkar, A. Tillack, M. Michalik and M. Beller, *Tetrahedron Lett.*, 2004, **45**, 3123–3126.

35 I. Bytschkov and S. Doye, *Eur. J. Org. Chem.*, 2003, **2003**, 935–946.

36 A. V. Lee and L. L. Schafer, *Eur. J. Inorg. Chem.*, 2007, 2243–2255.

37 S. Banerjee, Y. Shi, C. Cao and A. L. Odom, *J. Organomet. Chem.*, 2005, **690**, 5066–5077.

38 A. Tillack, H. Jiao, I. G. Castro, C. G. Hartung and M. Beller, *Chem. Eur. J.*, 2004, **10**, 2409–2420.

39 L. Ackermann and R. Born, *Tetrahedron Lett.*, 2004, **45**, 9541–9544.

40 N. Vujkovic, J. L. Fillol, B. D. Ward, H. Wadepohl, P. Mountford and L. H. Gade, *Organometallics*, 2008, **27**, 2518–2528.

41 B. D. Ward, A. Maisse-Francois, P. Mountford and L. H. Gade, *Chem. Commun.*, 2004, 704–705.

42 D. J. M. Trösch, P. E. Collier, A. Bashall, L. H. Gade, M. McPartlin, P. Mountford and S. Radojevic, *Organometallics*, 2001, **20**, 3308–3313.

43 A. Bashall, P. E. Collier, L. H. Gade, M. McPartlin, P. Mountford and D. J. M. Trösch, *Chem. Commun.*, 1998, 2555–2556.

44 J. D. Selby, C. D. Manley, A. D. Schwarz, E. Clot and P. Mountford, *Organometallics*, 2008, **27**, 6479–6494.

45 N. Vujkovic, B. D. Ward, A. Maisse-François, H. Wadepohl, P. Mountford and L. H. Gade, *Organometallics*, 2007, **26**, 5522–5534.

46 A. W. Addison, T. N. Rao, J. Reedijk, J. van Rijn and G. C. Verschoor, *J. Chem. Soc., Dalton Trans.*, 1984, 1349–1356.

47 S. Lorenzo, G. R. Lewis and I. Dance, *New J. Chem.*, 2000, **24**, 295–304.

48 J. H. Williams, *Acc. Chem. Res.*, 1993, **26**, 593–598.

49 C. R. Patrick and G. S. Prosser, *Nature*, 1960, 187, 1021.

50 C. Dai, P. Nguyen, T. B. Marder, T. B. Marder, A. J. Scott, W. Clegg, C. Viney and C. Viney, *Chem. Commun.*, 1999, 2493–2494.

51 N. Adams, A. R. Cowley, S. R. Dubberley, A. J. Sealey, M. E. G. Skinner and P. Mountford, *Chem. Commun.*, 2001, 2738–2739.

52 O. R. Lozman, R. J. Bushby and J. G. Vinter, *J. Chem. Soc. Perkin Trans. 2*, 2001, 1446–1452.

53 K. Reichenbächer, H. I. Süss and J. Hulliger, *Chem. Soc. Rev.*, 2005, **34**, 22–30.

54 L. R. Groom, A. F. Russell, A. D. Schwarz and P. Mountford, *Organometallics*, 2014, **33**, 1002–1019.

55 J. L. Kiplinger, T. G. Richmond and C. E. Osterberg, *Activation of Carbon-Fluorine Bonds by Metal Complexes*, 1994, vol. 94.

56 S. A. Scholl, G. T. Plundrich, H. Wadepohl and L. H. Gade, *Inorg. Chem.*, 2013, **52**, 10158–10166.

57 M. Sotoodeh, I. Leichtweis, H. W. Roesky, M. Noltemeyer and H.-G. Schmidt, *Chem. Ber.*, 1993, **126**, 913–919.

58 C. H. Winter, X. X. Zhou and M. J. Heeg, *Inorg. Chem.*, 1992, **31**, 1808–1815.

59 M. Klahn, P. Arndt, A. Spannenberg, A. Gansäuer and U. Rosenthal, *Organometallics*, 2008, **27**, 5846–5851.

60 R. Kickbusch and D. Lentz, *Chem. Commun.*, 2010, **46**, 2118–2120.

61 J. A. Bexrud, C. Li and L. L. Schäfer, *Organometallics*, 2007, **26**, 6366–6372.

62 J. L. Polse, R. A. Andersen and R. G. Bergman, *J. Am. Chem. Soc.*, 1995, **117**, 5393–5394.

63 H. M. Hoyt and R. G. Bergman, *Angew. Chem. Int. Ed. Engl.*, 2007, **46**, 5580–5582.

64 T. Chu, W. E. Piers, J. L. Dutton and M. Parvez, *Organometallics*, 2013, **32**, 1159–1165.

65 R. E. Blake, D. M. Antonelli, L. M. Henling, W. P. Schaefer, K. I. Hardcastle and J. E. Bercaw, *Organometallics*, 1998, **17**, 718–725.

66 H. E. Bryndza, L. K. Fong, R. A. Paciello, W. Tam and J. E. Bercaw, *J. Am. Chem. Soc.*, 1987, **109**, 1444–1456.

67 P. L. Holland, R. A. Andersen, R. G. Bergman, J. Huang and S. P. Nolan, *J. Am. Chem. Soc.*, 1997, **119**, 12800–12814.

68 P. L. Holland, R. A. Andersen and R. G. Bergman, *Comments Inorg. Chem.*, 1999, **21**, 115–129.

69 L. E. Schock and T. J. Marks, *J. Am. Chem. Soc.*, 1988, **110**, 7701–7715.

70 D. D. Wick and W. D. Jones, *Organometallics*, 1999, **18**, 495–505.

71 J. L. Bennett and P. T. Wolczanski, *J. Am. Chem. Soc.*, 1997, **119**, 10696–10719.

72 C. C. Cummins, S. M. Baxter and P. T. Wolczanski, *J. Am. Chem. Soc.*, 1988, **110**, 8731–8733.

73 C. C. Cummins, C. P. Schaller, G. D. Van Duyne, P. T. Wolczanski, A. W. E. Chan and R. Hoffmann, *J. Am. Chem. Soc.*, 1991, **113**, 2985–2994.

74 C. P. Schaller, C. C. Cummins, P. T. Wolczanski and N. York, *J. Am. Chem. Soc.*, 1996, **118**, 591–611.

75 L. M. Slaughter, P. T. Wolczanski, T. R. Klinckman and T. R. Cundari, *J. Am. Chem. Soc.*, 2000, **122**, 7953–7975.

76 P. J. Walsh, F. J. Hollander and R. G. Bergman, *J. Am. Chem. Soc.*, 1988, **110**, 8729–8731.

77 K. Manna, A. Ellern and A. D. Sadow, *Chem. Commun.*, 2010, **46**, 339–341.

78 M. Gómez-Gallego and M. A. Sierra, *Chem. Rev.*, 2011, **111**, 4857–963.

79 J. R. Webb, S. A. Burgess, T. R. Cundari and T. B. Gunnoe, *Dalton Trans.*, 2013, **42**, 16646–16665.

80 D. Balcells, E. Clot and O. Eisenstein, *Chem. Rev.*, 2010, **110**, 749–823.

81 T. H. Lowry and K. S. Richardson, *Mechanism and Theory in Organic Chemistry*, Harper and Row, New York, 1987.

82 B. K. Carpenter, *Determination of Reaction Mechanisms*, Wiley-Interscience, New York, 1984.

83 C. P. Schaller, J. B. Bonanno and P. T. Wolczanski, *J. Am. Chem. Soc.*, 1994, **116**, 4133–4134.

84 T. R. Cundari, T. R. Klinckman and P. T. Wolczanski, *J. Am. Chem. Soc.*, 2002, **124**, 1481–1487.

85 L. R. Groom, DPhil Thesis, University of Oxford, 2014.

86 L. E. N. Allan, G. J. Clarkson, D. J. Fox, A. L. Gott and P. Scott, *J. Am. Chem. Soc.*, 2010, **132**, 15308–15320.

87 A. L. Reznichenko and K. C. Hultzsch, *Organometallics*, 2010, **29**, 24–27.

88 A. L. Reznichenko and K. C. Hultzsch, *J. Am. Chem. Soc.*, 2012, **134**, 3300–3311.

89 M. G. Cushion, J. Meyer, A. Heath, A. D. Schwarz, I. Fernández, F. Breher and P. Mountford, *Organometallics*, 2010, **29**, 1174–1190.

90 B. Xie and P. Mountford, Unpublished results.

91 M. Slusarczyk and P. Mountford, Unpublished results.

Chapter Five

Evidence for the formation of a transient scandium borylimide and its small molecule reactivity

5.1 Overview

This Chapter will describe various attempts to prepare the first borylimido complex of a rare earth metal, namely scandium. Using a β-diketiminate (NacNac)-type supporting ligand incorporating a pendant NMe_2 donor group, the formation of a scandium methyl-borylamide will be described. Thermolysis reactions of this complex will then be explored, with such reactions in both the presence and absence of external bases giving unexpected C–H bond activations. The kinetics of these processes will be analysed, and evidence for the existence of a transient borylimide discussed. This will be further supported by trapping reactions with terminal and internal alkynes. Finally, modifications of both the boryl moiety and the supporting ligand set will be described, and the effects on the synthesis and reactivity of the resulting complexes explored. DFT and QTAIM studies will also be presented, with the bonding in a model scandium borylimide and its imido counterparts compared, followed by analysis of the relative energetics of reactions of these systems to explain the observed experimental outcomes.

5.2 Introduction

As introduced in Chapter One, the chemistry of terminal imido complexes of rare earth metals is considerably more scarce than that of their Group 4 analogues, and their successful isolation and structural characterisation have been much more recent.[1] A first factor which delayed such isolations is the tendency of the monomeric complexes to dimerise or form higher-nuclearity bridged clusters, especially for the larger lanthanides and yttrium.[2–14] Secondly, the highly polarised M=NR multiple bond is more reactive than its counterpart in Group 4 systems, meaning that undesired intra- or intermolecular activations may take place before the terminal imide can be isolated. For example, Mindiola and co-workers have reported on C–H bond activations of coordinated pyridine donors by P–N–P pincer ligand-supported scandium imides.[15–17] However, in recent years, a number of terminal imido complexes of scandium, the smallest rare earth metal, have been reported. Generally speaking, the successful syntheses of these have been achieved through two strategies: the incorporation of a large amount of steric bulk into both imido and supporting ligands, and the use of DMAP as a very strong Lewis base to stabilise the complexes. This use of DMAP was pioneered by Chen and co-workers, who reported the first terminal rare earth imido complex, $(L^1)Sc(NAr')(DMAP)$ (**1.47**, L^1 = $(Ar')NC(Me)CHC(Me)NCH_2CH_2NMe_2$), in 2010.[18] Addition of DMAP to

(L^1)Sc(Me)(NHAr') (**1.46**) at RT gave a six-coordinate DMAP-stabilised intermediate (**1.46'**), which eliminated methane under heating to yield the imide **1.47** (Scheme 5.1). The supporting ligand chosen was also considered to be of importance in obtaining this successful result. L^1 is a tridentate β-diketiminate (NacNac) ligand in which one N-substituent is the bulky Ar' group, and the second is a pendant $–CH_2CH_2NMe_2$ donor group. This gives a more flexible coordination framework around the scandium centre than a pincer ligand, and the hard N-donors are considered to provide a good electronic fit with the imido ligand.[1]

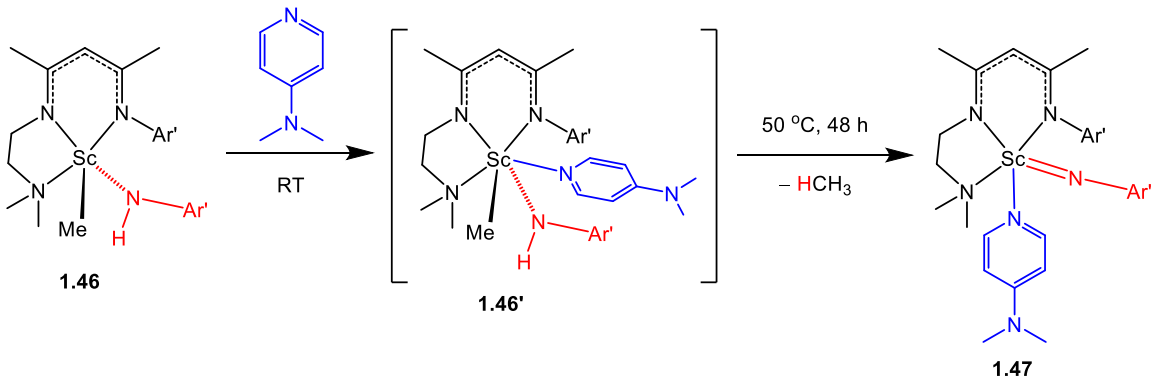

Scheme 5.1. Synthesis of (L^1)Sc(NAr')(DMAP) (**1.47**).[18]

This DMAP-based approach was later used by the research groups of both Piers and Cui to successfully form terminal scandium imides.[19,20] In the former case, (^{tBu}NacNac)Sc(Me)(NHAr') (**5.1**) reacted with DMAP at 50 °C over 5 days to form (^{tBu}NacNac)Sc(NAr')(DMAP) (**1.48**, Figure 5.1), with mechanistic studies showing that this proceeds *via* an intermediate in which intramolecular C–H bond activation of an Ar' methyl group has taken place at the Sc centre.[19] For the latter, the phosphazene ligand-supported alkyl-anilide {$N(PPh_2NPh)_2$}Sc(CH_2SiMe_3)(NHAr') in the presence of 2 equiv. DMAP underwent α-abstraction over 4 h at RT to yield the imide {$N(PPh_2NPh)_2$}Sc(NAr')$(DMAP)_2$ (**1.49**, Figure 5.1).[20] Chen and co-workers were later able to prepare an isolable terminal scandium imide without the need for DMAP. This was achieved through modification of their ligand set to incorporate a second pendant amine donor, making this now a (potentially) tetradentate ligand. From the alkyl-anilide (L^2)Sc(CH_2SiMe_3)(NHAr') (L^2 = (Ar')NC(Me)CHC(Me)$NCH_2CH_2N(Me)CH_2CH_2NMe_2$) in which the fourth donor atom of L^2 does not coordinate to the metal, heating at 50 °C for 3 days formed the imide (L^2)Sc(NAr') (**1.50**, Figure 5.1) in which L^2 has become tetradentate through the coordination of the second pendant amine donor.[21]

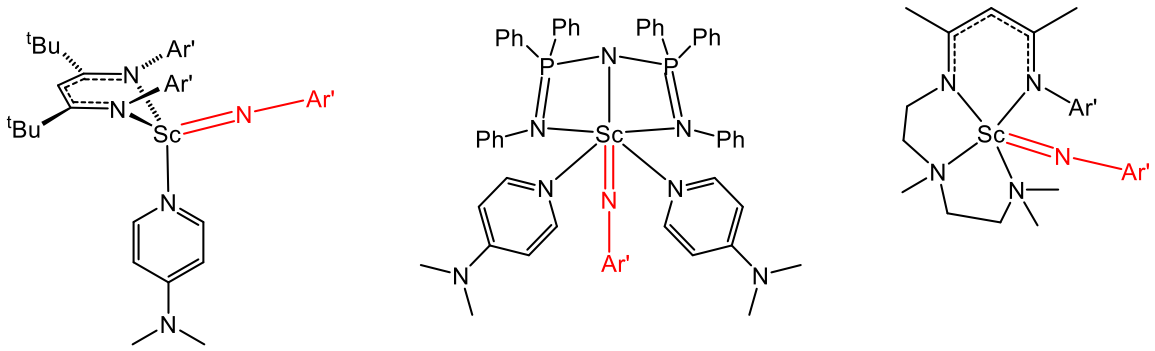

1.48 **1.49** **1.50**

Figure 5.1. Further examples of terminal imido complexes of scandium.[19–21]

Given the successful syntheses of a number of terminal scandium imides in recent years, the Author next decided to target the synthesis of a scandium borylimide. The incorporation of a large amount of steric bulk appears to be important in the formation of those terminal imides described above; indeed, all of those complexes have bulky 2,6-diisopropylphenylimido (–NAr') functional groups. Thus, it was postulated that the very bulky borylamine $H_2NB(NAr'CH)_2$ (**2.2**) would be similarly suitable for forming a stable borylimido complex. The initial success of Chen and co-workers in preparing **1.47**, and their subsequent reactivity studies on that imido complex with a wide range of substrates,[21–26] have demonstrated the suitability of the supporting ligand L^1 in this chemistry. Therefore, L^1 was chosen as the initial supporting ligand in these attempts to form a scandium borylimide, with $(L^1)ScCl_2$ (**5.2**) being used as the starting material.

5.3 Synthesis and characterisation of scandium borylamido complexes

By analogy to the preparation of $(L^1)Sc(Me)(NHAr')$ (**1.46**) by Chen and co-workers,[18] to $(L^1)ScCl_2$ (**5.2**) in THF was added 2 equiv. MeLi (1.6 M in Et_2O) to form the dimethylated complex $(L^1)ScMe_2$ (**5.3**), which was then reacted *in situ* with 1 equiv. $H_2NB(NAr'CH)_2$ (**2.2**) giving methane elimination over 60 h at RT (Scheme 5.2). After work-up, the methyl-borylamide $(L^1)Sc(Me)\{NHB(NAr'CH)_2\}$ (**36**) was isolated as an off-white powder in 53% yield. This reaction time was significantly longer than that required for the complete formation of **1.46** (24 h at RT), which presumably reflects steric hindrance in the approach of the bulkier borylamine to the scandium centre (compared with H_2NAr').

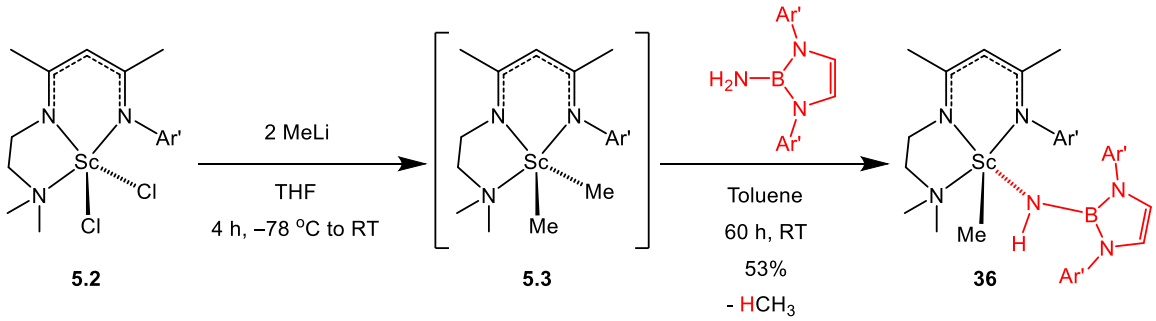

Scheme 5.2. Preparation of $(L^1)Sc(Me)\{NHB(NAr'CH)_2\}$ (**36**) from *in situ*-generated $(L^1)ScMe_2$ (**5.3**).

The ^1H (Figure 5.2) and ^{13}C NMR spectra of **36** are consistent with a C_1 symmetric species having one methyl ligand and one borylamido ligand in addition to the supporting ligand L^1. An NH singlet is observed at 3.29 ppm which, interestingly, is significantly upfield shifted compared to the corresponding NH resonance in **1.46** (5.70 ppm). Correspondingly, the amine protons of $H_2NB(NAr'CH)_2$ give a signal far upfield of that of the amine protons of H_2NAr' (1.19 *vs* 3.20 ppm). The resonance corresponding to the Sc–Me group of **36** is observed as a 3 H singlet at –0.90 ppm (*cf.* –0.49 ppm in **1.46**), with its ^{13}C resonance found at 24.3 ppm.

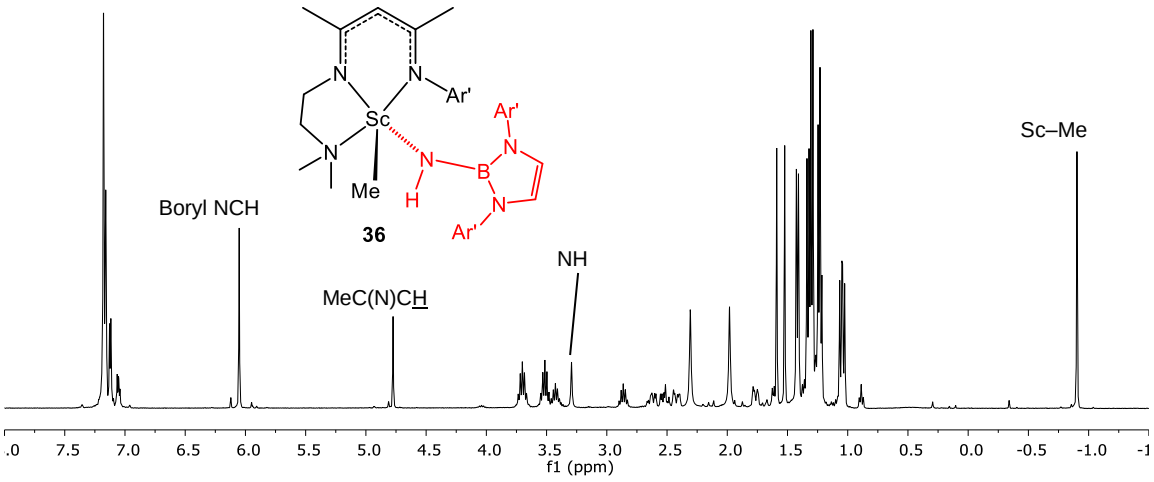

Figure 5.2. ^1H NMR spectrum (400.1 MHz) of $(L^1)Sc(Me)\{NHB(NAr'CH)_2\}$ (**36**) in C_6D_6 at 298 K.

Diffraction-quality crystals of **36** were successfully grown from a benzene solution at RT. The molecular solid state structure is shown in Figure 5.3, and selected bond distances and angles are listed in Table 5.1. Complex **36** has a monomeric, five-coordinate structure with square-based pyramidal geometry (τ = 0.02),[27] in which the tridentate L^1 and the methyl ligand form the base and N(1) of the borylamido ligand resides at the apex. The Sc(1)–N(1)

bond distance of 2.0629(8) Å is slightly longer (Δ = 0.016(3) Å) than the corresponding distance in the anilide **1.46** (2.047(3) Å), and the Sc–C bond distance of the methyl ligand of 2.273(1) Å is also longer than that in **1.46** (2.221(4) Å).[18] This probably reflects a steric effect in which the large bulk of the boryl moiety increases the crowding around the Sc centre, thus lengthening the bond distances to the metal, as well as the better donor ability of the NHB(NAr'CH)$_2$ ligand compared with NHAr'. Two further similar complexes have been crystallographically characterised: the methyl-anilide (^{tBu}NacNac)Sc(Me)(NHAr') (**5.1**) and its *tert*-butylamido analogue (**5.4**).[28] The Sc(1)–N(1) distance in **36** is also significantly longer than the corresponding distances in both **5.1** and **5.4**, these being 2.040(1) and 2.000(2) Å, respectively, presumably due to the higher coordination number, as well as increased steric bulk, in **36**. Similarly, the Sc–C bond of **36** is also longer than those in **5.1** and **5.4**: 2.212(2) and 2.229(2) Å respectively. In **36**, the borylamide hydrogen is close to a *cis* orientation with respect to the methyl group, with an H–N···Sc–C torsion angle of *ca* 32.2°. This is larger than the corresponding angle in **1.46** of *ca* 9.9°. Chen and co-workers commented that a small angle such as this would make the following α-abstraction process particularly facile.[18] However, it is noted that rotation about the Sc–NHR bond should itself be facile in the solution phase, and that coordination of DMAP to **1.46** prior to α-abstraction was proposed by that research group.

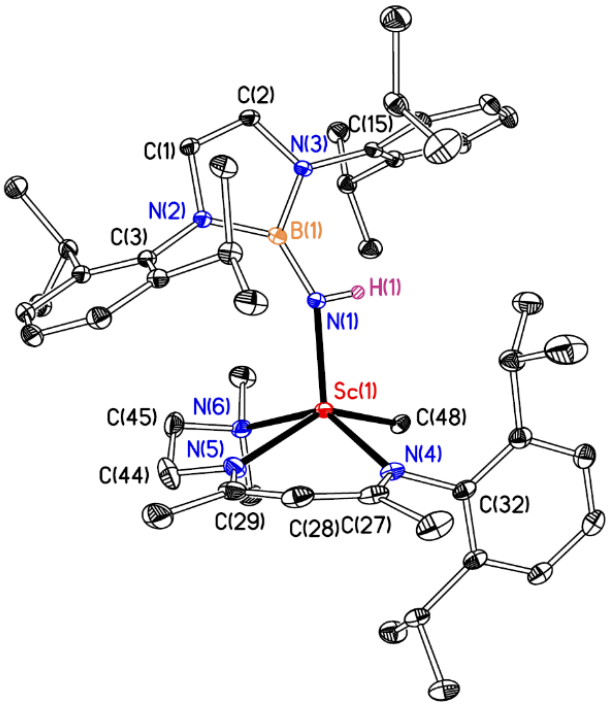

Figure 5.3. Displacement ellipsoid plot (20% probability) of (L^1)Sc(Me){NHB(NAr'CH)$_2$} (**36**). C-bound H atoms are omitted for clarity. H(1) is drawn as a sphere of arbitrary radius.

Table 5.1. Selected bond distances (Å) and angles (°) for $(L^1)Sc(Me)\{NHB(NAr'CH)_2\}$ (**36**) (τ = 0.02).

Sc(1)–N(1)	2.0629(8)	N(1)–Sc(1)–N(4)	118.10(3)
Sc(1)–N(4)	2.2047(9)	N(1)–Sc(1)–N(5)	111.87(4)
Sc(1)–N(5)	2.2085(9)	N(1)–Sc(1)–N(6)	100.49(3)
Sc(1)–N(6)	2.3199(9)	N(4)–Sc(1)–N(5)	82.15(4)
Sc(1)–C(48)	2.2730(10)	N(4)–Sc(1)–N(6)	140.38(3)
N(1)–B(1)	1.4179(13)	N(1)–Sc(1)– C(48)	104.03(4)
N(1)–H(1)	0.821(17)	N(4)–Sc(1)– C(48)	93.42(3)
		N(5)–Sc(1)– C(48)	141.40(4)
		N(6)–Sc(1)– C(48)	85.13(4)
		Sc(1)–N(1)–B(1)	152.36(7)
		Sc(1)–N(1)–H(1)	96.5(11)

Next, on the NMR tube scale in C_6D_6, $(L^1)ScCl_2$ (**5.2**) was reacted with 1 equiv. of the lithium borylamide $LiNHB(NAr'CH)_2$ (**5.5**) to give immediate quantitative conversion to the borylamide-chloride complex $(L^1)Sc\{NHB(NAr'CH)_2\}Cl$ (**37**, Equation 5.1) *via* salt metathesis. Unfortunately, this complex was found to be unstable to isolation on the preparative scale, with repeated attempts resulting in a large degree of decomposition which released the borylamine **2.2**. Therefore **37** was characterised on the NMR tube scale. Its ^1H and ^{13}C NMR spectra were found to be analogous to **36** other than the absence of resonances belonging to the methyl ligand. The borylamide NH singlet was observed at 3.72 ppm (*cf.* 3.29 ppm in **36**). Two *in situ* reactions of **37** were then performed on the NMR tube scale to test whether this complex could be converted to a borylimide. Firstly, 1 equiv. $Li[N(SiMe_3)_2]$ and 1 equiv. DMAP were added to a C_6D_6 solution of **37** in an attempted dehydrohalogenation reaction. Despite heating up to 80 °C, no reaction took place. Secondly, 2 equiv. DMAP were added with the rationale that the first equivalent may effect dehydrohalogenation to yield the pyridinium chloride salt and the second equivalent may stabilise the desired borylimido product. However, again no reaction was observed with heating of the mixture up to 80 °C. With the failure of these attempted reactions of **37**

to form a borylimido complex, focus was given to an alternative route: thermolysis reactions of the methyl-borylamido complex **36** which were expected to release methane *via* α-abstraction by analogy with the successful preparation of the arylimide **1.47**.[18]

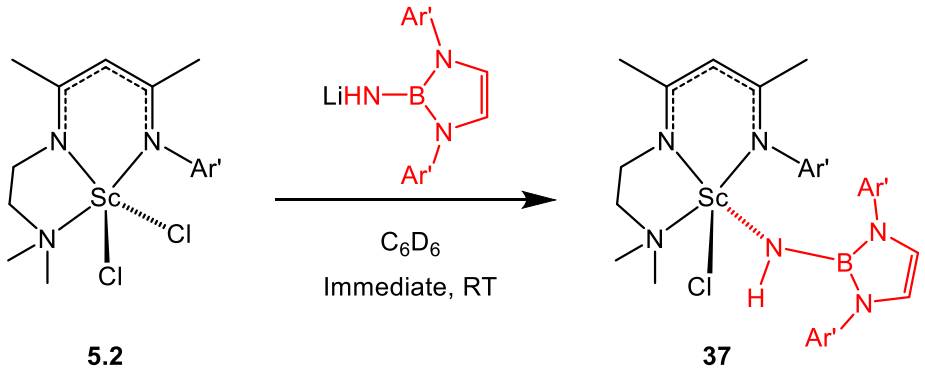

5.2 **37**

Equation 5.1

5.4 Thermolysis reactions of (L^1)Sc(Me){NHB(NAr'CH)$_2$} (36)

On the NMR tube scale in C_6D_6, three test thermolysis reactions of **36** were initially performed, these being in the presence of 1 equiv. pyridine or DMAP, as well as without the addition of an external base. Heating of the three solutions at 60 °C for *ca* 16 h led to quantitative conversion to three new species with the formation of methane also being observed. Initial inspection of the ^{1}H NMR spectra of all three products showed the presence of a broad singlet in each (between *ca* 2.8 and 3.1 ppm) which appeared to be an NH resonance of a borylamido ligand as no HSQC or HMBC ^{13}C correlations to those singlets were observed.

The three products were then each isolated on the preparative scale. For the base-free thermolysis, a toluene solution of **36** was heated at 60 °C for 16 h. After work-up, the product was isolated an off-white powder in 52% yield. Full analysis of its ^{1}H (Figure 5.4, top) and ^{13}C NMR spectra confirmed this to be the borylamido complex {MeC(NC$_6$H$_3$^{i}PrCH(Me)CH$_2$)CHC(Me)NCH$_2$CH$_2$NMe$_2$}Sc{NHB(NAr'CH)$_2$} (**38**) in which an isopropyl methyl group of the supporting ligand's Ar' moiety appears to have undergone intramolecular C–H activation at the metal centre, a so-called "tuck-in" reaction (Scheme 5.3). The ^{1}H NMR spectrum shows a broad singlet at 2.83 ppm which is assigned to the borylamide NH. The metallated methylene group gives an apparent triplet (1 H) at 0.22 ppm and a doublet of doublets (1 H) at –0.01 ppm due to the diastereotopic protons

coupling to the adjacent methine proton in addition to each other, whilst the scandium-bound carbon atom gives a ^{13}C signal at 32.0 ppm.

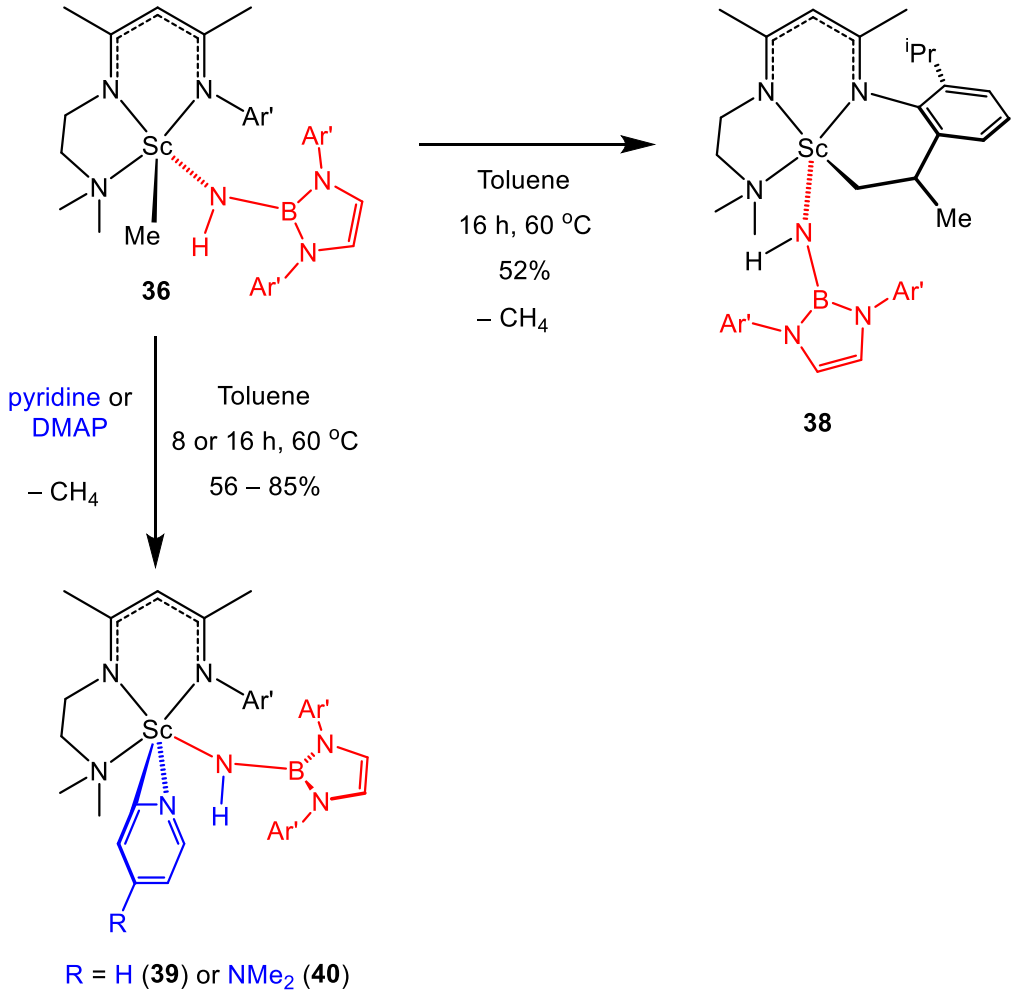

Scheme 5.3. Synthesis of {MeC($NC_6H_3{}^iPrCH(Me)CH_2$)CHC(Me)$NCH_2CH_2NMe_2$}Sc{NHB($NAr'CH)_2$} (**38**) and (L^1)Sc{NHB($NAr'CH)_2$}(η^2-4-NC_5H_3R) (R = H (**39**), NMe_2 (**40**)) from (L^1)Sc(Me){NHB($NAr'CH)_2$} (**36**).

In scaling up the thermolysis reactions in the presence of pyridine or DMAP, toluene solutions of **36** with each of those reagents were heated at 60 °C for 16 and 8 h, respectively. After work-up, the two products (L^1)Sc{NHB($NAr'CH)_2$}(η^2-4-NC_5H_3R) (R = H (**39**), NMe_2 (**40**)) were isolated in 56 and 85% yields, respectively, as pale yellow solids (Scheme 5.3). Full analysis of the ^1H and ^{13}C NMR spectra of the two complexes confirmed that they both have a borylamide ligand and an η^2-bound pyridyl ligand (or the DMAP counterpart) which has formed from C–H bond activation at the 2-position of the respective Lewis base. In the ^1H NMR spectrum of **39** (Figure 5.4, bottom), four multiplets belonging

to the η^2-pyridyl protons are observed at 6.89, 6.80 (two overlapping) and 6.48 ppm, and a broad NH singlet from the borylamide ligand is observed at 3.12 ppm. In the ^{13}C NMR spectrum, the Sc-bound carbon atom (the 2-position) of the pyridyl ligand gives a very lowfield-shifted resonance at 217.2 ppm. These spectral features are comparable to those of the pyridyl-bound anilido complex (PNP)Sc(NHAr')(η^2-NC_5H_4) (**1.44**, PNP = N{2-P^{i}Pr$_2$-4-C_6H_3Me}$_2$), which was prepared by Mindiola and co-workers through reaction of the methyl-anilide (PNP)Sc(Me)(NHAr') (**1.43**) with pyridine at RT.[15,16] In that compound, four multiplets were also observed in the ^1H NMR spectrum for the pyridyl ligands, with the Sc-bound carbon giving an identical ^{13}C chemical shift to **39** at 217.2 ppm. The crystallographic characterisation of complex **1.44** was also reported, and this confirmed the η^2-binding of the pyridyl ligand.[15] DFT calculations on **38** (*vide infra*) also support the η^2-binding of the pyridyl ligand in this complex.

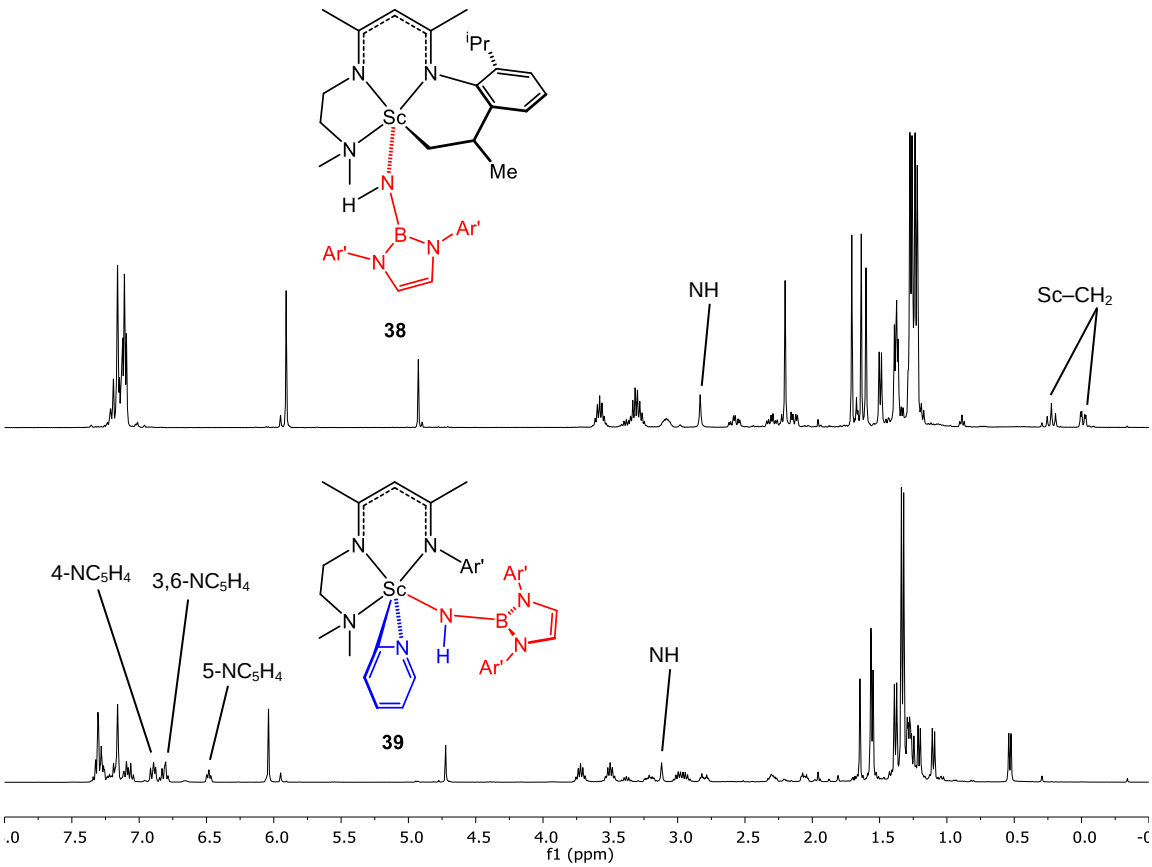

Figure 5.4. ^1H NMR spectra (400.1 MHz) of {MeC(NC_6H_3^{i}PrCH(Me)CH_2)CHC(Me)N$CH_2CH_2NMe_2$}Sc{NHB(NAr'CH)$_2$} (**38**, top) and (L^1)Sc{NHB(NAr'CH)$_2$}(η^2-NC_5H_4) (**39**, bottom) in C_6D_6 at 298 K.

The ^{1}H and ^{13}C NMR spectra of the DMAP counterpart **40** are analogous to those of **39**. Three multiplets are observed in the aromatic region of the ^{1}H NMR spectrum which correspond to the protons at the 3-, 5- and 6-positions of the η^2-bound ligand, and the borylamide NH gives a broad singlet at 3.07 ppm. Similarly, the Sc-bound carbon atom gives a ^{13}C signal at 212.8 ppm. These spectral features are also comparable to those of a previously reported complex: the DMAP-derived analogue of **1.44**, (PNP)Sc(NHAr')(η^2-4-$NC_5H_3NMe_2$) (**5.6**) which was similarly prepared from the methyl-anilide **1.43** and DMAP at RT.[16] The C–H bond activation processes which formed **1.44** and **5.6** were the subject of a full mechanistic study by Mindiola and co-workers,[16] and this will later be compared to the differing mechanism to be presented for the formation of **39** and **40** from **36**.

Unfortunately, the growth of diffraction-quality crystals of **39** and **40** proved to be elusive. However, diffraction-quality crystals of **38** were successfully grown from a benzene solution at RT. The molecular solid state structure is shown in Figure 5.5, and selected bond distances and angles are listed in Table 5.2. Complex **38** is confirmed to have a distorted square-based pyramidal geometry (τ = 0.35 and 0.37 for the two crystallographically independent molecules) similar to that of **36** in which one vertex of the basal plane is now a metallated methylene carbon which had been an isopropyl methyl group of the supporting ligand. This forms a new six-membered metallacycle with a distorted boat conformation. The borylamide functionality is again positioned at the pyramidal apex. The Sc(1)–N(1) bond distances of 2.0609(18) and 2.0649(18) Å are comparable to that in **36** (2.0629(8) Å). The Sc–C bond distances in the new metallated ligand are 2.249(2) and 2.247(2) Å, which are slightly shorter than the Sc–C bond distance in the methyl ligand of **36** (2.2730(10) Å). The structure of **38** may also be compared with that of the anilido analogue {$MeC(NC_6H_3{}^{i}PrCH(Me)CH_2)CHC(Me)NCH_2CH_2NMe_2$}Sc(NHAr') (**1.56**), which was prepared by Chen and co-workers by abstraction of the DMAP donor of **1.47** using an alkylated BBN derivative, $^{t}BuCH_2CH_2BC_8H_{14}$, followed by heating at 50 °C.[26] Mechanistic aspects of the formation of **1.56**, as well as that of **38**, will be discussed further later. The geometry of the molecular structure of **1.56** appears analogous to that of **38**, this being distorted square-based pyramidal also, with the anilido ligand sited at the pyramidal apex. The $Sc–N_{anilide}$ (2.078(2) Å) and Sc–C (2.260(2) Å) bond distances are both similar to the corresponding distances in **38**.

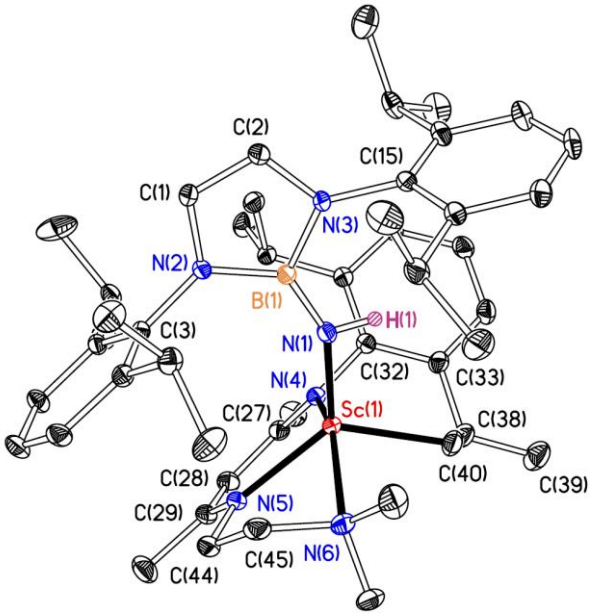

Figure 5.5. Displacement ellipsoid plot (20% probability) of {MeC(NC$_6$H$_3$^{i}PrCH(Me)CH$_2$)CHC(Me)NCH$_2$CH$_2$NMe$_2$}Sc{NHB(NAr'CH)$_2$} (**38**). C-bound H atoms are omitted for clarity. H(1) is drawn as a sphere of arbitrary radius.

Table 5.2. Selected bond distances (Å) and angles (^{o}) for {MeC(NC$_6$H$_3$^{i}PrCH(Me)CH$_2$)CHC(Me)NCH$_2$CH$_2$NMe$_2$}Sc{NHB(NAr'CH)$_2$} (**38**). Values in brackets are for the second crystallographically independent molecule (τ = 0.35 [0.37]).

Sc(1)–N(1)	2.0609(18) [2.0649(18)]	N(1)–Sc(1)–N(4)	114.35(7) [112.55(7)]
Sc(1)–N(4)	2.1738(19) [2.1853(17)]	N(1)–Sc(1)–N(5)	122.85(7) [127.08(7)]
Sc(1)–N(5)	2.1905(18) [2.2014(18)]	N(1)–Sc(1)–N(6)	96.40(8) [98.70(7)]
Sc(1)–N(6)	2.324(2) [2.3247(19)]	N(4)–Sc(1)–N(5)	83.86(7) [83.19(7)]
Sc(1)–C(40)	2.249(2) [2.247(2)]	N(4)–Sc(1)–N(6)	148.82(8) [148.49(7)]
N(1)–B(1)	1.412(3) [1.416(3)]	N(1)–Sc(1)–C(40)	108.03(9) [106.03(9)]
N(1)–H(1)	0.85(3) [0.91(3)]	N(4)–Sc(1)–C(40)	85.50(8) [84.76(7)]
		N(5)–Sc(1)–C(40)	127.84(9) [126.11(8)]
		N(6)–Sc(1)–C(40)	89.99(9) [90.61(8)]
		Sc(1)–N(1)–B(1)	153.96(15) [154.73(16)]
		Sc(1)–N(1)–H(1)	100(2) [99.0(18)]

Attention is now given to elucidating the mechanism of the formation of compounds **38**, **39** and **40**. The three thermolysis reactions of **36** which form these products were monitored by ^{1}H NMR arrays at 343 K. All of the reactions were found to follow first order kinetics as judged by linear semi-logarithmic plots of $-\ln([\mathbf{36}]/[\mathbf{36}]_0)$ *vs* time. Each monitored reaction was run in duplicate, and representative first order decay plots of the three reactions are shown in Figure 5.6 to at least 85% conversion (approximately three half-lives). The observed first order rate constants (k) for all three reactions are listed in Table 5.3. It can be seen that the three reactions have similar k values, thus it is initially proposed that they all share a common rate-determining step. It is significant that the thermolysis reactions in the presence of pyridine and DMAP to form **39** and **40** respectively have similar first order rate constants despite DMAP being a stronger nucleophile than pyridine by over two orders of magnitude.[29] This implies, therefore, that in those two reactions the coordination of the Lewis base to the metal centre is not involved in the rate-determining step.

Isotopic labelling was also used to shed light on the mechanism. (L^1)Sc(Me){NDB(NAr'CH)$_2$} (**36-*d*$_1$**) was first prepared using D$_2$NB(NAr'CH)$_2$ (**2.2-*d*$_2$**). Its ^{1}H NMR spectrum is identical to that of **36** other than the absence of the broad NH singlet. Upon thermolysis under the same conditions as **36**, **36-*d*$_1$** gave conversion exclusively to **38**; i.e. the product has a hydrogen at the borylamide site, not deuterium. This suggests that the deuterium was eliminated as DCH_3 prior to the intramolecular C–H bond activation of the supporting ligand CHMeMe group. An alternative mechanism in which the metalation occurs by σ-bond metathesis between Sc–Me and the isopropyl C–H bond would necessarily release CH_4 (there is no deuterium on the supporting ligand) and leave the ND-containing borylamide ligand intact. Unfortunately, the 1:1:1 triplet expected of DCH_3 in the ^{1}H NMR spectrum could not be observed as the region around 0.16 ppm contains product-based resonances which obscure it.

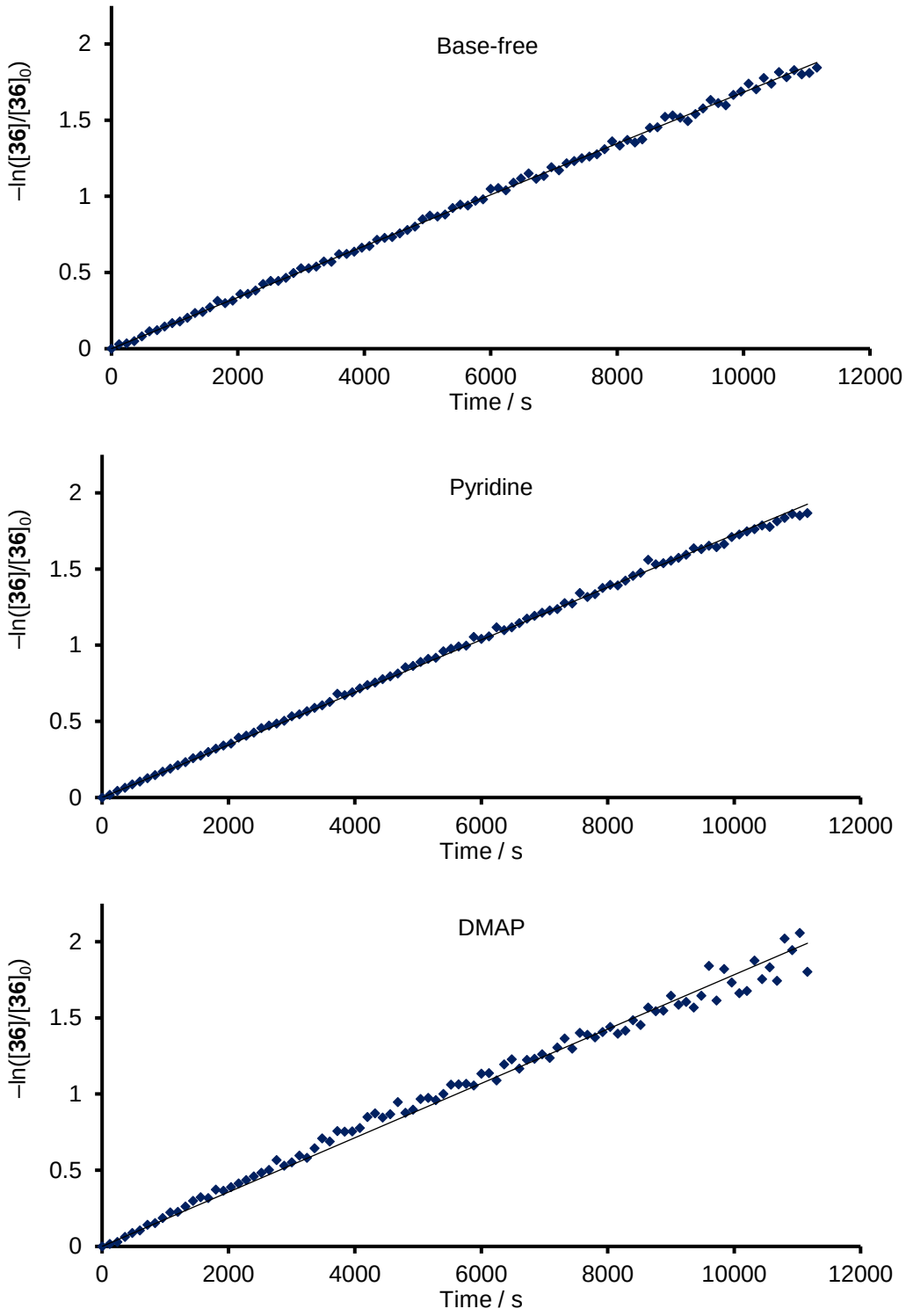

Figure 5.6. First order semi-logarithmic plots for the base-free thermolysis of (L^1)Sc(Me){NHB(NAr'CH)$_2$} (**36**) to form {MeC(NC$_6$H$_3$^{i}PrCH(Me)CH$_2$)CHC(Me)NCH$_2$CH$_2$NMe$_2$}Sc{NHB(NAr'CH)$_2$} (**38**, top), and with pyridine and DMAP to form (L^1)Sc{NHB(NAr'CH)$_2$}(η^2-4-NC$_5$H$_3$R) (R = H (**39**, middle), NMe$_2$ (**40**, bottom)) at 343 K in C$_6$D$_6$. (r^2 = 0.999, 0.999 and 0.989 respectively).

Table 5.3. First order rate constants obtained for the base-free thermolysis of $(L^1)Sc(Me)\{NHB(NAr'CH)_2\}$ (**36**) to form $\{MeC(NC_6H_3{}^iPrCH(Me)CH_2)CHC(Me)NCH_2CH_2NMe_2\}Sc\{NHB(NAr'CH)_2\}$ (**38**), and with pyridine and DMAP to form $(L^1)Sc\{NHB(NAr'CH)_2\}(\eta^2\text{-}4\text{-}NC_5H_3R)$ (R = H (**39**), NMe_2 (**40**)), in addition to isotopic variants, at 343 K in C_6D_6. Each reaction monitored was run in duplicate.[a]

Starting material	Reagent	Product	k / 10^{-5} s^{-1} (Run 1)	k / 10^{-5} s^{-1} (Run 2)
36	-	**38**	16.83(3)	15.56(5)
36-*d*$_1$	-	**38**	1.91(1)	1.82(1)
36	pyridine[b]	**39**	17.26(3)	16.90(5)
36	pyridine-d_5[b]	**39-*d*$_5$**	18.66(4)	18.34(8)
36	DMAP[b]	**40**	17.83(10)	18.04(12)

a. $[\mathbf{36}]_0 = 0.032$ mol dm^{-3}. *b.* [Lewis base]$_0 = 0.032$ mol dm^{-3}.

Next, the thermolysis of **36** in the presence of pyridine-d_5 was performed under the same conditions. The product was found to be exclusively $(L^1)Sc\{NDB(NAr'CH)_2\}(\eta^2\text{-}NC_5D_4)$ (**39-*d*$_5$**), and the singlet of CH_4 at 0.16 ppm was observed in the ^1H NMR spectrum of the reaction. The spectral features of **39-*d*$_5$** are identical to those of **39**, other than the absence of the borylamide NH singlet and all of the pyridyl multiplets. Similar to the base-free case, this result is also suggestive of methane release prior to the C–H bond activation of coordinated pyridine. An alternative σ-bond metathesis between Sc–Me and a C–D bond of the coordinated pyridine-d_5 would release DCH_3 and leave the NH-containing borylamide ligand intact. Following these isotope labelling studies, a combined mechanistic scheme for the three reactions may now be proposed (Scheme 5.4). Given that the three reactions have comparable first order rate constants, a common rate-determining step (RDS) is proposed which does not involve an added external base. Also, the isotope labelling studies described above established that this step occurs prior to the respective C–H bond activation in each case. Thus, this initial RDS is proposed to be α-hydrogen abstraction in **36** of the borylamide NH by the methyl ligand which leaves a highly reactive scandium borylimido complex $(L^1)Sc\{NB(NAr'CH)_2\}$ (**36'**) and releases methane. In the

absence of an external base, rapid C–H bond activation of a supporting ligand CHMeMe group then occurs at the Sc–N multiple bond (a 1,2-addition) to produce the tuck-in complex **38**. When pyridine or DMAP is present, this coordinates to the metal and then undergoes a similar rapid C–H bond activation across the Sc–N multiple bond.

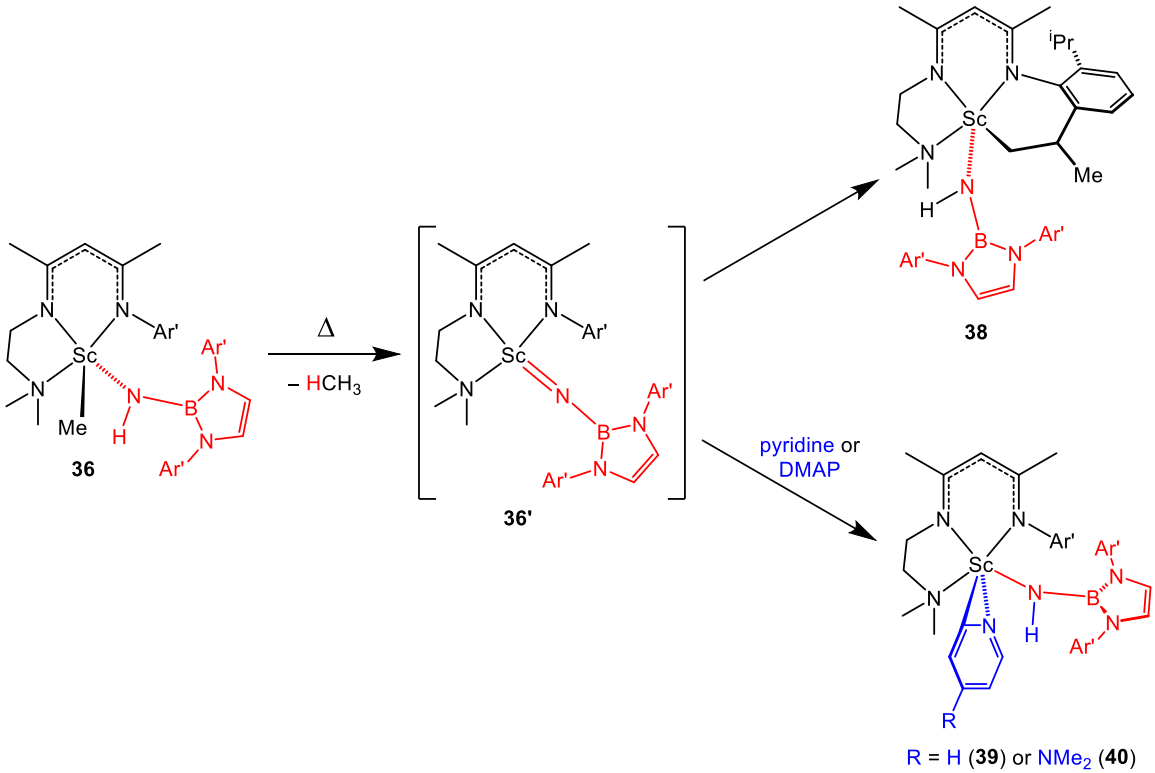

Scheme 5.4. Proposed pathways for the thermolysis reactions of $(L^1)Sc(Me)\{NHB(NAr'CH)_2\}$ (**36**) to form $\{MeC(NC_6H_3{}^iPrCH(Me)CH_2)CHC(Me)NCH_2CH_2NMe_2\}Sc\{NHB(NAr'CH)_2\}$ (**38**) and $(L^1)Sc\{NHB(NAr'CH)_2\}(\eta^2\text{-}4\text{-}NC_5H_3R)$ (R = H (**39**), NMe_2 (**40**)).

The base-free thermolysis of **36-*d*$_1$** to give **38**, and the reaction of **36** with pyridine-d_5, were each monitored by ^{1}H NMR arrays, and first order rate constants for the processes were obtained in the same manner as above (Table 5.3). In the former case, the thermolysis of **36-*d*$_1$** was found to be significantly slower than that of **36**, the respective *k* values being $1.91(1) \times 10^{-5}$ and $1.82(1) \times 10^{-5}$ s^{-1} (reaction performed in duplicate), and $16.83(3) \times 10^{-5}$ and $15.56(5) \times 10^{-5}$ s^{-1}. This gives a kinetic isotope effect (KIE) of between 8.15 and 9.25. As discussed in Chapter Four, a KIE of this magnitude is indicative of a process having a transition state in which the transfer of H is relatively linear.[30,31] The value obtained here is comparable to those KIEs reported by Wolczanski and co-workers for α-abstraction reactions in Group 4 and 5 systems which release methane or other alkanes

to yield imido functional groups,[32–36] as well as similar processes reported by a number of other research groups.[37–41] Moving on to the thermolysis reaction of **36** in the presence of pyridine-d_5, no significant difference was found between the observed first order rate constants from this reaction and the analogous one with protio pyridine. The k values measured are 18.66(4) × 10^{-5} and 18.34(8) × 10^{-5} s^{-1} (pyridine-d_5, in duplicate) and 17.26(3) × 10^{-5} and 16.90(5) × 10^{-5} s^{-1} (pyridine, in duplicate). These two results give further support to the pathways shown in Scheme 5.4. The presence of a large KIE for the breaking of the N–H bond in the starting material **36** is indicative of this taking place in the RDS, whilst the absence of a KIE for the C–H bond activation of the pyridine ligand is consistent with that step being rapid and taking place after the RDS and therefore having no influence on the overall rate of reaction.

This was then followed by competition reactions involving pyridine and DMAP in an attempt to further elucidate the mechanistic steps associated with coordination and C–H bond-activation of these Lewis bases. Firstly, thermolysis of **36** was carried out in the presence of an excess of both pyridine and pyridine-d_5 (1:5:5 ratio) on the NMR tube scale. Inspection of the final ^{1}H NMR spectrum (obtained after 8 h at 60 °C) showed the product isotopologues **39** and **39-*d*$_5$** to be formed in a 1:1 ratio, by integration of the N<u>H</u>B(NAr'CH)$_2$ resonance against the NacNac methine singlet. Similarly, thermolysis of **36** in the presence of an excess of both pyridine and DMAP (1:5:5 ratio) was performed, and this resulted in a product mixture of 53% **39** and 47% **40** after 8 h at 60 °C (measured by integration of the most upfield CH<u>Me</u>Me doublet in each compound). Together, the results of these two competition reactions suggest the presence of equilibria in the reaction mechanisms after the RDS, which give the effect of precluding a strong product or isotopologue selectivity in these cases. A schematic mechanistic profile is drawn in Figure 5.7 (considering reaction of pyridine only for clarity), and the proposed associated equilibria shown in Scheme 5.5. Simmons and Hartwig have described the ability of a number of different experimental techniques to reveal isotope effects in reactions having varying mechanistic profiles.[42] For such a profile as shown in Figure 5.7, in which the C–H bond cleavage step is a reversible process taking place after the RDS, parallel reactions which measure k_H and k_D cannot give a KIE; the C–H or C–D bond cleavage has no bearing on the rate of the overall reaction. Competition reactions which measure product distributions will also not give a large primary KIE due to the reversibility of the process, although a small isotope effect may be observed because the substitution of C–H for C–D can alter the concentrations of the

species on either side of the equilibrium by changing the relative values of the rate constants k_2 and k_{-2} (as defined in Scheme 5.5).

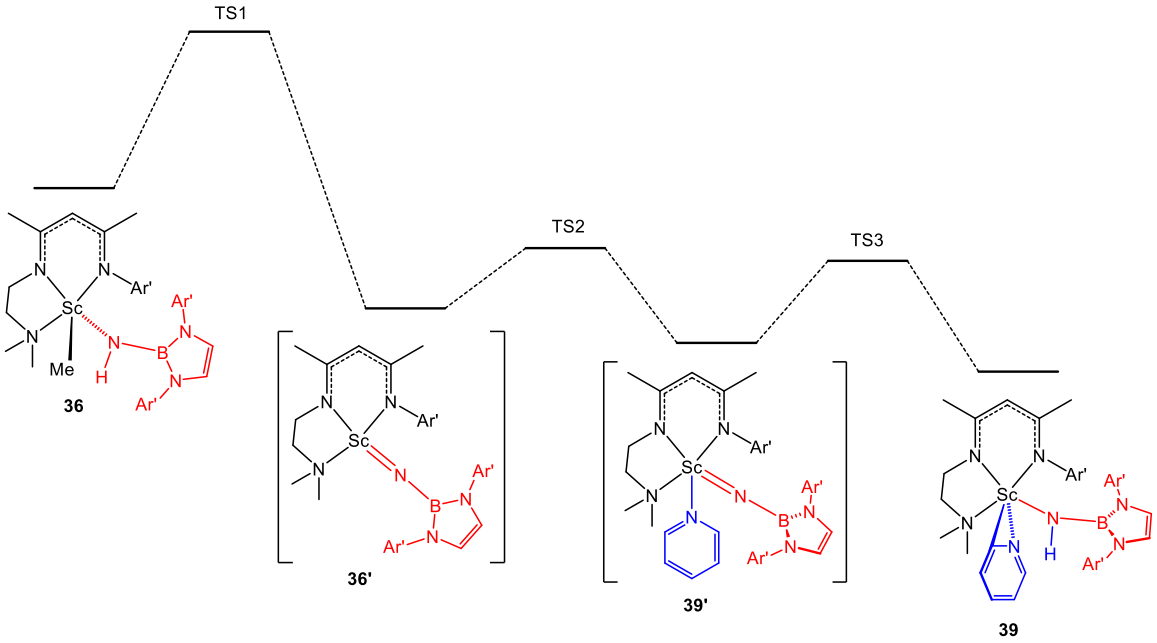

Figure 5.7. Schematic mechanistic profile of the thermolysis reaction of $(L^1)Sc(Me)\{NHB(NAr'CH)_2\}$ (**36**) with pyridine to give $(L^1)Sc\{NHB(NAr'CH)_2\}(\eta^2\text{-}NC_5H_4)$ (**39**). The activation barrier for TS1 is larger than that for either TS2 or TS3.

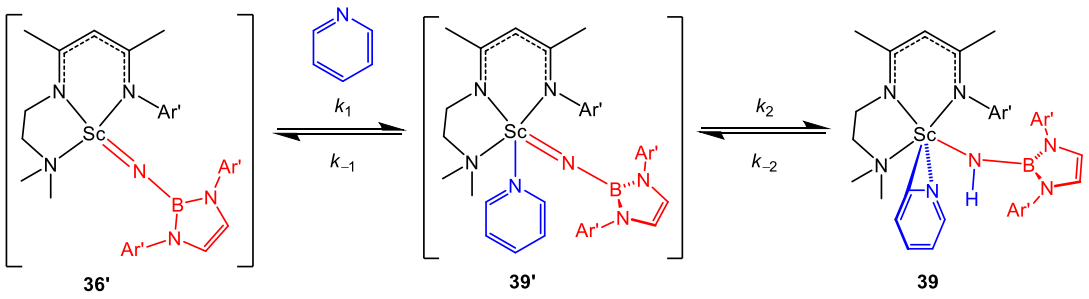

Scheme 5.5. Proposed equilibria in the formation of $(L^1)Sc\{NHB(NAr'CH)_2\}(\eta^2\text{-}NC_5H_4)$ (**39**) from $(L^1)Sc\{NB(NAr'CH)_2\}$ (**36'**).

The intermolecular competition of pyridine and pyridine-d_5 was found to give a negligible isotope effect (1.04). The product-determining step of this reaction is the k_2/k_{-2} step which has a rate of k_2[**39'**]. However, [**39'**] itself depends on the forward and reverse rate constants k_2 and k_{-2}, which may both be expected to vary with isotopic substitution, as well as depending on k_1 and k_{-1} of the pyridine coordination/dissociation step. Therefore the absence of an isotope effect here is not wholly unusual.[42] In order to isolate the C–H bond

activation step from the coordination/dissociation step, an *intramolecular* competition reaction was performed. This was achieved through thermolysis of **36** in the presence of 2-pyridine-d_1. In this way, coordination of that mono-deuterated ligand to the base-free borylimide **36'** gives a mono-deuterated pyridine-stabilised complex (**39'-*d*$_1$**), from which either C–H or C–D bond cleavage can take place in the (reversible) product-determining step. Performed in C_6D_6 at 60 °C over 8 h, this reaction resulted in an isotopomer mixture of 60% (L^1)Sc{NHB(NAr'CH)$_2$}(η^2-6-NC_5H_3D) (**39-*d*$_1$_C**) and 40% (L^1)Sc{NDB(NAr'CH)$_2$}(η^2-NC_5H_4) (**39-*d*$_1$_N**), giving an isotope effect of 1.5 (Scheme 5.6). The ratio of **39-*d*$_1$_C**:**39-*d*$_1$_N** remained constant throughout and after the reaction.

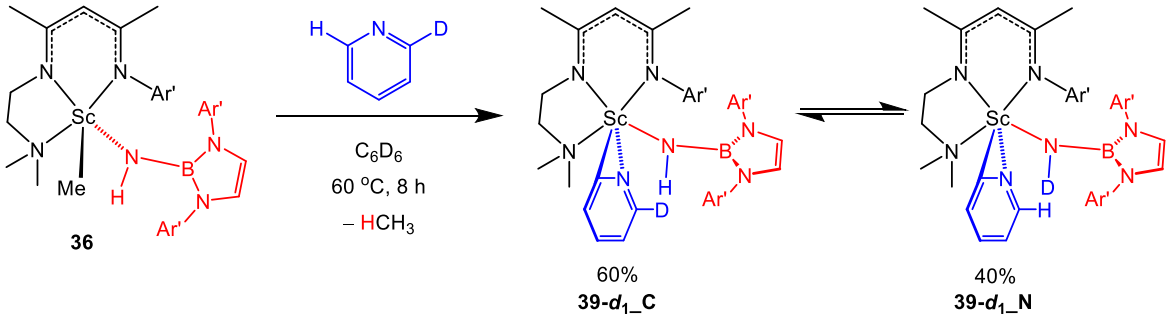

Scheme 5.6. Intramolecular competition reaction of (L^1)Sc(Me){NHB(NAr'CH)$_2$} (**36**) with 2-pyridine-d_1.

This small isotope effect value is indicative of it being an equilibrium isotope effect (EIE). As discussed in Chapter Four, EIEs are considered to reflect product mixtures of isotope-sensitive equilibria (ratios of KIEs) rather than being the KIE of a single step. By way of example, in a non-degenerate reaction described by Bergman, Andersen and co-workers, a metallacyclic complex Cp*$_2$Ti{CHC(Ph)O} (derived from [2+2] cycloaddition of HCCPh at a terminal oxo functionality) converts to the hydroxoacetylide Cp*$_2$Ti(OH)(CCPh) upon heating *via* a rate-determining C–H addition to a transient Ti=O bond.[43] An inverse EIE value of 0.781 was measured for this process (the ratio of two normal KIEs), which reflects the preference of deuterium to reside in a higher strength O–E bond (E = H or D) due to the greater zero point energy stabilisation.[30] Thus, substitution of H with D shifts the equilibrium further to the hydroxoacetylide side. In contrast, the intramolecular competition reaction of **36** with 2-pyridine-d_1 (which also has the heteroatom–H bond on the right of the equilibrium in Scheme 5.6) has given a *normal* EIE of 1.5. In this case, the two most isotope-sensitive bonds relevant to the equilibrium are the borylamide N–H bond and an sp^2 C–H bond of the bound pyridine. It is proposed, therefore, that in the equilibrium

between **39'** and **39**, deuterium favours residing in the relatively strong sp^2 bond, giving the isotopomer mixture described above, in which **39-*d*$_1$_C** is slightly predominant.

Returning to the competition reaction between pyridine and DMAP which resulted in a product mixture of 53% **39** and 47% **40**, this result again arises because the product-determining step is an equilibrium process which takes place after the RDS. Given the much greater nucleophilic strength of DMAP compared with pyridine,[29] this result highlights the fact that the addition of both pyridine and DMAP to the base-free intermediate **36'** must be reversible under the conditions of the reaction (60 °C), thereby not yielding **40** as the predominant product which would otherwise be expected.

Further to this, exchange reactions have shown the reversibility of both the k_1/k_{-1} and k_2/k_{-2} steps. Addition of 1 equiv. pyridine-d_5 to **39** on the NMR tube scale in C_6D_6 resulted in an equilibrium mixture of 56% **39** and 44% **39-*d*$_5$** after heating at 60 °C for 2 h. Similarly, upon heating at 60 °C, **39-*d*$_5$** with 1 equiv. pyridine gave an equilibrium mixture of 60% **39** and 40% **39-*d*$_5$**. These are both comparable to the isotopomer mixture obtained from the intramolecular competition using 2-pyridine-d_1. Also, heating a 1:1 mixture of **39** and DMAP at 60 °C for 2 h resulted in an equilibrium mixture of 50% **39** and 50% **40**, and a 1:1 mixture of **40** and pyridine under the same conditions gave an equilibrium mixture of 53% **39** and 47% **40**. These results are comparable to the mixture obtained from the intermolecular competition reaction of pyridine and DMAP with **36** described previously.

It was later found that further heating of **39** (16 h at 90 °C) resulted in conversion to the tuck-in complex **38**, although this was accompanied by some product decomposition to borylamine **2.2** as **38** is not thermally stable for long periods at this high temperature. Nevertheless, isotope labelling was successfully used to investigate this reaction further. Heating of **39-*d*$_5$** under the same conditions led to release only of pyridine-d_5, and giving exclusively **38** with no incorporation of deuterium. This implies that the release of pyridine occurs first to return to the base-free borylimido intermediate **36'**, which is then followed by intramolecular metalation (Scheme 5.7). This conversion from the kinetic product **39** to the thermodynamic product **38** is favoured by the entropic gain arising from the released pyridine at higher temperatures, and has been explored by DFT calculations described in Section 5.6. The equivalent process does not take place for the DMAP analogue **40**, for which heating at temperatures above 60 °C on the NMR tube scale results in conversion to a complex mixture of products which cannot be identified.

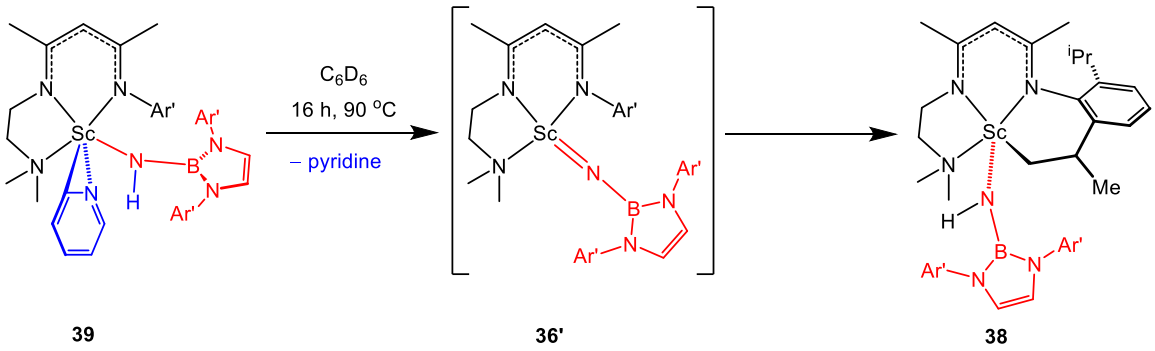

Scheme 5.7. Conversion of $(L^1)Sc\{NHB(NAr'CH)_2\}(\eta^2\text{-}NC_5H_4)$ (**39**) to $\{MeC(NC_6H_3{}^iPrCH(Me)CH_2)CHC(Me)NCH_2CH_2NMe_2\}Sc\{NHB(NAr'CH)_2\}$ (**38**) upon further heating.

Comparisons will now be drawn between the base-free thermolysis of **36** which forms the tuck-in complex **38** and similar reactions which have been reported in scandium imido systems, as well as between the C–H bond activation of pyridine or DMAP which forms **39** or **40**, respectively, and its literature precedents. As described above, Chen and co-workers used $^tBuCH_2CH_2BC_8H_{14}$ to abstract the Lewis base from the DMAP-stabilised borylimide **1.47**. Heating the base-free complex at 50 °C in the absence of any further added reagent gave quantitative conversion to the tuck-in complex **1.56**,[26] which is a direct structural analogue of **38** (*vide supra*). Following the formation of **38** from **36**, the Author prepared the methyl-anilido complex **1.46**, and heated it on the NMR tube scale in C_6D_6 to test if the analogous conversion to **1.56** would take place. With heating at 70 °C over 8 h, conversion to a mixture of products was observed, although inspection of the ^{1}H NMR spectrum showed the major product (*ca* 52% based on integration of the NacNac methine resonance) to be **1.56**. The half-life of the decay of **1.46** was measured to be *ca* 1.1 h, which is comparable to the half-life of **36** in conversion to **38** under the same conditions (*ca* 1.2 h). The Author also compared the behaviour of **1.46** and **36** with DMAP. Chen and co-workers had reported that DMAP coordinates rapidly to **1.46** at RT to give a six-coordinate intermediate (**1.46'**),[18] and inspection of the ^{1}H NMR spectrum of the NMR tube scale obtained here showed that this was the case. This contrasts starkly with the addition of DMAP to the methyl-borylamide **36**, for which no coordination to the metal is observed at RT. The difference here is proposed to have a steric basis; with **36** having a very bulky borylamido ligand, the addition of DMAP to give a six-coordinate intermediate would appear to be unfeasible. DFT studies (*vide infra*) support this conclusion. Upon heating, the C–H bond-activated product **40** is the only species observed in solution. The DMAP-

stabilised imido complex **1.47** was also prepared by the Author and heated at high temperatures on the NMR tube scale to test for a similar C–H bond activation. Despite extended heating at 90 °C in C_6D_6, **1.47** was found to be thermally stable, and no C–H bond activation of the coordinated DMAP (or indeed any other reaction) was found to take place.

In chemistry reported by Piers and co-workers, a NacNac-stabilised methyl-anilide (**5.1**) heated at 50 °C over 5 days in the presence of DMAP gave conversion to the DMAP-stabilised borylimide (^{tBu}NacNac)Sc(NAr')(DMAP) (**1.48**).[19] Mechanistic studies showed that this reaction proceeds *via* an intermediate in which intramolecular C–H bond activation of an Ar' methyl group from the supporting ligand has taken place at the Sc centre. In particular, when a mono-deuterated starting material, (^{tBu}NacNac)Sc(Me)(NDAr') (**5.1-*d*$_1$**), was heated with DMAP, only CH_4 (not DCH_3) was observed, signifying that the reaction was not proceeding *via* initial DMAP coordination followed by α-abstraction, but instead a rate-determining metalation which does not involve the anilido ligand, followed by DMAP-assisted H atom transfer from the anilido ligand to re-form the Ar' methyl group. In contrast, addition of DMAP to the borylamido tuck-in complex **38** gave no reaction at lower temperatures (up to 60 °C), whilst upon stronger heating up to 90 °C on the NMR tube scale in C_6D_6, conversion to a complex mixture of products was observed.

C–H bond activation reactions of coordinated pyridine by a scandium terminal imide have previously been reported by Mindiola and co-workers,[15–17] and a number of similar reactions by other early transition or rare earth metal systems have also been reported.[44–48] Heating of (PNP)Sc(Me)(NHAr') (**1.43**) in the presence of pyridine generates a transient scandium imide (PNP)Sc(NAr')(py) (**1.45**) which then (rapidly) activates a C–H bond of pyridine to form the pyridyl complex (PNP)Sc(NHAr')(η^2-NC_5H_4) (**1.44**). Mechanistic studies showed the reaction to be first order in both **1.43** and pyridine, and that pyridine coordinates to the metal centre of **1.43** *before* α-abstraction to generate the transient **1.45**.[16] This example of initial Lewis base coordination again contrasts with the thermolysis reactions of **36** which begin with the α-abstraction step to generate a transient borylimide. Furthermore, **1.43** was reacted with a number of substituted pyridine derivatives, and the kinetic profiles of these processes measured. Significantly, the reaction with DMAP was almost two orders of magnitude faster than that with pyridine, confirming the presence of the Lewis base in the rate equation of those reactions. This contrasts with the formation of **39** and **40**, which have comparable rates due to pyridine and DMAP coordinating only after the rate-determining step. In these cases, it is proposed that the coordination of the Lewis

base to form a six-coordinate intermediate is unfeasible due to the large steric bulk of the boryl moiety. This aspect will also be considered through DFT calculations to be presented in Section 5.6.

Finally, it was found that thermolysis of **36** in the presence of THF as external base resulted in quantitative conversion to **38** at 60 °C in C_6D_6. THF, being a weaker base than pyridine or DMAP, is unable to compete with the rapid intramolecular C–H bond activation process. Additionally, thermolysis was also tested with 2,6-dimethylpyridine, with the rationale that a borylimide adduct of a pyridine derivative without hydrogen atoms at the 2- or 6-positions may be stable. Unfortunately, heating at 60 °C in C_6D_6 resulted only in quantitative formation of the tuck-in complex **38**. The bulkier nature of this pyridine derivative significantly reduces its ability to coordinate to the metal, hence it is outcompeted by the intramolecular C–H bond activation.

5.5 Trapping of a transient scandium borylimide with alkynes

In order to gain further evidence of the existence of the transient borylimide **36'**, thermolysis reactions of the methyl-borylamido complex **36** were successfully performed in the presence of two alkynes. On the NMR tube scale, the reactions of 1 equiv. HCCTol or MeCCPh with **36** at 60 °C were each found to give quantitative conversion to two new products after 8 h. When performed on the preparative scale, the reaction of **36** with HCCTol was heated at 60 °C for 16 h in toluene. After work-up, the product, (L^1)Sc{NHB(NAr'CH)$_2$}(CCTol) (**41**) was isolated as an off-white powder in 50% yield (Scheme 5.8). The formation of this complex represents 1,2-addition of the alkyne C–H bond across the Sc–N multiple bond of **36'**. Similarly **36** was heated with MeCCPh in toluene at 60 °C for 16 h, and after work-up the azascandacyclobutene complex (L^1)Sc{N{B(NAr'CH)$_2$}C(Me)C(Ph)} (**42**) was isolated as a yellow powder in 48% yield. This reaction represents [2+2] cycloaddition of the internal alkyne across the Sc–N multiple bond of **36'**, giving excellent evidence of the existence of a transient borylimide. Attempted reactions with two further internal alkynes were unsuccessful. NMR tube scale thermolysis in the presence of MeCCMe resulted in a complex mixture of products from which none could be identified, whilst thermolysis in the presence of PhCCPh gave conversion to the tuck-in complex **38**, seemingly with no involvement of the bulkier internal alkyne.

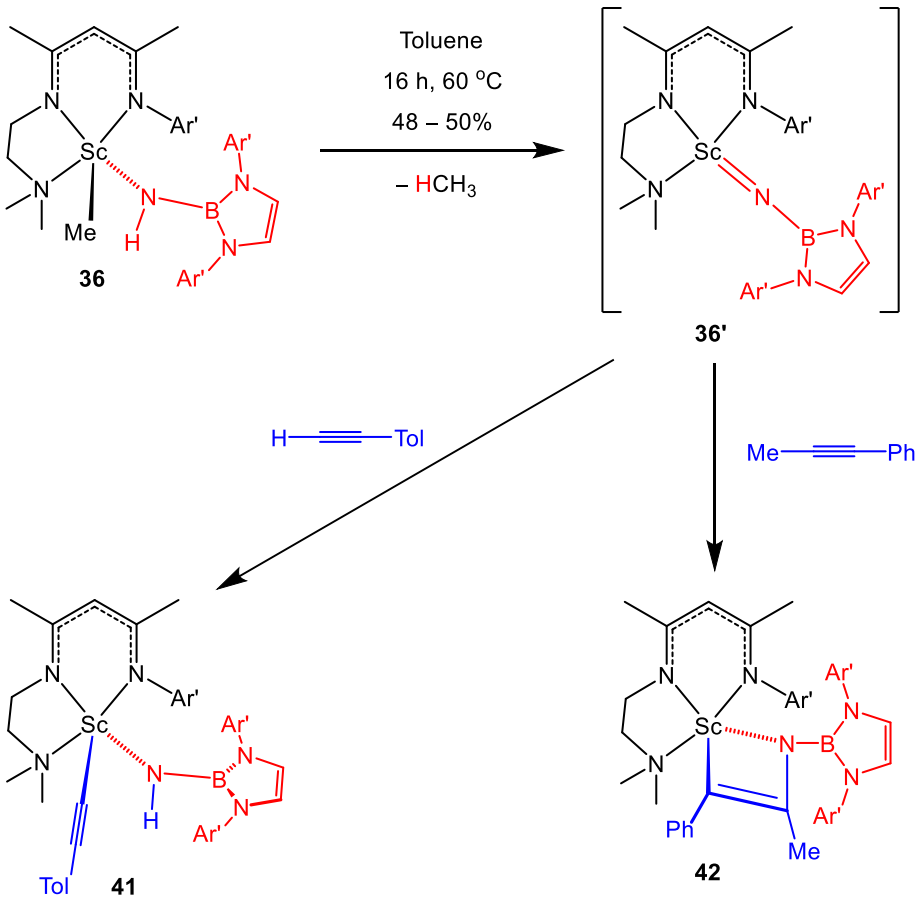

Scheme 5.8. Synthesis of $(L^1)Sc\{NHB(NAr'CH)_2\}(CCTol)$ (**41**) and $(L^1)Sc\{N\{B(NAr'CH)_2\}C(Me)C(Ph)\}$ (**42**) from $(L^1)Sc(Me)\{NHB(NAr'CH)_2\}$ (**36**).

The ^1H and ^{13}C NMR spectra of **41** are consistent with the molecule containing an acetylido functional group in addition to a borylamido ligand. The NH singlet of the latter ligand is found at 3.58 ppm, whilst the two acetylide carbons have ^{13}C resonances of 155.4 and 124.6 ppm for the carbons directly bonded to the metal and to the Tol group respectively. The ^{13}C spectrum of **42** is consistent with the azascandacyclobutene unit having anti-Markovnikov regiochemistry; of the two resonances belonging to the metallacycle, it is the downfield resonance (172.9 ppm) which features an HMBC correlation to an *o*-C_6H_5 proton and the upfield resonance (154.5 ppm) which features an HMBC correlation to the metallacycle methyl group. Diffraction-quality crystals of complex **42** were successfully grown from a benzene solution at RT. The molecular solid state structure is shown in Figure 5.8, and selected bond distances and angles are listed in Table 5.4.

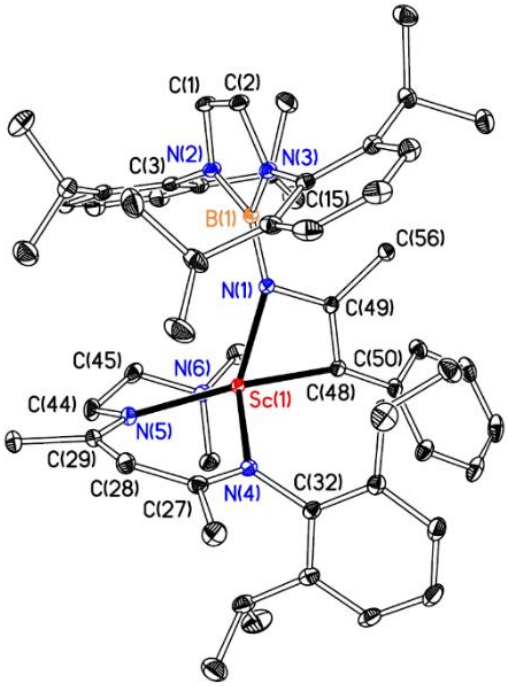

Figure 5.8. Displacement ellipsoid plot (20% probability) of (L^1)Sc{N{B(NAr'CH)$_2$}C(Me)C(Ph)} (**42**). H atoms are omitted for clarity.

Table 5.4. Selected bond distances (Å) and angles (°) for (L^1)Sc{N{B(NAr'CH)$_2$}C(Me)C(Ph)} (**42**) (τ = 0.53).

Sc(1)–N(1)	2.0528(7)	N(1)–Sc(1)–N(4)	120.76(3)
Sc(1)–N(4)	2.1984(7)	N(1)–Sc(1)–N(5)	120.53(3)
Sc(1)–N(5)	2.2247(7)	N(1)–Sc(1)–N(6)	109.35(3)
Sc(1)–N(6)	2.3169(7)	N(4)–Sc(1)–N(5)	82.41(3)
Sc(1)–C(48)	2.1578(8)	N(4)–Sc(1)–N(6)	129.86(3)
N(1)–B(1)	1.4397(11)	N(1)–Sc(1)–C(48)	70.12(3)
N(1)–C(49)	1.4393(10)	N(4)–Sc(1)–C(48)	105.55(3)
C(48)–C(49)	1.3706(11)	N(5)–Sc(1)–C(48)	161.59(3)
		N(6)–Sc(1)–C(48)	89.16(3)
		Sc(1)–N(1)–B(1)	151.33(6)
		Sc(1)–N(1)–C(49)	86.55(4)
		N(1)–C(49)–C(48)	118.93(7)

Complex **42** is confirmed to have a distorted five-coordinate geometry (τ = 0.53), with the bidentate N(1)–C(49)–C(48) unit of the metallacycle having anti-Markovnikov regiochemistry. The bite angle of the bidentate metallacycle unit is 70.12(3)°, which is considerably smaller than those bite angles seen in the diamide-amine-supported azatitanacyclobutenes **23**, **25** and **29** of 75.52(4), 77.19(6) and 75.34(10)° respectively. This arises from the larger radius of scandium relative to titanium meaning that the N(1)–C(49)–C(48) ligand is slightly further distant from the metal centre thus a smaller bite angle is necessary. The solid state structure of **42** may be compared with that of its direct analogue (L^1)Sc{N(Ar')C(Me)C(Ph)} (**1.54**), which was prepared by Chen and co-workers by abstraction of the DMAP from **1.47** using 9-BBN and subsequent reaction with MeCCPh at RT.[26] The metallacycle bite angle in **1.54** is comparable to that in **42**, being 69.92(13)°. The N_{im}–C and C=C bond lengths of the two complexes are also comparable, these being 1.4393(10) and 1.3706(11) Å, respectively, in **42**, and 1.441(5) and 1.368(5) Å, respectively, in **1.54**, indicating N–C single and C–C double bonds.

Additionally, a scandium anilide-acetylide, (^{tBu}NacNac)Sc(NHAr')(CCPh), was recently prepared by Piers and co-workers *via* C–H bond activation of HCCPh with the NacNac-supported arylimide **1.48** at 70 °C, and was crystallographically characterised.[19] Mechanistic studies showed that this formed after initial dissociation of the DMAP ligand, followed by 1,2-addition of the terminal alkyne C–H bond at the base-free imide, similar to the formation of **41** from the transient borylimide **36'**.

Next, the two reactions of **36** with HCCTol and MeCCPh which form **41** and **42** were monitored by ^{1}H NMR arrays at 343 K. Similar to those kinetic measurements of thermolysis reactions of **36** which were described above, the two reactions followed first order kinetics as shown by linear semi-logarithmic plots of –ln([**36**]/[**36**]$_0$) *vs* time. Each monitored reaction was run in duplicate, and representative first order decay plots of both reactions are shown in Figure 5.9 to at least 85% conversion (approximately three half-lives). The observed first order rate constants (k) are listed in Table 5.5. It can be seen that the k values for the two reactions are similar, and are also comparable to those previously listed in Table 5.3. This confirms that the formation of **41** and **42** proceed *via* the same RDS as those previous reactions: initial α-hydrogen abstraction releases methane to leave the transient borylimide **36'**, which then gives a rapid C–H bond activation with HCCTol or [2+2] cycloaddition with MeCCPh.

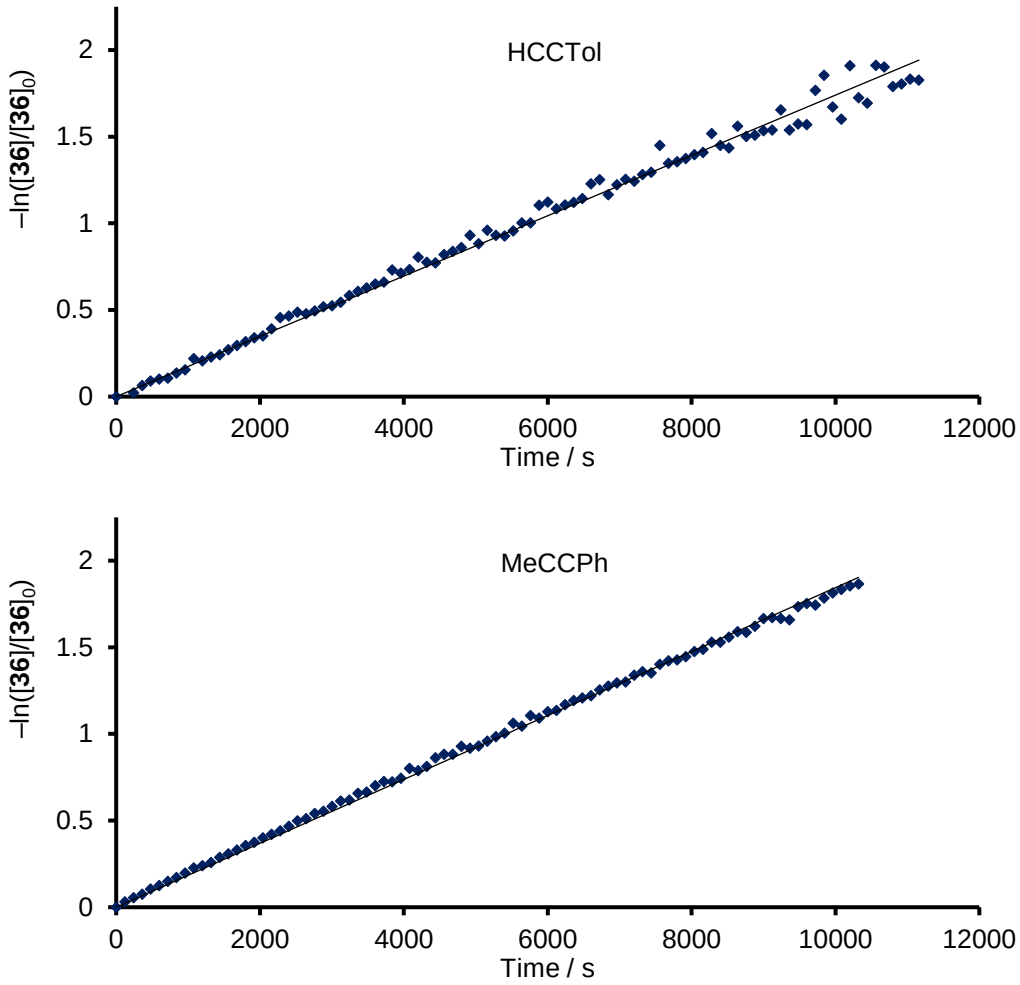

Figure 5.9. First order semi-logarithmic plots for the thermolysis of $(L^1)Sc(Me)\{NHB(NAr'CH)_2\}$ (**36**) with HCCTol and MeCCPh to form $(L^1)Sc\{NHB(NAr'CH)_2\}(CCTol)$ (**41**, top) and $(L^1)Sc\{N\{B(NAr'CH)_2\}C(Me)C(Ph)\}$ (**42**, bottom) at 343 K in C_6D_6. (r^2 = 0.991 and 0.998 respectively).

Table 5.5. First order rate constants obtained for the thermolysis of (L^1)Sc(Me){NHB(NAr'CH)$_2$} (**36**) with HCCTol and MeCCPh to form (L^1)Sc{NHB(NAr'CH)$_2$}(CCTol) (**41**) and (L^1)Sc{N{B(NAr'CH)$_2$}C(Me)C(Ph)} (**42**), in addition to isotopic variants, at 343 K in C_6D_6. Each reaction monitored was run in duplicate.[a]

Starting material	Reagent	Product	k / 10^{-5} s^{-1} (Run 1)	k / 10^{-5} s^{-1} (Run 2)
36	HCCTol[b]	**41**	16.94(10)	17.40(9)
36	DCCTol[b]	**41-*d*$_1$**	17.76(4)	17.34(5)
36	MeCCPh[b]	**42**	16.60(5)	18.44(4)

a. [**36**]$_0$ = 0.032 mol dm^{-3}. *b*. [alkyne]$_0$ = 0.032 mol dm^{-3}.

Furthermore, a reaction with DCCTol was found to give elimination of CH_4, and exclusive incorporation of deuterium at the borylamide site in (L^1)Sc{NDB(NAr'CH)$_2$}(CCTol) (**41-*d*$_1$**), giving additional support to this mechanism. As expected, no significant KIE was observed between the reactions of HCCTol and DCCTol as the C–H/D bond activation takes place after the RDS. An attempted competition reaction of **36** with HCCTol and DCCTol (1:5:5) could not be successfully analysed as the NH singlet overlaps with a ligand multiplet so cannot be integrated precisely. In a competition reaction of **36** with HCCTol and MeCCPh (1:5:5) at 60 °C in C_6D_6, 100% conversion to the acetylido complex **41** was observed, showing that the C–H bond activation of HCCTol is considerably faster than [2+2] cycloaddition of MeCCPh. In contrast to the pyridyl complex **39**, which was shown to form in a series of reversible steps, **41** and **42** form irreversibly from the borylimide **36'** as indicated by two attempted exchange reactions. Addition of 1 equiv. MeCCPh to **41** and heating up to 90 °C in C_6D_6 gave no exchange with the added alkyne, and **41** appeared to be thermally stable at this temperature. Addition of 1 equiv. HCCTol to **42** gave no reaction up to 90 °C, although at this temperature some decomposition to borylamine **2.2** was observed, which was also seen when **42** is heated on its own in C_6D_6 at 90 °C.

Finally, trapping of the base-free borylimide **36'** by MeCCPh was also achieved from other starting points. When the tuck-in complex **38** was heated at 100 °C in the presence of 1

equiv. MeCCPh, conversion to metallacycle **42** took place over 16 h (although accompanied by some decomposition to $H_2NB(NAr'CH)_2$ (**2.2**)). This indicates that, at that temperature, **38** reacts to re-form the isopropyl C–H bond and the borylimido ligand, before being rapidly trapped by the internal alkyne, with **42** being thermodynamically more stable than **38**. Heating of the pyridine C–H bond activation product **39** in the presence of 1 equiv. MeCCPh at 60 °C did not result in conversion to metallacycle **42**, despite previous exchange reactions showing that the association of pyridine to **36'** is reversible at 60 °C. However, in a competition reaction of $(L^1)Sc(Me)\{NHB(NAr'CH)_2\}$ (**36**) with pyridine and MeCCPh (1:5:5) at 60 °C, the exclusive formation of **39** was observed. It appears, therefore, that at this temperature, the reaction of **39** with MeCCPh remains under kinetic control. Although the pyridine ligand of **39'** may dissociate from the metal, its re-coordination is faster than alternative reaction with MeCCPh. At 90 °C, the reaction comes under thermodynamic control, giving quantitative conversion to **42** over 7.5 h. Starting from the DMAP C–H bond activation product **40**, again no reaction takes place with MeCCPh at 60 °C, whilst heating at 90°C resulted only in a complex mixture of products, which also takes place when **40** is heated at that temperature without any added reagent. Aspects of these reactions will be considered through DFT calculations presented in the following Section.

5.6 Computational studies of the thermolysis reactions of $(L^1)Sc(Me)\{NHB(NAr'CH)_2\}$ (36)

In this Section, DFT calculations on model scandium borylamides and borylimides, and their anilido and imido counterparts, will be used to shed more light on the differences between these systems with regards to the reactivity and stability of the respective scandium–nitrogen multiply bonded complexes. Firstly, however, an FMO analysis of model scandium imides and borylimides is presented, followed by a QTAIM analysis of the same model complexes.

DFT calculations (B3PW91 functional and Def2TZVP basis set) were performed on the small model complexes $\{(Ph)NC(Me)CHC(Me)NCH_2CH_2NMe_2\}Sc(NR)(py)$ (**6Q_R**; R = Me, Ph, $B(NHCH)_2$) by Prof. Philip Mountford. In order to study the underlying electronic interactions (without contribution from steric effects), the Ar' group of the L^1 ligand was modelled as a phenyl group, and the boryl moiety in **6Q_B(NHCH)2** was modelled as the much simpler $B(NHCH)_2$ group. Being representative of an alkylimide, an arylimide and a

borylimide, respectively, the FMOs of the three models **6Q_R** are comparable to those of the diamide-pyridine-supported model titanium complexes **1Q_R** (R = Me, Xyl, $B(NMeCH)_2$) described in Chapter Two. Beginning first with the FMOs of the model methylimide **6Q_Me**, Figure 5.10 (top) shows the two orthogonal π components that make up the formal Sc–N triple bond, these being the HOMO and HOMO–1. These are almost isoenergetic (–3.93 and –3.94 eV respectively) as the two π-symmetry lone pairs of the $[NMe]^{2-}$ fragment (Figure 3.5) are degenerate (C_{3v} symmetry) although they have different symmetries and mix with different acceptor orbitals at the metal centre.

Turning now to **6Q_Ph**, the HOMO and HOMO–1 again represent the two orthogonal π components of the Sc–N multiple bond (Figure 5.10, middle). The HOMO features an anti-bonding interaction between the Sc–N π bond and a filled π MO of the phenyl ring, thus this MO is destabilised relative to the HOMO of **6Q_Me** (–3.88 *vs* –3.93 eV). In contrast, the HOMO–1 of **6Q_Ph** is significantly stabilised compared to that in **6Q_Me** (–4.56 *vs* –3.94 eV) due to the electron-withdrawing nature of a phenyl group relative to methyl. Additionally, the HOMO–5 (–6.82 eV) is a counterpart of the HOMO which shows backbonding from a Sc–N π bond into an unfilled π orbital of the phenyl ring.

The FMOs of **6Q_B(NHCH)$_2$** featured in Figure 5.10 (bottom) are all comparable in form to those of **6Q_Ph**, though are consistently higher in energy due to the electropositive nature of boron. Again, the HOMO is the orbital which is destabilised by an antibonding interaction between the Sc–N π bond and a filled π orbital of the boryl ring, while the HOMO–3 in this case is its counterpart in which electron density is donated from a Sc–N π bond to an unoccupied π orbital of the boryl ring.

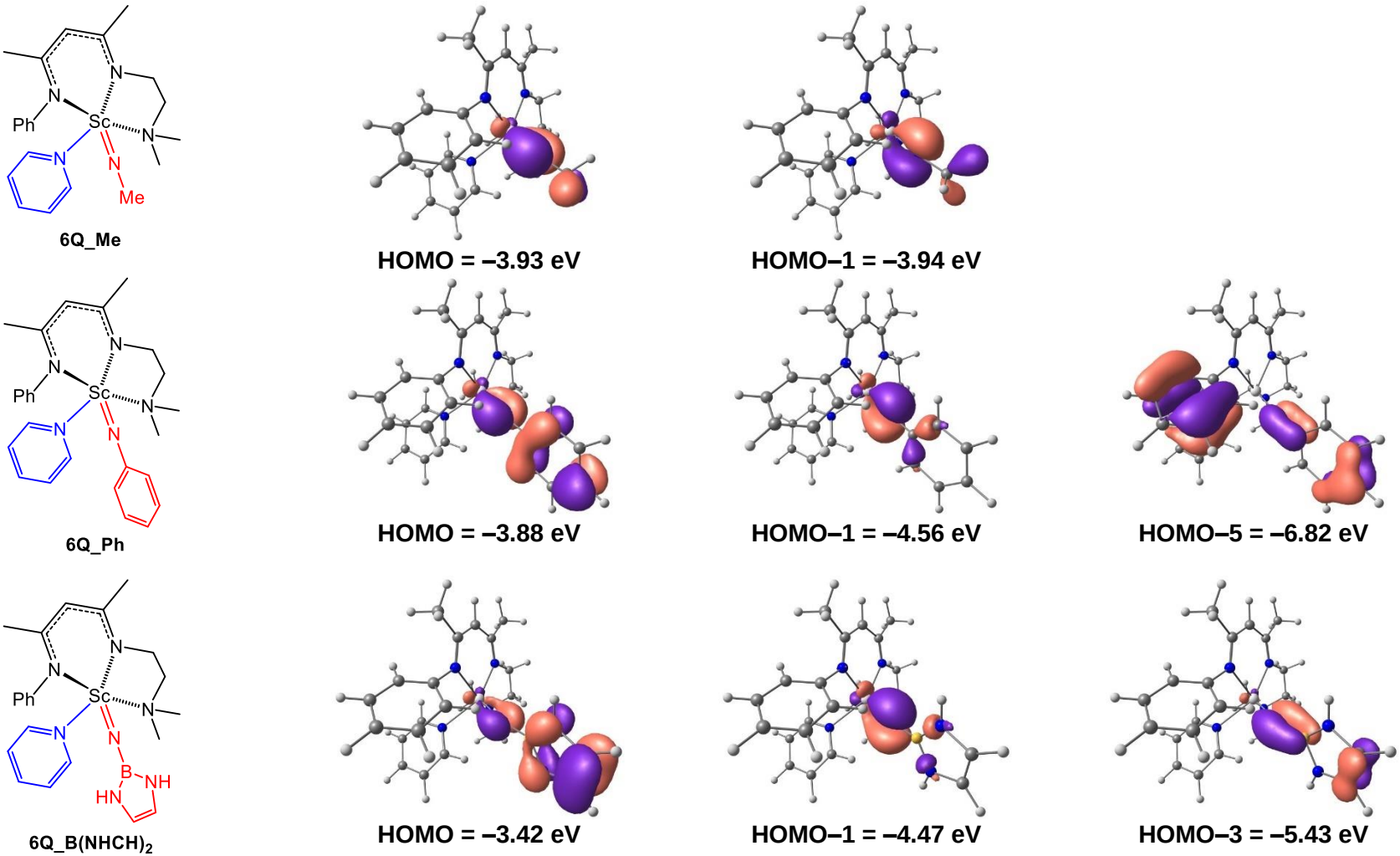

Figure 5.10. DFT model compounds {(Ph)NC(Me)CHC(Me)NCH$_2$CH$_2$NMe$_2$}Sc(NR)(py) (**6Q_R**; R = Me, Ph, B(NHCH)$_2$), and associated isosurfaces and energies of the π components of the Ti–N linkages

A QTAIM study was also performed on the three model complexes **6Q_R**,[49] and selected QTAIM data are shown in Table 5.6, along with the Sc–N_{im} bond distances in the optimised structures. As described in Chapters Two and Three, the delocalisation index, δ(A–B), of a bond A–B is a measure of the number of electron pairs shared between atoms A and B and can be related to the formal bond order.[50] In these model complexes, the δ(Sc–N_{im}) values are consistently smaller than δ(Ti–N_{im}) in the model titanium complexes **1Q_R** (Section 2.8), indicating a smaller degree of covalency in the more polar Sc–N_{im} bonds. Of the three models **6Q_R**, **6Q_Me** has the largest δ(Sc–N_{im}) value, which corresponds to the shortest Sc–N_{im} bond distance, while **6Q_Ph** has the smallest δ(Sc–N_{im}) value and the longest Sc–N_{im} bond distance, as the multiple bond is disrupted by π interactions with the phenyl ring (analogous to those described for arylimido functional groups in Chapters Two and Three). **6Q_B(NHCH)$_2$** has an intermediate δ value and Sc–N_{im} bond distance as there is less orbital mixing with the heteroaromatic ring. Similarly, the electron densities (ρ) at the BCPs of the Sc–N_{im} bonds in **6Q_R** are consistently smaller than the ρ values of the Ti–N_{im} bonds in **1Q_R**, this again indicating reduced covalency for the more polar Sc–N_{im} bonds. However, no clear trend is found in the variation of ρ among the three models **6Q_R** themselves.

This effect of a smaller degree of covalency is also seen in respect to the calculated charges (Q) on the NR fragments in **6Q_R**. For these anionic ligands, a higher negative charge remaining on the fragment indicates less of a covalent interaction as less negative charge is donated to the metal centre. For **6Q_R**, the Q(NR) values are in the range –1.229 (**6Q_Ph**) to –1.131 eV (**6Q_Me**) whilst in **1Q_R**, the Q(NR) values are much less negative, being in the range –0.987 (**1Q_Xyl**) to –0.884 (**1Q_Me**). The variation in Q(NR) across the three models **6Q_R** themselves follows the same trend as discussed above for the delocalisation indices; i.e. **6Q_Ph** incorporates the least covalent Sc–N_{im} linkage and has the longest Sc–N_{im} bond, whilst the bond is the most covalent (and shortest) for **6Q_Me**. Again, **6Q_B(NHCH)$_2$** has an intermediate Q(NB(NHCH)$_2$) value.

Table 5.6. Selected QTAIM data (atomic units) for the Sc–N_{im} bond in model complexes of the type {(Ph)NC(Me)CHC(Me)$NCH_2CH_2NMe_2$}Sc(NR)(py) (**6Q_R**; R = Me, Ph, $B(NHCH)_2$), Sc–N_{im} bond distances (*d*, Å) in the optimised structures, and charges (*Q*, units of *e*) of the model fragments (L is the model tridentate supporting ligand). Values for ρ (electron density), $\nabla^2\rho$ (electron density Laplacian), *H* (energy density) and ε (ellipticity) were obtained at the bond critical point. δ is the delocalisation index of the Sc–N_{im} bond.

	δ	ρ	$\nabla^2\rho$	ε	*H*	*d*(Sc–N_{im}) / Å	*Q*(L)	*Q*(Sc)	*Q*(py)	*Q*(NR)
6Q_Me	1.220	0.148	0.653	0.017	–0.052	1.809	–0.755	1.855	0.031	–1.131
6Q_Ph	1.083	0.141	0.613	0.074	–0.045	1.835	–0.706	1.894	0.041	–1.229
6Q_B(NHCH)$_2$	1.173	0.152	0.560	0.022	–0.056	1.829	–0.735	1.885	0.035	–1.186

Table 5.7. Selected QTAIM data (atomic units) for the Sc–N_{im} bond (fixed at 1.824 Å) in model complexes of the type {(Ph)NC(Me)CHC(Me)$NCH_2CH_2NMe_2$}Sc(NR)(py) (**6Q_R_fixed**; R = Me, Ph, $B(NHCH)_2$). All other bond metrics remain unchanged from the optimised structures. The bond dissociation energy (ΔE_{BD}, kcal mol^{-1}) is for Sc–N_{im} in **6Q_R** (to relaxed fragments).

	δ	ρ	$\nabla^2\rho$	ε	*H*	ΔE_{BD}	*Q*(L)	*Q*(Sc)	*Q*(py)	*Q*(NR)
6Q_Me_fixed	1.206	0.143	0.635	0.018	–0.047	99.1	–0.755	1.858	0.030	–1.133
6Q_Ph_fixed	1.093	0.144	0.627	0.073	–0.049	106.0	–0.707	1.892	0.041	–1.226
6Q_B(NHCH)$_2$_fixed	1.178	0.154	0.565	0.022	–0.058	116.7	–0.735	1.885	0.035	–1.185

As in the DFT and QTAIM study on model half-sandwich titanium complexes **2Q_R** presented in Chapter Three, the Sc–N_{im} bond of **6Q_Me** was extended from its value of 1.809 Å in its optimised structure to 1.850 Å. This resulted in the electronic SCF energy of the model complex increasing by only 0.3 kcal mol^{-1}, implying again that the strength of the bond is not strongly dependent on the bond distance. Indeed, the Sc–N_{im} bond dissociation energies of **6Q_R** (to relaxed fragments) were calculated to be 99.1 (R = Me), 106.0 (R = Ph) and 116.7 kcal mol^{-1} (R = $B(NHCH)_2$), which do not show a clear relationship to the trend in Sc–N_{im} bond distances across the three models.

As in Chapter Three, in order to see more clearly relationships between the QTAIM parameters and the Sc–N_{im} bond dissociation energies of **6Q_R**, a QTAIM study was next performed on variants of those model complexes (denoted **6Q_R_fixed**) in which the Sc–N_{im} bond distance is fixed at 1.824 Å which is the average of the three optimised distances. The newly calculated QTAIM parameters are listed in Table 5.7. Significantly, the electron densities, ρ, and the energy densities, H, at the BCPs now follow the same underlying trends as described for **2Q_R_fixed** in Chapter Three. In particular, the ρ values of **6Q_Me_fixed** and **6Q_Ph_fixed** are now similar, whilst that of **6Q_B(NHCH)$_2$_fixed** is significantly more positive, reflecting increased covalency of the bond with the σ-electron-releasing nature of the electropositive boryl group. Similarly, the H values of **6Q_Me_fixed** and **6Q_Ph_fixed** are also of similar magnitude, with that of **6Q_B(NHCH)$_2$_fixed** being significantly more negative, again reflecting the trend in σ-donor ability. A corresponding relationship is found with the Sc–N_{im} bond dissociation energies (ΔE_{BD}) in **6Q_R** (to relaxed fragments), also shown in Table 5.7, which follow the trend **6Q_Me < 6Q_Ph << 6Q_B(NHCH)$_2$**. This trend corresponds to the ρ and H values of **6Q_R_fixed** above which indicate that **6Q_B(NHCH)$_2$_fixed** has the most covalent, and therefore strongest, Sc–N_{im} bond (most positive ρ and most negative H), while the model imides have less covalent linkages (least for **6Q_Me_fixed**) giving lower bond dissociation energies. This result is consistent with the more in-depth analysis of bond dissociation energies provided for the half sandwich model complexes **2Q_R** in Chapter Three.

DFT calculations, including solvent and dispersion corrections, were performed by Simona Mellino on models of the various products of thermolysis reactions of (L^1)Sc(Me){NHB(NAr'CH)$_2$} (**36**) as described in previous Sections, as well as models of their analogues derived from the anilide (L^1)Sc(Me)(NHAr') (**1.46**). In these initial small

model calculations, the Ar' group is modelled as the smaller Xyl group in the imido- and amido-type ligands, giving –B(NXylCH)$_2$ as the model boryl moiety. However, given the role of an isopropyl group of the L^1 supporting ligand in the base-free tuck-in reaction, it was necessary to include L^1 in full. In the following scheme and discussion, the label **7Q** corresponds to borylamido and borylimido models, and **8Q** corresponds to the anilido and imido models incorporating a Xyl substituent. These models should give a good compromise between the full systems (too large to determine transition states (TSs)) and very small systems (do not realistically model the steric bulk) which are both described below.

Scheme 5.9 depicts the set of hypothetical reactions originating from the model methyl-borylamide (L^1)Sc(Me){NHB(NXylCH)$_2$} (**7Q_A**) and the analogous reactions originating from the model methyl-anilide (L^1)Sc(Me)(NHXyl) (**8Q_A**), along with G_{rel} values at 298 K for each of the model complexes (those for **7Q** in black, and those for **8Q** in red) as well as the G_{rel} values of selected transition states (shown in bold). G_{rel} values calculated at 343 K are shown in parentheses. In both systems, the G_{rel} values are relative to the model methyl-amido complexes **A**.

Several points arising from the calculated energetics in these two systems will now be discussed. Firstly, the α-abstraction step which forms the base-free (boryl)imido complexes **C** from **A** is calculated to be 1.9 kcal mol^{-1} more endergonic for the borylimido system compared with the imido system (the energies of **7Q_C** and **8Q_C** are +5.0 and +3.1 kcal mol^{-1} respectively). This is attributed to the higher N–H bond strength in the borylamido ligand of **7Q_A** which follows from the discussions in Chapter Three of the strong σ-donor ability of the borylimido fragment, and in turn arises from the electropositive nature of boron. The TS between **7Q_A** and **7Q_C** is also calculated to be higher in energy (in relative terms) than that between **8Q_A** and **8Q_C** (by 2.5 kcal mol^{-1} at 298 K and 2.8 kcal mol^{-1} at 343 K). In Section 5.4, the first order rate constant of the α-abstraction of the methyl-borylamide **36** was measured as 16.20(3) × 10^{-5} s^{-1} (average of two measurements, from the conversion of **36** to the tuck-in complex **38** at 343 K). From the Eyring equation, this results in an experimental measurement of $\Delta G_{343}^{\ddagger}$ of 26.1 kcal mol^{-1}, which compares well to the value of 27.4 kcal mol^{-1} calculated here at 343 K. The conversion of **7Q_C** to the tuck-in complex **7Q_D** proceeds with a comparable change in Gibbs free energy to its imido counterpart, the two processes having $\Delta_r G$ values of –11.0 and –11.2 kcal mol^{-1}, respectively, at 298 K. Thus, the gain of a stronger N–H bond for the borylimido compound

in this case does not appear to give a more favourable reaction. Entropic and enthalpic contributions to these reactions will later be considered through calculations on full systems including solvent and dispersion corrections (*vide infra*).

Next, the calculated reactions of **7Q_C** and **8Q_C** with the alkynes HCCTol and MeCCPh will be considered. For HCCTol, the metallacyclic complex **I** is calculated to be more stable than the acetylide complex **H** in both the imido and borylimido cases, by 4.5 and 6.6 kcal mol^{-1}, respectively, at 298 K. This is consistent with reactions of titanium borylimides with terminal alkynes described in Chapter Four, in which the thermodynamic product was shown to be the metallacyclic complex, although an acetylide formed by C–H bond activation could be isolated in some cases as a kinetic product. For example, $Ti(N_2N^{py})\{NB(NAr'CH)_2\}(py)$ (**7**) reacts with $HCCAr^F$ to form an acetylide as kinetic product at RT, and heating at 60 °C then resulted in conversion to a metallacycle as thermodynamic product. These calculations therefore imply that the experimental formation of the acetylide **41** from thermolysis of **36** in the presence of HCCTol is under kinetic control. Further heating of **41** (up to 100 °C), however, did not result in conversion to a metallacyclic product, with the kinetic barrier of returning to the imide **36'** from the highly stable **41** presumed to be insurmountable. The calculated G_{rel} values of the two alternative regioisomers of cycloadditions with MeCCPh show that the anti-Markovnikov isomer (**J**) is consistently lower in energy than the Markovnikov isomer (**K**), with a relative stabilisation, in the borylimido case of **7Q_J** *vs* **7Q_K**, of 9.5 kcal mol^{-1}. Experimentally, only the anti-Markovnikov metallacycle **42** was observed from the thermolysis of the methyl-borylimide **36**. It has been established, in titanium imido and hydrazido chemistry, that the anti-Markovnikov regioisomer is the electronically preferred isomer of alkyne cycloaddition (see Chapter Four).[51] Furthermore, the positioning of the phenyl group adjacent to the R substituent in the Markovnikov isomer models **K** is also sterically disfavoured, especially in the case of the large boryl moiety in **7Q_K**.

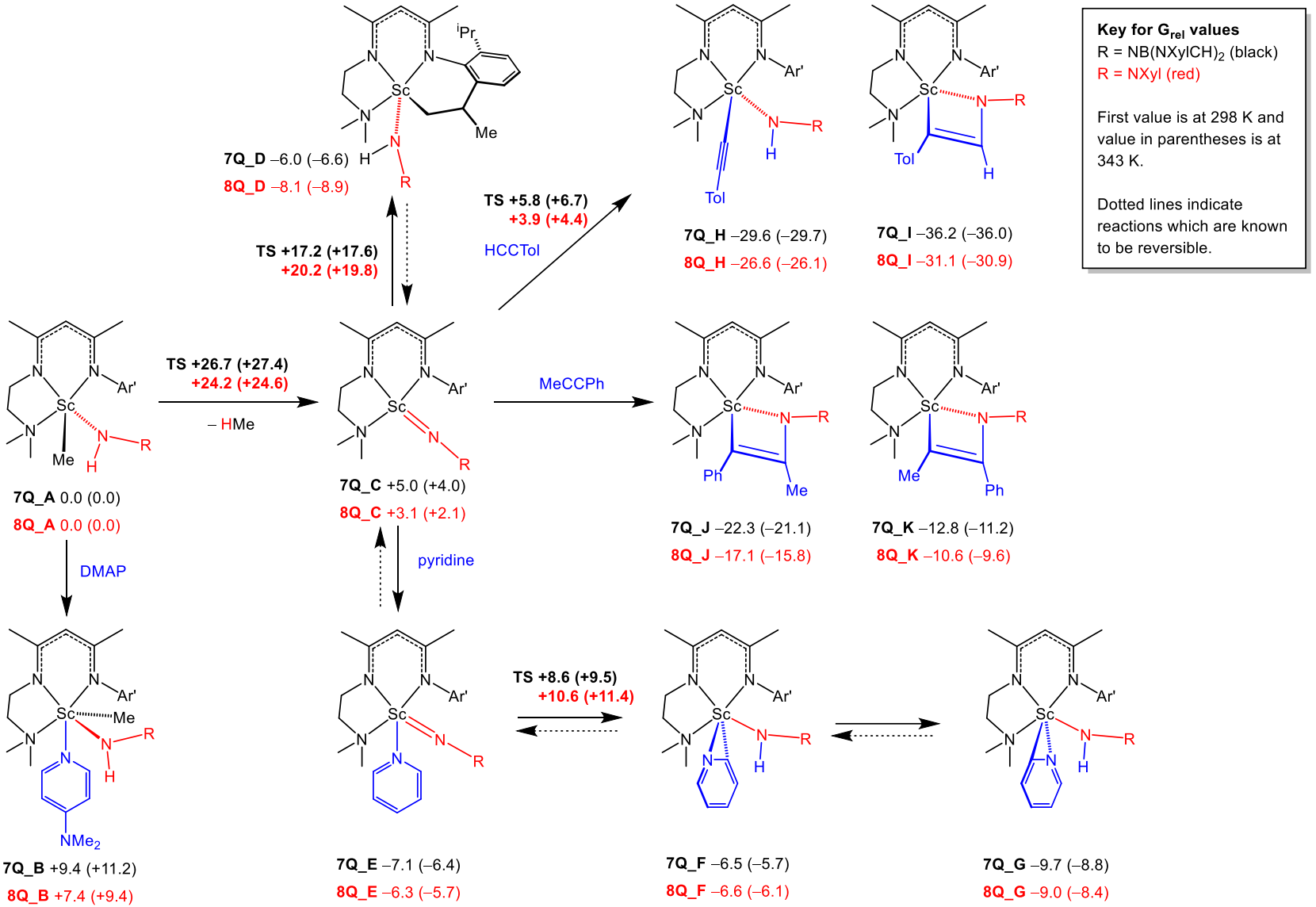

Scheme 5.9. Hypothetical reactions of a model methyl-borylamide **7Q_A** and a model methyl-anilide **8Q_A** with G_{rel} values (kcal mol^{-1}) at 298 K (black for **7Q** and red for **8Q**). G_{rel} values calculated at 343 K are shown in parentheses. Transition state (TS) G_{rel} values are in bold.

These calculations do not reveal a clear picture, however, of the C–H bond activations of bound pyridine. Experimentally, C–H bond activation of the putative pyridine-coordinated borylimide **39'** to give the η^2-pyridyl complex **39** is rapid, so **39'** cannot be observed, while Chen and co-workers found that the analogous reaction does not take place with the DMAP-stabilised arylimide (L^1)Sc(NAr')(DMAP) (**1.47**),[18] which is thermally stable up to 90 °C. These calculations give Δ_rG values of –2.6 kcal mol^{-1} at 298 K for the model borylimide **7Q_E** forming the most stable isomer of the pyridyl complex (**7Q_G**) and –2.7 kcal mol^{-1} for the analogous reaction in the imido system. The experimental differences in the imido and borylimido systems will therefore now be probed further through calculations on systems with full steric bulk.

DFT calculations were next performed by Prof. Philip Mountford on the same systems, although including the full steric bulk of both the supporting ligand L^1, and the boryl and Ar' moieties of the imido- and amido-type ligands. These calculations included solvent and dispersion corrections, and also explicitly analysed the enthalpic contribution (H_{rel}) to G_{rel} in each complex. Scheme 5.10 depicts this set of reactions in three cases. G_{rel} values (calculated at 298 K; H_{rel} in parentheses) typed in black denote the borylimido system **9Q** with R = $B(NAr'CH)_2$ and involving pyridine where relevant, those in blue denote the borylimido system **10Q** with R = $B(NAr'CH)_2$ and involving DMAP where relevant, and those in red denote the imido system **11Q** with R = Ar' and involving DMAP where relevant. G_{rel} values are also provided at 343 K (in square brackets). For clarity, those species which are observed experimentally have their G_{rel} and H_{rel} values in bold. In the discussion below, all G_{rel} and H_{rel} values described, and changes (Δ_r) between them, are those calculated at 298 K, unless stated otherwise. These model systems are too large to calculate TSs, but give the most accurate description of ground state (thermodynamic) preferences.

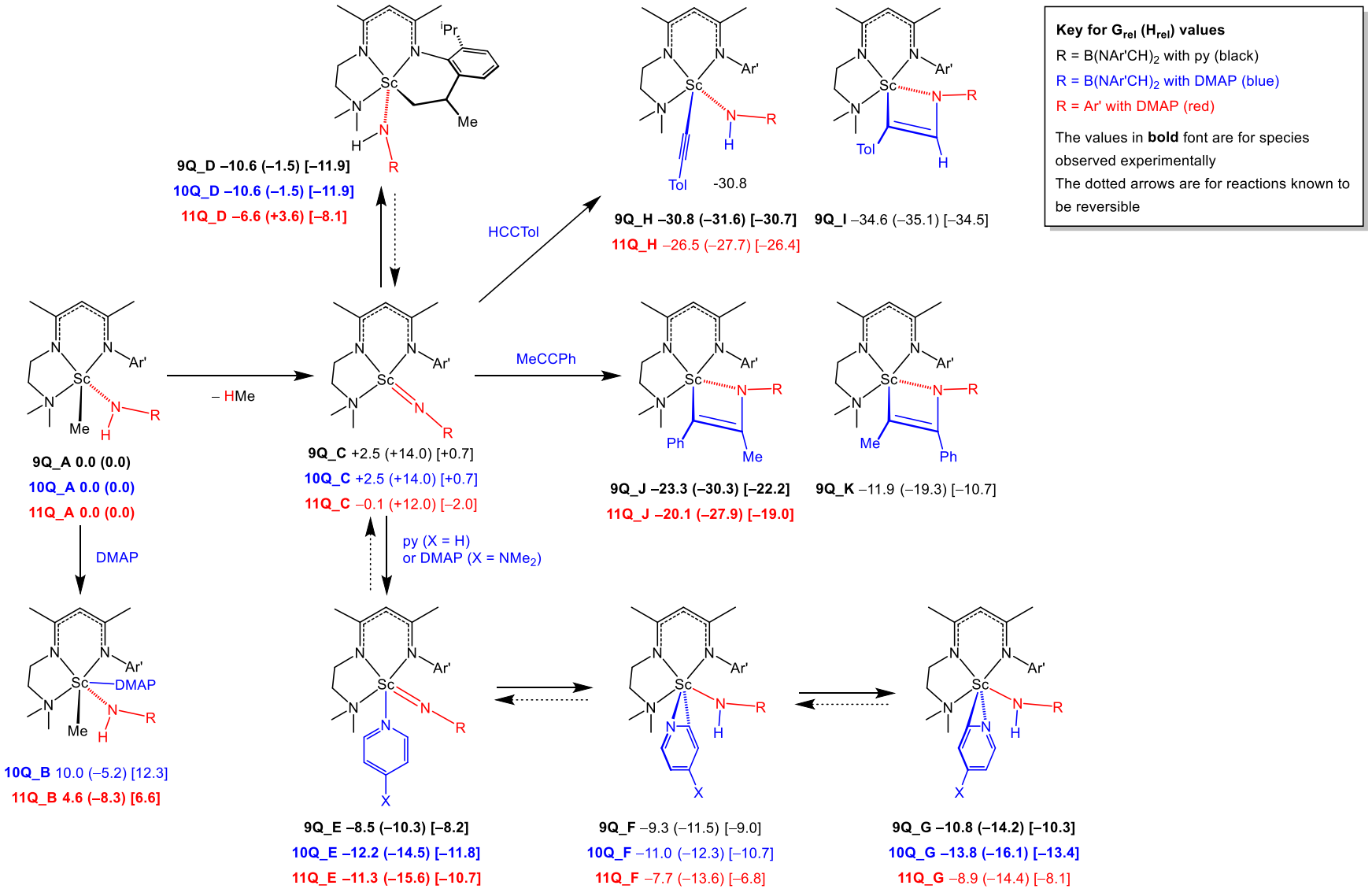

Scheme 5.10. Hypothetical reactions of a methyl-borylamide **9Q_A** and a model methyl-anilide **11Q_A** with G_{rel} values (and H_{rel} values in parentheses; both kcal mol^{-1}) calculated at 298 K. G_{rel} values calculated at 343 K are shown in square brackets. Refer to the Key for colour coding.

Firstly, the reactions with pyridine and DMAP will be considered. The addition of DMAP to **10Q_C** to give **10Q_E** is more favourable than the corresponding addition of pyridine to **9Q_C** to give **9Q_E** (Δ_rG = –14.7 *vs* –11.0 kcal mol^{-1}), arising from the stronger basicity of DMAP compared with pyridine. Moving to the next step which yields the first-formed η^2-pyridyl-type complexes **F**, this is found to be exergonic for pyridine in the system **9Q** (Δ_rG = –0.8 kcal mol^{-1} and Δ_rH = –1.2 kcal mol^{-1}) and endergonic for DMAP in the system **10Q** (Δ_rG = +1.2 kcal mol^{-1} and Δ_rH = +2.2 kcal mol^{-1}). This presumably arises (at least in part) as DMAP has a higher η^1-binding strength than pyridine in **E**, so has a relatively more unfavourable enthalpic contribution upon forming the η^2-pyridyl-type complexes **F**. Including the isomerisation to the more stable η^2-pyridyl-type complexes **G**, the overall C–H bond activation process for DMAP in **10Q** is also exergonic (Δ_rG = –1.6 kcal mol^{-1}), though less so than pyridine in **9Q** (Δ_rG = –2.3 kcal mol^{-1}).

Experimentally, the steps between complexes **C**, **E**, **F** and **G** are found to be reversible at 60 °C in the borylimido system. For example, reaction of the pyridyl complex (L^1)Sc{NHB(NAr'CH)$_2$}(η^2-NC$_5$H$_4$) (**39**) with 1 equiv. pyridine-d_5 at 60 °C resulted in an equilibrium mixture of 56% **39** and 44% **39-*d*$_5$** (the reverse reaction gave an equilibrium mixture of 60% **39** and 40% **39-*d*$_5$**), and a reaction of **39** with 1 equiv. DMAP at 60 °C resulted in an equilibrium mixture of 50% **39** and 50% of the DMAP analogue **40** (the reverse reaction gave an equilibrium mixture of 53% **39** and 47% **40**). Those exchange reactions suggested that **39** and **40** are similar in energy to give equilibrium mixtures close to equality. However, these DFT calculations showed the activated DMAP complex **10Q_G** to be 3.0 kcal mol^{-1} more stable than its pyridine counterpart. In enthalpy terms, however, the difference is less than 2 kcal mol^{-1} and within DFT precision for these large models. It is proposed that the interplay of opposing equilibria is responsible for the observed experimental outcome. In particular, coordination of DMAP is favoured over that of pyridine in the equilibrium between complexes of the type **C** and **E**, whilst the C–H bond activation of bound DMAP is disfavoured compared with that of pyridine in the equilibrium between complexes of the type **E** and **G**. This could, therefore, conceivably result in an approximately equal mixture of C–H bond activation products derived from pyridine and DMAP. In the imido system, the conversion of the DMAP adduct **11Q_E** to the first-formed C–H bond activation product **11Q_F** is more endergonic than the corresponding activation of DMAP in the borylimido system **10Q** (Δ_rG = +3.6 *vs* +1.2 kcal mol^{-1}), reflecting that a less strong N–H bond is formed in the anilido case than the borylimido

case. This is consistent with experimental results in which the DMAP-stabilised arylimide **1.47** is thermally stable and does not undergo an intramolecular C–H bond activation.

The addition of DMAP to the methyl complexes **A** to form the respective adducts (**B**) is also considered. Both reactions are found to be endergonic, though more so for the reaction in the borylamido system **10Q** (by 5.4 kcal mol^{-1}) due to the particularly unfavourable steric interactions in this six-coordinate complex containing the very bulky $B(NAr'CH)_2$ group. Although the experimentally successful formation of the anilide **11Q_B** would be expected to be exergonic, the large difference in Δ_rG between that reaction and the formation of **10Q_B** is consistent with the latter reaction not taking place in practice while the former reaction does. In these calculations on systems with full steric bulk it is suggested that the six-coordinate models **B** are not ideal representations of the true molecular conformations, so give higher than expected G_{rel} values. Considering these values in relative terms only, however, there is a clear distinction between **10Q_B** and **11Q_B** which is consistent with experimental outcomes.

Turning next to the formation of the tuck-in complexes **D** from the base-free multiply bonded complexes **C**, this process is found to be significantly more favourable for the borylimido system than the imido system (Δ_rG = –13.1 *vs* –6.5 kcal mol^{-1}). This difference primarily arises from a much greater negative enthalpic contribution in the former case (Δ_rH = –15.5 *vs* –8.4 kcal mol^{-1}) due to the stronger N–H bond which is formed in the borylamido ligand of **9Q_D**. The experimental conversion of the pyridyl complex **39** to the tuck-in complex **38** at 90 °C was described in Section 5.4, whilst the analogue derived from DMAP (**40**) does not form **38**, instead decomposing to a mixture of unidentified species at that temperature. The calculated G_{rel} values of the compounds **G** at 298 K show that, of the three, only the pyridyl-borylamido complex **9Q_G** is comparable in energy to its respective tuck-in complex **D** (–10.8 *vs* –10.6 kcal mol^{-1}). Calculated at 343 K, **9Q_D** becomes lower in energy than **9Q_G** (–11.9 *vs* –10.3 kcal mol^{-1}), this reflecting the increase in magnitude of the positive entropic contribution to this reaction which releases pyridine. This is now evidence to support the experimental conversion of **39** to **38** as a thermodynamic product at 90 °C. In contrast, the conversion of **10Q_G** to the tuck-in complex is 3.2 kcal mol^{-1} "uphill" at 298 K (1.5 kcal mol^{-1} "uphill" at 343 K), perhaps explaining why **38** cannot be accessed from **40**, giving instead deleterious side reactions.

The calculated Δ_rG values for reactions with HCCTol and MeCCPh confirm those trends that were seen in the small model systems. In particular, the experimentally observed anti-Markovnikov isomer of cycloaddition with MeCCPh (**9Q_J**) is 11.4 kcal mol^{-1} more stable than the Markovnikov isomer **9Q_K**, with the similar enthalpic difference of –11.0 kcal mol^{-1} confirming that this is dominated by Δ_rH and is little affected by entropic considerations. Additionally, the experimentally observed acetylide complex **9Q_H** is 3.8 kcal mol^{-1} less stable than the HCCTol metallacycle **9Q_I**, with again a similar difference in H_{rel} (+3.5 kcal mol^{-1}). Furthermore, the anilido complexes **11Q_H** and **11Q_J** are higher in energy than their borylamido counterparts (relative to the respective models **A**) by 4.3 and 3.2 kcal mol^{-1}, respectively, due to the weaker bonds formed to the NAr' fragment compared with those to the $NB(NAr'CH)_2$ fragment.

Finally, a series of complementary DFT calculations were performed on gas-phase systems having minimal steric bulk, and not including solvent or dispersion corrections. The modelling of ligands was the same as used in **6Q_R** at the beginning of this Section, replacing the Ar' groups of the L^1 supporting ligand and the arylimido ligand with phenyl groups, and using $NB(NHCH)_2$ as the model borylimido ligand. This strategy aimed to evaluate the underlying electronic preferences of reactivity without contributions from sterics or attractive dispersive effects. Scheme 5.11 summarises these hypothetical reactions for the model borylimido system denoted **12Q** and the model phenylimido system denoted **13Q**. The G_{rel} and H_{rel} values are here expressed relative to the base-free (boryl)imido complexes **C** to emphasis their central role in the reaction scheme. It is noted that the pyridine-stabilised models **D** are identical to **6Q_Ph** and **6Q_B(NHCH)$_2$** shown earlier in this Section, though will be referred to here using the **D** notation for consistent comparison with the other species in Scheme 5.11.

Looking first at the α-abstraction reactions of the methyl complexes **A** in a reverse sense of hypothetical C–H bond activations of methane, the formation of the methyl-borylamide **12Q_A** from **12Q_C** is 3.6 kcal mol^{-1} more exergonic than the analogous reaction in the imido system **13Q**. With the entropic contributions to the two reactions being comparable, this shows that the difference in Δ_rG is dominated by the difference in Δ_rH. Indeed, the difference in Δ_rH between the two reactions is calculated as 4.2 kcal mol^{-1}. These results highlight the higher strength of N–H bonds formed to borylimido fragments compared with imido fragments which has been discussed previously.

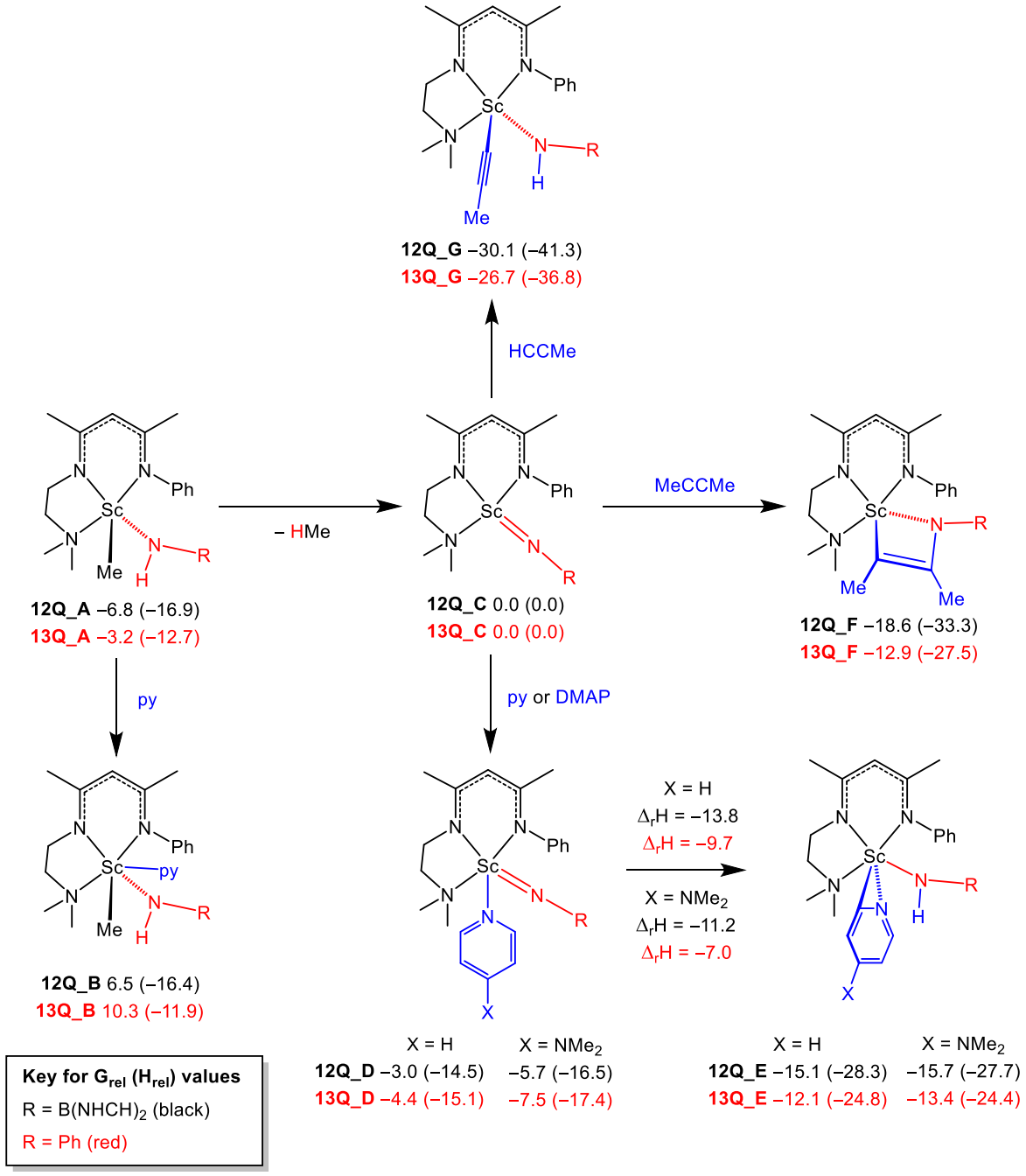

Scheme 5.11. Hypothetical reactions of a model methyl-borylamide **12Q_A** and a model methyl-anilide **13Q_A** with G_{rel} values (and H_{rel} values in parentheses; both kcal mol^{-1}) calculated at 298 K. Those values for **12Q** are in black, and those for **13Q** are in red, and all are expressed relative to the base-free (boryl)imido complexes **C**.

The formation of the pyridine adducts **D** from **C** is found to be more favourable in the imido system **13Q** than the borylimido system **12Q** (by 1.4 kcal mol^{-1}). This probably reflects the fact that the borylimido ligand has a greater σ-donor ability than the phenylimido ligand (as discussed for the models **6Q_R**), thus reducing the ability of the Sc centre to accept

electron density from the pyridine ligand. This results in a weaker Sc–N_{py} bond, and a less favourable enthalpic contribution, in the borylimido system. Inspection of the two optimised structures **D** reveals that the Sc–N_{py} bond is slightly shorter in **13Q_D** than **12Q_D** (2.373 *vs* 2.379 Å), giving support to this interpretation. Looking next at the C–H bond activations of complexes **D**, as expected this process is more favourable in the borylimido system **12Q** than the imido system **13Q**. The enthalpic contributions, $\Delta_r H$, are –13.8 and –9.7 kcal mol^{-1} respectively, which again highlights the higher relative strength of N–H bonds to borylimido fragments. As in the calculations on the full system described above, coordination of DMAP to the base-free complexes **C** is more favourable than coordination of pyridine, by 2.7 kcal mol^{-1} in the borylimides **12Q** and 3.1 kcal mol^{-1} in the imides **13Q**. The C–H bond activation of coordinated DMAP is found to be less favourable than that of pyridine (the enthalpic difference being 2.6 kcal mol^{-1} for **12Q** and 2.7 kcal mol^{-1} for **13Q**), with the reasoning that moving to η^2-binding is relatively disfavoured for the Lewis base with stronger η^1-binding, as described previously.

It is noted, however, that both the model imido and borylimido systems predict that C–H bond activation of bound pyridine and DMAP should be favourable, whereas experimentally this occurs for the transient borylimide **36'** but not for the DMAP-stabilised arylimide **1.47**. These calculations on small models, and the full system calculations above, suggest that the experimental differences in these systems arise from a combination of the electronic favouring of borylamido N–H bonds and the increased stability of η^1-coordination of DMAP relative to its η^2-pyridyl derivative compared with pyridine relative to an η^2-pyridyl ligand.

The addition of pyridine to the methyl-amido complexes **A** to form the respective adducts (**B**) is also considered. Compared with the formation of the adducts **D** described above, $\Delta_r G$ in the two systems are much more similar, being +13.3 and +13.5 kcal mol^{-1} in the borylamido system **12Q** and anilido system **13Q**, respectively. These endergonic processes are dominated by the large, negative entropic contribution which accompanies the formation of the crowded six-coordinate species. As Chen and co-workers described the formation of a DMAP adduct of the methyl-anilide **1.46** at RT, the coordination of DMAP to an analogous borylamido species would also be expected to occur. Experimentally, DMAP did not coordinate to the methyl-borylamide **36** prior to α-abstraction, so this difference is ascribed to the very large steric bulk of the borylamido moiety, as supported by the calculations on larger systems which were described above.

Additionally, the formation of the metallacyclic products **F** from **C** is favoured for the borylimido system **12Q** by 5.7 kcal mol^{-1} over the imido system **13Q**, and similarly, the formation of the model acetylide-borylamide **12G** is favoured by 3.4 kcal mol^{-1} over its anilido counterpart. The enthalpic contributions to these differences is 5.8 kcal mol^{-1} for **F** and 4.5 kcal mol^{-1} for **G**, again highlighting the higher strength of bonds formed to borylimido fragments relative to arylimido fragments.

5.7 Attempted incorporation of alternative alkyl ligands

It was next decided to attempt to prepare an analogue of the methyl-borylamide **36** having alternative alkyl ligands, $–CH_2SiMe_3$ or $–CH_2{}^tBu$, with the rationale that release of the respective alkane by α-abstraction may occur more readily, or at lower temperatures, thus making an isolable borylimide. Using a trimethylsilylmethyl group ($–CH_2SiMe_3$), only one sequence of reactions was found to give an alkyl-borylamide: the chloride complex **37** was reacted with $LiCH_2SiMe_3$ on the NMR tube scale to produce $(L^1)Sc(CH_2SiMe_3)\{NHB(NAr'CH)_2\}$. Heating of this on the NMR tube scale *in situ* unfortunately resulted only in conversion to the tuck-in complex **38**, and at a slower rate than from **36**; complete conversion was achieved after 40 h at 60 °C, (*cf*. 8 h from **36**). Moving to the *neo*-pentyl group (Np = $CH_2{}^tBu$), which was expected to be eliminated in a more facile manner,[52,53] the complex $Sc(Np)_3(THF)_2$ (**5.7**) was prepared as described by Tilley and co-workers.[54] It was found that addition of $H_2NB(NAr'CH)_2$ (**2.2**) to this complex was rapid, giving $Sc(Np)_2\{NHB(NAr'CH)_2\}(THF)_2$ as putative intermediate, although a second protonolysis step of addition of L^1–H required heating at 60 °C, so unsurprisingly this also led to conversion to **38** after 40 h at that temperature. The reverse sequence of steps, i.e. addition of L^1–H and then **2.2**, also required heating at 60 °C, although in this case gave a small amount of conversion to **38**, along with complex decomposition.

5.8 Scandium borylamides incorporating a new boryl moiety and a modified supporting ligand set

As explored in Section 5.4, a transient borylimide $(L^1)Sc\{NB(NAr'CH)_2\}$ (**36'**) was successfully formed from **36**. However, under the conditions required for its formation (60 °C or above), the complex gave rapid C–H bond activations, including with coordinated Lewis bases intended to stabilise it. Therefore, it was next decided to modify both the

borylamine starting material and the supporting ligand set to test if these changes could result in an isolable borylimido complex.

Firstly, a new borylamine, $H_2NB(N^iPr)_2C_6H_4$ (**5.8**), was introduced. Its preparation was first achieved by another DPhil student in our research group,[55] by reaction of the known bromoborane, $BrB(N^iPr)_2C_6H_4$,[56] in hexane solution with liquid ammonia. Having isopropyl groups as N-substituents it is expected to be much less sterically demanding than $H_2NB(NAr'CH)_2$ (**2.2**). An analogous reaction to that which formed **36** was carried out; i.e. $(L^1)ScCl_2$ (**5.2**) was methylated with 2 equiv. MeLi, then reacted *in situ* with 1 equiv. $H_2NB(N^iPr)_2C_6H_4$ (**5.8**) in toluene at RT to form $(L^1)Sc(Me)\{NHB(N^iPr)_2C_6H_4\}$ (**43**) as an off-white powder in 56% yield after work-up (Scheme 5.12). The reduced sterics in this case appeared to increase the rate of the reaction, giving complete conversion to **43** after 16 h, rather than the 60 h required for **36**.

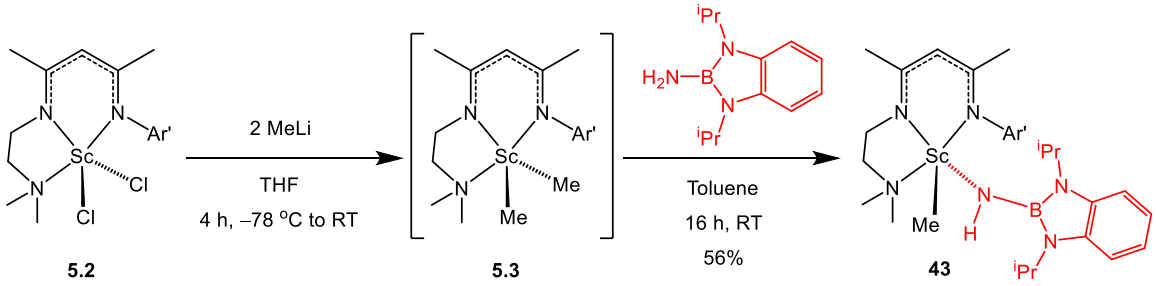

Scheme 5.12. Preparation of $(L^1)Sc(Me)\{NHB(N^iPr)_2C_6H_4\}$ (**43**) from *in situ*-generated $(L^1)ScMe_2$ (**5.3**).

The ^1H and ^{13}C NMR spectra of **43** are comparable to those of **36**. The Sc–Me ^1H resonance is observed at –0.56 ppm and the ^{13}C resonance at 23.1 ppm. A broad NH singlet is observed at 3.90 ppm (though is overlapping with the isopropyl septet from the boryl moiety). The set of ^1H signals attributed to the new boryl group include that septet (2 H) and two doublets (6 H each) corresponding to the isopropyl groups and a complex multiplet (4 H) arising from all the protons of the *o*-phenylene group forming the boryl backbone. The ^{11}B signal of **43** was observed to be 24.1 ppm, which is similar to that in borylamido complexes incorporating the previously described $–NHB(NAr'CH)_2$ ligand. For example, the ^{11}B resonance in **36** is found at 23.3 ppm.

Within the course of the preparation of **43**, a second species was detected in the ^1H NMR spectrum of the crude reaction mixture. Close inspection of the resonances showed that this was the bis(borylamide) $(L^1)Sc\{NHB(N^iPr)_2C_6H_4\}_2$ (**44**). This was later rationally prepared

through the same reaction using 2 equiv. **5.8**. After work-up, complex **44** was isolated as an off-white powder in 41% yield. The ^{1}H NMR spectrum of **44** clearly shows the presence of two primary borylamido ligands, with a 4 H septet at 3.96 ppm and two 12 H doublets at 1.55 and 1.38 ppm corresponding to the four isopropyl groups over the two ligands. A broad NH singlet (2 H) is seen at 3.25 ppm. The ^{11}B signal of **44** is of identical chemical shift (24.1 ppm) as in **43**.

Diffraction-quality crystals of the bis(borylamide) **44** were successfully grown from a hexane solution. The molecular solid state structure is shown in Figure 5.11, and selected bond distances and angles are listed in Table 5.8. Molecules of **44** have a distorted five-coordinate geometry (τ = 0.54 and 0.57 for the two crystallographically independent molecules) in which the supporting ligand (L^1) binds meridionally. The four Sc–N bond distances (two ligands in two crystallographically independent molecules) of the borylamide ligands in **44** are found in a range between 2.0388(18) and 2.0712(18) Å, so are similar to the distance of 2.0629(8) Å in the methyl-borylamide **36**. The Sc–N–B bond angles in **44**, however, are significantly smaller than those in borylamido complexes with the –NHB(NAr'CH)$_2$ ligand. In this bis(borylamide) they are found in a range between 142.37(14) and 146.48(16)°, whereas, for example, the angle is 152.36° in **36**. This probably corresponds to the greatly reduced sterics of the newly incorporated boryl moiety allowing the bond angle to approach closer to the ideal sp^2 value (120°).

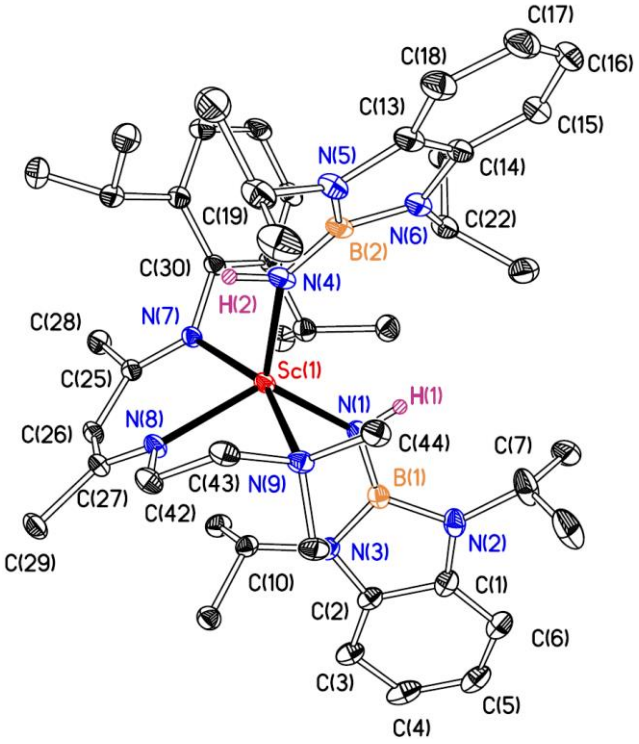

Figure 5.11. Displacement ellipsoid plot (20% probability) of $(L^1)Sc\{NHB(N^iPr)_2C_6H_4\}_2$ (**44**). C-bound H atoms are omitted for clarity. H(1) and H(2) are drawn as spheres of arbitrary radius.

Table 5.8. Selected bond distances (Å) and angles (°) for $(L^1)Sc\{NHB(N^iPr)_2C_6H_4\}_2$ (**44**). Values in brackets are for the second crystallographically independent molecule (τ = 0.54 [0.57]).

Sc(1)–N(1)	2.0712(18) [2.0669(18)]	N(1)–Sc(1)–N(4)	118.98(8) [119.31(8)]
Sc(1)–N(4)	2.0388(18) [2.0417(17)]	N(1)–Sc(1)–N(7)	104.85(6) [104.18(7)]
Sc(1)–N(7)	2.2102(15) [2.2136(16)]	N(1)–Sc(1)–N(8)	125.40(7) [123.68(7)]
Sc(1)–N(8)	2.1754(15) [2.1701(16)]	N(1)–Sc(1)–N(9)	87.87(6) [89.48(7)]
Sc(1)–N(9)	2.3386(16) [2.3503(17)]	N(4)–Sc(1)–N(7)	98.65(7) [98.71(7)]
N(1)–B(1)	1.406(3) [1.407(3)]	N(4)–Sc(1)–N(8)	112.47(8) [114.49(8)]
N(1)–H(1)	0.876(10) [0.877(10)]	N(4)–Sc(1)–N(9)	90.37(7) [89.44(7)]
N(4)–B(2)	1.409(3) [1.399(3)]	N(7)–Sc(1)–N(9)	158.00(6) [157.73(6)]
N(4)–H(2)	0.895(10) [0.890(10)]	Sc(1)–N(1)–B(1)	142.37(14) [145.83(15)]
		Sc(1)–N(4)–B(2)	145.46(17) [146.48(16)]

Upon isolation of the bis(borylamide) **44**, an NMR tube scale test reaction was performed with DMAP, with the possibility of this displacing one of the borylamido ligands and forming a borylimide *via* proton transfer and accompanying borylamine release. Unfortunately, despite heating at 90 °C in C_6D_6 for an extended period of time, no reaction was observed and **44** appeared to be thermally stable at this temperature. Focus therefore turned to thermolysis reactions of the new methyl-borylamide **43**. NMR tube scale reactions were performed between **43** and both pyridine and DMAP, as well as without the addition of an external base. However, all of these were found to form a mixture of products. The base-free thermolysis was attempted on the preparative scale, although no single product could be isolated. Nevertheless, some diffraction-quality crystals grew from the reaction mixture, and were found to be $[\{MeC(NAr')CHC(CH_2)NCH_2CH_2NMe_2\}Sc\{NHB(N^iPr)_2C_6H_4\}]_2$, a dimeric complex formed by intermolecular C–H bond activation of the methyl group at the β-position of the NacNac ligand by a second scandium centre, forming an eight membered metallacycle (Appendix, A3). Deprotonation at this site in NacNac ligands is not uncommon, and the non-innocence of ligands of this type has recently been reviewed by Clement and Arnold.[57] In particular, an analogous dimeric scandium complex with an eight-membered metallacycle has been reported by Roesky and co-workers.[58] Thus, it appears that the move to a boryl functionality with reduced steric demand has resulted in a loss of control over the reactivity of the borylamido complex. Significantly, the observation of an intermolecular C–H bond activation to produce a dimer is different behaviour to the borylamide **36** which incorporates the bulkier $–NHB(NAr'CH)_2$ ligand and gave only *intramolecular* C–H bond activations; presumably an intermolecular dimerisation in that case would be unfeasible due to steric constraints.

Next, complexes with the modified ligand L^2 were targeted, this ligand (which has the potential to be tetradentate) previously being used by Chen and co-workers to prepare the only example of a scandium terminal imide not stabilised by DMAP, $(L^2)Sc(NAr')$ (**1.50**).[21] It was thought that the presence of an extra internal donor may stabilise the desired borylimido complex, and hoped that this would not be susceptible to intramolecular C–H bond activations. Initially, an analogous route to that which formed **1.50** was attempted. $(L^2)Sc(CH_2SiMe_3)_2$ (**5.9**) and $H_2NB(NAr'CH)_2$ (**2.2**) were mixed on the NMR tube scale in C_6D_6, although no reaction was observed between the two compounds up to 60 °C, and at higher temperatures decomposition of the starting material was observed. The analogous

reaction with $H_2NB(N^iPr)_2C_6H_4$ (**5.8**) similarly did not proceed. In contrast, $(L^2)Sc(CH_2SiMe_3)(NHAr')$ (**5.10**) was prepared by Chen and co-workers with H_2NAr' at 50 °C.[21] In an alternative sequence of ligand additions, **2.2** was added to $Sc(CH_2SiMe_3)_3(THF)_2$ (**5.11**) in a first rapid protonolysis step at RT, followed by a second protonolysis with addition of L^2–H at RT, to successfully form the alkyl-borylamide $(L^2)Sc(CH_2SiMe_3)\{NHB(NAr'CH)_2\}$ (**45**). On the preparative scale, the two steps were carried out in toluene sequentially at RT, and **45** was isolated as a pale yellow solid in 73% yield (Scheme 5.13).

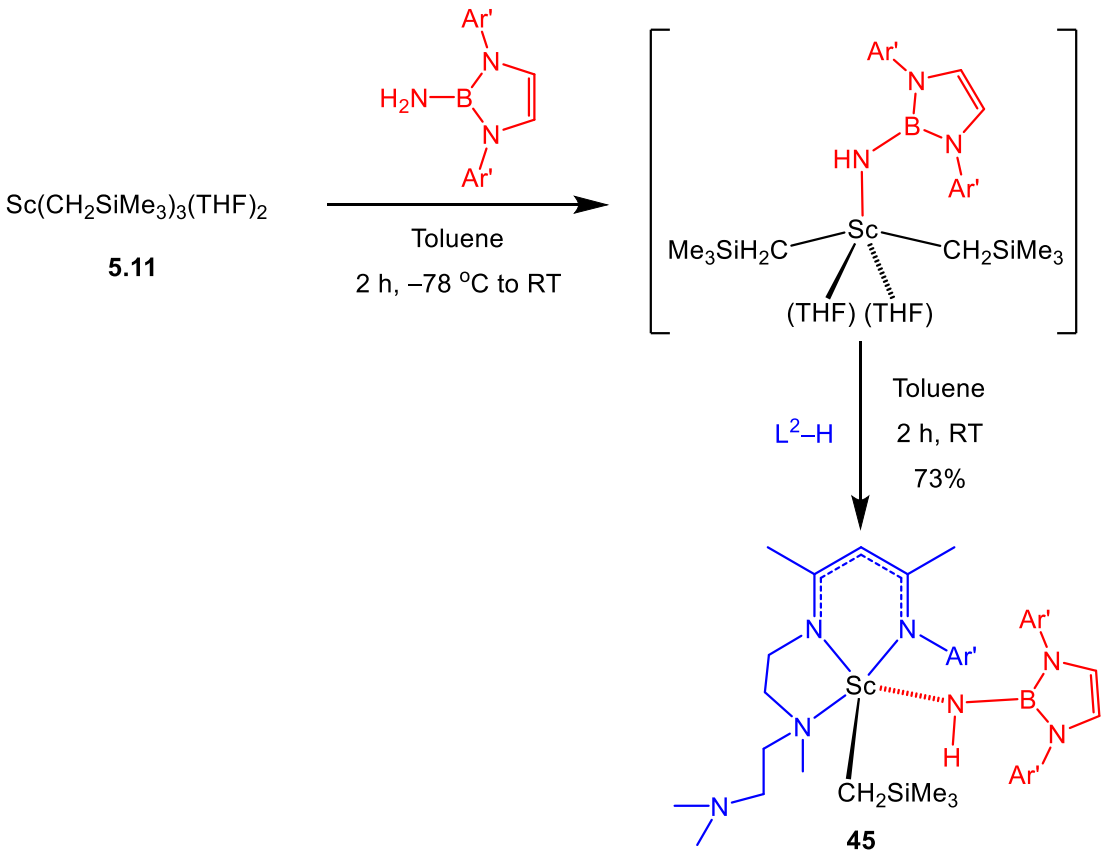

Scheme 5.13. Synthesis of $(L^2)Sc(CH_2SiMe_3)\{NHB(NAr'CH)_2\}$ (**45**) from $Sc(CH_2SiMe_3)_3(THF)_2$ (**5.11**), $H_2NB(NAr'CH)_2$ (**2.2**) and L^2–H.

The ^{1}H NMR spectrum of **45** is consistent with the complex having one borylamide ligand (a broad NH singlet is found at 3.36 ppm) and one CH_2SiMe_3 ligand (a sharp 9 H singlet is observed at –0.14 ppm and a broad 2 H singlet at –0.86 ppm). The resonances belonging to the L^2 ligand suggest that this is bound in a three-coordinate fashion. In particular, both methyl groups of the pendant NMe_2 appear to be chemically equivalent, so giving a single 6 H singlet at 2.01 ppm. If the nitrogen were bound to the metal centre, the two methyl

groups would be expected to be chemically inequivalent, as is the case in the spectrum of **1.50**.[21] This is therefore consistent with the scandium centre in **45** being five-coordinate.

Upon heating of borylamide **45** in C_6D_6 solution, no reaction was observed at 60 °C, whilst heating at 80 °C led to complete decomposition of the starting material over 6 h, based on the observation of borylamine **2.2** and multiple L^2 ligand environments in the ^{1}H NMR spectrum. In contrast, the imido complex **1.50** was prepared by Chen and co-workers from **5.10** at 50 °C over 3 days.[21] It is proposed that, in the formation of **1.50**, coordination of the fourth (pendant) donor is necessary to favour the release of $SiMe_4$ through α-abstraction. In the case of **45**, the large steric bulk of the borylamido ligand is expected to make this step (which makes the scandium centre six-coordinate) unfeasible, thus at high temperatures only complex decomposition is observed.

Consequently, salt metathesis reactions from the starting material $ScCl_3(THF)_3$ were next targeted. Firstly, that complex was reacted with 1 equiv. $LiNHB(NAr'CH)_2$ (**5.5**) although this resulted in decomposition of the scandium species at RT and giving **2.2** as the only boryl environment observed in the ^{1}H NMR spectra. Next, $ScCl_3(THF)_3$ was reacted with 1 equiv. Li[L^2] on the NMR tube scale in C_6D_6. This gave quantitative conversion to a species formulated as (L^2)$ScCl_2$. Unfortunately, this complex was found to be unstable to isolation on the preparative scale, and an *in situ* NMR tube scale reaction with **5.5** again gave decomposition to **2.2**. It is perhaps notable that Chen and co-workers appear to have avoided salt metathesis reactions of complexes incorporating the L^2 ligand; whilst **1.47** was prepared from (L^1)$ScMe_2$ (**5.3**, formed by salt metathesis of (L^1)$ScCl_2$ (**5.2**) with MeLi),[18] **1.50** was prepared instead through a route only involving protonolysis from (L^2)$Sc(CH_2SiMe_3)_2$ (**5.9**).[21]

Returning to the *neo*-pentyl starting material, $Sc(Np)_3(THF)_2$ (**5.7**),[54] addition of L^2–H gave a putative bis(*neo*-pentyl) complex (L^2)$Sc(Np)_2$ which appeared analogous to (L^2)$Sc(CH_2SiMe_3)_2$ (**5.9**) according to NMR spectroscopy. Upon addition of borylamine **2.2** to this compound *in situ* on the NMR tube scale, a complex mixture of products was observed to form at RT. Alternatively, reaction between **5.7** and **2.2** gave the putative complex $Sc(Np)_2\{NHB(NAr'CH)_2\}(THF)_2$ on the NMR tube scale in C_6D_6. However, addition of L^2–H to this resulted in the immediate formation of **2.2** and multiple ligand environments. Both of these routes were also attempted with the alternative borylamine $H_2NB(N^iPr)_2C_6H_4$ (**5.8**), although these were similarly unsuccessful. Thus, the putative

neo-pentyl complexes formed here are observed to be considerably less stable than the trimethylsilylmethyl complex **45**, meaning that these routes have not been synthetically useful.

5.9 Conclusions and Outlook

This Chapter has explored attempts to form the first borylimido complexes of a rare earth metal, namely scandium. From the starting material $(L^1)ScCl_2$ (**5.2**) which incorporates a NacNac supporting ligand with a pendant NMe_2 donor group, was formed the methyl-borylamide $(L^1)Sc(Me)\{NHB(NAr'CH)_2\}$ (**36**). Thermolysis reactions of this complex were then performed. In the absence of external base, an intramolecular sp^3 C–H bond activation of an isopropyl group on the supporting ligand takes place, forming the tuck-in complex $\{MeC(NC_6H_3{}^iPrCH(Me)CH_2)CHC(Me)NCH_2CH_2NMe_2\}Sc\{NHB(NAr'CH)_2\}$ (**38**). Thermolysis in the presence of pyridine or DMAP forms the pyridyl-type complexes $(L^1)Sc\{NHB(NAr'CH)_2\}(\eta^2\text{-}4\text{-}NC_5H_3R)$ (R = H (**39**), NMe_2 (**40**)), by (sp^2) C–H bond activation at the 2-position of coordinated pyridine or DMAP, respectively. Kinetic analysis showed that all of these reactions proceed with comparable first order rate constants, showing that they share a common rate-determining step: initial α-abstraction to release methane and generate the transient borylimido complex $(L^1)Sc\{NB(NAr'CH)_2\}$ (**36'**). Following this step, the respective C–H bond activations are rapid. This mechanism was also supported by isotope labelling studies.

Further evidence of the existence of **36'** was next sought from trapping reactions with two alkynes. Thermolysis of **36** in the presence of HCCTol produced the acetylido complex $(L^1)Sc\{NHB(NAr'CH)_2\}(CCTol)$ (**41**) *via* C–H bond activation at the sp centre, thus completing the set of sp, sp^2 and sp^3 C–H bond activations by **36'**. Thermolysis of **36** in the presence of the internal alkyne MeCCPh instead produced the azascandacyclobutene complex $(L^1)Sc\{N\{B(NAr'CH)_2\}C(Me)C(Ph)\}$ (**42**) by [2+2] cycloaddition across the multiple bond of **36'**, thus giving excellent evidence for its existence. Furthermore, the first order rate constants of these two reactions were found to be comparable to those described previously, so confirming the common RDS.

A combined DFT and QTAIM study on model scandium alkylimides, arylimides and borylimides confirmed that borylimides are expected to be comparable to arylimides structurally, due to the similar π effects arising from the aryl ring and aromatic boryl ring. Meanwhile, scandium borylimides are calculated to have stronger scandium–nitrogen

multiple bonds than their imido counterparts due to the strong σ-donating nature of the boryl moiety. Calculations performed on the reaction products of a model base-free borylimide, and its arylimido counterpart, with a number of substrates resulted in an analysis of the relative energetics of these processes. It was shown that C–H bond activations are more favourable in the borylimido case, due to the higher strength of the N–H bond formed in a borylamido ligand compared with that in an anilido ligand. Other bonds formed to a borylimido fragment, such as the C–N bond in the metallacyclic product of a [2+2] cycloaddition, are also found to be stronger than those to arylimido fragments, as shown by the more favourable enthalpic contribution to free energy of the process in which it is formed.

Next, a new methyl-borylamide (L^1)Sc(Me){NHB(N^iPr)$_2C_6H_4$} (**43**) was prepared using a borylamine with a much reduced steric profile, $H_2NB(N^iPr)_2C_6H_4$ (**5.8**). When thermolysis reactions of **43** were attempted, the smaller steric profile appeared to lead to a loss of control over the reactivity compared with that of **36**, with complex mixtures of products observed. A modified supporting ligand L^2 was also investigated, this having the potential to act as a tetradentate ligand, so giving more stability to the desired borylimido complex. An alkyl-borylamide, (L^2)Sc(CH_2SiMe_3){NHB(NAr'CH)$_2$} (**45**), was successfully prepared, although this did not eliminate $SiMe_4$ at temperatures below that which caused total complex decomposition. It is proposed that the large steric bulk of the boryl functionality prevents the coordination of the terminal NMe_2 group of the L^2 supporting ligand, which is necessary to promote the elimination of the alkane.

To summarise, excellent evidence has been obtained to support the formation of the transient scandium borylimido complex **36'**. Unfortunately attempts to modify both the borylamine starting material and the supporting ligand set have not resulted in the formation of an isolable complex. The DFT calculations described above showed that a scandium borylimide is particularly prone to undergoing C–H bond activations, including undesired intramolecular activation of a supporting ligand. Future attempts to form an isolable scandium borylimide may focus on the development of new, robust supporting ligands for which such processes are less likely.

5.10 References

1 O. T. Summerscales and J. C. Gordon, *RSC Adv.*, 2013, **3**, 6682–6692.

2 G. R. Giesbrecht and J. C. Gordon, *Dalton Trans.*, 2004, 2387–2393.

3 D. Schädle, C. Schädle, K. W. Törnroos and R. Anwander, *Organometallics*, 2012, **31**, 5101–5107.

4 D. Schädle, C. Schädle, D. Schneider, C. Maichle-Mössmer and R. Anwander, *Organometallics*, 2015, **34**, 4994–5008.

5 K. D. Conroy, W. E. Piers and M. Parvez, *Organometallics*, 2009, **28**, 6228–6233.

6 A. A. Trifonov, M. N. Bochkarev, H. Schumann and J. Loebel, *Angew. Chem. Int. Ed. Engl.*, 1991, **30**, 1149–1151.

7 Z. Xie, S. Wang, Q. Yang and T. C. W. Mak, *Organometallics*, 1999, **18**, 1578–1579.

8 S. Wang, Q. Yang, T. C. W. Mak and Z. Xie, *Organometallics*, 1999, **18**, 5511–5517.

9 H. Chan, H. Li and Z. Xie, *Chem. Commun.*, 2002, 652–653.

10 J. C. Gordon, G. R. Giesbrecht, D. L. Clark, P. J. Hay, D. W. Keogh, R. Poli, B. L. Scott and J. G. Watkin, *Organometallics*, 2002, **21**, 4726–4734.

11 D. J. Beetstra, A. Meetsma, B. Hessen and J. H. Teuben, *Organometallics*, 2003, **22**, 4372–4374.

12 A. G. Avent, P. B. Hitchcock, A. V Khvostov, M. F. Lappert and A. V Protchenko, *Dalton Trans.*, 2004, 2272–2280.

13 D. Cui, M. Nishiura and Z. Hou, *Angew. Chem. Int. Ed.*, 2005, **44**, 959–962.

14 C.-L. Pan, W. Chen, S. Song, H. Zhang and X. Li, *Inorg. Chem.*, 2009, **48**, 6344–6346.

15 J. Scott, F. Basuli, A. R. Fout, J. C. Huffman and D. J. Mindiola, *Angew. Chem. Int. Ed.*, 2008, **47**, 8502–8505.

16 B. F. Wicker, H. Fan, A. K. Hickey, M. G. Crestani, J. Scott, M. Pink and D. J. Mindiola, *J. Am. Chem. Soc.*, 2012, **134**, 20081–20096.

17 B. F. Wicker, J. Scott, A. R. Fout, M. Pink and D. J. Mindiola, *Organometallics*, 2011, **30**, 2453–2456.

18 E. Lu, Y. Li and Y. Chen, *Chem. Commun.*, 2010, **46**, 4469–4471.

19 T. Chu, W. E. Piers, J. L. Dutton and M. Parvez, *Organometallics*, 2013, **32**, 1159–1165.

20 W. Rong, J. Cheng, Z. Mou, H. Xie and D. Cui, *Organometallics*, 2013, **32**, 5523–5529.

21 E. Lu, J. Chu, Y. Chen, M. V Borzov and G. Li, *Chem. Commun.*, 2011, **47**, 743–745.

22 J. Chu, E. Lu, Z. Liu, Y. Chen, X. Leng and H. Song, *Angew. Chem. Int. Ed.*, 2011, **50**, 7677–7680.

23 E. Lu, Q. Zhou, Y. Li, J. Chu, Y. Chen, X. Leng and J. Sun, *Chem. Commun.*, 2012, **48**, 3403–3405.

24 J. Chu, C. E. Kefalidis, L. Maron, X. Leng and Y. Chen, *J. Am. Chem. Soc.*, 2013, **135**, 8165–8168.

25 J. Chu, E. Lu, Y. Chen and X. Leng, *Organometallics*, 2013, **32**, 1137–1140.

26 J. Chu, X. Han, C. E. Kefalidis, J. Zhou, L. Maron, X. Leng and Y. Chen, *J. Am. Chem. Soc.*, 2014, **136**, 10894–10897.

27 A. W. Addison, T. N. Rao, J. Reedijk, J. van Rijn and G. C. Verschoor, *J. Chem. Soc., Dalton Trans.*, 1984, 1349–1356.

28 L. K. Knight, W. E. Piers, P. Fleurat-Lessard, M. Parvez and R. McDonald, *Organometallics*, 2004, **23**, 2087–2094.

29 F. Brotzel, B. Kempf, T. Singer, H. Zipse and H. Mayr, *Chem. Eur. J.*, 2007, **13**, 336–345.

30 T. H. Lowry and K. S. Richardson, *Mechanism and Theory in Organic Chemistry*, Harper and Row, New York, 1987.

31 B. K. Carpenter, *Determination of Reaction Mechanisms*, Wiley-Interscience, New York, 1984.

32 J. L. Bennett and P. T. Wolczanski, *J. Am. Chem. Soc.*, 1997, **119**, 10696–10719.

33 C. C. Cummins, S. M. Baxter and P. T. Wolczanski, *J. Am. Chem. Soc.*, 1988, **110**, 8731–8733.

34 C. C. Cummins, C. P. Schaller, G. D. Van Duyne, P. T. Wolczanski, A. W. E. Chan and R. Hoffmann, *J. Am. Chem. Soc.*, 1991, **113**, 2985–2994.

35 C. P. Schaller, C. C. Cummins, P. T. Wolczanski and N. York, *J. Am. Chem. Soc.*, 1996, **118**, 591–611.

36 L. M. Slaughter, P. T. Wolczanski, T. R. Klinckman and T. R. Cundari, *J. Am. Chem. Soc.*, 2000, **122**, 7953–7975.

37 K. Manna, A. Ellern and A. D. Sadow, *Chem. Commun.*, 2010, **46**, 339–341.

38 P. J. Walsh, F. J. Hollander and R. G. Bergman, *J. Am. Chem. Soc.*, 1988, **110**, 8729–8731.

39 M. Gómez-Gallego and M. A. Sierra, *Chem. Rev.*, 2011, **111**, 4857–963.

40 J. R. Webb, S. A. Burgess, T. R. Cundari and T. B. Gunnoe, *Dalton Trans.*, 2013, **42**, 16646–16665.

41 D. Balcells, E. Clot and O. Eisenstein, *Chem. Rev.*, 2010, **110**, 749–823.

42 E. M. Simmons and J. F. Hartwig, *Angew. Chem. Int. Ed.*, 2012, **51**, 3066–3072.

43 J. L. Polse, R. A. Andersen and R. G. Bergman, *J. Am. Chem. Soc.*, 1995, **117**, 5393–5394.

44 A. S. Guram and R. F. Jordan, *Organometallics*, 1991, **10**, 3470–3479.

45 R. F. Jordan and A. S. Guram, *Organometallics*, 1990, **9**, 2116–2123.

46 R. F. Jordan, D. Taylor and N. Baenziger, *Organometallics*, 1990, **9**, 1546–1557.

47 B.-J. Deelman, W. M. Stevels, J. H. Teuben, M. T. Lakin and A. L. Spek, *Organometallics*, 1994, **13**, 3881–3891.

48 K. H. Den Haan, Y. Wielstra and J. H. Teuben, *Organometallics*, 1987, **6**, 2053–2060.

49 R. F. W. Bader, *Atoms in Molecules: A Quantum Theory*, Oxford University Press, Oxford, 1990.

50 X. Fradera, M. A. Austen and R. F. W. Bader, *J. Phys. Chem. A*, 1999, **103**, 304–314.

51 A. D. Schofield, A. Nova, J. D. Selby, C. D. Manley, A. D. Schwarz, E. Clot and P. Mountford, *J. Am. Chem. Soc.*, 2010, **132**, 10484–10497.

52 R. R. Schrock and J. D. Fellmann, *J. Am. Chem. Soc.*, 1978, **100**, 3359–3370.

53 P. D. Bolton, N. Adams, E. Clot, A. R. Cowley, P. J. Wilson, M. Schröder and P. Mountford, *Organometallics*, 2006, **25**, 5549–5565.

54 D. S. Levine, T. D. Tilley and R. A. Andersen, *Organometallics*, 2015, **34**, 4647–4655.

55 B. Xie and P. Mountford, Unpublished results.

56 L. Weber, J. Kahlert, L. Böhling, A. Brockhinke, H.-G. Stammler, B. Neumann, R. A. Harder, P. J. Low and M. A. Fox, *Dalton Trans.*, 2013, **42**, 2266–81.

57 C. Camp and J. Arnold, *Dalton Trans.*, 2016, **45**, 14462–14498.

58 A. M. Neculai, H. W. Roesky, D. Neculai and J. Magull, *Organometallics*, 2001, **20**, 5501–5503.

Chapter Six

Experimental details and characterising data

6.1 General methods and implementation

All manipulations were carried out using standard Schlenk line or dry-box techniques under an atmosphere of argon or dinitrogen. Solvents were either degassed by sparging with dinitrogen and dried by passing through a column of the appropriate drying agent[1] or refluxed over sodium (toluene), potassium (THF), Na/K alloy (Et_2O) or CaH_2 (pyridine) and distilled. Deuterated solvents were dried over sodium (toluene-d_8), potassium (C_6D_6), CaH_2 (pyridine-d_5) or P_2O_5 (CD_2Cl_2), distilled under reduced pressure and stored under argon in Teflon valve ampoules. Unless otherwise stated NMR samples were prepared under dinitrogen in 5 mm Wilmad 507-PP tubes fitted with J. Young Teflon valves. ^{1}H, $^{13}C\{^{1}H\}$, $^{11}B\{^{1}H\}$, $^{19}F\{^{1}H\}$ and ^{2}H spectra were recorded on a Bruker Ascend 400 NMR spectrometer, a Bruker Avance III 500 NMR spectrometer or on a Bruker AVC 500 spectrometer fitted with a ^{13}C cryoprobe. Unless otherwise stated, all NMR spectra were recorded at 298 K. ^{1}H and $^{13}C\{^{1}H\}$ and spectra were referenced internally to residual protio-solvent (^{1}H) or solvent (^{13}C) resonances, and are reported relative to tetramethylsilane (δ = 0 ppm). ^{2}H NMR spectra were referenced to the natural abundance deuterium resonance of the protio solvent. ^{19}F and ^{11}B NMR specra were referenced externally to $CFCl_3$ and $Et_2O{\cdot}BF_3$ respectively. Assignments were confirmed as necessary with the use of two dimensional ^{1}H–^{1}H, ^{13}C–^{1}H and ^{19}F–^{19}F correlation experiments. Chemical shifts are quoted in δ (ppm) and coupling constants in Hz. Unless otherwise stated, IR spectra were recorded on a Thermo Scientific Nicolet iS5 FTIR spectrometer and samples prepared in a dry-box using NaCl plates as a Nujol mull or as a thin film. The data are quoted in wavenumbers (cm^{-1}). Mass spectra were recorded by the mass spectrometry service of Oxford University's Department of Chemistry. Elemental analyses were carried out by the Elemental Analysis Service at the London Metropolitan University.

6.2 Literature preparations

$Ti(NMe_2)_2Cl_2$,[2] $H_2NB(NAr'CH)_2$ (**2.2**),[3] H_2NBMes_2,[4,5] $(\mu\text{-}H_2N)_2(BC_8H_{14})_2$,[6] Me_3[6]aneN_3,[7] $Li_2N_2^{SiMe_3}N^{Me}$,[8] $H_2N_2^{ArF}N^{Me}$,[9] $Li_2N_2^{iPr}N^{Me}$,[10] $Li_2N_2N^{py}$,[11] $Li_2N_2^{pyr}N^{Me}$,[12] Cp*Ti(N^tBu)Cl(py) (**1.8**),[13] Li[hpp],[14] $LiN^{pyr}N^{Me_2}$,[15] NaCp,[16] Li[$MeC(N^iPr)_2$],[17] $BrB(NAr'CH)_2$,[18] $HCCAr^F$,[19,20] $DCCAr^F$,[21] $(L^1)ScCl_2$ (**5.2**),[22] $LiNHB(NAr'CH)_2$ (**5.5**),[3] 2-pyridine-d_1,[23] $LiCH_2SiMe_3$,[24] LiNp,[25,26] $Sc(Np)_3(THF)_2$ (**5.7**),[27] $H_2NB(N^iPr)_2C_6H_4$ (**5.8**),[28] $Sc(CH_2SiMe_3)_3(THF)_2$ (**5.11**),[29] L^2–H[30] and $(L^2)Sc(CH_2SiMe_3)_2$ (**5.9**),[30] were synthesised according to literature procedures, either by the Author or other members of

the Mountford Group (see below). $Li_2N_2^{ArF}N^{Me}$ was prepared by reaction of $H_2N_2^{ArF}N^{Me}$ with 2.2 equiv. ^{n}BuLi (1.6 M in hexane) in hexane solution, in analogy to preparations of $Li_2N_2^{SiMe_3}N^{Me}$ and $Li_2N_2^{iPr}N^{Me}$.[8,10] DCCTol was prepared by reaction of HCCTol with 1.1 equiv. ^{n}BuLi (1.6 M in hexanes) in THF and quenching with D_2O, then extraction into Et_2O and drying over $MgSO_4$.

Me_3[6]aneN_3, $Li_2N_2^{pyr}N^{Me}$, $LiN^{pyr}N^{Me_2}$ and NaCp were provided by Dr Andrew Schwarz; $Li_2N_2^{SiMe_3}N^{Me}$ and $Li_2N_2^{ArF}N^{Me}$ were provided by Simona Mellino; $Li_2N_2^{iPr}N^{Me}$ was provided by Dr Laura Stevenson; Li[MeC(N^{i}Pr)$_2$] was provided by Dr Laura Groom.

All other reagents were purchased from commercial suppliers, and (for liquid reagents) degassed before use, unless specified otherwise. $H_2N^{t}Bu$, H_2NXyl, HCCTol and MeCCPh were dried over CaH_2 and distilled before use. H_2NTol and DMAP were sublimed under dynamic vacuum at 100 °C and transferred to the dry-box.

Procedure for deuteration of H_2NB(NAr'CH)$_2$ (2.2). Inert atmosphere techniques were used throughout. To a hexane solution (10 mL) of H_2NB(NAr'CH)$_2$ (0.490 g, 1.21 mmol) was added D_2O (10 mL) and NaOD (40% w/w in D_2O, 12 μL, 0.162 mmol), and the mixture stirred at RT for 16 h. After this time, DCl (35% w/w in D_2O, 22 μL, 0.162 mmol) was added, and the mixture stirred for 30 mins. The hexane fraction was then decanted away, and the remaining aqueous fraction extracted with hexane (10 mL). The combined hexane fractions were then dried over $CaCl_2$ for 16 h, filtered, and the volatiles removed under reduced pressure to afford D_2NB(NAr'CH)$_2$ (**2.2-*d*$_2$**) as an off-white powder. Yield: 0.310 g (63%). ^{1}H NMR analysis indicated >98% deuteration.

6.3 X-ray data collection and processing parameters

Crystals were mounted on glass fibers using perfluoropolyether oil and cooled rapidly in a stream of cold N_2 using an Oxford Cryosystems Cryostream unit. Diffraction data were measured using either an Enraf-Nonius KappaCCD or Agilent Technologies Supernova diffractometer using Mo-K_α or Cu-K_α radiation, respectively. As appropriate, absorption and decay corrections were applied to the data and equivalent reflections merged.[31] The structures were solved with SIR92[32] or Superflip,[33] and further refinements and all other crystallographic calculations were performed using the CRYSTALS program suite.[34] Other details of the structure solutions and refinements are given in the individual CIFs contained in the CD Appendix.

6.4 Computational details

DFT calculations described in this Thesis were performed by Philip Mountford and Simona Mellino at The University of Oxford in collaboration with Dr Eric Clot at Université Montpellier 2. Geometry optimisations were performed with the Gaussian09 package[35] at the B3PW91 level of hybrid density functional theory,[36,37] with inclusion of Grimme's D3(bj) correction[38,39] in the optimisation process except for sterically-pruned model systems. For geometry optimisations in the gas phase all atoms were represented by the Def2-SVP basis set.[40] For sterically-pruned model systems additional single-point calculations were carried out on the optimised geometry using the Def2-TZVP basis set.[41] For systems with realistic steric bulk, single-point calculations took into account both solvent and dispersion effects. The solvent (benzene) influence was taken into consideration through single point calculations on the gas-phase optimized geometry with SCRF calculations within the SMD model.[42] For the SCRF calculations all the atoms were treated with a Def2-TZVP basis set.[41] Influence of the dispersion forces was also considered by computing the D3(bj) corrections.[38,39] SCF energies reported in this work are for gas-phase model systems using the Def2-TZVP basis set. For larger systems (Def2-TZVP basis sets) the Gibbs free energies and enthalpies were obtained by summing the SMD energy, the gas-phase Gibbs or enthalpy contribution at 298 K (or another temperature where specified) obtained from the geometry optimisations, and the D3(bj) correction. The NBO analyses were carried out using NBO 6.0,[43] on wavefunctions computed with B3PW91 in the gas phase with the Def2 family of basis sets for all atoms. Atoms-in-molecules analyses were performed using the AIMALL programme,[44] using Gaussian09 wavefunction files as input.

6.5 Experimental details and characterising data for Chapter Two

Ti{NB(NAr'CH)$_2$}Cl$_2$(NHMe$_2$)$_2$ (1). To a solution of Ti(NMe$_2$)$_2$Cl$_2$ (1.36 g, 6.58 mmol) in toluene (10 mL) was slowly added a solution of H$_2$NB(NAr'CH)$_2$ (**2.2**, 2.52 g, 6.25 mmol) in toluene (10 mL), at –78 °C. The mixture was allowed to warm to RT, upon which it became a red/brown slurry. After stirring for 30 mins, all solids had dissolved, leaving a deep red solution, which was stirred at RT for a further 2.5 h. The volatiles were then removed under reduced pressure to leave a red-brown, waxy solid. The product was triturated in hexane, yielding **1** as an orange-brown powder. Yield: 3.01 g (79%).

Diffraction-quality crystals were grown from a saturated hexane solution at room temperature.

^{1}H NMR (C_6D_6, 400.1 MHz): δ 7.13 (6 H, overlapping 2 × m, *m*- and *p*-$C_6\underline{H}_3{}^{i}Pr_2$), 5.73 (2 H, s, NCH), 3.53 (4 H, sept., ^{3}J = 6.9 Hz, C<u>H</u>MeMe), 2.67 (2 H, sept., ^{3}J = 6.1 Hz, N<u>H</u>Me_2), 1.92 (12 H, d, ^{3}J = 6.1 Hz, NH<u>Me</u>$_2$), 1.56 (12 H, d, ^{3}J = 6.9 Hz, CH<u>Me</u>Me), 1.24 (12 H, d, ^{3}J = 6.9 Hz, CHMe<u>Me</u>) ppm. ^{13}C{^{1}H} NMR (C_6D_6, 100.6 MHz): δ 146.8 (*i*-<u>C</u>$_6H_3{}^{i}Pr_2$), 140.2 (*o*-<u>C</u>$_6H_3{}^{i}Pr_2$), 127.2 (*p*-<u>C</u>$_6H_3{}^{i}Pr_2$), 123.3 (*m*-<u>C</u>$_6H_3{}^{i}Pr_2$), 115.5 (NCH), 40.0 (NH<u>Me</u>$_2$), 28.4 (<u>C</u>HMeMe), 24.2 (CHMe<u>Me</u>), 24.0 (CH<u>Me</u>Me) ppm. ^{11}B{^{1}H} NMR (C_6D_6, 128.4 MHz): δ 14.2 ppm. IR (NaCl plates, Nujol mull, cm^{-1}): 3289 (w, non-bridging N–H), 3277 (w, hydrogen bonded N–H), 1586 (m), 1260 (w), 1180 (w), 1076 (w), 1025 (m), 983 (m), 890 (m), 798 (m), 686 (w), 652 (m). IR (NaCl cell, CH_2Cl_2, ν(N–H), cm^{-1}): 3288. Anal. found (calcd. for $C_{30}H_{50}BCl_2N_5Ti$): C, 58.95 (59.04); H, 8.18 (8.26); N, 11.37 (11.47)%.

Ti{NB(NAr'CH)$_2$}Cl$_2$(Me$_3$[6]aneN$_3$) (2). To a solution of Ti{NB(NAr'CH)$_2$}Cl$_2$(NHMe$_2$)$_2$ (**1**, 0.250 g, 0.410 mmol) in toluene (10 mL) at – 78 °C was added Me$_3$[6]aneN$_3$ (57.5 μL, 0.409 mmol). The solution was then allowed to warm to RT, and stirred for 3 h, after which time it had become an orange slurry. The slurry was concentrated (by ~75%) and filtered, then the resulting solid washed with hexane (3 × 2 mL) and dried *in vacuo*, yielding **2** as a pale orange powder. Yield: 0.154 g (58%).

^{1}H NMR (C_6D_6, 400.1 MHz): δ 7.27 (6 H, overlapping 2 × m, *m*- and *p*-$C_6\underline{H}_3{}^{i}Pr_2$), 5.83 (2 H, s, NCH), 4.00 (1 H, d, ^{2}J = 7.3 Hz, CH_2 *trans* to NB(NAr'CH)$_2$), 3.56 (4 H, sept., ^{3}J = 6.9 Hz, C<u>H</u>MeMe), 3.33 (2 H, d, ^{2}J = 7.9 Hz, CH_2 *trans* to Cl), 2.24 (1 H, d, ^{2}J = 7.3 Hz, CH_2 *trans* to NB(NAr'CH)$_2$), 1.95 (2 H, d, ^{2}J = 7.9 Hz, CH_2 *trans* to Cl), 1.87 (6 H, s, NMe *trans* to Cl), 1.66 (12 H, d, ^{3}J = 6.9 Hz, CH<u>Me</u>Me), 1.48 (3 H, s, NMe *trans* to NB(NAr'CH)$_2$), 1.31 (12 H, d, ^{3}J = 6.9 Hz, CHMe<u>Me</u>) ppm. ^{13}C{^{1}H} NMR (C_6D_6, 100.6 MHz): δ 147.3 (*o*-<u>C</u>$_6H_3{}^{i}Pr_2$), 141.0 (*i*-<u>C</u>$_6H_3{}^{i}Pr_2$), 127.4 (*p*-<u>C</u>$_6H_3{}^{i}Pr_2$), 123.7 (*m*-<u>C</u>$_6H_3{}^{i}Pr_2$), 116.5 (NCH), 77.0 (CH_2 *trans* to Cl), 76.0 (CH_2 *trans* to NB(NAr'CH)$_2$), 40.6 (NMe *trans* to Cl), 36.8 (NMe *trans* to NB(NAr'CH)$_2$), 29.3 (<u>C</u>HMeMe), 25.5 (CHMe<u>Me</u>), 24.6 (CH<u>Me</u>Me) ppm. ^{11}B{^{1}H} NMR (C_6D_6, 128.4 MHz): δ 13.4 ppm. IR (NaCl plates, Nujol mull, cm^{-1}): 1595 (m), 1459 (s), 1380 (s), 1273 (m), 1260 (m), 1175 (w), 1113 (w), 1083 (m), 935 (w), 899 (w), 799 (m), 758 (w), 721 (w), 657 (w). Anal. found (calcd. for $C_{32}H_{51}BCl_2N_6Ti$): C, 56.28 (59.19); H, 7.46 (7.92); N, 12.75 (12.94)%. Repeated attempts

to obtain an elemental analysis with satisfactory % C values failed, presumably due to incomplete combustion of the compound.

Ti{NB(NAr'CH)$_2$}Cl$_2$(py)$_3$ (3). To a Schlenk flask containing Ti{NB(NAr'CH)$_2$}Cl$_2$(NHMe$_2$)$_2$ (**1**, 3.00 g, 4.92 mmol) was added pyridine (5 mL). The brown solution was stirred at room temperature for 10 mins, and then the volatiles removed under reduced pressure to give a yellow-brown waxy solid, which was triturated in hexane (10 mL) to yield **3** as a bright yellow powder. Yield: 3.30 g (89%). Diffraction-quality crystals were grown from a saturated hexane solution at 5 °C.

^{1}H NMR (C$_6$D$_6$, 400.1 MHz): δ 8.72 (4 H, d, ^3J = 4.9 Hz, 2,6-py *cis* to NB(NAr'CH)$_2$), 8.63 (2 H, br. m, 2,6-py *trans* to NB(NAr'CH)$_2$), 7.13–7.06 (6 H, overlapping 2 × m, *m*- and *p*-C$_6$H$_3$^{i}Pr$_2$), 6.89 (1 H, br. m, 4-py *trans* to NB(NAr'CH)$_2$), 6.77 (2 H, t, ^3J = 7.6 Hz, 4-py *cis* to NB(NAr'CH)$_2$), 6.57 (2 H, br. m, 3,5-py *trans* to NB(NAr'CH)$_2$), 6.40 (4 H, m, 3,5-py *cis* to NB(NAr'CH)$_2$), 5.70 (2 H, s, NCH), 3.63 (4 H, sept., ^3J = 6.9 Hz, CHMeMe), 1.50 (12 H, d, ^3J = 6.9 Hz, CHMeMe), 1.26 (12 H, d, ^3J = 6.9 Hz, CHMeMe) ppm. ^{13}C{^{1}H} NMR (C$_6$D$_6$, 100.6 MHz): δ 151.6 (2,6-py *cis* to NB(NAr'CH)$_2$), 150.8 (2,6-py *trans* to NB(NAr'CH)$_2$), 147.3 (*o*-C$_6$H$_3$^{i}Pr$_2$), 140.9 (*i*-C$_6$H$_3$^{i}Pr$_2$), 137.3 (4-py *cis* to NB(NAr'CH)$_2$), 135.7 (4-py *trans* to NB(NAr'CH)$_2$), 127.4 (*p*-C$_6$H$_3$^{i}Pr$_2$), 123.7 (3,5-py *cis* to NB(NAr'CH)$_2$), 123.6 (*m*-C$_6$H$_3$^{i}Pr$_2$), 123.4 (3,5-py *trans* to NB(NAr'CH)$_2$), 116.2 (NCH), 28.8 (CHMeMe), 24.5 (CHMeMe), 24.3 (CHMeMe) ppm. ^{11}B{^{1}H} NMR (C$_6$D$_6$, 128.4 MHz): δ 13.8 ppm. IR (NaCl plates, Nujol mull, cm^{-1}): 3072 (w), 1606 (s), 1219 (s), 1117 (m), 1102 (m), 1073 (m), 1043 (m), 1015 (m), 896 (s), 802 (m), 710 (w), 698 (w), 686 (m), 667 (w), 646 (m), 638 (w), 616 (w). Anal. found (calcd. for C$_{41}$H$_{51}$BCl$_2$N$_6$Ti): C, 64.84 (65.01); H, 6.86 (6.79); N, 10.94 (11.09)%.

Alternative "one-pot" synthesis of Ti{NB(NAr'CH)$_2$}Cl$_2$(py)$_3$ (3). To a solution of Ti(NMe$_2$)$_2$Cl$_2$ (1.54 g, 7.42 mmol) in toluene (15 mL) was slowly added a solution of H$_2$NB(NAr'CH)$_2$ (**2.2**, 3.00 g, 7.42 mmol) in toluene (15 mL), at –78 °C. The mixture was allowed to warm to RT, upon which it became a red/brown slurry. After stirring for 30 mins, all solids had dissolved, leaving a deep red solution, which was stirred at RT for a further 2.5 h. The volatiles were then removed under reduced pressure to leave a red-brown, waxy solid. This was then dissolved in pyridine (10 mL) and stirred at RT for 10 mins. The volatiles were again removed under reduced pressure, to give **3** as a yellow-brown, waxy solid, which was triturated in hexane (10 mL) to yield a bright yellow powder. Yield: 5.31

g (94%). The ^{1}H NMR spectrum was identical to that of a sample prepared from isolated **1**.

Ti(N$_2^{SiMe_3}$N^{Me}){NB(NAr'CH)$_2$}(py) (4). To a Schlenk flask containing Ti{NB(NAr'CH)$_2$}Cl$_2$(py)$_3$ (**3**, 1.48 g, 1.95 mmol) and Li$_2$N$_2^{SiMe_3}$N^{Me} (0.534 g, 1.95 mmol), was added toluene (30 mL) at –78 °C. The mixture was allowed to warm to room temperature and then stirred for 1 h, after which it had become a dark brown suspension. The volatiles were removed under reduced pressure, and the product extracted into pentane (4 × 20 mL). Removal of the solvent under reduced pressure, followed by drying *in vacuo*, resulted in **4** as an orange powder. Yield: 1.24 g (79%). Diffraction-quality crystals were grown from a concentrated hexane solution at 5 °C.

^{1}H NMR (C$_6$D$_6$, 400.1 MHz): δ 8.11 (2 H, m, 2,6-py), 7.24 (6 H, overlapping 2 × m, *m*- and *p*-C$_6$H$_3^{i}$Pr$_2$), 6.76 (1 H, m, 4-py), 6.48 (2 H, m, 3,5-py), 5.89 (2 H, s, NCH), 3.77 (4 H, sept., ^{3}J = 6.8 Hz, CHMeMe), 3.33 (4 H, t, ^{3}J = 5.8 Hz, CH$_2$NSiMe$_3$), 2.61 (2 H, m, CH$_2$NMe), 2.29 (2 H, m, CH$_2$NMe), 1.66 (3 H, s, NMe), 1.56 (12 H, d, ^{3}J = 6.8 Hz, CHMeMe), 1.32 (12 H, d, ^{3}J = 6.8 Hz, CHMeMe), –0.07 (18 H, s, SiMe$_3$) ppm. ^{13}C{^{1}H} NMR (C$_6$D$_6$, 100.6 MHz): δ 154.0 (2,6-py), 147.9 (*o*-C$_6$H$_3^{i}$Pr$_2$), 143.2 (*i*-C$_6$H$_3^{i}$Pr$_2$), 137.9 (4-py), 126.7 (*m*-C$_6$H$_3^{i}$Pr$_2$), 123.6 (*p*-C$_6$H$_3^{i}$Pr$_2$), 123.5 (3,5-py), 117.1 (NCH), 61.2 (CH$_2$NMe), 47.9 (CH$_2$NSiMe$_3$), 46.0 (NMe), 28.7 (CHMeMe), 26.1 (CHMeMe), 24.6 (CHMeMe), 1.7 (SiMe$_3$) ppm. ^{11}B{^{1}H} NMR (C$_6$D$_6$, 128.4 MHz): δ 14.9 ppm. IR (NaCl plates, Nujol mull, cm^{-1}): 1930 (w), 1860 (w), 1650 (w), 1602 (s), 1559 (m), 1406 (m), 1340 (w), 1270 (m), 1238 (s), 1213 (w), 1175 (m), 1137 (w), 1089 (m), 1066 (m), 1040 (m), 966 (m), 934 (m), 922 (w), 876 (w), 828 (s), 758 (w), 740 (w), 694 (m), 668 (m), 646 (m). EI-MS: *m*/*z* = 708 [*M* – py]$^{+}$ (25%). Anal. found (calcd. for C$_{42}$H$_{70}$BN$_7$Si$_2$Ti): C, 63.95 (64.02); H, 8.84 (8.96); N, 12.33 (12.44)%.

Ti(N$_2^{ArF}$N^{Me}){NB(NAr'CH)$_2$}(py) (5). To a Schlenk flask containing Ti{NB(NAr'CH)$_2$}Cl$_2$(py)$_3$ (**3**, 1.50 g, 1.98 mmol) and Li$_2$N$_2^{ArF}$N^{Me} (0.913 g, 1.98 mmol), was added toluene (20 mL) at –78 °C. The mixture was allowed to warm to room temperature and then stirred for 1 hour, after which it had become a dark red suspension. The volatiles were removed under reduced pressure, and the product extracted into pentane (3 × 15 mL). The solvent was removed from the combined extracts under reduced pressure, yielding **5** as a deep red solid, which was then dried *in vacuo*. Yield: 1.51 g (78%). Diffraction-quality crystals were grown from a concentrated pentane solution at 5 °C.

^{1}H NMR (C_6D_6, 400.1 MHz): δ 7.88 (2 H, m, 2,6-py), 7.18 – 7.10 (6 H, overlapping 2 × m with residual protio solvent resonance, *m*- and *p*-$C_6\underline{H}_3{}^{i}Pr_2$), 6.46 (1 H, m, 3,5-py), 6.09 (2 H, m, 4-py), 5.79 (2 H, s, NCH), 3.60 (4 H, sept., ^{3}J = 6.9 Hz, C<u>H</u>MeMe), 3.47 (2 H, m, C<u>H</u>$_2$NAr^{F}), 3.20 (2 H, m, C<u>H</u>$_2$NAr^{F}), 2.49 (2 H, m, C<u>H</u>$_2$NMe), 2.28 (2 H, m, C<u>H</u>$_2$NMe), 1.96 (3 H, s, NMe), 1.28 (12 H, d, ^{3}J = 6.9 Hz, CH<u>Me</u>Me), 1.26 (12 H, d, ^{3}J = 6.9 Hz, CHMe<u>Me</u>) ppm. ^{13}C{^{1}H} NMR (C_6D_6, 100.6 MHz): δ 151.4 (2,6-py), 147.6 (*i*-<u>C</u>$_6$H$_3{}^{i}$Pr$_2$), 144.4 (*o*-C_6F_5), 141.4 (*o*-<u>C</u>$_6$H$_3{}^{i}$Pr$_2$), 139.5 (*m*-C_6F_5), 138.3 (4-py), 137.0 (*i*-C_6F_5), 133.7 (*p*-C_6F_5), 126.9 (*p*-<u>C</u>$_6$H$_3{}^{i}$Pr$_2$), 123.7 (3,5-py), 123.6 (*m*-<u>C</u>$_6$H$_3{}^{i}$Pr$_2$), 116.8 (NCH), 56.7 (<u>C</u>H$_2$NMe), 52.4 (<u>C</u>H$_2$NC$_6F_5$), 46.2 (NMe), 28.6 (<u>C</u>HMeMe), 25.6 (CHMe<u>Me</u>), 23.2 (CH<u>Me</u>Me) ppm. ^{11}B{^{1}H} NMR (C_6D_6, 128.4 MHz): δ 14.7 ppm. ^{19}F{^{1}H} NMR (C_6D_6, 376.5 MHz): δ –149.4 (2 F, d, ^{3}J = 22.4 Hz, *o*-C_6F_5), –166.0 (2 F, app. t, app. ^{3}J = 22.4 Hz, *m*-C_6F_5), –169.9 (1 F, t, ^{3}J = 22.4 Hz, *p*-C_6F_5) ppm. IR (NaCl plates, Nujol mull, cm^{-1}): 3084 (w), 2608 (w), 2459 (w), 1997 (w), 1605 (w), 1583 (m), 1507 (m), 1491 (m), 1446 (w), 1406 (m), 1368 (s), 1303 (m), 1259 (m), 1157 (m), 1114 (w), 1086 (w), 1065 (m), 982 (s), 931 (w), 897 (w), 862 (m), 806 (w), 765 (m), 752 (w), 702 (m), 668 (w), 640 (w). EI-MS: *m*/*z* = 896 [*M* – py]$^{+}$ (4%). Anal. found (calcd. for $C_{48}H_{52}BF_{10}N_7Ti$): C, 59.17 (59.09); H, 5.36 (5.37); N, 9.98 (10.05)%.

Ti(N$_2{}^{iPr}$N^{Me}){NB(NAr'CH)$_2$}(py) (6). To a Schlenk flask containing Ti{NB(NAr'CH)$_2$}Cl$_2$(py)$_3$ (**3**, 1.50 g, 1.98 mmol) and Li$_2$N$_2{}^{iPr}$N^{Me} (0.422 g, 1.98 mmol) was added toluene (30 mL) at –78 °C. The mixture was allowed to warm to RT, and then stirred for 3 h, after which time it had become a deep red suspension. The volatiles were removed under reduced pressure, and the product extracted into pentane (4 × 15 mL). The solvent was removed from the combined extracts under reduced pressure, resulting in **6** as a red solid, which was then dried *in vacuo*. Yield: 1.27 g (88%). Diffraction-quality crystals were grown from a concentrated pentane solution at 5 °C.

^{1}H NMR (C_6D_6, 400.1 MHz): δ 8.01 (2 H, m, 2,6-py), 7.25 (6 H, overlapping 2 × m, *m*- and *p*-$C_6\underline{H}_3{}^{i}Pr_2$), 6.76 (1 H, m, 4-py), 6.40 (2 H, m, 3,5-py), 5.90 (2 H, s, NCH), 3.87 (4 H, sept., ^{3}J = 6.9 Hz, C_6H_3(C<u>H</u>MeMe)$_2$), 3.76 (2 H, sept., ^{3}J = 6.5 Hz, NC<u>H</u>MeMe) 3.29 (2 H, m, C<u>H</u>$_2$N^{i}Pr), 3.08 (2 H, m, C<u>H</u>$_2$N^{i}Pr), 2.77 (2 H, m, C<u>H</u>$_2$NMe), 2.29 (2 H, m, C<u>H</u>$_2$NMe), 1.55 (3 H, s, NMe), 1.50 (12 H, d, ^{3}J = 6.9 Hz, C_6H_3(CH<u>Me</u>Me)$_2$), 1.41 (6 H, d, ^{3}J = 6.5 Hz, NCH<u>Me</u>Me), 1.37 (12 H, d, ^{3}J = 6.9 Hz, C_6H_3(CHMe<u>Me</u>)$_2$), 0.66 (6 H, d, ^{3}J = 6.5 Hz, NCHMe<u>Me</u>) ppm. ^{13}C{^{1}H} NMR (C_6D_6, 100.6 MHz): δ 152.9 (2,6-py), 148.1 (*o*-<u>C</u>$_6$H$_3{}^{i}$Pr$_2$), 143.8 (*i*-<u>C</u>$_6$H$_3{}^{i}$Pr$_2$), 137.1 (4-py), 126.4 (*p*-<u>C</u>$_6$H$_3{}^{i}$Pr$_2$), 123.3 (overlapping *m*-<u>C</u>$_6$H$_3{}^{i}$Pr$_2$ and

3,5-py), 116.8 (NCH), 58.7 (CH$_2$NMe), 51.4 (NCHMeMe), 45.1 (CH$_2$N^{i}Pr), 45.0 (NMe), 28.7 (C$_6$H$_3$(CHMeMe)$_2$), 25.2 (C$_6$H$_3$(CHMeMe)$_2$), 24.3 (C$_6$H$_3$(CHMeMe)$_2$), 21.5 (NCHMeMe), 21.1 (NCHMeMe) ppm. ^{11}B{^{1}H} NMR (C$_6$D$_6$, 128.4 MHz): δ 15.2 ppm. IR (NaCl plates, Nujol mull, cm^{-1}): 2777 (w), 2653 (w), 1601 (s), 1543 (w), 1443 (w), 1422 (m), 1359 (s), 1350 (m), 1337 (s), 1308 (m), 1287 (w), 1272 (w), 1239 (w), 1210 (m), 1179 (w), 1139 (w), 1065 (m), 1040 (w), 1013 (w), 999 (m), 930 (w), 895 (w), 879 (w), 814 (w), 763 (m), 755 (w), 699 (m), 668 (m), 640 (m). Anal. found (calcd. for C$_{42}$H$_{66}$BN$_7$Ti): C, 69.23 (69.32); H, 9.31 (9.14); N, 13.55 (13.47)%.

Ti(N$_2$N^{py}){NB(NAr'CH)$_2$}(py) (7). To a Schlenk flask containing Ti{NB(NAr'CH)$_2$}Cl$_2$(py)$_3$ (**3**, 1.50 g, 1.98 mmol) and Li$_2$N$_2$N^{py} (0.668 g, 2.08 mmol) was added toluene (25 mL) at –78 °C. The mixture was allowed to warm to room temperature and then stirred for 3 h, after which it had become a dark orange suspension. The volatiles were removed under reduced pressure, and the product extracted into hexane (2 × 20 mL). The solvent was removed from the combined extracts under reduced pressure, resulting in **7** as an orange solid, which was dried *in vacuo*. Yield: 1.38 g (83%). Diffraction-quality crystals were grown from a concentrated pentane solution cooled to 5 °C.

^{1}H NMR (C$_6$D$_6$, 400.1 MHz): δ 8.70 (2 H, d, ^3J = 4.6 Hz, 2,6-py), 8.05 (1 H, br. m, 6-C$_5$H$_4$N), 7.18 (6 H, overlapping 2 × m, *m*- and *p*-C$_6$H$_3$^{i}Pr$_2$), 7.03 (1 H, m, 4-py), 6.88 (1 H, m, 4-C$_5$H$_4$N), 6.70 (1 H, d, ^3J = 8.0 Hz, 3-C$_5$H$_4$N), 6.53 (3 H, m, overlapping 3,5-py and 5-C$_5$H$_4$N), 5.89 (2 H, s, NCH), 3.90 (4 H, sept., ^3J = 6.9 Hz, CHMeMe), 3.36 (2 H, d, ^2J = 12.4 Hz, NCH$_2$), 3.09 (2 H, d, ^2J = 12.4 Hz, NCH$_2$), 1.40 (12 H, d, ^3J = 6.9 Hz, CHMeMe), 1.34 (12 H, d, ^3J = 6.9 Hz, CHMeMe), 0.94 (3 H, s, CMe), 0.09 (18 H, s, SiMe$_3$) ppm. ^{13}C{^{1}H} NMR (C$_6$D$_6$, 100.6 MHz): δ 159.6 (2-C$_5$H$_4$N), 150.9 (2,6-py), 150.6 (6-C$_5$H$_4$N), 147.6 (*o*-C$_6$H$_3$^{i}Pr$_2$), 143.2 (*i*-C$_6$H$_3$^{i}Pr$_2$), 137.1 (4-py), 136.6 (4-C$_5$H$_4$N), 126.6 (*p*-C$_6$H$_3$^{i}Pr$_2$), 123.7 (*m*-C$_6$H$_3$^{i}Pr$_2$), 123.3 (3,5-py), 121.2 (5-C$_5$H$_4$N), 119.9 (3-C$_5$H$_4$N), 117.3 (NCH), 63.9 (NCH$_2$), 45.3 (CMe), 28.5 (CHMeMe), 26.2 (CHMeMe), 24.4 (CHMeMe), 24.0 (CMe), 1.0 (SiMe$_3$) ppm. ^{11}B{^{1}H} NMR (C$_6$D$_6$, 128.4 MHz): δ 14.5 ppm. IR (NaCl plates, Nujol mull, cm^{-1}): 2781 (w), 1601 (s), 1570 (m), 1240 (m), 1209 (w), 1177 (w), 1113 (m), 1053 (s), 994 (m), 952 (w), 892 (m), 875 (w), 829 (m), 775 (w), 762 (m), 701 (m), 668 (m), 643 (m), 560 (w). EI-MS: *m*/*z* = 756 [*M* – py]$^+$ (38%). Anal. found (calcd. for C$_{46}$H$_{70}$BN$_7$Si$_2$Ti): C, 65.95 (66.09); H, 8.58 (8.44); N, 11.88 (11.73)%.

Ti($N_2^{pyr}N^{Me}$){NB(NAr'CH)$_2$}(py)$_2$ (8). To a Schlenk flask containing Ti{NB(NAr'CH)$_2$}Cl$_2$(py)$_3$ (**3**, 0.500 g, 0.660 mmol) and $Li_2N_2N^{py}$ (0.139 g, 0.693 mmol) was added toluene at –78 °C. The mixture was allowed to warm to RT and then stirred for 45 minutes, after which time it had become a deep red suspension. The volatiles were removed under reduced pressure, and then the product extracted into Et_2O (3 × 10 mL). The combined extracts were concentrated by ~75% and cooled to –80 °C, resulting in the formation of **8** as a pale orange powder, which was then washed with pentane (5 mL) and dried *in vacuo*. Yield: 0.180 g (34%). Diffraction-quality crystals were grown from a concentrated Et_2O solution at 5 °C.

^{1}H NMR (C_6D_6, 400.1 MHz): δ 7.98 (2 H, m, 2-pyr), 7.80 (2 H, d, ^3J = 4.9 Hz, 2,6-py), 7.69 (2 H, d, ^3J = 4.9 Hz, 2,6-py), 6.82 (6 H, overlapping 2 × m, *m*- and *p*-$C_6\underline{H}_3{}^iPr_2$), 6.78 (2 H, m, 3-pyr), 6.65 (1 H, t, ^3J = 7.5 Hz, 4-py), 6.54 (1 H, t, ^3J = 7.5 Hz, 4-py), 6.26 (2 H, d, ^3J = 2.25 Hz, 4-pyr), 6.22 (2 H, m, 3,5-py), 6.13 (2 H, m, 3,5-py), 5.68 (2 H, s, NCH), 3.65 (4 H, sept., ^3J = 6.9 Hz, C<u>H</u>MeMe), 2.98 (4 H, s, NC<u>H</u>$_2$pyr), 1.48 (12 H, d, ^3J = 6.9 Hz, CH<u>Me</u>Me), 1.27 (3 H, s, NMe), 1.24 (12 H, d, ^3J = 6.9 Hz, CHMe<u>Me</u>) ppm. ^{13}C{^{1}H} NMR (C_6D_6, 100.6 MHz): δ 115.8 (2,6-py), 150.6 (2,6-py), 146.1 (*o*-<u>C</u>$_6$H$_3{}^iPr_2$), 141.6 (*i*-<u>C</u>$_6$H$_3{}^iPr_2$), 139.1 (5-pyr), 137.4 (4-py), 137.1 (4-py), 130.6 (2-pyr), 126.7 (*p*-<u>C</u>$_6$H$_3{}^iPr_2$), 124.2 (3,5-py), 123.8 (3,5-py), 123.0 (*m*-<u>C</u>$_6$H$_3{}^iPr_2$), 116.9 (NCH), 108.9 (3-pyr), 104.1 (4-pyr), 60.0 (N<u>C</u>H$_2$pyr), 44.7 (NMe), 28.6 (<u>C</u>HMeMe), 25.4 (CHMe<u>Me</u>), 24.1 (CH<u>Me</u>Me) ppm. ^{11}B{^{1}H} NMR (C_6D_6, 128.4 MHz): δ 13.2 ppm. IR (NaCl plates, Nujol mull, cm^{-1}): 3076 (w), 3055 (w), 2011 (w), 1867 (w), 1602 (s), 1585 (w), 1543 (w), 1417 (m), 1331 (w), 1320 (m), 1287 (w), 1275 (w), 1242 (w), 1218 (s), 1185 (m), 1172 (m), 1128 (w), 1116 (m), 1106 (m), 1040 (m), 1029 (m), 1010 (m), 973 (s), 932 (w), 891 (m), 876 (m), 860 (m), 760 (m), 740 (m), 700 (w), 664 (w), 654 (m), 632 (m), 621 (w). Anal. found (calcd. for $C_{47}H_{59}BN_8Ti$): C, 70.92 (71.03); H, 7.57 (7.48); N, 13.96 (14.10)%.

6.6 Experimental details and characterising data for Chapter Three

Cp*Ti{NB(NAr'CH)$_2$}Cl(py) (9). To a Schlenk flask were added Cp*Ti(N^{t}Bu)Cl(py) (**1.8**, 2.00 g, 5.42 mmol) and H_2NB(NAr'CH)$_2$ (**2.2**, 1.97 g, 4.88 mmol). The two solids were heated with stirring to 140 °C, at which temperature they melted to form a dark brown oil. Repeated, brief exposures to a dynamic vacuum resulted in bubbling of the oil as H_2N^tBu was released; the cessation of bubbling and no further diminishment of the vacuum (as measured by a Pirani gauge) indicated reaction completion. The oil was allowed to cool

to RT, forming a deep red glassy solid, which was triturated in hexane (10 mL) to yield **9** as a red powder, before washing with further hexane (2 × 10 ml) and drying *in vacuo*. Yield: 2.02 g (59%). Diffraction-quality crystals were grown from a saturated benzene/hexane solution at RT.

^{1}H NMR (C_6D_6, 400.1 MHz): δ 7.88 (2 H, d, ^{3}J = 4.7 Hz, 2,6-py), 7.25 (2 H, dd, ^{3}J = 7.8 Hz, ^{4}J = 1.5 Hz, *m*-$C_6\underline{H}_3{}^{i}Pr_2$ closest to py), 7.17–7.12 (2 H, m overlapping with residual protio solvent resonance, *p*-$C_6\underline{H}_3{}^{i}Pr_2$), 7.00 (2 H, dd, ^{3}J = 7.8 Hz, ^{4}J = 1.5 Hz, *m*-$C_6\underline{H}_3{}^{i}Pr_2$ closest to Cl), 6.65 (1 H, t, ^{3}J = 7.8 Hz, 4-py), 6.22 (2 H, m, 3,5-py), 5.87 (2 H, s, NCH), 3.92 (2 H, sept., ^{3}J = 6.9 Hz, C<u>H</u>MeMe closest to py), 3.67 (2 H, sept., ^{3}J = 6.9 Hz, C<u>H</u>MeMe closest to Cl), 1.71 (15 H, s, C_5Me_5), 1.61 (6 H, d, ^{3}J = 6.8 Hz, CH<u>Me</u>Me closest to py), 1.31 (12 H, app. t, app. ^{3}J = 7.3 Hz, overlapping CHMe<u>Me</u> closest to py and CH<u>Me</u>Me closest to Cl), 1.26 (6 H, d, ^{3}J = 6.8 Hz, CHMe<u>Me</u> closest to Cl) ppm. ^{13}C{^{1}H} NMR (C_6D_6, 100.6 MHz): δ 150.4 (2,6-py), 147.3 (*o*-$\underline{C}_6H_3{}^{i}Pr_2$ closest to Cl), 147.0 (*o*-$\underline{C}_6H_3{}^{i}Pr_2$ to py), 141.9 (*i*-$\underline{C}_6H_3{}^{i}Pr_2$), 126.9 (*p*-$\underline{C}_6H_3{}^{i}Pr_2$), 123.8 (3,5-py), 123.8 (*m*-$\underline{C}_6H_3{}^{i}Pr_2$ closest to Cl), 123.1 (*m*-$\underline{C}_6H_3{}^{i}Pr_2$ closest to py), 121.8 ($\underline{C}_5Me_5$), 116.9 (NCH), 29.0 (<u>C</u>HMeMe closest to py), 28.4 (<u>C</u>HMeMe closest to Cl), 26.0 (CHMe<u>Me</u> closest to Cl), 24.9 (CHMe<u>Me</u> closest to py), 24.2 (CH<u>Me</u>Me closest to Cl), 23.6 (CH<u>Me</u>Me closest to py), 12.0 ($C_5\underline{Me}_5$) ppm. ^{11}B{^{1}H} NMR (C_6D_6, 128.4 MHz): δ 15.5 ppm. IR (NaCl plates, Nujol mull, cm^{-1}): 3583 (w), 3064 (m), 2724 (m), 1936 (w), 1868 (w), 1801 (w), 1663 (m), 1606 (s), 1585 (w), 1328 (m), 1308 (w), 1275 (m), 1215 (m), 1178 (w), 1154 (m), 1114 (m), 1070 (m), 1046 (m), 1017 (w), 1009 (w), 894 (m), 883 (w), 803 (m), 763 (m), 755 (m), 721 (w), 681 (w), 651 (s). EI-MS: *m*/*z* = 698 [*M*]$^{+}$ (1%). Anal. found (calcd. for $C_{41}H_{56}BClN_4Ti$): C, 70.35 (70.45); H, 7.95 (8.07); N, 7.95 (8.01)%.

Alternative NMR tube scale synthesis of Cp*Ti{NB(NAr'CH)$_2$}Cl(py) (9). To an NMR tube fitted with a J. Youngs valve was added a C_6D_6 solution (0.6 mL) of Ti{NB(NAr'CH)$_2$}Cl$_2$(py)$_3$ (**3**, 0.0192 g, 0.0253 mmol) and LiCp* (0.0360 g, 0.0253 mmol). The tube was heated at 70 °C for 72 h, after which the ^{1}H NMR spectrum indicated quantitative conversion to **9**.

Cp*Ti(hpp){NB(NAr'CH)$_2$} (10). To a Schlenk tube containing Cp*Ti{NB(NAr'CH)$_2$}Cl(py) (**9**, 1.50 g, 2.15 mmol) and Li[hpp] (0.311 g, 2.15 mmol), was added toluene (20 mL) at –78 °C. The mixture was allowed to warm to RT and then stirred at 50 °C for 16 h, after which time it had turned dark brown. The volatiles were

removed under reduced pressure, and then the product extracted into pentane (5 × 20 mL). Removal of the pentane under reduced pressure resulted in a brown waxy solid, which was triturated in hexane (10 mL) to produce **10** as a brown powder, which was then dried *in vacuo*. Yield: 1.05 g (68%). Diffraction-quality crystals were grown from a saturated hexane solution.

^{1}H NMR (C_6D_6, 400.1 MHz): δ 7.22 (6 H, overlapping 2 × m, *m*- and *p*-$C_6\underline{H}_3{}^{i}Pr_2$), 5.89 (2 H, s, NCH), 3.55 (4 H, sept., ^{3}J = 6.9 Hz, C<u>H</u>MeMe), 2.86 (2 H, m, TiNC<u>H</u>$_2$), 2.71 (2 H, m, N_2CNCH_2), 2.48 (4 H, overlapping 2 × m, TiNC<u>H</u>$_2$ and N_2CNCH_2), 1.87 (15 H, s, C_5Me_5), 1.45 (12 H, d, ^{3}J = 6.8 Hz, CH<u>Me</u>Me), 1.39 (4 H, m, $CH_2C\underline{H}_2CH_2$), 1.29 (12 H, d, ^{3}J = 6.8 Hz, CHMe<u>Me</u>) ppm. ^{13}C{^{1}H} NMR (C_6D_6, 100.6 MHz): δ 151.7 (N_2CN), 147.1 (*o*-$\underline{C}_6H_3{}^{i}Pr_2$), 142.2 (*i*-$\underline{C}_6H_3{}^{i}Pr_2$), 126.3 (*p*-$\underline{C}_6H_3{}^{i}Pr_2$), 123.3 (*m*-$\underline{C}_6H_3{}^{i}Pr_2$), 120.1 ($\underline{C}_5Me_5$), 116.0 (NCH), 47.1 ($N_2CN\underline{C}H_2$), 43.5 (TiN<u>C</u>H$_2$), 28.6 (<u>C</u>HMeMe), 25.0 (CHMe<u>Me</u>), 24.4 (CH<u>Me</u>Me), 24.0 ($CH_2\underline{C}H_2CH_2$), 11.5 ($C_5\underline{Me}_5$) ppm. ^{11}B{^{1}H} NMR (C_6D_6, 128.4 MHz): δ 14.6 ppm. IR (NaCl plates, Nujol mull, cm^{-1}): 2728 (w), 1584 (w), 1543 (m), 1499 (s), 1319 (w), 1295 (m), 1261 (m), 1202 (w), 1147 (w), 1099 (w), 802 (m), 762 (w), 721 (w), 668 (w), 648 (w). EI-MS: *m*/*z* = 722 [*M*]$^{+}$ (1%). Anal. found (calcd. for $C_{43}H_{63}BN_6Ti$): C, 71.35 (71.46); H, 8.90 (8.79); N, 11.57 (11.63)%.

Cp*Ti(N^{pyr}N^{Me_2}){NB(NAr'CH)$_2$} (11). To a Schlenk tube containing Cp*Ti{NB(NAr'CH)$_2$}Cl(py) (**9**, 0.600 g, 0.858 mmol) and LiN^{pyr}N^{Me_2} (0.112 g, 0.858 mmol), was added toluene (10 mL) at –78 °C. The mixture was allowed to warm to RT and then stirred at 50 °C for 16 h, after which time it had turned dark brown. The volatiles were removed under reduced pressure, and then the product extracted into pentane (3 × 10 mL). The extracts were concentrated by ~70% under reduced pressure, and cooled to 5 °C; after 16 h, dark brown crystalline **11** had formed. After isolation of the crystals, a second crop was obtained at the same conditions. Total yield: 0.432 g (71%). Diffraction-quality crystals were grown from a concentrated hexane solution at 5 °C.

^{1}H NMR (C_6D_6, 400.1 MHz): δ 7.22–7.15 (6 H, overlapping 2 × m with residual protio solvent resonance, *m*- and *p*-$C_6\underline{H}_3{}^{i}Pr_2$), 6.77 (1 H, m, 2-pyr), 6.52 (1 H, m, 3-pyr), 6.33 (1 H, m, 4-pyr), 5.90 (2 H, s, NCH), 4.63 (1 H, d, ^{2}J = 12.5 Hz, C<u>H</u>$_2$NMe$_2$), 3.62 (2 H, sept., ^{3}J = 6.9 Hz, C<u>H</u>MeMe closest to pyr), 3.44 (2 H, sept., ^{3}J = 6.9 Hz, C<u>H</u>MeMe closest to NMe$_2$), 2.93 (1 H, d, ^{2}J = 12.5 Hz, C<u>H</u>$_2$NMe$_2$), 1.77 (15 H, s, C_5Me_5), 1.57 (3 H, s, N<u>Me</u>Me), 1.51 (3 H, s, NMe<u>Me</u>), 1.46 (6 H, d, ^{3}J = 6.9 Hz, CH<u>Me</u>Me closest to NMe$_2$),

1.29 (6 H, d, ^3J = 6.9 Hz, CHMeMe closest to pyr), 1.24 (6 H, d, ^3J = 6.9 Hz, CHMeMe closest to NMe_2), 1.15 (6 H, d, ^3J = 6.9 Hz, CHMeMe closest to pyr) ppm. $^{13}C\{^1H\}$ NMR (C_6D_6, 100.6 MHz): δ 147.0 (*o*-$C_6H_3{}^iPr_2$ closest to pyr), 146.8 (*o*-$C_6H_3{}^iPr_2$ closest to NMe_2), 142.0 (*i*-$C_6H_3{}^iPr_2$), 132.2 (5-pyr), 126.9 (*p*-$C_6H_3{}^iPr_2$), 124.0 (*m*-$C_6H_3{}^iPr_2$ closest to NMe_2), 123.3 (*m*-$C_6H_3{}^iPr_2$ closest to pyr), 122.5 (C_5Me_5), 117.2 (NCH), 107.9 (3-pyr), 105.7 (4-pyr), 63.5 (CH_2NMe_2), 49.5 (NMeMe), 47.5 (NMeMe), 29.1 (CHMeMe closest to pyr), 28.4 (CHMeMe closest to NMe_2), 27.2 (CHMeMe closest to NMe_2), 25.5 (CHMeMe closest to pyr), 23.3 (CHMeMe closest to NMe_2), 23.0 (CHMeMe closest to pyr), 12.2 (C_5Me_5) ppm. $^{11}B\{^1H\}$ NMR (C_6D_6, 128.4 MHz): δ 15.3 ppm. IR (NaCl plates, Nujol mull, cm^{-1}): 3115 (w), 3062 (w), 2727 (w), 1931 (w), 1866 (w), 1584 (m), 1557 (w), 1273 (m), 1260 (m), 1223 (m), 1184 (s), 1163 (s), 1139 (w), 1117 (m), 1105 (w), 1068 (m), 981 (m), 959 (s), 889 (m), 844 (m), 802 (m), 760 (s), 722 (m), 668 (m), 656 (m). EI-MS: *m*/*z* = 707 $[M]^+$ (12%). Anal. found (calcd. for $C_{43}H_{62}BN_5Ti$): C, 72.83 (72.98); H, 9.00 (8.83); N, 9.85 (9.90)%.

$Cp_2Ti\{NB(NAr'CH)_2\}(py)$ (12). To a Schlenk flask containing $Ti\{NB(NAr'CH)_2\}Cl_2(py)_3$ (**3**, 0.500 g, 0.660 mmol) and NaCp (0.122 g, 1.39 mmol) was added toluene (10 mL) at –78 °C. The mixture was allowed to warm to RT, and then stirred for 3 h, after which it had become a deep brown suspension. The volatiles were removed under reduced pressure, and the product extracted into pentane (4 × 10 mL). The combined extracts were evaporated to dryness, giving **12** as an orange powder. Yield: 0.253 g (58%). Diffraction-quality crystals were grown from a concentrated pentane solution at 5 °C.

^1H NMR (C_6D_6, 400.1 MHz): δ 7.96 (2 H, d, ^3J = 4.9 Hz, 2,6-py), 7.31–7.25 (6 H, overlapping 2 × m, *m*- and *p*-$C_6H_3{}^iPr_2$), 6.71 (1 H, t, ^3J = 7.7 Hz, 4-py), 6.23 (2 H, m, 3,5-py), 5.94 (2 H, s, NCH), 5.69 (10 H, s, C_5H_5), 3.74 (4 H, sept., ^3J = 6.9 Hz, CHMeMe), 1.49 (12 H, d, ^3J = 6.9 Hz, CHMeMe), 1.30 (12 H, d, ^3J = 6.9 Hz, CHMeMe) ppm. $^{13}C\{^1H\}$ NMR (C_6D_6, 100.6 MHz): δ 155.1 (2,6-py), 147.5 (*o*-$C_6H_3{}^iPr_2$), 142.2 (*i*-$C_6H_3{}^iPr_2$), 136.4 (4-py), 127.0 (*m*-$C_6H_3{}^iPr_2$), 123.7 (*p*-$C_6H_3{}^iPr_2$), 123.6 (3,5-py), 117.2 (NCH), 111.4 (C_5H_5), 28.9 (CHMeMe), 25.7 (CHMeMe), 23.6 (CHMeMe) ppm. $^{11}B\{^1H\}$ NMR (C_6D_6, 128.4 MHz): δ 18.0 ppm. IR (NaCl plates, Nujol mull, cm^{-1}): 1602 (m), 1583 (w), 1543 (m), 1403 (w), 1215 (m), 1178 (w), 1068 (m), 1023 (m), 936 (w), 883 (w), 863 (s), 763 (w), 699 (m), 668 (m), 653 (w). EI-MS: *m*/*z* = 580 $[M - py]^+$ (4%). Anal. found (calcd. for $C_{41}H_{51}BN_4Ti$): C, 74.61 (74.78); H, 7.96 (7.81); N, 8.64 (8.51)%.

CpTi{NB(NAr'CH)$_2$}Cl(py) (13). A mixture of Ti{NB(NAr'CH)$_2$}Cl$_2$(py)$_3$ (**3**, 0.811 g, 1.07 mmol) and Cp$_2$Ti{NB(NAr'CH)$_2$}(py) (**12**, 0.700 g, 1.07 mmol) in toluene (25 mL) was stirred at 70 °C for 5 days, after which the volatiles were removed under reduced pressure. The product was triturated in hexane (10 mL) and filtered, affording **13** as a deep brown solid. Yield: 1.01 g (75%).

^{1}H NMR (C$_6$D$_6$, 400.1 MHz): δ 7.85 (2 H, d, ^3J = 4.6 Hz, 2,6-py), 7.24 – 7.23 (6 H, overlapping 2 × m, *m*- and *p*-C$_6$H$_3$^{i}Pr$_2$), 6.67 (1 H, t, ^3J = 7.4 Hz, 4-py), 6.27 (2 H, m, 3,5-py), 5.93 (5 H, s, C$_5$H$_5$), 5.89 (2 H, s, NCH), 3.62 (4 H, sept., ^3J = 6.8 Hz, CHMeMe), 1.57 (6 H, d, ^3J = 6.8 Hz, CHMeMe), 1.49 (6 H, d, ^3J = 6.8 Hz, CHMeMe), 1.29 (12 H, app. t, app. ^3J = 6.4 Hz, CHMeMe) ppm. ^{13}C{^{1}H} NMR (C$_6$D$_6$, 100.6 MHz): δ 152.2 (2,6-py), 147.05 (*o*-C$_6$H$_3$^{i}Pr$_2$), 146.8 (*o*-C$_6$H$_3$^{i}Pr$_2$), 140.3 (*i*-C$_6$H$_3$^{i}Pr$_2$), 137.8 (4-py), 126.8 (*m*-C$_6$H$_3$^{i}Pr$_2$), 123.7 (3,5-py), 123.4 (*p*-C$_6$H$_3$^{i}Pr$_2$), 123.0 (*p*-C$_6$H$_3$^{i}Pr$_2$), 115.7 (NCH), 112.4 (C$_5$H$_5$), 28.4 (CHMeMe), 24.6 (CHMeMe), 24.3 (CHMeMe), 23.9 (CHMeMe), 23.7 (CHMeMe) ppm. ^{11}B{^{1}H} NMR (C$_6$D$_6$, 128.4 MHz): δ 16.0 ppm. IR (NaCl plates, Nujol mull, cm^{-1}): 3063 (m), 1869 (w), 1800 (w), 1715 (w), 1661 (w), 1604 (s), 1416 (s), 1331 (m), 1275 (m), 1238 (w), 1214 (m), 1179 (w), 1119 (m), 1046 (w), 934 (w), 900 (m), 880 (w), 770 (w), 760 (m), 700 (m), 668 (w), 652 (m). Anal. found (calcd. for C$_{36}$H$_{46}$BClN$_4$Ti): C, 68.70 (68.75); H, 7.47 (7.37); N, 8.81 (8.91)%.

CpTi{MeC(N^{i}Pr)$_2$}{NB(NAr'CH)$_2$} (14). A mixture of CpTi{NB(NAr'CH)$_2$}Cl(py) (**13**, 0.500 g, 0.795 mmol) and Li[MeC(N^{i}Pr)$_2$] (0.118 g, 0.795 mmol) in toluene (15 mL) was heated at 50 °C for 16 h. The volatiles were then removed under reduced pressure and the product extracted into pentane (3 × 10 mL). Removal of the solvent under reduced pressure afforded **14** as a brown, waxy solid. Yield: 0.380 g (73%).

^{1}H NMR (C$_6$D$_6$, 400.1 MHz): δ 7.27 (6 H, overlapping 2 × m, *m*- and *p*-C$_6$H$_3$^{i}Pr$_2$), 6.04 (5 H, s, C$_5$H$_5$), 5.81 (2 H, s, NCH), 3.50 (4 H, sept., ^3J = 6.9 Hz, C$_6$H$_3$(CHMeMe)$_2$), 3.32 (2 H, sept., ^3J = 6.3 Hz, MeC(NCHMeMe)$_2$), 1.48 (12 H, d, ^3J = 6.9 Hz, C$_6$H$_3$(CHMeMe)$_2$), 1.47 (3 H, s overlapped with C$_6$H$_3$(CHMeMe)$_2$ resonance, MeC(N^{i}Pr)$_2$), 1.29 (12 H, d, ^3J = 6.9 Hz, C$_6$H$_3$(CHMeMe)$_2$), 0.78 (6 H, d, ^3J = 6.3 Hz, MeC(NCHMeMe)$_2$), 0.59 (6 H, d, ^3J = 6.3 Hz, MeC(NCHMeMe)$_2$) ppm. ^{13}C{^{1}H} NMR (C$_6$D$_6$, 100.6 MHz): δ 159.44 (MeC(N^{i}Pr)$_2$), 147.0 (*o*-C$_6$H$_3$^{i}Pr$_2$), 141.5 (*i*-C$_6$H$_3$^{i}Pr$_2$), 127.0 (*p*-C$_6$H$_3$^{i}Pr$_2$), 123.4 (*m*-C$_6$H$_3$^{i}Pr$_2$), 116.9 (NCH), 112.0 (C$_5$H$_5$), 48.4 (MeC(NCHMeMe)$_2$), 28.7 (C$_6$H$_3$(CHMeMe)$_2$), 25.4 (MeC(NCHMeMe)$_2$), 24.8 (C$_6$H$_3$(CHMeMe)$_2$), 24.4

($C_6H_3(CH\underline{Me}Me)_2$), 24.3 ($MeC(NCHMe\underline{Me})_2$), 10.5 ($\underline{Me}C(N^iPr)_2$) ppm. $^{11}B\{^1H\}$ NMR (C_6D_6, 128.4 MHz): δ 15.1 ppm. IR (NaCl plates, Nujol mull, cm^{-1}): 3484 (w), 3409 (m), 1652 (w), 1597 (s), 1552 (w), 1361 (s), 1330 (m), 1275 (m), 1221 (m), 1142 (w), 1120 (s), 1072 (w), 1058 (w), 935 (m), 894 (w), 763 (m), 696 (w), 654 (m). Anal. found (calcd. for $C_{39}H_{58}BN_5Ti$): C, 71.30 (71.45); H, 8.78 (8.92); N, 10.52 (10.68)%.

Reaction of Cp*Ti(hpp){NB(NAr'CH)$_2$} (10) with CO_2: synthesis of [Cp*Ti(hpp)(μ-O)]$_2$ (17) and OCNB(NAr'CH)$_2$ (15). A solution of Cp*Ti(hpp){NB(NAr'CH)$_2$} (**10**, 0.400 g, 0.553 mmol) in benzene (10 mL) was freeze-pump-thaw-degassed three times. The solution was then exposed to CO_2 at a pressure of *ca* 1.1 atm. After 5 minutes the solution had turned orange, and the mixture was left to stir at RT for 2.5 days. The volatiles were then removed under reduced pressure, and the crude mixture separated with hexane (3 × 10 mL). The filtrate was concentrated to 10 mL and cooled to –80 °C overnight, after which pale yellow crystals of **15** had formed. Yield: 0.0910 g (38%). Diffraction-quality crystals of **15** were grown from a hexane solution at –30 °C. **17** was isolated as the yellow solid remaining from the separation. Yield: 0.153 g (82%). Diffraction-quality crystals of **17** were grown from a benzene solution at RT.

*Data for [Cp*Ti(hpp)(μ-O)]$_2$ (**17**, major isomer).* ^1H NMR (CD_2Cl_2, 400.1 MHz): δ 4.17 (2 H, m, $TiNCH_2$), 3.43 (2 H, m, $TiNCH_2$), 3.27 (4 H, m overlapping with minor isomer, N_2CNCH_2), 1.98 (4 H, m, $CH_2C\underline{H}_2CH_2$), 1.85 (15 H, s, C_5Me_5) ppm. $^{13}C\{^1H\}$ NMR (C_6D_6, 100.6 MHz): δ 154.0 (N_2CN), 122.3 ($\underline{C}_5Me_5$), 50.1 ($N_2CN\underline{C}H_2$), 48.7 ($TiNCH_2$), 23.3 ($CH_2\underline{C}H_2CH_2$), 12.0 ($C_5\underline{Me}_5$) ppm.

*Data for [Cp*Ti(hpp)(μ-O)]$_2$ (**17**, minor isomer).* ^1H NMR (CD_2Cl_2, 400.1 MHz): δ 3.94 (2 H, m, $TiNCH_2$), 3.27 (4 H, m overlapping with minor isomer, N_2CNCH_2), 3.03 (2 H, m, $TiNCH_2$), 1.91 (4 H, m, $CH_2C\underline{H}_2CH_2$), 1.84 (15 H, s, C_5Me_5) ppm. $^{13}C\{^1H\}$ NMR (CD_2Cl_2, 100.6 MHz): δ 152.8 (N_2CN), 121.3 ($\underline{C}_5Me_5$), 50.1 ($N_2CN\underline{C}H_2$), 43.5 ($TiNCH_2$), 23.1 ($CH_2\underline{C}H_2CH_2$), 11.9 ($C_5\underline{Me}_5$) ppm.

*Common data for [Cp*Ti(hpp)(μ-O)]$_2$ (**17**).* IR (NaCl plates, Nujol mull, cm^{-1}): 1792 (w), 1771 (w), 1733 (w), 1667 (s), 1579 (s), 1504 (s), 1395 (m), 1350 (m), 1318 (s), 1212 (s), 1173 (m), 1115 (m), 1067 (m), 978 (m), 943 (m), 904 (m), 864 (s), 757 (w), 670 (s). EI-MS: m/z = 539 $[M - Cp^*]^+$ (100%). Anal. found (calcd. for $C_{34}H_{54}N_6O_2Ti_2$): C, 60.32 (60.54); H, 7.91 (8.07); N, 12.29 (12.46)%.

*Data for OCNB(NAr'CH)$_2$ (**15**).* ^{1}H NMR (C_6D_6, 400.1 MHz): δ 7.23 – 7.12 (6 H, overlapping 2 × m with residual protio solvent resonance, *m*- and *p*-$C_6\underline{H}_3{}^i Pr_2$), 5.95 (2 H, s, NCH), 3.14 (4 H, sept., ^3J = 6.9 Hz, C<u>H</u>MeMe), 1.26 (12 H, d, ^3J = 6.9 Hz, CH<u>Me</u>Me), 1.19 (12 H, d, ^3J = 6.9 Hz, CHMe<u>Me</u>) ppm. $^{13}C\{^1H\}$ NMR (C_6D_6, 125.7 MHz): δ 146.5 (*o*-$\underline{C}_6H_3{}^i Pr_2$), 136.8 (*i*-$\underline{C}_6H_3{}^i Pr_2$), 128.5 (*p*-$\underline{C}_6H_3{}^i Pr_2$), 125.7 (NCO), 123.9 (*m*-$\underline{C}_6H_3{}^i Pr_2$), 118.2 (NCH), 28.9 (<u>C</u>HMeMe), 24.4 (CH<u>Me</u>Me), 24.1 (CHMe<u>Me</u>) ppm. $^{11}B\{^1H\}$ NMR (C_6D_6, 128.4 MHz): δ 17.8 ppm. IR (NaCl plates, Nujol mull, cm^{-1}): 3117 (w), 3070 (w), 3028 (w), 2388 (w), 2305 (s, NCO as stretch), 1940 (m), 1868 (m), 1715 (w), 1682 (w), 1587 (w), 1573 (w), 1537 (s), 1502 (s), 1407 (m), 1360 (m), 1231 (m), 1192 (m), 1179 (w), 1116 (w), 1102 (w), 1059 (m), 1041 (w), 937 (m), 910 (m), 760 (m), 692 (m), 668 (w), 649 (m), 597 (w). EI-HRMS: *m/z* found (calcd. for $C_{27}H_{36}BN_3O$, $[M]^+$) 429.2957 (429.2951). Anal. found (calcd. for $C_{27}H_{36}BN_3O$): C, 75.44 (75.52); H, 8.54 (8.45); N, 9.63 (9.79)%.

Independent synthesis of OCNB(NAr'CH)$_2$ (15). To a Schlenk flask containing BrB(NAr'CH)$_2$ (0.400 g, 0.856 mmol) and AgOCN (0.128 g, 0.856 mmol) was added MeCN (15 mL). The mixture was stirred for 16 hours, resulting in a dark grey suspension. The solvent was removed under reduced pressure, and the product extracted into hexane (3 × 10 mL). Removal of the solvent under reduced pressure, followed by drying *in vacuo* gave **15** as an off-white powder. Yield: 0.261 g (71%). The ^{1}H NMR spectrum was identical to that of the sample prepared from the borylimide **10**.

Reaction of Cp*Ti(hpp){NB(NAr'CH)$_2$} (10) with CS$_2$: synthesis of [Cp*Ti(hpp)(μ-S)]$_2$ (18) and SCNB(NAr'CH)$_2$ (16). To a solution of Cp*Ti(hpp){NB(NAr'CH)$_2$} (**10**, 0.400 g, 0.553 mmol) in toluene (15 mL) was added CS_2 (134 μL, 2.21 mmol). The mixture was heated to 80 °C, then stirred for 3.5 days. The volatiles were then removed under reduced pressure, and the crude mixture separated with hexane (3 × 5 mL). The filtrate was concentrated to 5 mL and cooled to –80 °C overnight, after which pale green crystals of **16** had formed. Yield: 0.106 g (43%). Diffraction-quality crystals of **16** were grown from a hexane solution at –30 °C. **18** was isolated as the red solid remaining from the separation. Yield: 0.103 g (53%). Diffraction-quality crystals of **18** were grown from a benzene solution at RT.

*Data for [Cp*Ti(hpp)(μ-S)]$_2$ (**18**).* ^{1}H NMR (C_6D_6, 400.1 MHz): δ 3.65 (2 H, m, TiNC$\underline{H}_2$), 3.11 (2 H, m, TiNC$\underline{H}_2$), 2.94 (2 H, m, N_2CNC$\underline{H}_2$), 2.60 (2 H, m, N_2CNC$\underline{H}_2$), 2.36 (15 H, s, C_5Me_5), 1.70 (4 H, m, $CH_2C\underline{H}_2CH_2$) ppm. $^{13}C\{^1H\}$ NMR (C_6D_6, 125.7 MHz): δ 153.6

(N_2CN), 124.3 ($\underline{C}_5Me_5$), 46.8 ($N_2CN\underline{C}H_2$), 46.6 ($TiNCH_2$), 24.7 ($CH_2\underline{C}H_2CH_2$), 14.1 ($C_5\underline{Me}_5$) ppm. IR (NaCl plates, Nujol mull, cm^{-1}): 2040 (s), 1993 (w), 1623 (m), 1556 (s), 1523 (s), 1436 (s), 1354 (m), 1316 (s), 1295 (s), 1280 (m), 1199 (s), 1145 (m), 1114 (w), 1099 (m), 1068 (s), 881 (w), 806 (m), 740 (m). EI-MS: *m*/*z* = 433 $[M - Cp^* - hpp]^+$ (1%). Anal. found (calcd. for $C_{34}H_{54}N_6S_2Ti_2$): C, 57.59 (57.79); H, 7.56 (7.70); N, 11.78 (11.89)%.

*Data for SCNB{N(Ar')CH}₂ (**16**).* ^{1}H NMR (C_6D_6, 400.1 MHz): δ 7.22 – 7.11 (6 H, overlapping 2 × m with residual protio solvent resonance, *m*- and *p*-$C_6\underline{H}_3{}^i Pr_2$), 5.91 (2 H, s, NCH), 3.10 (4 H, sept., ^3J = 6.9 Hz, C<u>H</u>MeMe), 1.30 (12 H, d, ^3J = 6.9 Hz, CH<u>Me</u>Me), 1.18 (12 H, d, ^3J = 6.9 Hz, CHMe<u>Me</u>) ppm. $^{13}C\{^1H\}$ NMR (C_6D_6, 125.7 MHz): δ 146.3 (*o*-$\underline{C}_6H_3{}^i Pr_2$), 143.2 (NCS), 136.4 (*i*-$\underline{C}_6H_3{}^i Pr_2$), 128.6 (*p*-$\underline{C}_6H_3{}^i Pr_2$), 123.9 (*m*-$\underline{C}_6H_3{}^i Pr_2$), 118.6 (NCH), 28.9 (<u>C</u>HMeMe), 24.5 (CH<u>Me</u>Me), 24.0 (CHMe<u>Me</u>) ppm. $^{11}B\{^1H\}$ NMR (C_6D_6, 128.4 MHz): δ 16.0 ppm. IR (NaCl plates, Nujol mull, cm^{-1}): 3111 (w), 3071 (w), 2176 (m), 2092 (s, NCS as stretch), 1943 (w), 1707 (w), 1614 (w), 1590 (m), 1549 (m), 1505 (m), 1413 (m), 1394 (m), 1343 (w), 1328 (m), 1280 (w), 1230 (w), 1197 (w), 1182 (m), 1116 (m), 1101 (w), 1058 (m), 992 (w), 935 (w), 913 (m), 855 (m), 759 (s), 696 (m), 668 (m), 659 (m), 649 (m). FI-HRMS: *m/z* found (calcd. for $C_{27}H_{36}BN_3S$, $[M]^+$) 445.2722 (445.2723). Anal. found (calcd. for $C_{27}H_{36}BN_3S$): C, 72.94 (72.80); H, 8.25 (8.15); N, 9.51 (9.43)%.

Independent synthesis of SCNB(NAr'CH)₂ (16). To a Schlenk flask containing BrB{N(Dipp)CH}₂ (0.400 g, 0.856 mmol) and AgSCN (0.142 g, 0.856 mmol) was added MeCN (15 mL). The mixture was stirred for 16 hours, resulting in a dark grey suspension. The solvent was removed under reduced pressure, and the product extracted into hexane (3 × 10 mL). Removal of the solvent under reduced pressure, followed by drying *in vacuo* gave **16** as an off-white powder. Yield: 0.310 g (81%). The ^{1}H NMR spectrum was identical to that of the sample prepared from the borylimide **10**.

Reaction of Cp*Ti(N^{pyr}N^{Me_2}){NB(NAr'CH)₂} (11) with CO₂: synthesis of [Cp*Ti(N^{pyr}N^{Me_2})(μ-O)]₂ (19) and OCNB{N(Ar')CH}₂ (15). A solution of Cp*Ti(N^{pyr}N^{Me_2}){NB(NAr'CH)₂} (**11**, 0.500 g, 0.706 mmol) in benzene (10 mL) was freeze-pump-thaw-degassed three times. The solution was then exposed to CO_2 at a pressure of *ca* 1.1 atm. After 30 minutes the solution had turned orange, and the volatiles were then removed under reduced pressure to leave an orange oil. Trituration in pentane (5

mL), followed by washing with more pentane (2 × 5 mL), left **19** as a yellow solid, which was recrystallised from warm hexane at –30 °C. Yield: 0.0430 g (19%). Removal of the solvent from the combined washings left impure **15**, which was then recrystallized from warm hexane at –30 °C. Yield: 0.156 g (51%).

*Data for [Cp*Ti($N^{pyr}N^{Me_2}$)(μ-O)]$_2$ (**19**).* ^{1}H NMR (C_6D_6, 400.1 MHz): δ 7.72 (2 H, m, 2-pyr), 6.25 (2 H, m, 4-pyr), 6.16 (2 H, m, 3-pyr), 3.90 (4 H, br. s, C$\underline{H}_2$NMe$_2$), 2.27 (12 H, s, NMe$_2$), 2.00 (30 H, s, C_5Me_5) ppm. ^{13}C{^{1}H} NMR (C_6D_6, 100.6 MHz): δ 133.3 (5-pyr), 126.2 ($\underline{C}_5Me_5$), 121.9 (2-pyr), 115.1 (4-pyr), 111.3 (3-pyr), 56.8 ($\underline{C}H_2NMe_2$), 45.6 (NMe$_2$), 11.5 ($C_5\underline{Me}_5$) ppm. IR (NaCl plates, Nujol mull, cm^{-1}): 1868 (w), 1748 (w), 1731 (w), 1715 (w), 1704 (w), 1698 (w), 1682 (w), 1647 (s), 1588 (m), 1547 (m), 1396 (w), 1314 (m), 1242 (w), 1133 (m), 851 (m), 758 (w), 668 (m). A satisfactory elemental analysis of **19** could not be obtained.

Cp*Ti(hpp)(N^{t}Bu) (20). To a Schlenk flask containing Cp*Ti(N^{t}Bu)Cl(py) (**1.8**, 1.00 g, 2.71 mmol) and Li[hpp] (0.394 g, 2.71 mmol) was added toluene (20 mL) at –78 °C. The mixture was allowed to warm to room temperature, then heated to 40 °C and stirred for 16 h, a colour change from red to brown being observed in this time. The volatiles were then removed under vacuum and the product extracted into pentane (3 × 10 mL), then dried *in vacuo* to yield **20** as a deep red, waxy solid. Yield: 0.905 g (85%). Diffraction-quality crystals were grown from a concentrated pentane solution at room temperature.

^{1}H NMR (C_6D_6, 400.1 MHz): δ 3.27 (2 H, m, TiNC$\underline{H}_2$), 3.19 (2 H, m, TiNC$\underline{H}_2$), 2.72 (2 H, m, N$_2$CNC$\underline{H}_2$), 2.60 (2 H, m, N$_2$CNC$\underline{H}_2$), 2.19 (15 H, s, C_5Me_5), 1.60 (4 H, m, CH$_2$C$\underline{H}_2$CH$_2$), 1.23 (9 H, s, CMe$_3$) ppm. ^{13}C{^{1}H} NMR (C_6D_6, 100.6 MHz): δ 153.4 (N$_2$CN), 118.9 ($\underline{C}_5Me_5$), 66.7 ($\underline{C}Me_3$), 47.9 (N$_2$C$\underline{C}$H$_2$), 45.5 (TiNCH$_2$), 34.0 (C$\underline{Me}_3$), 24.4 (CH$_2\underline{C}$H$_2$CH$_2$), 12.1 ($C_5\underline{Me}_5$) ppm. IR (NaCl plates, Nujol mull, cm^{-1}): 2047 (s), 1943 (w), 1792 (w), 1772 (w), 1749 (w), 1734 (w), 1717 (w), 1670 (m), 1635 (m), 1600 (m), 1110 (m), 977 (w), 932 (w), 879 (m), 701 (w). EI-HRMS: *m/z* found (calcd. for $C_{21}H_{36}N_4Ti$, [*M*]$^+$) 392.2422 (392.2419). Anal. found (calcd. for $C_{21}H_{36}N_4Ti$): C, 64.09 (64.28); H, 9.16 (9.25); N, 13.98 (14.28)%.

NMR tube scale reaction of Cp*Ti(hpp)(N^{t}Bu) (20) and H$_2$NB(NAr'CH)$_2$ (2.2). A C_6D_6 solution (0.6 mL) of Cp*Ti(hpp)(N^{t}Bu) (**20**, 14.9 mg, 0.0380 mmol) and H$_2$NB(NAr'CH)$_2$ (**2.2**, 15.3 mg, 0.0380 mmol) was introduced into an NMR tube equipped with a J. Young Teflon valve. The reaction was monitored by ^{1}H NMR spectroscopy. After 16 h at 50 °C,

there had been *ca* 30% conversion to Cp*Ti(hpp){NB(NAr'CH)$_2$} (**10**) as measured by integrations of the NCH resonances in **10** and **2.2**. No further changes in the reaction mixture were observed, indicating this was the final equilibrium mixture.

NMR tube scale reaction of Cp*Ti(hpp){NB(NAr'CH)$_2$} (10) and H$_2$N^{t}Bu. To a C_6D_6 solution (0.6 mL) of Cp*Ti(hpp){NB(NAr'CH)$_2$} (**10**, 15.0 mg, 0.0208 mmol) in an NMR tube equipped with a J. Young Teflon valve was added H$_2$N^{t}Bu (2.2 μL, 0.0208 mmol). The reaction was monitored by ^{1}H NMR spectroscopy. After 16 h at RT, there had been *ca* 70% conversion to H$_2$NB(NAr'CH)$_2$ as measured by integrations of the NCH resonances in **10** and **2.2**. No further changes in the reaction mixture were observed, indicating this was the final equilibrium mixture.

Cp*Ti(hpp)(NHTol)$_2$ (21). To a solution of Cp*Ti(hpp)(N^{t}Bu) (**20**, 0.300 g, 0.765 mmol) in toluene (10 mL) was added a solution of H$_2$NTol (0.164 g, 1.53 mmol) in toluene (10 mL) at –78 °C, then the mixture stirred for 3 h at RT. The volatiles were removed under reduced pressure to leave a red-brown, waxy solid which was then triturated in hexane (10 mL). **21** was isolated as the resultant deep red solid, which was then dried *in vacuo*. Yield: 0.330 g (81%). Diffraction-quality crystals were grown from a benzene solution at RT.

^{1}H NMR (C_6D_6, 400.1 MHz): δ 8.08 (2 H, br. s, N<u>H</u>Tol), 6.92 (4 H, d, ^3J = 8.3 Hz, *o*-C$_6$<u>H</u>$_4$Me), 6.88 (4 H, d, ^3J = 8.3 Hz, *m*-C$_6$<u>H</u>$_4$Me), 3.03 (4 H, m, TiNC<u>H</u>$_2$), 2.45 (4 H, m, N$_2$CNC<u>H</u>$_2$), 2.12 (6 H, s, C$_6$H$_4$<u>Me</u>) 2.00 (15 H, s, C$_5$Me$_5$), 1.38 (4 H, m, CH$_2$C<u>H</u>$_2$CH$_2$) ppm. ^{13}C{^{1}H} NMR (C_6D_6, 100.6 MHz): δ 157.3 (N$_2$CN), 152.6 (*i*-<u>C</u>$_6$H$_4$Me), 129.4 (*m*-<u>C</u>$_6$H$_4$Me), 126.3 (*p*-<u>C</u>$_6$H$_4$Me), 126.3 (<u>C</u>$_5$Me$_5$), 117.7 (*o*-<u>C</u>$_6$H$_4$Me), 46.3 (N$_2$CN<u>C</u>H$_2$), 42.7 (TiNCH$_2$), 24.4 (CH$_2$<u>C</u>H$_2$CH$_2$), 20.9 (C$_6$H$_3$<u>Me</u>$_2$), 12.0 (C$_5$<u>Me</u>$_5$) ppm. IR (NaCl plates, Nujol mull, cm^{-1}): 3365 (w, N–H), 3336 (w, N–H), 1603 (w), 1567 (m), 1526 (m), 1498 (m), 1320 (w), 1200 (m), 1144 (m), 853 (m), 809 (s), 668 (m). EI-MS: *m*/*z* = 426 [*M* – TolNH$_2$]$^+$ (40%). Anal. found (calcd. for $C_{31}H_{43}N_5Ti$): C, 69.59 (69.78); H, 8.24 (8.12); N, 13.01 (13.13)%.

NMR tube scale synthesis of Cp*Ti(hpp)(NHTol)$_2$ (21). To a C_6D_6 solution (0.6 mL) of Cp*Ti(hpp){NB(NAr'CH)$_2$} (**10**) (15.0 mg, 0.0208 mmol) in an NMR tube equipped with a J. Young Teflon valve was added H$_2$NTol (4.4 mg, 0.0416 mmol), giving an immediate colour change from deep red to red-brown. The ^{1}H NMR spectrum demonstrated quantitative conversion to Cp*Ti(hpp)(NHTol)$_2$ (**21**) and H$_2$NB(NAr'CH)$_2$, with resonances identical to those described above.

Cp*Ti(hpp)(NXyl) (22). To a solution of Cp*Ti(hpp)(N^{t}Bu) (**20**, 0.810 g, 2.07 mmol) in toluene (15 mL) was added H_2NXyl (280 μL, 2.27 mmol), and the mixture stirred at RT for 90 mins. The volatiles were removed under reduced pressure, then the product washed with hexane (3 × 10 mL) before being dried *in vacuo* to leave **22** as a green-brown solid. Yield: 0.500 g (55%).

^{1}H NMR (C_6D_6, 400.1 MHz): δ 7.07 (2 H, d, ^3J = 7.4 Hz, *m*-$C_6\underline{H}_3Me_2$), 6.71 (1 H, t, ^3J = 7.4 Hz, *p*-$C_6\underline{H}_3Me_2$), 3.23 (2 H, m, TiNC$\underline{H}_2$), 3.14 (2 H, m, TiNC$\underline{H}_2$), 2.59 (2 H, m, N_2CNC$\underline{H}_2$), 2.48 (2 H, m, N_2CNC$\underline{H}_2$), 2.29 (6 H, s, $C_6H_3\underline{Me}_2$) 2.05 (15 H, s, C_5Me_5), 1.49 (4 H, m, $CH_2C\underline{H}_2CH_2$) ppm. ^{13}C{^{1}H} NMR (C_6D_6, 100.6 MHz): δ 159.1 (*i*-$\underline{C}_6H_3Me_2$), 152.2 ($N_2\underline{C}N$), 130.5 (*o*-$\underline{C}_6H_3Me_2$), 127.5 (*m*-$\underline{C}_6H_3Me_2$), 120.0 ($\underline{C}_5Me_5$), 117.8 (*p*-$\underline{C}_6H_3Me_2$), 47.0 ($N_2CN\underline{C}H_2$), 44.5 (TiNCH_2), 23.9 ($CH_2\underline{C}H_2CH_2$), 19.7 ($C_6H_3\underline{Me}_2$), 12.1 ($C_5\underline{Me}_5$) ppm. IR (NaCl plates, Nujol mull, cm^{-1}): 1620 (w), 1556 (m), 1537 (m), 1404 (w), 1317 (m), 1295 (s), 1202 (m), 1146 (w), 1093 (w), 1068 (w), 1024 (w), 952 (w), 755 (m), 740 (m), 701 (w). EI-HRMS: *m/z* found (calcd. for $C_{25}H_{36}N_4Ti$, $[M]^+$) 440.2428 (440.2419). Anal. found (calcd. for $C_{25}H_{36}N_4Ti$): C, 65.08 (68.17); H, 8.78 (8.24); N, 12.16 (12.72)%. Repeated attempts to obtain an elemental analysis with satisfactory % C values failed, presumably due to incomplete combustion of the compound.

NMR tube scale synthesis of Cp*Ti(hpp)(NXyl) (22). To a C_6D_6 solution (0.6 mL) of Cp*Ti(hpp){NB(NAr'CH)$_2$} (**10**, 15.0 mg, 0.0208 mmol) in an NMR tube equipped with a J. Young Teflon valve was added H_2NXyl (2.6 μL, 0.0208 mmol), giving an immediate colour change from deep red to green-brown. The ^{1}H NMR spectrum demonstrated quantitative conversion to Cp*Ti(hpp)(NXyl) (**22**) and H_2NB(NAr'CH)$_2$, with resonances identical to those described above.

6.7 Experimental details and characterising data for Chapter Four

Ti($N_2^{SiMe_3}N^{Me}$){N{B(NAr'CH)$_2$}C(H)C(Tol)} (23). To a solution of Ti($N_2^{SiMe_3}N^{Me}$){NB(NAr'CH)$_2$}(py) (**4**, 0.291 g, 0.369 mmol) in toluene (10 mL) was added HCCTol (47 μL, 0.369 mmol) at RT, giving an immediate colour change to deep red-brown. The reaction mixture was stirred at RT for 1 h, after which the volatiles were removed under reduced pressure, giving **23** as a deep brown, waxy solid. Yield: 0.206 g (68%). Diffraction-quality crystals were grown from a sample of the isolated waxy solid left at RT.

^{1}H NMR (C_6D_6, 400.1 MHz): δ 10.51 (1 H, s, TiC=CH), 7.23 (2 H, d, ^{3}J = 8.0 Hz, *m*-$C_6\underline{H}_4$Me), 7.18 – 7.11 (6 H, overlapping 2 × m residual protio solvent resonance, *m*- and *p*-$C_6\underline{H}_3{}^{i}Pr_2$), 7.08 (2 H, d, ^{3}J = 8.0 Hz, *o*-$C_6\underline{H}_4$Me), 6.18 (2 H, s, NCH), 3.45 (6 H, overlapping sept. and m, C<u>H</u>MeMe and C$\underline{H}_2$NSiMe$_3$), 3.09 (2 H, m, C$\underline{H}_2$NSiMe$_3$), 2.65 (2 H, m, C$\underline{H}_2$NMe), 2.15 (3 H, s, $C_6H_4\underline{Me}$), 2.13 (3 H, s, NMe), 1.92 (2 H, m, C$\underline{H}_2$NMe), 1.30 (12 H, d, ^{3}J = 6.9 Hz, CH<u>Me</u>Me), 1.21 (12 H, d, ^{3}J = 6.9 Hz, CHMe<u>Me</u>), 0.12 (18 H, s, SiMe$_3$) ppm. ^{13}C{^{1}H} NMR (C_6D_6, 100.6 MHz): δ 205.3 (Ti<u>C</u>=CH), 162.7 (TiC=<u>C</u>H), 146.5 (*o*-$\underline{C}_6H_3{}^{i}Pr_2$), 144.3 (*i*-$\underline{C}_6H_4$Me), 139.7 (*i*-$\underline{C}_6H_3{}^{i}Pr_2$), 133.6 (*p*-$\underline{C}_6H_4$Me), 128.7 (*o*-$\underline{C}_6H_4$Me), 128.0 (*p*-$\underline{C}_6H_3{}^{i}Pr_2$), 127.6 (*m*-$\underline{C}_6H_4$Me), 124.2 (*m*-$\underline{C}_6H_3{}^{i}Pr_2$), 118.9 (NCH), 57.5 ($\underline{C}H_2$NMe), 51.2 (C$\underline{H}_2$NSiMe$_3$), 43.1 (NMe), 29.0 (C<u>H</u>MeMe), 26.4 (CHMe<u>Me</u>), 23.7 (CH<u>Me</u>Me), 21.2 ($C_6H_4\underline{Me}$), 2.8 (SiMe$_3$) ppm. ^{11}B{^{1}H} NMR (C_6D_6, 128.4 MHz): δ 23.8 ppm. IR (NaCl plates, Nujol mull, cm^{-1}): 3406 (w), 1657 (s), 1585 (w), 1504 (m), 1487 (s), 1406 (m), 1362 (s), 1328 (m), 1277 (w), 1245 (s), 1179 (w), 1155 (w), 1117 (s), 1060 (w), 1042 (w), 986 (w), 926 (m), 837 (s), 805 (m), 762 (m), 681 (m), 647 (m). EI-MS: *m*/*z* = 519 [TolC(H)=C(H)N(H)B(NAr'CH)$_2$]$^{+}$ (92%). Anal. found (calcd. for $C_{46}H_{73}BN_6Si_2Ti$): C, 66.82 (66.97); H, 8.84 (8.92); N, 10.01 (10.19)%.

Ti(N$_2^{SiMe_3}$N^{Me}){N{B(NAr'CH)$_2$}C(H)C(Ar^{F})} (24). To a solution of Ti(N$_2^{SiMe_3}$N^{Me}){NB(NAr'CH)$_2$}(py) (**4**, 0.261 g, 0.331 mmol) in hexane (15 mL) was added HCCAr^{F} (44 μL, 0.331 mmol) at RT, giving an immediate colour change to deep red/brown. The reaction mixture was stirred at RT for 1 h, after which the volatiles were removed under reduced pressure, giving **24** as a deep brown waxy solid. Yield: 0.198 g (66%).

Major isomer: ^{1}H NMR (C_6D_6, 400.1 MHz): δ 10.43 (br. s overlapping with minor isomer, TiC=CH), 7.22 – 7.11 (overlapping 2 × m with minor isomer and residual protio solvent resonance, *m*- and *p*-$C_6\underline{H}_3{}^{i}Pr_2$), 6.11 (2 H, s, NCH), 3.39 (4 H, sept., ^{3}J = 6.9 Hz, C<u>H</u>MeMe), 3.02 (2 H, m, C$\underline{H}_2$NSiMe$_3$), 2.62 (2 H, m, C$\underline{H}_2$NMe), 1.97 (3 H, s, NMe), 1.89 (2 H, m, C$\underline{H}_2$NMe), 1.29 (12 H, d, ^{3}J = 6.9 Hz, CH<u>Me</u>Me), 1.20 (12 H, d, ^{3}J = 6.9 Hz, CHMe<u>Me</u>) 0.02 (18 H, s, SiMe$_3$) ppm. A second resonance assigned to C$\underline{H}_2$NSiMe$_3$ is found to be subsumed by the C<u>H</u>MeMe resonance at 3.39 ppm, as observed by HSQC and HMBC spectra. ^{13}C{^{1}H} NMR (C_6D_6, 125.7 MHz): δ 179.4 (Ti<u>C</u>=CH), 161.8 (TiC=<u>C</u>H), 147.2 (*o*-$\underline{C}_6H_3{}^{i}Pr_2$), 143.7 (m, *o*-$C_6F_5$), 141.8 (m, *m*-$C_6F_5$), 139.5 (*i*-$\underline{C}_6H_3{}^{i}Pr_2$), 136.5 (m, *p*-$C_6F_5$), 124.2 (*m*-$\underline{C}_6H_3{}^{i}Pr_2$), 121.2 (m, *i*-$C_6F_5$), 119.2 (NCH), 57.8 ($\underline{C}H_2$NMe), 51.0 ($\underline{C}H_2$NSiMe$_3$), 43.3 (NMe), 29.0 (<u>C</u>HMeMe), 26.3 (CHMe<u>Me</u>), 23.7 (CH<u>Me</u>Me), 1.9 (SiMe$_3$) ppm. The

p-C$_6$H$_3$^{i}Pr$_2$ resonance is subsumed by the solvent resonance. ^{19}F{^{1}H} NMR (C$_6$D$_6$, 376.5 MHz): –140.4 (2 F, d, ^3J = 21.6 Hz, *o*-C$_6$F$_5$), –163.1 (1 F, t, ^3J = 21.5 Hz, *p*-C$_6$F$_5$), –165.4 (2 F, m, *m*-C$_6$F$_5$) ppm.

Minor isomer: ^{1}H NMR (C$_6$D$_6$, 400.1 MHz): δ 10.43 (br. s overlapping with major isomer, TiC=CH), 7.22 – 7.11 (overlapping 2 × m with minor isomer and residual protio solvent resonance, *m*- and *p*-C$_6$H$_3$^{i}Pr$_2$), 6.04 (2 H, s, NCH), 3.43 (4 H, sept., ^3J = 6.9 Hz, CHMeMe), 3.19 (2 H, m, CH$_2$NSiMe$_3$), 2.89 (2 H, m, CH$_2$NSiMe$_3$), 2.42 (2 H, m, CH$_2$NMe), 2.16 (3 H, s, NMe), 2.02 (2 H, m, CH$_2$NMe), 1.43 (12 H, d, ^3J = 6.9 Hz, CHMeMe), 1.23 (12 H, d, ^3J = 6.9 Hz, CHMeMe), 0.23 (18 H, s, SiMe$_3$) ppm. ^{13}C{^{1}H} NMR (C$_6$D$_6$, 125.7 MHz): δ 179.4 (TiC=CH), 161.8 (TiC=CH), 146.5 (*o*-C$_6$H$_3$^{i}Pr$_2$), 139.1 (*i*-C$_6$H$_3$^{i}Pr$_2$), 127.6 (*p*-C$_6$H$_3$^{i}Pr$_2$), 124.1 (*m*-C$_6$H$_3$^{i}Pr$_2$), 117.7 (NCH), 59.3 (CH$_2$NMe), 50.8 (CH$_2$SiMe$_3$), 47.3 (NMe), 28.7 (CHMeMe), 26.0 (CHMeMe), 23.8 (CHMeMe), 2.2 (SiMe$_3$) ppm. Those resonances belonging to the TiC(Ar^F)=CH rings could not be satisfactorily assigned. ^{19}F{^{1}H} NMR (C$_6$D$_6$, 376.5 MHz): –136.9 (2 F, m, *o*-C$_6$F$_5$), –157.8 (1 F, t, ^3J = 21.3 Hz, *p*-C$_6$F$_5$), –163.9 (2 F, m, *m*-C$_6$F$_5$) ppm.

Common data: ^{11}B{^{1}H} NMR (C$_6$D$_6$, 128.4 MHz): δ 23.4 ppm. IR (NaCl plates, Nujol mull, cm^{-1}): 3522 (w), 3391 (m), 1832 (w), 1866 (w), 1797 (w), 1655 (m), 1637 (m), 1586 (m), 1510 (m), 1201 (m), 1180 (m), 1117 (s), 1031 (s), 960 (s), 909 (s), 837 (s), 759 (m), 674 (m), 651 (m), 604 (m), 556 (m). EI-MS: *m*/*z* = 595 [Ar^{F}C(H)=C(H)N(H)B(NAr'CH)$_2$]$^+$ (100%). Anal. found (calcd. for C$_{45}$H$_{66}$BF$_5$N$_6$Si$_2$Ti): C, 59.71 (59.99); H, 7.13 (7.38); N, 9.32 (9.33)%.

Ti(N$_2$^{ArF}N^{Me}){N{B(NAr'CH)$_2$}C(H)C(Tol)} (25). To a solution of Ti(N$_2$^{ArF}N^{Me}){NB(NAr'CH)$_2$}(py) (**5**, 0.499 g, 0.511 mmol) in toluene (10 mL) was added HCCTol (65 µL, 0.511 mmol) at RT, giving an immediate colour change to deep red. The reaction mixture was stirred for 20 minutes, after which the volatiles were removed under reduced pressure, to yield **25** as a deep red solid, which was then dried *in vacuo*. Yield: 0.395 g (76%). Diffraction-quality crystals were grown from a concentrated hexane solution at 5 °C.

^{1}H NMR (C$_6$D$_6$, 400.1 MHz): δ 11.61 (1 H, s, TiC=CH), 7.27 – 7.19 (6 H, overlapping 2 × m, *m*- and *p*-C$_6$H$_3$^{i}Pr$_2$), 6.65 (2 H, d, ^3J = 7.9 Hz, *o*-C$_6$H$_4$Me), 6.12 (2 H, d, ^3J = 7.9 Hz, *m*-C$_6$H$_4$Me), 6.01 (2 H, s, NCH), 3.67 (2 H, m, CH$_2$NAr^F), 3.49 (4 H, sept., ^3J = 6.9 Hz, CHMeMe), 3.10 (2 H, m, CH$_2$NAr^F), 2.95 (2 H, m, CH$_2$NMe), 2.19 (2 H, m, CH$_2$NMe),

1.86 (3 H, s, $C_6H_4\underline{Me}$), 1.28 (24 H, app. t, app. ^3J = 7.5 Hz, CH$\underline{Me}$Me), 1.27 (3 H, s, NMe) ppm. $^{13}C\{^1H\}$ NMR (C_6D_6, 125.8 MHz): δ 217.2 (Ti$\underline{C}$=CH), 163.8 (TiC=$\underline{C}$H), 147.5 (*o*-$\underline{C}_6H_3{}^iPr_2$), 143.3 (m, *o*-$C_6F_5$), 141.4 (m, *p*-$C_6F_5$), 140.8 (*i*-$\underline{C}_6H_3{}^iPr_2$), 137.2 (*i*-$\underline{C}_6H_4Me$), 136.7 (m, *m*-$C_6F_5$), 135.7 (*p*-$\underline{C}_6H_4Me$), 133.3 (td, $^2J_{C–F}$ = 14.3 Hz, $^3J_{C–F}$ = 3.7 Hz, *i*-C_6F_5), 129.3 (*p*-$\underline{C}_6H_3{}^iPr_2$), 128.6 (*m*-$\underline{C}_6H_4Me$), 126.3 (*o*-$\underline{C}_6H_4Me$), 124.5 (*m*-$\underline{C}_6H_3{}^iPr_2$), 119.2 (NCH), 56.8 ($\underline{C}H_2NAr^F$), 55.9 ($\underline{C}H_2NMe$), 41.4 (NMe), 29.0 ($\underline{C}HMeMe$), 25.0 (CH$\underline{Me}$Me), 23.4 (CHMe$\underline{Me}$), 20.8 ($C_6H_4\underline{Me}$) ppm. $^{11}B\{^1H\}$ NMR (C_6D_6, 128.4 MHz): δ 21.9 ppm. $^{19}F\{^1H\}$ NMR (C_6D_6, 376.5 MHz): –150.1 (2 F, m, *o*-C_6F_5), –166.1 (2 F, m, *m*-C_6F_5), –167.0 (1 F, t, ^3J = 21.9 Hz, *p*-C_6F_5). IR (NaCl plates, Nujol mull, cm^{-1}): 3407 (w), 3067 (w), 1942 (w), 1658 (m), 1625 (w), 1583 (m), 1496 (s), 1408 (w), 1391 (m), 1349 (w), 1278 (w), 1207 (m), 1118 (w), 1065 (w), 982 (s), 937 (w), 901 (m), 861 (m), 816 (w), 769 (m), 694 (w), 650 (m). EI-MS: *m*/*z* = 1012 $[M]^+$ (10%). Anal. found (calcd. for $C_{52}H_{55}BF_{10}N_6Ti$): C, 61.54 (61.67); H, 5.65 (5.47); N, 8.12 (8.30)%.

Ti{MeN(CH$_2$CH$_2$NAr^F){CH$_2$CH$_2$NC$_6$F$_4$C(Ar^F)=CHNB(NAr'CH)$_2$}}(F) (26). To a solution of Ti($N_2{}^{ArF}N^{Me}$){NB(NAr'CH)$_2$}(py) (**5**, 0.300 g, 0.307 mmol) in toluene (10 mL) was added HCCAr^F (41 μL, 0.307 mmol) at RT, giving an immediate colour change to deep red. The reaction mixture was heated to 60 °C and stirred for 16 h, after which the volatiles were removed under reduced pressure, resulting in a deep brown, waxy solid. Washing with hexane (5 mL) gave **26** as a yellow-orange solid. Yield: 0.191 g (57%). Diffraction-quality crystals were grown from a concentrated C_6D_6 solution at RT.

^1H NMR (C_6D_6, 400.1 MHz): δ 7.29 (2 H, t, ^3J = 7.6 Hz, *p*-$C_6\underline{H}_3{}^iPr_2$), 7.18 (2 H, d, ^3J = 7.6 Hz, m_a-$C_6\underline{H}_3{}^iPr_2$), 6.99 (2 H, d, ^3J = 7.6 Hz, m_b-$C_6\underline{H}_3{}^iPr_2$), 6.72 (1 H, s, NC($\underline{H}$)=CAr^F), 5.89 (2 H, s, NCH), 4.11 (1 H, m, MeNCH$_2$C$\underline{H}_2$NC$_6$F$_4$), 3.31 (4 H, overlapping 2 × sept., C$\underline{H}_a$MeMe and C$\underline{H}_b$MeMe), 3.05 (1 H, m, MeNC$\underline{H}_2$CH$_2$NC$_6$F$_4$), 2.98 (3 H, overlapping 3 × m, MeNCH$_2$C$\underline{H}_2$NC$_6$F$_4$, MeNCH$_2$C$\underline{H}_2$NC$_6$F$_5$ and MeNC$\underline{H}_2$CH$_2$NC$_6$F$_5$), 2.72 (1 H, m, MeNCH$_2$C$\underline{H}_2$NC$_6$F$_5$), 2.33 (3 H, s, NMe), 1.99 (1 H, m, MeNC$\underline{H}_2$CH$_2$NC$_6$F$_5$), 1.74 (1 H, m, MeNC$\underline{H}_2$CH$_2$NC$_6$F$_4$), 1.44 (6 H, d, ^3J = 6.8 Hz, CH$\underline{Me}_a$Me), 1.22 (6 H, d, ^3J = 6.8 Hz, CH$\underline{Me}_b$Me), 1.17 (6 H, d, ^3J = 6.8 Hz, CHMe$\underline{Me}_a$), 1.05 (6 H, d, ^3J = 6.8 Hz, CHMe$\underline{Me}_b$) ppm. $^{13}C\{^1H\}$ NMR (C_6D_6, 125.7 MHz): δ 146.8 (o_a-$\underline{C}_6H_3{}^iPr_2$), 145.8 ($o_b$-$\underline{C}_6H_3{}^iPr_2$), 139.1 (*i*-$\underline{C}_6H_3{}^iPr_2$), 138.4 (N$\underline{C}$(H)=CAr^F), 128.4 (*p*-$\underline{C}_6H_3{}^iPr_2$), 124.1 ($m_a$-$\underline{C}_6H_3{}^iPr_2$), 122.9 ($m_b$-$\underline{C}_6H_3{}^iPr_2$), 119.8 (NCH), 109.7 (NC(H)=$\underline{C}$Ar^F), 56.1 (MeNCH$_2\underline{C}$H$_2$NC$_6$F$_5$), 55.7 (MeN$\underline{C}$H$_2$CH$_2$NC$_6$F$_5$), 53.9 (MeNCH$_2\underline{C}$H$_2$NC$_6$F$_4$), 52.0 (MeN$\underline{C}$H$_2$CH$_2$NC$_6$F$_4$), 43.5 (NMe), 28.6 ($\underline{C}$HMeMe), 26.7 (CHMe$\underline{Me}_b$), 26.5 (CHMe$\underline{Me}_a$), 23.5 (CH$\underline{Me}_a$Me), 22.3

(CHMe$_b$Me) ppm. Those resonances belonging to the NAr^F and C_6F_4 rings could not be satisfactorily assigned. $^{11}B\{^1H\}$ NMR (C_6D_6, 128.4 MHz): δ 22.4 ppm. $^{19}F\{^1H\}$ NMR (C_6D_6, 376.5 MHz): –100.0 (s, TiF), –134.0 (1 F, dd, ^3J = 24.0 Hz, ^4J = 5.7 Hz, δ-C_6F_4), –140.5 (1 F, m, ligand *o*-C_6F_5), –142.6 (1 F, br. m, alkene *o*-C_6F_5), –142.8 (1 F, d, ^3J = 22.0 Hz, ligand *o*-C_6F_5), –145.0 (1 F, dd, ^3J = 20.5 Hz, ^4J = 7.8 Hz, β-C_6F_4), –147.0 (1 F, br. m, alkene *o*-C_6F_5), –156.0 (1 F, t, ^3J = 21.3 Hz, ligand *p*-C_6F_5), –157.5 (1 F, app. t, app. *J* = 21.4 Hz, α-C_6F_4), –160.1 (1 F, br. m, alkene *m*-C_6F_5), –162.0 (1 F, t, ^3J = 21.3 Hz, alkene *p*-C_6F_5), –162.4 (1 F, app. t, *J* = 23.5 Hz, γ-C_6F_4), –163.0 (2 F, overlapping 2 × m, ligand *m*-C_6F_5), –168.5 (1 F, br. m, alkene *m*-C_6F_5) ppm. IR (NaCl plates, Nujol mull, cm^{-1}): 1637 (w), 1610 (w), 1574 (w), 1521 (s), 1500 (s), 1389 (s), 1345 (m), 1332 (m), 1287 (m), 1208 (w), 1115 (w), 1086 (m), 1023 (m), 996 (s), 986 (s), 944 (w), 910 (w), 901 (w), 886 (w), 857 (w), 811 (w), 758 (m), 738 (m), 691 (m), 656 (m), 600 (m). EI-MS: *m*/*z* = 1088 $[M]^+$ (1%). Anal. found (calcd. for $C_{51}H_{48}BF_{15}N_6Ti$): C, 56.05 (56.27); H, 4.47 (4.44); N, 7.65 (7.72)%.

NMR tube scale synthesis of Ti(N$_2^{ArF}$N^{Me}){N{B(NAr'CH)$_2$}C(H)C(Ar^F)} (27). To an NMR tube fitted with a J. Youngs valve was added a solution of Ti(N$_2^{ArF}$N^{Me}){NB(NAr'CH)$_2$}(py) (**5**, 0.0150 g, 0.0153 mmol) and B(Ar^F)$_3$ (0.0078 g, 0.0153 mmol) in C_6D_6 (0.6 mL). HCCAr^F (2.0 μL, 0.0153 mmol) was added *via* microsyringe, followed by an immediate colour change to very deep brown. Conversion to **27** and [py–B(Ar^F)$_3$] was found to be quantitative.

Major isomer: ^1H NMR (C_6D_6, 400.1 MHz): δ 11.51 (1 H, s, TiC=CH), 7.26 – 7.17 (multiple m overlapping with minor isomer, *m*- and *p*-C$_6$H$_3$^{i}Pr$_2$), 5.98 (2 H, s, NCH), 3.46 (4 H, sept. overlapping with minor isomer, CHMeMe), 2.91 (multiple m overlapping with minor isomer, CH$_2$NAr^F and CH$_2$NMe), 2.12 (2 H, m, CH$_2$NMe), 1.26 (multiple m overlapping with minor isomer, NMe and CHMeMe) ppm. $^{13}C\{^1H\}$ NMR (C_6D_6, 125.7 MHz): δ 194.1 (TiC=CH), 162.6 (TiC=CH), 147.2 (*o*-C$_6$H$_3$^{i}Pr$_2$), 140.1 (*i*-C$_6$H$_3$^{i}Pr$_2$), 128.4 (*p*-C$_6$H$_3$^{i}Pr$_2$), 124.9 (*m*-C$_6$H$_3$^{i}Pr$_2$), 119.6 (NCH), 56.4 (CH$_2$NMe), 55.8 (CH$_2$NAr^F), 41.6 (NMe), 28.9 (CHMeMe), 25.3 (CHMeMe), 23.2 (CHMeMe) ppm. Those resonances belonging to the NAr^F and TiC(Ar^F)=CH rings could not be satisfactorily assigned.

Minor isomer: ^1H NMR (C_6D_6, 400.1 MHz): δ 11.30 (1 H, s, TiC=CH), 7.26 – 7.17 (multiple m overlapping with major isomer, *m*- and *p*-C$_6$H$_3$^{i}Pr$_2$), 6.10 (2 H, s, NCH), 3.76 (4 H, m, CH$_2$NAr^F), 3.46 (4 H, sept. overlapping with major isomer, CHMeMe), 2.91 (m

overlapping with major isomer, C$\underline{H}_2$NMe), 2.74 (3 H, s, NMe) 1.93 (2 H, m, C$\underline{H}_2$NMe), 1.26 (multiple m overlapping with major isomer, CH$\underline{Me}$Me) ppm. $^{13}C\{^1H\}$ NMR (C_6D_6, 125.7 MHz): δ 201.1 (Ti$\underline{C}$=CH), 160.2 (TiC=$\underline{C}$H), 146.0 (*o*-$\underline{C}_6H_3{}^iPr_2$), 124.3 (*m*-$\underline{C}_6H_3{}^iPr_2$), 118.8 (NCH), 56.9 ($\underline{C}H_2$NMe), 55.4 ($\underline{C}H_2NAr^F$), 37.8 (NMe), 29.0 ($\underline{C}$HMeMe), 25.9 (CH$\underline{Me}$Me), 23.1 (CHMe$\underline{Me}$) ppm. Those resonances belonging to the NAr^F and TiC($\underline{Ar^F}$)=CH rings, and the *i*-$\underline{C}_6H_3{}^iPr_2$ resonance could not be satisfactorily assigned. The *p*-$\underline{C}_6H_3{}^iPr_2$ resonance is subsumed by the solvent resonance.

Common data: $^{11}B\{^1H\}$ NMR (C_6D_6, 128.4 MHz): δ 22.6 ppm.

Ti{MeN(CH$_2$CH$_2$NAr^F){CH$_2$CH$_2$NC$_6$F$_4$C(Tol)=CHNB(NAr'CH)$_2$}}(F) (28). To a solution of Ti($N_2{}^{ArF}N^{Me}$){NB(NAr'CH)$_2$}(py) (**5**, 0.290 g, 0.297 mmol) in toluene (10 mL) was added HCCTol (38 µL, 0.297 mmol) at RT, giving an immediate colour change to deep red. The reaction mixture was heated to 70 °C and stirred for 3.5 h, after which the volatiles were removed under reduced pressure, resulting in an orange waxy solid. Washing with hexane (3 × 10 mL) gave **28** as a yellow-orange solid. Yield: 0.141 g (47%). Diffraction-quality crystals were grown from a concentrated hexane solution at RT.

^1H NMR (C_6D_6, 400.1 MHz): δ 7.31 (2 H, t, ^3J = 7.7 Hz, *p*-$C_6\underline{H}_3{}^iPr_2$), 7.15 (2 H, d, ^3J = 7.7 Hz, m_a-$C_6\underline{H}_3{}^iPr_2$), 7.10 (2 H, d, ^3J = 7.7 Hz, m_b-$C_6\underline{H}_3{}^iPr_2$), 6.93 (4 H, m, $C_6\underline{H}_4$Me), 6.59 (1 H, s, NC($\underline{H}$)=CTol), 5.98 (2 H, s, BNCH), 4.28 (1 H, m, MeNCH$_2$C$\underline{H}_2$NC$_6$F$_4$), 3.51 (2 H, sept., ^3J = 6.9 Hz, C$\underline{H}_a$MeMe), 3.34 (2 H, sept., ^3J = 6.9 Hz, C$\underline{H}_b$MeMe), 3.14 (2 H, overlapping 2 × m, MeNC$\underline{H}_2$CH$_2$NC$_6$F$_4$ and MeNC$\underline{H}_2$CH$_2$NC$_6$F$_5$), 2.82 (3 H, overlapping 2 × m, MeNCH$_2$C$\underline{H}_2$NC$_6$F$_4$ and MeNCH$_2$C$\underline{H}_2$NC$_6$F$_5$), 2.37 (3 H, s, NMe), 2.17 (3 H, s, $C_6H_4\underline{Me}$), 2.03 (1 H, m, MeNC$\underline{H}_2$CH$_2$NC$_6$F$_5$), 1.76 (1 H, m, MeNC$\underline{H}_2$CH$_2$NC$_6$F$_4$), 1.40 (12 H, d, ^3J = 6.9 Hz, overlapped CH$\underline{Me}_a$Me and CH$\underline{Me}_b$Me), 1.18 (6 H, d, ^3J = 6.9 Hz, CHMe$\underline{Me}_b$), 1.13 (6 H, d, ^3J = 6.9 Hz, CHMe$\underline{Me}_a$). $^{13}C\{^1H\}$ NMR (C_6D_6, 100.6 MHz): δ 146.9 (o_a-$\underline{C}_6H_3{}^iPr_2$), 145.9 ($o_b$-$\underline{C}_6H_3{}^iPr_2$), 138.7 ($i_a$-$\underline{C}_6H_3{}^iPr_2$), 138.0 (*i*-$\underline{C}_6H_4$Me), 137.9 ($i_b$-$\underline{C}_6H_3{}^iPr_2$), 130.2 (N$\underline{C}$(H)=CTol), 129.4 (*o*-$\underline{C}_6H_4$Me), 129.3 (*p*-$\underline{C}_6H_4$Me), 126.4 (*m*-$\underline{C}_6H_4$Me), 124.0 ($m_a$-$\underline{C}_6H_3{}^iPr_2$), 123.0 ($m_b$-$\underline{C}_6H_3{}^iPr_2$), 119.4 (NCH), 114.6 (NC(H)=$\underline{C}$Tol), 55.1 (MeNCH$_2\underline{C}$H$_2$NC$_6$F$_5$), 55.5 (MeN$\underline{C}$H$_2$CH$_2$NC$_6$F$_5$), 54.0 (MeNCH$_2\underline{C}$H$_2$NC$_6$F$_4$), 51.7 (MeN$\underline{C}$H$_2$CH$_2$NC$_6$F$_4$), 43.2 (NMe), 28.6 ($\underline{C}$H$_a$MeMe), 28.3 ($\underline{C}$H$_b$MeMe), 26.7 (CHMe$\underline{Me}_a$), 26.2 (CHMe$\underline{Me}_b$), 23.9 (CH$\underline{Me}_a$Me), 22.9 (CH$\underline{Me}_b$Me), 21.0 ($C_6H_4\underline{Me}$) ppm. Those resonances belonging to the NAr^F and C_6F_4 rings could not be satisfactorily assigned. $^{11}B\{^1H\}$ NMR (C_6D_6, 128.4 MHz): δ 22.9 ppm. $^{19}F\{^1H\}$ NMR

(C_6D_6, 376.5 MHz): –102.5 (s, TiF), –128.9 (1 F, m, δ-C_6F_4), –146.4 (1 F, dd, ^3J = 20.2 Hz, ^4J = 7.8 Hz, β-C_6F_4), –147.0 (2 F, d, ^3J = 23.4 Hz, *o*-C_6F_5), –158.1 (1 F, app. t, app. ^3J = 21.0 Hz, α-C_6F_4), –163.0 (1 F, m, *p*-C_6F_5), –163.3 (2 F, m, *m*-C_6F_5), –164.8 (1 F, app. t, *J* = 23.1 Hz, γ-C_6F_4) ppm. IR (NaCl plates, Nujol mull, cm^{-1}): 1634 (w), 1607 (w), 1586 (w), 1557 (w), 1502 (s), 1363 (s), 1335 (s), 1289 (m), 1203 (w), 1115 (m), 1060 (s), 997 (s), 989 (s), 951 (w), 899 (m), 858 (m), 821 (w), 786 (w), 758 (m), 690 (w), 656 (m), 623 (m), 601 (m). EI-MS: *m*/*z* = 1012 $[M]^+$ (100%). Anal. found (calcd. for $C_{52}H_{55}BF_{10}N_6Ti$): C, 61.47 (61.67); H, 5.61 (5.47); N, 8.11 (8.30)%.

NMR tube scale synthesis of Ti{MeN(CH$_2$CH$_2$NAr^F){CH$_2$CH$_2$NC$_6$F$_4$C(Tol)=CHNB(NAr'CH)$_2$}}(F) (28). To an NMR tube fitted with a J. Youngs valve was added a solution of Ti($N_2^{ArF}N^{Me}$){N{B(NAr'CH)$_2$}C(H)C(Tol)} (**25**, 0.0150 g, 0.0148 mmol) in C_6D_6 (0.6 mL), and the tube heated to 60 °C for 16 h, after which time the ^{1}H NMR spectrum indicated quantitative conversion to **28**.

Kinetic measurements for the conversion of Ti($N_2^{ArF}N^{Me}$){N{B(NAr'CH)$_2$}C(H)C(Tol)} (25) to Ti{MeN(CH$_2$CH$_2$NAr^F){CH$_2$CH$_2$NC$_6$F$_4$C(Tol)=CHNB(NAr'CH)$_2$}}(F) (28). The general procedure is as follows. In a dry-box, a C_6D_6 solution (0.6 mL) of Ti($N_2^{ArF}N^{Me}$){N{B(NAr'CH)$_2$}C(H)C(Tol)} (**25**, 0.0156 g, 0.0154 mmol) was transferred to an NMR tube fitted with a J. Youngs valve. A blank C_6D_6 sample was added to the NMR probe at RT, locked and shimmed, and the probe heated to the relevant temperature (327, 330, 333, 336 or 339 K). After thermal equilibration, the experimental sample replaced the blank sample, the shimming was checked and an array was set up to record a ^{1}H NMR spectrum (4 scans) every 120 s. The formation of **28** was calculated by measuring the integral of NMe. First order rate constants were obtained from linear plots of –ln(1–([**28**]/[**28**]$_{final}$)) *vs* time.

Kinetic measurements for the conversion of Ti($N_2^{ArF}N^{Me}$){N{B(NAr'CH)$_2$}C(H)C(Ar^F)} (27) to Ti{MeN(CH$_2$CH$_2$NAr^F){CH$_2$CH$_2$NC$_6$F$_4$C(Ar^F)=CHNB(NAr'CH)$_2$}}(F) (26). The general procedure is as follows. In a dry-box, Ti($N_2^{ArF}N^{Me}$){NB(NAr'CH)$_2$}(py) (**5**, 0.0150 g, 0.0154 mmol) and B(Ar^F)$_3$ (0.0079 g, 0.0154 mmol) were mixed in C_6D_6 (0.6 mL), and the mixture transferred to an NMR tube fitted with a J. Youngs valve. Next, HCCAr^F (2.0

μL, 0.0154 mmol) was added *via* microsyringe, giving immediate conversion to **27**. A blank C_6D_6 sample was added to the NMR probe at RT, locked and shimmed, and the probe heated to the relevant temperature (327, 330, 333, 336 or 339 K). After thermal equilibration, the experimental sample replaced the blank sample, the shimming was checked and an array was set up to record a ^{1}H NMR spectrum (4 scans) every 120 s. The formation of **26** was calculated by measuring the integral of NMe. First order rate constants were obtained from linear plots of $-\ln(1-([\mathbf{26}]/[\mathbf{26}]_{final}))$ *vs* time.

Ti(N$_2^{iPr}$N^{Me}){N{B(NAr'CH)$_2$}C(H)C(Tol)} (29). To a solution of Ti(N$_2^{iPr}$N^{Me}){NB(NAr'CH)$_2$}(py) (**6**, 0.500 g, 0.687 mmol) in toluene (15 mL) was added HCCTol (87 μL, 0.686 mmol) at RT, giving an immediate colour change to deep brown. The mixture was stirred for 1 h, then the volatiles removed under reduced pressure. The product was dissolved in hexane (5 mL), concentrated to 2 mL then cooled to –30 °C, resulting in large, deep brown crystals of **29**. Yield: 0.228 g (43%). Diffraction-quality crystals were grown from a concentrated hexane solution at 5 °C.

*Major isomer (**cis-29**)*: ^{1}H NMR (C_6D_6, 400.1 MHz): δ 10.32 (1 H, s, TiC=CH), 7.32 – 7.20 (6 H, overlapping 2 × m with minor isomer, *m*- and *p*-C$_6$H$_3$^{i}Pr$_2$), 7.04 (2 H, d, ^3J = 8.0 Hz, *o*-C$_6$H$_4$Me), 6.93 (2 H, d, ^3J = 8.0 Hz, *m*-C$_6$H$_4$Me), 5.99 (2 H, s, BNCH), 4.26 (2 H, sept., ^3J = 6.7 Hz, NCHMeMe), 3.56 (4 H, sept. overlapping with minor isomer, ^3J = 6.9 Hz, C$_6$H$_3$(CHMe$_2$)$_2$), 3.40 (2 H, m, CH$_2$N^{i}Pr), 2.99 (4 H, overlapping 2 × m with minor isomer, CH$_2$N^{i}Pr and CH$_2$NMe), 2.21 (2 H, m, CH$_2$NMe), 2.14 (3 H, s, C$_6$H$_4$Me), 1.29 (12 H, d overlapping with minor isomer, ^3J = 6.9 Hz, C$_6$H$_3$(CHMeMe)$_2$), 1.08 (3 H, s, NMe), 1.00 (6 H, d, ^3J = 6.7 Hz, NCHMeMe), 0.91 (6 H, d, ^3J = 6.7 Hz, NCHMeMe) ppm. ^{13}C{^{1}H} NMR (C_6D_6, 100.6 MHz): δ 209.5 (TiC=CH), 148.9 (TiC=CH), 147.3 (*o*-C$_6$H$_3$^{i}Pr$_2$), 142.0 (*i*-C$_6$H$_3$^{i}Pr$_2$), 139.7 (*i*-C$_6$H$_4$Me), 133.5 (*p*-C$_6$H$_4$Me), 129.2 (*o*-C$_6$H$_4$Me), 127.5 (*p*-C$_6$H$_3$^{i}Pr$_2$), 127.0 (*m*-C$_6$H$_4$Me), 124.1 (*m*-C$_6$H$_3$^{i}Pr$_2$), 118.6 (BNCH), 57.2 (NCHMeMe), 56.9 (CH$_2$NMe), 47.2 (CH$_2$N^{i}Pr), 41.5 (NMe), 28.9 (C$_6$H$_3$(CHMeMe)$_2$), 24.6 (C$_6$H$_3$(CHMeMe)$_2$), 23.9 (C$_6$H$_3$(CHMeMe)$_2$), 23.6 (NCHMeMe), 22.2 (NCHMeMe), 21.2 (C$_6$H$_4$Me) ppm.

*Minor isomer (**trans-29**)*: ^{1}H NMR (C_6D_6, 400.1 MHz): δ 9.35 (1 H, s, TiC=CH), 7.32 – 7.20 (6 H, overlapping 2 × m with major isomer, *m*- and *p*-C$_6$H$_3$^{i}Pr$_2$), 6.94 (2 H, overlapping with major isomer, *o*-C$_6$H$_4$Me), 6.71 (2 H, d, ^3J = 8.0 Hz, *m*-C$_6$H$_4$Me), 6.02 (2 H, s, BNCH), 4.18 (2 H, sept., ^3J = 6.7 Hz, NCHMeMe), 3.56 (2 H, sept. overlapping with major isomer,

^{3}J = 6.9 Hz, $C_6H_3(C\underline{H}Me_2)_2$), 3.25 (2 H, m, $C\underline{H}_2N^iPr$), 2.99 (4 H, overlapping 2 × m with major isomer, $C\underline{H}_2N^iPr$ and $C\underline{H}_2NMe$), 2.42 (2 H, m, $C\underline{H}_2NMe$), 2.09 (3 H, s, $C_6H_4\underline{Me}$), 1.35 (12 H, d, ^{3}J = 6.9 Hz, $C_6H_3(CH\underline{Me}Me)_2$, 1.30 (3 H, s, NMe), 1.29 (12 H, d overlapping with major isomer, ^{3}J = 6.9 Hz, $C_6H_3(CH\underline{Me}Me)_2$), 0.95 (6 H, d, ^{3}J = 6.7 Hz, NCH$\underline{Me}$Me), 0.76 (6 H, d, ^{3}J = 6.7 Hz, NCHMe$\underline{Me}$) ppm. $^{13}C\{^{1}H\}$ NMR (C_6D_6, 100.6 MHz): δ 196.7 (Ti$\underline{C}$=CH), 147.2 (*o*-$\underline{C}_6H_3{}^iPr_2$), 144.8 (*i*-$\underline{C}_6H_4Me$), 143.5 (TiC=$\underline{C}$H), 141.3 (*i*-$\underline{C}_6H_3{}^iPr_2$), 132.6 (*p*-$\underline{C}_6H_4Me$), 129.0 (*o*-$\underline{C}_6H_4Me$), 127.5 (*p*-$\underline{C}_6H_3{}^iPr_2$), 125.7 (*m*-$\underline{C}_6H_4Me$), 123.9 (*m*-$\underline{C}_6H_3{}^iPr_2$), 119.6 (BNCH), 57.1 ($\underline{C}H_2NMe$), 54.4 (N$\underline{C}$HMeMe), 46.7 ($\underline{C}H_2N^iPr$), 43.8 (NMe), 25.9 ($C_6H_3(\underline{C}HMeMe)_2$), 23.7 ($C_6H_3(CH\underline{MeMe})_2$), 23.7 (NCH$\underline{Me}$Me), 21.6 (NCHMe$\underline{Me}$), 21.0 ($C_6H_4\underline{Me}$) ppm.

Common data: $^{11}B\{^{1}H\}$ NMR (C_6D_6, 128.4 MHz): 22.1 ppm. IR (NaCl plates, Nujol mull, cm^{-1}): 2078 (w), 1930 (w), 1867 (w), 1656 (s), 1585 (m), 1568 (w), 1504 (m), 1487 (m), 1361 (m), 1276 (m), 1227 (w), 1116 (m), 1104 (m), 1042 (w), 994 (w), 944 (m), 898 (w), 762 (m), 648 (m). EI-MS: *m*/*z* = 519 $[TolC(H)=C(H)N(H)B(NAr'CH)_2]^+$ (95%). Anal. found (calcd. for $C_{46}H_{69}BN_6Ti$): C, 72.12 (72.24); H, 9.09 (9.09); N, 10.88 (10.99)%.

Ti($N_2^{iPr}N^{Me}$){NHB(NAr'CH)$_2$}(CCAr^F) (30). To a solution of Ti($N_2^{iPr}N^{Me}$){NB(NAr'CH)$_2$}(py) (**6**, 0.300 g, 0.412 mmol) in hexane (15 mL) was added HCCAr^F (55 µL, 0.412 mmol) at RT. The mixture was stirred for 1 h, then the volatiles removed under reduced pressure to yield **30** as a yellow-orange solid. Yield: 0.178 g (51%).

^{1}H NMR (C_6D_6, 400.1 MHz): δ 7.21 – 7.19 (6 H, overlapping 2 × m with minor isomer, *m*- and *p*-$C_6\underline{H}_3{}^iPr_2$), 6.58 (1 H, s, N$\underline{H}$B(NAr'CH)$_2$), 5.89 (2 H, s, BNCH), 5.00 (2 H, sept., ^{3}J = 6.3 Hz, NC$\underline{H}$MeMe), 3.49 (4 H, sept., ^{3}J = 6.9 Hz, $C_6H_3(C\underline{H}MeMe)_2$), 3.27 (2 H, m, $C\underline{H}_2N^iPr$), 2.87 (2 H, m, $C\underline{H}_2N^iPr$), 2.74 (2 H, m, $C\underline{H}_2NMe$), 2.07 (2 H, m, $C\underline{H}_2NMe$), 1.99 (3 H, s, NMe), 1.45 (12 H, d, ^{3}J = 6.9 Hz, $C_6H_3(CH\underline{Me}Me)_2$), 1.28 (12 H, d, ^{3}J = 6.9 Hz, $C_6H_3(CHMe\underline{Me})_2$), 1.25 (6 H, d, ^{3}J = 6.3 Hz, NCHMe$\underline{Me}$), 0.42 (6 H, d, ^{3}J = 6.3 Hz, NCHMe$\underline{Me}$) ppm. $^{13}C\{^{1}H\}$ NMR (C_6D_6, 125.7 MHz): δ 162.0 (Ti$\underline{C}$CAr^F), 148.9 (m, *o*-C_6F_5) 147.2 (*o*-$\underline{C}_6H_3{}^iPr_2$), 140.2 (*i*-$\underline{C}_6H_3{}^iPr_2$), 138.7 (m, *p*-$C_6F_5$), 136.9 (m, *m*-$C_6F_5$), 124.0 (*m*-$\underline{C}_6H_3{}^iPr_2$), 123.9 (*p*-$\underline{C}_6H_3{}^iPr_2$), 117.8 (BNCH), 103.2 (td, $^{2}J_{C-F}$ = 18.9 Hz, $^{3}J_{C-F}$ = 3.7 Hz, *i*-C_6F_5), 83.7 (TiC$\underline{C}$Ar^F), 57.9 ($\underline{C}H_2NMe$), 52.3 (N$\underline{C}$HMeMe), 47.2 ($\underline{C}H_2N^iPr$), 45.8 (NMe), 28.8 ($C_6H_3(\underline{C}HMeMe)_2$), 24.9 ($C_6H_3(CHMe\underline{Me})_2$), 24.1 ($C_6H_3(CH\underline{Me}Me)_2$), 21.1 (NCH$\underline{Me}$Me), 19.6 (NCHMe$\underline{Me}$) ppm. $^{11}B\{^{1}H\}$ NMR (C_6D_6, 128.4 MHz): 23.0 ppm. $^{19}F\{^{1}H\}$ NMR (C_6D_6, 376.5 MHz): –138.9 (2 F, m, *o*-C_6F_5), –159.1 (1 F, t, ^{3}J = 21.7 Hz,

p-C_6F_5), –164.4 (2 F, m, *m*-C_6F_5). IR (NaCl plates, Nujol mull, cm^{-1}): 3484 (w), 3409 (m), 3208 (w), 2094 (w, ν(C≡C)), 1596 (m), 1512 (s), 1493 (s), 1416 (s), 1398 (s), 1339 (s), 1277 (m), 1181 (m), 1140 (m), 1109 (m), 1060 (m), 991 (s), 959 (s), 938 (m), 905 (w), 868 (w), 824 (m), 787 (m), 758 (s), 713 (w), 658 (m), 630 (w), 605 (m). EI-MS: *m*/*z* = 595 $[Ar^FC(H)=C(H)N(H)B(NAr'CH)_2]^+$ (<1%). Anal. found (calcd. for $C_{45}H_{62}BF_5N_6Ti$): C, 64.02 (64.29); H, 7.56 (7.43); N, 9.91 (10.00)%.

NMR tube scale synthesis of $Ti(H_2N_2^{iPr}N^{Me})\{NB(NAr'CH)_2\}(CCAr^F)_2$ (31). To an NMR tube fitted with a J. Youngs valve was added a solution of $Ti(N_2^{iPr}N^{Me})\{NB(NAr'CH)_2\}$(py) (**6**, 0.0150 g, 0.0206 mmol) in C_6D_6 (0.6 mL). Upon addition of $HCCAr^F$ (20 equiv., 55.0 μL, 0.412 mmol) *via* microsyringe, a colour change to orange was observed, and giving *ca* 93% conversion to **31**, as measured by ^{1}H NMR integration.

^{1}H NMR (C_6D_6, 500.3 MHz): δ 7.18 – 7.11 (6 H, overlapping 2 × m with residual protio solvent resonance, *m*- and *p*-$C_6\underline{H}_3{}^iPr_2$), 5.68 (2 H, s, BNCH), 3.71 (2 H, app. dd, *J* = 12.4, 3.3 Hz, $\underline{H}N^iPr$), 3.61 (4 H, sept., ^3J = 6.9 Hz, $C_6H_3(C\underline{H}MeMe)_2$), 3.48 (2 H, app. td, *J* = 12.4, 3.3 Hz, $C\underline{H}_2NMe$), 2.37 (4 H, overlapping 2 × m, $NC\underline{H}MeMe$ and $C\underline{H}_2N^iPr$), 2.17 (2 H, app. d, app. *J* = 12.8 Hz, $C\underline{H}_2N^iPr$), 2.07 (3 H, s, NMe), 1.69 (12 H, d, ^3J = 6.9 Hz, $C_6H_3(CH\underline{Me}Me)_2$), 1.64 (2 H, app. dd, app. *J* = 12.4, 2.6 Hz, $C\underline{H}_2NMe$), 1.30 (12 H, d, ^3J = 6.9 Hz, $C_6H_3(CHMe\underline{Me})_2$), 1.24 (6 H, d, ^3J = 6.5 Hz, $NCH\underline{Me}Me$), 0.63 (6 H, d, ^3J = 6.5 Hz, $NCHMe\underline{Me}$) ppm. $^{13}C\{^1H\}$ NMR (C_6D_6, 125.7 MHz): δ 166.0 (Ti$\underline{C}$C), 162.6 (Ti$\underline{C}$C), 150.3 (o_a-$\underline{C}_6H_3{}^iPr_2$), 149.1 (m, *o*-$C_6F_5$), 147.3 ($o_b$-$\underline{C}_6H_3{}^iPr_2$), 147.1 (m, *o*-$C_6F_5$), 143.0 (m, *p*-$C_6F_5$), 141.6 ($i_b$-$\underline{C}_6H_3{}^iPr_2$), 140.9 (m, *p*-$C_6F_5$), 138.6 (m, *m*-$C_6F_5$), 136.6 (m, *m*-$C_6F_5$), 135.3 ($i_a$-$\underline{C}_6H_3{}^iPr_2$), 128.6 ($p_b$-$\underline{C}_6H_3{}^iPr_2$), 127.3 ($p_a$-$\underline{C}_6H_3{}^iPr_2$), 123.7 ($m_b$-$\underline{C}_6H_3{}^iPr_2$), 123.5 ($m_a$-$\underline{C}_6H_3{}^iPr_2$), 116.6 (BNCH), 103.8 (td, $^2J_{C-F}$ = 19.1 Hz, $^3J_{C-F}$ = 3.0 Hz, *i*-C_6F_5), 96.0 (TiC$\underline{C}$), 95.5 (TiC$\underline{C}$), 57.7 ($\underline{C}H_2NMe$), 50.6 ($N\underline{C}HMeMe$), 45.4 (NMe), 40.2 ($\underline{C}H_2N^iPr$), 28.8 ($C_6H_3(\underline{C}HMeMe)_2$), 24.9 ($C_6H_3(CH\underline{Me}Me)_2$), 24.6 ($C_6H_3(CHMe\underline{Me})_2$), 24.0 ($NCH\underline{Me}Me$), 19.1 ($NCHMe\underline{Me}$) ppm. $^{11}B\{^1H\}$ NMR (C_6D_6, 128.4 MHz): δ 13.3 ppm. $^{19}F\{^1H\}$ NMR (C_6D_6, 376.5 MHz): δ –139.7 (4 F, m, overlapping o_a-C_6F_5 and o_a-C_6F_5), –158.3 (1 F, t, ^3J = 21.5 Hz, p_a-C_6F_5), –159.7 (1 F, t, ^3J = 21.5 Hz, p_b-C_6F_5), –163.8 (2 F, m, m_a-C_6F_5), –164.6 (2 F, m, m_a-C_6F_5) ppm.

$Ti(N_2^{iPr}N^{Me})\{N\{B(NAr'CH)_2\}C(H)C(Ar^F)\}$ (32). To a solution of $Ti(N_2^{iPr}N^{Me})\{NB(NAr'CH)_2\}$(py) (**6**, 0.300 g, 0.412 mmol) in toluene (10 mL) was added

$HCCAr^F$ (55 µL, 0.412 mmol) at RT. The mixture was heated to 60 °C, stirred for 16 h and then the volatiles removed under reduced pressure to yield **32** as a brown, waxy solid. Yield: 0.253 g (73%).

*Major isomer (**trans-32**)*: ^{1}H NMR (C_6D_6, 500.3 MHz): δ 9.29 (1 H, s, TiC=CH), 7.28 – 7.17 (multiple m overlapping with minor isomer, *m*- and *p*-$C_6\underline{H}_3{}^i Pr_2$), 5.97 (2 H, s, BNCH), 4.27 (2 H, sept. overlapping with minor isomer, ^3J = 6.5 Hz, NC<u>H</u>MeMe), 3.50 (4 H, sept. overlapping with minor isomer, ^3J = 6.9 Hz, $C_6H_3(C\underline{H}MeMe)_2$), 3.22 (2 H, m, $C\underline{H}_2N^iPr$), 2.89 (4 H, overlapping 2 × m, $C\underline{H}_2NMe$ and $C\underline{H}_2N^iPr$), 2.40 (2 H, m, $C\underline{H}_2NMe$), 1.89 (3 H, s, NMe), 1.37 (12 H, d, ^3J = 6.9 Hz, $C_6H_3(CH\underline{Me}Me)_2$), 1.29 – 1.25 (12 H, d overlapping with minor isomer, $C_6H_3(CHMe\underline{Me})_2$), 0.97 (6 H, d, ^3J = 6.5 Hz, NCH<u>Me</u>Me), 0.71 (6 H, d, ^3J = 6.5 Hz, NCHMe<u>Me</u>) ppm. $^{13}C\{^1H\}$ NMR (C_6D_6, 125.7 MHz): δ 168.7 (Ti<u>C</u>=CH), 147.6 (TiC=<u>C</u>H), 147.0 (*o*-$\underline{C}_6H_3{}^i Pr_2$), 142.7 (m, *o*-$C_6F_5$), 140.8 (*i*-$\underline{C}_6H_3{}^i Pr_2$), 140.4 (m, *m*-$C_6F_5$), 136.9 (m, *p*-$C_6F_5$), 127.8 (*p*-$\underline{C}_6H_3{}^i Pr_2$), 124.0 (*m*-$\underline{C}_6H_3{}^i Pr_2$), 122.2 (td, $^2J_{C–F}$ = 17.9 Hz, $^3J_{C–F}$ = 3.5 Hz, *i*-C_6F_5), 119.9 (BNCH), 56.8 ($\underline{C}H_2NMe$), 54.7 (N<u>C</u>HMeMe), 46.8 ($\underline{C}H_2N^iPr$), 43.4 (NMe), 28.9 ($C_6H_3(\underline{C}HMeMe)_2$), 25.9 ($C_6H_3(CHMe\underline{Me})_2$), 23.7 ($C_6H_3(CH\underline{Me}Me)_2$), 23.0 (NCH<u>Me</u>Me), 21.5 (NCHMe<u>Me</u>) ppm. $^{19}F\{^1H\}$ NMR (C_6D_6, 376.5 MHz): –144.1 (2 F, m, *o*-C_6F_5), –164.5 (1 F, t, ^3J = 21.5 Hz, *p*-C_6F_5), –165.6 (2 F, m, *m*-C_6F_5).

*Minor isomer (**cis-32**)*: ^{1}H NMR (C_6D_6, 500.3 MHz): δ 10.32 (1 H, s, TiC=CH), 7.28 – 7.17 (multiple m overlapping with major isomer, *m*- and *p*-$C_6\underline{H}_3{}^i Pr_2$), 6.17 (2 H, s, BNCH), 4.27 (2 H, sept. overlapping with major isomer, ^3J = 6.5 Hz, NC<u>H</u>MeMe), 3.50 (4 H, sept. overlapping with major isomer, ^3J = 6.9 Hz, $C_6H_3(C\underline{H}MeMe)_2$), 3.31 (2 H, m, $C\underline{H}_2N^iPr$), 2.95 (2 H, m, $C\underline{H}_2N^iPr$), 2.75 (2 H, m, CH_2NMe), 2.17 (2 H, m, CH_2NMe), 1.29 – 1.25 (24 H, 2 × d overlapping with major isomer, $C_6H_3(CHMe\underline{Me})_2$), 1.10 (3 H, s, NMe), 0.94 (6 H, d, ^3J = 6.5 Hz, NCH<u>Me</u>Me), 0.90 (6 H, d, ^3J = 6.5 Hz, NCHMe<u>Me</u>) ppm. $^{13}C\{^1H\}$ NMR (C_6D_6, 125.7 MHz): δ 183.3 (Ti<u>C</u>=CH), 149.7 (TiC=<u>C</u>H), 146.9 (*o*-$\underline{C}_6H_3{}^i Pr_2$), 141.2 (*i*-$\underline{C}_6H_3{}^i Pr_2$), 127.7 (*p*-$\underline{C}_6H_3{}^i Pr_2$), 124.1 (*m*-$\underline{C}_6H_3{}^i Pr_2$), 120.2 (NCH), 57.1 (N<u>C</u>HMeMe), 57.0 ($\underline{C}H_2NMe$), 47.3 ($\underline{C}H_2N^iPr$), 41.3 (NMe), 28.9 ($C_6H_3(\underline{C}HMeMe)_2$), 24.9 ($C_6H_3(CHMe\underline{Me})_2$), 23.9 ($C_6H_3(CH\underline{Me}Me)_2$), 22.2 (NCH<u>Me</u>Me), 22.1 (NCHMe<u>Me</u>) ppm. Those resonances belonging to the Ar^F ring could not be satisfactorily assigned. $^{19}F\{^1H\}$ NMR (C_6D_6, 376.5 MHz): δ –141.7 (2 F, m, *o*-C_6F_5), –164.9 (1 F, t, ^3J = 21.5 Hz, *p*-C_6F_5), –166.2 (2 F, m, *m*-C_6F_5) ppm.

Common data: $^{11}B\{^1H\}$ NMR (C_6D_6, 128.4 MHz): 22.7 ppm. IR (NaCl plates, Nujol mull, cm^{-1}): 3438 (w), 3065 (w), 1929 (w), 1655 (m), 1638 (m), 1585 (m), 1512 (s), 1415 (s), 1288 (w), 1228 (w), 1203 (w), 1176 (w), 1117 (m), 1007 (m), 989 (m), 976 (m), 960 (s), 940 (w), 898 (w), 888 (w), 865 (w), 823 (s), 759 (s), 674 (w), 649 (w), 620 (w), 606 (m), 566 (w). EI-MS: *m*/*z* = 595 $[Ar^FC(H)=C(H)N(H)B(NAr'CH)_2]^+$ (100%). Anal. found (calcd. for $C_{45}H_{62}BF_5N_6Ti$): C, 64.09 (64.29); H, 7.59 (7.43); N, 9.90 (10.00)%.

NMR tube scale synthesis of Ti($N_2^{iPr}N^{Me}$){N{B(NAr'CH)$_2$}C(H)C(Ar^F)} (32). To an NMR tube fitted with a J. Youngs valve was added a solution of Ti($N_2^{iPr}N^{Me}$){NHB(NAr'CH)$_2$}(CCAr^F) (**30**, 0.0150 g, 0.0178 mmol) in C_6D_6 (0.6 mL). The tube was heated at 70 °C for 16 h, after which time the ^1H NMR spectrum indicated quantitative conversion to **32**.

Ti(N_2N^{py}){N{B(NAr'CH)$_2$}C(H)C(Tol)} (33). To a solution of Ti(N_2N^{py}){NB(NAr'CH)$_2$}(py) (**7**, 0.300 g, 0.359 mmol) in toluene (10 mL) was added HCCTol (46 µL, 0.359 mmol) at RT. The mixture was heated to 60 °C and stirred for 2 h, then the volatiles removed under reduced pressure. The dark brown waxy solid was then dissolved in hexane (10 mL), concentrated to ~5 mL and cooled to 5 °C, resulting in deep brown, diffraction-quality crystals of **33**. Yield: 0.076 g (24%).

^1H NMR (C_6D_6, 400.1 MHz): δ 9.56 (1 H, s, TiC=CH), 9.07 (1 H, d, ^3J = 4.3 Hz, 6-C_5H_4N), 7.35 (2 H, d, ^3J = 8.0 Hz, *m*-$C_6\underline{H}_4Me$), 7.20 – 7.09 (9 H, 5 × m overlapping with residual protio solvent resonance, *m*- and *p*-$C_6\underline{H}_3{}^iPr_2$ and 3,4,5-C_5H_4N), 6.88 (2 H, d, ^3J = 8.0 Hz, *o*-$C_6\underline{H}_4Me$), 6.21 (2 H, s, NCH), 4.07 (2 H, d, ^2J = 12.3 Hz, NCH_2), 3.55 (4 H, sept., ^3J = 6.9 Hz, C$\underline{H}$MeMe), 3.22 (2 H, d, ^2J = 12.3 Hz, NCH_2), 2.18 (3 H, s, $C_6H_4\underline{Me}$), 1.29 (12 H, d, ^3J = 6.9 Hz, CH$\underline{Me}$Me), 1.15 (3 H, s, CMe), 1.12 (12 H, d, ^3J = 6.9 Hz, CHMe$\underline{Me}$), –0.26 (18 H, s, $SiMe_3$) ppm. $^{13}C\{^1H\}$ NMR (C_6D_6, 125.7 MHz): δ 210.6 (Ti$\underline{C}$=CH), 162.0 (2-C_5H_4N), 154.9 (TiC=$\underline{C}$H), 146.9 (*o*-$\underline{C}_6H_3{}^iPr_2$), 146.7 (6-$C_5H_4N$), 143.0 (5-$C_5H_4N$), 140.0 (*i*-$\underline{C}_6H_3{}^iPr_2$), 138.5 (4-$C_5H_4N$), 132.1 (*p*-$\underline{C}_6H_4Me$), 129.2 (*p*-$\underline{C}_6H_3{}^iPr_2$), 127.6 (3-$C_5H_4N$), 124.9 (*m*-$\underline{C}_6H_4Me$), 123.9 (*m*-$\underline{C}_6H_3{}^iPr_2$), 121.1 (*i*-$\underline{C}_6H_4Me$), 120.0 (*o*-$\underline{C}_6H_4Me$), 119.2 (NCH), 63.4 ($NCH_2$), 51.0 ($\underline{C}$Me), 29.0 ($\underline{C}$HMeMe), 26.5 (CH$\underline{Me}$Me), 23.8 (CHMe$\underline{Me}$), 22.7 ($C\underline{Me}$), 21.3 ($C_6H_4\underline{Me}$), 0.44 ($SiMe_3$) ppm. $^{11}B\{^1H\}$ NMR (C_6D_6, 128.4 MHz): 25.5 ppm. IR (NaCl plates, Nujol mull, cm^{-1}): 3437 (w), 1656 (m), 1601 (w), 1587 (m), 1571 (w), 1403 (s), 1246 (s), 1179 (w), 1159 (w), 1140 (w), 1115 (w), 1059 (m), 915 (m), 856 (s), 837 (s), 806 (m), 780 (w), 762 (m), 683 (w), 645 (m). EI-MS: *m*/*z* = 519

$[TolC(H)=C(H)N(H)B(NAr'CH)_2]^+$ (8%). Anal. found (calcd. for $C_{50}H_{73}BN_6Si_2Ti$): C, 68.66 (68.79); H, 8.52 (8.43); N, 9.51 (9.63)%.

$Ti(N_2N^{py})\{NHB(NAr'CH)_2\}(CCAr^F)$ (34). To a solution of $Ti(N_2N^{py})\{NB(NAr'CH)_2\}(py)$ (**7**, 0.300 g, 0.359 mmol) in toluene (10 mL) was added $HCCAr^F$ (47.5 μL, 0.359 mmol) at RT, then the mixture left to stir for 24 h, resulting in a deep red-brown solution. The volatiles were then removed under reduced pressure, and the crude product dissolved in hexane (10 mL). This solution was concentrated to ~5 mL and cooled to 5 °C, resulting in orange, diffraction-quality crystals of **34**. Yield: 0.075 g (22%).

^{1}H NMR (C_6D_6, 400.1 MHz): δ 9.11 (1 H, d, ^3J = 5.3 Hz, 6-C_5H_4N), 7.25 – 7.18 (6 H, overlapping 2 × m, *m*- and *p*-$C_6\underline{H}_3{}^i Pr_2$), 7.13 (1 H, m, 4-$C_5H_4N$), 6.88 (1 H, m, 5-$C_5H_4N$), 6.82 (1 H, d, ^3J = 7.9 Hz, 3-C_5H_4N), 6.08 (1 H, s, N$\underline{H}$B(NAr'CH)$_2$), 6.01 (2 H, s, NCH), 3.99 (2 H, d, ^2J = 12.8 Hz, NCH_2), 3.44 (4 H, sept., ^3J = 6.9 Hz, C$\underline{H}$MeMe), 3.16 (2 H, d, ^2J = 12.8 Hz, NCH_2), 1.28 (12 H, d, ^3J = 6.9 Hz, CH$\underline{Me}$Me), 1.26 (6 H, d, ^3J = 6.9 Hz, CHMe$\underline{Me}_a$), 1.19 (6 H, br. m, CHMe$\underline{Me}_b$), 1.06 (3 H, s, C$\underline{Me}$), 0.01 (18 H, s, $SiMe_3$) ppm. ^{13}C{^{1}H} NMR (C_6D_6, 100.6 MHz): δ 162.0 (2-C_5H_4N), 161.1 (Ti$\underline{C}$CAr^F), 148.7 (m, *o*-C_6F_5), 147.6 (*o*$_a$-$\underline{C}_6H_3{}^i Pr_2$), 147.5 (6-$C_5H_4N$), 147.2 (*o*$_a$-$\underline{C}_6H_3{}^i Pr_2$), 139.7 (*i*-$\underline{C}_6H_3{}^i Pr_2$), 138.8 (m, *p*-$C_6F_5$), 138.5 (4-$C_5H_4N$), 136.9 (m, *m*-$C_6F_5$), 127.6 (*p*-$\underline{C}_6H_3{}^i Pr_2$), 124.3 (*m*$_a$-$\underline{C}_6H_3{}^i Pr_2$), 123.9 (*m*$_a$-$\underline{C}_6H_3{}^i Pr_2$), 121.2 (5-$C_5H_4N$), 119.5 (3-$C_5H_4N$), 118.0 (NCH), 103.6 (td, $^2J_{C–F}$ = 19.0 Hz, $^3J_{C–F}$ = 3.7 Hz, *i*-C_6F_5), 87.6 (TiC$\underline{C}$Ar^F), 64.5 (NCH_2), 49.7 ($\underline{C}$Me), 28.7 ($\underline{C}$HMeMe), 25.7 (CH$\underline{Me}$Me), 24.4 (CHMe$\underline{Me}_b$), 24.3 (CHMe$\underline{Me}_a$), 22.8 (C$\underline{Me}$), –0.34 ($SiMe_3$) ppm. ^{11}B{^{1}H} NMR (C_6D_6, 128.4 MHz): 23.0 ppm. ^{19}F{^{1}H} NMR (C_6D_6, 376.5 MHz): –138.8 (2 F, m, *o*-C_6F_5), –159.8 (1 F, t, ^3J = 21.4 Hz, *p*-C_6F_5), –164.7 (2 F, m, *m*-C_6F_5) ppm. IR (NaCl plates, Nujol mull, cm^{-1}): 3484 (w), 3409 (w), 3213 (w), 2096 (m , ν(C≡C)), 1604 (m), 1575 (w), 1512 (s), 1492 (s), 1354 (s), 1326 (w), 1289 (w), 1275 (w), 1184 (w), 1141 (m), 1112 (m), 1059 (m), 1047 (m), 989 (s), 958 (s), 913 (s), 890 (w), 839 (s), 808 (m), 754 (m), 688 (w), 657 (m), 645 (w), 611 (m). EI-MS: *m*/*z* = 595 $[Ar^FC(H)=C(H)N(H)B(NAr'CH)_2]^+$ (56%). Anal. found (calcd. for $C_{49}H_{66}BF_5N_6Si_2Ti$): C, 61.89 (62.02); H, 7.13 (7.01); N, 9.01 (8.86)%.

Kinetic isotope effect measurements for the reaction of $Ti(N_2N^{py})\{NB(NAr'CH)_2\}$ (7) with $HCCAr^F$ to form $Ti(N_2N^{py})\{NHB(NAr'CH)_2\}(CCAr^F)$ (34). To a C_6D_6 solution (0.6 mL) of $Ti(N_2N^{py})\{NB(NAr'CH)_2\}(py)$ (**7**, 0.0150 g, 0.0179 mmol) in an NMR tube equipped with a J. Youngs valve was added $HCCAr^F$ or $DCCAr^F$ (2.4 μL, 0.0179 mmol)

via microsyringe. The NMR tube was transferred to a temperature-regulated (298 K) probe, and the reaction monitored by ^{1}H NMR spectroscopy using an array which recorded spectra (4 scans) every 120 s. The formation of **34** (or **34-*d*$_1$**) was calculated by measuring the integral of an NCH_2 resonance. Initial rate constants were obtained from plots of [**34**] *vs* time using *Origin*.

Competition reaction of Ti(N$_2$N^{py}){NB(NAr'CH)$_2$}(py) (7) with HCCAr^F and DCCAr^F. To a C_6D_6 solution (0.3 mL) of Ti(N_2N^{py}){NB(NAr'CH)$_2$}(py) (**7**, 0.0100 g, 0.0120 mmol) in an NMR tube fitted with a J. Youngs valve was added a C_6D_6 solution (0.3 mL) of $HCCAr^F$ (7.9 μL, 0.0598 mmol) and $DCCAr^F$ (8.0 μL, 0.0598 mmol). The mixture was then left at RT for 16 h, with ^{1}H NMR integration showing the products to be 87% **34** and 13% **34-*d*$_1$**.

Ti(N$_2$N^{py}){N{B(NAr'CH)$_2$}C(H)C(Ar^F)} (35). To a solution of Ti(N_2N^{py}){NB(NAr'CH)$_2$}(py) (**7**, 0.267 g, 0.319 mmol) in toluene (10 mL) was added $HCCAr^F$ (42.5 μL, 0.359 mmol) at RT, then the mixture heated to 60 °C and stirred for 40 h, resulting in a deep brown solution. The volatiles were then removed under reduced pressure, and **35** isolated as a deep brown, waxy solid. Yield: 0.195 g (64%).

^{1}H NMR (C_6D_6, 500.3 MHz): δ 10.05 (1 H, s, TiC=CH), 9.04 (1 H, d, ^{3}J = 5.2 Hz, 6-C_5H_4N), 7.25 – 7.17 (6 H, overlapping 2 × m, *m*- and *p*-$C_6\underline{H}_3{}^{i}Pr_2$), 7.10 (1 H, m, 4-$C_5H_4N$), 6.89 (1 H, m, 5-$C_5H_4N$), 6.85 (1 H, d, ^{3}J = 8.1 Hz, 3-C_5H_4N), 6.20 (2 H, s, NCH), 4.09 (2 H, d, ^{2}J = 12.4 Hz, NCH_2), 3.46 (4 H, sept., ^{3}J = 6.9 Hz, C$\underline{H}$MeMe), 3.12 (2 H, d, ^{2}J = 6.9 Hz, NCH_2), 1.28 (6 H, d, ^{3}J = 6.9 Hz, CH$\underline{Me}_a$Me), 1.26 (12 H, d, ^{3}J = 6.9 Hz, CHMe$\underline{Me}$), 1.10 (3 H, s, CMe), 1.08 (6 H, br. m, CH$\underline{Me}_b$Me), –0.28 (18 H, s, $SiMe_3$) ppm. ^{13}C{^{1}H} NMR (C_6D_6, 125.7 MHz): δ 177.9 (Ti$\underline{C}$=CH), 161.4 (TiC=$\underline{C}$H), 161.2 (2-C_5H_4N), 147.6 (*o*-$C_6\underline{H}_3{}^{i}Pr_2$), 146.4 (6-$C_5H_4N$), 142.9 (m, *o*-$C_6F_5$), 140.9 (m, *m*-$C_6F_5$), 139.5 (*i*-$C_6\underline{H}_3{}^{i}Pr_2$), 138.9 (4-$C_5H_4N$), 137.4 (m, *p*-$C_6F_5$), 127.6 (*p*-$C_6\underline{H}_3{}^{i}Pr_2$), 124.0 (*m*-$C_6\underline{H}_3{}^{i}Pr_2$), 121.4 (5-$C_5H_4N$), 120.2 (3-$C_5H_4N$), 119.5 (td, $^{2}J_{C–F}$ = 14.5 Hz, $^{3}J_{C–F}$ = 4.5 Hz, *i*-C_6F_5), 119.3 (NCH), 63.4 (NCH_2), 50.4 ($\underline{C}$Me), 28.6 ($\underline{C}$HMeMe), 26.6 (CHMe$\underline{Me}$), 24.4 (CH$\underline{Me}$Me), 23.4 (C$\underline{Me}$), 0.01 ($SiMe_3$) ppm. ^{11}B{^{1}H} NMR (C_6D_6, 128.4 MHz): 25.0 ppm. ^{19}F{^{1}H} NMR (C_6D_6, 376.5 MHz): –141.5 (2 F, m, *o*-C_6F_5), –166.9 (2 F, m, *m*-C_6F_5), –168.5 (1 F, tt, ^{3}J = 21.6 Hz, ^{4}J 4.1 Hz, *p*-C_6F_5) ppm. IR (NaCl plates, Nujol mull, cm^{-1}): 3522 (w), 3436 (w), 3391 (w), 1931 (w), 1865 (w), 1655 (m), 1638 (m), 1602 (m), 1587 (s), 1506 (s), 1327 (m), 1209 (m), 1180 (w), 1116 (m), 1059 (s), 959 (s), 913 (s), 856 (s), 780 (m), 758 (s), 675

(m), 646 (m), 604 (m). EI-MS: *m*/*z* = 595 $[Ar^FC(H)=C(H)N(H)B(NAr'CH)_2]^+$ (4%). Anal. found (calcd. for $C_{49}H_{66}BF_5N_6Si_2Ti$): C, 61.88 (62.02); H, 7.10 (7.01); N, 9.02 (8.86)%.

NMR tube scale synthesis of Ti(N_2N^{py}){N{B(NAr'CH)$_2$}C(H)C(Ar^F)} (35). To an NMR tube fitted with a J. Youngs valve was added a solution of Ti(N_2N^{py}){NHB(NAr'CH)$_2$}($CCAr^F$) (**34**, 0.0150 g, 0.0158 mmol) in C_6D_6 (0.6 mL). The tube was heated at 70 °C for 18 h, after which time the ^{1}H NMR spectrum indicated quantitative conversion to **35**.

Kinetic isotope effect measurements for the conversion of Ti(N_2N^{py}){NHB(NAr'CH)$_2$}($CCAr^F$) (34) to Ti(N_2N^{py}){N{B(NAr'CH)$_2$}C(H)C(Ar^F)} (35). A C_6D_6 solution (0.6 mL) of Ti(N_2N^{py}){NHB(NAr'CH)$_2$}($CCAr^F$) (**34**, 0.0150 g, 0.0158 mmol) or **34-*d*$_1$** was transferred to an NMR tube equipped with a J. Youngs valve. A blank C_6D_6 sample was added to the NMR probe at RT, locked and shimmed, and the probe heated to 343 K. After thermal equilibration, the experimental sample replaced the blank sample, the shimming was checked and an array was set up to record a ^{1}H NMR spectrum (4 scans) every 120 s (or every 600 s for **34-*d*$_1$**). The decay of **34** was calculated by measuring the integral of an NCH_2 doublet. First order rate constants were obtained from linear plots of –ln([**34**]/[**34**]$_0$) *vs* time.

NMR tube scale reaction of Ti(N_2N^{py}){N{B(NAr'CH)$_2$}C(H)C(Tol)} (33) with H_2N^tBu. To a C_6D_6 solution (0.6 mL) of Ti(N_2N^{py}){N{B(NAr'CH)$_2$}C(H)C(Tol)} (**33**, 0.0150 g, 0.0172 mmol) in an NMR tube equipped with a J. Youngs valve was added H_2N^tBu (1.8 μL, 0.0172 mmol) and pyridine (1.4 μL, 0.0172 mmol). After heating at 60 °C for 24 h, quantitative conversion of the boryl moiety to TolC(H)=C(H)N(H)B(NAr'CH)$_2$ (**4.9**) had taken place, with the ^{1}H NMR spectrum showing signals consistent with those of isolated **4.9**.[28] The identity of the titanium-containing species in solution could not be ascertained.

6.8 Experimental details and characterising data for Chapter Five

(L^1)Sc(Me){NHB(NAr'CH)$_2$} (36). To a solution of (L^1)$ScCl_2$ (**5.2,** 0.950 g, 2.14 mmol) in THF (25 mL) at –78 °C was added MeLi (1.6 M in Et_2O, 2.7 mL, 4.28 mmol). The mixture was allowed to warm to RT, then stirred for 4 h. The volatiles were then removed under reduced pressure, and the residue extracted with toluene (25 mL). The extracts were transferred into a Schlenk tube containing $H_2NB(NAr'CH)_2$ (**2.2**, 0.862 g, 2.14 mmol), and this mixture stirred for 60 h at RT. After this time, the volatiles were removed under reduced pressure, and the resulting waxy solid triturated in hexane (5 mL). After drying *in*

vacuo, **36** was isolated as an off-white powder. Yield: 0.898 g (53%). Diffraction-quality crystals were grown from a benzene solution at RT.

^{1}H NMR (C_6D_6, 400.1 MHz): δ 7.18 (6 H, overlapping 2 × m, boryl *m*- and *p*-$C_6\underline{H}_3{}^{i}Pr_2$), 7.13 (2 H, d, ^{3}J = 4.6 Hz, NacNac *m*-$C_6\underline{H}_3{}^{i}Pr_2$), 7.05 (1 H, t, ^{3}J = 4.6 Hz, NacNac *p*-$C_6\underline{H}_3{}^{i}Pr_2$), 6.05 (2 H, s, NCH), 4.77 (1 H, s, MeC(N)C$\underline{H}$), 3.70 (2 H, sept., ^{3}J = 6.9 Hz, boryl C$\underline{H}_a$MeMe), 3.51 (2 H, sept., ^{3}J = 6.9 Hz, boryl C$\underline{H}_b$MeMe), 3.43 (1 H, sept., ^{3}J = 6.8 Hz, NacNac C$\underline{H}_a$MeMe), 3.29 (1 H, s, NH), 2.86 (1 H, sept., ^{3}J = 6.8 Hz, NacNac C$\underline{H}_b$MeMe), 2.63 (1 H, m, C$\underline{H}_2$NC(Me)), 2.53 (1 H, m, C$\underline{H}_2$NMe$_2$), 2.44 (1 H, m, C$\underline{H}_2$NC(Me)), 2.31 (3 H, s, NMe$_2$), 1.98 (3 H, s, NMe$_2$), 1.77 (1 H, m, C$\underline{H}_2$NMe$_2$), 1.59 (3 H, s, $\underline{Me}$C(N)CH), 1.52 (3 H, s, $\underline{Me}$C(N)CH), 1.42 (6 H, d, ^{3}J = 6.9 Hz, boryl CH$\underline{Me}_a$Me), 1.33 (6 H, d, ^{3}J = 6.9 Hz, boryl CH$\underline{Me}_b$Me), 1.30 (9 H, overlapping 2 × d, boryl CHMe$\underline{Me}_b$ and NacNac CH$\underline{Me}_a$Me), 1.23 (9 H, overlapping 2 × d, boryl CHMe$\underline{Me}_a$ and NacNac CH$\underline{Me}_b$Me), 1.06 (3 H, d, ^{3}J = 6.8 Hz, NacNac CHMe$\underline{Me}_b$), 1.04 (3 H, d, ^{3}J = 6.8 Hz, NacNac CHMe$\underline{Me}_a$), –0.90 (3 H, s, ScMe) ppm. ^{13}C{^{1}H} NMR (C_6D_6, 100.6 MHz): δ 166.3 (Me$\underline{C}$(N)CH), 165.5 (Me$\underline{C}$(N)CH), 147.5 (NacNac *o*-$\underline{C}_6H_3{}^{i}Pr_2$), 147.4 (boryl *o*-$\underline{C}_6H_3{}^{i}Pr_2$), 146.9 (boryl *o*-$\underline{C}_6H_3{}^{i}Pr_2$), 142.9 (NacNac *i*-$\underline{C}_6H_3{}^{i}Pr_2$), 141.9 (boryl *i*-$\underline{C}_6H_3{}^{i}Pr_2$), 141.3 (boryl *i*-$\underline{C}_6H_3{}^{i}Pr_2$), 126.7 (boryl *p*-$\underline{C}_6H_3{}^{i}Pr_2$), 125.6 (NacNac *p*-$\underline{C}_6H_3{}^{i}Pr_2$), 124.1 (NacNac *m*-$\underline{C}_6H_3{}^{i}Pr_2$), 124.0 (boryl *m*-$\underline{C}_6H_3{}^{i}Pr_2$), 123.6 (boryl *m*-$\underline{C}_6H_3{}^{i}Pr_2$), 117.5 (NCH), 99.5 (MeC(N)$\underline{C}$H), 58.8 ($\underline{C}H_2NMe_2$), 48.2 (NMe$_2$), 46.8 ($\underline{C}H_2NC(Me)$), 42.7 (NMe$_2$), 29.0 (boryl $\underline{C}_a$HMeMe), 28.3 (NacNac $\underline{C}_b$HMeMe), 28.2 (boryl $\underline{C}_b$HMeMe), 28.1 (NacNac $\underline{C}_a$HMeMe), 26.1 (boryl CHMe$\underline{Me}_b$), 25.9 (boryl CHMe$\underline{Me}_a$), 25.0 (NacNac CH$\underline{Me}_a$Me), 24.8 ($\underline{Me}$C(N)CH), 24.7 (NacNac CHMe$\underline{Me}_b$), 24.4 (NacNac CH$\underline{Me}_b$Me), 24.3 (ScMe), 24.2 (boryl CH$\underline{Me}_b$Me), 24.0 (NacNac CHMe$\underline{Me}_a$), 23.4 ($\underline{Me}$C(N)CH), 22.8 (boryl CH$\underline{Me}_a$Me) ppm. ^{11}B{^{1}H} NMR (C_6D_6, 128.4 MHz): δ 23.3 ppm. IR (NaCl plates, Nujol mull, cm^{-1}): 3212 (w, N–H), 3056 (w), 1930 (w), 1863 (w), 1581 (w), 1546 (m), 1523 (s), 1497 (m), 1416 (s), 1359 (s), 1345 (s), 1317 (m), 1254 (m), 1180 (m), 1138 (w), 1115 (w), 1103 (w), 1067 (w), 1052 (w), 1024 (m), 962 (w), 937 (m), 878 (w), 845 (w), 806 (w), 790 (m), 766 (m), 750 (s), 706 (w), 649 (m). Anal. found (calcd. for $C_{48}H_{74}BN_6Sc$): C, 72.68 (72.89); H, 9.55 (9.43); N, 10.50 (10.63)%.

(L^{1})Sc(Me){NDB(NAr'CH)$_2$} (36-*d*$_1$) was prepared analogously to **36**, using (L^{1})ScCl$_2$ (**5.2**, 0.225 g, 0.506 mmol), MeLi (1.6 M in Et$_2$O, 0.63 mL, 1.01 mmol) and D$_2$NB(NAr'CH)$_2$ (**2.2-*d*$_2$**, 0.205 g, 0.506 mmol). Yield: 0.103 g (26%). The ^{1}H NMR spectrum was identical to that of **36**, other than the absence of the NH resonance.

NMR tube scale synthesis of (L^1)Sc{NHB(NAr'CH)$_2$}Cl (37). A mixture of (L^1)ScCl$_2$ (**5.2**, 0.0150 g, 0.0338 mmol) and LiNHB(NAr'CH)$_2$ (**5.5**, 0.0138 g, 0.0338 mmol) in C_6D_6 (0.6 mL) was transferred to an NMR tube fitted with a J. Youngs valve. The ^{1}H NMR spectrum indicated quantitative conversion to **37** at RT.

^{1}H NMR (C_6D_6, 400.1 MHz): δ 7.19 – 7.05 (overlapping 4 × m, boryl and NacNac *m*- and *p*-C$_6$H$_3^i$Pr$_2$), 6.02 (2 H, s, NCH), 4.81 (1 H, s, MeC(N)CH), 3.72 (1 H, s, NH), 3.61 (2 H, sept., ^3J = 6.9 Hz, boryl CH$_a$MeMe), 3.48 (2 H, sept., ^3J = 6.9 Hz, boryl CH$_b$MeMe), 3.25 (1 H, sept., ^3J = 6.8 Hz, NacNac CH$_a$MeMe), 2.67 (3 H, overlapping 2 × m, NacNac CH$_b$MeMe and CH$_2$NMe$_2$), 2.58 (1 H, m, CH$_2$NC(Me)), 2.47 (1 H, m, CH$_2$NC(Me)), 2.37 (3 H, s, NMe$_2$), 2.02 (3 H, s, NMe$_2$), 1.70 (1 H, m, CH$_2$NMe$_2$), 1.54 (3 H, s, MeC(N)CH), 1.50 (3 H, s, MeC(N)CH), 1.46 (6 H, d, ^3J = 6.9 Hz, boryl CHMe$_a$Me), 1.33 (6 H, d, ^3J = 6.9 Hz, boryl CHMe$_b$Me), 1.28 (12 H, overlapping 3 × d, boryl CHMeMe$_a$, NacNac CHMe$_a$Me and NacNac CHMe$_b$Me), 1.23 (6 H, d, ^3J = 6.9 Hz, boryl CHMeMe$_b$), 1.13 (3 H, d, ^3J = 6.8 Hz, NacNac CHMeMe$_a$), 1.02 (3 H, d, ^3J = 6.8 Hz, NacNac CHMeMe$_b$) ppm. ^{13}C{^{1}H} NMR (C_6D_6, 100.6 MHz): δ 166.9 (MeC(N)CH), 166.2 (MeC(N)CH), 147.8 (NacNac *o*-C$_6$H$_3^i$Pr$_2$), 147.5 (boryl *o*-C$_6$H$_3^i$Pr$_2$), 147.0 (boryl *o*-C$_6$H$_3^i$Pr$_2$), 142.9 (NacNac *i*-C$_6$H$_3^i$Pr$_2$), 141.3 (boryl *i*-C$_6$H$_3^i$Pr$_2$), 141.0 (boryl *i*-C$_6$H$_3^i$Pr$_2$), 126.9 (boryl *p*-C$_6$H$_3^i$Pr$_2$), 125.9 (NacNac *p*-C$_6$H$_3^i$Pr$_2$), 124.2 (NacNac *m*-C$_6$H$_3^i$Pr$_2$), 124.0 (boryl *m*-C$_6$H$_3^i$Pr$_2$), 123.8 (boryl *m*-C$_6$H$_3^i$Pr$_2$), 123.5 (NacNac *m*-C$_6$H$_3^i$Pr$_2$), 117.6 (NCH), 100.2 (MeC(N)CH), 58.5 (CH$_2$NMe$_2$), 48.9 (NMe$_2$), 46.9 (CH$_2$NC(Me)), 42.3 (NMe$_2$), 29.0 (boryl C$_a$HMeMe), 28.4 (NacNac C$_a$HMeMe and C$_b$HMeMe), 28.3 (boryl C$_b$HMeMe), 26.0 (boryl CHMeMe$_b$), 25.9 (boryl CHMeMe$_a$), 24.9 (NacNac CHMe$_a$Me and MeC(N)CH), 24.6 (NacNac CHMe$_b$Me), 24.4 (NacNac CHMeMe$_b$), 24.2 (NacNac CHMeMe$_a$), 24.1 (boryl CHMe$_b$Me), 23.3 (MeC(N)CH), 23.0 (boryl CHMe$_a$Me) ppm. ^{11}B{^{1}H} NMR (C_6D_6, 128.4 MHz): δ 22.9 ppm.

{MeC(NC$_6$H$_3^i$PrCH(Me)CH$_2$)CHC(Me)NCH$_2$CH$_2$NMe$_2$}Sc{NHB(NAr'CH)$_2$} (38). A toluene solution (7.5 mL) of (L^1)Sc(Me){NHB(NAr'CH)$_2$} (**36**, 0.197 g, 0.249 mmol) was heated at 60 °C for 16 h. The volatiles were removed under reduced pressure, and the resulting residue washed with hexane (2 × 2 mL) to afford **38** as an off-white powder. Yield: 0.100 g (52%). Diffraction-quality crystals were grown from a benzene solution at RT.

^{1}H NMR (C_6D_6, 400.1 MHz): δ 7.21 – 7.09 (overlapping 4 × m, boryl and NacNac *m*- and *p*-$C_6\underline{H}_3{}^{i}Pr_2$), 5.91 (2 H, s, NCH), 4.93 (1 H, s, MeC(N)C$\underline{H}$), 3.58 (2 H, sept., ^{3}J = 6.9 Hz, boryl C$\underline{H}_a$MeMe), 3.31 (3 H, overlapping 2 × m, boryl C$\underline{H}_b$MeMe and NacNac C$\underline{H}$MeMe), 3.09 (1 H, m, ScCH$_2$C$\underline{H}$Me), 2.83 (1 H, s, NH), 2.58 (1 H, td, ^{2}J = 13.5 Hz, ^{3}J = 5.5 Hz, C$\underline{H}_2$NC(Me)), 2.30 (1 H, td, ^{2}J = 13.5 Hz, ^{3}J = 5.5 Hz, C$\underline{H}_2$NMe$_2$), 2.20 (3 H, s, NMe$_2$), 2.13 (1 H, dd, ^{2}J = 13.5 Hz, ^{3}J = 5.5 Hz, C$\underline{H}_2$NC(Me)), 1.71 (3 H, s, $\underline{Me}$C(N)CH), 1.64 (3 H, s, $\underline{Me}$C(N)CH), 1.60 (3 H, s, NMe$_2$), 1.50 (3 H, d, ^{3}J = 6.8 Hz, NacNac CH$\underline{Me}$Me), 1.37 (6 H, overlapping 2 × d, NacNac CHMe$\underline{Me}$ and ScCH$_2$CH$\underline{Me}$), 1.34 (1 H, m, C$\underline{H}_2$NMe$_2$), 1.27 (12 H, d, ^{3}J = 6.9 Hz, boryl CH$\underline{Me}$Me), 1.23 (12 H, d, ^{3}J = 6.9 Hz, boryl CHMe$\underline{Me}$), 0.22 (1 H, app. t, app. *J* = 12.2 Hz, ScC$\underline{H}_2$), –0.01 (1 H, dd, ^{2}J = 12.2 Hz, ^{3}J = 3.3 Hz) ppm. ^{13}C{^{1}H} NMR (C_6D_6, 100.6 MHz): δ 166.4 (Me$\underline{C}$(N)CH), 164.8 (Me$\underline{C}$(N)CH), 147.8 (boryl *o*-$\underline{C}_6H_3{}^{i}Pr_2$), 147.6 (NacNac *o*-$\underline{C}_6H_3{}^{i}Pr_2$), 147.2 (boryl *o*-$\underline{C}_6H_3{}^{i}Pr_2$), 143.9 (NacNac *i*-$\underline{C}_6H_3{}^{i}Pr_2$), 141.9 (boryl *i*-$\underline{C}_6H_3{}^{i}Pr_2$), 141.2 (boryl *i*-$\underline{C}_6H_3{}^{i}Pr_2$), 126.8 (boryl *p*-$\underline{C}_6H_3{}^{i}Pr_2$), 125.5 (NacNac *p*-$\underline{C}_6H_3{}^{i}Pr_2$), 124.1 (boryl *m*-$\underline{C}_6H_3{}^{i}Pr_2$), 123.9 (NacNac *m*-$\underline{C}_6H_3{}^{i}Pr_2$), 123.0 (boryl *m*-$\underline{C}_6H_3{}^{i}Pr_2$), 122.0 (NacNac *m*-$\underline{C}_6H_3{}^{i}Pr_2$), 117.8 (NCH), 98.5 (MeC(N)$\underline{C}$H), 54.4 ($\underline{C}$H$_2$NMe$_2$), 48.1 (NMe$_2$), 47.0 ($\underline{C}$H$_2$NC(Me)), 42.3 (NMe$_2$), 38.1 (ScCH$_2\underline{C}$HMe), 32.0 (ScCH$_2$), 29.0 (boryl $\underline{C}_a$HMeMe), 27.9 (boryl $\underline{C}_b$HMeMe), 27.6 (NacNac $\underline{C}$HMeMe), 26.7 (boryl CH$\underline{Me}_a$Me), 26.1 (boryl CHMe$\underline{Me}_a$ and NacNac CH$\underline{Me}$Me), 25.8 (ScCH$_2$CH$\underline{Me}$), 24.4 (boryl CHMe$\underline{Me}_b$), 23.6 (NacNac CHMe$\underline{Me}$), 23.2 ($\underline{Me}$C(N)CH), 22.5 (boryl CH$\underline{Me}_b$Me), 22.3 ($\underline{Me}$C(N)CH) ppm. ^{11}B{^{1}H} NMR (C_6D_6, 128.4 MHz): δ 23.3 ppm. IR (NaCl plates, Nujol mull, cm^{-1}): 3210 (w, N–H), 3059 (w), 2360 (w), 1922 (w), 1857 (w), 1793 (w), 1583 (w), 1530 (s), 1360 (s) 1334 (s), 1319 (m), 1273 (m), 1229 (w), 1176 (m), 1136 (m), 1115 (w), 1047 (m), 970 (m), 938 (m), 878 (m), 846 (w), 805 (m), 787 (w), 763 (s), 748 (s), 707 (m), 650 (m). Anal. found (calcd. for $C_{47}H_{70}BN_6Sc$): C, 72.71 (72.85); H, 9.21 (9.11); N, 10.95 (10.85)%.

(L^{1})Sc{NHB(NAr'CH)$_2$}(η^{2}-NC$_5$H$_4$) (39). To a toluene solution (8 mL) of (L^{1})Sc(Me){NHB(NAr'CH)$_2$} (**36**, 0.197 g, 0.249 mmol) was added pyridine (40 μL, 0.498 mmol) at RT. The mixture was heated to 60 °C and stirred for 16 h, after which the volatiles were removed under reduced pressure, to afford **39** as an off-white solid, which was then dried *in vacuo*. Yield: 0.120 g (56%).

^{1}H NMR (C_6D_6, 400.1 MHz): δ 7.32 – 7.26 (5 H, overlapping m, boryl and NacNac *m*- and *p*-$C_6\underline{H}_3{}^{i}Pr_2$), 7.11 – 7.04 (3 H, overlapping m, boryl and NacNac *m*- and *p*-$C_6\underline{H}_3{}^{i}Pr_2$), 6.89 (2 H, overlapping 2 × m, 4-NC$_5$H$_4$ and boryl *m*-$C_6\underline{H}_3{}^{i}Pr_2$), 6.80 (2 H, overlapping 2 × m,

3- and 6-NC_5H_4), 6.48 (1 H, m, 5-NC_5H_4), 6.04 (2 H, s, NCH), 4.72 (1 H, s, MeC(N)C<u>H</u>), 3.72 (2 H, sept., ^3J = 6.9 Hz, boryl C<u>H</u>$_a$MeMe), 3.50 (2 H, sept., ^3J = 6.9 Hz, boryl C<u>H</u>$_b$MeMe), 3.21 (1 H, m, C<u>H</u>$_2$NC(Me)), 3.12 (1 H, s, NH), 2.96 (2 H, overlapping 2 × sept., NacNac C<u>H</u>MeMe), 2.80 (1 H, m, C<u>H</u>$_2$NC(Me)), 2.30 (1 H, m, C<u>H</u>$_2$$NMe_2$), 2.06 (1 H, m, C<u>H</u>$_2$$NMe_2$), 1.65 (3 H, s, <u>Me</u>C(N)CH), 1.56 (6 H, s, NMe_2), 1.55 (3 H, s, <u>Me</u>C(N)CH), 1.38 (6 H, d, ^3J = 6.9 Hz, boryl CH$_a$<u>Me</u>Me), 1.34 (18 H, overlapping 3 × d, boryl CH<u>Me</u>$_b$Me and CHMe<u>Me</u>), 1.28 (3 H, d, ^3J = 6.7 Hz, NacNac CH<u>Me</u>$_b$Me), 1.20 (3 H, d, ^3J = 6.7 Hz, NacNac CHMe<u>Me</u>$_b$), 1.10 (3 H, d, ^3J = 6.7 Hz, NacNac CH<u>Me</u>$_a$Me), 0.53 (3 H, d, ^3J = 6.7 Hz, NacNac CHMe<u>Me</u>$_a$) ppm. $^{13}C\{^1H\}$ NMR (C_6D_6, 100.6 MHz): δ 217.2 (2-NC_5H_4), 165.4 (Me<u>C</u>(N)CH), 165.3 (Me<u>C</u>(N)CH), 149.8 (NacNac *o*-<u>C</u>$_6$H$_3$^{i}Pr$_2$), 148.0 (boryl *o*-<u>C</u>$_6$H$_3$^{i}Pr$_2$), 147.6 (boryl *o*-<u>C</u>$_6$H$_3$^{i}Pr$_2$), 144.1 (4-NC_5H_4), 142.7 (boryl *i*-<u>C</u>$_6$H$_3$^{i}Pr$_2$), 142.1 (boryl *i*-<u>C</u>$_6$H$_3$^{i}Pr$_2$), 141.5 (NacNac *i*-<u>C</u>$_6$H$_3$^{i}Pr$_2$), 132.0 (6-NC_5H_4), 128.6 (3-NC_5H_4), 126.4 (boryl *p*-<u>C</u>$_6$H$_3$^{i}Pr$_2$), 124.5 (NacNac *p*-<u>C</u>$_6$H$_3$^{i}Pr$_2$), 123.6 (boryl *m*-<u>C</u>$_6$H$_3$^{i}Pr$_2$), 123.5 (NacNac *m*-<u>C</u>$_6$H$_3$^{i}Pr$_2$), 123.4 (boryl *m*-<u>C</u>$_6$H$_3$^{i}Pr$_2$), 123.1 (NacNac *m*-<u>C</u>$_6$H$_3$^{i}Pr$_2$), 120.7 (5-NC_5H_4), 117.7 (NCH), 99.5 (MeC(N)<u>C</u>H), 60.4 (<u>C</u>H$_2$$NMe_2$), 47.2 (<u>C</u>H$_2$NC(Me)), 46.3 ($NMe_2$), 28.9 (boryl <u>C</u>$_a$HMeMe), 28.3 (boryl <u>C</u>$_b$HMeMe), 28.1 (NacNac <u>C</u>$_a$HMeMe), 28.0 (NacNac <u>C</u>$_b$HMeMe), 26.1 (boryl CHMe<u>Me</u>$_b$), 25.8 (boryl CHMe<u>Me</u>$_a$), 24.7 (NacNac CHMe<u>Me</u>$_b$ and boryl CH<u>Me</u>$_b$Me), 24.5 (NacNac CHMe<u>Me</u>$_a$), 24.4 (<u>Me</u>C(N)CH and NacNac CH<u>Me</u>$_b$Me), 23.2 (boryl CH<u>Me</u>$_a$Me), 22.6 (<u>Me</u>C(N)CH) ppm. $^{11}B\{^1H\}$ NMR (C_6D_6, 128.4 MHz): δ 23.5 ppm. IR (NaCl plates, Nujol mull, cm^{-1}): 3174 (br., w, N–H), 1921 (w), 1856 (w), 1790 (w), 1622 (w), 1583 (m), 1544 (s), 1521 (s), 1337 (s), 1320 (s), 1274 (m), 1254 (s), 1206 (w), 1180 (m), 1132 (w), 1101 (m), 1055 (m), 998 (w), 961 (w), 937 (m), 874 (m), 846 (w), 805 (m), 762 (s), 745 (s), 704 (w), 671 (w), 653 (m), 625 (w). A satisfactory elemental analysis of **39** could not be obtained, due to high compound sensitivity and/or incomplete combustion, as described by Mindiola and co-workers for analogous compounds.[45]

(L^1)Sc{NHB(NAr'CH)$_2$}(η^2-4-$NC_5H_3NMe_2$) (40). To a mixture of (L^1)Sc(Me){NHB(NAr'CH)$_2$} (**36**, 0.050 g, 0.0632 mmol) and DMAP (0.008 g, 0.0632 mmol) was added toluene (2 mL) at RT. The mixture was heated to 60 °C and stirred for 8 h, after which the volatiles were removed under reduced pressure, to afford **40** as a pale yellow, waxy solid, which was then dried *in vacuo*. Yield: 0.048 g (85%).

^1H NMR (C_6D_6, 400.1 MHz): δ 8.44 (1 H, br. m, 6-NC_5<u>H</u>$_3$$NMe_2$), 7.34 – 7.29 (5 H, overlapping m, boryl and NacNac *m*- and *p*-C_6<u>H</u>$_3$^{i}Pr$_2$), 7.19 – 7.05 (3 H, overlapping m,

boryl and NacNac *m*- and *p*-$C_6\underline{H}_3{}^iPr_2$), 6.95 (1 H, m, boryl *m*-$C_6\underline{H}_3{}^iPr_2$), 6.76 (1 H, d, ^3J = 6.2 Hz, 3-$NC_5\underline{H}_3NMe_2$), 6.06 (2 H, s, NCH), 5.97 (1 H, m, 5-$NC_5\underline{H}_3NMe_2$), 4.73 (1 H, s, MeC(N)C$\underline{H}$), 3.78 (2 H, sept., ^3J = 6.9 Hz, boryl C$\underline{H}_a$MeMe), 3.56 (2 H, sept., ^3J = 6.9 Hz, boryl C$\underline{H}_b$MeMe), 3.30 (1 H, m, C$\underline{H}_2$NC(Me)), 3.07 (1 H, s, NH), 2.99 (2 H, overlapping 2 × sept., NacNac C$\underline{H}$MeMe), 2.83 (1 H, m, C$\underline{H}_2$NC(Me)), 2.39 (7 H, overlapping s and m, $NC_5H_3N\underline{Me}_2$ and C$\underline{H}_2NMe_2$), 2.05 (1 H, m, C$\underline{H}_2NMe_2$), 1.72 (6 H, s, $CH_2N\underline{Me}_2$), 1.68 (3 H, s, $\underline{Me}$C(N)CH), 1.56 (3 H, s, $\underline{Me}$C(N)CH), 1.45 (6 H, d, ^3J = 6.9 Hz, boryl $CH_a\underline{Me}Me$), 1.40 (6 H, d, ^3J = 6.9 Hz, boryl $CH\underline{Me}_bMe$), 1.35 (15 H, overlapping 3 × d, boryl $CHMe\underline{Me}_a$, $CHMe\underline{Me}_b$ and NacNac $CH\underline{Me}_bMe$), 1.23 (3 H, d, ^3J = 6.7 Hz, NacNac $CH\underline{Me}_aMe$), 1.14 (3 H, d, ^3J = 6.7 Hz, NacNac $CHMe\underline{Me}_b$), 0.61 (3 H, d, ^3J = 6.7 Hz, NacNac $CHMe\underline{Me}_a$) ppm. $^{13}C\{^1H\}$ NMR (C_6D_6, 100.6 MHz): δ 212.8 (2-$NC_5H_3NMe_2$), 165.2 (Me$\underline{C}$(N)CH), 165.1 (Me$\underline{C}$(N)CH), 151.6 (4-$NC_5H_3NMe_2$), 150.3 (NacNac *o*-$\underline{C}_6H_3{}^iPr_2$), 148.0 (boryl *o*-$\underline{C}_6H_3{}^iPr_2$), 147.7 (boryl *o*-$\underline{C}_6H_3{}^iPr_2$), 143.2 (3-$NC_5H_3NMe_2$), 143.0 (boryl *i*-$\underline{C}_6H_3{}^iPr_2$), 142.6 (NacNac *i*-$\underline{C}_6H_3{}^iPr_2$), 141.7 (NacNac *i*-$\underline{C}_6H_3{}^iPr_2$), 126.2 (NacNac *m*-$\underline{C}_6H_3{}^iPr_2$), 124.1 (boryl *p*-$\underline{C}_6H_3{}^iPr_2$), 124.0 (boryl *m*-$\underline{C}_6H_3{}^iPr_2$), 123.6 (6-$NC_5H_3NMe_2$), 123.3 (boryl *m*-$\underline{C}_6H_3{}^iPr_2$), 122.9 (NacNac *p*-$\underline{C}_6H_3{}^iPr_2$), 117.7 (NCH), 106.0 (5-$NC_5H_3NMe_2$), 99.4 (MeC(N)$\underline{C}$H), 60.5 ($\underline{C}H_2NMe_2$), 47.3 ($\underline{C}H_2NC(Me)$), 46.5 (CH_2NMe_2), 38.8 ($NC_5H_3N\underline{Me}_2$), 28.9 (boryl $\underline{C}_aHMeMe$), 28.4 (boryl $\underline{C}_bHMeMe$), 28.0 (NacNac $\underline{C}$HMeMe), 26.1 (boryl $CHMe\underline{Me}_a$ and $CHMe\underline{Me}_b$), 25.7 (NacNac $CH\underline{Me}_aMe$), 25.2 (NacNac $CH\underline{Me}_bMe$), 24.8 (boryl $CH\underline{Me}_bMe$ and $\underline{Me}$C(N)CH), 24.4 (NacNac $CHMe\underline{Me}_a$ and $CHMe\underline{Me}_b$), 23.3 (boryl $CH\underline{Me}_aMe$), 22.5 ($\underline{Me}$C(N)CH) ppm. $^{11}B\{^1H\}$ NMR (C_6D_6, 128.4 MHz): δ 23.5 ppm. IR (NaCl plates, Nujol mull, cm^{-1}): 3175 (br., w, N–H), 1596 (w), 1580 (s), 1544 (m), 1519 (s), 1359 (s), 1337 (m), 1320 (m), 1274 (w), 1229 (w), 1179 (w), 1118 (w), 1102 (w), 1056 (w), 996 (w), 937 (w), 874 (w), 846 (w), 805 (m), 763 (m), 745 (m), 704 (w), 687 (w), 652 (m). A satisfactory elemental analysis of **40** could not be obtained, due to high compound sensitivity and/or incomplete combustion, as described by Mindiola and co-workers for analogous compounds.[45]

Competition reaction of (L[1])Sc(Me){NHB(NAr'CH)$_2$} (36) with pyridine and pyridine-*d*$_5$. To a C_6D_6 solution (0.6 mL) of (L[1])Sc(Me){NHB(NAr'CH)$_2$} (**36**, 0.0100 g, 0.0126 mmol) in an NMR tube fitted with a J. Youngs valve was added pyridine (5.1 μL, 0.0632 mmol) and pyridine-d_5 (5.1 μL, 0.0632 mmol). The mixture was then heated at 60 °C for 8 h, with ^{1}H NMR integration showing the products to be 51% **39** and 49% **39-*d*$_5$**.

Competition reaction of (L^1)Sc(Me){NHB(NAr'CH)$_2$} (36) with pyridine and DMAP. To a C_6D_6 solution (0.6 mL) of (L^1)Sc(Me){NHB(NAr'CH)$_2$} (**36**, 0.0100 g, 0.0126 mmol) and DMAP (0.0077 g, 0.0632 mmol) in an NMR tube fitted with a J. Youngs valve was added pyridine (5.1 μL, 0.0632 mmol). The mixture was then heated at 60 °C for 8 h, with ^{1}H NMR integration showing the products to be 53% **39** and 47% **40**.

Intramolecular competition reaction of (L^1)Sc(Me){NHB(NAr'CH)$_2$} (36) with 2-pyridine-*d*$_1$. To a C_6D_6 solution (0.6 mL) of (L^1)Sc(Me){NHB(NAr'CH)$_2$} (**36**, 0.0150 g, 0.0190 mmol) in an NMR tube fitted with a J. Youngs valve was added 2-pyridine-d_1 (1.6 μL, 0.0190 mmol). The mixture was then heated at 60 °C for 8 h, with ^{1}H NMR integration showing the products to be 60% **39-*d*$_1$_C** and 40% **39-*d*$_1$_N**.

Exchange reaction of (L^1)Sc{NHB(NAr'CH)$_2$}(η^2-NC$_5$H$_4$) (39) with pyridine-*d*$_5$. To a C_6D_6 solution (0.6 mL) of (L^1)Sc{NHB(NAr'CH)$_2$}(η^2-NC$_5$H$_4$) (**39**, 0.0162 g, 0.0190 mmol) in an NMR tube fitted with a J. Youngs valve was added pyridine-d_5 (1.5 μL, 0.0190 mmol). The mixture was then heated at 60 °C for 2 h, with ^{1}H NMR integration showing the equilibrium mixture to be 56% **39** and 44% **39-*d*$_5$**. The reverse reaction (starting with **39-*d*$_5$**) resulted in an equilibrium mixture of 60% **39** and 40% **39-*d*$_5$**, under the same conditions.

Exchange reaction of (L^1)Sc{NHB(NAr'CH)$_2$}(η^2-NC$_5$H$_4$) (39) with DMAP. A C_6D_6 solution (0.6 mL) of (L^1)Sc{NHB(NAr'CH)$_2$}(η^2-NC$_5$H$_4$) (**39**, 0.0150 g, 0.0176 mmol) and DMAP (0.0022 g, 0.0176 mmol) was transferred to an NMR tube fitted with a J. Youngs valve. The mixture was then heated at 60 °C for 2 h, with ^{1}H NMR integration showing the equilibrium mixture to be 50% **39** and 50% **40**. The reverse reaction (starting with **40**) resulted in an equilibrium mixture of 53% **39** and 47% **40**.

NMR tube scale conversion of (L^1)Sc{NHB(NAr'CH)$_2$}(η^2-NC$_5$H$_4$) (39) to {MeC(NC$_6$H$_3$^{i}PrCH(Me)CH$_2$)CHC(Me)NCH$_2$CH$_2$NMe$_2$}Sc{NHB(NAr'CH)$_2$} (38). A C_6D_6 solution (0.6 mL) of (L^1)Sc{NHB(NAr'CH)$_2$}(η^2-NC$_5$H$_4$) (**39**, 0.0150 g, 0.0176 mmol) was transferred to an NMR tube fitted with a J. Youngs valve, and heated to 90 °C for 16 h. After this time, all of **39** had been consumed, giving partial conversion to **38** and pyridine, in addition to some decomposition which released H$_2$NB(NAr'CH)$_2$ (**2.2**).

(L^1)Sc{NHB(NAr'CH)$_2$}(CCTol) (41). To a toluene solution (8 mL) of (L^1)Sc(Me){NHB(NAr'CH)$_2$} (**36**, 0.199 g, 0.251 mmol) was added HCCTol (32 μL, 0.251 mmol) at RT. The mixture was heated to 60 °C and stirred for 16 h, after which the volatiles

were removed under reduced pressure. The yellow waxy solid was washed with hexane (2 mL) to afford **41** as an off-white powder, which was then dried *in vacuo*. Yield: 0.112 g (50%).

^{1}H NMR (C_6D_6, 400.1 MHz): δ 7.18 (overlapping 4 × m, boryl and NacNac *m*- and *p*-$C_6\underline{H}_3{}^{i}Pr_2$), 7.11 (2 H, d, ^{3}J = 8.2 Hz, *m*-$C_6\underline{H}_4Me$), 6.90 (2 H, d, ^{3}J = 8.2 Hz, *o*-$C_6\underline{H}_4Me$), 6.05 (2 H, s, NCH), 4.85 (1 H, s, MeC(N)C$\underline{H}$), 3.72 (2 H, sept., ^{3}J = 6.9 Hz, boryl C$\underline{H}_a$MeMe), 3.58 (1 H, s, NH), 3.50 (2 H, sept., boryl C$\underline{H}_b$MeMe), 3.31 (1 H, sept., ^{3}J = 6.7 Hz, NacNac C$\underline{H}_a$MeMe), 2.77 (1 H, sept., ^{3}J = 6.7 Hz, NacNac C$\underline{H}_b$MeMe), 2.71 (3 H, s, NMe_2), 2.67 (2 H, overlapping 2 × m, C$\underline{H}_2NMe_2$ and C$\underline{H}_2$NC(Me)), 2.36 (1 H, m, C$\underline{H}_2$NC(Me)), 2.22 (3 H, s, NMe_2), 2.05 (3 H, s, $C_6H_4\underline{Me}$), 1.79 (1 H, m, C$\underline{H}_2NMe_2$), 1.56 (3 H, s, $\underline{Me}$C(N)CH), 1.54 (3 H, s, $\underline{Me}$C(N)CH), 1.52 (6 H, d, ^{3}J = 6.9 Hz, boryl CH$\underline{Me}_a$Me), 1.34 (9 H, overlapping 2 × d, NacNac CH$\underline{Me}_b$Me and boryl CH$\underline{Me}_b$Me), 1.28 (9 H, overlapping 2 × d, NacNac CH$\underline{Me}_a$Me and boryl CHMe$\underline{Me}_b$), 1.23 (6 H, d, ^{3}J = 6.9 Hz, boryl CHMe$\underline{Me}_a$), 1.09 (3 H, d, ^{3}J = 6.7 Hz, NacNac CHMe$\underline{Me}_b$), 1.04 (3 H, d, ^{3}J = 6.7 Hz, CHMe$\underline{Me}_a$) ppm. ^{13}C{^{1}H} NMR (C_6D_6, 100.6 MHz): δ 166.6 (Me$\underline{C}$(N)CH), 166.4 (Me$\underline{C}$(N)CH), 155.4 (Sc$\underline{C}$CTol), 147.7 (boryl *o*-$\underline{C}_6H_3{}^{i}Pr_2$), 147.6 (boryl *o*-$\underline{C}_6H_3{}^{i}Pr_2$), 146.9 (NacNac *o*-$\underline{C}_6H_3{}^{i}Pr_2$), 143.4 (NacNac *i*-$\underline{C}_6H_3{}^{i}Pr_2$), 142.4 (boryl *i*-$\underline{C}_6H_3{}^{i}Pr_2$), 141.1 (boryl *i*-$\underline{C}_6H_3{}^{i}Pr_2$), 138.7 (*i*-$\underline{C}_6H_4Me$), 135.1 (*p*-$\underline{C}_6H_4Me$), 132.1 (*m*-$\underline{C}_6H_4Me$), 128.9 (*o*-$\underline{C}_6H_4Me$), 126.8 (boryl *p*-$\underline{C}_6H_3{}^{i}Pr_2$), 125.8 (NacNac *p*-$\underline{C}_6H_3{}^{i}Pr_2$), 124.6 (Sc$\underline{C}$CTol), 123.9 (boryl *m*-$\underline{C}_6H_3{}^{i}Pr_2$), 123.5 (NacNac *m*-$\underline{C}_6H_3{}^{i}Pr_2$), 117.5 (NCH), 100.2 (MeC(N)$\underline{C}$H), 58.5 ($\underline{C}H_2NMe_2$), 48.8 (NMe_2), 46.9 ($\underline{C}H_2$NC(Me)), 42.3 (NMe_2), 29.1 (boryl $\underline{C}_a$HMeMe), 28.6 (NacNac $\underline{C}_a$HMeMe), 28.4 (NacNac $\underline{C}_b$HMeMe), 28.2 (boryl $\underline{C}_b$HMeMe), 26.1 (boryl CHMe$\underline{Me}_b$), 26.0 (boryl CHMe$\underline{Me}_a$), 24.9 (NacNac CH$\underline{Me}_b$Me), 24.7 ($\underline{Me}$C(N)CH), 24.5 (NacNac CH$\underline{Me}_a$Me), 24.3 (boryl CH$\underline{Me}_b$Me), 23.8 (NacNac CHMe$\underline{Me}_a$), 23.3 (NacNac CHMe$\underline{Me}_b$), 23.0 (boryl CH$\underline{Me}_a$Me), 21.3 ($C_6H_4\underline{Me}$) ppm. ^{11}B{^{1}H} NMR (C_6D_6, 128.4 MHz): δ 22.9 ppm. IR (NaCl plates, Nujol mull, cm^{-1}): 3195 (w, N–H), 2074 (w), 1902 (w), 1793 (w), 1584 (w), 1541 (m), 1525 (s), 1505 (m), 1415 (s), 1359 (s), 1339 (s), 1316 (m), 1255 (m), 1199 (m), 1178 (m), 1134 (w), 1102 (w), 1054 (m), 963 (w), 937 (w), 879 (w), 847 (w), 819 (m), 807 (m), 764 (m), 751 (s), 708 (w), 651 (m). Anal. found (calcd. for $C_{56}H_{78}BN_6Sc$): C, 72.16 (75.49); H, 9.00 (8.82); N, 9.33 (9.43)%. Repeated attempts to obtain an elemental analysis with satisfactory % C values failed, presumably due to incomplete combustion of the compound.

(L^1)Sc{N{B(NAr'CH)$_2$}C(Me)C(Ph)} (42). To a toluene solution (8 mL) of (L^1)Sc(Me){NHB(NAr'CH)$_2$} (0.197 g, 0.249 mmol) was added MeCCPh (31.5 μL, 0.252 mmol) at RT. The mixture was heated to 60 °C and stirred for 16 h, after which the volatiles were removed under reduced pressure. The orange waxy solid was washed with hexane (2 × 2 mL) to afford **42** as a yellow powder, which was then dried *in vacuo*. Yield: 0.106 g (48%). Diffraction-quality crystals were grown from a benzene solution at RT.

^{1}H NMR (C_6D_6, 400.1 MHz): δ 7.26 – 7.06 (overlapping 5 × m, boryl and NacNac *m*- and *p*-$C_6\underline{H}_3{}^i\mathrm{Pr}_2$ and *m*-C_6H_5), 6.85 (1 H, t, ^3J = 7.2 Hz, *p*-C_6H_5), 6.17 (2 H, s, NCH), 5.90 (2 H, d, ^3J = 7.2 Hz, *o*-C_6H_5), 4.89 (1 H, s, MeC(N)C$\underline{H}$), 3.65 (2 H, sept., ^3J = 6.9 Hz, boryl C$\underline{H}_a$MeMe), 3.48 (2 H, sept., boryl C$\underline{H}_b$MeMe), 3.00 (1 H, sept., ^3J = 6.7 Hz, NacNac C$\underline{H}_a$MeMe), 2.93 (1 H, m, C$\underline{H}_2$NC(Me)), 2.70 (1 H, m, C$\underline{H}_2$NC(Me)), 2.58 (3 H, s, ScC=C$\underline{\mathrm{Me}}$), 2.44 (1 H, sept., ^3J = 6.7 Hz, NacNac C$\underline{H}_b$MeMe), 1.81 (3 H, s, NMe_2), 1.73 (3 H, s, $\underline{\mathrm{Me}}$C(N)CH), 1.64 (3 H, s, NMe_2), 1.61 (3 H, s, $\underline{\mathrm{Me}}$C(N)CH), 1.51 (1 H, s, C$\underline{H}_2\mathrm{NMe}_2$), 1.38 (7 H, overlapping m and d, boryl CH$\underline{\mathrm{Me}}_a$Me and C$\underline{H}_2\mathrm{NMe}_2$), 1.24 (18 H, overlapping 3 × d, boryl CH$\underline{\mathrm{Me}}_b$Me and CHMe$\underline{\mathrm{Me}}$), 1.13 (3 H, d, ^3J = 6.7 Hz, NacNac CH$\underline{\mathrm{Me}}_a$Me), 1.10 (3 H, d, ^3J = 6.7 Hz, NacNac CH$\underline{\mathrm{Me}}_b$Me), 1.04 (3 H, d, ^3J = 6.7 Hz, NacNac CHMe$\underline{\mathrm{Me}}_a$), 0.42 (3 H, d, ^3J = 6.7 Hz, NacNac CHMe$\underline{\mathrm{Me}}_b$) ppm. ^{13}C{^{1}H} NMR (C_6D_6, 100.6 MHz): δ 172.9 (Sc$\underline{\mathrm{C}}$=CMe), 166.8 (Me$\underline{\mathrm{C}}$(N)CH), 165.8 (Me$\underline{\mathrm{C}}$(N)CH), 154.5 (ScC=$\underline{\mathrm{C}}$Me), 147.3 (boryl *o*-$\underline{\mathrm{C}}_6\mathrm{H}_3{}^i\mathrm{Pr}_2$), 146.9 (boryl *o*-$\underline{\mathrm{C}}_6\mathrm{H}_3{}^i\mathrm{Pr}_2$), 144.5 (NacNac *o*-$\underline{\mathrm{C}}_6\mathrm{H}_3{}^i\mathrm{Pr}_2$), 142.1 (boryl *i*-$\underline{\mathrm{C}}_6\mathrm{H}_3{}^i\mathrm{Pr}_2$), 141.7 (NacNac *i*-$\underline{\mathrm{C}}_6\mathrm{H}_3{}^i\mathrm{Pr}_2$), 127.5 (*i*-$C_6H_5$), 127.4 (*m*-$C_6H_5$), 127.1 (*o*-$C_6H_5$), 125.6 (NacNac *p*-$\underline{\mathrm{C}}_6\mathrm{H}_3{}^i\mathrm{Pr}_2$), 125.2 (NacNac *m*-$\underline{\mathrm{C}}_6\mathrm{H}_3{}^i\mathrm{Pr}_2$), 124.4 (boryl *p*-$\underline{\mathrm{C}}_6\mathrm{H}_3{}^i\mathrm{Pr}_2$), 123.7 (boryl *m*-$\underline{\mathrm{C}}_6\mathrm{H}_3{}^i\mathrm{Pr}_2$), 123.5 (NacNac *m*-$\underline{\mathrm{C}}_6\mathrm{H}_3{}^i\mathrm{Pr}_2$), 120.3 (*p*-$C_6H_5$), 119.1 (NCH), 100.0 (MeC(N)$\underline{\mathrm{C}}$H), 58.6 ($\underline{\mathrm{C}}\mathrm{H}_2\mathrm{NMe}_2$), 48.5 ($\mathrm{NMe}_2$), 47.0 ($\underline{\mathrm{C}}\mathrm{H}_2$NC(Me)), 42.5 ($\mathrm{NMe}_2$), 29.6 (boryl $\underline{\mathrm{C}}_a$HMeMe), 28.7 (NacNac $\underline{\mathrm{C}}$HMeMe), 28.4 (boryl $\underline{\mathrm{C}}_b$HMeMe), 26.2 (NacNac CH$\underline{\mathrm{Me}}_b$Me), 25.8 (boryl CHMe$\underline{\mathrm{Me}}_a$ and CH$\underline{\mathrm{Me}}_b$Me), 25.2 ($\underline{\mathrm{Me}}$C(N)CH), 24.9 (NacNac CH$\underline{\mathrm{Me}}_a$Me and CHMe$\underline{\mathrm{Me}}_a$), 24.0 (boryl CHMe$\underline{\mathrm{Me}}_b$), 23.0 ($\underline{\mathrm{Me}}$C(N)CH), 22.9 (NacNac CHMe$\underline{\mathrm{Me}}_b$), 22.7 (boryl CH$\underline{\mathrm{Me}}_a$Me), 21.8 (ScC=C$\underline{\mathrm{Me}}$) ppm. ^{11}B{^{1}H} NMR (C_6D_6, 128.4 MHz): δ 24.6 ppm. IR (NaCl plates, Nujol mull, cm^{-1}): 1928 (w), 1862 (w), 1797 (w), 1580 (m), 1548 (m), 1524 (s), 1407 (s), 1339 (s), 1315 (s), 1269 (m), 1244 (m), 1203 (m), 1181 (w), 1170 (w), 1119 (w), 1101 (w), 1066 (w), 998 (w), 965 (w), 935 (w), 903 (w), 879 (w), 849 (w), 841 (w), 818 (m), 803 (m), 766 (m), 750 (m), 700 (m), 673 (w). Anal. found (calcd. for $C_{56}H_{78}BN_6Sc$): C, 75.35 (75.49); H, 8.87 (8.82); N, 9.33 (9.43)%.

Competition reaction of (L^1)Sc(Me){NHB(NAr'CH)$_2$} (36) with HCCTol and MeCCPh. To a C_6D_6 solution (0.6 mL) of (L^1)Sc(Me){NHB(NAr'CH)$_2$} (**36**, 0.0100 g, 0.0126 mmol) in an NMR tube fitted with a J. Youngs valve was added HCCTol (8.0 μL, 0.0632 mmol) and MeCCPh (7.9 μL, 0.0632 mmol). The mixture was then heated at 60 °C for 16 h, with ^{1}H NMR integration showing the product to be 100% (L^1)Sc{NHB(NAr'CH)$_2$}(CCTol) (**41**).

Competition reaction of (L^1)Sc(Me){NHB(NAr'CH)$_2$} (36) with pyridine and MeCCPh. To a C_6D_6 solution (0.6 mL) of (L^1)Sc(Me){NHB(NAr'CH)$_2$} (**36**, 0.0150 g, 0.0190 mmol) in an NMR tube fitted with a J. Youngs valve was added pyridine (8.2 μL, 0.0948 mmol) and MeCCPh 11.9 μL, 0.0948 mmol). The mixture was then heated at 60 °C for 16 h, with ^{1}H NMR integration showing the product to be 100% (L^1)Sc{NHB(NAr'CH)$_2$}(η^2-NC$_5$H$_4$) (**41**).

NMR tube scale conversion of (L^1)Sc{NHB(NAr'CH)$_2$}(η^2-NC$_5$H$_4$) (39) to (L^1)Sc{N{B(NAr'CH)$_2$}C(Me)C(Ph)} (42). A C_6D_6 solution (0.6 mL) of (L^1)Sc{NHB(NAr'CH)$_2$}(η^2-NC$_5$H$_4$) (**39**, 0.0162 g, 0.0190 mmol) was transferred to an NMR tube fitted with a J. Youngs valve, and MeCCPh (2.4 μL, 0.0190 mmol) added *via* microsyringe. The mixture was heated to 90 °C for 8 h, after which time, all of **39** had been consumed, giving partial conversion to **42** and pyridine, in addition to some decomposition which released H$_2$NB(NAr'CH)$_2$ (**2.2**).

NMR tube scale conversion of {MeC(NC$_6$H$_3$^{i}PrCH(Me)CH$_2$)CHC(Me)NCH$_2$CH$_2$NMe$_2$}Sc{NHB(NAr'CH)$_2$} (38) to (L^1)Sc{N{B(NAr'CH)$_2$}C(Me)C(Ph)} (42). A C_6D_6 solution (0.6 mL) of {MeC(NC$_6$H$_3$^{i}PrCH(Me)CH$_2$)CHC(Me)NCH$_2$CH$_2$NMe$_2$}Sc{NHB(NAr'CH)$_2$} (**38**, 0.0147 g, 0.0190 mmol) was transferred to an NMR tube fitted with a J. Youngs valve, and MeCCPh (2.4 μL, 0.0190 mmol) added *via* microsyringe. The mixture was heated to 100 °C for 16 h, after which time, all of **38** had been consumed, giving partial conversion to **42**, in addition to some decomposition which released H$_2$NB(NAr'CH)$_2$ (**2.2**).

Kinetic measurements for thermolysis reactions of (L^1)Sc(Me){NB(NAr'CH)$_2$} (36). The general procedure is as follows. In a dry-box, a C_6D_6 solution (0.6 mL) of (L^1)Sc(Me){NB(NAr'CH)$_2$} (**36**, 0.0150 g, 0.0190 mmol) was transferred to an NMR tube fitted with a J. Youngs valve. For liquid reagents (pyridine, pyridine-d_5, HCCTol, DCCTol, MeCCPh), 1 equiv. of the respective reagent was added to the tube *via* microsyringe before

sealing. For DMAP, a combined solution of **36** and DMAP was mixed before transferring to the tube. A blank C_6D_6 sample was added to the NMR probe at RT, locked and shimmed, and the probe heated to 343 K. After thermal equilibration, the experimental sample replaced the blank sample, the shimming was checked and an array was set up to record a ^{1}H NMR spectrum (4 scans) every 120 s. The decay of **36** was calculated by measuring the integral of Sc–Me. First order rate constants were obtained from linear plots of –ln([**36**]/[**36**]$_0$)) *vs* time.

NMR tube scale reaction of (L^1)Sc{NHB(NAr'CH)$_2$}Cl (37) with LiCH$_2$SiMe$_3$. (L^1)Sc{NHB(NAr'CH)$_2$}Cl (**37**, 0.0338 mmol) was prepared on the NMR tube scale in C_6D_6 as described above. To the solution in an NMR tube fitted with a J. Youngs valve was added LiCH$_2$SiMe$_3$ (0.0032 g, 0.0338 mmol) giving immediate conversion to (L^1)Sc(CH$_2$SiMe$_3$){NHB(NAr'CH)$_2$}. Heating the NMR tube at 60 °C resulted in quantitative conversion to {MeC(NC$_6$H$_3$^{i}PrCH(Me)CH$_2$)CHC(Me)NCH$_2$CH$_2$NMe$_2$}Sc{NHB(NAr'CH)$_2$} (**38**) after 40 h.

NMR tube scale reaction of Sc(Np)$_3$(THF)$_2$ (5.7) with H$_2$NB(NAr'CH)$_2$ (2.2) and L^1–H. A mixture of Sc(Np)$_3$(THF)$_2$ (**5.7**, 0.0150 g, 0.0373 mmol) and H$_2$NB(NAr'CH)$_2$ (**2.2**, 0.0150 g, 0.0373 mmol) in C_6D_6 (0.6 mL) was transferred to an NMR tube fitted with a J. Youngs valve, with quantitative conversion to Sc(Np)$_2${NHB(NAr'CH)$_2$}(THF)$_2$ taking place. L^1–H (0.0122 g, 0.0373 mmol) was then added, and after heating at 60 °C for 40 h, quantitative conversion to **38** had taken place.

(L^1)Sc(Me){NHB(N^{i}Pr)$_2$C$_6$H$_4$} (43). To a solution of (L^1)ScCl$_2$ (**5.2**, 0.970 g, 2.18 mmol) in THF (30 mL) at –78 °C was added MeLi (1.6 M in Et$_2$O, 2.75 mL, 4.37 mmol). The mixture was allowed to warm to RT, then stirred for 3 h. The volatiles were then removed under reduced pressure, and the residue extracted with toluene (30 mL). The extracts were transferred into a Schlenk tube containing H$_2$NB(N^{i}Pr)$_2$C$_6$H$_4$ (**5.8**, 0.474 g, 2.18 mmol), and this mixture was then stirred for 16 h at RT. After this time, the volatiles were removed under reduced pressure, and the resulting waxy solid washed with hexane (3 × 6 mL). After drying *in vacuo*, **43** was isolated as an off-white powder. Yield: 0.741 g (56%).

^{1}H NMR (C_6D_6, 400.1 MHz): δ 7.20 (3 H, overlapping 2 × m, NacNac *m*- and *p*-C$_6$H$_3$^{i}Pr$_2$), 7.06 (4 H, m, boryl 2,3,4,5-C$_6$H$_4$), 4.91 (1 H, s, MeC(N)CH), 3.89 (3 H, overlapping s and m, NH and boryl CHMeMe), 3.79 (1 H, sept., ^3J = 6.8 Hz, NacNac CH$_a$MeMe), 3.11 (1 H,

sept., ^{3}J = 6.8 Hz, NacNac C$\underline{H}_b$MeMe), 2.89 (1 H, m, C$\underline{H}_2$NC(Me)), 2.83 (1 H, m, C$\underline{H}_2$NC(Me)), 2.43 (1 H, m, C$\underline{H}_2$NMe$_2$), 2.19 (1 H, m, C$\underline{H}_2$NMe$_2$), 2.16 (3 H, s, NMe$_2$), 2.08 (3 H, s, NMe$_2$), 1.68 (3 H, s, $\underline{Me}$C(N)CH), 1.66 (3 H, s, $\underline{Me}$C(N)CH), 1.49 (6 H, d, ^{3}J = 7.0 Hz, boryl CH$\underline{Me}$Me), 1.45 (3 H, d, ^{3}J = 6.8 Hz, NacNac CH$\underline{Me}_a$Me), 1.38 (9 H, overlapping 2 × d, NacNac CH$\underline{Me}_b$Me and boryl CHMe$\underline{Me}$), 1.15 (6 H, overlapping 2 × d, NacNac CHMe$\underline{Me}_a$ and CHMe$\underline{Me}_b$), –0.56 (3 H, s, ScMe) ppm. ^{13}C{^{1}H} NMR (C_6D_6, 100.6 MHz): δ 166.9 (Me$\underline{C}$(N)CH), 166.6 (Me$\underline{C}$(N)CH), 145.5 (*i*-$\underline{C}_6H_3{}^{i}Pr_2$), 143.5 (*o*-$\underline{C}_6H_3{}^{i}Pr_2$), 142.7 (*o*-$\underline{C}_6H_3{}^{i}Pr_2$), 137.8 (1,6-$C_6H_4$), 126.2 (*p*-$\underline{C}_6H_3{}^{i}Pr_2$), 124.5 (*m*-$\underline{C}_6H_3{}^{i}Pr_2$), 124.1 (*m*-$\underline{C}_6H_3{}^{i}Pr_2$), 116.9 (2,5-$C_6H_4$), 108.93 (3,4-$C_6H_4$), 98.7 (MeC(N)$\underline{C}$H), 57.5 ($\underline{C}H_2NMe_2$), 47.7 ($\underline{C}H_2$NC(Me)), 47.0 (NMe$_2$), 45.5 (boryl $\underline{C}$HMeMe), 44.4 (NMe$_2$), 28.7 (NacNac $\underline{C}_b$HMeMe), 28.0 (NacNac $\underline{C}_a$HMeMe), 25.9 (NacNac CH$\underline{Me}_a$Me), 25.4 (NacNac CHMe$\underline{Me}_a$), 24.8 (NacNac CHMe$\underline{Me}_b$), 24.6 ($\underline{Me}$C(N)CH), 24.3 (NacNac CH$\underline{Me}_b$Me), 23.3 ($\underline{Me}$C(N)CH), 23.1 (ScMe), 22.3 (boryl CH$\underline{MeMe}$) ppm. ^{11}B{^{1}H} NMR (C_6D_6, 128.4 MHz): δ 24.1 ppm. IR (NaCl plates, Nujol mull, cm^{-1}): 3181 (br., w, N–H), 1593 (m), 1524 (s), 1484 (s), 1339 (s), 1321 (s), 1139 (m), 1128 (m), 1115 (m), 1101 (m), 1070 (w), 1056 (w), 958 (w), 937 (m), 910 (w), 893 (w), 863 (w), 839 (w), 761 (m), 748 (w), 704 (m), 681 (w), 663 (m), 614 (m). Anal. found (calcd. for $C_{34}H_{56}BN_6Sc$): C, 62.17 (67.54); H, 9.41 (9.34); N, 11.75 (13.90)%. Repeated attempts to obtain an elemental analysis with satisfactory % C values failed, presumably due to incomplete combustion of the compound.

(L^{1})Sc{NHB(N^{i}Pr)$_2$C$_6$H$_4$}$_2$ (44). To a solution of (L^{1})ScCl$_2$ (**5.2**, 0.314 g, 0.706 mmol) in THF (10 mL) at –78 °C was added MeLi (1.6 M in Et$_2$O, 0.88 mL, 1.41 mmol). The mixture was allowed to warm to RT, then stirred for 3 h. The volatiles were then removed under reduced pressure, and the residue extracted with toluene (10 mL). The extracts were transferred into a Schlenk tube containing H$_2$NB(N^{i}Pr)$_2$C$_6$H$_4$ (**5.8**, 0.307 g, 1.41 mmol), and this mixture was then stirred for 16 h at RT. After this time, the volatiles were removed under reduced pressure, and the resulting waxy solid washed with hexane (6 × 2 mL). After drying *in vacuo*, **44** was isolated as an off-white powder. Yield: 0.232 g (41%). Diffraction-quality crystals were grown from a concentrated hexane solution at 5 °C.

^{1}H NMR (C_6D_6, 400.1 MHz): δ 7.13 (4 H, m, 3,4-C_6H_4), 7.06 (3 H, overlapping 2 × m, NacNac *m*- and *p*-$C_6\underline{H}_3{}^{i}Pr_2$), 7.01 (4 H, m, 2,5-$C_6H_4$), 4.91 (1 H, s, MeC(N)C$\underline{H}$), 3.96 (4 H, sept., ^{3}J = 7.0 Hz, boryl C$\underline{H}$MeMe), 3.42 (2 H, sept., ^{3}J = 6.8 Hz, NacNac C$\underline{H}$MeMe), 3.25 (2 H, s, NH), 2.83 (2 H, t, ^{3}J = 6.0 Hz, C$\underline{H}_2$NC(Me)), 2.37 (2 H, t, ^{3}J = 6.0 Hz, C$\underline{H}_2$NMe$_2$),

1.97 (6 H, s, NMe_2), 1.67 (3 H, s, MeC(N)CH), 1.64 (3 H, s, MeC(N)CH), 1.55 (12 H, d, ^3J = 7.0 Hz, boryl CHMeMe), 1.38 (12 H, d, ^3J = 7.0 Hz, boryl CHMeMe), 1.27 (6 H, d, ^3J = 6.8 Hz, NacNac CHMeMe), 1.09 (6 H, d, ^3J = 6.8 Hz, NacNac CHMeMe) ppm. $^{13}C\{^1H\}$ NMR (C_6D_6, 100.6 MHz): δ 167.5 (MeC(N)CH), 167.0 (MeC(N)CH), 144.9 (*i*-$C_6H_3{}^iPr_2$), 143.6 (*o*-$C_6H_3{}^iPr_2$), 137.3 (1,6-C_6H_4), 126.6 (*p*-$C_6H_3{}^iPr_2$), 124.5 (*m*-$C_6H_3{}^iPr_2$), 116.9 (2,5-C_6H_4), 110.2 (3,4-C_6H_4), 98.9 (MeC(N)CH), 56.5 (CH_2NMe_2), 48.2 ($CH_2NC(Me)$), 46.5 (NMe_2), 45.7 (boryl CHMeMe), 28.3 (NacNac CHMeMe), 25.7 (NacNac CHMeMe), 25.2 (NacNac CHMeMe), 24.7 (MeC(N)CH), 23.4 (MeC(N)CH), 22.0 (boryl CHMeMe), 21.7 (boryl CHMeMe) ppm. $^{11}B\{^1H\}$ NMR (C_6D_6, 128.4 MHz): δ 24.1 ppm. IR (NaCl plates, Nujol mull, cm^{-1}): 3179 (br., w, N–H), 1593 (m), 1527 (s), 1483 (s), 1438 (s), 1417 (s), 1317 (s), 1290 (s), 1232 (w), 1173 (m), 1157 (w), 1139 (m), 1106 (w), 1064 (w), 958 (w), 937 (m), 909 (w), 892 (w), 844 (w), 763 (w), 699 (m), 662 (m), 612 (m). Anal. found (calcd. for $C_{45}H_{72}B_2N_9Sc$): C, 66.86 (67.08); H, 8.85 (9.01); N, 15.49 (15.65)%.

(L^2)Sc(CH_2SiMe_3){NHB(NAr'CH)$_2$} (45). To a Schlenk tube containing $Sc(CH_2SiMe_3)_3(THF)_2$ (**5.11**, 0.500 g, 1.11 mmol) and $H_2NB(NAr'CH)_2$ (**2.2**, 0.447 g, 1.11 mmol) was added toluene (20 mL) at –78 °C. The mixture was allowed to warm to RT and then stirred for 2 h. After this time, the pale yellow solution was transferred into another Schlenk tube containing L^2–H (0.429 g, 1.11 mmol) at RT and then stirred for another 2 h. The volatiles were then removed under reduced pressure to obtain **45** as a pale yellow solid. Yield: 0.749 g (73%).

^1H NMR (C_6D_6, 400.1 MHz): δ 7.21 (6 H, overlapping 2 × m, boryl *m*- and *p*-$C_6H_3{}^iPr_2$), 7.16 (2 H, overlapping with residual protio solvent resonance, NacNac *m*- and *p*-$C_6H_3{}^iPr_2$), 7.04 (1 H, dd, ^3J = 7.0, 2.3 Hz, NacNac *m*-$C_6H_3{}^iPr_2$), 5.95 (2 H, s, NCH), 4.68 (1 H, s, MeC(N)CH), 3.54 (4 H, overlapping 2 × sept., boryl CHMeMe), 3.37 (3 H, overlapping s and m, NH and NacNac CHMeMe), 3.05 (2 H, m, $CH_2CH_2NMe_2$), 2.84 (3 H, overlapping 3 × m, $CH_2NC(Me)$ and CH_2NMe), 2.63 (1 H, m, CH_2NMe), 2.47 (3 H, s, NMe), 2.19 (1 H, m, CH_2NMe_2), 2.13 (1 H, m, CH_2NMe_2), 2.01 (6 H, s, NMe_2), 1.61 (3 H, s, MeC(N)CH), 1.47 (6 H, overlapping s and d, MeC(N)CH and NacNac CHMeMe), 1.44 (6 H, d, ^3J = 6.9 Hz, boryl CHMeMe), 1.40 (6 H, d, ^3J = 6.9 Hz, boryl CHMeMe), 1.31 (15 H, overlapping 3 × d, boryl CHMeMe and NacNac CHMeMe), 1.25 (3 H, d, ^3J = 6.8 Hz, NacNac CHMeMe), 0.98 (3 H, d, ^3J = 6.8 Hz, NacNac CHMeMe), –0.14 (9 H, s, $SiMe_3$), –0.86 (2 H, s, CH_2SiMe_3) ppm. $^{13}C\{^1H\}$ NMR (C_6D_6, 100.6 MHz): δ 166.2 (MeC(N)CH), 165.7 (MeC(N)CH), 148.8 (NacNac *o*-$C_6H_3{}^iPr_2$), 147.6 (NacNac *o*-$C_6H_3{}^iPr_2$), 147.2 (boryl

o-$\underline{C}_6H_3{}^iPr_2$), 142.7 (NacNac *i*-$\underline{C}_6H_3{}^iPr_2$), 142.0 (boryl *i*-$\underline{C}_6H_3{}^iPr_2$), 141.8 (boryl *i*-$\underline{C}_6H_3{}^iPr_2$), 126.9 (boryl *p*-$\underline{C}_6H_3{}^iPr_2$), 125.8 (NacNac *p*-$\underline{C}_6H_3{}^iPr_2$), 124.7 (NacNac *p*-$\underline{C}_6H_3{}^iPr_2$), 124.0 (NacNac *m*-$\underline{C}_6H_3{}^iPr_2$), 123.9 (boryl and NacNac *m*-$\underline{C}_6H_3{}^iPr_2$), 123.7 (boryl *m*-$\underline{C}_6H_3{}^iPr_2$), 118.1 (NCH), 99.6 (MeC(N)$\underline{C}$H), 53.2 ($\underline{C}H_2NMe$), 52.2 ($\underline{C}H_2NMe_2$), 50.3 ($\underline{C}H_2CH_2NMe_2$), 47.1 ($\underline{C}H_2NC(Me)$), 45.8 ($NMe_2$), 43.4 (NMe), 38.5 ($\underline{C}H_2SiMe_3$), 29.1 (boryl $\underline{C}$HMeMe), 28.6 (NacNac $\underline{C}$HMeMe), 28.5 (boryl $\underline{C}$HMeMe), 28.0 (NacNac $\underline{C}$HMeMe), 26.3 (boryl CH$\underline{Me}$Me), 26.0 ($\underline{Me}$C(N)CH), 25.7 (boryl CH$\underline{Me}$Me), 25.5 ($\underline{Me}$C(N)CH), 25.0 (NacNac CH$\underline{Me}$Me), 24.4 (NacNac CH$\underline{Me}$Me), 24.3 (NacNac CH$\underline{Me}$Me), 24.0 (boryl CH$\underline{Me}$Me), 23.5 (NacNac CH$\underline{Me}$Me), 23.4 (boryl CH$\underline{Me}$Me), 4.3 ($SiMe_3$) ppm. $^{11}B\{^1H\}$ NMR (C_6D_6, 128.4 MHz): δ 23.0 ppm. IR (NaCl plates, Nujol mull, cm^{-1}): 3174 (br., w, N–H), 1924 (w), 1859 (w), 1792 (w), 1661 (w), 1583 (m), 1529 (s), 1178 (m), 1133 (m), 1098 (s), 964 (m), 936 (m), 832 (s), 747 (s), 705 (m), 655 (m), 598 (w). Anal. found (calcd. for $C_{54}H_{89}BN_7ScSi$): C, 65.90 (70.48); H, 9.42 (9.75); N, 10.45 (10.66)%. Repeated attempts to obtain an elemental analysis with satisfactory % C values failed, presumably due to incomplete combustion of the compound.

6.9 References

1 A. B. Pangborn, M. A. Giardello, R. H. Grubbs, R. K. Rosen and F. J. Timmers, *Organometallics*, 1996, **15**, 1518–1520.

2 M. Froneman, D. L. Cheney and T. A. Modro, *Phosphorus. Sulfur. Silicon Relat. Elem.*, 1990, **47**, 273–281.

3 T. J. Hadlington, J. A. B. Abdalla, R. Tirfoin, S. Aldridge and C. Jones, *Chem. Commun.*, 2016, **52**, 1717–1720.

4 G. E. Coates and J. G. Livingstone, *J. Chem. Soc.*, 1961, 4909–4911.

5 R. A. Bartlett, H. Chen, H. V. R. Dias, M. M. Olmstead and P. P. Power, *J. Am. Chem. Soc.*, 1988, **110**, 446–449.

6 R. Köster and G. Seidel, *Justus Liebigs Ann. Chem.*, 1977, **1977**, 1837–1846.

7 C. W. Hoerr, E. Rapkin, A. E. Brake, K. N. Warner and H. J. Harwood, *J. Am. Chem. Soc.*, 1956, **78**, 4667–4670.

8 B. D. Ward, S. R. Dubberley, A. Maisse-Francois, L. H. Gade and P. Mountford, *J. Chem. Soc., Dalton Trans.*, 2002, **2**, 4649–4657.

9 F. V. Cochran, P. J. Bonitatebus and R. R. Schrock, *Organometallics*, 2000, **19**, 2414–2416.

10 J. L. Fauré, H. Gornitzka, R. Réau, D. Stalke and G. Bertrand, *Eur. J. Inorg. Chem.*,

1999, **1999**, 2295–2299.

11 C. H. Galka, D. J. M. Trosch, M. Schubart, L. H. Gade, S. Radojevic, I. J. Scowen and M. McPartlin, *Eur. J. Inorg. Chem.*, 2000, 2577–2583.

12 J. T. Ciszewski, J. F. Harrison and A. L. Odom, *Inorg. Chem.*, 2004, **43**, 3605–3617.

13 S. C. Dunn, P. Mountford and D. A. Robson, *J. Chem. Soc. Dalton Trans.*, 1997, **2**, 293–304.

14 M. P. Coles and P. B. Hitchcock, *Organometallics*, 2003, **22**, 5201–5211.

15 J.-H. Huang, L.-S. Chi, F.-M. Huang, P.-C. Kuo, C.-C. Zhou, G.-H. Lee and S.-M. Peng, *J. Chinese Chem. Soc.*, 2000, **47**, 895–900.

16 E. O. Fischer and H. P. Hofmann, *Angew. Chem.*, 1957, **69**, 639–640.

17 M. P. Coles, D. C. Swenson, R. F. Jordan and V. G. Young, *Organometallics*, 1997, **16**, 5183–5194.

18 Y. Segawa, Y. Suzuki, M. Yamashita and K. Nozaki, *J. Am. Chem. Soc.*, 2008, **130**, 16069–16079.

19 T. Nishikawa, A. Ino and M. Isobe, *Tetrahedron*, 1994, **50**, 1449–1468.

20 Z. Yadong and W. Jianxun, *J. Fluor. Chem.*, 1990, 47, 533–535.

21 L. C. Stevenson, DPhil Thesis, University of Oxford, 2015.

22 E. Lu, Y. Li and Y. Chen, *Chem. Commun.*, 2010, **46**, 4469–4471.

23 B. Liu, Y. Huang, J. Lan, F. Song and J. You, *Chem. Sci.*, 2013, **4**, 2163–2167.

24 C. Tessier-Youngs, O. T. Beachley, J. P. Oliver and K. Butcher, in *Inorganic Syntheses, Volume 24*, ed. J. M. Shreeve, John Wiley & Sons, Inc., Hoboken, NJ, USA, 1986, pp. 95–97.

25 R. R. Schrock and J. D. Fellmann, *J. Am. Chem. Soc.*, 1978, **100**, 3359–3370.

26 C. Morton, *ChemSpider SyntheticPages*, 2001, http://cssp.chemspider.com/120.

27 D. S. Levine, T. D. Tilley and R. A. Andersen, *Organometallics*, 2015, **34**, 4647–4655.

28 B. Xie and P. Mountford, Unpublished results.

29 M. F. Lappert and R. Pearce, *J. Chem. Soc. Chem. Commun.*, 1973, 126.

30 E. Lu, J. Chu, Y. Chen, M. V Borzov and G. Li, *Chem. Commun.*, 2011, **47**, 743–745.

31 Z. Otwinowski and W. Minor, *Processing of X-ray Diffraction Data Collected in Oscillation Mode*, Academic press, New York, 1997.

32 A. Altomare, G. Cascarano, G. Giacovazzo, A. Guagliardi, M. C. Burla, G. Polidori and M. Camalli, *J. Appl. Crystallogr.*, 1994, **27**, 435.

33 L. Palatinus and G. Chapuis, *J. Appl. Cryst.*, 2007, **40**, 786–790.

34 P. W. Betteridge, J. R. Cooper, R. I. Cooper, K. Prout and D. J. Watkin, *J. Appl. Cryst.*, 2003, **36**, 1487.

35 M. J. Frisch, G. W. Trucks, H. B. Schlegel, G. E. Scuseria, M. A. Robb, J. R. Cheeseman, G. Scalmani, V. Barone, B. Mennucci, G. A. Petersson, H. Nakatsuji, M. Caricato, X. Li, H. P. Hratchian, A. F. Izmaylov, J. Bloino, G. Zheng, J. L. Sonnenberg, M. Hada, M. Ehara, K. Toyota, R. Fukuda, J. Hasegawa, M. Ishida, T. Nakajima, Y. Honda, O. Kitao, H. Nakai, T. Vreven, J. A. Montgomery Jr., J. E. Peralta, F. Ogliaro, M. J. Bearpark, J. Heyd, E. N. Brothers, K. N. Kudin, V. N. Staroverov, R. Kobayashi, J. Normand, K. Raghavachari, A. P. Rendell, J. C. Burant, S. S. Iyengar, J. Tomasi, M. Cossi, N. Rega, N. J. Millam, M. Klene, J. E. Knox, J. B. Cross, V. Bakken, C. Adamo, J. Jaramillo, R. Gomperts, R. E. Stratmann, O. Yazyev, A. J. Austin, R. Cammi, C. Pomelli, J. W. Ochterski, R. L. Martin, K. Morokuma, V. G. Zakrzewski, G. A. Voth, P. Salvador, J. J. Dannenberg, S. Dapprich, A. D. Daniels, Ö. Farkas, J. B. Foresman, J. V Ortiz, J. Cioslowski and D. J. Fox, *Gaussian 09, Revision. D.01, Gaussian Inc., Wallingford CT*, 2013.

36 A. D. Becke, *J. Chem. Phys.*, 1993, **98**, 5648–5652.

37 J. P. Perdew and Y. Wang, *Phys. Rev. B*, 1992, **45**, 13244–13249.

38 S. Grimme, J. Antony, S. Ehrlich and H. Krieg, *J. Chem. Phys.*, 2010, **132**, 154104–154119.

39 S. Grimme, S. Ehrlich and L. Goerigk, *J. Comput. Chem.*, 2011, **32**, 1456–1465.

40 A. Schäfer, H. Horn and R. Ahlrichs, *J. Chem. Phys.*, 1992, **97**, 2571–2577.

41 F. Weigend and R. Ahlrichs, *Phys. Chem. Chem. Phys.*, 2005, **7**, 3297–3305.

42 A. V. Marenich, C. J. Cramer and D. G. Truhlar, *J. Phys. Chem. B*, 2009, **113**, 6378–6396.

43 E. D. Glendening, J. K. Badenhoop, A. E. Reed, J. Carpenter, J. A. Bohmann, C. M. Morales, C. R. Landis and F. Weinhold, *NBO 6.0, Theoretical Chemistry Institute, University of Wisconsin, Madison*, 2013.

44 T. A. Keith, *AIMAll (Version 16.10.31), TK Gristmill Software, Overland Park KS, USA*, 2016.

45 B. F. Wicker, H. Fan, A. K. Hickey, M. G. Crestani, J. Scott, M. Pink and D. J. Mindiola, *J. Am. Chem. Soc.*, 2012, **134**, 20081–20096.

Appendix

A1 Comparison of DFT model systems containing {MeC(NMe)$_2$} and hpp ligands

To test the validity of using CpTi{MeC(NMe)$_2$}{NB(NMeCH)$_2$} (**2Q_B(NMeCH)$_2$**) as a model for the real compound Cp*Ti(hpp){NB(NAr'CH)$_2$} (**10**), in particular the use of the N-methyl-substituted amidinate rather than the guanidinate ligand hpp, calculations were also run on the hpp-supported model CpTi(hpp)(NMe) (**14Q_Me**) and compared with **2Q_Me**. The three highest occupied MOs of each model are displayed in Figure A1, along with their energies. It is found that these MOs of **14Q_Me** are analogous in form to those of **2Q_Me** although are consistently higher in energy, possibly arising from the guanidinate nitrogen making the ligand more electron rich. The HOMO of each model is predominantly made up of ligand-based lone pairs (at energies of –5.49 and –5.31 eV for **2Q_Me** and **14Q_Me** respectively). The HOMO–1 is the π_v MO, and the HOMO–2– is the π_h MO in each case. Structurally, the optimised models are extremely similar; selected bond metrics are shown in Table A1.

Table A1. DFT-calculated bond distances (Å) and angles (°) for the model compounds CpTi{MeC(NMe)$_2$}(NMe) (**2Q_Me**) and CpTi(hpp)(NMe) (**14Q_Me**). Cp$_{cent}$ refers to the computed Cp ring centroid.

Parameter	**2Q_Me**	**14Q_Me**
Ti–N$_{im}$	1.679	1.679
Ti–N$_{ligand}$	2.090, 2.097	2.088, 2.094
Ti–Cp$_{cent}$	2.091	2.098
Cp$_{cent}$–Ti–N$_{im}$	122.8	122.2

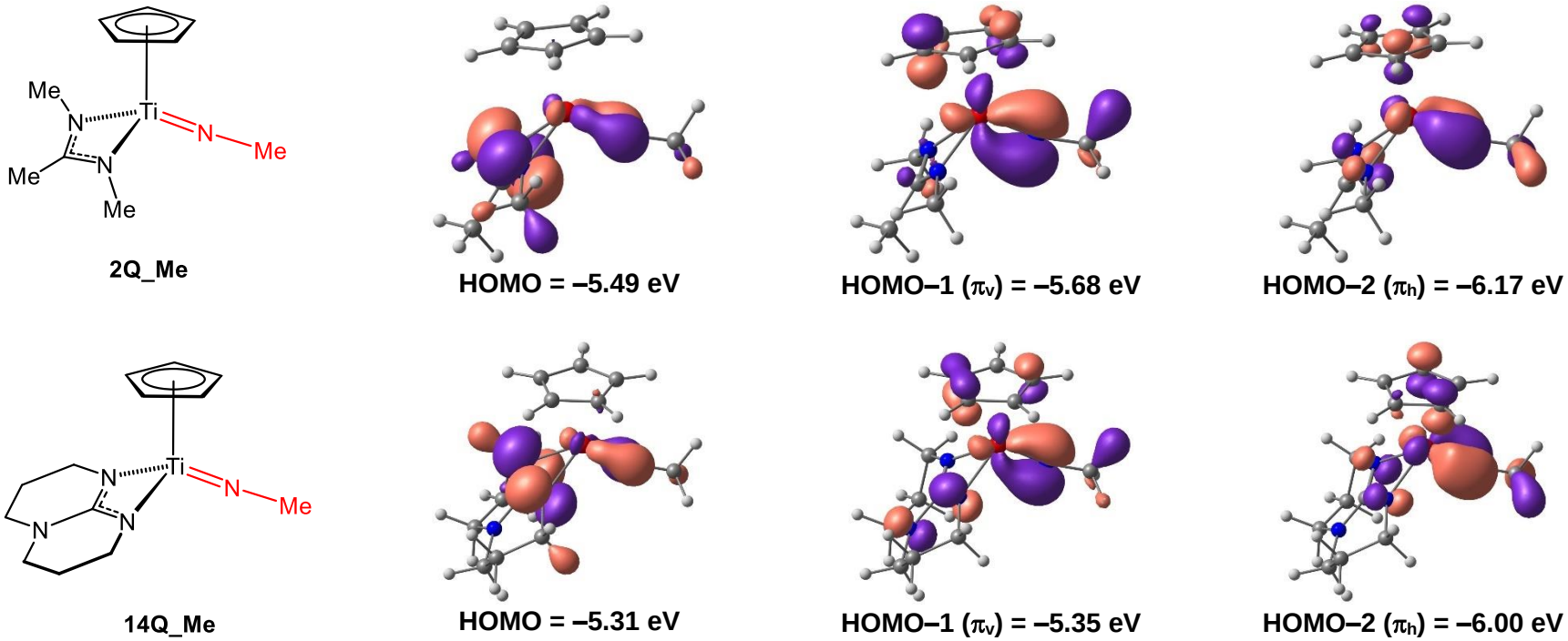

Figure A1. DFT model compounds CpTi{MeC(NMe)$_2$}(NMe) (**2Q_Me**, top) and CpTi(hpp)(NMe) (**14Q_Me**, bottom), and associated isosurfaces and energies of the three highest occupied MOs..

For the families of model compounds **2Q_R** and **14Q_R** (R = Me, Ph, Xyl, BMe_2, $B(NMeCH)_2$ in both cases), the Ti–N_{im} bond dissociation energies (ΔE_{BD}) were calculated. These are listed in Table A2, and compared graphically in Figure A2. It is apparent that the bond dissociation energies of the hpp-supported models **14Q_R** are consistently lower than their counterparts **2Q_R**. The *y*-intercept of 21.67 kcal mol^{-1} in Figure A2 represents the intrinsic difference between the two systems, which is attributed to differences in relaxation energies of the respective fragments. This is confirmed by considering the exchange energies of **2Q_Me** and **14Q_Me** with amines H_2NR to give **2Q_Me** or **14Q_Me** and H_2NMe, which are found to be comparable between the two systems (Table A2). MO analysis of the triplet CpTi{$MeC(NMe)_2$} and CpTi(hpp) fragments shows that in the former case, the highest energy SOMO is a metal–amidinate antibonding MO, whereas for the latter, this is a non-bonding MO (in fact a pure metal d orbital). Thus, the CpTi{$MeC(NMe)_2$} fragment is destabilised relative to the hpp-analogue and gains much less of a negative contribution to its ΔE_{BD} values from the relaxation of this fragment.

Table A2. DFT-calculated Ti–N_{im} bond dissociation energies (ΔE_{BD}, kcal mol^{-1}) in the model compounds CpTi{$MeC(NMe)_2$}(NMe) (**2Q_R**) and CpTi(hpp)(NMe) (**14Q_R**); R = Me, Ph, Xyl, BMe_2, $B(NMeCH)_2$, along with exchange energies (ΔE_{exch}, kcal mol^{-1}) for **2Q_Me** or **14Q_Me** with H_2NR to give **2Q_R** or **14Q_R** and H_2NMe.

R	ΔE_{BD} (**2Q_R**)	ΔE_{BD} (**14Q_R**)	ΔE_{exch} (**2Q_R**)	ΔE_{exch} (**14Q_R**)
Me	109.7	91.2	-	-
Ph	108.2	90.4	–1.8	–2.5
Xyl	105.3	87.3	–1.3	–1.8
BMe_2	132.3	115.4	11.7	10.2
$B(NMeCH)_2$	119.6	102.0	0.8	0.03

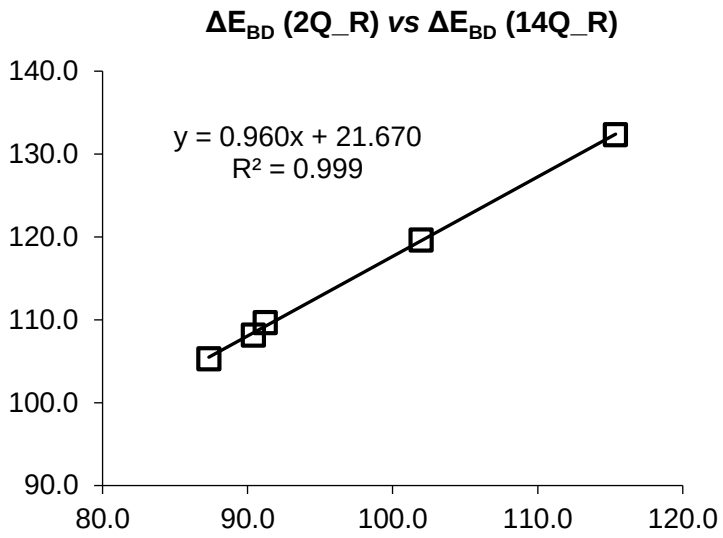

Figure A2. Plot of DFT-calculated Ti–N_{im} bond dissociation energies (ΔE_{BD}, kcal mol^{-1}) in the model compounds CpTi{$MeC(NMe)_2$}(NMe) (**2Q_R**) *vs* those in CpTi(hpp)(NMe) (**14Q_R**); R = Me, Ph, Xyl, BMe_2, $B(NMeCH)_2$.

A2 Additional kinetic data for Chapter Four

Table A3. First order rate constants obtained for the conversion of $Ti(N_2^{ArF}N^{Me})\{N\{B(NAr'CH)_2\}C(H)C(Tol)\}$ (**25**) to $Ti\{MeN(CH_2CH_2NAr^F)\{CH_2CH_2NC_6F_4C(Tol)=CHNB(NAr'CH)_2\}\}(F)$ (**28**), described in Chapter Four.

Temperature K	Notes	k_{obs} / 10^{-5} s^{-1}
327		8.15(2)
330		10.34(1)
333		11.04(3)
333	Double [**25**]	12.72(2)
336		15.18(2)
339		18.41(6)

Unless otherwise stated, $[\mathbf{25}]_0 = [\mathbf{28}]_{final} = 0.026$ mol dm^{-3}.

Table A4. First order rate constants obtained for the conversion of $Ti(N_2^{ArF}N^{Me})\{N\{B(NAr'CH)_2\}C(H)C(Ar^F)\}$ (**27**) to $Ti\{MeN(CH_2CH_2NAr^F)\{CH_2CH_2NC_6F_4C(Ar^F)=CHNB(NAr'CH)_2\}\}(F)$ (**26**), described in Chapter Four.

Temperature K	Notes	k_{obs} / 10^{-5} s^{-1}
327		6.60(2)
330		8.35(2)
333		9.32(3)
336		11.82(1)
336	Double [**27**]	12.63(2)
339		14.97(1)

Unless otherwise stated, $[\mathbf{27}]_0 = [\mathbf{26}]_{final} = 0.026$ mol dm^{-3}.

A3 Additional crystallographic structure for Chapter Five

Figure A3. Displacement ellipsoid plot (20% probability) of [{MeC(NAr')CHC(CH_2)($NCH_2CH_2NMe_2$)}Sc{NHB($N^iPr)_2C_6H_4$}]$_2$, as described in Chapter Five. Atoms carrying the suffix 'A' are related to their counterparts by the symmetry operator [–*x*, 1–*y*, 1–*z*].

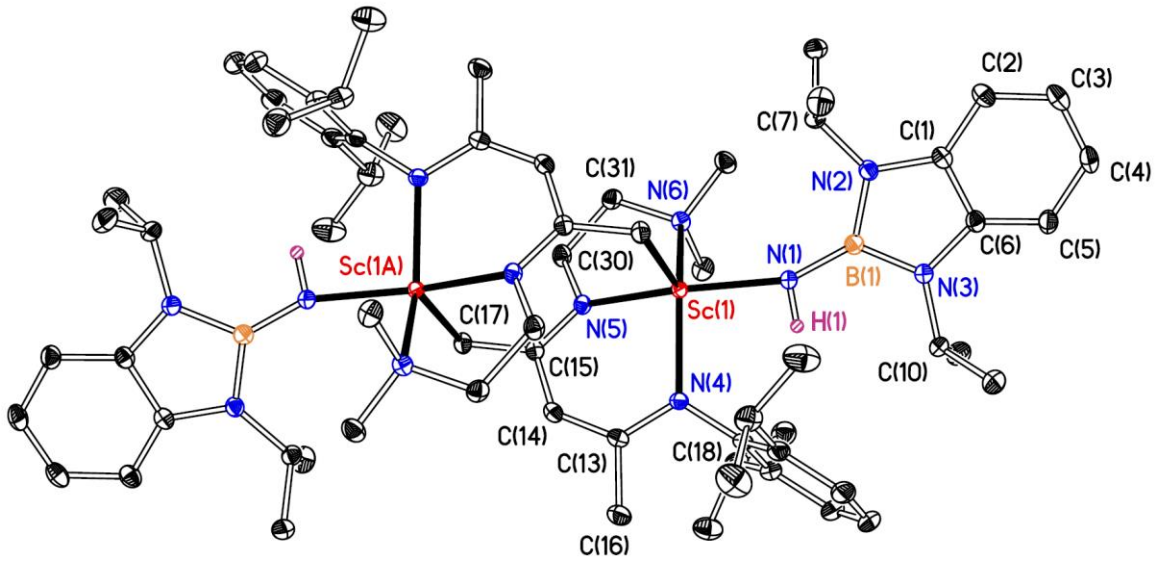

Table A5. Selected bond distances (Å) and angles (°) for [{MeC(NAr')CHC(CH_2)($NCH_2CH_2NMe_2$)}Sc{NHB($N^iPr)_2C_6H_4$}]$_2$.

Sc(1)–N(1)	2.0922(15)	N(1)–Sc(1)–N(4)	94.77(6)
Sc(1)–N(4)	2.1420(14)	N(1)–Sc(1)–N(5)	153.59(6)
Sc(1)–N(5)	2.1873(14)	N(1)–Sc(1)–N(6)	88.28(5)
Sc(1)–N(6)	2.3460(14)	N(4)–Sc(1)–N(5)	85.84(5)
Sc(1)–C(17)	2.3333(17)	N(1)–Sc(1)– C(17)	103.24(6)
N(1)–B(1)	1.412(2)	Sc(1)–N(1)–B(1)	156.18(13)
N(1)–H(1)	0.91(3)	Sc(1)–N(1)–H(1)	95.3(17)